The Dissertation Committee for Stephanie Wafforn certifies that this is the approved version of the following dissertation:

Geo- and Thermochronology of the Ertsberg-Grasberg Cu-Au Mining District, west New Guinea, Indonesia

Committee:

Mark Cloos, Co-Supervisor

Daniel F. Stockli, Co-Supervisor

James Richard Kyle

Sarah C. Penniston-Dorland

Jeremy P. Richards

Geo- and Thermochronology of the Ertsberg-Grasberg Cu-Au Mining District, west New Guinea, Indonesia

by

Stephanie Wafforn, BS; MS

Dissertation

Presented to the Faculty of the Graduate School of

The University of Texas at Austin

in Partial Fulfillment

of the Requirements

for the Degree of

Doctor of Philosophy

The University of Texas at Austin

May, 2017

Acknowledgements

First and foremost I want to thank my advisors, Mark Cloos and Danny Stockli, for their guidance and mentorship throughout this journey. I am so very proud of what we've accomplished with this dissertation. The countless hours that Mark and I have spent discussing the geology of the Ertsberg-Grasberg mining district and the fundamentals of porphyry copper deposit genesis have helped make me the scientist that I am today. I also have to thank my committee members, Richard Kyle, Sarah Penniston-Dorland, and Jeremy Richard, for their help and input throughout the course of this dissertation. Their comments, edits, and challenges have certainly improved this dissertation.

So many others have contributed to the success of this work. The continued logistical and financial support of Freeport McMoRan has been integral in making the Ertsberg Project a success. I want to thank Clyde Leys for helpful discussions and facilitating the two site visits, and Reza Al Furqan, Pandji Muhammad, Apun Permana, Nimrod Msen, and Hari for their help in the core shed and beyond. I would also like to thank the UT Chron lab managers, Lisa Stockli and Des Patterson, for their technical support throughout the completion of the geochronology and thermochronology analyses.

It has taken an army of undergraduate workers to help with all of the mineral separation, slab polishing, and petrography required to make this project a success, and I am incredibly grateful for their hard work. Jacob Makis has been involved with this project almost as long as I have, and completed a huge amount of mineral separation and sample preparation for this project. I also want to thank Drew McPeak, Grace Hartzell, Emily Frank, Fawwaz Aziz, Barret Yeager, Emilie Bowman, Alan Morales Sandoval, Dana Downs, and Eytan Orent for their hard work on the Ertsberg-Grasberg Project.

Lastly, a huge thank you to my family and friends for supporting me throughout this endeavor. Mum, Dad, and Miles – I love you! Patrick came into my life towards the end of this project, and has willingly endured the long work hours and random geology rants. I will always be grateful for your support during this time in our lives together. And of course, I would not have made it this far without Scattered Oaks Farm as my sanctuary and escape. It seems fitting to end my acknowledgements with a nod to Fuller, my heart horse.

Geo- and Thermochronology of the Ertsberg-Grasberg Cu-Au Mining District, west New Guinea, Indonesia

Stephanie Wafforn, PhD

The University of Texas at Austin, 2017

Co-Supervisors: Mark Cloos and Daniel F. Stockli

The prolific Ertsberg-Grasberg Cu-Au mining district, located on the island of New Guinea in Indonesia, is host to the supergiant Grasberg porphyry copper deposit, and multiple giant skarns. The well-studied nature of the district provides geologic context for high resolution geochronology and thermochronology studies. The supergiant Grasberg porphyry copper deposit is hosted in the Grasberg Igneous Complex. Intrusions were dated using the novel zircon U/Pb depth profiling technique, and age results show the magmatic system was active from 3.6-3.1 Ma. Cu-Au mineralization initiated following intrusion of the MGI (3.22 ± 0.04 Ma) and predates the EKI (3.20 ± 0.04 Ma) and LKI (3.09 ± 0.05 Ma). Based on these cross-cutting relationships, the high grade core of the Grasberg deposit formed in less than 100 to 220 kyr. Age results for the Ertsberg pluton (31-2.8 Ma) and other minor intrusions shows that magmatism in the district took less than 1 myr.

Zircon and apatite (U-Th)/He ages from a 2.2 km vertical profile in the Grasberg deposit record minimum cooling rates of 25°C/10 kyr near surface and 4°C/10 kyr at depth. These results indicate Grasberg ore formation occurred immediately following maar volcanism and was short-lived. Rapid cooling of surface samples precludes the presence of a 2 km volcanic edifice overlying the orebody. Rapid cooling at 2 km depth necessitates emplacement into cold country rock. As copper sulfide precipitation is temperature dependent, the tightness of isotherms in the ore zone contributes to the localization of copper mineralization into a small volume, resulting in an extraordinarily high ore grades.

Garnet samples from the Big Gossan skarn were dated using the newly developed LA-ICP-MS garnet U/Pb chronometer. Age results show the skarn formed between 2.9–2.7 Ma, over a timespan of approximately 200 kyr. High U contents (10-100 ppm) and a consistent common Pb composition improve precision, and garnet ages agree with external age constraints. This study demonstrates that andradite garnet U/Pb chronometry can be a robust dating technique for constraining the timing and duration of skarn-forming hydrothermal systems.

Table of Contents

List of Tables

List of Figures

Introductory Notes

This dissertation is a collection of seven chapters that discuss the geochronology and thermochronology of intrusions in the Ertsberg-Grasberg mining district, and the implications for the sequence of events, the duration of magmatic-hydrothermal fluid flow, and the critical factors leading to porphyry and skarn type ore formation.

Chapters 1 presents the results of zircon U/Pb (LA-ICP-MS) dating of the Grasberg Igneous Complex (n=45 samples), where cross-cutting relationships constrain the duration of magmatic-hydrothermal flow. Chapter 2 discusses the results of zircon and apatite (U-Th)/He dating of samples from a 2.2 km vertical profile through the Grasberg porphyry copper deposit, and the implications of rapid cooling for ore formation. Chapter 3 presents garnet U/Pb ages for eight samples from the Big Gossan skarn, measured using the newly developed andradite garnet U/Pb LA-ICP-MS chronometer. Chapters 4 expands the zircon U/Pb geochronology to nearly all intrusions known in the district (n=63), establishing the sequence of magmatic events, and Chapter 5 expands the zircon and apatite (U-Th)/He thermochronology to the Ertsberg pluton, North Grasberg, Wanagon and the HEAT Road dikes, confirming that intrusions in the district cooled rapidly and river incision rates near the crest of the mountain range are high. Chapter 6 focuses on the preliminary dating results for garnet samples from Dom (n=2) and Kucing Liar (n=1). Chapter 7 evaluates the volume and flux of magma and hydrothermal fluids required to both supply and transport the extraordinarily large metal abundances in the district, using the duration estimates presented in the preceding chapters.

Chapter 1: Zircon U/Pb Geochronology of the Grasberg Igneous Complex

ABSTRACT

The Grasberg porphyry copper deposit, located in Papua, Indonesia, contains one of the largest resources of copper and gold in the world (2000 Mt at 1 wt. % Cu and 1 g/ton Au). Copper and gold mineralization is hosted in the Pliocene Grasberg Igneous Complex (GIC), which includes the Dalam phase, the Main Grasberg Intrusion (MGI), and the Kali Dikes. At the pit level, well-defined cross-cutting relationships show that main stage Cu-Au mineralization is hosted in the MGI and cross-cut by the Late Kali Dikes. Intrusions were dated using the novel tape mount, zircon U/Pb method, where zircons are mounted on double-sided tape and the crystal face is ablated. This technique makes it possible to isolate only the outermost, youngest zircon growth zones, such that when 30 zircon analyses from a single sample are plotted on a Tera Wasserburg diagram the resultant lower intercept age almost always has a precision of ±0.1 myr. Composite ages are calculated by compiling all zircon analyses from three or more samples of the same intrusion, thus improving the statistics and reducing the uncertainties (±0.05 myr).

LA-ICP-MS zircon U/Pb dating of intrusions that host and cross-cut ore grade mineralization provide tight constraints on the maximum duration of hydrothermal fluid flow. Dalam phase magmatism was multi-stage, with intrusive and extrusive activity between 3.6 to 3.3 Ma. Main phase copper mineralization initiated following intrusion of the MGI (3.22 ± 0.04 Ma, x=9 samples, n=233 zircons,) and predates the Late Kali Dikes (3.09 ± 0.05 Ma, x=3, n=88). The bulk of the Cu-Au mineralization is also post-dated by the Early Kali Dikes (3.20 ± 0.04 Ma, x=5, n=141). Based on these cross-cutting relationships, and taking into account the analytical errors, the high grade core of the Grasberg deposit formed in at most 100 to 220 kyr.

INTRODUCTION

The island of New Guinea hosts three major economic ore deposits, including the prolific Ertsberg-Grasberg mining district, OK Tedi, and Porgera. New Guinea was created during the largest and most recent island arc-continent collision. The northern half of the island comprises an ocean island arc complex and the southern half of the island comprises deformed passive margin strata deposited on the northern edge of Australian continental crust (Figure 1-1) (Dewey and Bird, 1970; Hamilton, 1979; Weiland and Cloos, 1996; Quarles van Ufford and Cloos, 2005). The shape of New Guinea is often described as a bird, where the bird's body can be divided into four tectonic terranes: from south to north these are the foreland basin, the Central Range fold and thrust belt, a metamorphic belt, and an accreted island arc complex. Two distinct phases of deformation created the Central Range (Quarles van Ufford and Cloos, 2005). The first pre-collision phase began at approximately 12 Ma, when kilometer-scale folds and subsidiary reverse and thrust faults developed as Australian strata were bulldozed in a northern dipping oceanic subduction zone (Figure 1-2). The second phase of collisional tectonism occurred between 8 Ma and 2 Ma, when the continental part of the Australian plate jammed the subduction zone (Cloos et al., 2005). Breakoff of the oceanic end of the Australian plate, and decompression melting of the asthenospheric mantle, resulted in a short-lived but large magmatic event. This magmatic event was ultimately responsible for ore formation in the Ertsberg-Grasberg mining district (Cloos et al., 2005). Housh and McMahon (2000) show that mafic magma assimilated a large volume of the lower crust, most likely in a large chamber near the Moho, prior to ascent to a batholithic magma chamber in the upper crust (Figure 1-3) (Cloos, 2001). Structural analysis by Sapiie (1998) showed the Grasberg Igneous Complex (GIC) was emplaced into a pull-apart connection between sinistral strike-slip faults in the Central Range during this time (Sapiie and Cloos, 2004). Here, and elsewhere, the strike-slip structural setting appears to be critical in providing pathways for magma ascent and focused hydrothermal fluid flow (see Richards, 2003; 2009; 2011), and for enabling a prolonged throttled discharge from the fluid charged cupola (Cloos and Sapiie, 2013).

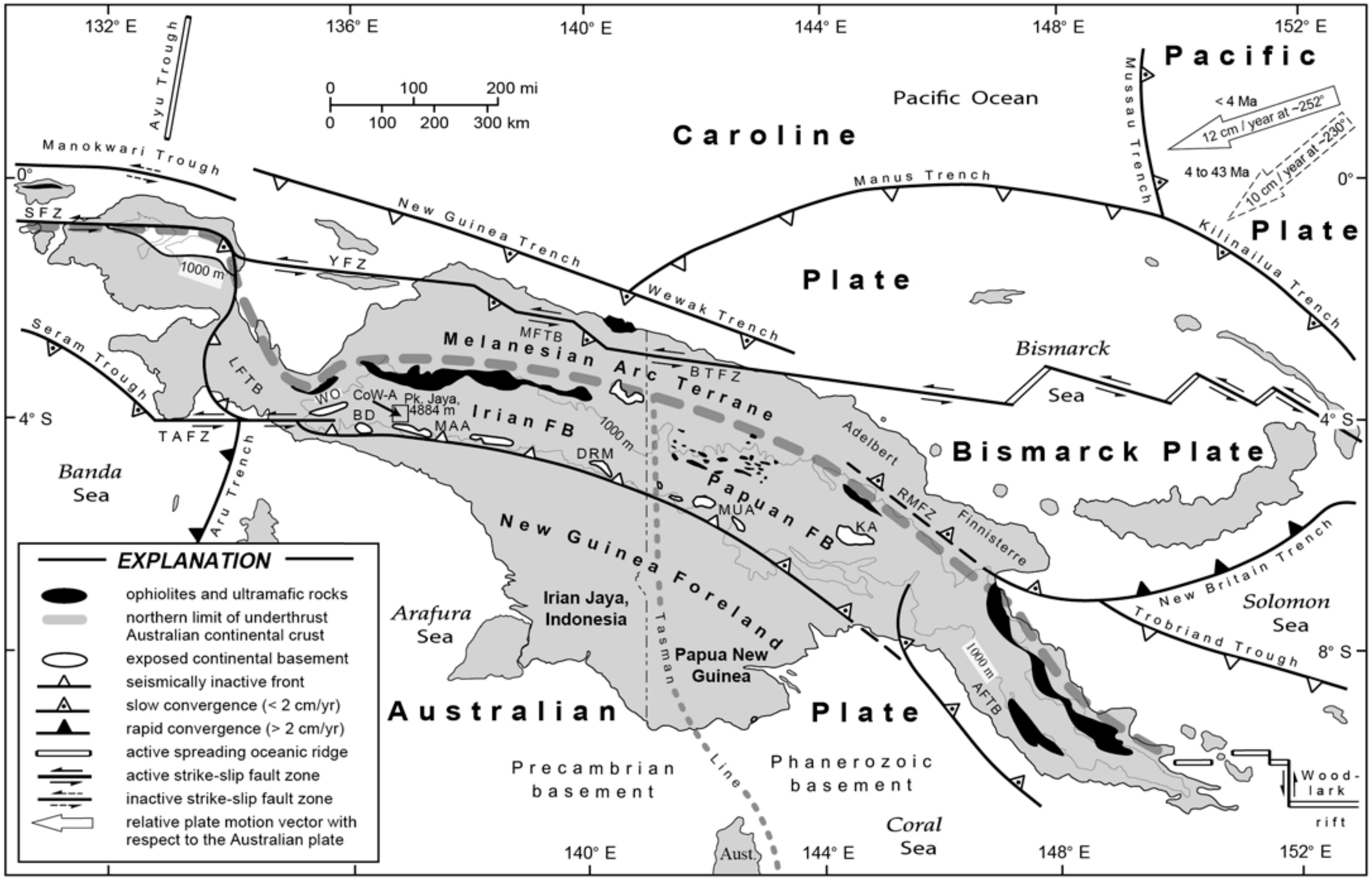

Figure 1-1. Tectonic map of New Guinea with outcrops of Australian continental basement and ophiolite highlighting the Central Range between the Australian and Pacific plates. The Central Range consists of the following tectonostratigraphic provinces, from west to east: the Lengguru fold-and-thrust belt (LFTB), the Weyland over-thrust (WO), Irian fold belt (FB), and Papuan fold belt. Other tectonic features include AFTB - Aure fold-and-thrust belt, BD - Baupo dome, BTFZ - Bewani-Torricelli fault zone, DRM Digul Range monocline, KA - Kubor anticline, MAA - Mapenduma anticline, MUA – Muller anticline, MFTB - Mamberamo fold and-thrust belt, RMFZ - Ramu-Markham fault zone, SFZ - Sorong fault zone, TAFZ - Tarera-Aiduna fault zone, YFZ - Yapen fault zone. Simplified from Hamilton (1979), Cooper and Taylor (1987), and Dow et al. (1986). From Weiland and Cloos (1996) and Sapiie et al. (1999).

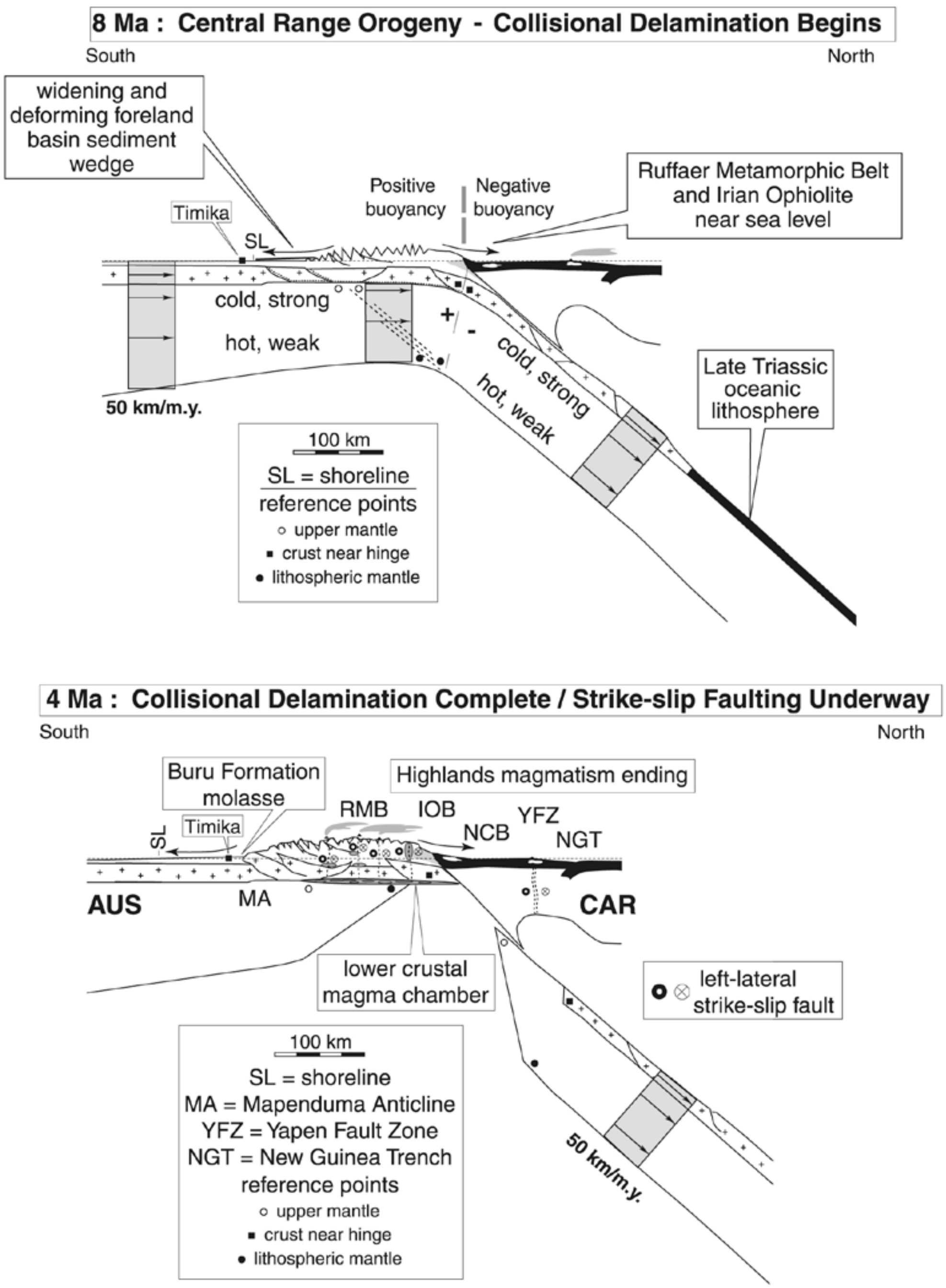

Figure 1-2. (Above) Cross section at 8 Ma showing the initial stage of jamming of the Australian passive margin against the Pacific Plate. As the Australian continental lithosphere jams the subduction zone, delamination begins as the slabs pull force is translated updip in the upper part of the plate. (Below) Cross section showing the lithosphere at 2 Ma once delamination is complete. Upwelling of the asthenosphere where the plate breaks away results in decompression melting. The magma generation event is short-lived. Pooling of the mafic magma at the Moho leads to lower crustal assimilation. From Cloos et al. (2005).

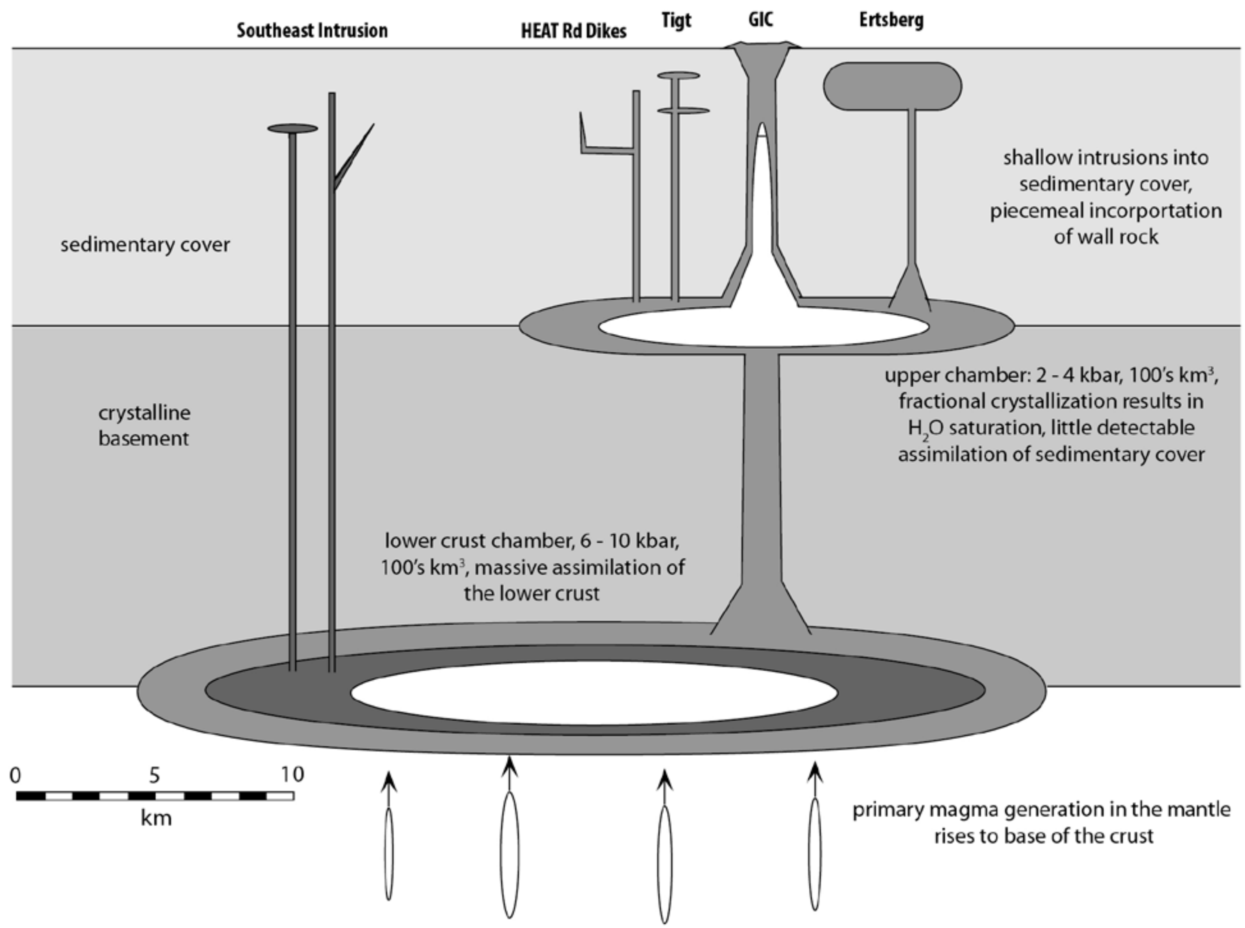

Figure 1-3. Schematic diagram illustrating the feeder stock and batholithic magma chambers inferred to underlie the Ertsberg-Grasberg mining district. The lower magma chamber is where mafic magma, generated by decompression melting of the asthenospheric and lithospheric mantle during slab delamination, pooled at the interface between the continental crust and the mantle. Assimilation of lower crust takes place in this magma chamber. Similarly, buoyancy forces act to create an upper crustal magma chamber at the contact between crystalline basement and the sedimentary cover. The pathways for magma ascent are created primarily by pull-apart zones between strike-slip faults. After Cloos (2001).

In the mining district, drilling reveals that the GIC intruded into sedimentary strata of the Jurassic-Cretaceous Kembelangan and Tertiary New Guinea Groups (Figure 1-4) (Flint, 1972; MacDonald and Arnold, 1994; McMahon, 1994; McDowell et al., 1996). The Kembelangan Group is regionally extensive and consists of interlayered carbonaceous siltstone and mudstone and fine-grained quartz sandstones with minor shale (Quarles van Ufford, 1996). The New Guinea Limestone Group overlies the Kembelangan and is well exposed in the mining district. Much interest centers on the magmatic evolution of the GIC, which comprises three main phases: the Dalam Phase, the Main Grasberg Intrusion (MGI) and the Kali Dikes (Figure 1-5) (MacDonald and Arnold, 1994; Leys et al., 2012). The Dalam Phase includes four mappable units: the Dalam Andesite, a greenish coarsely porphyritic hornblende-biotite andesite, the Dalam Fragmental, a monomict autobreccia, the Dalam Volcanic, a matrix-supported polymict breccia, and the Tertiary Volcaniclastic Sediments (Tvs), a 100 m thick sequence of fine-grained tuffaceous strata (Sapiie and Cloos, 2013). Below ~3500 m these units grade into crystalline plutonic rock, logged as the highly altered Dalam Diorite. The MGI is a conical plug that was emplaced into the still hot center of the Dalam units (Paterson and Cloos, 2005a). The intrusion comprises highly altered quartz monzonite to quartz monzodiorite with a nearly equigranular texture. The Kali Phase is a NW striking wedge-shaped nest of dikes that was divisible above ~3700 m elevation into an early and late phase. Diking relationships are more complex with depth, where more phases of the Kali Dikes are recognized (Pollard and Taylor, 2002; Bowman, 2017). Above 3700 m elevation the Early Kali Dikes are restricted in area, forming an ellipsoidal zone tens of meters across near the center of the GIC. Above 3700 m elevation the Late Kali Dikes clearly post-date most high-grade ore mineralization (Penniston-Dorland, 1997) and have abundant fresh magmatic feldspars, biotite, and hornblende.

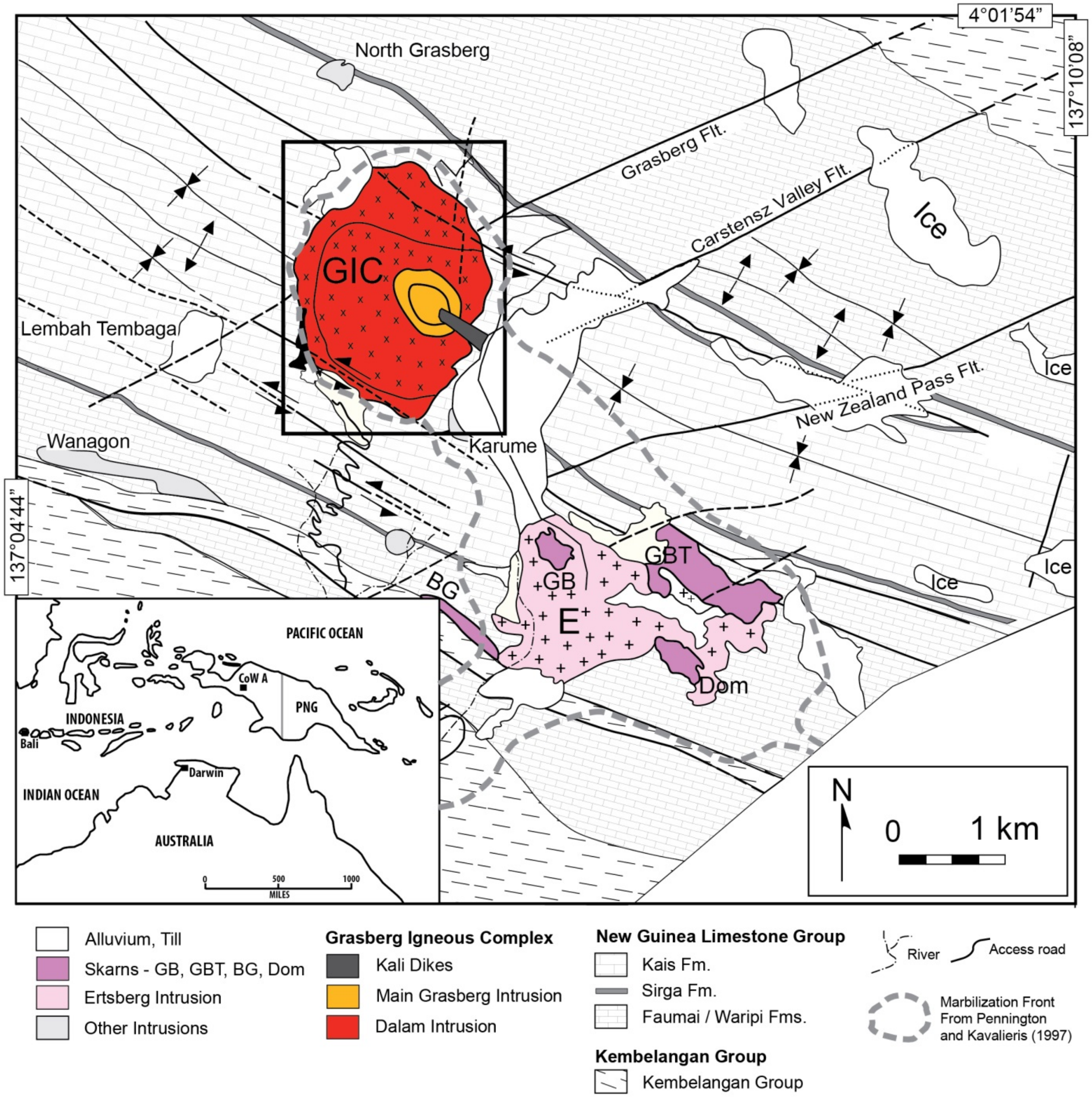

Figure 1-4. Map of the Ertsberg-Grasberg mining district modified from Paterson and Cloos (2005a). Black box shows the location of Figure 1-5. Inset map shows the location of the Ertsberg-Grasberg mining district, labeled CoWA (Contract of Work area A), in Papua, Indonesia. Skarns: GB - Gunung Bijih (Ertsberg), GBT – Gunung Bijih Timur (Ertsberg East), BG - Big Gossan.

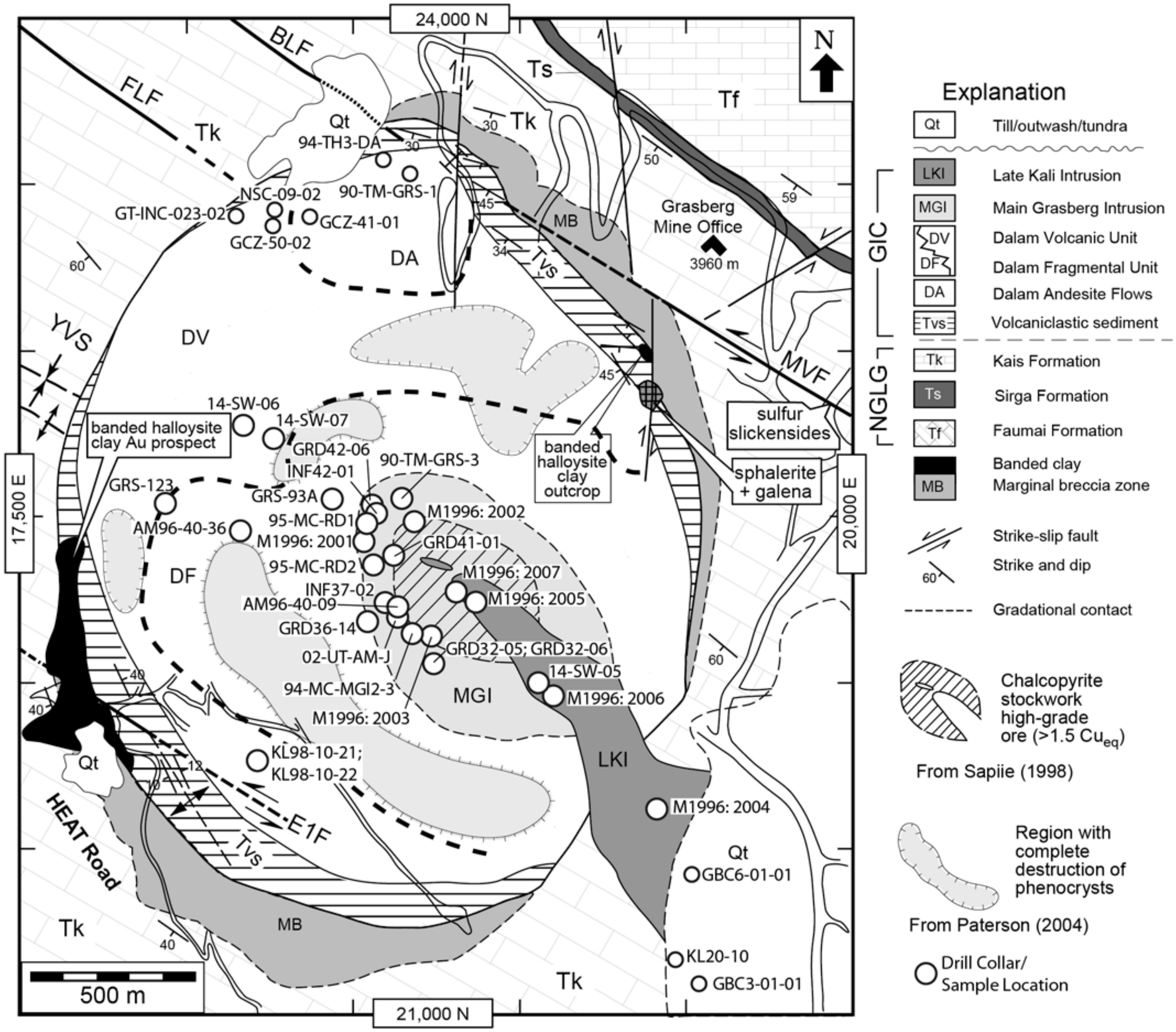

Figure 1-5. Geology of the Grasberg Igneous Complex (GIC) at the ~3900 m elevation. Modified from Suwardy (1995), Sapiie (1998), and Paterson and Cloos (2005a). Locations for outcrop samples and drill hole collars for core samples are shown in the black circles.

Mineralizing fluids in the Grasberg system ascended near the center of the GIC (Van Nort et al., 1991), as evidenced by the decreasing alteration intensity outwards from the center of the stock. According to Penniston-Dorland (2001), above 3700 m elevation there are two distinct stages of vein formation. Stage 1a occurred following emplacement of the MGI and is characterized by a quartz ± magnetite stockwork. This is defined as a 3D dilatational network, with a 200 to 300 m diameter zone commonly containing areas with greater than 50% veins per cubic meter (Sapiie and Cloos, 2013). Stage 1b makes up the majority of the high grade ore and comprises both vein-hosted and disseminated chalcopyrite and bornite, which increases in abundance with depth. Stage 2 occurred after intrusion of the Kali Phase Dikes, and is characterized by the presence of abundant biotite and rare K-feldspar veins with very minor associated copper sulfide (Penniston-Dorland, 2001).

Porphyry Copper Deposits

Mining of porphyry copper deposits in the United States began as early as 1870. Initial mining efforts in Arizona, Utah, and Nevada included selective underground mining and local smelting operations of high-grade copper oxide and sulfide bearing ores. Parsons (1933) documented the financing, engineering, and development of a dozen porphyry copper deposits, stating that the expanded use of electricity in the 20th century would not have been possible without the large and steady supply of copper. The first compilation of porphyry copper deposit descriptions by Titley and Hicks (1966) was followed up by the seminal paper by Lowell and Guilbert (1970) describing the patterns of alteration and mineralization that guide exploration programs. Another notable early contribution was the description of the El Salvador porphyry copper deposit, located in Chile, by Gustafson and Hunt (1975), who described several classes of veins that are now recognized in deposits worldwide.

Modern porphyry copper deposit models largely focus on the magmatic-hydrothermal processes that lead to fluid exsolution, metal transport, hypogene mineralization and alteration (summarized in Seedorff et al., 2005; Sillitoe, 2005; 2010). Porphyry systems span the upper 4-6 km of the crust, and are associated with a stock. Giant deposits must be connected to a larger parental batholith at depth (Cloos, 2001; Richards, 2005). While the source of metals in porphyry systems was initially up for debate, with models ranging from a magmatic source (Gustafson and Hunt, 1975; Burnham, 1979; Dilles, 1987) to leaching of metals from the wall rocks by circulating, hot meteoric fluids (Henley and McNabb, 1978; Norton, 1982), it is now understood that copper is scavenged from a melt by chlorine-rich magmatic-hydrothermal fluids. A summary of the overall picture is that oxidizing, hydrous (1-4 wt.% H_2O) magmas emplaced into the upper crust becomes saturated with a fluid phase (Burnham and Ohmoto, 1980; Candela and Holland, 1984; Cline and Bodnar, 1991). The strong pressure-dependence on the partitioning of chlorine, and this copper, into the fluid phase means that the bulk of the batholith must be deeper than 2 kbar, or 6 km depth (Shinohara et al., 1989; Cline and Bodnar, 1991). A stock geometry facilitates the localization of both the magma and the magmatic-hydrothermal fluid flow such that an ore body is able to precipitate in the overlying crust.

Bubbling Magma Chambers and Throttling Cupolas

When a stock is emplaced into cold country rock, steep lateral thermal gradients will result in a zone of transition from mobile to solidified magma (Cloos, 2001). At depths where the magma is H_2O unsaturated, feldspars and quartz must crystallize for the magma to become fluid saturated. Bubbles should first form in the shallow parts of the system. When the amount of bubble formation is sufficient, buoyant magma will rise along the sidewalls. This is a self-enhancing process, because buoyancy increases as the bubbles expand during ascent. Eventually, bubbles grow large enough to rise on their own, separating from the magma to collect below a cupola (Figure 1-6). Degassed magma will then sink in the middle of the stock. The cupola becomes charged with a copper-rich fluid when the bubbling front reaches depths of ~6 km, as the partitioning of chlorine, and thus copper, is strongly pressure dependent (Candela and Holland, 1984; Shinohara et al., 1989). A porphyry copper deposit can form when copper-rich hydrothermal fluids collect beneath a fluid-charged cupola and ascend into the overlying rock mass, either through pervasive infiltration fluid flow, which results in the characteristic alteration halos of Lowell and Gilbert (1970) or in extension fractures that form veins. When copper-rich fluid generation occurs in a steady and prolonged fashion, a giant porphyry copper deposit can form.

Draining of the fluid charged cupola must be a critical step in the formation of porphyry copper deposits, as the creation of pockets of supercritical fluid is probably a common precursor to explosive discharge and eruption of a magmatic system. Cloos and Sapiie (2013) conclude that strike-slip faulting is the key mechanism that causes periodic draining of fluid from beneath a cupola. Strike-slip faulting generates pull-apart zones, which provides a pathway for emplacement of the stock. Continued movement after emplacement as rapid, earthquake generating fault slip events create extension fractures in the hot and ductile carapace of the stock above the cupola (Figure 1-7). Hydrothermal fluids in the fluid charged cupola will jet into the extension fractures, decompress, and cool, resulting in the precipitation of vein minerals, including copper sulfides when the fluids contain sufficient copper and sulfur. Earthquake recurrence rates on a decadal scale would allow sufficient time for the cupola to be re-charged with fluid, while also acting as a safety valve for the release of the fluids, preventing explosive eruption. This process is appropriately termed the “throttling cupola”.

This is the tectono-magmatic framework for which this study provides the refined geochronology needed to evaluate the magmatic and hydrothermal fluxes that led to ore formation in one of the largest ore bodies on Earth.

Deep-Seated Bubbling: Stock-Batholith Chamber

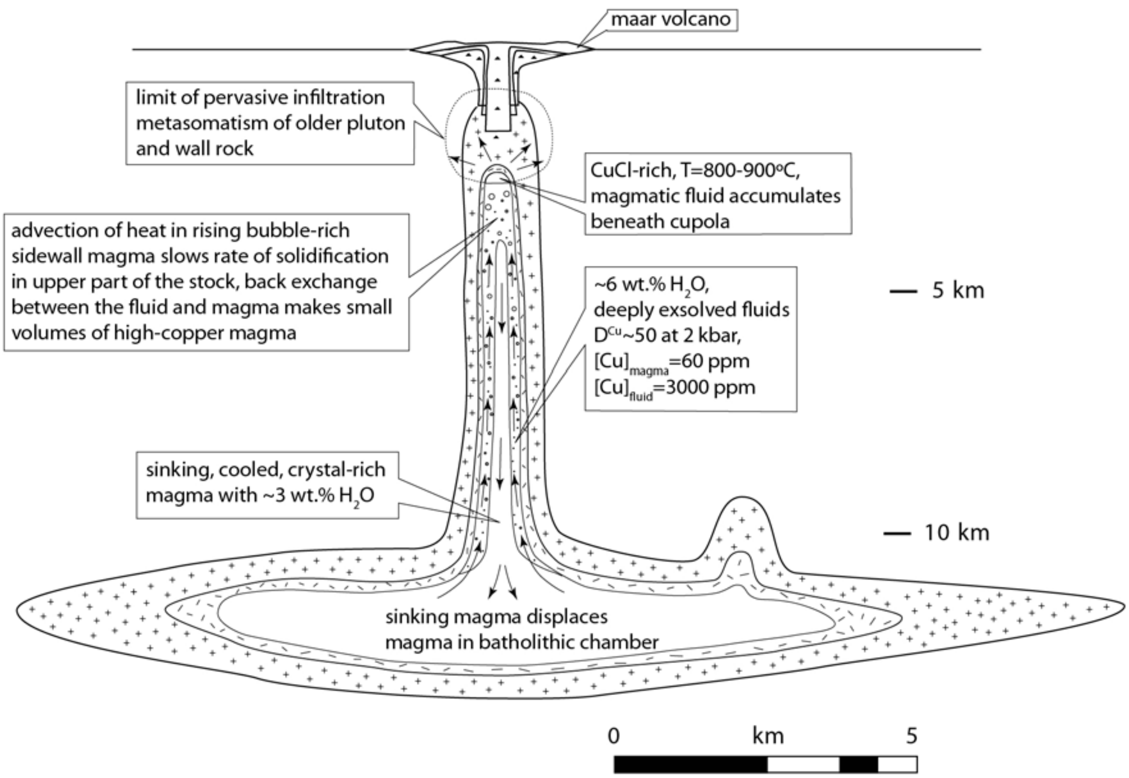

Figure 1-6. Schematic diagram of a bubbling stock connected to a batholithic magma chamber in the upper crust. As sidewall magma crystallizes quartz and feldspar the melt reaches fluid saturation. As fluid bubbles are generated the magma can start to buoyantly rise along the sidewalls. Bubbles grow and become sufficiently large that they separate and collect below the cupola. Degassed magma sinks down the middle of the stock. When the bubbling front becomes sufficiently deep (greater than ~ 6 km) chlorine, and thus copper, will experience strong partitioning into the fluid phase. As bubble-bearing magma continues to rise along the sidewalls, the cupola becomes charged with copper-rich hydrothermal fluids. D_{Cu} = copper partitioning coefficient. Modified from Cloos (2001).

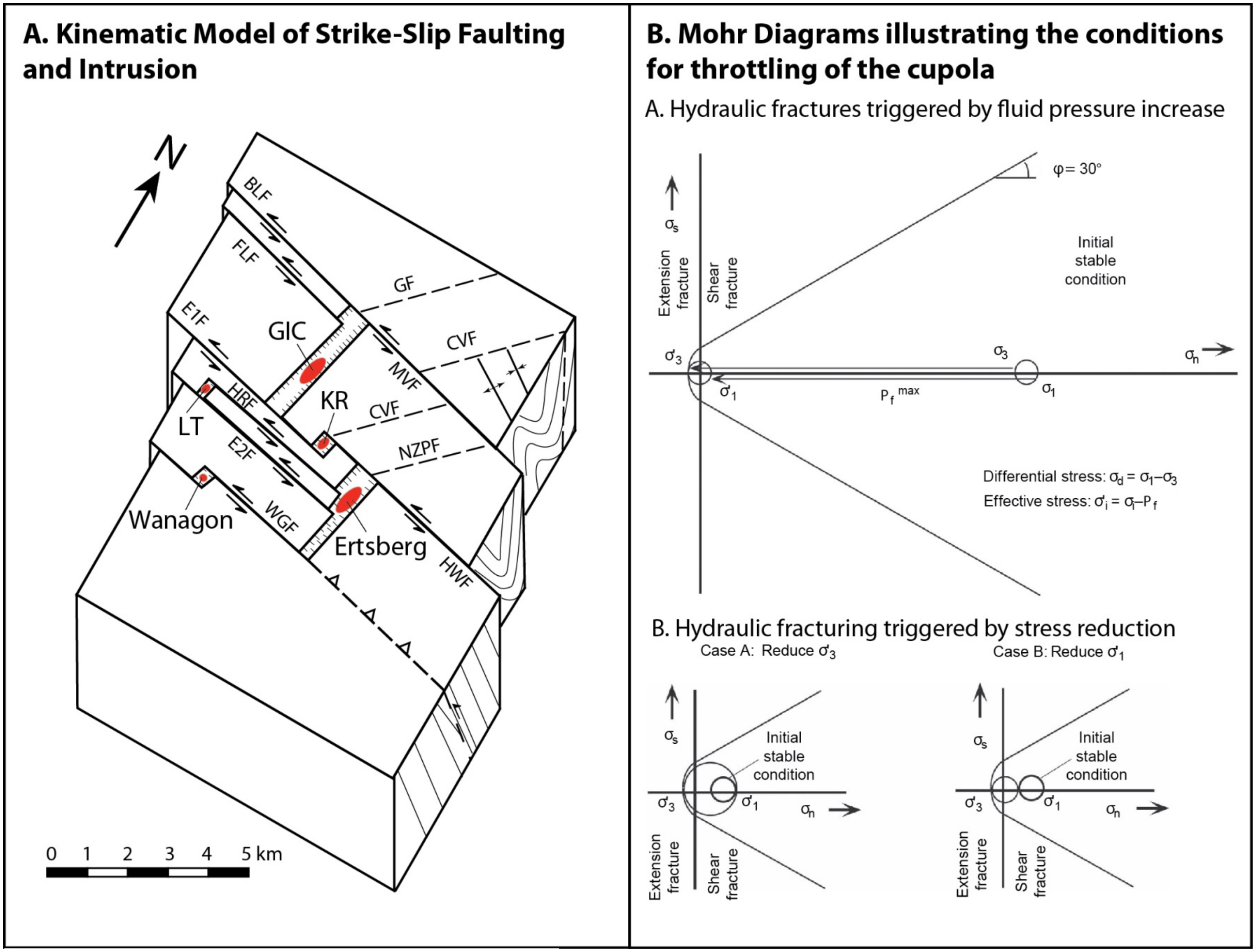

Figure 1-7. Continued next page.

Figure 1-7. (A) Block diagram illustrating the relationship between the strike-slip pull-apart zones and intrusion emplacement. Faults: MVF – Meren Valley Fault; E1F – Ertsberg No. 1 fault; HRF – HEAT Road fault; E2F – Ertsberg No. 2 fault; WGF – Wanagon fault; BLF – Barat Laut fault; FLF – Fairy Lakes fault; HWF – Hanging Wall fault; GF – Grasberg fault; CVF – Carstenz Valley fault; NZPF – New Zealand Pass fault. From Sapiie and Cloos (2004). (B) Mohr diagrams illustrating the ways to achieve extension fracturing of the cupola roof: A. Conventional hydraulic fracturing driven by an increase in the fluid pressure. B. Hydraulic fracturing driven by a local reduction in lateral stress as rapid slip dilates a pull-apart zone connecting sub-parallel strike-slip faults. Given that the rock above the cupola is at near magmatic temperatures the differential stresses between slip events will be low and the fluid pressures will be near lithostatic values. A reduction in stress in the σ_1 or σ_3 direction can drive extension fracturing, tapping the fluid-charged cupola and resulting in vein formation. From Cloos and Sapiie (2013).

Previous Geochronology Work

For almost 25 years a single K-Ar age of 3.10 ± 0.12 Ma from an uncharacterized sample of the Ertsberg pluton collected near the tramway terminal was the primary constraint on the age of magmatism and mineralization in the district (Titley, 1975). McDowell et al. (1996) performed K-Ar dating of magmatic biotite from 15 of the "freshest" samples and found that the intrusions fall within a 2 myr time window between 4.5 and 2.5 Ma (Figure 1-8). All samples from McDowell et al. (1996) were re-dated using the zircon U/Pb technique as part of this study. Pollard et al. (2005) reported 10 biotite $^{40}Ar/^{39}Ar$ ages for the Dalam and nearby Ertsberg intrusion.

Another geochronologic constraint for the history of the district comes from apatite fission track analysis of eight magmatic samples that yielded pooled ages between 3.7 ± 0.9 Ma and 2.0 ± 0.3 Ma (Weiland and Cloos, 1996). The wide track length distribution and the presence of long, etchable fission tracks (mean length >14 µm) indicates rapid cooling, an expectation for shallow intrusions. Weiland and Cloos (1996) also found a distinct difference in unroofing rate from ~0.3 km/myr for the igneous rocks near the GIC, at the crest of the range, to ~1.7 km/myr for the sedimentary section along the access road on the southern flank. Here we report 45 zircon U/Pb ages for intrusions in the GIC, measured using the novel tape-mounted method pioneered by Trautman (2013), which allows isolation of the youngest growth zones for high precision zircon U-Pb ages.

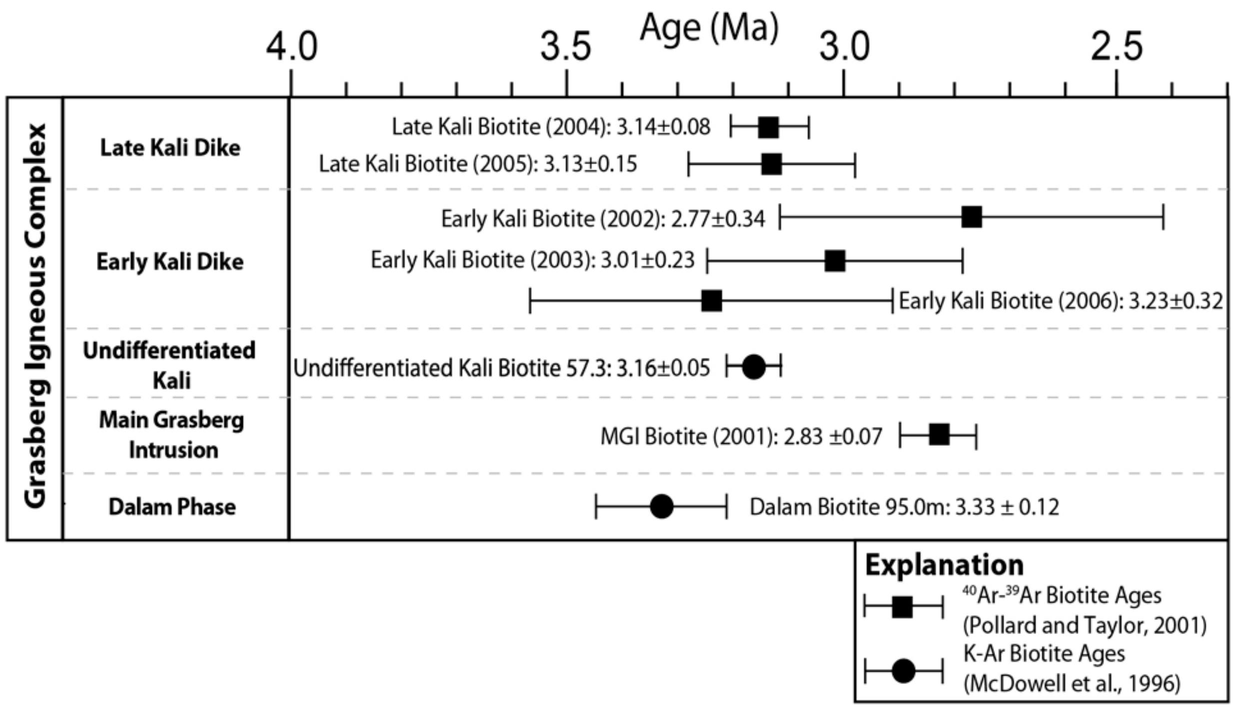

Figure 1-8. Geochronologic information available for the GIC prior to this study. Biotite K-Ar ages from McDowell et al. (1996) and biotite Ar/Ar ages from Pollard and Taylor (2001). It is not possible to distinguish the MGI and the Kali Dikes based on the K-Ar and Ar/Ar ages.

MOTIVATION

One of the major insufficiently understood questions in the genesis of supergiant porphyry copper deposits, like the Grasberg deposit, is how long the mineralizing hydrothermal system is active in order to deposit the large volumes of copper and gold (Von Quadt et al., 2011; Chiaradia et al., 2013). This is important because the duration of the hydrothermal system is a fundamental parameter for any quantitative modeling of magma and hydrothermal fluid fluxes that create porphyry copper deposits. The most common approach taken to address this question combines zircon U/Pb crystallization ages of intrusions with biotite $^{40}Ar/^{39}Ar$ cooling ages of hydrothermal alteration. The most thorough studies of this kind are in El Teniente (Maksaev et al., 2004), Bajo de la Alumbrera (Harris et al., 2008), and Chuquicamata (zircon U/Pb LA-ICP-MS and SHRIMP dating; Ballard et al., 2001). The combination of data indicates that the intrusive centers and their associated hydrothermal systems were active over time spans of 1 to 2 million years. Notably, only one study is known where igneous cross-cutting relationships provide direct constraints on the duration of the ore-forming hydrothermal system. At Cerro Rico de Potosi, an epithermal silver deposit where high precision $^{40}Ar/^{39}Ar$ dating of sanidine and biotite from pre- and post-ore mineralization intrusions showed that the hydrothermal system was active for ~200,000 years (Rice et al., 2005). See Appendix A for a compilation of duration estimates for magmatic-hydrothermal systems.

A different approach to constrain the duration of hydrothermal activity was undertaken on a modern analogue: Simmons and Brown (2006) measured gold fluxes in hydrothermal fluids from the active Ladolam hydrothermal system in Papua New Guinea. They found that with the current gold flux of 24 kg/yr the entire deposit could have formed in as little as 55,000 years. Numerical modeling of hydrothermal systems indicate activity may be long lived. Cathles et al. (1997) modeled convective cooling of an ore-forming intrusion and found that under optimal conditions a single large intrusion can sustain a hydrothermal system for up to 800,000 years. These studies illustrate the uncertainty in the duration of ore-forming hydrothermal systems, which could last anywhere from tens of thousands of years to millions of years.

The motivation for this study is to report zircon U/Pb ages for the magmatic phases in the Grasberg Igneous Complex, which hosts the supergiant Grasberg porphyry copper deposit. Dated cross-cutting relationships constrain the maximum duration of magmatism and hydrothermal fluid flow. Zircon and apatite (U-Th)/He ages date when high-temperature (>210°C) hydrothermal fluid flow must have ceased. The zircon U/Pb ages also provide a refined context needed to evaluate the geochemical and isotopic evolution of the system.

ANALYTICAL TECHNIQUES

LA-ICP-MS Zircon U/Pb Dating

Zircon crystals were separated from drill core and hand samples using conventional heavy liquid and magnetic separation techniques. Handpicked zircon crystals (most crystals are euhedral and between 60 to 120 µm) were mounted on a double-sided piece of tape attached to an epoxy puck, following the procedures pioneered by Trautman (2013) (Figure 1-9). Each grain was carefully mounted such that a flat crystal face was facing upwards. The epoxy mount was then placed in the sample cell with no additional sample preparation.

All analyses were completed at the University of Texas at Austin, where the lab facilities include a magnetic sector, single collector Element2 HR-ICP-MS with an attached PhotonMachine Analyte G.2 Excimer Laser with a large-volume Helex sample. The Analyte G.2 has the advantage of superior optics, allowing spots to be selected on the surface of each individual zircon crystal, and the Helex sample cell minimizes the required sample volume and reduces the sample wash-out time to <0.3 s, a critical factor for depth profiling (Smye and Stockli, 2014). Data acquisition parameters optimized for signal strength were 30 µm spot size, 10 Hz repetition rate, and a 4 mJ energy set point. The instrument was tuned in order to maximize ^{238}U counts and minimize the interferences from oxide masses (UO <0.5%).

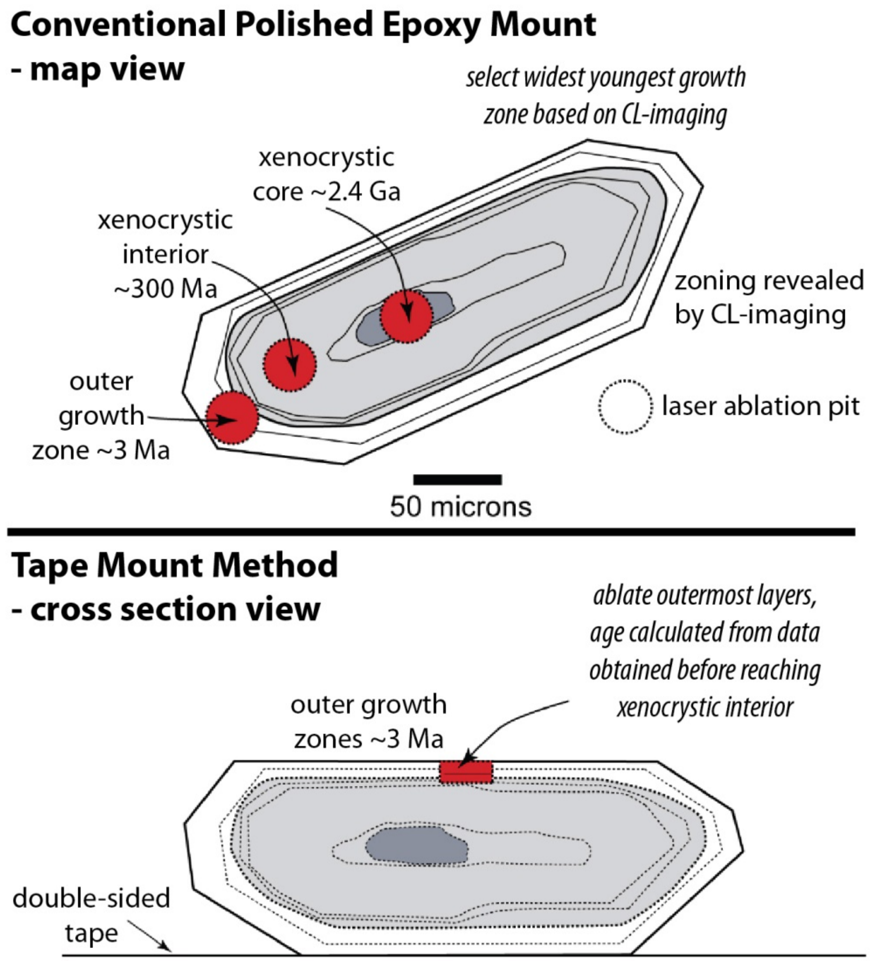

Figure 1-9. Schematic diagram comparing the conventional polished epoxy mount and the new tape mount method. For the conventional mount zircons are polished and the youngest growth zones are selected based on CL imaging. In the new tape mount method, whole zircon grains are mounted on double sided tape and the laser ablates into the side, maximizing the ability to isolate the youngest growth zone. From Trautman (2013).

Data reduction is accomplished using the Iolite software package (on the IGOR Pro platform). The magnitude of inter-element fractionation changes with depth in the laser pit, where more refractory elements are preferentially retained, forming a condensate at the bottom of the ablation pit, and more volatile elements are preferentially partitioned into the vapor phase. A matrix-matched standard, GJ1, is used to correct for U-Pb fractionation and for instrument mass bias. As the objective is to date only the most recent phase of zircon growth, the youngest growth zones are isolated to calculate an age. The advantage of ablating the sides of the zircon in order to isolate the outermost, youngest growth zones, and plotting the ±30 zircon analyses from one intrusion on the same Tera-Wasserburg plot (Figure 1-10) (Tera and Wasserburg, 1972), is that the resultant zircon U/Pb ages are highly precise (±0.1 myr). Composite ages are calculated by compiling all zircon analyses from samples of the same intrusion (n typically greater than 100 individual age determinations), thus improving the statistics and reducing the uncertainties to the second decimal place (±0.05 myr). Based on the cross-cutting relationships between the intrusions, specifically the highly mineralized MGI and the post-mineralization Kali Dikes, it is possible to place tight constraints on the duration of the hydrothermal fluid flow that produced the bulk of the Grasberg ore body.

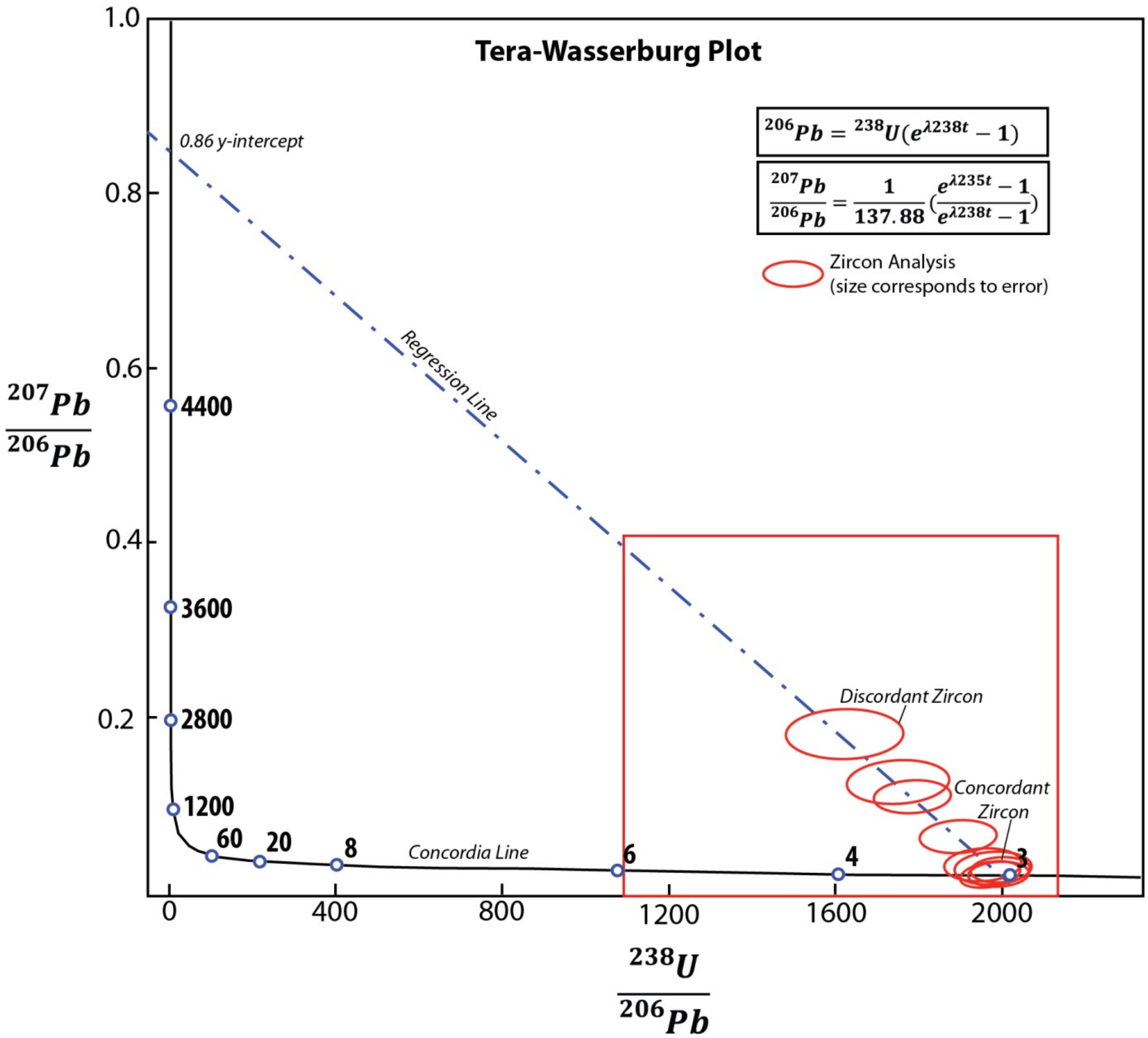

Figure 1-10. Tera-Wasserburg concordia diagram showing examples of discordant and concordant zircons. The intercept between the regression line and the Concordia is the common lead corrected sample age. Red box shows the location of the data plots shown in this chapter.

Age Corrections

Two corrections are necessary to obtain the age of crystallization. The first correction accounts for any common lead incorporated into the zircon crystal. The second correction accounts for initial Th disequilibrium, which is necessary as these zircons are less than 10 Ma (Scharer, 1984). Common lead is corrected by plotting the zircon analyses from a single sample on a Tera-Wasserburg diagram, where samples with variable amounts of incorporated common lead will plot along a single common lead mixing line. The y-axis of the Discordia line is pinned based on the whole rock $^{207}Pb/^{206}Pb$ ratio (Cloos, pers. comm.), the $^{207}Pb/^{206}Pb$ common lead ratio measured in the skarn garnets (see Chapter 3 and 6), and a preliminary study of common lead in feldspars, which are all consistent at ~0.86. The lower intercept between the Discordia line and Concordia is taken as the age and uncertainty of the sample.

The initial Th disequilibrium correction is applied to the sample age in order to account for the time it takes for the zircons to reach secular equilibrium. The Th/U ratio of most zircons is less than the Th/U ratio of the magma, which results in the near exclusion of ^{230}Th from the zircon crystal structure. The initial scarcity of ^{230}Th in the zircon causes disequilibrium in the ^{238}U radioactive decay chain, which ultimately results in a deficit in radiogenic ^{206}Pb. In order to correct for this deficit, it is assumed that the whole rock Th/U ratio reflects the Th/U ratio of the parental magma that is co-genetic with the zircons. The correction is calculated using the equations in Scharer (1984) (see Ito, 2014 for an example dating 0.1 Ma zircons from the Toya Tephra, Japan). The Th/U ratio of the rock was assumed based on the whole rock geochemistry database for rocks in the GIC. The magnitude of the correction is typically between 0.07 to 0.11 myr (see Figure B-1 in Appendix B), but may be as low as 0.04. The reported age for each sample includes both the common lead corrected zircon age and the correction for Th disequilibrium.

Geochemical Analyses

The geochronology was done to determine the age of magmatism in all parts of the GIC. Many of the rock samples are highly altered, but some are "fresh" enough to evaluate the evolution of the magmatic system over time. Since initial studies in the district by McMahon, "fresh" rocks have been identified at the outcrop, drill core, and hand sample scale based on a lack of visible pervasive hydrothermal alteration and a scarcity of veining. Samples were examined in detail using polished slabs and thin sections in order to verify the freshness prior to selection for analysis. Selected samples were crushed to ~5mm size pieces and then inspected using a binocular microscope to remove any visibly altered pieces, micro veins, or xenoliths. The fragments were powdered in a ceramic puck mill to obtain 100 to 250 grams of powder. Major element geochemistry analyses were performed by SGS in Vancouver, Canada. The ICM90A package was selected for major and trace elements. Following the geochemical analysis, the data were filtered based on the S content (excluding samples with S contents >2 wt%). High S content was taken as cryptic evidence of pervasive alteration at magmatic temperatures. The samples selected for the plots reflect the best available samples representing the Dalam (n=1), MGI (n=5), and Kali Dikes (n=7) magmas. The MGI predates ore formation and the Kali Dikes post-date most, if not all, hydrothermal mineralization.

Sr-Nd Isotope Analyses

All of the samples included in the age-geochemistry compilation were also analyzed for their Sr and Nd isotopic ratios, as part of an ongoing study by Cloos. Measurements were completed in the UT Austin isotope labs by Eric James, Todd Housh, and Staci Loewy. Analyses were made in static multicollector mode on a Finnigan MAT 261 and on a Thermo Scientific Triton TIMS. The procedure is outlined in Housh and McMahon (2000) and Cloos (in prep).

RESULTS

Zircon U/Pb Ages

Forty-five zircon U/Pb ages have been collected for samples from the GIC. Age results are shown in Figure 1-11 and composite Tera-Wasserburg diagrams for each of the intrusions are shown in Figure 1-12 (see Figure 1-5 and Appendix C for sample locations, Appendix D for polished slab photos, Appendix E for zircon U/Pb data, and Appendix F for Tera-Wasserburg diagrams). The results show that the Dalam Phase of magmatism occurred over a protracted time window between 3.6 and 3.3 Ma. The lack of a sharp contact between the MGI and the Dalam indicates that the MGI intruded into the still hot center of the Dalam Phase (Paterson and Cloos, 2005a). The MGI is a small intrusion (<1 km^3) and the texture does not vary significantly with depth, therefore it is interpreted as one pulse of magmatism that slowly cooled. This interpretation is supported by the zircon U/Pb ages of 10 MGI samples, which do not show a significant spread, and overlap within error. The MGI intrusion has a composite zircon U/Pb age of 3.22 ± 0.04 Ma (x=9 samples (5 "fresh" and 4 mineralized), n=233 zircons). Much of the MGI is highly altered, as it hosts high-grade ore, but two parts of the intrusion, the "Ring Dike" zone near ~3700 m elevation and a deeper MGI zone at ~3000 m elevation near the Amole drifts, were in locations that escaped intense alteration. The "Ring Dike" was named for the crescent shape of the fresh part of the MGI above 3700 m, and was originally mapped and interpreted as a later intrusion. The name is a misnomer, but retained here for the anomalously fresh part of the MGI. Samples from the "Ring Dike" have zircon U/Pb ages that overlap with the highly mineralized MGI (Figure 1-13), supporting the field and petrographic evidence that this is a less altered zone in the MGI.

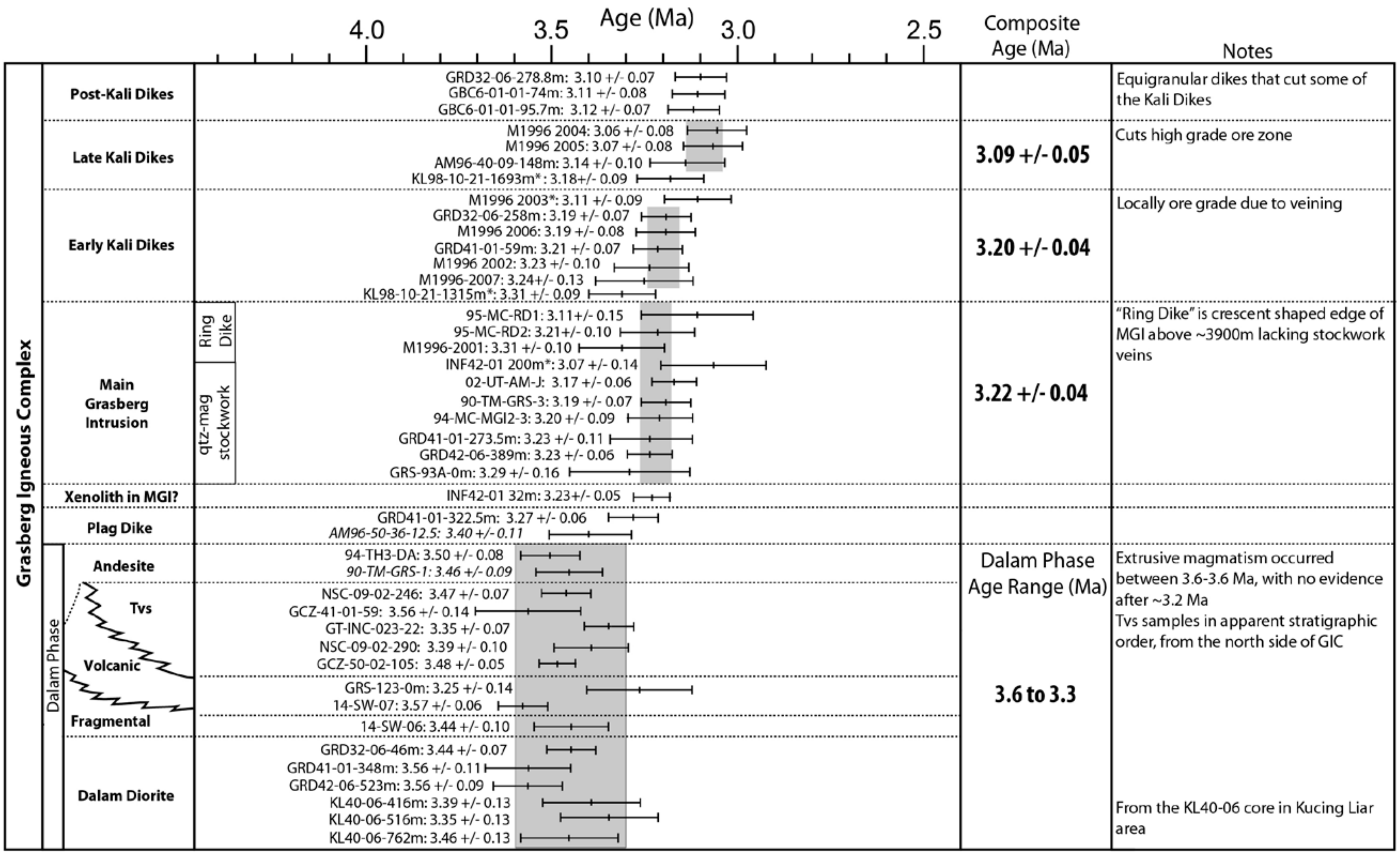

Figure 1-11. Age table showing the zircon U/Pb age and uncertainty for each dated sample in the GIC. Each sample included in the composite ages have been confirmed as part of the same intrusion based on polished slabs and petrographic analysis. * indicates samples that were not petrographically identical and therefore were not included in the composite age calculation.

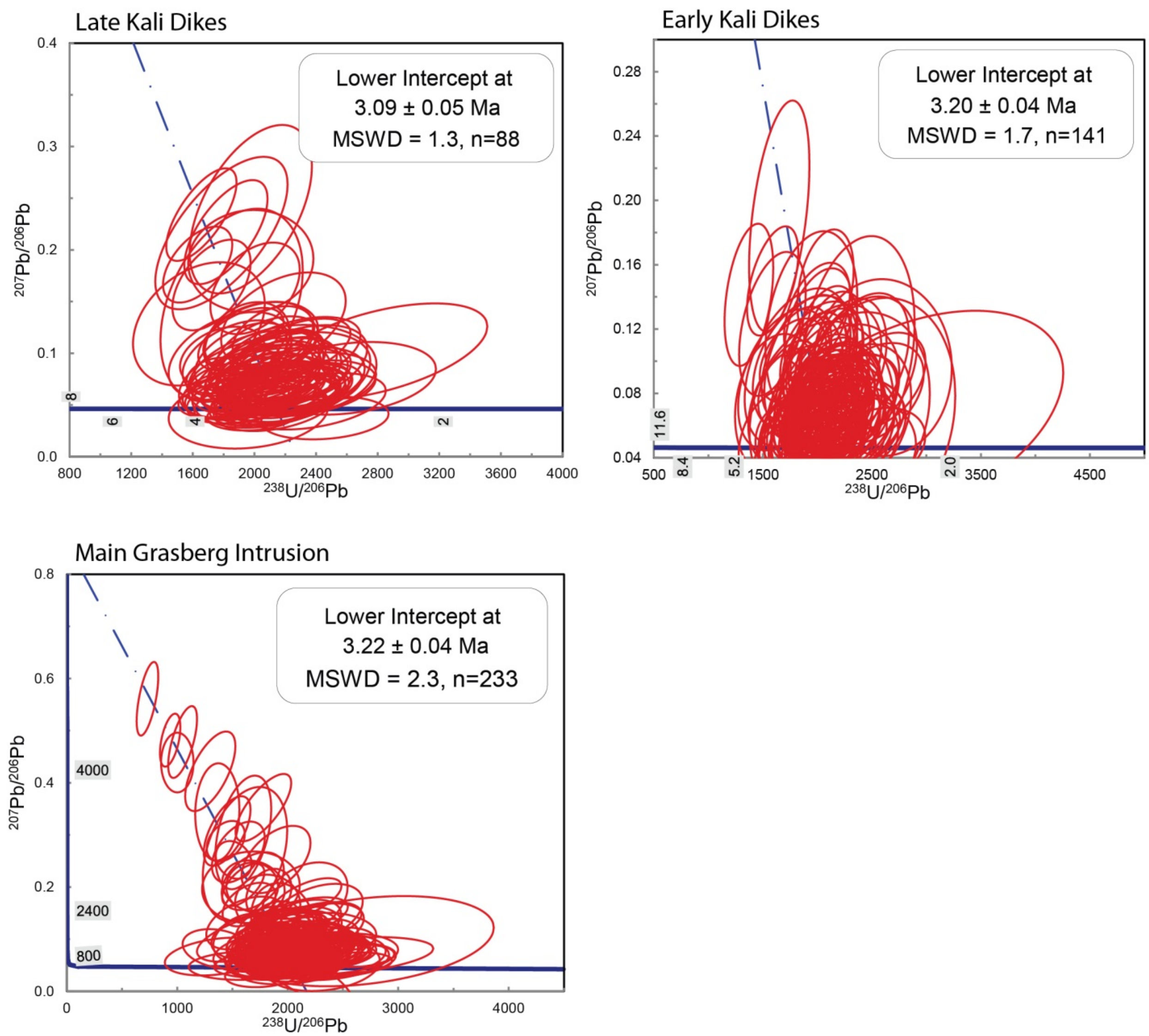

Figure 1-12. Composite Tera-Wasserburg diagrams for the Main Grasberg Intrusion, the Early Kali Dikes and the Late Kali Dikes. Data-point error ellipses are 2σ.

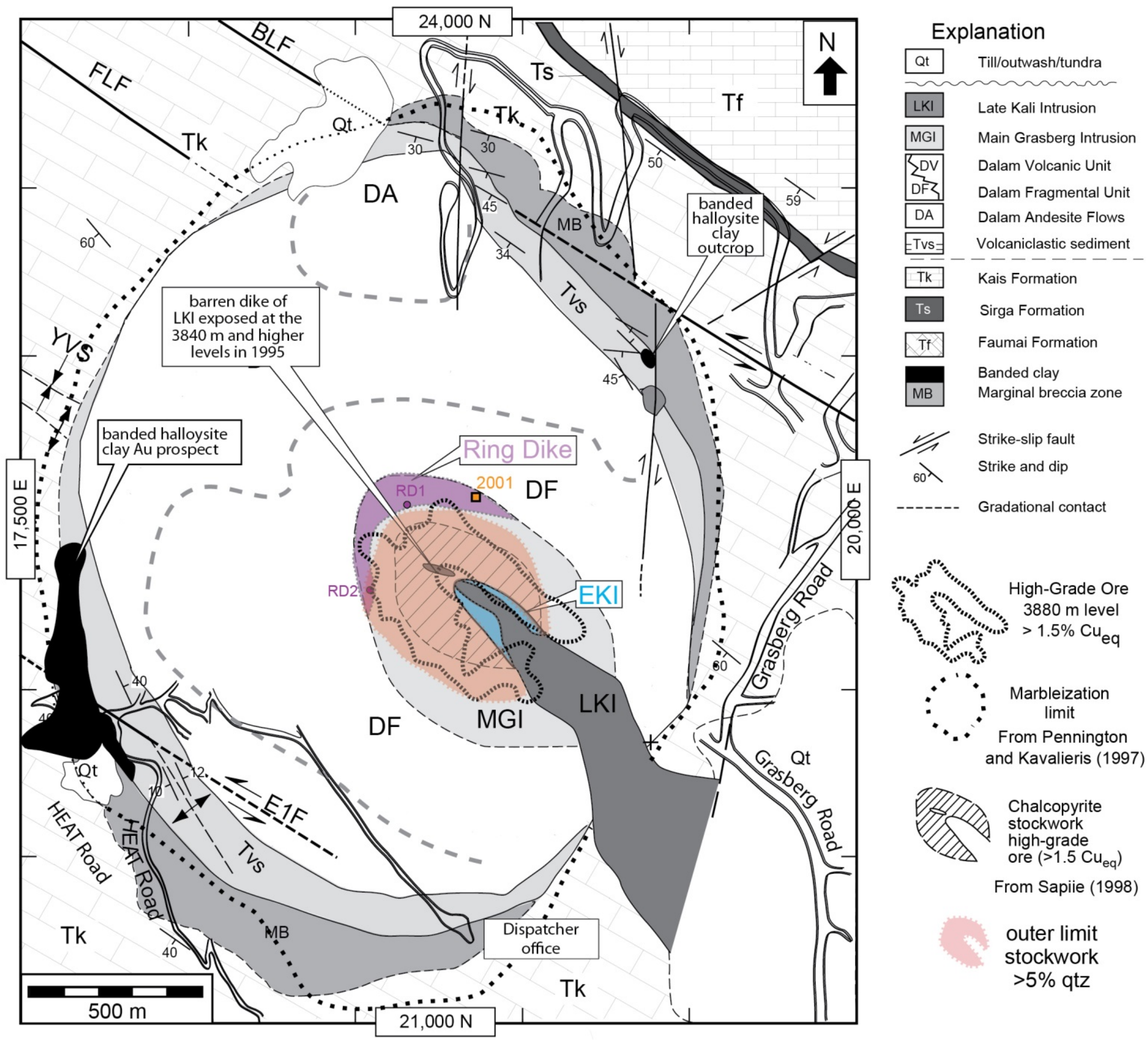

Figure 1-13. Geology of the Grasberg Igneous Complex (GIC) at the ~3900 m elevation, showing the location of the "Ring Dike Complex" in purple. The "Ring Dike" sample locations are marked. The crescent shape of the "Ring Dike" is not due to intrusion, but is rather an area with much less stockwork veining. Modified from Suwardy (1995), Sapiie (1998), and Paterson and Cloos (2005a).

The Kali Dikes phase of magmatism is the youngest in the GIC. At the pit level, above 3700 m, the Kali Dikes were divisible into an Early Kali Intrusion (EKI) and a Late Kali Intrusion (LKI) (MacDonald and Arnold, 1994). While marginal parts of the Kali have ore grade mineralization below 3500 m, the LKI clearly cuts the high-grade ore zone to the depths exposed in the open pit and is treated as waste rock. At the level of the Amole drifts (~3045 m) there are multiple phases of the Kali, and the intrusion is more accurately described as a series of nested dikes (Bowman, 2017). The geochronology data set, which includes open pit and drill core samples from various depths, reflects the complicated nature of the Kali Dikes. Samples identified as EKI based on pit mapping and polished slab inspection have a composite zircon U/Pb age of 3.20 ± 0.04 Ma (x= 5, n=141). This age overlaps within error with the MGI. The volumetrically minor EKI is generally viewed as a near-end of mineralization plug (Figure 1-14). Samples identified as LKI have a composite zircon age of 3.09 ± 0.05 Ma (x= 3, n=88). These samples clearly postdate high-grade ore formation, and this provides the fundamental timing constraint on the duration of the hydrothermal system.

Zircon Core Ages

An advantage of the tape mount method that arises from isolating the youngest growth zones of the zircon, to precisely date the outer most bands of zircon growth, is that information from the inner growth zones, or xenocrystic cores, is also retrieved. When the outermost growth zone is less than the depth of laser ablation (~16 µm), the age of inner growth zones and/ or xenocrystic cores are obtained. Of the 45 dated samples from the GIC, 74 crystals yielded data that enabled resolution of the concordant ages of xenocrystic cores. The data set for these cores reveals that ~50% of the 74 measured inner growth zones are between 200 and 335 Ma, which corresponds to magmatism during the Tasman Orogeny in Australia (Edwards et al., 1990) (Figure 1-15; see Appendix G for zircon core U/Pb data). About 40% of the xenocrystic cores were Proterozoic in age, predominantly ranging between 1300 and 2300 Ma.

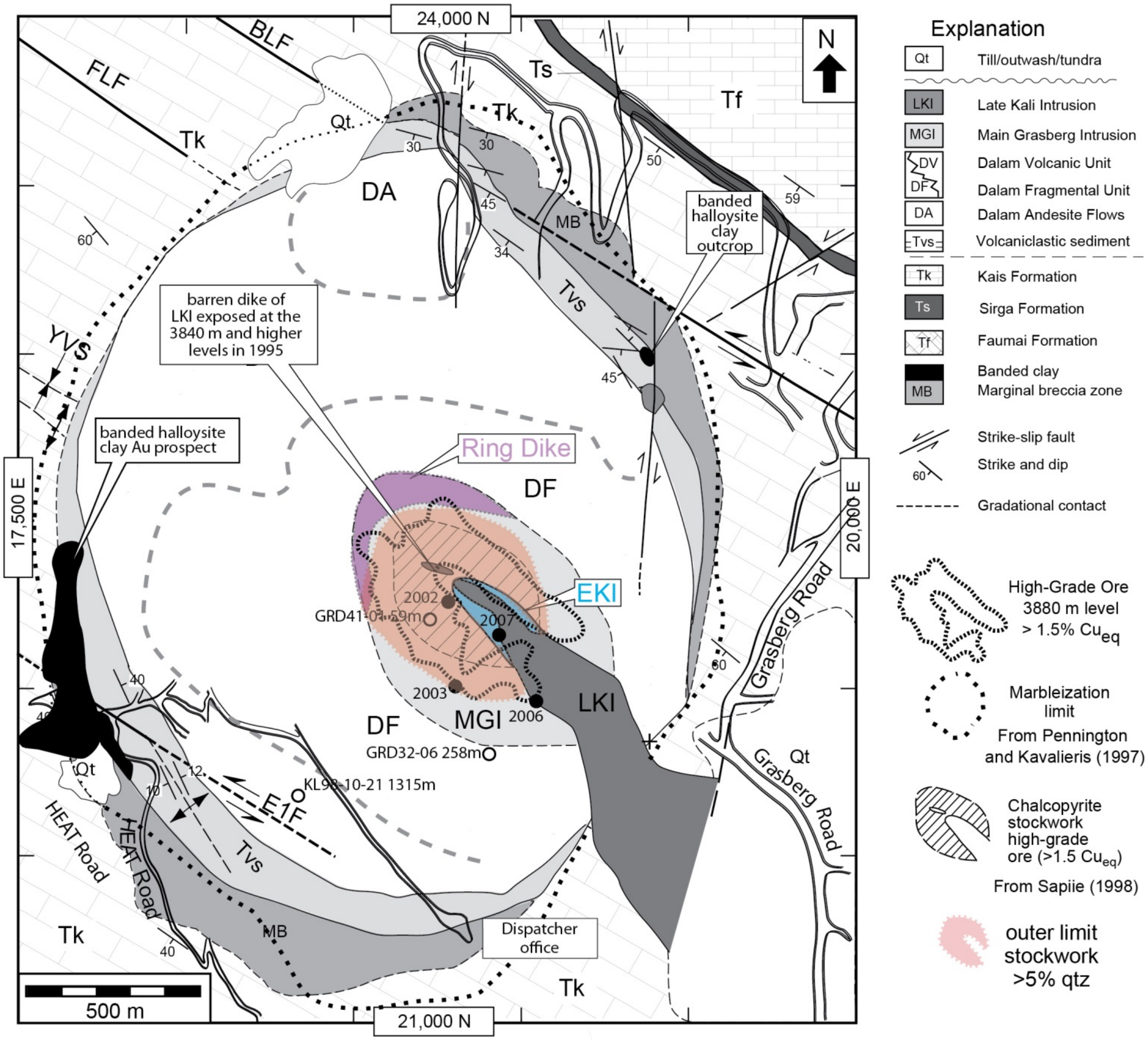

Figure 1-14. Geology of the Grasberg Igneous Complex (GIC) at the ~3900 m elevation, showing the location of the Early Kali Intrusion (EKI) in blue. EKI outcrop samples are marked with a solid black circle and EKI drill hole samples are marked with an open black circle denoting the collar location. Modified from Suwardy (1995), Sapiie (1998), and Paterson and Cloos (2005a).

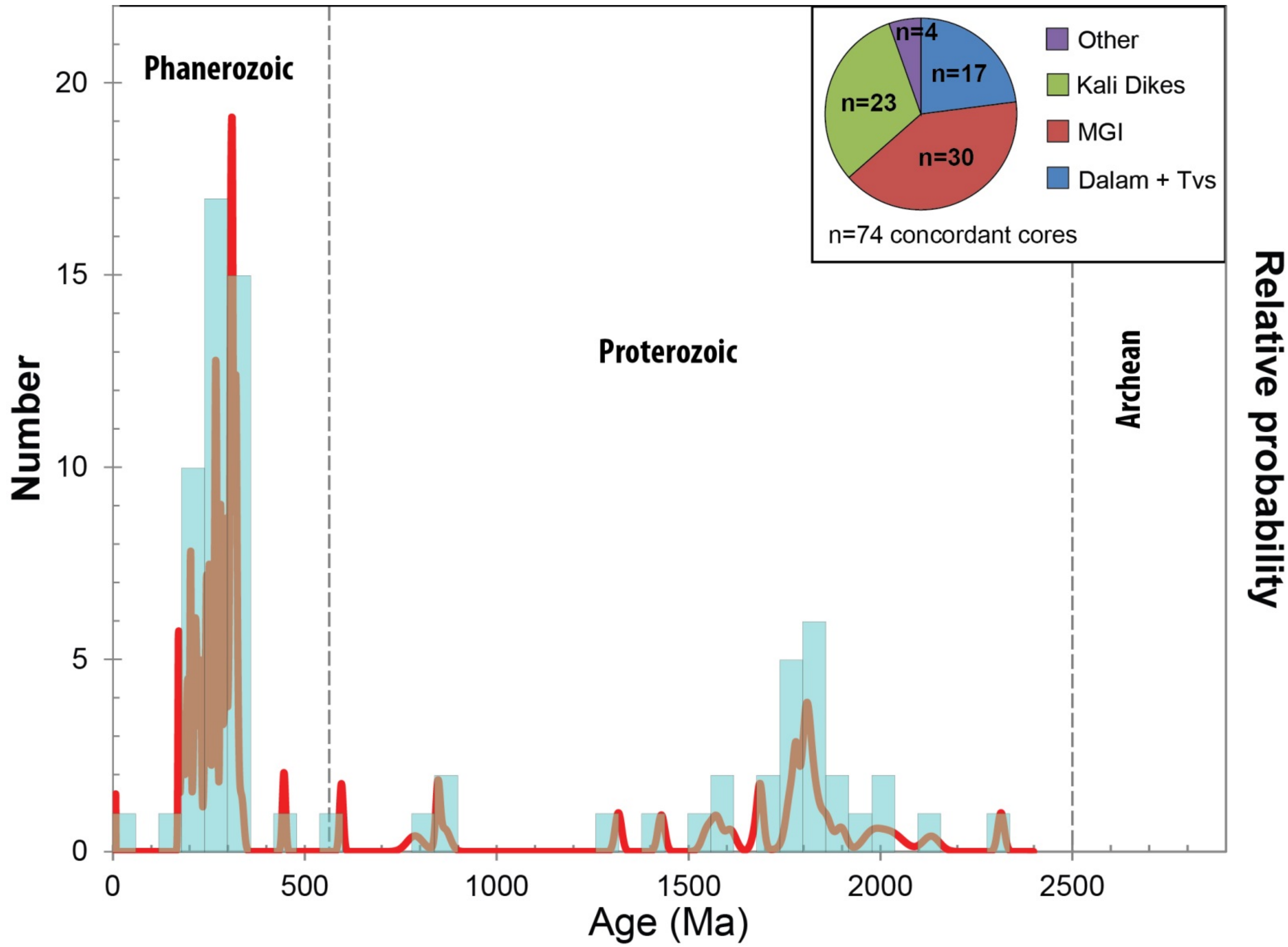

Figure 1-15. Probability density diagram showing the age distribution of concordant zircon interior growth zones for intrusions in the Grasberg Igneous Complex (n=74 from 45 samples). "Other" includes the Plag Dike and the Post-Kali Dikes. The most prominent age peak is between 200-400 Ma, with fewer cores in the Proterozoic.

Before these data were obtained there was speculation as to the nature of the assimilated lower crust beneath the Ertsberg-Grasberg mining district. Housh and McMahon (2000) went to extensive efforts to date zircons using the TIMS method in order to resolve the age of magmatism and age of xenocrystic cores. The near absence of Archean inner growth zones in zircons from the GIC strongly suggests that the lower crust underlying the parental magma chamber and the Grasberg porphyry deposit is primarily composed of Proterozoic intrusions and metamorphic units. Van Dongen et al. (2010) report similar results for the Ok Tedi porphyry Cu-Au deposit, located near the international border between Indonesia and Papua New Guinea, where zircons from the 1.1 to 1.4 Ma deposit have xenocrystic cores that are only as old as ~1.8 Ga.

Geochronometer Comparison

New zircon U/Pb ages for the intrusive phases of the GIC allows for a re-evaluation of the previous geochronology for the GIC. Grasberg samples from the McDowell et al. (1996) study were reprocessed for the zircons and dated using the tape mount method. New results show that for four of the five samples from the GIC the biotite K-Ar ages overlap with the zircon U/Pb ages (Figure 1-16). For the 2002 sample, the biotite K-Ar age is 0.46 myr younger than the zircon U/Pb age, which could be attributed to Ar loss. An unpublished biotite $^{40}Ar/^{39}Ar$ age is also available for the 2004 sample from the McDowell et al. suite (Cloos, unpublished data). The biotite $^{40}Ar/^{39}Ar$ plateau age is 0.12 myr younger than the zircon U/Pb age and 0.20 myr younger the biotite K-Ar age.

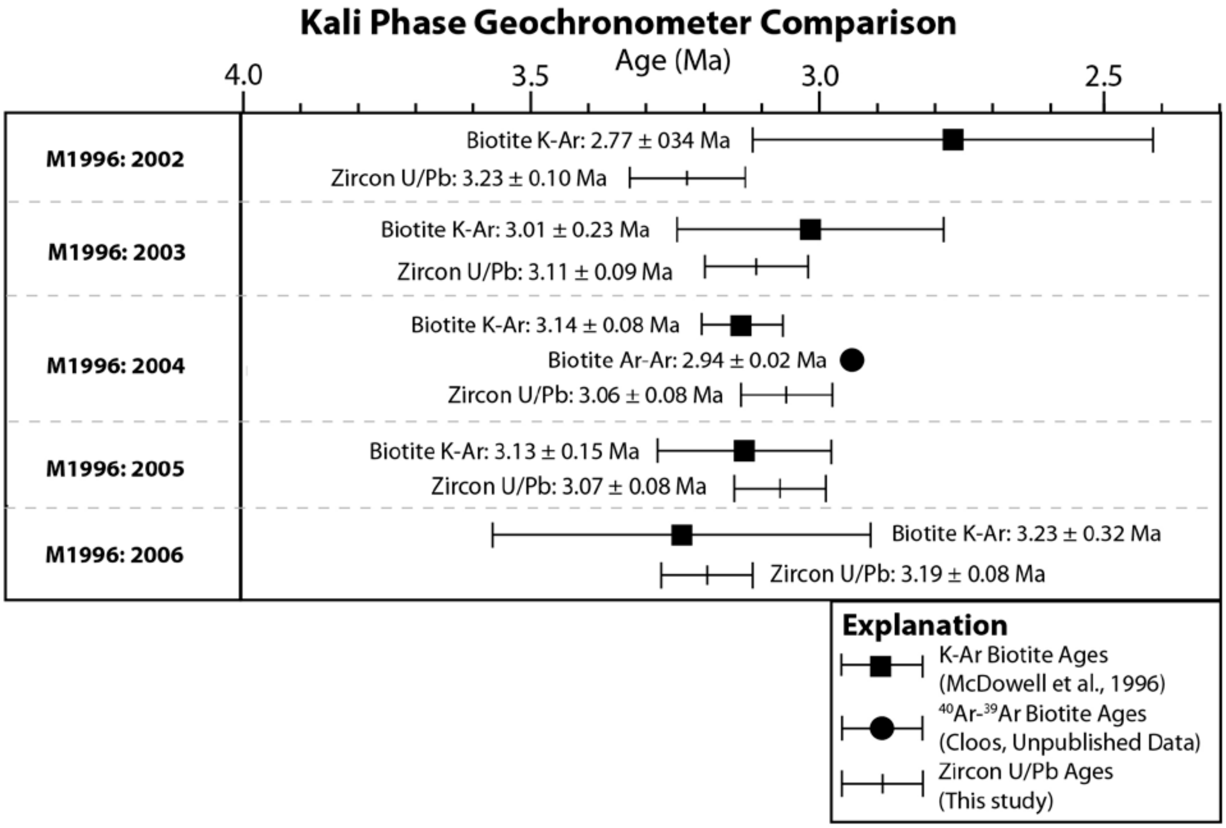

Figure 1-16. Comparison between biotite K-Ar ages (McDowell et al., 1996), biotite Ar-Ar ages (Cloos, unpublished data), and zircon U/Pb ages (this study) for five samples from the Kali Phase. All ages were measured on the same samples to allow for a direct age comparison.

Geochemistry Results

In most porphyry copper deposit ore systems, the ability to evaluate the evolution of the magmatic systems is complicated by the overprint of hydrothermal alteration. In order to avoid the alteration overprint, “fresh” igneous rock samples were sought from the least altered parts of the GIC. As most of the Dalam samples are highly altered, this study primary focuses on the differences between the MGI (n=5) and the Kali Dikes (n=7). After removing minor amounts of quartz veins and altered pieces from these samples, the composition of the analyzed powders are taken to reflect the composition of the magma.

Analysis of the major element vs. age plots reveals increasing SiO_2 and decreasing MgO from the MGI to the Kali, indicating magma recharge with a more felsic melt (Figure 1-17). P_2O_5 also decreases with time, which indicates that apatite was one of the early crystalizing phases. While the other elements do not show systematic patterns, the elements Al, Ca, K, and Na are all strongly correlated, which is expected if feldspar fractionation played a significant role in the evolution of the magma. Taking SiO_2 content as an indicator of fractionation, with increasing differentiation the SiO_2, Al_2O_3, and K_2O are higher, whereas the MgO, FeO, Fe_2O_3, and the P_2O_5 are lower (Figure 1-18).

According to these data the ore metal abundances in the “fresh” intrusions are 10 to 800 ppm Cu, 2-120 ppb Au, 4-16 ppm Pb, and 20-80 ppm Zn (Figure 1-19). For Au, Pb, and Zn the values for the Dalam (n=1), MGI (n=4), and Kali Dikes (n=7) are similar, and they are all similar to normal intermediate magmas. The Cu values in the MGI (between 600 to 1600 ppm), however, are high relative to mature arc rocks (mean of 60 ± 43 ppm Cu) and island arc rocks (94 ± 59 ppm Cu) (compilation by Richards, 2015).

Elevated copper values in the Kali samples are explained by back reaction of ascending copper rich fluid and the magma near the top of the stock. As there is a negative correlation between pressure and the partitioning coefficient for chlorine, there is an expectation that as copper-rich bubbles rise along the edges of stock the pressure decreases should drive a back reaction that would increase the copper content of the residual magma that became the Kali. As such, magma at the top of the stock is enriched in copper relative to the rest of the batholith. The high copper content of the MGI is best explained as a result of fluid-rock interaction at near-magmatic temperatures.

Sr-Nd Isotopes Results

Strontium and neodymium isotopes are used to evaluate magmatic sources and to compare intrusions. Here we report Sr and Nd isotopic ratios for dated samples from the GIC. Magmas are characterized by εNd values between −10.7 and −19.2 and $^{87}Sr/^{86}Sr$ ratios between 0.70619 and 0.70714 (Figure 1-20). The isotopic ratios for the Dalam, MGI, and Kali magmatic phases are distinct, and this is the most direct evidence for two episodes of magma chamber recharge. Based on the evolution of the isotopic composition between the intrusions, the upper crustal parental magma chamber was recharged with a more mafic, mantle derived magma between the Dalam and the MGI, and a more felsic, crustal enriched, magma between the MGI and the Kali.

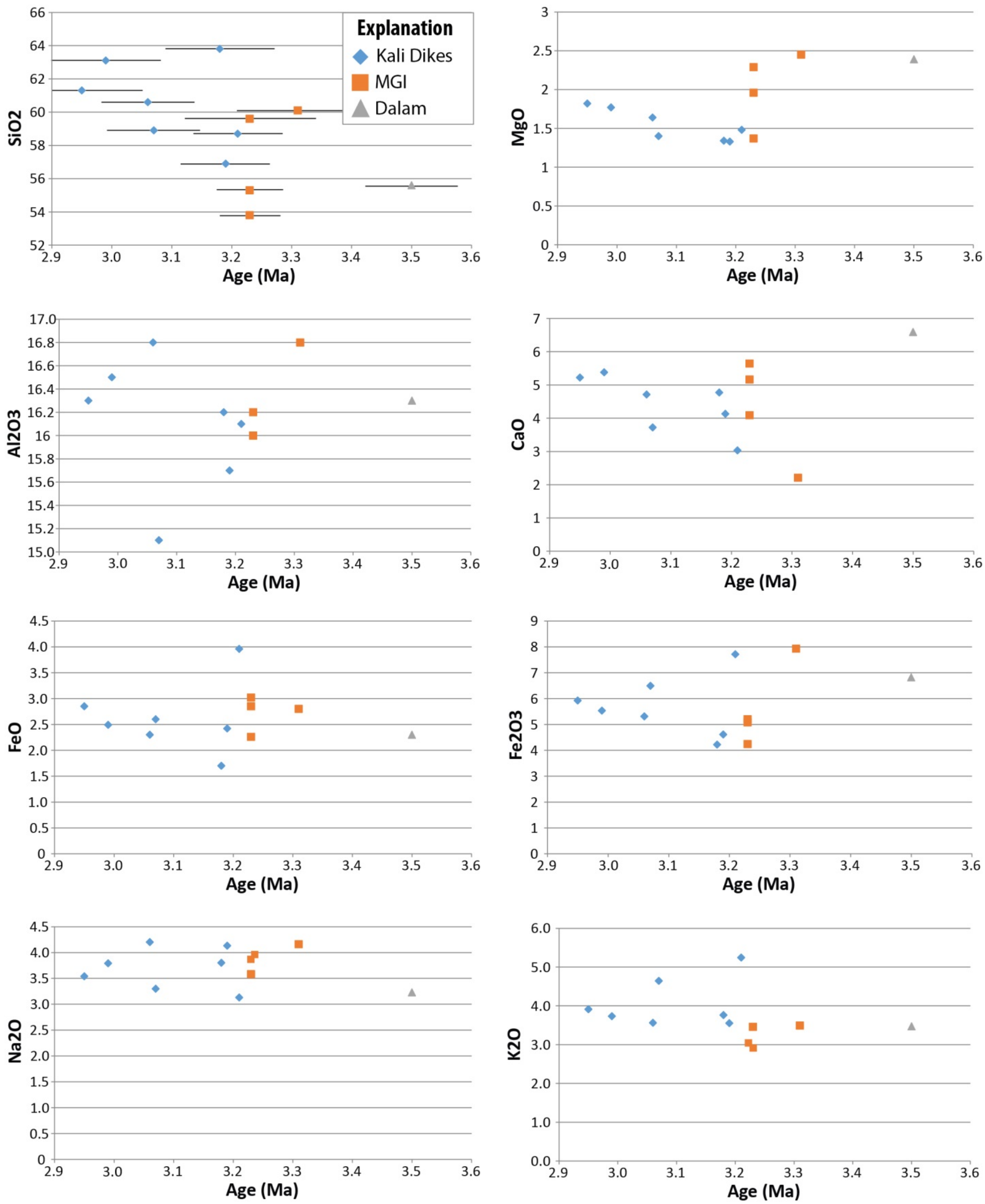

Figure 1-17. Major element geochemistry vs. age. SiO_2 increases with time whereas MgO decreases with time, suggesting the parental magma chamber changed between MGI and Kali Phase magmatism. Black bars show age uncertainties (top left plot).

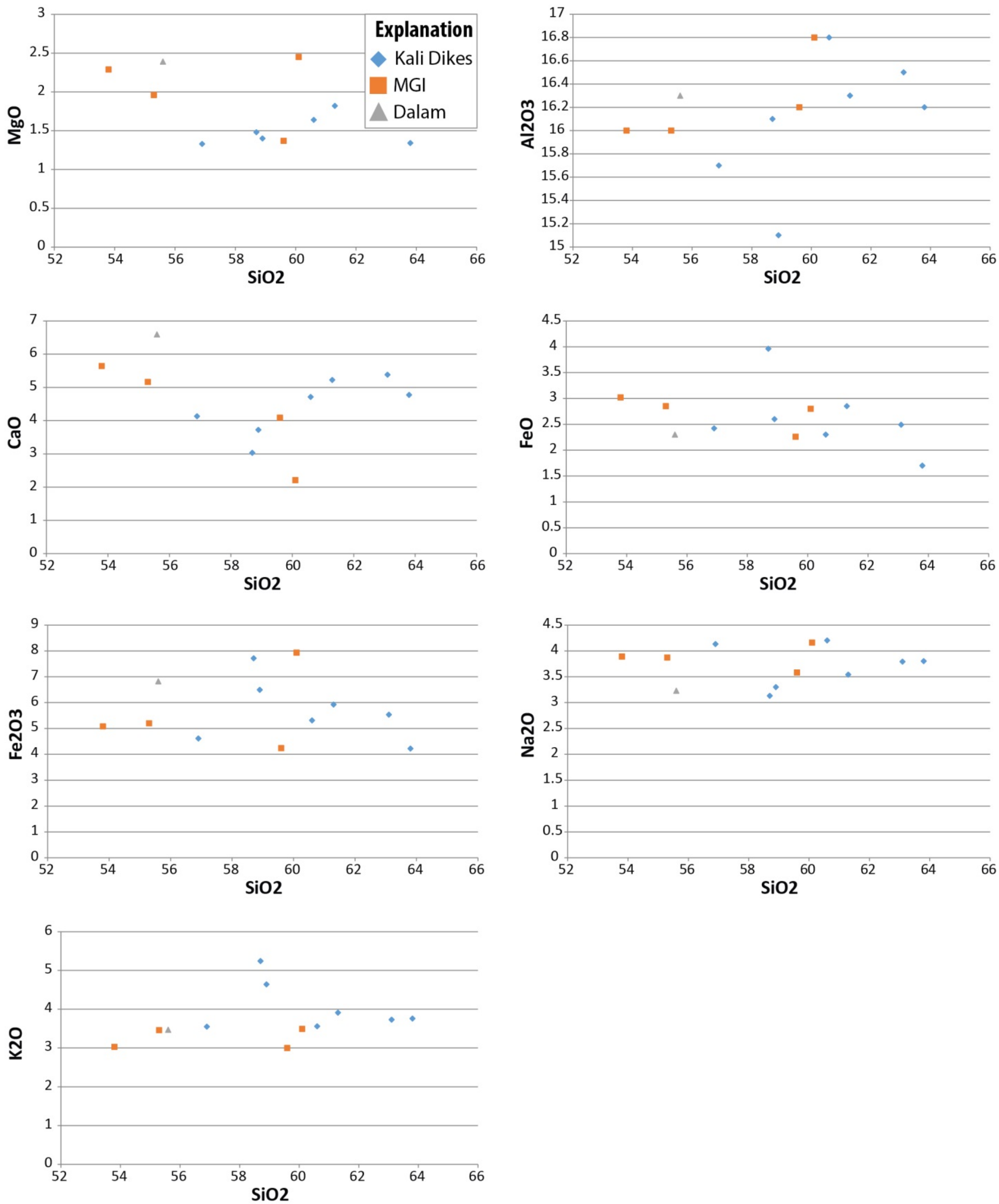

Figure 1-18. Major element geochemistry vs. SiO_2.

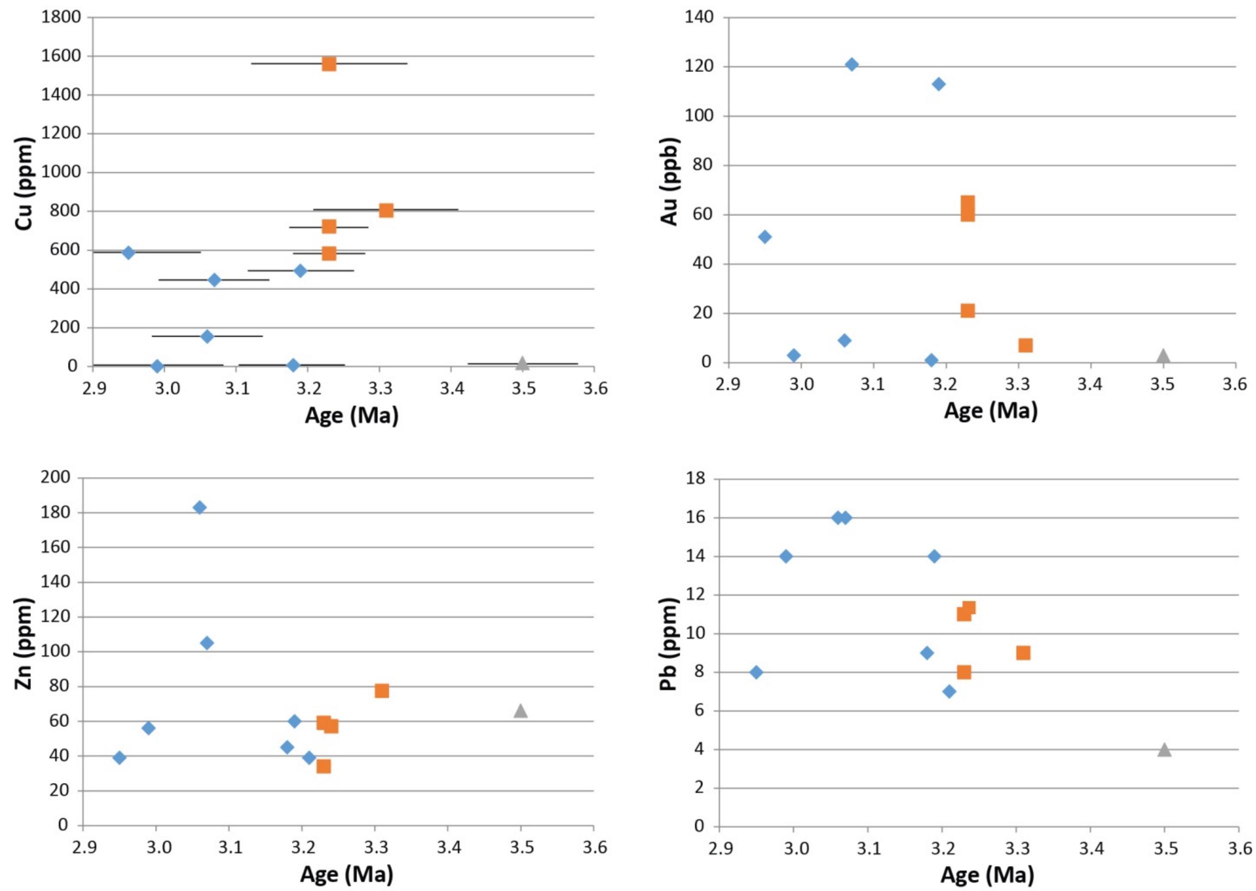

Figure 1-19. Plots showing the metal content vs. age for samples from the GIC. Black bars show age uncertainties (top left plot). Care was taken to only include fresh igneous samples, such that the metal contents reflect the metal content of the magmas.

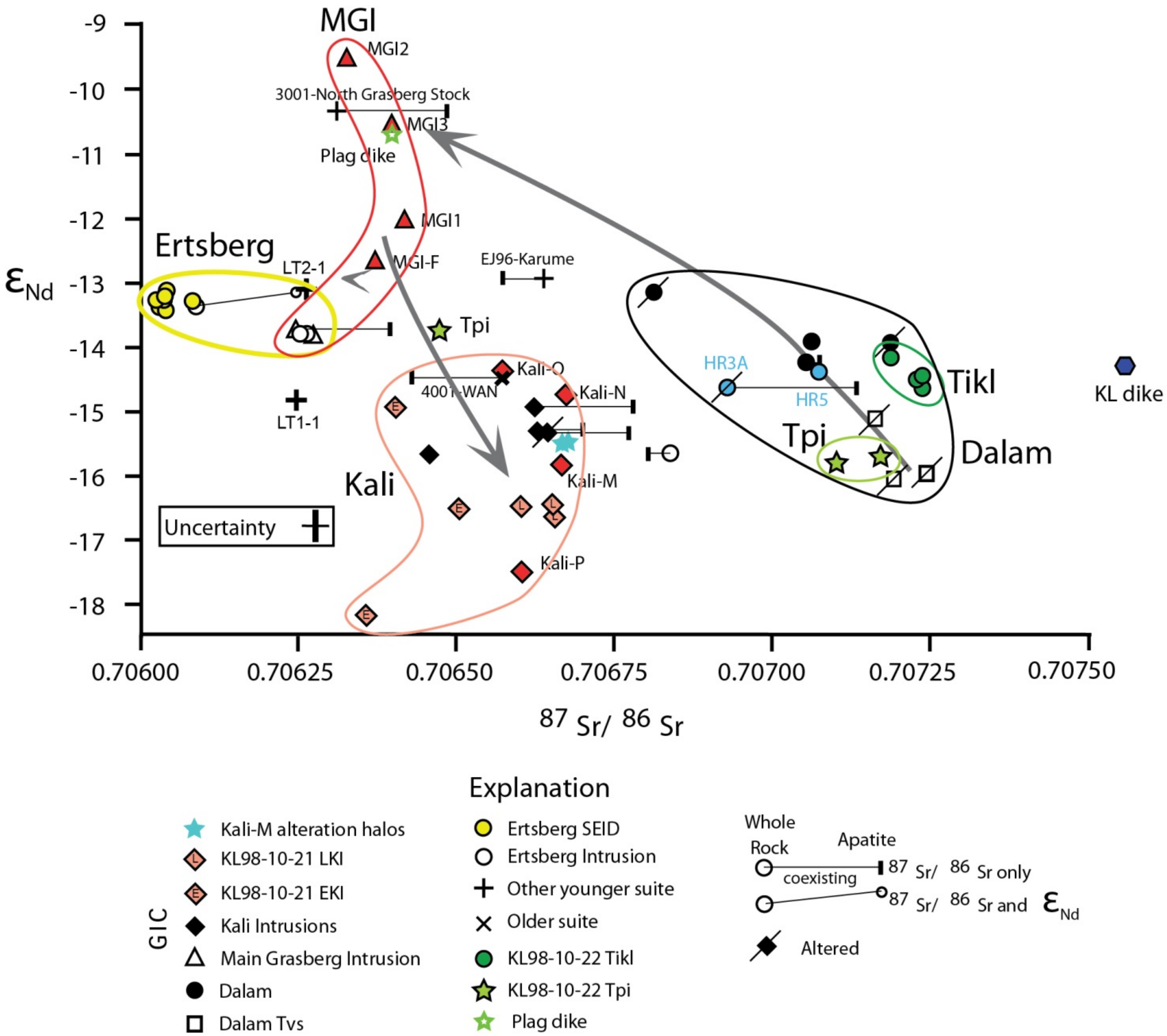

Figure 1-20. Plot showing the εNd and 87Sr/86Sr isotopic compositions for samples from the Ertsberg-Grasberg mining district. The diagram shows three recharge events; one between the Dalam and the MGI, one between the MGI and the Kali, and one between the Kali and the Ertsberg pluton (see Chapter 4). Data from Housh and McMahon (2000) and Cloos, pers. comm. (2016). Modified from Trautman (2013).

DISCUSSION

Duration of hydrothermal fluid flow and magmatism

Chiaradia et al. (2013) and Tapster et al. (2015) argued that it is not possible to constrain the maximum duration of hydrothermal fluid flow by dating intrusions using zircon U/Pb LA-ICP-MS techniques, as the precision of the method is insufficient and the ages may record protracted crystallization along the mush zones of the magma chamber. In the case of the GIC, there is a fundamental cross-cutting relationship that puts direct constraints on the maximum duration of hydrothermal fluid flow. The age difference was resolvable in this study using the LA-ICP-MS technique for two reasons. The tape mount method was used and the Grasberg system has the advantage of being an optimal age (~3 Ma). The zircon U/Pb LA-ICP-MS method typically has analytical uncertainties of 1-2%, which for a 3 Ma zircon corresponds to uncertainties of ±0.03 to 0.06 myr (see Chiaradia et al., 2013 Figure 2; Schoene, 2014). By dating multiple zircons and using the age intercept on the Tera-Wasserburg diagram, the statistical precision is improved towards the 1% level.

In the Grasberg porphyry copper deposit, above the 3700 m level, both the EKI and the LKI cross-cut the bulk of the high-grade ore mineralization. Taking the composite ages of the MGI (3.22 ± 0.04 Ma, x=5, n=233), the EKI (3.20 ± 0.04 Ma, x=5, n=141), and the LKI (3.09 ± 0.05 Ma, x=3, n=88), the maximum duration of hydrothermal fluid flow that produced the bulk of the high grade ore was between 100 to 220 kyr, depending on whether the EKI or the LKI is taken as the cross-cutting constraint (Figure 1-21). The entire GIC, from the oldest dated part of the Dalam to the youngest Kali Dike, formed in a timespan of ~600 kyr.

Evolution of the GIC

Based on the zircon U/Pb and the geochemistry data presented above, it is possible to refine the temporal evolution of the GIC, which is shown schematically in Figure 1-22. The Dalam Phase is the oldest magmatic event. Some magmatism was extrusive and included phreomagmatic events in a maar caldera type setting, as evidenced by the Tvs unit, which is present on the northern and southwest sides of the GIC, and includes wood fragments (see MacDonald and Arnold, 1994; Paterson and Cloos, 2005a). The MGI intruded into the still hot core of the Dalam Phase, as the borders with the Dalam lack chilled margins. The uniform and equigranular texture of the MGI indicates it intruded as a single pulse (Paterson and Cloos, 2005a). The shape of the MGI narrows with depth (Figure 1-21). This can be explained by initial intrusion as a normal stock, about 300 m across, with a zone of crystallized sidewall magma that is thickest at the top and narrows along the sidewalls. The bulbous shape of the MGI could reflect the shape of the cupola when mineralization occurred, or it could be a manifestation of the downwards migration of the cupola due to withdraw of magma before intrusion of the Kali Dikes. In this case, as the mobile magma withdraws the original width of the stock is be maintained at the top but as the width of crystallized sidewall magma becomes narrower at depth, the void left by the retreating magma contracts.

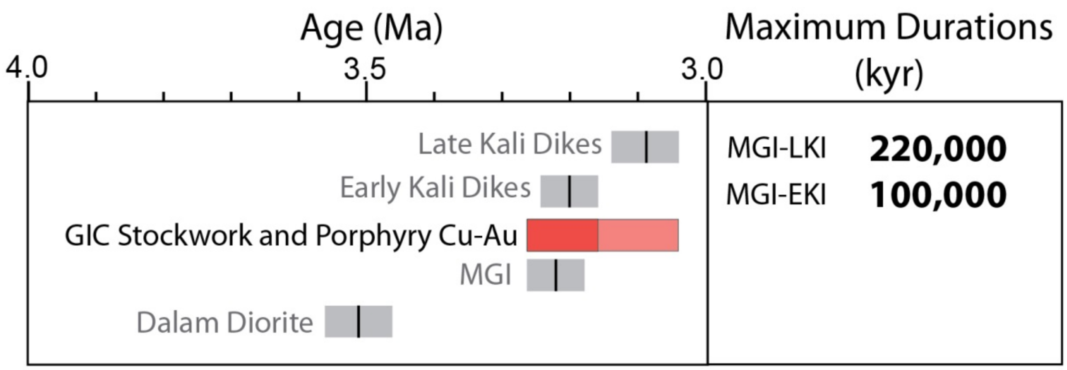

Figure 1-21. Plot showing the composite zircon U/Pb ages for cross-cutting intrusions in the GIC. The maximum duration of ore formation is constrained by the oldest age for the MGI (3.22 ± 0.04 Ma) and the youngest age for the Early Kali Dikes (3.20 ± 0.04 Ma) and the Late Kali Dikes (3.09 ± 0.05 Ma). Based on these ages, hydrothermal fluid flow responsible for the bulk of the high grade copper and gold mineralization lasted for at most 100 to 220 kyr.

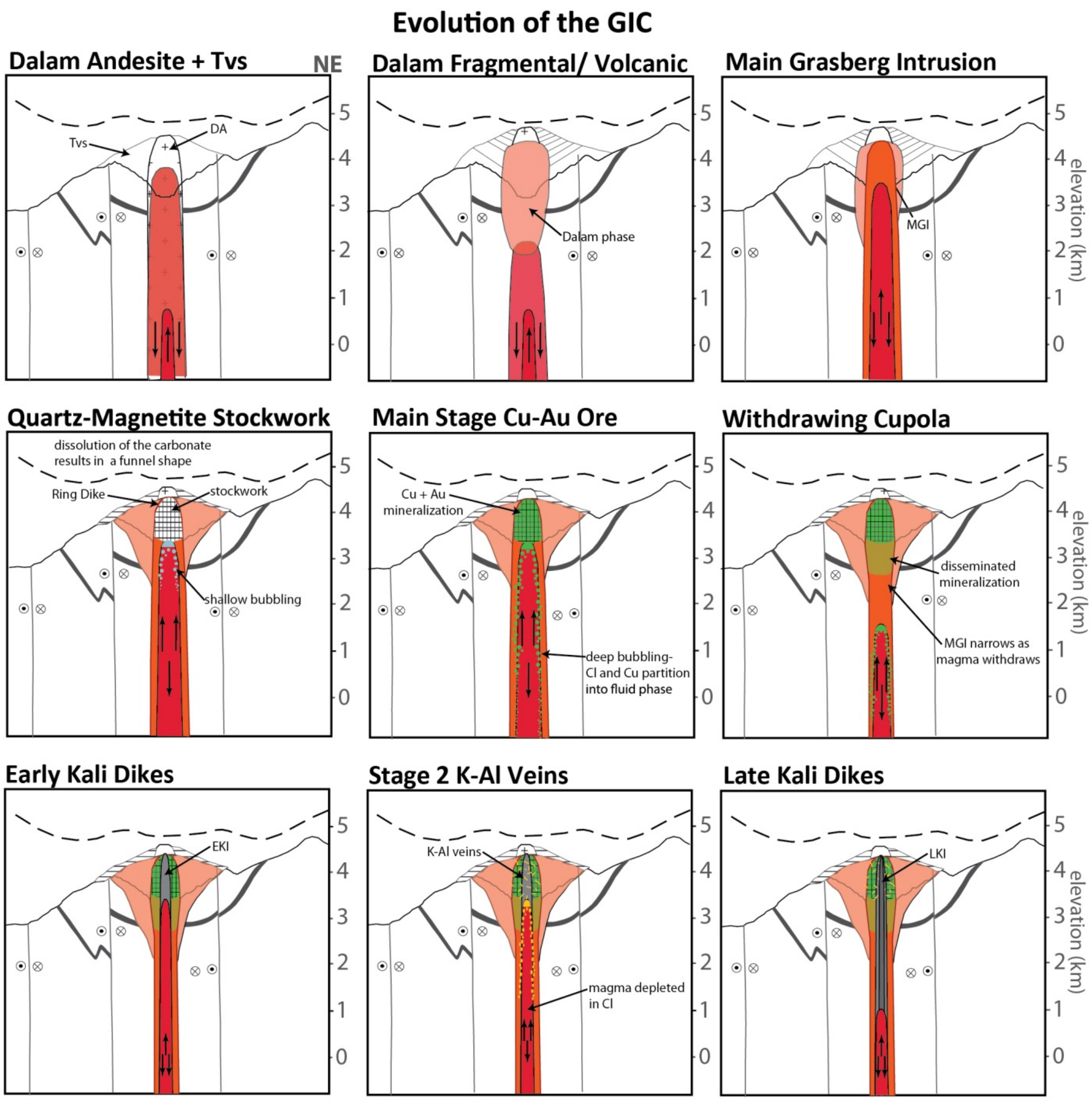

Figure 1-22. Schematic diagram showing the evolution of the GIC. The first igneous activity in the GIC is the Dalam Phase, which includes the Dalam Andesite, Tvs, Dalam Fragmental, and Dalam Volcanic. The MGI was the next intrusion, and is the host rock for the quartz magnetite stockwork and the main stage Cu and Au mineralization. The bubbling front evolved downwards between the two stages of mineralization, allowing Cl and Cu to partition efficiently into the fluid phase. The MGI narrows with depth, which is interpreted to be the result of lessening magma supply and cupola withdrawal. The EKI cuts the MGI and associated mineralization, and re-development of the bubbling front in Cl-depleted magma results in the formation of Stage 2 k-feldspar and biotite veins. The final igneous event is the LKI, which cuts the main stage mineralization and provides a temporal constrain on the duration of hydrothermal activity. After Cloos (2001).

The MGI is the host for the main stage Cu-Au ore mineralization (MacDonald and Arnold, 1994; Penniston-Dorland, 2001). The earliest part of the ore forming system is a barren quartz-magnetite stockwork (Stage 1a), which occurs between the pre-mining surface and ~3500 m elevation. The volume of quartz veining decreases from greater than 25-50 % in the center of the quartz-stockwork zone to < 10 % at the 3000 m elevation level in the MGI. Based on a reconnaissance study of the quartz-magnetite stockwork zone, there is a change in the nature of the copper ore from the stockwork zone down to the 3000 m elevation. In the high-grade core of the ore zone, above 3700 m elevation, the quartz-magnetite stockwork is overprinted by a network of chalcopyrite veinlets (Stage 1b), and the bulk of the ore is in veins, whereas in the core of the system below 3500 m, copper ore occurs both as veins and as disseminations. The change in mineralization style with depth in the MGI indicates that the stockwork zone responded differently than the deeper disseminated zone. The quartz-magnetite stockwork zone formed when the fluid-charged cupola was located above ~3500 m. At this time the rocks directly overlying the cupola were at near-magmatic temperatures, and thus the differential stress was low. When an earthquake occurred, the pull-apart in which the GIC was emplaced rapidly extended, creating tectonic extension fracturing in the hot rock above the cupola (see Cloos and Sapiie, 2013). Collapse of the rock mass overlying the cupola as the fluid moved upwards resulted in near instantaneous 3D dilatation. Cooling and decompression of the fluids as they filled in between the collapsed rock fragments, precipitating quartz and magnetite, formed the stockwork zone. Quartz and magnetite were the dominant minerals precipitated above ~500°C, and chalcopyrite, bornite, and other minerals, precipitated below ~500°C (Williams-Jones and Heinrich, 2005, and references therein).

Zircon U/Pb dating of the Kali Dikes helps confirm that, while above 3700 m the Kali Dikes can be divided into the EKI and the LKI, the classification scheme becomes more complicated at depth. Based on samples that were identified as the EKI and the LKI in the open pit, the ages of the dikes are 3.20 ± 0.04 Ma (x=5, n=141) and 3.09 ± 0.05 Ma (x=3, n=88) respectively. The age dispersion suggests that the EKI is closer in age to the MGI, and occurred shortly following intrusion of the MGI and formation of the bulk of the high-grade ore zone. In contrast, the LKI is resolvably younger than the MGI and essentially non-mineralized at the level of the open pit. At depth in the GIC, accessed by drilling, it is not always possible to distinguish between the EKI and LKI, and the unit identified as EKI above 3700 m elevation may be absent (Cloos, pers. comm.). At the 3000 m elevation level of the Amole drifts it is clear that there are more than two Kali-Phase diking events (Bowman, 2017). The Kali Dikes samples from deeper than ~3700 m show a range of ages between 3.2 and 3.0 Ma.

Implications for the magmatic system

Knowledge of the GIC evolution is deduced based on field relationships and the robust geochronology throughout the complex presented in this study. The evolution of the parental magma chamber, based on the geochemistry, shows a modest fractionation trend between the MGI and the Kali Dikes, and a significant recharge and mixing event, based on the different Sr and Nd isotopic compositions between the magmatic phases of the GIC. The compositional trends, or lack thereof, which show minimal correlation between SiO_2 and the other major elements indicate that the parental magma comprised sources with varying degrees of fractional crystallization. Bowman (2017) postulates a major recharge event added enough heat to cause cessation of mineralization. This study shows the re-initiation of cooling that led to the formation of ore bodies elsewhere in the district (see Chapter 4). A change in the location of mineralization is explained as a result of changes in the pattern of faulting in the crust above the parental batholith.

The overall similarity in the geochemical character of the Dalam, MGI and Kali Dikes indicates the magma chamber was well-mixed and actively convecting. Sr and Nd isotope data show that the magma chamber experienced two major recharge pulses during the lifetime of the GIC. A recharge event post-dated the Dalam and pre-dated the MGI plug. Another recharge event occurred between the MGI and Kali. This event corresponds to the abrupt shut-off of the hydrothermal system (Paterson and Cloos, 2005b), and may have played a role in initiating the intrusion of the Kali Dikes.

CONCLUSIONS

By using the novel LA-ICP-MS tape-mount zircon U/Pb method to isolate the youngest growth zones, and plotting all of the zircon analyses from a single intrusion on a composite Tera-Wasserburg diagram, it is possible to achieve high precision (±0.05 myr). New composite zircon U/Pb ages for the GIC show resolvable differences between emplacement of the Dalam, the MGI and the LKI. Based on these results the Dalam Phase took place between 3.6 to 3.3 Ma, the MGI was emplaced at 3.22 ± 0.04 Ma (x=5, n=233), and the EKI and LKI were emplaced at 3.20 ± 0.04 Ma (x=5, n=141) and 3.09 ± 0.05 Ma (x=3, n=88) respectively.

Fundamental cross-cutting relationships in the GIC place direct constraints on the maximum duration of hydrothermal fluid flow: both the EKI and the LKI cross-cut the bulk of the high grade mineralization. Based on the composite ages and analytical errors for the MGI, EKI, and LKI, the maximum duration of hydrothermal fluid flow was between 100 to 220 kyr. The entire GIC, from the oldest dated part of the Dalam to the youngest Kali Dike, formed in a timespan of ~600 kyr.

Chapter 2: Rapid Cooling of the Grasberg Porphyry Copper Deposit and Implications for High Grade Ore Formation

ABSTRACT

Classical porphyry copper deposit genetic models infer that ore bodies form in association with long-lived, subduction zone volcanoes, where magmatism and hydrothermal fluid discharge takes place over millions of years. This study presents zircon and apatite (U-Th)/He ages (zHe and aHe) from a 2.2 km vertical profile in the center of the supergiant Grasberg deposit. Volcanic samples from the top of the profile cooled below ~210°C immediately following eruption between 3.5 to 3.3 Ma (zHe ages of 3.4±0.1 and 3.3±0.3 Ma). Samples from the Kali Dikes at 2.2 km depth, which crystallized at 3.1±0.1 Ma, cooled more slowly (zHe age of 2.1±0.3 Ma). Throughout the vertical profile aHe ages, which record cooling to ~110°C, are less than 0.6 m.y. younger than the zHe ages. The minimum cooling rate from 700°C to 210°C was 25°C/10 kyr near the surface and 4°C/10 kyr at 2 km depth. These results indicate Grasberg ore formation occurred immediately following maar volcanism, was short-lived, and the system cooled rapidly. Such rapid cooling of near-surface samples precludes the presence of a 2 km tall volcanic edifice overlying the orebody. The slower, but still overall rapid, cooling at 2 km depth necessitates emplacement into cold country rock. As most copper sulfides precipitate from fluids between about 500 to 300°C, the tightness of vertical and lateral isotherms contribute to the localization of copper mineralization into a small volume, one of the critical factors leading to the formation of an extraordinarily high grade copper-gold ore zone.

INTRODUCTION

The Ertsberg-Grasberg mining district, located in Papua, Indonesia, contains one of the single largest recoverable resources of copper and gold in the world. The supergiant, high-grade Grasberg deposit (2000 Mt at 1 wt. % Cu and 1 g/ton Au; Leys et al., 2012) is associated with latest Pliocene quartz diorite to quartz monzonite intrusions emplaced into sedimentary strata of the Cretaceous and Tertiary Kembelangan and New Guinea Limestone Groups (MacDonald and

Arnold, 1994; McMahon, 1994). Chapter 1 reports the geochronological history of the magmatic system. The oldest magmatic activity in the Grasberg Igneous Complex (GIC) is the Dalam Phase, which took place between 3.6 – 3.3 Ma. The Main Grasberg Intrusion (MGI), a cone-shaped plug that hosts much of the high-grade ore, was emplaced at 3.2 Ma. The youngest magmatic activity is the Kali, a series of dikes emplaced between 3.2 and 3.1 Ma which form a wedge shaped composite intrusion that cross-cuts the main stage copper mineralization (Penniston-Dorland, 2001; Paterson and Cloos, 2005a). The young age of the GIC (3.6-3.1 Ma) provides a unique opportunity to study a porphyry copper system that has not experienced significant post-mineralization tectonic dismemberment or thermal overprinting.

Field relationships and petrological studies provide two lines of evidence that indicate the top of the Grasberg deposit formed at depths less than 1 km and experienced a rapid shut-off to the hydrothermal system (Paterson and Cloos, 2005b). First, there is a lack of evidence for a towering volcanic cone above the Grasberg deposit. A 2 km cone would have a radius of 4 to 5 km. Second, the banded clay unit, located on the northeast and southwest boundary of the GIC, consists of laminated halloysite clays that appear to be the roots of a boiling mudpot field, through which acidic fluids discharged. The limited extent of overprinting between the high-T biotite + magnetite core alteration zone and the low-T sericite + pyrite ± anhydrite alteration zone (in a 500 m annular region around the core of the deposit, less than 1% by volume of the biotite is altered to sericite; Paterson and Cloos, 2005b) indicates that there was very little fluid flow as the core of the system cooled to temperatures below ~300°C. To better constrain the timing and rate of cooling in this remarkable deposit, zHe and aHe ages are presented from two vertical profiles, which span 2.5 km in the center of the GIC. The quantification of cooling rates has several implications for the generation of the supergiant orebody.

Recent publications suggest that gas-brine mixing reactions (Blundy et al., 2015), sulfur-dioxide flux and chemisorption reactions (Henley et al., 2015), and sulfide melt transport by adherence to vapor bubbles (Mungall et al., 2015) are the critical factors leading to the generation of porphyry copper deposits. However, none of these processes explain why porphyry copper deposits are rare when intermediate magmas with ore-forming potential are relatively common (e.g. Mt. Pinatubo 1991 eruption; Pasteris, 1996). Even more critically, none of these mechanisms provide an explanation for what factors focus hydrothermal fluids into a restricted volume or a tall column, as is the case in the GIC. While the necessary magma chemistry (including volatile content) appears to be commonplace, the necessary structural plumbing for magma ascent and focusing of hydrothermal fluid discharge is apparently less common (Cloos, 2001). A factor neglected in all reports, partially because of the lack of ability to assess it, is the cooling rate of the magmatic and hydrothermal systems. Cooling rate must be important, as it can govern the rate of fluid generation, and tight isotherms associated with rapid cooling can localize ore mineral precipitation. Where heat loss is the key factor controlling fluid generation, then the cooling rate of the magma controls the rate of fluid exsolution. Steep thermal gradients across the margins of a parental stock emplaced into cold country rock will lead to rapid crystallization (Cloos, 2001). The crystallization of quartz and feldspar will cause volatile contents to build up to the point of saturation. Once bubbles are generated at sufficient depths (greater than 6 km) chlorine, and thus copper (Candela and Holland, 1984), will experience strong partitioning into the fluid phase (Shinohara et al., 1989). Copper-rich hydrothermal fluids, located in bubbling magma ascending along the side-walls of the stock, can separate to collect in a cupola at the top of the stock (Cloos, 2001). Mineralizing fluids then ascend from the charged cupola, through both infiltration fluid flow and during vein-forming events. When this is prolonged, a porphyry copper ore body can form. Tightly spaced, steep isotherms cause faster heat loss from the magma chamber, which promotes steady production of copper-rich hydrothermal fluids. Tightly spaced, near horizontal isotherms in the ore-forming zone help localize sulfide precipitation, enhancing the potential of forming a high-grade ore body.

ANALYTICAL TECHNIQUES

Zircon and apatite (U-Th)/He analyses were completed at the University of Texas at Austin. Lengths and widths of euhedral, inclusion-free crystals were measured using a binocular microscope (180x) and loaded into 1 x 0.5 mm Pt tubes. Samples in Pt tubes were heated to approximately 1300°C for 10 minutes for zircon and ~1050°C for 5 minutes for apatite using a PhotonMachines 75W diode laser. Extracted ^{4}He was spiked with a ^{3}He tracer, cryogenically purified, and measured using a Blasers Prisma QMS-200 quadrapole noble gas mass spectrometer. ^{4}He contents were calculated by isotope dilution using a manometrically calibrated ^{4}He standard.

After He measurement, apatite grains, left in Pt tubes, were spiked with ^{230}Th and ^{235}U and dissolved using HNO_3 and heating to 90°C for 1 hour. Deionized water was subsequently added to the solution. Zircon grains were extracted from the Pt tubes, spiked with ^{230}Th and ^{235}U, and dissolved using a two-step HF-HNO_3 pressure vessel dissolution procedure. The resultant solution was analyzed for $^{238}U/^{235}U$ and $^{232}Th/^{230}Th$ ratios using a self-aspirating micro-concentric nebulizer on a ThermoFisher Element2 double-focusing magnetic sector HR-ICP-MS. Reported ages are given a standard 2σ error of 8% (Reiners et al., 2002; Stockli, pers. comm.).

RESULTS

Zircon and Apatite (U-Th)/He Ages

Twenty-five years of drilling and mining at the Grasberg porphyry copper deposit allows a unique opportunity to study a 2.2 km vertical cross section through the deposit. Samples collected from the open pit, exploration drill holes, and a deep drill hole (KL98-10-21) that extends from 3.0 km to ~1.4 km elevation, complete a 600 m vertical profile in the pre-ore MGI and a 2 km vertical profile in the post-ore Kali Dikes (Figure 2-1) (See Appendix H for sample locations). Zircon and Apatite (U-Th)/He aliquot ages are in Appendix J and Appendix K. Essentially identical zircon U/Pb and zHe ages in the samples above 3 km elevation for both the MGI (3.2±0.1 Ma and 3.2±0.3 Ma, respectively) and the Late Kali Intrusion (3.1±0.1 Ma and 3.1±0.2 Ma, respectively) indicates extremely rapid cooling from >700°C to <210°C. Furthermore, samples from the volcaniclastic sedimentary unit (Tvs) (zircon U/Pb age range from 3.6 to 3.3 Ma) show instantaneous cooling followed emplacement (zHe age 3.3±0.3 Ma to

3.1±0.5 Ma). While surface samples cooled rapidly, deeper samples record slower cooling; the sample from 1.4 km elevation in the Kali Intrusion has a zHe age of 2.1±0.3 Ma. That volcanic samples cooled rapidly is no surprise, but if a 2 km volcanic edifice once towered over the GIC, samples from the center would have been buried by at least 2 km and only cooled to <210°C long after hydrothermal activity ceased. That the intrusive rocks at the center of the GIC, above the hydrothermal system record immediate cooling is strong evidence that the system lacked a towering volcanic edifice.

AHe ages in the Kali Intrusion vertical profile show that an additional ~100°C of cooling took approximately 0.6 myr, and no more than 1 myr, even at depths of 2 km. Younging of the aHe ages with depth from 2.9±0.2 Ma at 3.3 km elevation to 2.1±0.3 Ma at 1.9 km elevation illustrates slightly more protracted cooling at depth, but overall rapid cooling is recorded down to a depth of 2.2 km. Collectively, these results show that the MGI cooled rapidly following intrusion and crystallization at 3.2 Ma. Subsequent emplacement of the Kali Intrusion did not provide enough heat to reset the zHe ages in the sampled parts of the MGI, suggesting that the dikes were volumetrically minor, with a thermal footprint that did not extend far into the MGI.

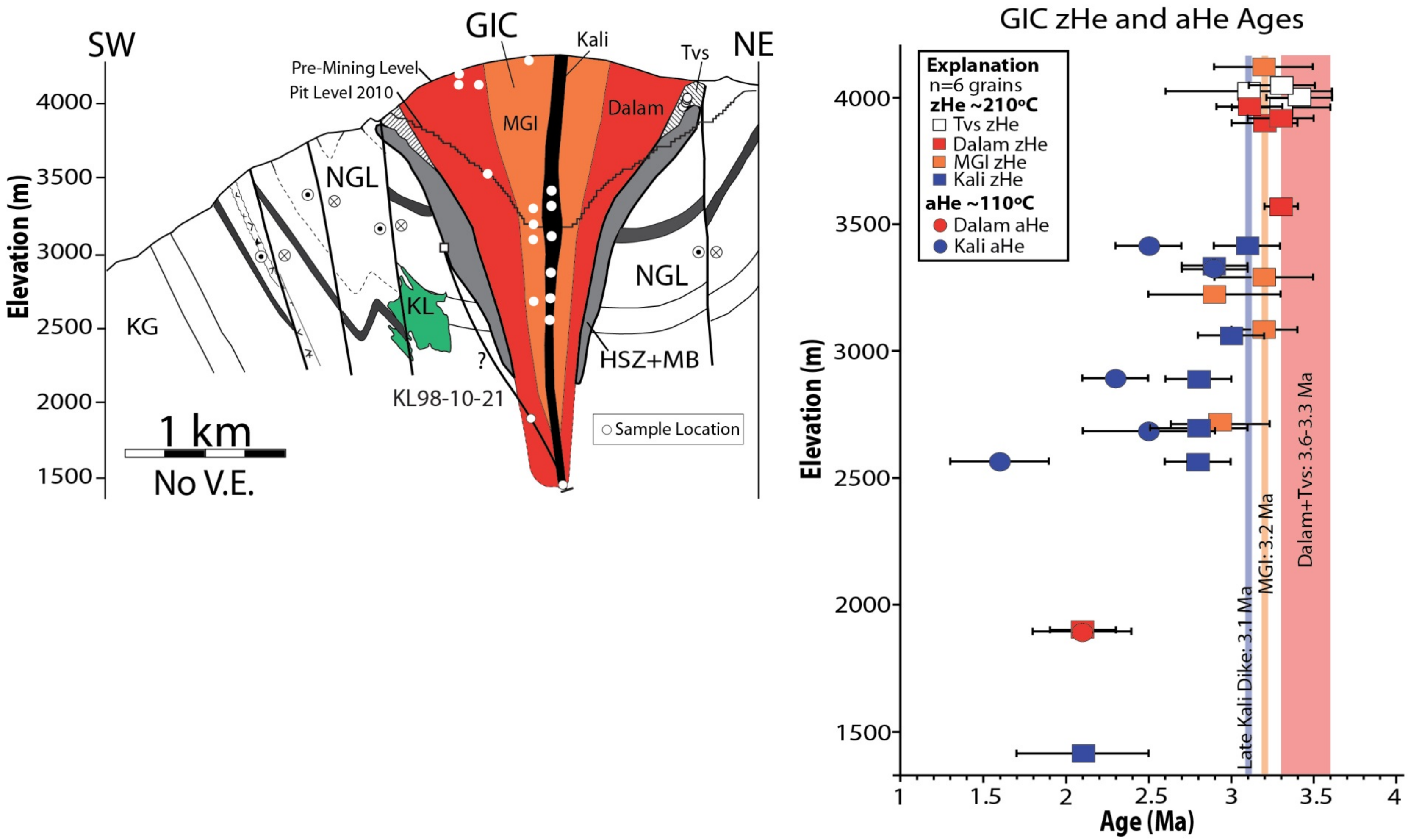

Figure 2-1. Cross section of the Grasberg Igneous Complex (left) showing sample locations for the MGI and Kali vertical profiles, and the Dalam and Tvs samples. Plot showing zHe and aHe ages for all samples (right). Bars show helium age and uncertainty. Colored vertical lines show the zircon U/Pb crystallization age for each magmatic phase. NGL - New Guinea Limestone Group, KG - Kembelangan Group, KL - Kucing Liar Skarn, HSZ + MB - Heavy Sulfide Zone + Marginal Breccia.

Closure Temperatures and Cooling Rates

Helium loss from zircon and apatite occurs through thermally activated volume diffusion. In order to quantitatively interpret the zHe ages, it is important to understand the diffusion kinetics and retentivity of helium for low radiation damage Grasberg zircons (Guenthner et al., 2013). ^{4}He diffusion experiments were conducted on two zircons from the MGI (Farley et al., 1999), and the results show that bulk helium diffusion, despite the low radiation damage, is not anomalously low and is consistent with published experimental data on zircon (Appendix I) (Reiners et al., 2004)**.** The zircon U/Pb, zHe, and aHe ages show that the magmatic and hydrothermal system that formed the Grasberg orebody cooled rapidly. “Effective” closure temperatures, calculated iteratively for the observed cooling rate (~500°C/myr) using the Dodson equation (Dodson, 1973), the experimentally derived zircon diffusion kinetics, and published apatite helium diffusion kinetics (Farley, 2000), are ~210°C and ~110°C for zircon and apatite respectively.

U/Pb crystallization ages and the low-temperature thermochronology data allow for a determination of the cooling rates from zircon crystallization at >700°C to the zircon helium closure temperature at ~210°C (Table 2-1) and the apatite closure temperature at ~110°C. In the Kali Dike the minimum cooling rate is 25°C/10 kyr near the surface, 10°C/10 kyr at 1 km depth, and 4°C/10 kyr at 2 km depth (Figure 2-2). The Tvs samples, located at 4 km elevation, record rapid cooling rates from 25 to 10°C/10kyr. The minimum cooling rate from 210°C to 110°C in the Kali Dike ranges from 2 to 1°C/10kyr. All evidence indicates the multi-stage GIC was emplaced, crystallized, and cooled to near-ambient conditions in less than one million years.

Table 2-1. Minimum Cooling Rates from 700 to 210°C

							Minimum Cooling Rates	
Sample	**Intrusion**	**Elevation (m)**	**Zr U/Pb Age (Ma)**	**Zr U/Pb Uncertainty (Ma)**	**zHe Age (Ma)**	**zHe Uncertainty (Ma)**	**(°C/Ma)**	**°C/10kyr**
GCZ-41-01-59m	Tvs	4020	3.6	0.1	3.3	0.2	980	**10**
NSC-09-02-246m	Tvs	4020	3.5	0.1	3.1	0.5	544	**5**
GT-1NC-023-22m	Tvs	4010	3.4	0.1	3.4	0.2	2450	**25**
GCZ-50-02-105m-1	Tvs	3960	3.5	0.1	3.3	0.3	980	**10**
14-SW-06	Dalam	3500	3.4	0.1	3.3	0.1	2473	**25**
14-SW-05	Kali	3415	3.1	0.1	3.1	0.2	2450	**25**
INF37-02-75m	Kali	3320	3.1	0.1	2.9	0.2	1225	**12**
INF42-01-250m	MGI	3300	3.2	0.1	3.2	0.3	1633	**16**
14-SW-02	MGI	3235	3.2	0.1	2.9	0.4	710	**7**
INF37-02-275m	Kali	3120	3.1	0.1	3	0.2	1633	**16**
INF42-01-50m	MGI	3100	3.2	0.1	3.2	0.2	2583	**26**
AM96-40-01-148m	Kali	2893	3.1	0.1	2.8	0.2	980	**10**
GRD42-06-362m	MGI	2700	3.2	0.1	2.9	0.3	868	**9**
AM96-40-01-344.7m	Kali	2696	3.1	0.1	2.8	0.3	817	**8**
AM96-40-01-477m	Kali	2564	3.1	0.1	2.8	0.2	980	**10**
KL98-10-21-1192m	Dalam	1902	3.4	0.1	2.1	0.2	327	**3**
KL98-10-21-1693m	Kali	1414	3.1	0.1	2.1	0.4	350	**4**

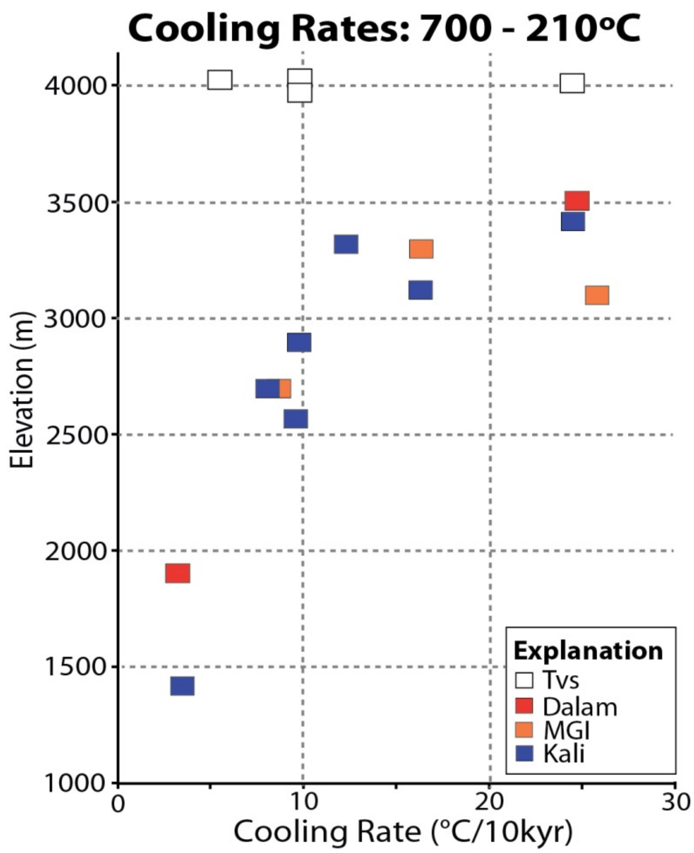

Figure 2-2. Cooling rate plot showing depth vs. cooling rate from 700°C to 210°C for each sample with zircon U/Pb and zircon (U-Th)/He ages.

DISCUSSION

Steep Thermal Gradients

The low-temperature thermochronology data provide a quantitative understanding of the previously reported field and petrographic evidence (Paterson and Cloos, 2005b), described above, that suggested an abrupt shut off to the hydrothermal system in the GIC, as cooling to temperatures below 300°C was not concurrent with substantial hydrothermal alteration forming phyllic or argillic assemblages.

Steep vertical thermal gradients indicate steep lateral thermal gradients, which is not surprising as the GIC was emplaced into the youngest strata capping the sequence of deformed Jurassic-Cretaceous clastic sedimentary rocks and Paleocene-Miocene shelf carbonates deposited on the northern passive margin of the Australian continent (Quarles van Ufford and Cloos, 2005; Cloos et al., 2005). While the hydrothermal event that created the orebody was remarkably large, the GIC has a narrow thermal footprint. The marble halo is <100 m wide at the surface, and remains narrow at 1 km depth (Pennington and Kavalieris, 1997). This small thermal footprint indicates none of the intrusions acted as long-lived feeders for a large volcanic center, as such a magma conduit would have heated the wall rock.

Volcanic Edifice

Several questions about the GIC can be addressed with the new thermochronology data. AHe ages provide a basis to evaluate the size of the volcanic edifice associated with the Grasberg ore deposit. Classical genetic models for porphyry copper mineralization typically assume that ore formation occurs beneath a 1-3 km tall strato- or composite volcano (Sillitoe and Bonham, 1984; Seedorff et al., 2010; Sillitoe, 2010). While a <1 km volcano can form quickly, a 2+ km tall volcanic edifice probably requires 100+ kyr of magmatic activity, resulting in lateral thermal gradients that create a contact aureole that enlarges over time as pulses of magma intrude to build a large volcano. Furthermore, if a 2+ km tall volcano once capped the GIC, very high erosion rates would be necessary to destroy all evidence in much less than 3 million years, as discussed below (Figure 2-3).

AHe ages of 3.0 to 2.0 Ma are not consistent with a long-lived magmatic center. If this was a typical long-lived subduction zone volcanic arc setting, as in Java or Japan, elevated geothermal gradients (50+ °C/km) would have developed near centers of volcanism. Thus, the aHe ages (which represent cooling < 110°C) from 2 km depth should be much younger than 2.0 Ma. The vertical profile would also be expected to exhibit more pronounced younging between the 4 km elevation surface samples and 2 km depth samples. Instead, this is a collisional setting. The folding and faulting that upturned bedding and made the spectacular alpine scenery should have created sub-normal thermal gradients before the magmatic intrusions rise from below. The Tvs and near-surface Kali samples show cooling immediately after emplacement, zHe and aHe sample pairs show rapid cooling between 210°C and 110°C, and the youngest aHe ages, which are from the deepest sampled parts of the GIC, indicate cooling to less than 110°C within 1 myr of emplacement. These results would not be expected if a 2+ km volcanic edifice towered above the GIC. Furthermore, while it may seem possible that glacial erosion rates could destroy a 1-3 km tall stratovolcano in 3 million years, glaciation in the Central Range did not initiate until the Pleistocene (Brown, 1990), after the aHe samples had already cooled below 110°C. The data indicate that maar-style volcanism occurred around 3.6-3.3 Ma, followed by passive intrusion of the MGI and the Kali Dikes with no associated volcanism.

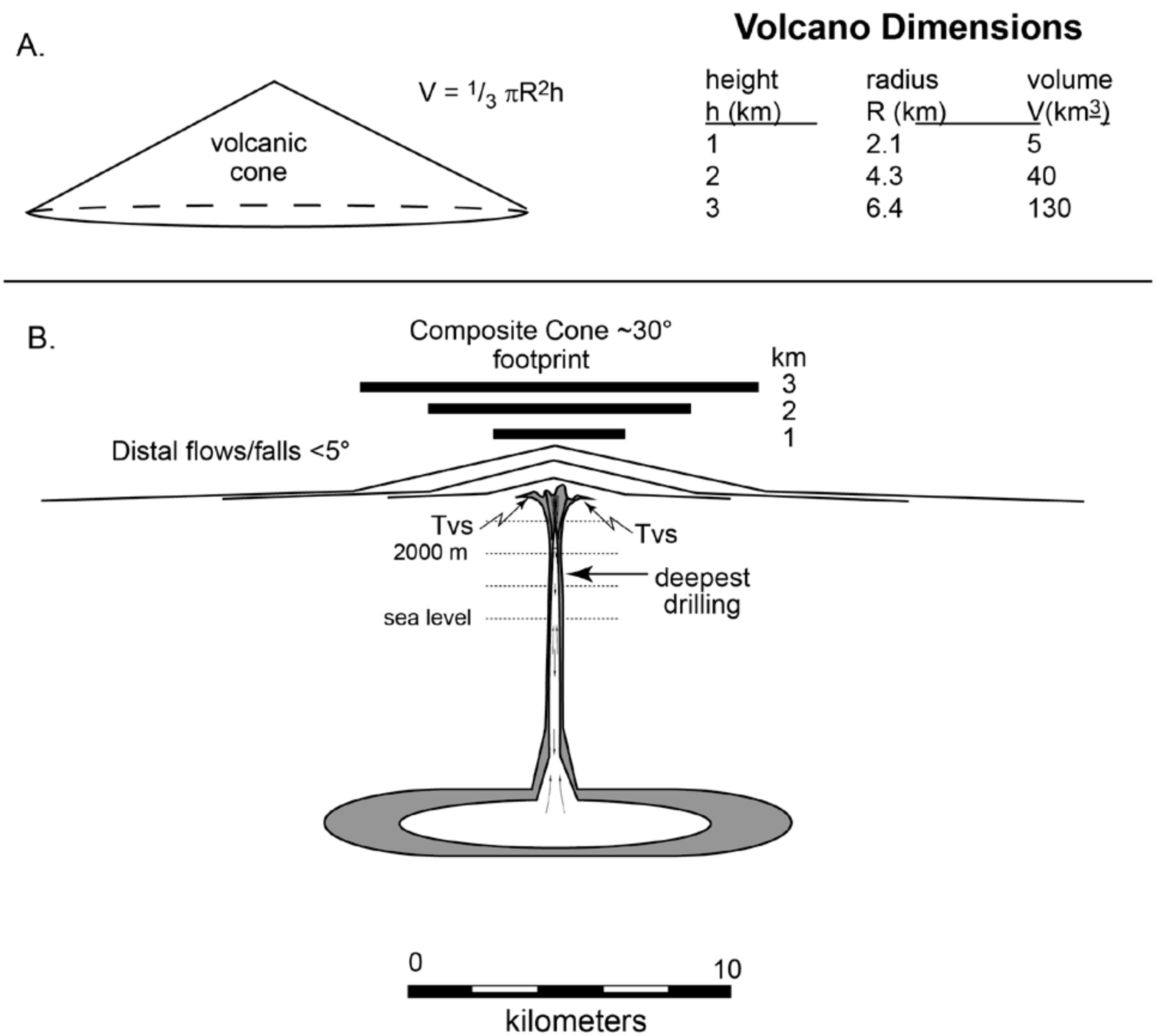

Volcano Dimensions

height h (km)	radius R (km)	volume V(km^3)
1	2.1	5
2	4.3	40
3	6.4	130

Figure 2-3. Diagram showing (A) the dimensions of a 1 to 3 km tall composite volcano, and (B) the footprint of a 1 to 3 km tall composite volcano had it existed above the GIC. The rapid cooling rates to the depths of the deepest drilling, the lack of field evidence for a tall composite volcanic cone, and the presence of halloysite clays in the banded clay unit preclude the presence of a towering composite volcano above the GIC.

Implications for Ore Genesis

Rapid cooling at depths as great as 2.2 km in the GIC indicates steep thermal gradients in the wall rock, which is only possible if the magmatic history was short-lived and the intrusions were emplaced into cold country rock. The direct implications of this inference are: (1) the isotherms within the ore-forming zone were tightly spaced, and (2) thermal gradients at the top of the stock were also relatively high, at least to depths of several km. Tight spacing of isotherms near the surface will localize deposition of copper-bearing sulfide minerals into a restricted volume, a key contributor in forming high grade hypogene mineralization (see William-Jones and Heinrich, 2005 and references therein) (Figure 2-4). Additionally, heat loss is faster where thermal gradients are steep. This leads to more rapid crystallization along the margins of the parental stock/ batholith. Heat loss controlled fluid generation would be steady compared to fluid generation from episodic recharge of the magma chamber by volatile-releasing magma (Figure 2-5).

All data indicate that the top of the Grasberg system cooled rapidly. Extrapolating downwards, it is envisioned that once magma in a stock reaches fluid saturation at pressures greater than ~2 kbar (or depths greater than 6 km) chlorine, and thus copper and other metals, experience strong partitioning into the fluid phase (Candela and Holland, 1984; Shinohara et al., 1989; Cline and Bodnar, 1991; Metrich and Rutherford, 1992). Once bubble-bearing magma along the sidewalls of a crystallizing stock becomes buoyant, it rises until such time that the bubbles are able to separate and collect in a cupola (Cloos, 2001). Mineralization results from infiltration fluid flow, that creates the characteristic alteration halos of Lowell and Gilbert (1970), and episodic rupturing of the cupola, which allows the copper-rich fluids to form veins in the overlying rock mass. Strike-slip faulting coeval with cupola charging causes pull-apart extension, which creates pathways for magma ascent and focuses hydrothermal fluid flow (Cloos and Sapiie, 2013; Sapiie and Cloos, 2013). Tightly spaced isotherms localize copper-sulfide deposition, resulting in a high grade porphyry copper-type orebody. The efficiency of steady deep-seated fluid generation, cupola charging, and localization of copper sulfide deposition is greatest when the parental magma chamber is emplaced into cold country rock. High T/P gradients near arcs may be the primary reason porphyry copper deposit mineralization is absent in some subduction zones (e.g. Java and Japan).

Recent publications have focused on the starting magmatic conditions and fluid chemistry that may lead to porphyry copper-type mineralization: Blundy et al. (2015) conclude the porphyry copper ore formation is a two-stage process involving copper enrichment of a brine, followed by copper sulfide precipitation triggered by sulfur-rich magmatic-gas release from an under-plated mafic magma. Henley et al. (2015) state that efficient generation of a porphyry deposit is spurred by chemisorption reactions between sulfur dioxide gas and calcic feldspar, which generates anhydrite and hydrogen sulfide gas, thus triggering the precipitation of copper sulfide minerals. Alternatively, Mungall et al. (2015) believe that the fundamental problem in porphyry deposit formation is the upwards transport mechanism of sulfur and metals, and describe a process whereby copper sulfide melt droplets adhere to vapor bubbles, forming compound droplets that float.

None of these workers postulate factors that explain why porphyry copper deposits are rare but magmatic systems with similar compositions are common, nor what are the special factors that make supergiant deposits such as Grasberg. In most deposits, the passive nature of alteration zonation indicates there was steady and prolonged fluid production and localization of hydrothermal fluid flow and copper sulfide deposition. As discussed, a combination of structural plumbing for focusing the ascent of magma and hydrothermal fluids and wall rock thermal structure are critical, especially for the creation of supergiant deposits such as Grasberg.

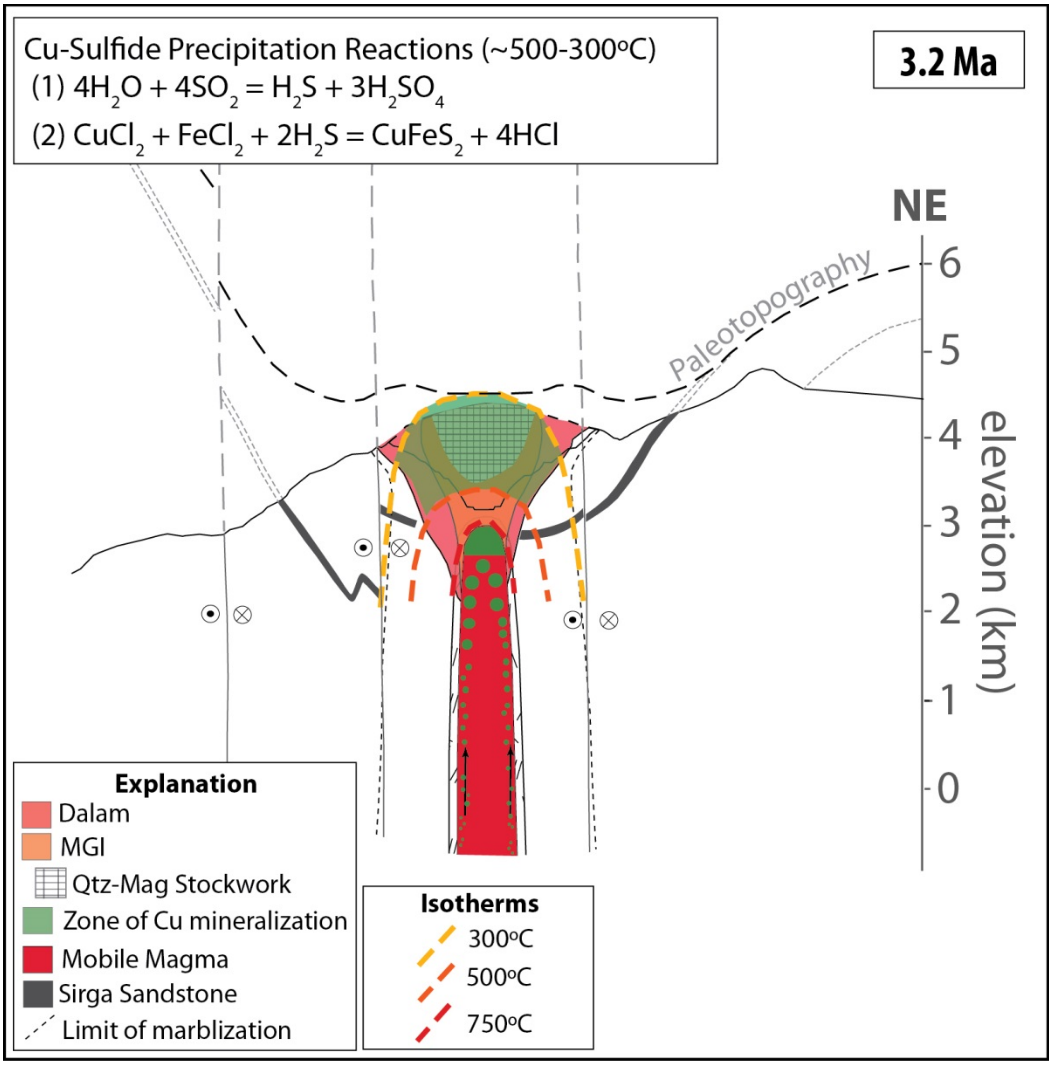

Figure 2-4. Schematic diagram showing how tight spacing of isotherms in the ore zone limits the volume of mineralized rock , resulting in higher ore grades. Isotherms at 750ºC, 500ºC, and 300ºC are shown in red to orange. The area of copper sulfide precipitation is shown in green. Paleotopography, which reflects the shape of the maar volcano, is shown in dashed lines.

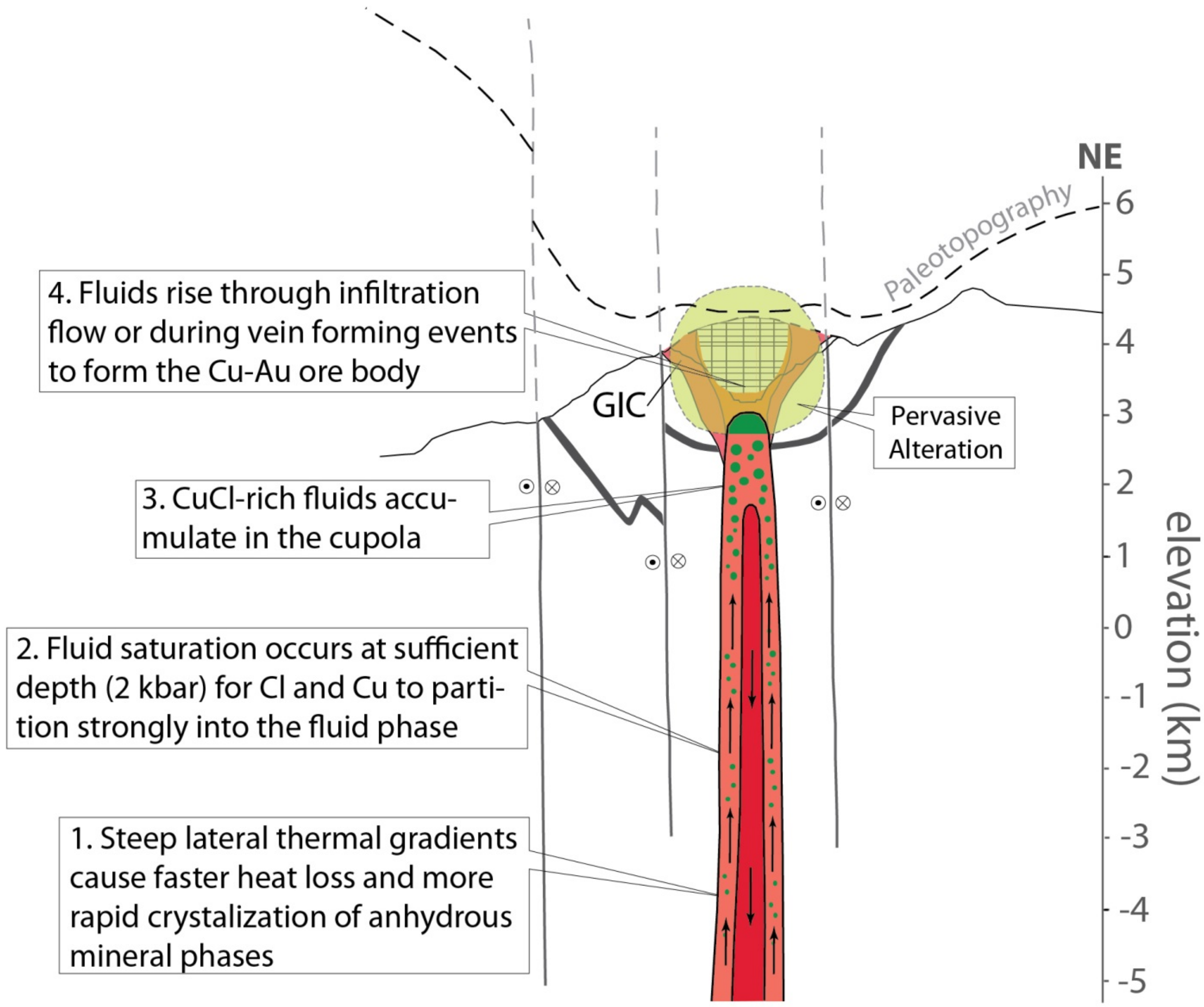

Figure 2-5. Schematic diagram of the stock associated with the Grasberg porphyry copper deposit (modified from Cloos, 2001). Fluid exsolution and bubbling occurs along the sidewall of the stock. Bubble-bearing magma rises until the bubbles are sufficiently large to separate and collect beneath the cupola. Periodic extension fracturing in the strike-slip pull-apart zone leads to hydrothermal vein formation and pervasive fluid infiltration results in the concentric alteration zones characteristic of porphyry copper deposits. Theoretical maar volcano topography and 3.2 Ma paleotopography shown in dashed lines.

Any model for porphyry copper deposit formation must also account for the observation that porphyry copper deposits rarely form during periods of steady state subduction volcanism but during periods characterized by a change in the tectonic style (Tosdal and Richards, 2001; Cloos and Housh, 2008; Mpodozis and Cornejo, 2012). Based on the cooling rates presented in this study, the near lack of porphyry copper deposits in tectonic settings such as modern day Java or Japan can be explained by high geothermal gradients: the isotherms along the margins of the stock are too widely spaced to facilitate efficient deep-seated crystallization and bubbling at the appropriate depths for Cl and Cu partitioning into the fluid phase. Conversely, periods of mineralization in the prolific South American metal belts correspond to times when the speed and angle of subduction were changing (Mpodozis and Cornejo, 2008). Magmas in new volcanic arcs will be emplaced into cold country rocks. During these time periods the thermal conditions in the country rock are normal (i.e. cold) and thus the cooling rates experienced by the first intrusions are high.

CONCLUSIONS

The major discoveries and implications of this study are:

1. For near-surface samples, above ~3 km elevation, in the GIC, the zircon U/Pb and zHe ages are essentially identical, indicating extremely rapid cooling from >700°C to <210°C. AHe ages in the Kali Intrusion vertical profile show that an additional ~100°C of cooling took approximately 0.6 myr, and no more than 1 myr, even at depths of 2 km. Minimum cooling rates in the Kali Dikes are 25°C/10 kyr near the surface, 10°C/10 kyr at 1 km depth, and 4°C/10 kyr at 2 km depth.
2. Based on the high cooling rates recorded in the GIC, the supergiant Grasberg porphyry copper deposit did not form in association with a long-lived volcanic edifice: instead the parental magma chamber was emplaced into cold country rock and steep thermal gradients localized copper-gold mineralization. The rate of heat loss out the sides of the stock controls the rate of fluid saturation, and the efficiency

of copper-rich fluid generation. Tightly spaced isotherms in the ore zone limit the volume of rock in which the copper sulfides precipitate. These factors, in conjunction with the exceptional structural control, resulted in a remarkably high-grade porphyry copper ore body.

Chapter 3: Andradite garnet U/Pb geochronology of the Big Gossan Skarn, Ertsberg-Grasberg Mining District, Indonesia

Abstract

The Big Gossan skarn is located in the prolific Ertsberg-Grasberg mining district, on the island of New Guinea in eastern Indonesia. Although it is small in size compared to the giant ore bodies in the district, Big Gossan has the highest ore grades (71 million tonnes at 2.39 wt% Cu and 0.91 ppm Au). Big Gossan was emplaced into the steeply upturned southern limb of the Yellow Valley Syncline near the conformable contact between the Ekmai sandstone and Waripi dolomitic limestone, adjacent to the western edge of the 3.1 – 2.8 Ma Ertsberg diorite. Garnets from Big Gossan were directly dated using the LA-ICP-MS U-Pb method. Analyses of eight garnet samples show that the Big Gossan skarn formed between ~2.9 – 2.7 Ma. To constrain reproducibility, one sample was dated twice, four months apart, producing overlapping ages of 2.75 ± 0.03 Ma (n=150 spots) and 2.73 ± 0.06 Ma (n=50 spots) (lower intercept age, Tera-Wasserburg concordia). This precision was achievable due to the high U contents (10-100 ppm) and consistent common Pb composition of Big Gossan garnets. Andradite garnet U/Pb ages are compatible with district-wide zircon U/Pb geochronology and the one existing phlogopite $^{40}Ar/^{39}Ar$ age for the deposit. The new garnet ages show that Big Gossan was one of the last ore-forming events in the Ertsberg-Grasberg district, and that skarn formation took place over less than ~200 kyr. This study demonstrates that andradite garnet U/Pb chronometry can be a robust dating technique for constraining the timing and duration of skarn-forming hydrothermal systems.

Introduction

Skarn ore deposits are major sources for a variety of elements, including Fe, W, Cu, Au, Mo and REEs. Cu- and Au-rich skarns commonly occur in the same mining districts as porphyry copper deposits. Both ore systems form as a result of magmatic-hydrothermal fluid exsolution from an intermediate magma emplaced into the upper crust (Burnham, 1979; Candela, 1989;

Hedenquist and Lowenstern, 1994; Baker et al., 2004; Candela and Piccoli, 2005). Fluid exsolution must occur in a prolonged fashion, at sufficient depths for chlorine, and thus copper, to be partitioned into a copper-rich hydrothermal fluid (Candela and Holland, 1984; Shinohara et al., 1989; Cline and Bodnar, 1991; Metrich and Rutherford, 1992; Williams et al., 1995). Once these conditions are met, the governing factor for whether a porphyry deposit or a skarn deposit may form is whether the magmatic fluids pass through an igneous host rock or carbonate wall rock (Meinert et al., 2005; Sillitoe, 2010). Skarn ore systems can be large (e.g. Ertsberg East, OK Tedi, Mines Gaspe), but have highly variable ore grades and complex mineralogy, making mining and beneficiation practices more difficult. Despite the potential challenges, they remain exploration targets for a variety of base and precious metals.

A major question in many skarn deposits is the timing of ore formation. Geochronology and thermochronology results from porphyry-related magmatic-hydrothermal systems, including zircon U/Pb, biotite Ar/Ar, and hornblende Ar/Ar ages, show that magmatic and hydrothermal activity may be protracted over millions of years (e.g. Chuquicamata, Ballard et al., 2001; El Teniente, Maksaev et al., 2004; Rio Blanco, Deckart et al., 2005) or may occur over a brief time period, on the order of 10,000 to 100,000 years (e.g. Potrerillos District, Marsh et al., 1997; Bajo de la Alumbrera, von Quadt et al., 2011; Far Southeast, Arribas et al., 1995). Similar geochronology studies of skarn systems are rare, due to a lack of dateable primary skarn minerals, challenges identifying causative intrusions, or a lack of cross-cutting relationships that may constrain the duration of magmatic hydrothermal activity. Two recent studies dated hydrothermal zircon and baddeleyite in order to constrain the timing of skarn formation: Deng et al. (2015) dated 56 hydrothermal zircons from four Fe-skarn systems in the Early Cretaceous Handan-Xingtai district, located in the North China craton, using LA-ICP-MS U-Pb techniques and found that the ages clustered between two time periods, from 137 to 133 Ma and from 131 to 128 Ma. Zhao et al. (2016) dated five hydrothermal zircons from the Late Cretaceous Tengtie iron deposit in South China using the SIMS U-Pb technique, and concluded that the deposit formed in less than several million years.

This study presents eight andradite garnet U/Pb ages from the Big Gossan skarn, located in the prolific Ertsberg-Grasberg mining district, on the Indonesian side of the island of New Guinea (Leys et al., 2012). Ages were measured using LA-ICP-MS techniques, a new method for garnets developed at the University of Texas at Austin (Seman et al., in review). The andradite garnets from the Big Gossan skarn are an ideal test of this new method given their relatively high U concentrations (10-100 ppm U), the relatively homogenous distribution of U throughout the garnet, and the well-behaved nature of the common lead. The young age of mineralization in the Ertsberg-Grasberg district (3.6 to 2.7 Ma) also allows for the measurement of highly precise ages for the skarn (Chiaradia et al., 2013; Schoene, 2014), as well as avoiding complexities resulting from tectonic-magmatic-hydrothermal overprinting that has affected many older skarn systems.

Geology of the Big Gossan Skarn

The Big Gossan skarn is small compared to the giant Grasberg porphyry copper deposit or the Ertsberg East Skarn System (Figure 3-1), but large compared to many copper-bearing skarns (e.g. Meinert et al., 2005). It contains the highest average copper grades in the mining district, with 71 million tonnes of ore at 2.39 wt% Cu and 0.91 ppm Au (assuming a 1 wt% Cu cutoff grade; Leys et al., 2012). The Big Gossan skarn developed in the steeply upturned southern limb of the Yellow Valley Syncline, near the contact between the Ekmai Formation and the Waripi dolomitic limestone, close to the southwestern margin of the Ertsberg Intrusion (Meinert et al., 1997; Gregory, 2004). The ore body (up to 1100 m along strike, 4-60 m thick, and >700 m in vertical extent) is localized at the intersection between strike-slip faults (Gregory, 2004). In contrast to the other skarns in the Ertsberg-Grasberg district, including Dom, Ertsberg, Ertsberg East, and Kucing Liar (Mertig et al., 1994), Big Gossan skarn is dominated by garnet and pyroxene, with a ratio of 1:2. The predominant sulfide mineral is chalcopyrite, with local concentrations of up to 20% pyrite, and <1% sphalerite, galena, and pyrrhotite.

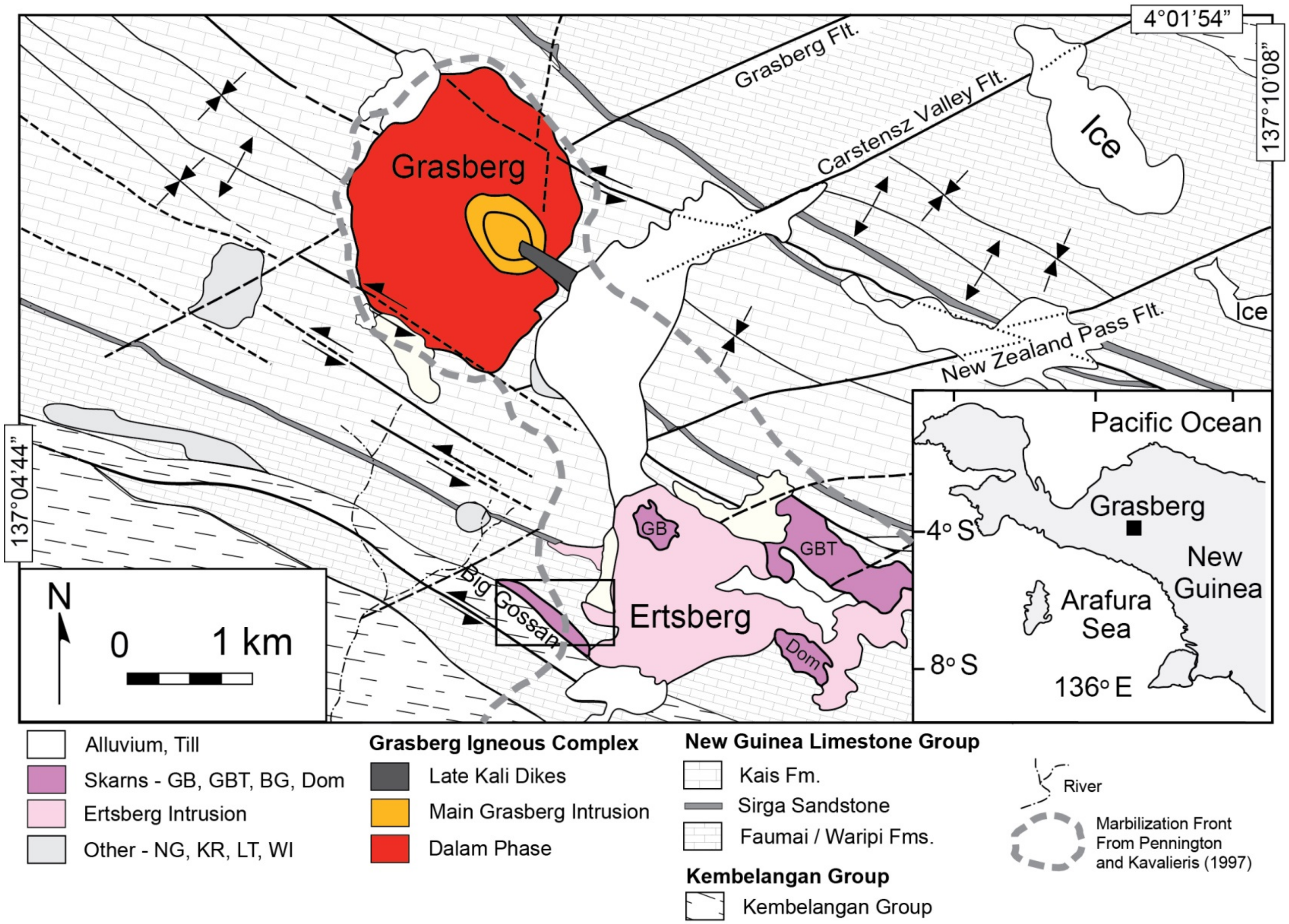

Figure 3-1. Map of the Ertsberg Mining District showing the location of the Big Gossan skarn. Modified from Paterson and Cloos (2005). Skarns: GB - Gunung Bijih, GBT - Gunung Bijih Timur (upper part of the Ertsberg East Skarn System). Black box shows the location of the map in Figure 3-2.

Previous Work

Garnets are an attractive mineral phase to target for dating as they are a ubiquitous phase in calc-silicate skarns and the garnet-bearing mineral assemblage may record the P-T conditions of prograde metamorphic reactions (Burton and O'Nions, 1991; Baxter and Sherer, 2013). Dating garnets became possible in the 1990's due to improvements in mass spectrometry, with the most commonly used radiometric systems being Sm/Nd and Lu/Hf (Scherer et al., 2000; Smit et al., 2013). In comparison to the established techniques, garnet LA-ICP-MS U-Pb dating has the advantage of being an in-situ technique; large inclusions can be visually screened out during laser spot selection or during data analysis, only small sample volumes are required, and the closure temperature of the U-Pb system is high. Burton et al. (1995) evaluated diffusion of Pb and other cations in garnet and found that Pb does not readily diffuse, even at temperatures up to 900°C, which is higher than U-Pb in monazite ($T_c = 725 \pm 25$°C; Parrish, 1990) and Sm-Nd in garnet ($T_c = 600 \pm 30$°C; Mezger et al., 1992).

Mezger et al. (1989) made the first attempt to use the U/Pb radiometric system to date garnet using the ID-TIMS method. They used garnet U/Pb ages to date the timing of melting and staurolite breakdown during prograde metamorphism, the timing of migmatization, and the timing of late granitic intrusions in the late Archean Pikwitonei granulite domain in Manitoba, Canada. ID-TIMS garnet U/Pb ages are obtained by completely dissolving the garnet crystal (including any inclusions) and measuring the U and Pb isotopes. If the U content of the garnet is dominated by the inclusions, then the garnet may simply act as a "container" for the inclusions (DeWolf et al., 1996), with the low rates of diffusion for U and Pb in garnet protecting the inclusions from isotopic resetting due to diffusive Pb loss, re-equilibration, recrystallization, or alteration by external fluids (Lima et al., 2012; Jung and Mezger, 2003). In this case the measured age would be that of the inclusion, and not the garnet.

While inclusions are the primary concern when using the ID-TIMS technique, they are not the sole source of radiogenic elements. Haack and Gramse (1972) investigated the fission track densities of 43 garnets from a suite of skarn samples from around the globe, and found that the U concentrations in andradite and spessartine garnets (estimated concentrations ranged from 30 ppb to 35 ppm) were sufficiently high to potentially measure a fission track age. DeWolf et al. (1996) also found that grossular-andradite garnets from Cascade Slide (Adirondacks, NY) showed little variation in fission track density, indicating that U is homogenously distributed throughout the garnet crystal structure. Conversely, almandine garnets from the metamorphic Pikwitonei Granulite Domain (Manitoba, Canada) and from the Wind River Range (Wyoming, USA) showed localization of fission tracks around micron scale monazite inclusions, indicating that the radiogenic elements were largely inclusion-hosted. The DeWolf et al. (1997) study demonstrates that the distribution of U, either in inclusions or in the garnet crystal structure, is strongly composition dependent. Experimental work aimed at testing the accommodation of REE and U in synthetic garnets also found that the incorporation of U in garnet is highly composition dependent (Yudintsev et al., 2002). The high U concentration in skarn grossular-andradite garnets (between 1 and 100 ppm) make it at excellent target for LA-ICP-MS dating, particularly as inclusions can be easily detected and avoided.

ANALYTICAL TECHNIQUES

Samples were collected from the mine drifts in the Big Gossan underground and from drill core (Figure 3-2). Large garnets (0.3-1 cm in size) were separated from the samples using a chisel and the fragments were visually inspected for inclusions. Five large crystals were selected from each sample, mounted in epoxy, and polished to expose a clean face of the garnet rim. Sample BG14W-07 65m was selected for core-rim age experiments due to the presence of multiple cm-scale garnet crystals. Three garnets from this sample were cut in half using a slow speed saw, and then mounted in epoxy. Backscattered electron images were collected in order to evaluate the zoning within the garnet crystals prior to analysis.

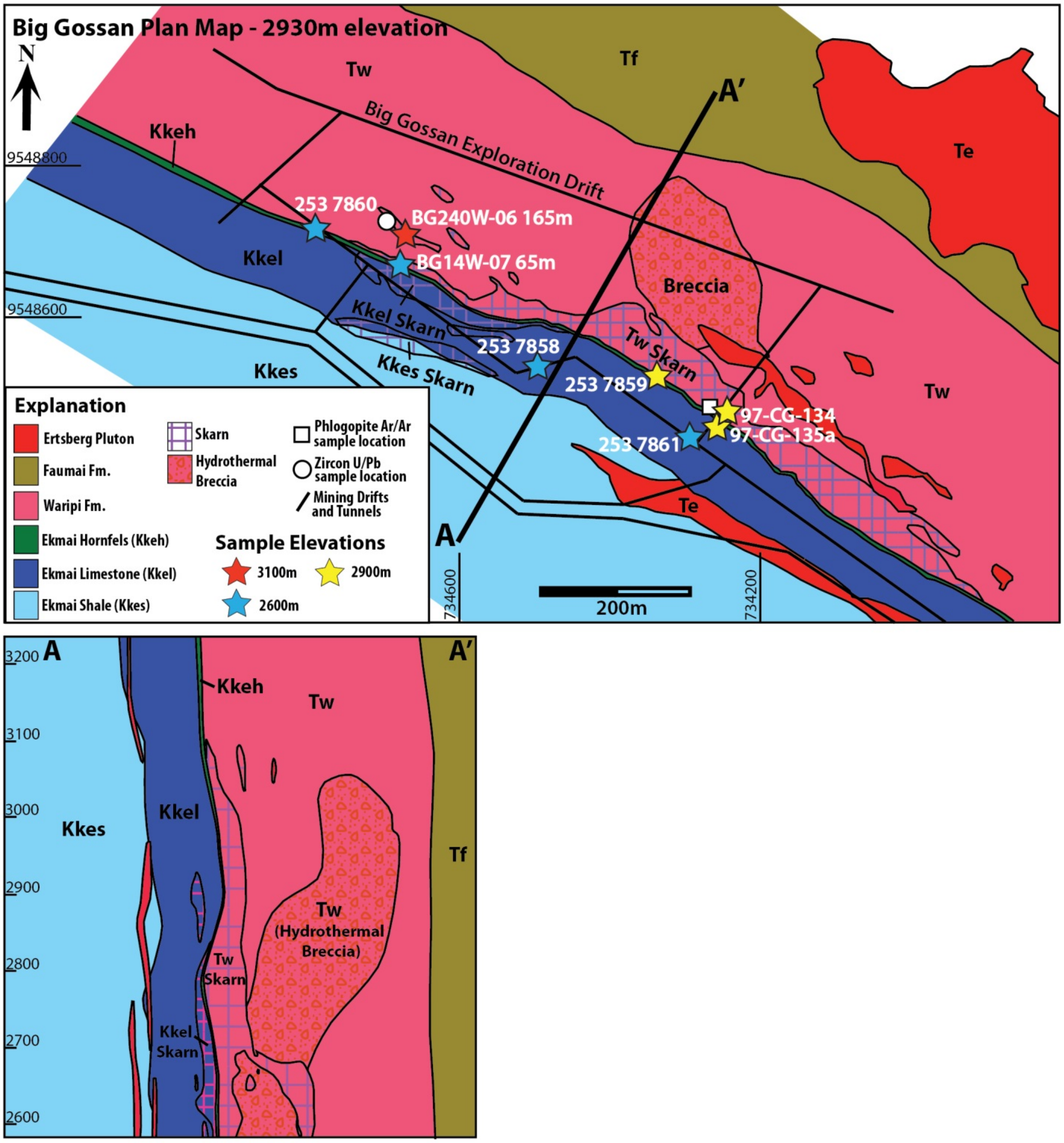

Figure 3-2. (Above) Plan map of the Big Gossan skarn at 2930m elevation. Sample locations are projected onto the plan map with the elevation denoted by color. Approximate location of the phlogopite Ar/Ar sample from Prendergast et al. (2005). (Left) Cross section of the Big Gossan skarn ore body from A-A'.

Garnet U/Pb analyses were completed at the University of Texas at Austin, using a single collector ThermoFisher Element2 ICP-MS with an attached PhotonMachine Analyte G.2 193 nm ArF Excimer Laser and large-volume Helex sample. The method of Seman et al. (submitted) was used to acquire data: garnets were ablated for 30 s (10 Hz repetition rate, 6 mJ energy, 17% beam attenuation, resulting in a fluence rate of 1.67 J/cm^2) using a large 110 µm spot size in order to maximize count rates. The instrument was tuned in order to maximize ^{238}U counts and minimize the interferences from oxide masses (UO <0.5%). In order to determine which primary standard is most appropriate for "high U" garnets data reduction was completed twice: once using a Willsboro garnet primary standard (Seman et al., in review) and once using GJ1, a Sri Lankan zircon primary standard. Although the zircon is not a matrix-matched standard, the wide laser pits (shallow depth) seem to minimize the effects of downhole fractionation, as there were no differences in age when using the first 10 seconds of the ablation compared to the full 30 seconds of ablation. Furthermore, the ages calculated using the Willsboro garnet as a primary standard overlapped within error with the ages calculated using GJ1. However, as the propagation of isotopic ratio uncertainties favors GJ1, which has a considerably more precise TIMS calibration, the ages reported here were calculated with GJ1 as the primary standard. This standardization was adopted because of the remarkable agreement with external age constraints (discussed below).

Data were processed using the Iolite software package (Paton et al. 2011) and ages were calculated using Isoplot v.4 (Ludwig, 1998). Given the heterogeneous distribution of common Pb in the Big Gossan garnets, we use a linear regression in Tera-Wasserburg space, where the lower Concordia intercept and its uncertainty are reported as the common lead corrected sample age and uncertainty (Tera and Wasserburg, 1972).

GARNET U/PB AGE RESULTS

Eight andradite garnet samples from the Big Gossan skarn were selected for dating. Sample locations are spatially varied, covering 600 m laterally and 500 m vertically throughout the skarn (Figure 3-2). Compositional zoning from core to rim has been previously noted in Big Gossan garnets (Meinert et al., 1997); therefore, for seven of the eight samples polished rims were targeted for dating in order to avoid potential complications from analyzing multiple growth zones. One sample with cm-size garnets was selected for experiments in order to determine if there is a detectable age difference between the cores and the rims of the polished central sections. BSE images show the garnet surfaces that were targeted (Figure 3-3).

Garnet U/Pb age data are reported in Appendix L. Tera-Wasserburg plots for seven garnet samples show there is one composition of common lead, as all of the error ellipses for the 50 – 60 laser spot analyses lie along a single mixing line (Figure 3-4). Variations in uranium and common lead concentrations result in a spread of data points along the mixing line, allowing for a robust common lead mixing line to be regressed, such that the reported lower intercept age is precise (errors between 0.03 and 0.2 Ma). The common lead corrected age for each garnet sample is shown in Table 3-1. All of the garnet U/Pb ages overlap within error, and there is no spatial pattern to the ages. Garnet U/Pb ages constrain the time window of Big Gossan skarn formation between 2.9 and 2.7 Ma, making the Big Gossan skarn the last ore-forming event in the mining district.

Duplicates

In order to test the reproducibility of the ages two kinds of duplicates were analyzed: (1) the same sample was analyzed twice, and (2) two samples from meters apart along the same drift in the Big Gossan skarn were analyzed. Garnets from sample BG-240W-06 165m were dated twice over the course of four months (January 2016 and April 2016), and the ages from each run are 2.75±0.03 Ma (n=154 spots) and 2.73±0.06 Ma (n=50 spots) (Figure 3-5). The agreement of the age and analytical error is remarkable. Two samples collected ~10 meters apart along the same drift, 97-CG-134 and 97-CG-135a, have ages of 2.84±0.11 Ma and 2.72±0.05 Ma respectively, which overlap within error. Collectively, the ability to reproduce duplicate ages indicates that the garnet U/Pb chronometer is robust and reliable.

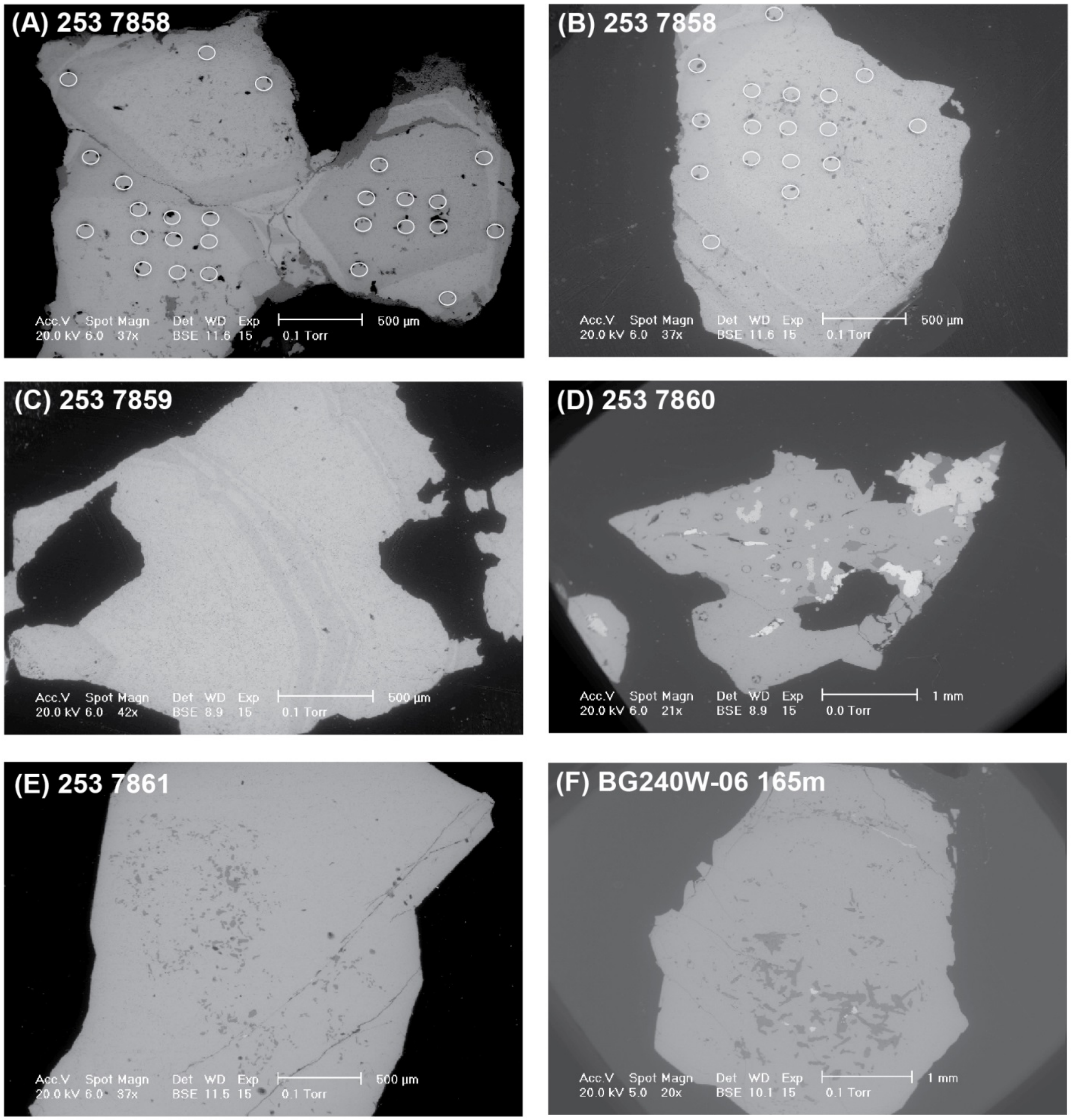

Figure 3-3. Backscattered Electron Images (BSE) of dated garnets. 110 µm laser spots shown in white circles. A. One large garnet grain showing three subgrains with three to four growth zones along the rims. Spots show laser pits. B. Garnet grain showing two to three growth zones along the rim. C. Faint zoning within an otherwise compositionally uniform grain. D. Garnet grain with bright sulfide and dark pyroxene inclusions. E. Garnet grain with 20 µm dark pyroxene inclusions. F. Single grain with dark pyroxene inclusions in the center and inclusion-free garnet along the edge.

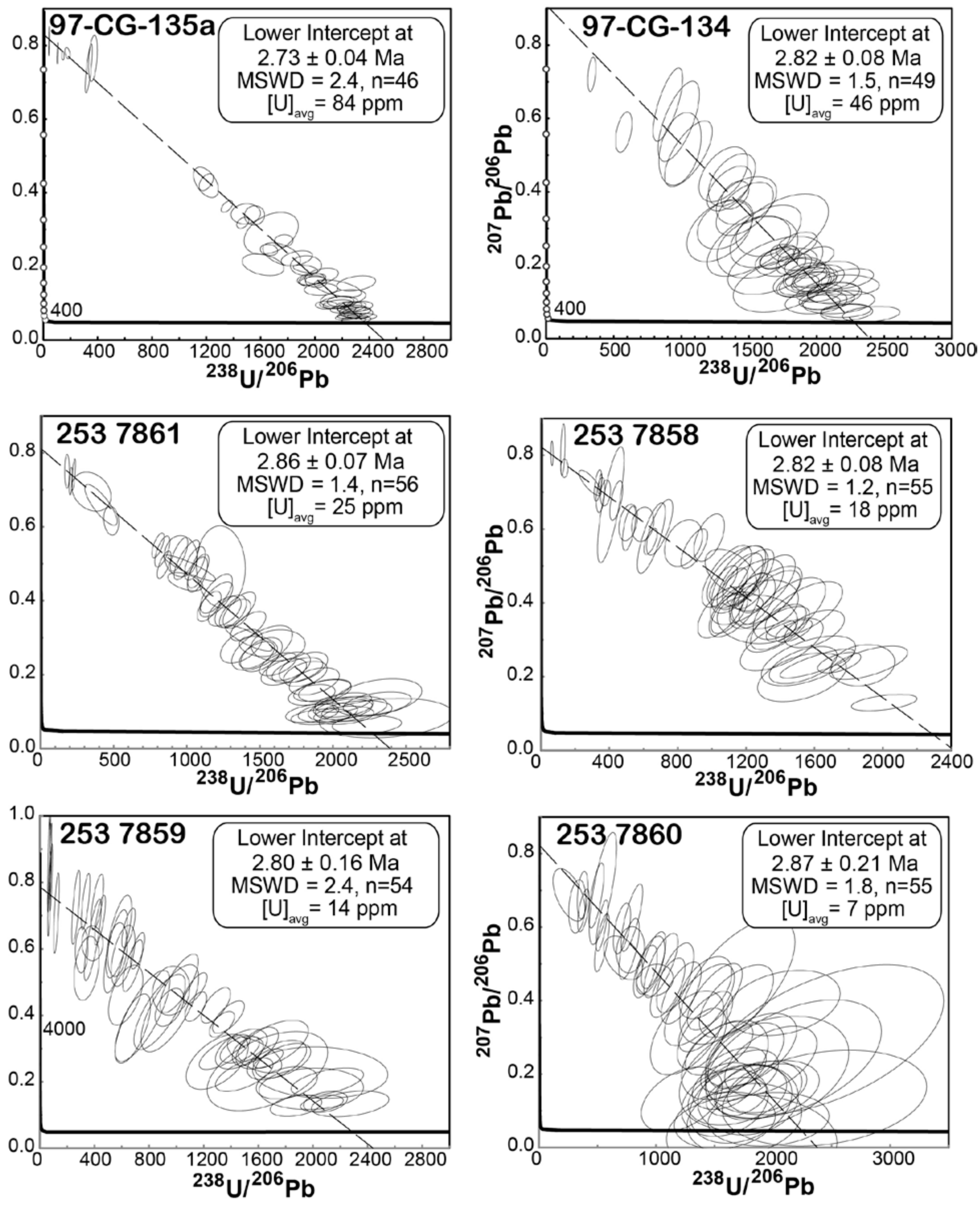

Figure 3-4. Tera-Wasserburg diagrams for six of the garnet U/Pb samples. Lower intercept ages are reported. Data-point error ellipses are 2σ.

Table 3-1. Garnet Sample Locations

sample ID	Sample location	Coordinate			Formation	Protolith	Associated skarn gangue minerals	Associated Mineralization	Garnet details
		Easting	Northing	Elevation (m)					
BG240W-06 165m	Drill Core	734838	9548716	3026	Tw	Dolomite	Actinolite-tremolite, dipside, anhydrite, sphalerite, quartz, magnetite	Chalcopyrite, pyrite	Brown Garnet (Andradite), coarse to very coarse grained
BG14W-07 65m	Drill Core	734927	9548464	2549	Tw	Dolomite	Garnet, chlorite, epidote, magnetite, tremolite, anhydrite	Chalcopyrite, pyrite	Brown Garnet (Andadite), moderate to course grain
97-CG-134	Drift Sample	734837	9548635	3016	Tw	Dolomite	Garnet, anhydrite, epidote, quartz, calcite, hematite	Chalcopyrite, pyrite	Brown Garnet (Andadite), moderate to course grain
97-CG-135a	Drift Sample	734832	9548645	3016	Tw	Dolomite	Garnet, tremolite, anhdyrite, epidote, quartz, dolomite, hematite	Chalcopyrite, pyrite	Brown Garnet (Andadite), moderate to course grain
2537858	BG2640L XC29	734748	9548583	2647	Tw	Dolomite	Anhydrite, diopside, epidote, sphalerite, magnetite	Chalcopyrite, pyrite	Brown Garnet (Andradite), coarse to very coarse grained
2537859	BG2860L XC40	734919	9548523	2866	Tw	Dolomite	Actinolite-tremolite, garnets, sphalerite, hematite, epidote	Chalcopyrite, pyrite	Brown Garnet (Andradite), coarse to very coarse grained
2537860	BG2600L XC15	734562	9548685	2613	Tw	Dolomite	Diopside, actinolite, tremolite, anhydrite, magnetite	Chalcopyrite, pyrite	Brown Garnet (Andradite), coarse to very coarse grained
2537861	BG2560L XC45	734963	9548473	2568	Tw	Dolomite	Diopside, anhydrite, quartz, epidote, magnetite	Chalcopyrite, pyrite	Brown Garnet (Andradite), coarse to very coarse grained

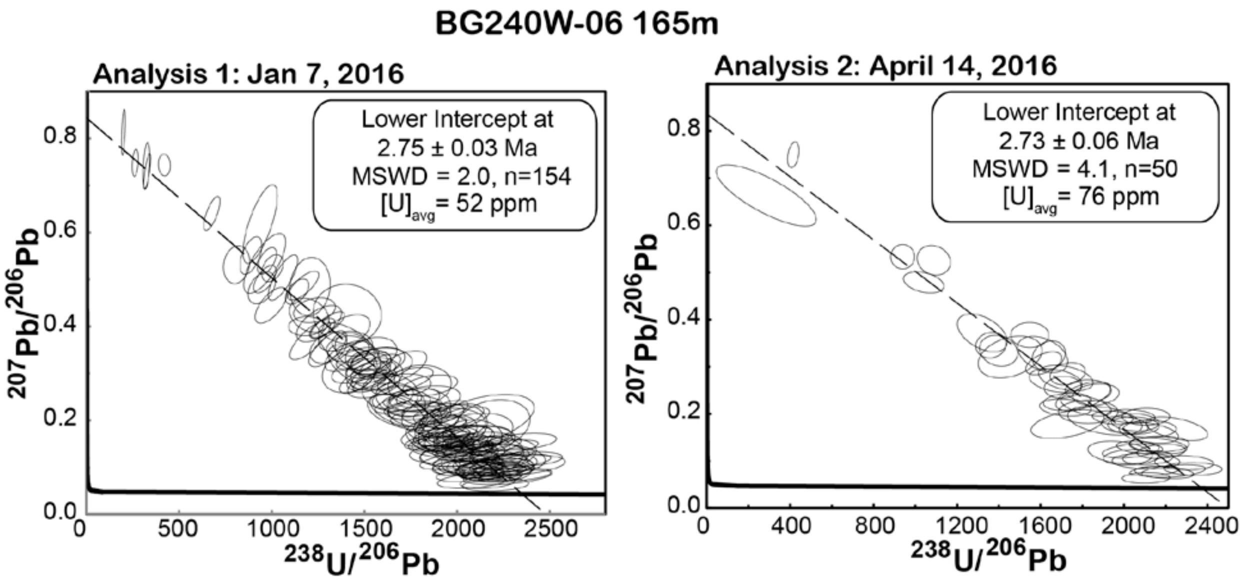

Figure 3-5. Tera-Wasserburg diagrams for the duplicate analyses of sample BG240W-06 165m. Both of the ages overlap within error. Data-point error ellipses are 2σ.

Core-Rim Ages

The new andradite garnet U/Pb geochronometer also has the potential to constrain the duration of individual garnet growth within the skarn system. Furthermore, dating individual garnet crystals has the potential to provide insight into the spatial growth of the skarn system through time. In order to test the ability to measure the duration of garnet growth, three garnets from sample BG14W-07 65m were cut for central sections. These results show that, while the cores trended older for all three garnet crystals analyzed, the cores and the rims overlapped in error (Figure 3-6). Based on compiled core and rim analyses for sample BG14W-07 65m, the cores are 2.78±0.05 Ma and the rims are 2.72±0.04 Ma. These age results suggest that the garnets formed rapidly.

External Age Constraints

The Big Gossan skarn is an ideal place to test the accuracy of the garnet U/Pb chronometer, as there is excellent age control for the skarn based on field relationships, phlogopite $^{40}Ar/^{39}Ar$ ages, and extensive zircon U/Pb dating throughout the district (Figure 3-7). Gregory (2004) mapped fault patterns in the mine drifts and discovered that while abundant faults are present in the country rock, the skarn itself contains few faults. This indicates the skarn formed late in the faulting history of this part of the district. Prendergast et al. (2005) reported a phlogopite $^{40}Ar/^{39}Ar$ age of 2.82 ± 0.04 Ma, which overlaps with the Big Gossan garnet U/Pb ages (location shown in Figure 3-2). Additionally, extensive zircon U/Pb dating in the mining district has constrained the timing of the Grasberg Igneous Complex between 3.6 to 3.1 Ma (see Chapter 1). The nearby Ertsberg pluton spans a time period between 3.1 to 2.8 Ma (see Chapter 4). Only one strongly altered dike has been identified in the Big Gossan area, and a zircon U/Pb age of 3.0 ± 0.1 Ma confirms that it pre-dates skarn hydrothermal activity (location is shown in Figure 3-2). U/Pb ages for garnets from the Big Gossan skarn, between 2.9 – 2.7 Ma, are in agreement with all external age constraints.

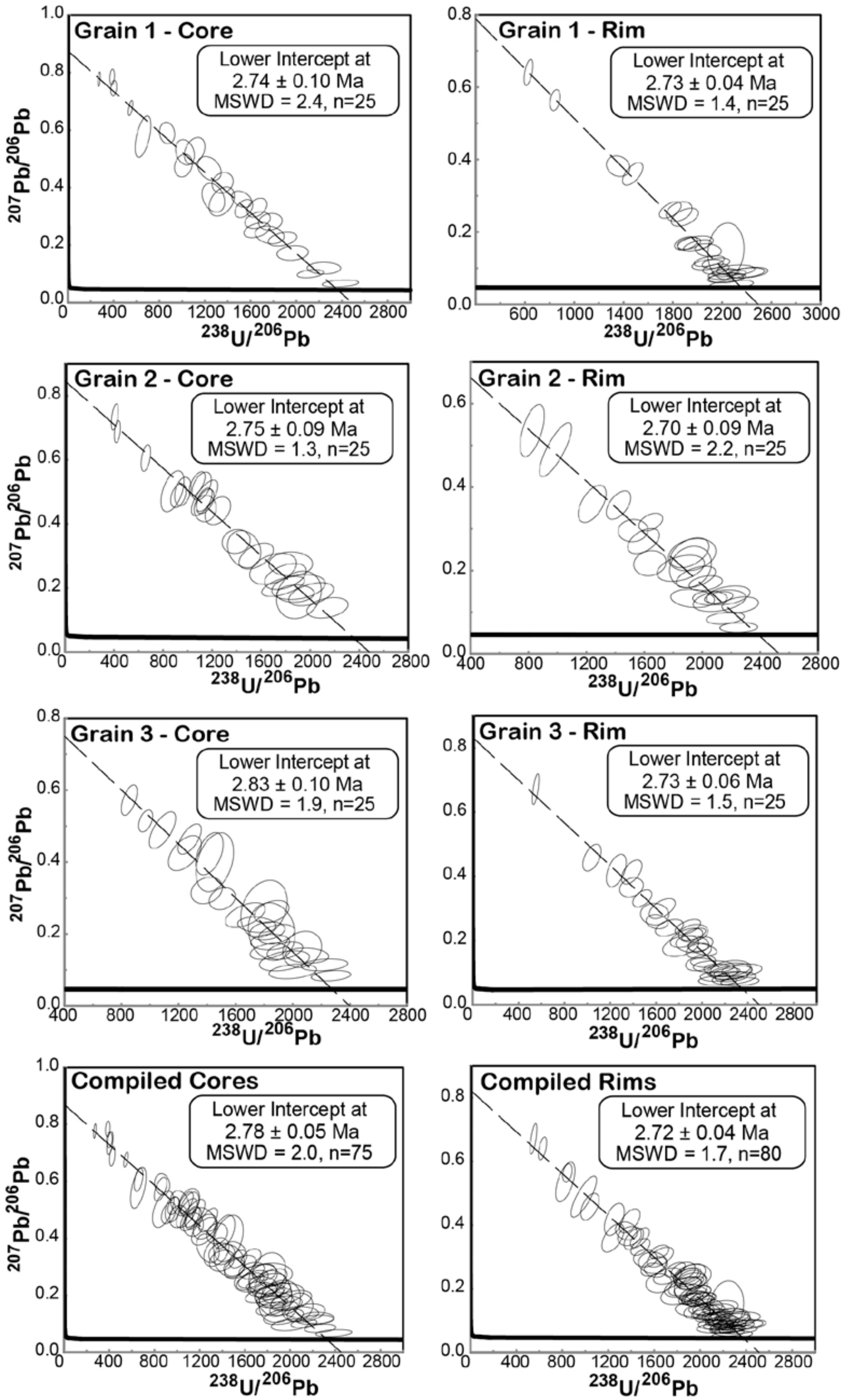

Figure 3-6. Continued next page.

Figure 3-6. Tera-Wasserburg diagrams showing the results of rim-core dating experiments for three garnet grains from the BG14W-07 65m sample. Each large garnet was cut in half, mounted in epoxy, and polished. Grids of spots were placed in the core and around the rim in order to maximize the potential for dating cores and rims. In each case the core age trends older, but the ages overlap within error. Data-point error ellipses are 2σ.

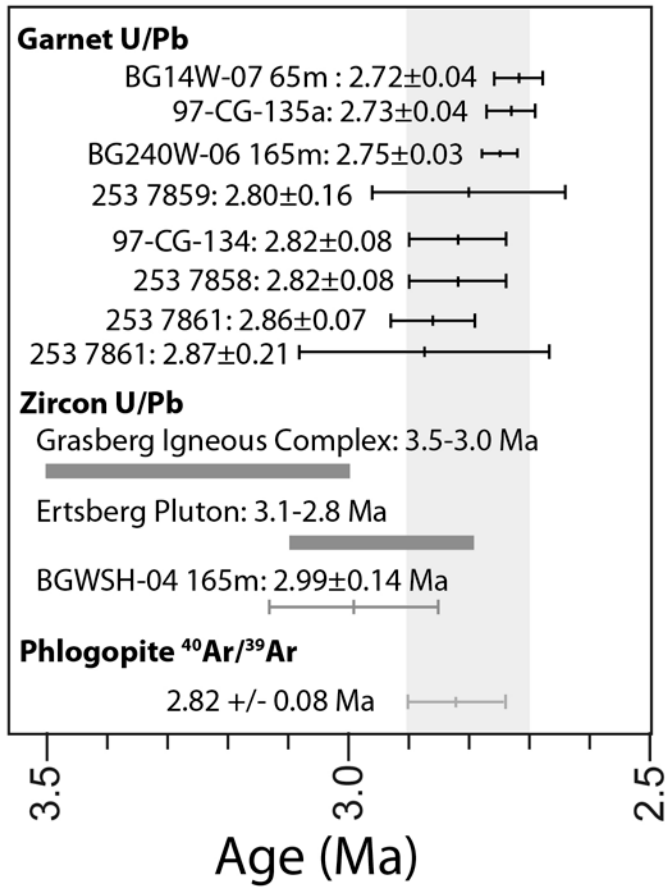

Figure 3-7. Summary plot showing the external age constraints for the garnet U/Pb ages. Zircon U/Pb ages from Wafforn (Chapter 1), sample BG WSH-04 165m from a hydrothermally altered dike that pre-dates the Big Gossan skarn, and phlogopite $^{40}Ar/^{39}Ar$ ages Prendergast et al. (2005). Shaded grey bar from 2.9 to 2.7 Ma shows the age range of the Big Gossan skarn based on the garnet U/Pb ages. All ages shown with 2σ sigma error.

DISCUSSION

One of the advantages of in-situ garnet dating is the ability to directly date the growth of skarn garnet. This is a significant advance compared to the traditional approach of dating the crystallization age of causative intrusions (where one can easily be identified) and the phlogopite, biotite, or potassium feldspar Ar/Ar cooling age. The age results for the Big Gossan skarn do not show a systematic spatial pattern that records the pattern of skarn growth. However, as the precision is reported to as good as ±0.03 myr, the possibility remains that a finer scale sampling may resolve the spatial evolution of this skarn body.

Given that Big Gossan is a hydrothermal skarn, it is most likely that the hydrothermal fluid system responsible for the calc-silicate alteration of the Waripi host rock was also responsible for the Cu and Au ore mineralization. All of the garnet crystallization ages fall within a time period between 2.9 and 2.7 Ma, suggesting that the duration of hydrothermal fluid flow was on the order of ~200 kyr (Figure 3-6).

U and Pb in Garnet

One of the outcomes of in-situ garnet U/Pb dating is the ability to detect the distribution of U. The U concentration in Big Gossan garnets ranges from 5-100 ppm. Th concentrations are significantly lower, typically < 1 ppm. Although the U concentration varies between garnets, the internal distribution of radiogenic elements is remarkably consistent, and little to no zoning was observed (Figure 3-8). The determination that U can have a homogenous distribution makes andradite garnet a feasible target for LA-ICP-MS U/Pb dating.

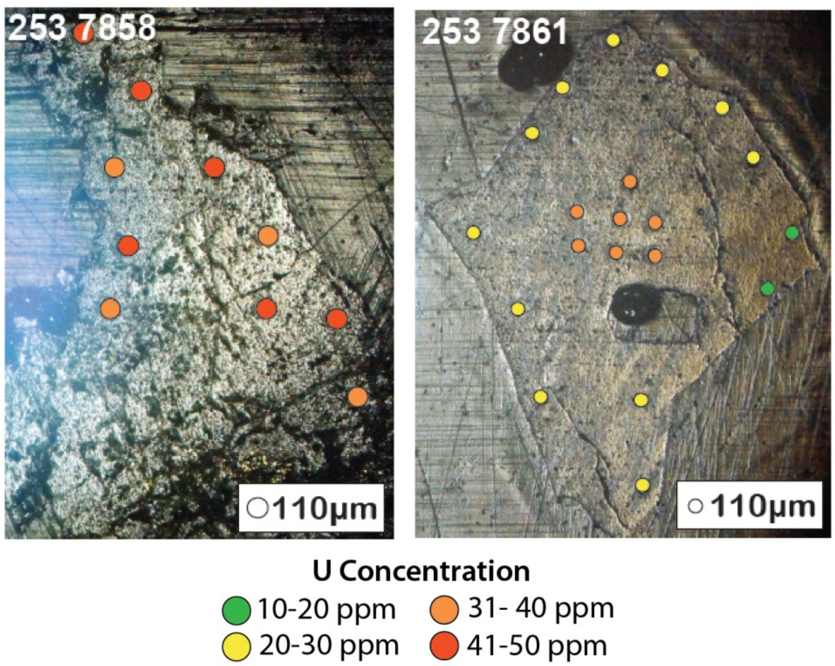

Figure 3-8. Reflected light images from samples 253 7858 and 253 7861 showing the location of laser spots on the polished garnet rims. Each spot is color coded based on the measured uranium concentration.

Garnet composition has a significant control on trace element abundances. DeWolf et al. (1996) found that andradite-rich garnets ($Ca_3Fe_2(SiO_4)_3$) are more likely to have higher concentrations of REE, U and Th, suggesting that the larger atomic size of Fe^{3+} relative to Al^{3+} may permit substitution of the larger cations. There are two possibilities for the location of U in the Big Gossan garnets: it could occur in micro-inclusions, homogenously distributed throughout the garnets, or stoichiometrically in the garnet. While micro-inclusions cannot be ruled out, none are visible in the ESEM images, and the homogenous distribution of U in the laser pits suggests that the U is stoichiometric.

Naturally occurring uranium garnet, named elbrusite-(Zr), has a chemical formula of $Ca_3U_xZr_{(2-x)}Fe_3O_{12}$. Guo et al. (2016) synthesized uranium bearing garnets, and using X-ray photoelectron and absorption spectroscopies determined that uranium occurred in a pentavalent and hexavalent oxidation state. Using transmission ^{57}Fe-Mossbauer spectroscopy they also show that that the iron is tetrahedrally coordinated as Fe^{3+}. Based on these results it seems plausible that uranium occurs in the octahedral site in the Big Gossan garnets.

Lead in the garnets is clearly a mix of common lead and radiogenic lead (see Tera-Wasserburg diagrams in Figure 3-4). In this case, the consistent composition of the common lead, and the variation in the concentration of lead in the garnet crystal, creates a spread in the data along a single mixing line in Tera-Wasserburg space. The y-intercept on the Tera-Wasserburg diagram represents the $^{207}Pb/^{206}Pb$ ratio for the common lead in the system: the ~0.86 value is consistent with feldspar and whole rock common lead ratio for the district (Cloos, unpublished data). The results of this study suggest that common lead is co-located with radiogenic lead in the garnet crystal.

CONCLUSIONS

The remarkable agreement between Big Gossan andradite garnet U/Pb ages and external age constraints, and the ability to duplicate ages, provides good evidence that the andradite garnet U/Pb chronometer can be a robust dating technique. The ability to directly date the timing of hydrothermal skarn formation is a significant addition to the geochronologist's toolkit in skarn systems, which have traditionally been difficult to constrain. Based on the results presented here, the prerequisites for precise and robust andradite garnet U/Pb ages for garnets that are ~3 Ma are > 5 ppm U, such that sufficient radiogenic lead is produced, and a single, consistent common lead composition. If these two requirements are met, the radiogenic lead and common lead form a single mixing line that allows robust regression line in Tera-Wasserburg space. All of the andradite garnet U/Pb ages for the Big Gossan skarn are between 2.9 and 2.7 Ma, confirm that the Big Gossan skarn is one of the last major ore-forming event in the Ertsberg-Grasberg mining district.

Chapter 4: Zircon U/Pb Geochronology of the Ertsberg-Grasberg Mining District, Papua, Indonesia

INTRODUCTION

Zircon U/Pb dating is a powerful tool for establishing the crystallization ages of magmatic intrusions. The refractory nature of zircon means that it can be unaffected by the hydrothermal alteration and mineralization that forms mining districts. The primary motivations for this study are to constrain the duration of magmatism in the district and to evaluate the geochemical and isotopic evolution of the magmatic system. Furthermore, where cross-cutting intrusions are identified it is possible to constrain the maximum duration of magmatic-hydrothermal fluid flow.

Intrusions in the District

McMahon (1994) sampled sixteen distinctive intrusive bodies in the Ertsberg-Grasberg district, with most being small dikes and plugs. The largest of the igneous bodies are the Ertsberg pluton (10-20 km^3) and the Grasberg Igneous Complex (~3 km^3) (Figure 4-1) (discussed in Chapter 1). The Ertsberg pluton ranges from slightly porphyritic to equigranular in texture, with grain sizes ranging from 0.5 to 2 mm. Euhedral to subhedral K-feldspar grains are interlocked with euhedral to subhedral plagioclase, with interstitial quartz. Clinopyroxene is the main mafic phase, with small amounts of primary biotite. Based on the modal mineralogy, the Ertsberg pluton is a quartz monzodiorite to a monzogranite.

Of the minor intrusions in the district the Karume is the largest, with a volume of ~2 km^3. Only the western margin of the intrusion was exposed at the surface, but drilling results beneath the Carstenzsweide Valley indicate it is an irregular ovoid in shape. The Karume is distinguished from other intrusions in the district based on its large, cm-scale potassium-feldspar phenocrysts. The North Grasberg plug is located to the northwest of the GIC, and has a diameter of ~300 m. The intrusion has a porphyritic texture, with plagioclase as the main phenocryst phase, and locally contains xenoliths of the sedimentary wall rocks. The Wanagon Sill is a tabular intrusion that outcrops southwest of the GIC. The sill is up to 200 m thick, exposed for 1.7 km along strike, and has a porphyritic texture.

The Kay intrusion belongs to the lower-K suite defined by McMahon (1994). It is a roughly circular plug, with a diameter of 300 m, that was emplaced into Faumai Formation to the west of the Ertsberg pluton.

Trautman (2013) described two additional intrusions that were previously unknown: the Tertiary Intrusion Gajah Tidur, "Tigt" (previously known as Tikl) and the Tertiary Pliocene Intrusion, "Tpi." Both intrusions were encountered during a super deep drilling program, where two 1700 m cores (KL98-10-21 and KL98-10-22) were collared at the 3000 m elevation of the Amole Drift. On was angled to go through the Kucing Liar Skarn and the other was angled to reach the deepest intercepts of the GIC. The Tigt intercept is ~550 m long, and is characterized by pervasively altered rock. Magmatic phenocrysts include feldspar, amphibole, and biotite, but in most cases alteration has resulted in the partial to total replacement of magmatic phases with sericite, biotite, chlorite, carbonate, and opaques. A remarkable feature of the Tigt is the quartz stockwork zone, which extends throughout the Tigt and includes meter-long core segments that are volumetrically ~40% to > 95% vein quartz. The Tigt is cut by the Tpi dikes, which are less altered and less mineralized. Twenty-nine Tpi dike intercepts were in the core, and they vary in size from 3 cm to 2.3 m.

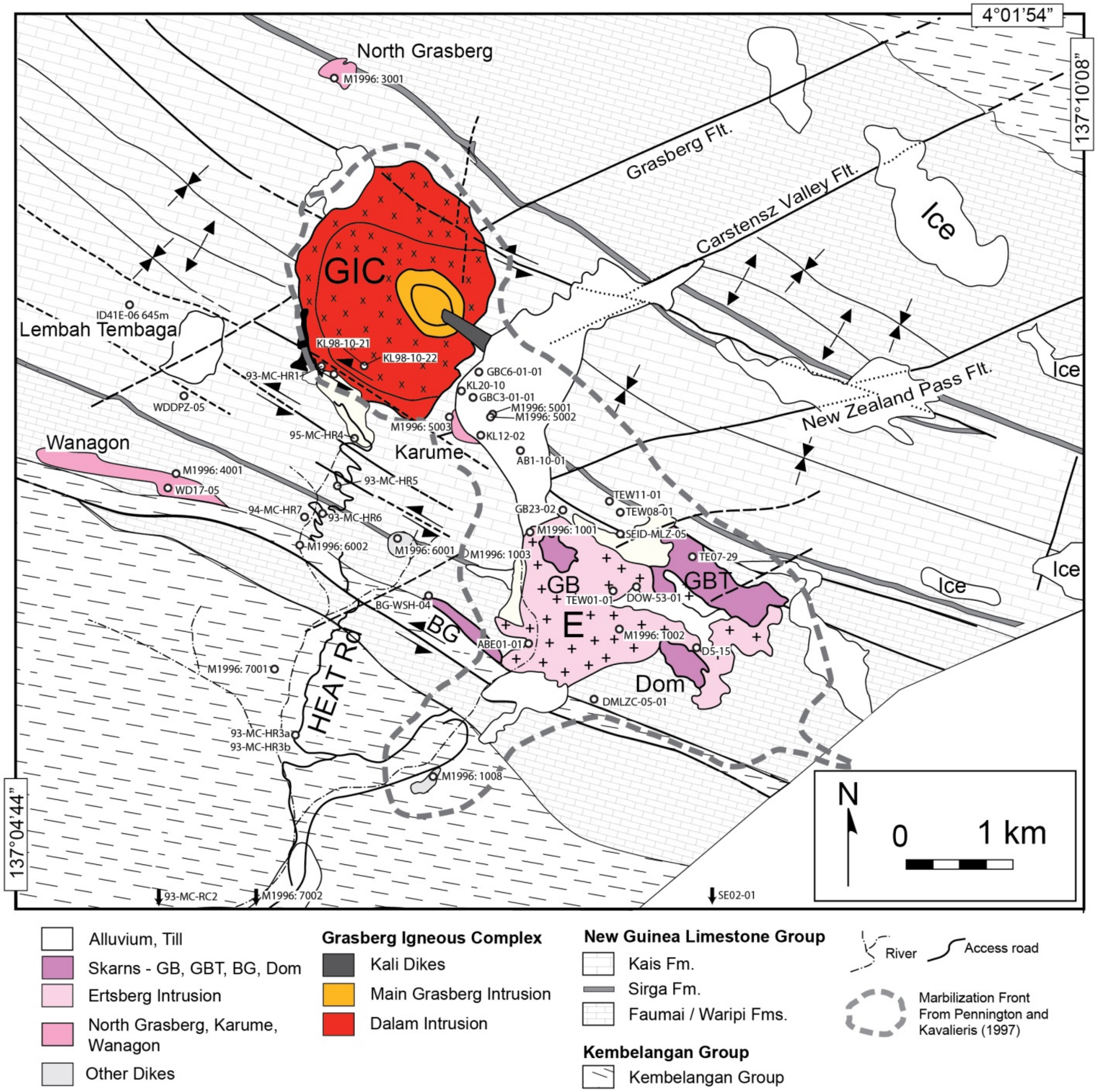

Figure 4-1. Simplified geologic map of the Ertsberg-Grasberg mining district showing drill hole collars/ outcrop locations for each of zircon U/Pb samples (black circles). Modified from Paterson and Cloos (2005). Skarns: GB - Gunung Bijih (Ertsberg), GBT - Gunung Bijih Timur (Ertsberg East), BG - Big Gossan.

Previous Geochronology

A single K-Ar age of 3.10 ± 0.12 Ma from an uncharacterized sample of the Ertsberg pluton collected near the tramway terminal by Delos Flint was the primary constraint on the age of magmatism and mineralization in the district (Titley, 1975). With the advent of the UT Ertsberg Project a sample set of "fresh" intrusions was collected by Timothy McMahon for petrographic analysis and K-Ar dating. McDowell et al. (1996) reported 15 biotite K-Ar ages for nine distinct intermediate igneous intrusions in the Ertsberg-Grasberg mining district (see Table 4-1 and Figure 4-2). The ages ranged from 3.8 to 2.6 Ma, with one outlier at 4.4 Ma, leading to the conclusion that magmatism in the Ertsberg-Grasberg mining district took place over a time window of approximately 2 million years. Pollard et al. (2005) reported ten $^{40}Ar/^{39}Ar$ ages for hydrothermal biotite sampled from the Dalam and the nearby Ertsberg intrusions. These are largely in agreement with the results of McDowell et al. (1996). New (2006) reported seven phlogopite, biotite, and muscovite $^{40}Ar/^{39}Ar$ ages for samples from the Kucing Liar skarn. The age results ranged between 3.42 ± 0.04 Ma and 3.19 ± 0.03 Ma. Additionally, Prendergast et al. (2005) report one phlogopite $^{40}Ar/^{39}Ar$ age for the Big Gossan skarn (2.82 ± 0.08 Ma) and one K-feldspar/adularia $^{40}Ar/^{39}Ar$ age for the Wanagon Sill (3.61 ± 0.06 Ma). All ages are reported here with 2 sigma error.

Table 4-1. Ertsberg-Grasberg Mining District Geochronology Pre-2013. After Trautman, 2013 and New, 2006

Sample	Mineral	Method	Lithology	Age (Ma)	Error (Ma)	Source
A96-43-5 275.0m	Muscovite	^{40}Ar-^{39}Ar	Grasberg	3.16	0.35	Pollard et al., 2001
A96-43-5 68.5m	Biotite	^{40}Ar-^{39}Ar	Grasberg (KalI)	3.13	0.05	Pollard et al., 2001
A96-41-3 92.5m	Biotite	^{40}Ar-^{39}Ar	Grasberg	3.07	0.01	Pollard et al., 2001
A96-36-4 150.1m	Biotite	^{40}Ar-^{39}Ar	Grasberg	3.02	0.06	Pollard et al., 2001
Unnamed	Molybdenite	Re-Os	Grasberg	2.9	0.3	Mathur et al., 2005
Unnamed	Sulfides	Re-Os	Grasberg	2.89	0.1	Mathur et al., 2005
B42 DOZ	Phlogopite	^{40}Ar-^{39}Ar	Ertsberg East	2.94	0.1	Pollard et al., 2001
B43 GBT-A	Phlogopite	^{40}Ar-^{39}Ar	Ertsberg East	2.8	0.03	Pollard et al., 2001
B41 DOZ	Phlogopite	^{40}Ar-^{39}Ar	Ertsberg East	2.73	0.07	Pollard et al., 2001
DZ5-04 290.2m	Biotite	^{40}Ar-^{39}Ar	Ertsberg East	2.71	0.04	Pollard et al., 2001
Unnamed	Molybdenite	Re-Os	Ertsberg East	2.54	0.1	Mathur et al., 2005
1001	Biotite	K-Ar	Ertsberg East	3	0.08	McDowell et al., 1996
1002	Biotite	K-Ar	Ertsberg East	2.65	0.12	McDowell et al., 1996
1003	Biotite	K-Ar	Ertsberg East	3.09	0.25	McDowell et al., 1996
DZ5-06 269.3m	Biotite	^{40}Ar-^{39}Ar	Ertsberg East	2.67	0.03	Pollard et al., 2005
2001	Biotite	K-Ar	Grasberg	2.83	0.07	McDowell et al., 1996
2002	Biotite	K-Ar	Grasberg	2.77	0.34	McDowell et al., 1996
2003	Biotite	K-Ar	Grasberg	3.01	0.23	McDowell et al., 1996
2004	Biotite	K-Ar	Grasberg	3.14	0.08	McDowell et al., 1996
2005	Biotite	K-Ar	Grasberg	3.13	0.15	McDowell et al., 1996
2006	Biotite	K-Ar	Grasberg	3.23	0.32	McDowell et al., 1996
A96-40-5 95.0m	Biotite	^{40}Ar-^{39}Ar	Grasberg	3.33	0.12	Pollard et al., 2005
A96-41-2 172.5m	Biotite	^{40}Ar-^{39}Ar	Grasberg	3.06	0.04	Pollard et al., 2005
A96-43-5 57.3m	Biotite	^{40}Ar-^{39}Ar	Grasberg (KalI)	3.16	0.05	Pollard et al., 2005
3001	Biotite	K-Ar	North Grasberg	3.5	0.23	McDowell et al., 1996
3002	Biotite	K-Ar	North Grasberg	3.04	0.14	McDowell et al., 1996
LT 1-5 953m	Biotite	^{40}Ar-^{39}Ar	Lembah Tembaga	3.51	0.02	Pollard et al., 2005
4001	Biotite	K-Ar	Wanagon	3.81	0.06	McDowell et al., 1996
4002	Biotite	K-Ar	Wanagon	3.46	0.06	McDowell et al., 1996
5001	Biotite	K-Ar	Karume*	3.13	0.09	McDowell et al., 1996
6001	Biotite	K-Ar	Kay	4.44	0.1	McDowell et al., 1996

Table 4-1. Continued.

				Plateau Age			Isochron Age			
Sample	**Mineral**	**Method**	**Lithology**	**Age (Ma)**	**Error (Ma)**	**MSWD**	**Age (Ma)**	**Error (Ma)**	**MSWD**	**Source**
KL28-1 360.3m	Phlogopite	^{40}Ar-^{39}Ar	Fault	3.41	0.04		3.42	0.04	1.7	New, 2006
KL32-8 331.0m	Phlogopite	^{40}Ar-^{39}Ar	Limestone	3.27	0.03	1.5	3.28	0.04	1.6	New, 2006
KL32-5 539.6m	Biotite	^{40}Ar-^{39}Ar	Fault	3.34	0.02	1.5	3.28	0.04	1	New, 2006
KL32-5 652.4m	Biotite	^{40}Ar-^{39}Ar	Shale	3.23	0.04	3	3.2	0.04	4.7	New, 2006
KL20-9 465.3m	Biotite	^{40}Ar-^{39}Ar	Shale	3.18	0.02	0.5	3.19	0.03	3	New, 2006
KL32-8 455.9m	Muscovite	^{40}Ar-^{39}Ar	Shale	3.18	0.02	0.42	3.18	0.16	4.2	New, 2006
KL32-1 255.7m	Muscovite	^{40}Ar-^{39}Ar	Fault	3.45	0.06	1.6	3.54	0.12	2.3	New, 2006

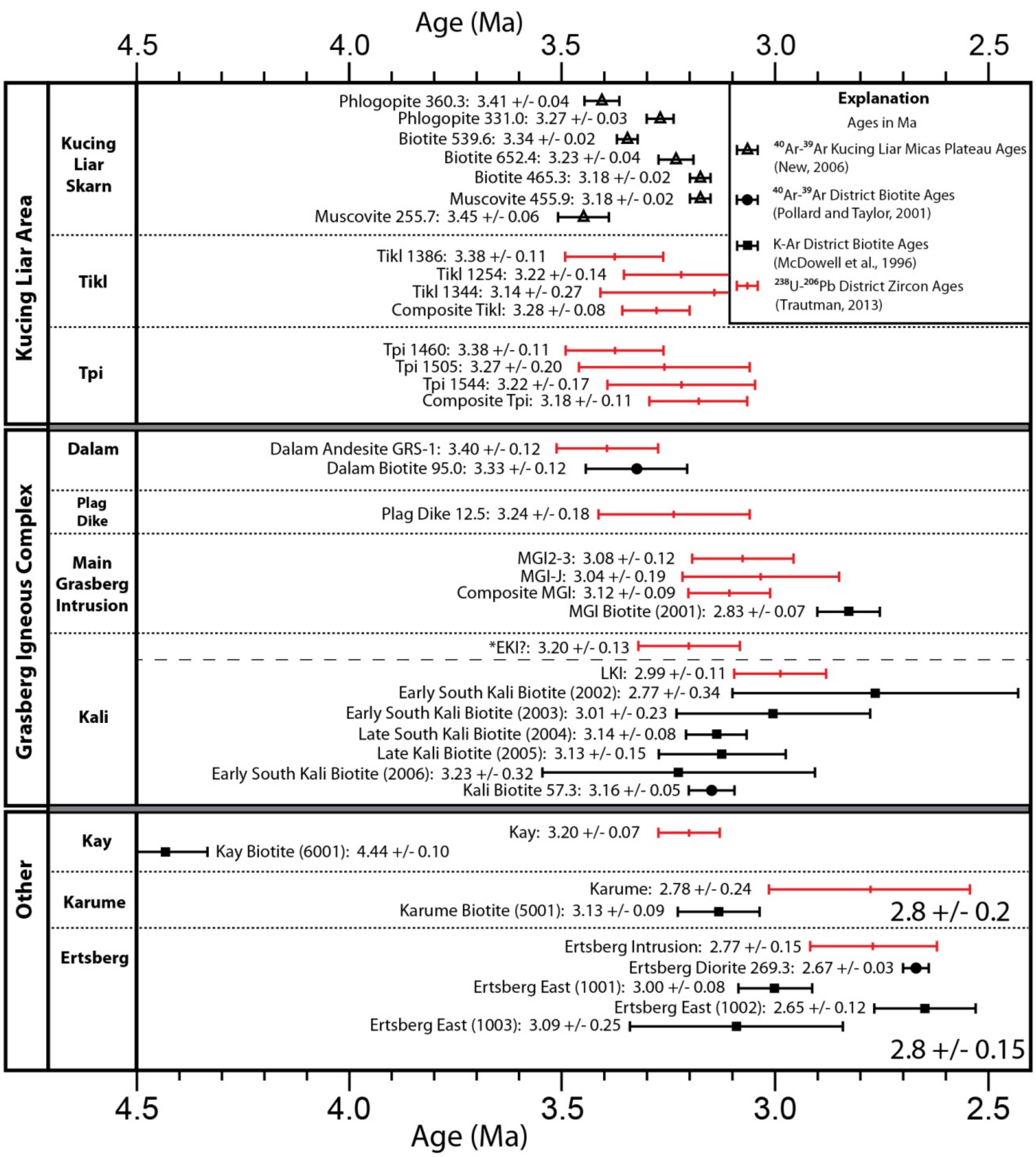

Figure 4-2. Summary table of the previous geochronology in the district. Kucing Liar mica ages are plateau ages from New (2006). Zircon U/Pb ages from Trautman (2013) were determined using the tape mount method. Modified from Trautman (2013).

ANALYTICAL TECHNIQUES

In this study, magmatic crystallization ages were determined for all units in the district using the zircon U/Pb LA-ICPMS technique. Chapter 1 presents the analytical procedures; a short summary is provided here. Zircons are separated from crushed and pulverized, kilogram-sized drill core or outcrop samples using standard heavy liquid and magnetic separation techniques. Hand-picked euhedral zircons are mounted on an epoxy puck using double-sided tape. The zircons are oriented such that they are laying on a flat face. The zircons are then placed in the laser sample chamber and the sides are ablated, using six shots to "pre-clean" the surface and remove any surface contamination and 300 shots to ablate the zircon to a depth of about 15 µm. The resultant aerosol is analyzed in a magnetic sector, single collector Element2 HR-ICP-MS. Data were reduced using the Iolite software package, and ages are corrected for initial common lead and initial Th disequilibrium. A complete discussion of these corrections is provided in Appendix B.

Ablating the sides of the zircon sequentially samples the outermost, youngest growth zones. Plotting the analyses for ±30 zircons from one intrusion on the same Tera Wasserburg diagram yields ages with remarkable statistical precision. This procedure makes it possible to differentiate between magmatic events (at time scales of ±0.1 m.y.). For some intrusions "composite ages" were calculated by compiling all of the zircon analyses from seemingly identical samples of the same intrusion (typically n is greater than 100 individual age determinations). When possible, this improved statistics and reduced the calculated uncertainties to the second decimal place (±0.05 m.y.).

Since UT studies began in 1989, "fresh" samples of the intrusions have been sought for geochemical analysis. Most samples were collected by G. Atwood, T. McMahon, M. Cloos, M. Trautman, and S. Wafforn. Processing procedures for geochemistry samples are described in Chapter 1; in short, approximately one kg of fresh rock samples were crushed into pea size pieces, and these pieces were visually inspected to remove fragments that contained veins or alteration. Only the fresh pieces were powdered and sent for analysis. Geochemistry analyses were completed by SGS using the ICM90A and ICP95A packages.

RESULTS

Zircon U/Pb Age Results

Zircon U/Pb ages have been measured for each of the named major intrusions and many of the minor intrusions in the Ertsberg-Grasberg mining district (Figure 4-1) (see Appendix C for sample coordinates, Appendix D for polished slab photos, and Appendix E for zircon U/Pb age results). The Grasberg Igneous Complex ages are reported in Chapter 1, the Ertsberg pluton ages are reported in Figure 4-3, and the ages for the remaining intrusions are reported in Figure 4-4.

Results show that the oldest intrusion in CoW-A is the Southeast Intrusion (which lies just inside the southeastern CoW-A boundary), which has an age of 4.38 ± 0.15 Ma. Inside the 4 km wide strike-slip fault corridor that hosts all of the major ore deposits in the district (Sapiie and Cloos, 2004), the oldest intrusions are the Wanagon Sill (3.56 ± 0.07 Ma, x = 2 samples, n = 56 zircons) and the Lembah Tembaga Intrusion (3.49 ± 0.07 Ma, x = 2 samples, n = 52 zircons). The North Grasberg (3.40 ± 0.17 Ma) and Kay (3.34 ± 0.05 Ma) plugs also occur early in the magmatic history of the district. The GIC is a long-lived magmatic center with activity over a time period between 3.6 to 3.1 Ma (see Chapter 1).

Sampling of the Tigt intrusion is limited to intercepts from two super-deep drill holes (KL98-10-21 and KL98-10-22). Based on the age results from these samples, the Tigt intrusion was emplaced at 3.38 ± 0.05 Ma (x=5, n=110 zircons), post-dating the Dalam Phase but pre-dating the MGI in the GIC. Trautman (2013) reports that the Tpi dikes cut the Tigt intrusion, however the four dated samples range in age between 3.48 and 3.30 Ma. The supergiant Kucing Liar (KL) skarn is hypothesized to be associated with the Tigt intrusions (Leys et al., 2012). The phlogopite, muscovite, and biotite $^{40}Ar/^{39}Ar$ ages from the KL skarn reported by New (2006) range between 3.42 ± 0.04 Ma and 3.19 ± 0.03 Ma. The crystallization age of the Tigt and the cooling age of skarn minerals indicate the Kucing Liar skarn is the oldest ore-forming event in the district.

The Karume, which has a distinct texture with large, cm scale potassium feldspar phenocrysts in a quartzo-feldspathic matrix, intruded concurrent with the GIC. The spread in ages for the four Karume samples suggests prolonged intrusion and/or cooling between 3.4 and 3.1 Ma. A separate magma chamber source is now postulated for the Karume, as it seems unlikely that the same magma chamber that produced the plagioclase-dominated porphyries in the district would spontaneously form large potassium-feldspar phenocrysts.

Much work was done on the Ertsberg pluton because the map pattern and drilling indicates it is the largest intrusion in the district with a volume of at least 10 to 20 km^3 (McMahon, 1999) and there has been debate about its mode of emplacement. Twenty-two samples have been dated and the ages range from 3.1 to 2.8 Ma. The ages suggest a continuous period of zircon crystallization throughout the solidification of the Ertsberg pluton. As the oldest ages are closest to the margins of the pluton, the spatial pattern suggests that the pluton was intruded as one pulse of magma that cooled relatively slowly (Figure 4-5). The youngest dated intrusion in the district is a dike in the Ertsberg pluton, which has a crystallization age of 2.76 ± 0.07 Ma (sample GBC3-01-01 1033.2m, location shown in Figure 4-1).

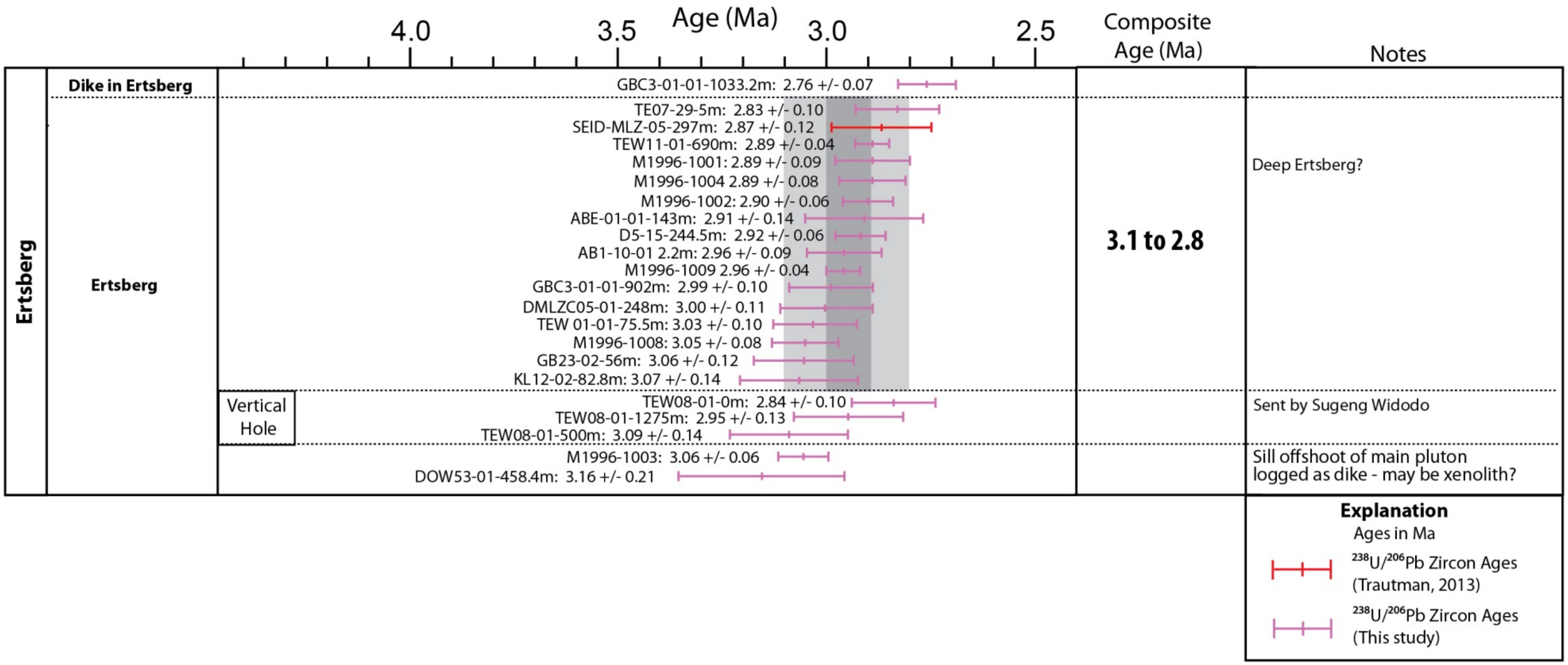

Figure 4-3. Zircon U-Pb crystallization ages for the Ertsberg pluton. Taking into account the ages and uncertainties, the Ertsberg pluton crystallized between 3.1 to 2.8 Ma; however the time range may be even narrower, between 3.0 to 2.9 Ma. Bars indicate the sample age and uncertainty.

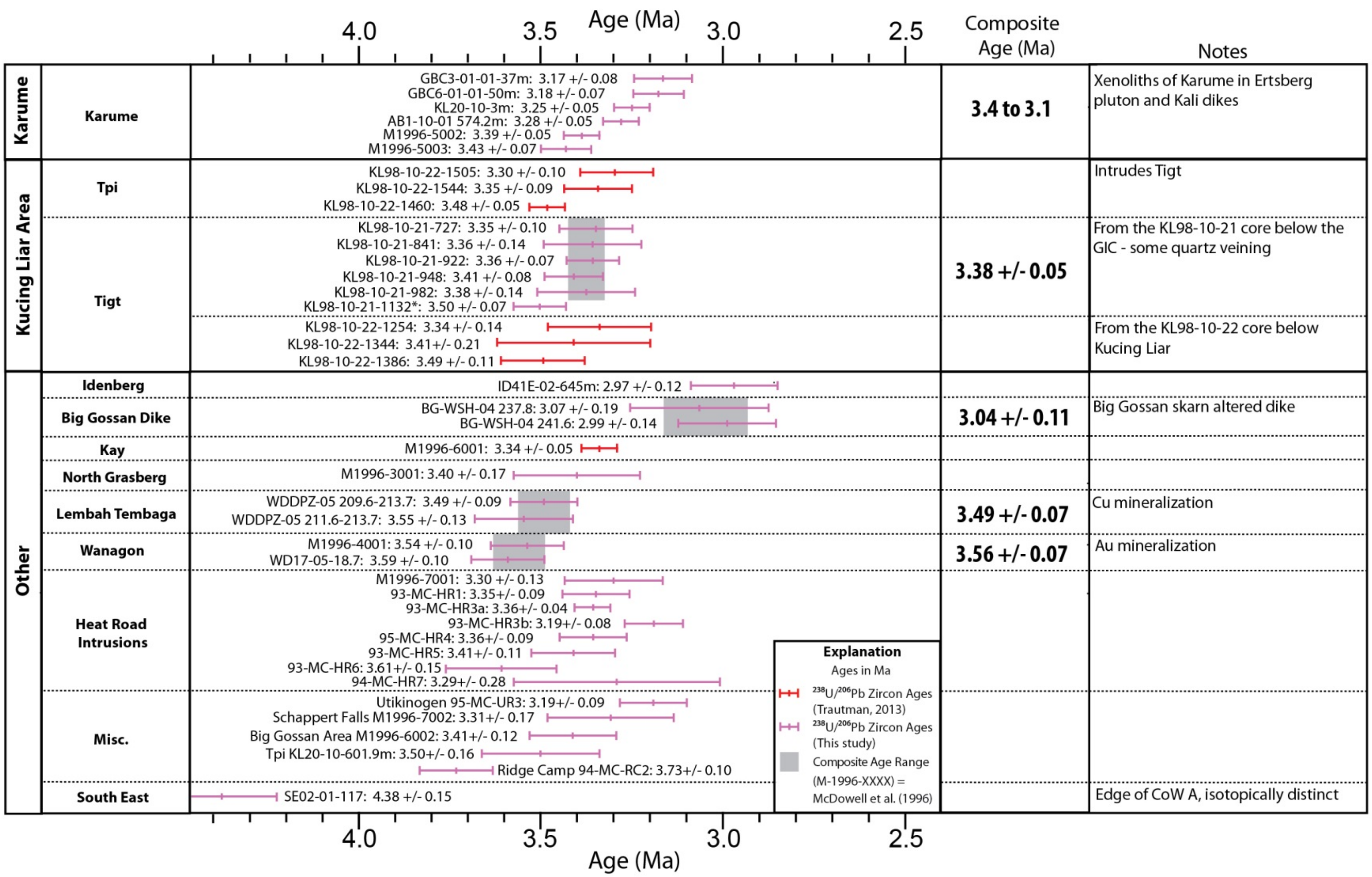

Figure 4-4. Zircon U-Pb crystallization ages for intrusions in the Ertsberg-Grasberg district. See Chapter 1 for Grasberg Igneous Complex Ages and Figure 4-3 for Ertsberg pluton ages. Bars indicate the sample age and uncertainty. Composite ages are calculated using all individual zircons from samples which have been classified as part of the intrusion based on petrographic analysis. Any sample that was petrographically different from the bulk character of the intrusion was not included in the composite age (these samples are indicated with a *). Composite ages illustrated by the grey boxes, which include the age and error range.

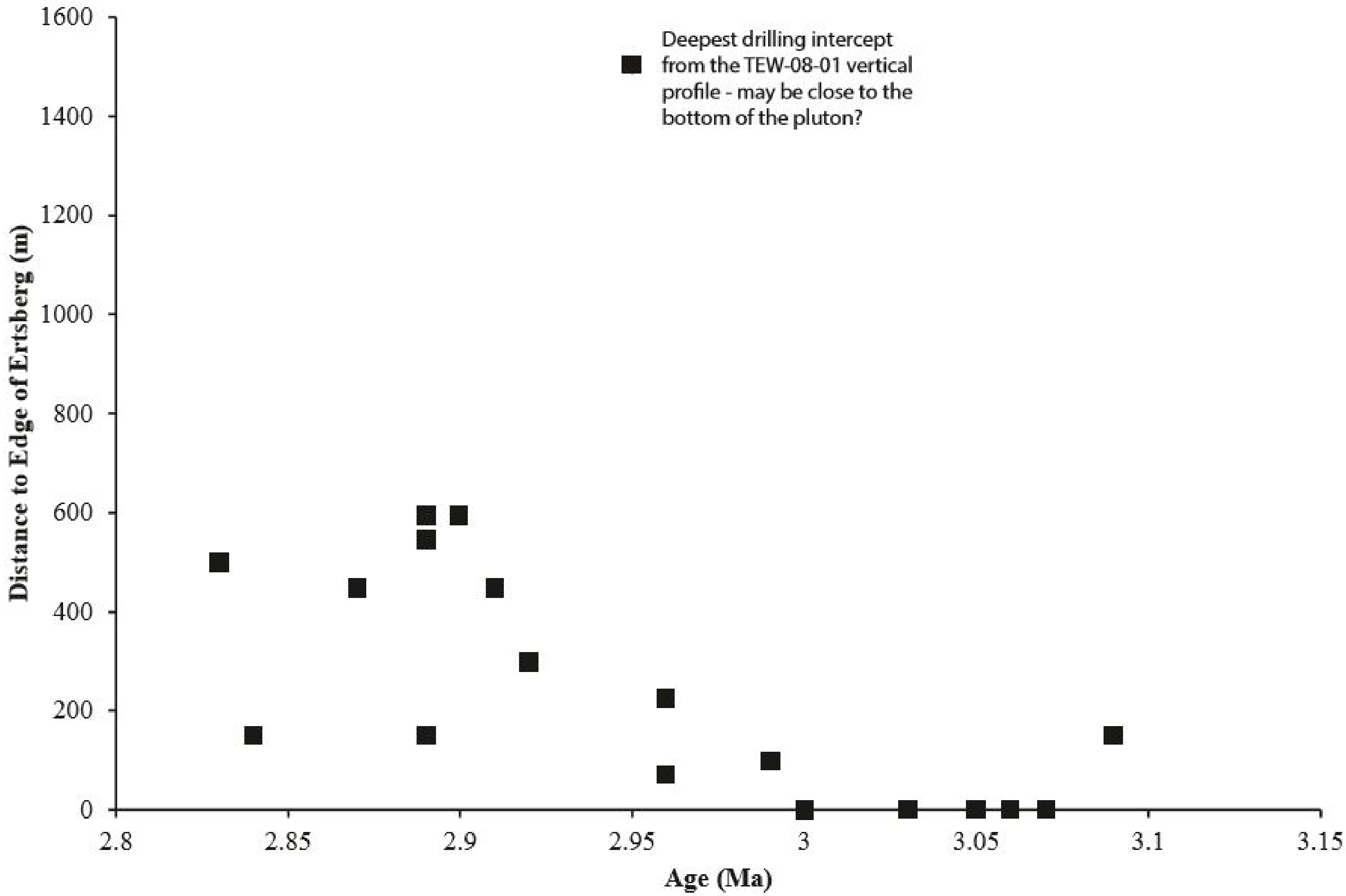

Figure 4-5. Plot showing the relationship between the age of the Ertsberg samples and the distance from the margin of the pluton. Samples closest to the margin crystallized early and samples further for the margin crystallized later. This age relationship suggest that the pluton crystallized from the edges towards the center.

Duplicates and Cross-Cutting Relationships

As of 12/01/2015, five duplicates were analyzed to assess the reproducibility of the ages (see Figure 4-6). The duplicates comprise two splits of the zircons recovered during a single mineral separation. The ages of all the duplicates overlap within uncertainty. The ABE-01-01 143m sample was analyzed three times on three different dates and each time the ages overlap within ±0.1 Ma. These duplicates, in addition to the consistency between all 108 samples dated, confirms that the LA-ICP-MS ages reported in this study can be regarded as precise to the first decimal place (±0.1 myr).

Five sets of samples with known cross cutting relationships were collected during the 2014 field season (see Figure 4-6 for ages and Figure 4-7 for polished slab photos). The zircon U/Pb age dates obtained the expected age relationships for three of these sample pairs, including samples of the Ertsberg pluton and a dike in the Ertsberg pluton, a Kali sample and a post-Kali dike sample, and a set of samples including Kali, MGI, Plag Dike, and Dalam. The fourth sample set was originally interpreted as a Kali dike and a post-Kali dike, however thin section analysis revealed that both samples came from the same intrusion. This interpretation agrees with the age results, which are essentially identical. The fifth cross cutting sample set was interpreted by core-loggers as an MGI sample and a “cross-cutting dike”. As the ages reveal that the “dike” is older than the intrusion, it is concluded that the “dike” is in fact a large xenolith within the MGI.

Zircon Interior Growth Zones

Using the novel tape mount method developed at UT Austin, the sides of the zircon are ablated, making pits that are 15 to 17 µm deep. The advantage of the tape mount method is that the youngest growth zone are sequentially analyzed, increasing the precision of the age. Additionally, if an ablation pit reaches an interior part of a zircon with a different age, an overgrowth relationship is identified. The data can be used to calculate the ages for the outer part of the zircon and the xenocrystic cores. Zones with concordant older ages were detected in 8% of the 3680 zircons analyzed. Highly discordant cores were detected in approximately 5% of the analyzed zircons. The significance of the highly discordant cores is uncertain and not considered further. In some small intrusions, such as the HEAT Road dikes, the outer growth zones are very thin, and most of the zircon is an older core. The width and cooling rate of the intrusion must be a significant control on the thickness of new zircon growth.

The ages of the interior growth zones are shown in Figure 4-8. The majority of the concordant cores, 46%, are between 200 to 400 Ma, which broadly corresponds to the age of the magmatic and metamorphic rocks created by the Tasman orogeny in eastern Australia (Edwards et al., 1990). Another 38% are Proterozoic in age, predominately ranging between 1500 and 2500 Ma. The near absence of Archean age cores (n=8 out of 282) strongly suggests that the lower crust assimilant that made up a large component of the parental magmas (Housh and McMahon, 2000) was most likely a combination of magmatic and metamorphic units of Tasman and Proterozoic age. As the laser ablation pits typically do not extend to the center of the zircon, additional analysis of conventional polished grain mounts might reveal more evidence of reworked Archean material.

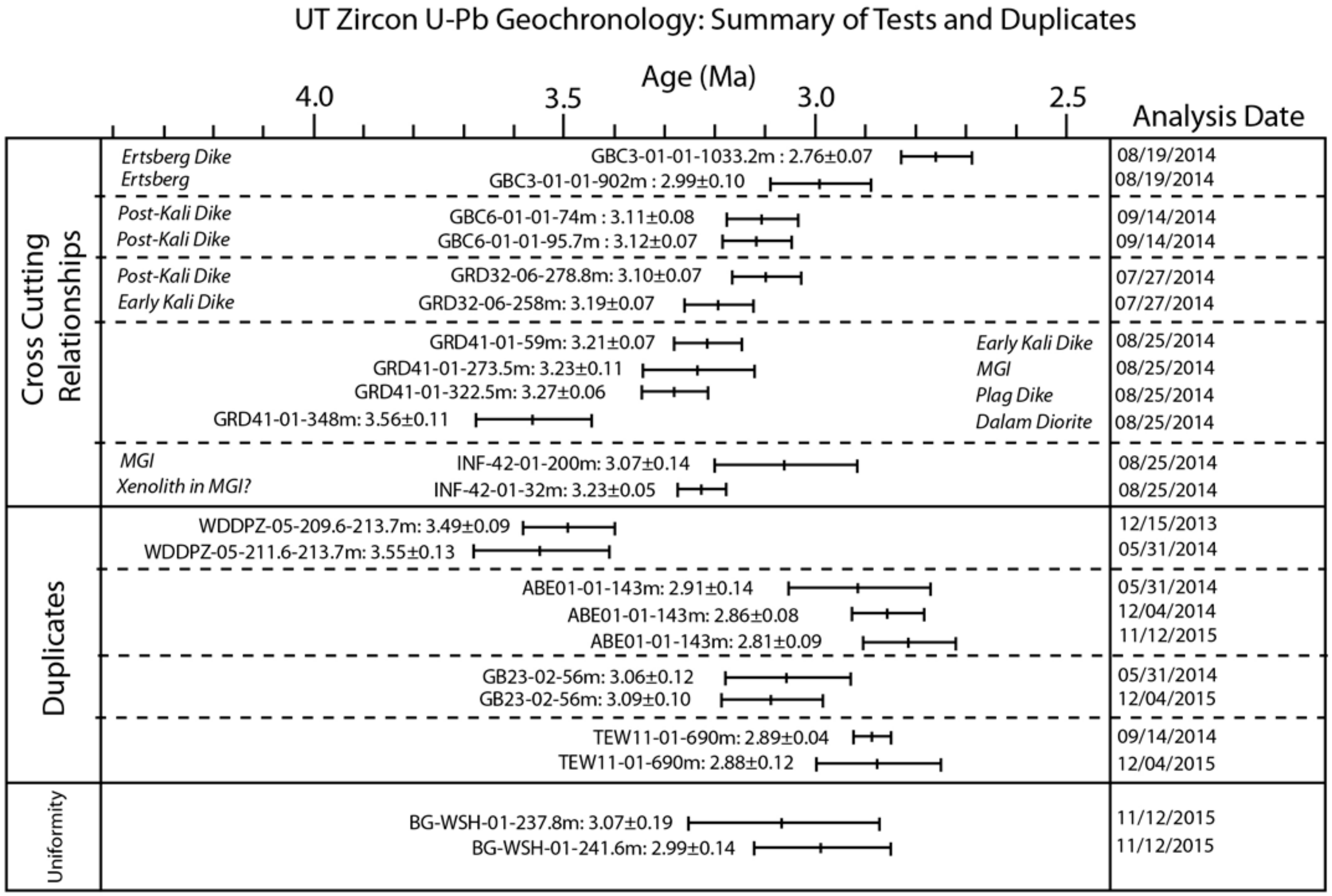

Figure 4-6. Summary diagram showing the cross-cutting relationships and the duplicates that were used to test the zircon U/Pb LA-ICP-MS method. The uniformity test dated two adjacent samples from the same intrusion in the same drill-core in order to test that the age remained the same.

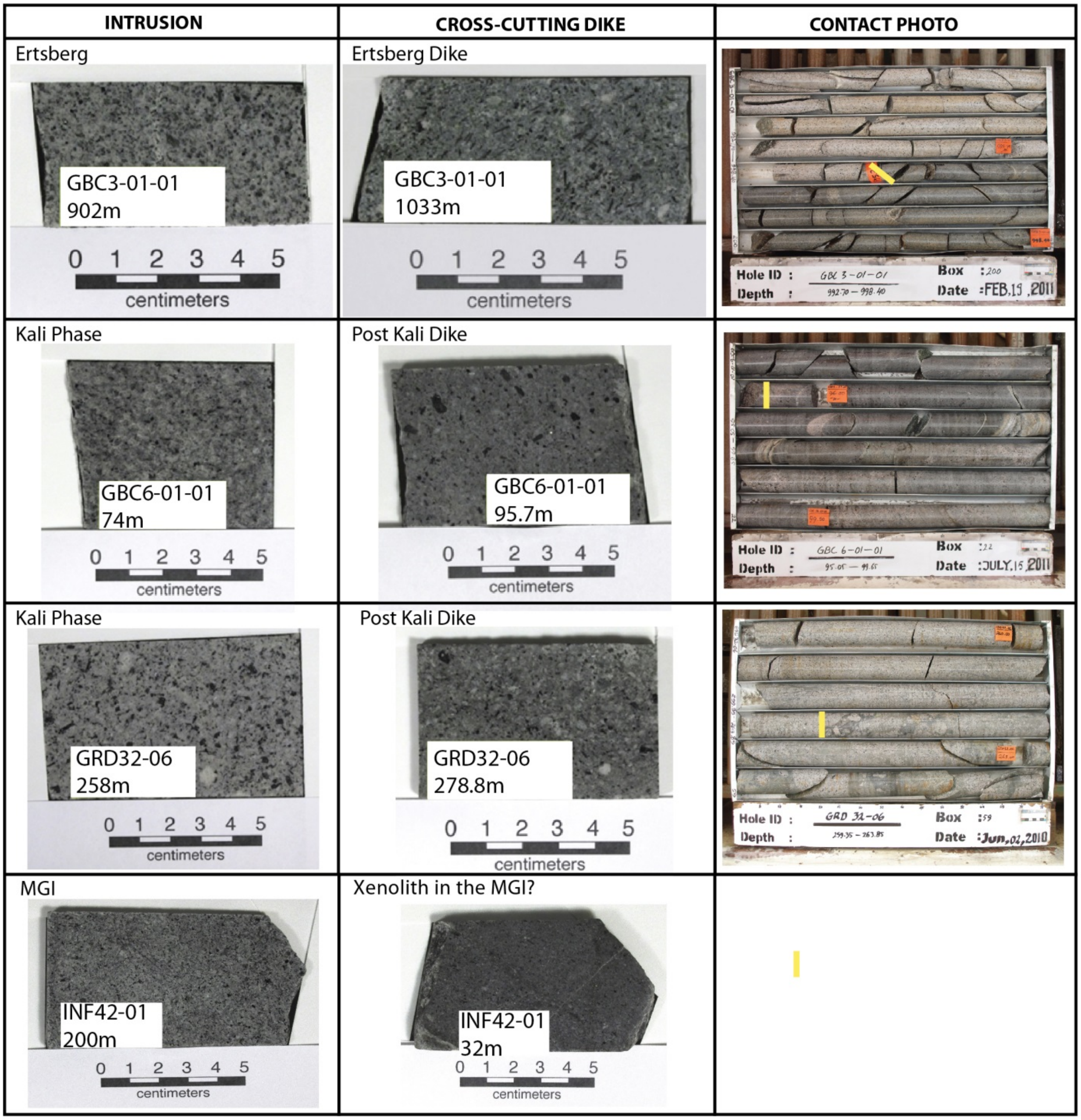

Figure 4-7. Slab photos of the intrusions and cross-cutting dike samples that were dated in order to test the precision of the zircon U/Pb geochronometer. Contacts are marked with a yellow line.

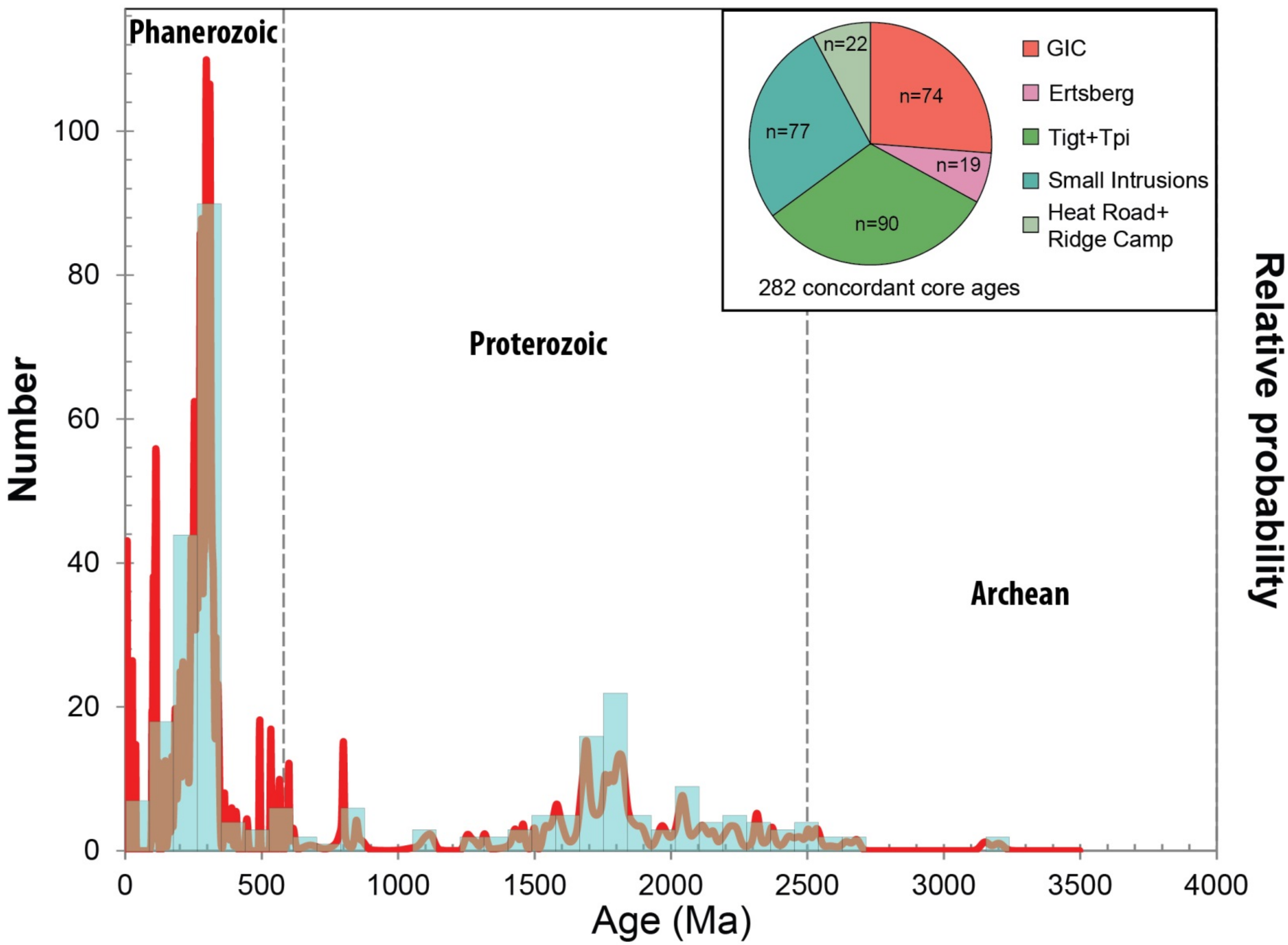

Figure 4-8. Probability density diagram showing the age distribution of concordant zircon interior growth zones for intrusions in the Ertsberg-Grasberg mining district. "Small Intrusions" includes the Karume, Big Gossan area dike, Kay, North Grasberg, Lembah Tembaga, and Wanagon. The most prominent age peaks are between 200-400 Ma and broadly in the Proterozoic.

Geochemical Evolution of Magmas in the District

The zircon U/Pb age data provides a temporal context to evaluate the geochemical evolution of the Ertsberg-Grasberg district. Overall, the major elements, including SiO_2, Al_2O_3, Na_2O, MnO, K_2O, and P_2O_5, do not show obvious trends (see Figure 4-9), whereas MgO, CaO, FeO, Fe_2O_3, and TiO_2 show an increasing trend through time. These results indicate that the magmatic system was becoming more mafic. This is most likely accomplished through magma recharge in the parental, lower crustal, magma chamber, where the source of the recharging melt is predominately melt from the asthenospheric and lithospheric mantle.

Taking SiO_2 as an indicator of the degree of fractionation in the parental magma chamber, there is a negative correlation between the degree of fractionation and the MgO, FeO, Fe_2O_3, and the P_2O_5 (Figure 4-10). The remaining major elements show no statistically significant correlation with increasing or decreasing SiO_2. Note that the overall lack of pattern in the major elements vs. SiO_2 suggests that fractional crystallization is not the most prominent magmatic process taking place in the parental magma chamber. Furthermore, the wide variation in SiO_2, between 53-65%, suggests that magmas with varying degrees of fractional crystallization were sampled throughout the lifetime of the district. Collectively, this suggests that magma recharge is the dominant process affecting the geochemical character of the inferred mid-crustal magma chamber over time.

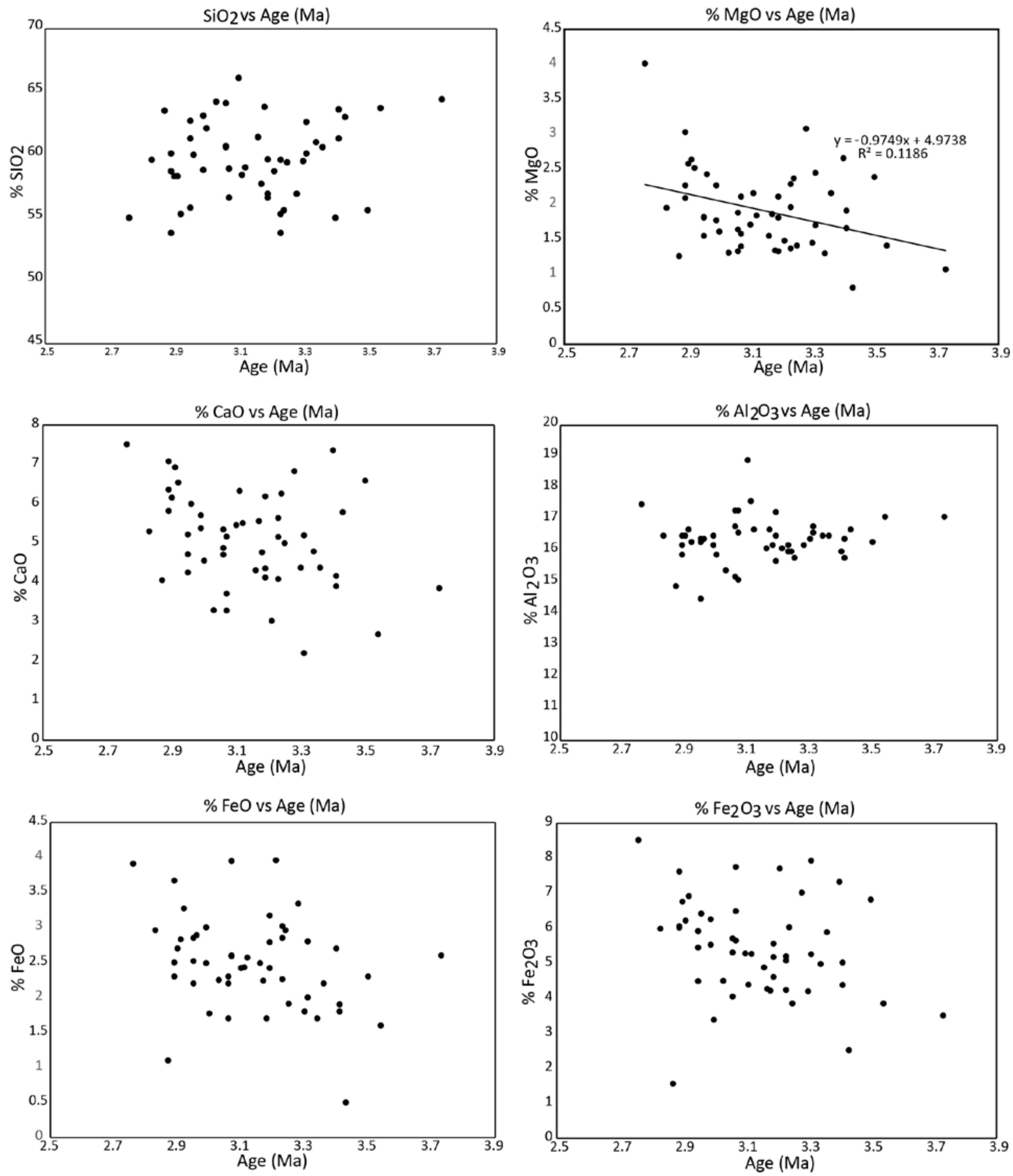

Figure 4-9. Geochemistry plots showing the major elements vs. age (Ma). All of the analyses shown on these diagrams have been filtered such that only fresh samples are included. These analyses are taken to represent the chemical composition of the parental magma.

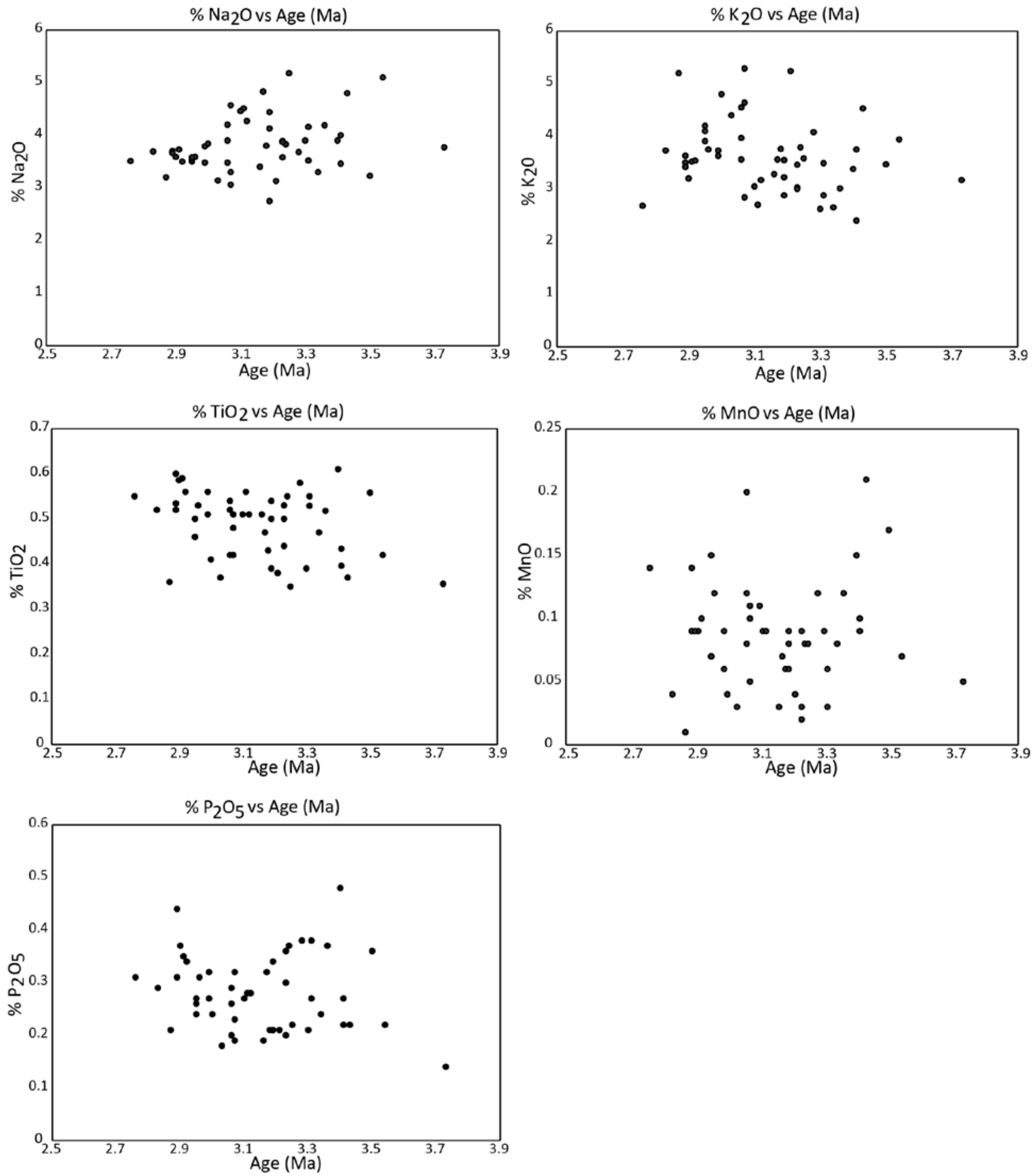

Figure 4-9. Continued

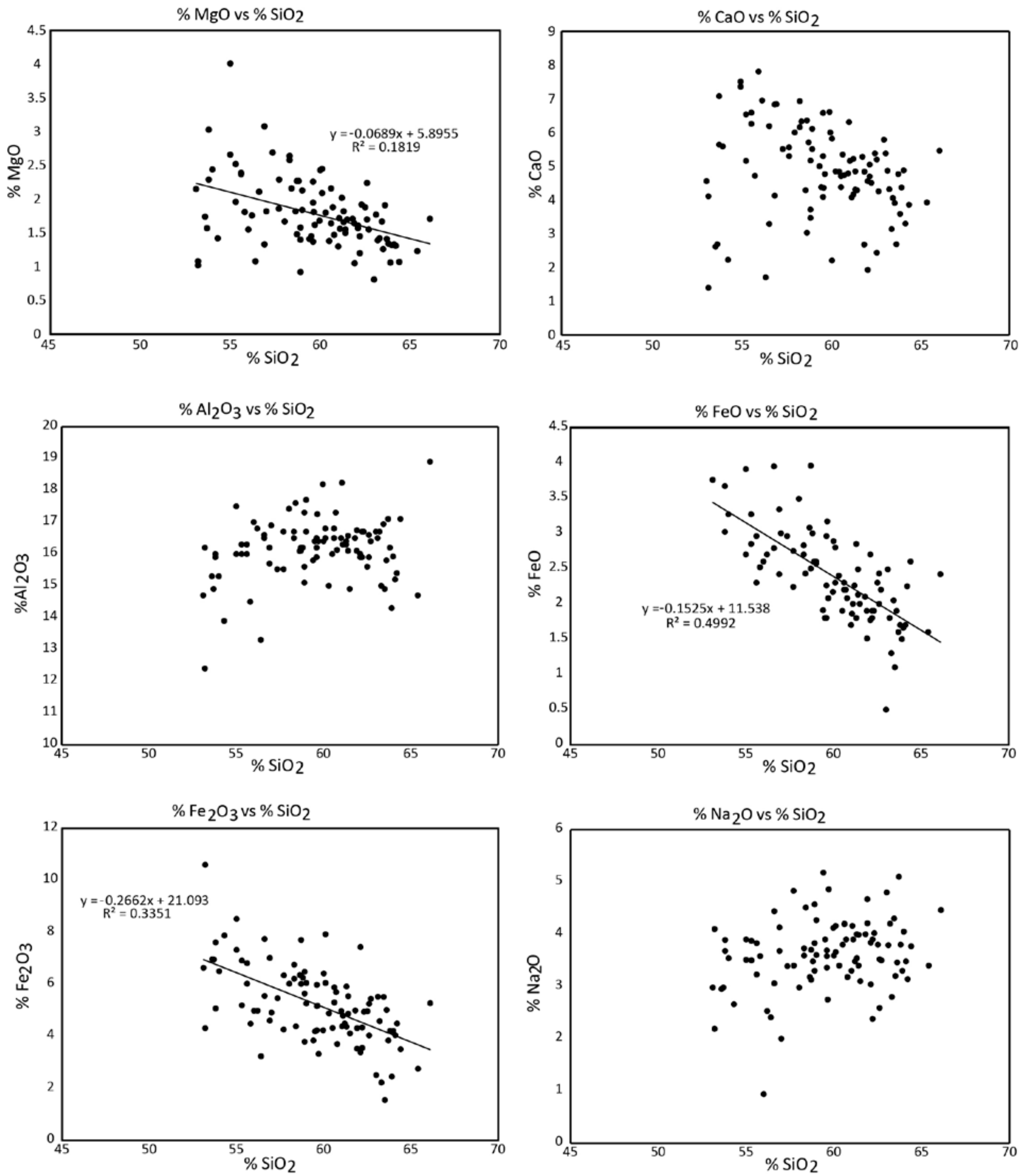

Figure 4-10. Geochemistry plots showing the major elements vs. SiO2. All of the analyses shown on these diagrams have been filtered such that only fresh samples are included. These analyses are taken to represent the chemical composition of the parental magma.

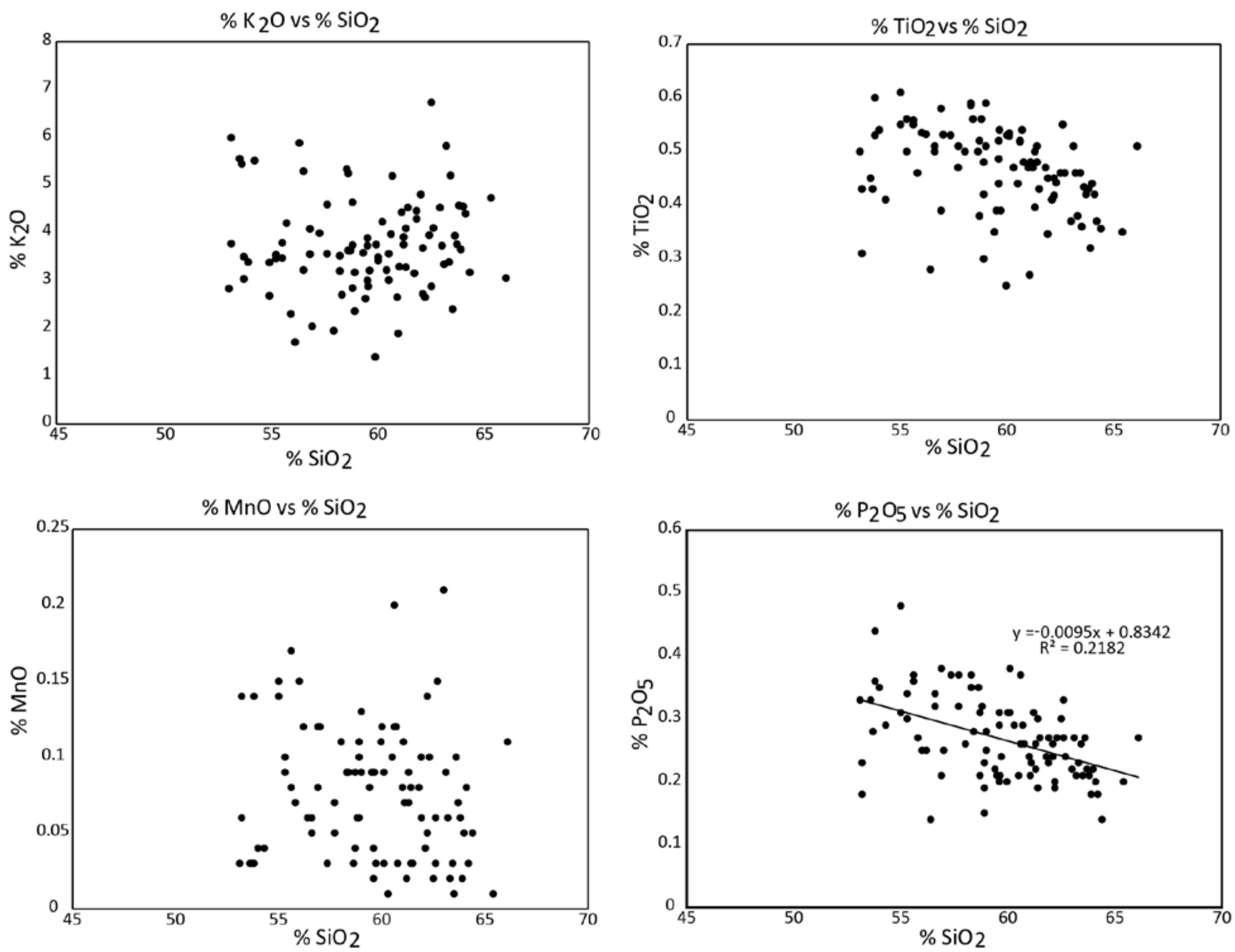

Figure 4-10. Continued

DISCUSSION

Sequence of Events in the Ertsberg-Grasberg Mining Distrct

The duration of magmatism in the Ertsberg-Grasberg mining district is well constrained by the new zircon U/Pb geochronology (Figure 4-11). Figure 4-12 is a schematic diagram that illustrates the sequencing of events. The oldest intrusions in the district are the Wanagon Sill (3.56 ± 0.07 Ma, x = 2 samples, n = 56 zircons) and the Lembah Tembaga intrusions (3.49 ± 0.07 Ma, x = 2 samples, n = 52 zircons), and the youngest dated intrusion in the district is one sample of a dike in the Ertsberg pluton (2.76 ± 0.07 Ma, x = 1 sample, n = 32 zircons). Based on these age constraints magmatism in the district lasted for less than one million years. This is comparable to the results of the study by McDowell et al. (1996) who concluded magmatism in the district lasted approximately 1.8 million years. As discussed in Chapter 1, magmatism forming the GIC lasted for at most 600 kyr**,** main stage hydrothermal fluid flow occurred lasted for at most 100 to 220 kyr, and crystallization of the Ertsberg pluton spans an age range of approximately 300 kyr (Figure 4-11)**.**

With the exception of the supergiant Grasberg porphyry copper deposit, the duration of hydrothermal fluid flow in each of the mineralizing centers has not been constrained by dating intrusions that cross-cut the mineralization. It is, however, possible to place constraints on the relative timing of each ore forming systems based on the zircon U/Pb crystallization ages of the intrusions, and their (U-Th)/He cooling ages, which date cooling to temperatures less than ~200°C, which is less than the temperature of the ore-forming fluids.

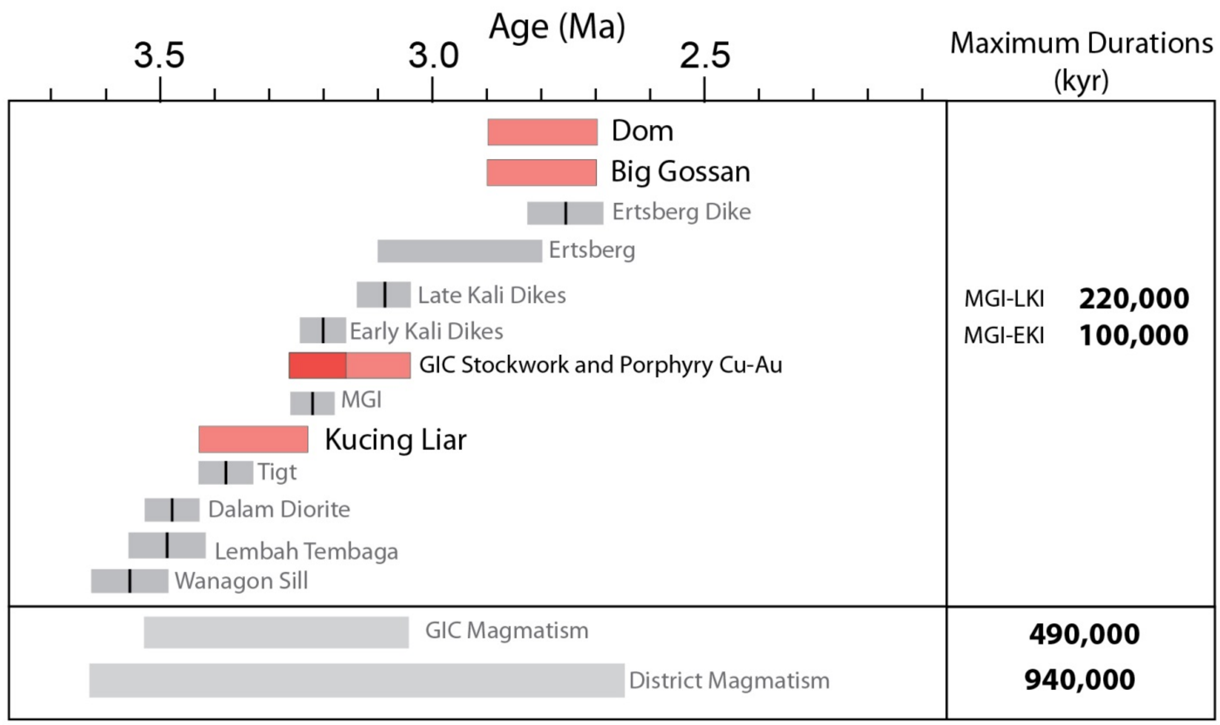

Figure 4-11. Plot showing the composite zircon U/Pb ages for important intrusions in the Ertsberg-Grasberg mining district. The best constraints for the maximum duration of hydrothermal fluid flow are in the Grasberg porphyry copper deposit. The interpreted duration for the Kucing Liar skarn, Big Gossan and Dom are also shown. Intrusion ages are shown in grey boxes and ore bodies are shown in red boxes.

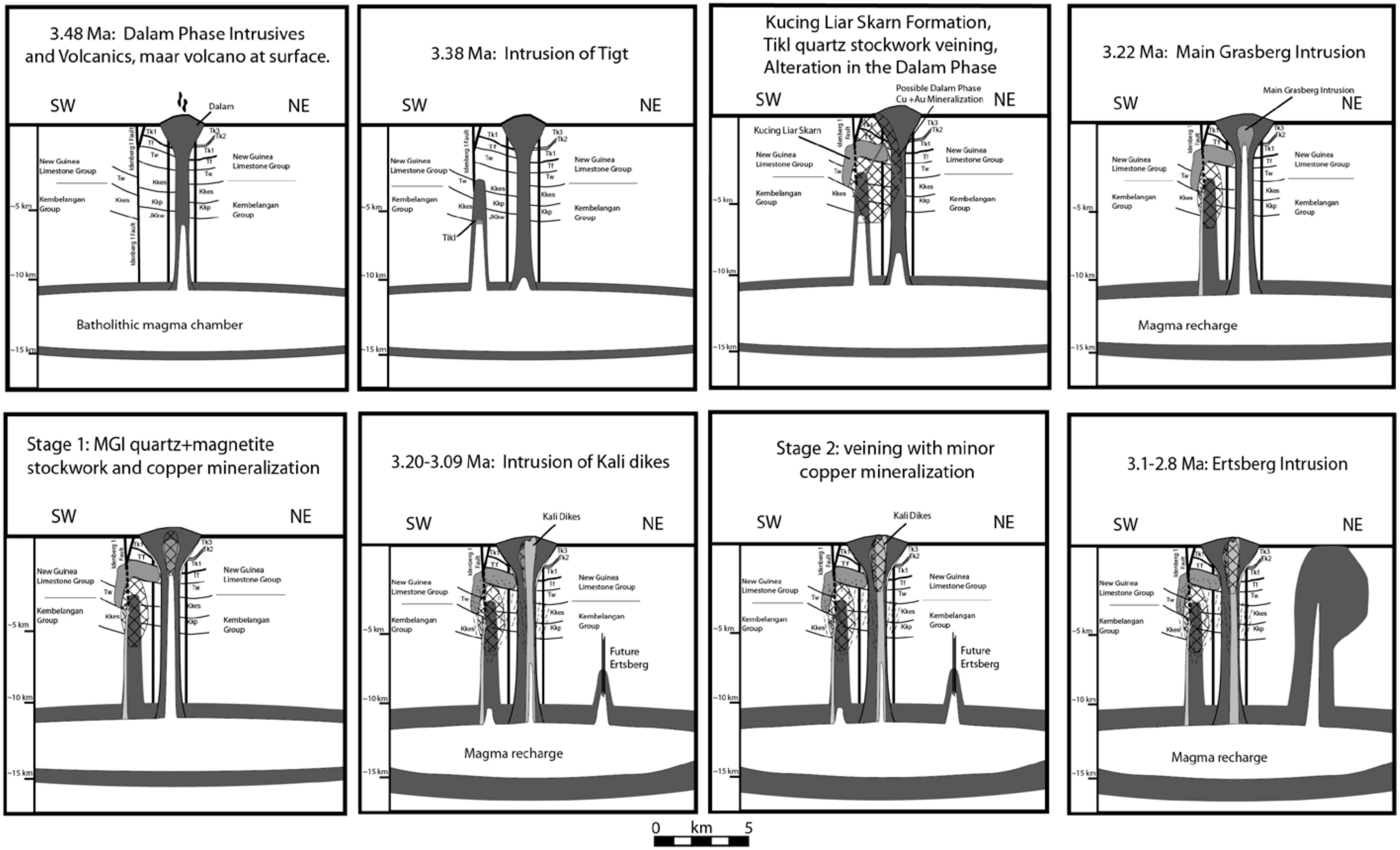

Figure 4-12. Continued next page.

Figure 4-12. Sequence of in the Ertsberg-Grasberg District, including intrusion of Tigt and the Kucing Liar skarn, each of the mineralization events in the GIC, and intrusion of the Ertsberg pluton. The Ertsberg East Skarn System and Ertsberg porphyry formed following intrusion of the Ertsberg pluton; it is unknown whether the Ertsberg skarn pre-dates or post-dates the Ertsberg.

The oldest mineralization center in the district is the Kucing Liar skarn. There is an additional challenge in estimating the duration of hydrothermal fluid flow in the Kucing Liar skarn, as the causative intrusion has not been conclusively identified. Based on the spatial association between the Tigt intrusion and the Kucing Liar skarn, and the presence of an intense quartz stockwork (up to 90% quartz, per meter length segment of core) in the Tigt intrusion, Leys et al. (2012) hypothesize that the Tigt is from the parental intrusion for the skarn. Zircon U/Pb crystallization ages for the Tigt intrusion range between approximately 3.4 and 3.3 Ma. New (2006) reported $^{40}Ar/^{39}Ar$ cooling ages for hydrothermal biotite and phlogopite from the Kucing Liar skarn (see Table 4-1). The skarn ages are approximately 3.2 ± 0.05 Ma. Based on the crystallization age of the Tigt and the cooling ages in the Kucing Liar skarn the best estimate for the duration of hydrothermal fluid flow responsible for skarn formation is ~100 to 200 kyr. It is possible that the hydrothermal fluid flow responsible for the Kucing Liar skarn could have also caused an early phase of hydrothermal alteration in the pre-existing Dalam phase. Following the formation of the Kucing Liar Skarn, magmatism and hydrothermal fluid flow jumped to the GIC, after the MGI was emplaced.

The main stage of Grasberg copper and gold mineralization followed intrusion of the MGI. The fundamental cross-cutting relationship is that the Late Kali Dikes cross cut the high grade copper and gold mineralization. As reported above, the maximum duration of hydrothermal fluid flow responsible for the supergiant Grasberg porphyry copper deposit is between 100 to 220 kyr. Figure 4-11b shows the relative sequence of events in the Kucing Liar Skarn and the GIC.

Seven garnet samples from the Big Gossan skarn have been dated using the innovative LA-ICP-MS garnet U/Pb technique. The results, which are discussed in Chapter 3, show that all garnet samples in the Big Gossan skarn formed between 2.9 and 2.7 Ma, which suggest that prograde skarn formation occurred over a time period of ~200 kyr.

Cross cutting dike relationships have yet to be identified in the Ertsberg porphyry deposit or the Ertsberg East skarn. Based on zircon U/Pb ages the Ertsberg pluton crystallized between

3.1 and 2.8 Ma. Phlogopite and biotite $^{40}Ar/^{39}Ar$ cooling ages reported by Pollard et al. (2001) range between 2.94 ± 0.10 Ma and 2.71 ± 0.04 Ma, which suggests that mineralization in the Ertsberg porphyry and Ertsberg East Skarn System occurred over a time period of no more than ~300 kyr.

Based on the reported timing and age ranges for each of the mineralizing centers in the Ertsberg-Grasberg mining district, all of the ore deposits are temporally district. Over a period of time between ~3.6and 2.8 Ma, four giant ore deposits and a number of smaller ore systems (including Wanagon and Dom), which have not been addressed in this analysis, were emplaced into a relatively narrow 4 km wide strike-slip corridor.

CONCLUSIONS

1. Zircon U/Pb ages have been measured using the depth-profiling LA-ICPMS technique for 108 samples in the Ertsberg-Grasberg mining district. The results show that magmatism in the district took place over a time window of less than one million years.
2. The Kucing Liar skarn, the Grasberg porphyry copper deposit, and the Big Gossan and Dom skarns each formed at distinct times. Zircon U/Pb ages reported here and hydrothermal biotite and phlogopite Ar/Ar ages from New (2006) indicate that the Kucing Liar skarn formed between 3.4 to 3.2 Ma. The supergiant Grasberg deposit formed between 3.22 ± 0.04 Ma and 3.09 ± 0.05 Ma, and there was little to no overlap with the Kucing Liar Skarn. The coeval Big Gossan and Dom skarns, which formed between ~2.9 to 2.7 Ma were the last ore forming events in the district.
3. Concordant interior growth zones were measured for 5% of the zircons analyzed, and the results show that the lower crust assimilant includes ~300 Ma intrusions related to the Tasman Orogeny and Proterozoic basement units. There is little evidence for Archean age rock units in the lower crust below the Ertsberg-Grasberg mining district.

Chapter 5: Thermal History of the Ertsberg-Grasberg Mining District, Papua, Indonesia

INTRODUCTION AND MOTIVATION

Traditional dating techniques, including zircon U/Pb and Ar/Ar chronometers provide insight into both the magmatic crystallization history and the intermediate cooling temperatures (500 to 300°C) of intrusions associated with hydrothermal systems. The low temperature cooling history (< 210°C), which could record either cooling of the hydrothermal system to ambient conditions or cooling associated with exhumation, is delineated using the zircon and apatite (U-Th)/He thermochronometers (abbreviated as zHe and aHe). Low temperature cooling ages provide a unique opportunity to understand the cooling rates associated with magmatic-hydrothermal ore systems, and the erosion rates that lead to unroofing and exposure of ore deposits at the surface of the Earth (McInnnes et al., 2005; Wilkinson and Kesler, 2007).

Zircon and apatite (U-Th)/He age results for the GIC are reported in Chapter 2. The results showed very fast cooling rates (20°C/10 kyr at surface and 2°C/10 kyr at 2.5 km depth), which were interpreted to reflect emplacement into cold country rock (see Chapter 2). Tightly spaced horizontal isotherms in the ore zone restricts the precipitation of copper sulfide minerals into a small rock volume, resulting in a high grade orebody. High lateral thermal gradients at the depths where fluids exsolve leads to rapid heat loss from a cooling stock. Rapid crystallization of anhydrous mineral phases along the sidewalls of the stock increases the flux of magmatic-hydrothermal fluid generation. Steady and prolonged fluid generation can occur when fluid production is controlled by the rate of heat loss, ultimately governing the rate of cupola charging with copper rich hydrothermal fluids (Cloos, 2001; Cloos and Sapiie, 2013).

To supplement the GIC vertical profiles, samples were collected from a vertical profile (drill hole TEW-08-01) and from spatially varied locations throughout the Ertsberg pluton (Figure 5-1). The motivation for dating these samples was to evaluate the magmatic cooling rates in the Ertsberg pluton. In addition to the Ertsberg samples, a suite of six samples was collected from the AB1-10-01 core, a unique drill core that was drilled horizontally, at 2528 m elevation, underneath the Carstenszweide Valley, between the Ertsberg pluton and the GIC. The core is collared in the Ertsberg intrusion, but also contains an Ertsberg-Kali contact and intervals of Karume and Plag Dike. Each of these intrusions has a different magmatic crystallization age (see Chapter 4, Figure 4-3), making it possible to differentiate between a magmatic cooling age and an erosional cooling age. This unique dataset provides information on the thermal footprints of the two large intrusive centers in the district.

In addition to vertical profiles, it is possible to evaluate the thermal history of an intrusion by applying multiple geo- and thermo-chronometers to a single sample. Five samples originally dated by McDowell et al. (1996) using the biotite K-Ar technique, were also dated by Brad Hacker at Stanford University using biotite Ar/Ar (unpublished data; Cloos, pers. comm.), and by Weiland and Cloos (1996) using apatite fission track (AFT). By dating these samples using the zHe and aHe techniques it is possible to constrain the thermal history of a single sample from a magmatic crystallization temperature of ~700°C, through to the low temperature cooling. These thermal profiles supplement the cooling rates measured in the vertical profiles, and provide an alternative tool for verifying the interpretation that intrusions in the district were emplaced into cold country rock, a critical premise for the interpretations discussed in Chapter 2, namely that rapid cooling is a fundamental contributing factor for supergiant ore body formation.

The low temperature thermochronometry dating undertaken in the Ertsberg-Grasberg mining district provides a new constraint on the thermal histories associated with both porphyry Cu-Au and skarn style mineralization. Furthermore, determining the extent of thermal halos associated with each of the intrusive centers and their associated mineralization could provide a unique dataset for refining exploration models for similar systems (Hickey et al., 2014). More conventionally, by evaluating the cooling rate profiles, and assuming a plausible geothermal gradient, it is possible to constrain the paleo-topographic profile and the depth of emplacement at the time of mineralization, and determine the denudation rate near the spine of the Central Range (see Stockli, 2005).

Geothermal Gradients at 3 Ma

Intrusions in the Ertsberg-Grasberg mining district were emplaced into passive margin siliciclastic and carbonate units that had been folded and faulted during the collision between the Australian continent and the Pacific Plate (Weiland and Cloos, 1996; Sapiie, 1999; Cloos et al., 2005). Geothermal gradients on similar continental passive margins are typically 20 to 30 °C/km, depending on the heat flow in the region (Pribnow et al., 2000; Goutorbe et al., 2008). Given that the Australian passive margin sequence was subsequently bulldozed and thickened during the recent arc-continent collision, the geothermal gradient prior to emplacement of the intrusions was probably 10 to 20 °C/km. The observation that the GIC was emplaced into cold country rock (see Chapter 2) suggests that the lower end of these values, perhaps between 15 - 20°C/km, is a plausible estimate for the geothermal gradient at 3 Ma.

The present day geothermal gradient measured in the deep workings of the Ertsberg-Grasberg mining district is 11-13 °C/km (Freeport, unpublished data). Such low geothermal gradient develop in mountain terranes with deep valleys due to advective heat loss as groundwater flows down and away from the crest of the mountain because of deep river valley incision, such as in the East and West Agahwagon Valleys.

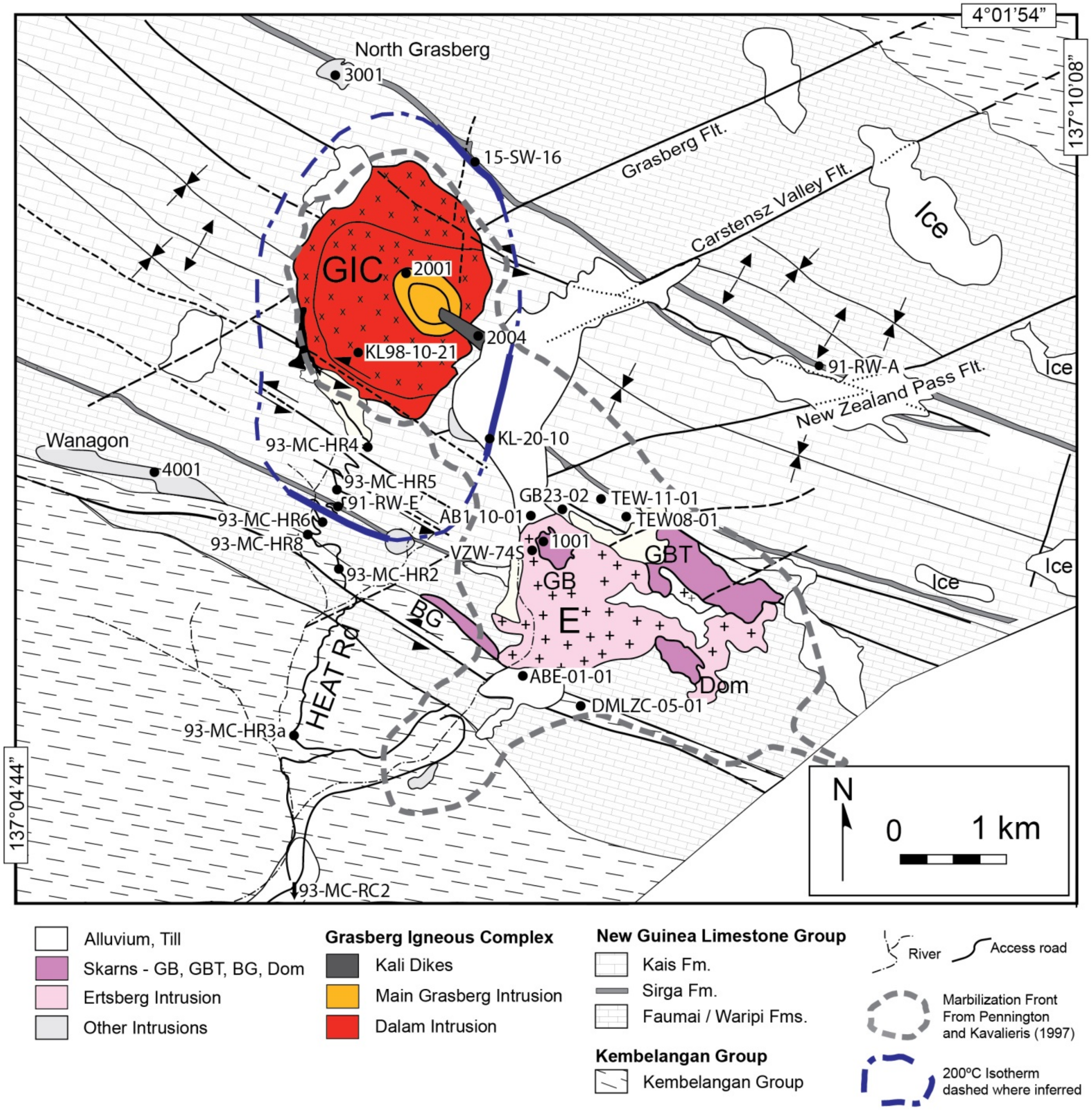

Figure 5-1. Simplified geologic map of the Ertsberg-Grasberg mining district showing drill hole collars/ outcrop locations for each of the (U-Th)/He samples (black circles). Modified from Paterson and Cloos (2005). Skarns: GB - Gunung Bijih (Ertsberg), GBT - Gunung Bijih Timur (Ertsberg East), BG - Big Gossan.

ANALYTICAL TECHNIQUES

Apatite and zircon (U-Th)/He analyses were completed at the University of Texas at Austin. The (U-Th)/He chronometer is based on the fact that the radioactive elements ^{238}U, ^{235}U, and ^{232}Th decay to their stable daughter products by a chain of alpha decays. Each radioactive parent produces 8, 7, and 6 ^{4}He particles respectively. The age is calculated using the following equation:

$$^{4}He=8\,^{238}U(e^{\lambda 238t}-1)+7(^{238}U/137.88)(e^{\lambda 235t}-1)+6\,^{232}Th(e^{\lambda 232t}-1)+^{147}Sm(e^{\lambda 147t}-1) \quad (1)$$

The calculated age is a cooling age, because when the mineral is above the mineral's closure temperature (nominally ~180°C for zircon and 70°C for apatite given a cooling rate of 10°C/myr) helium is able to readily diffuse out of the grain. Once the mineral cools past the "closure temperature," the loss of helium by diffusion out of the crystal is negligible and the helium atoms start to accumulate. The chronometer records the time at which the grain passed through its partial retention zone.

There is an added complexity in interpreting the cooling ages for minerals in the Ertsberg-Grasberg mining district, as the observed rapid cooling rates of ~5°C/ 10 kyr means that the nominal closure temperature will be too low (Dodson, 1973). In order to understand the diffusion kinetics for the very young Grasberg zircons (which will be relatively radiation damage free; Guenthner et al., 2013), diffusion experiments were conducted on six zircons (using the techniques described by Farley et al. (1999)). The results are shown in Appendix I**.** By iteratively solving the Dodson equation using the experimentally determined diffusion kinetics for zircon, and using the Flowers et al. (2009) radiation damage model for apatite, the effective closure temperatures reported herein are ~210°C for zircon and ~100°C for apatite (Figure 5-2).

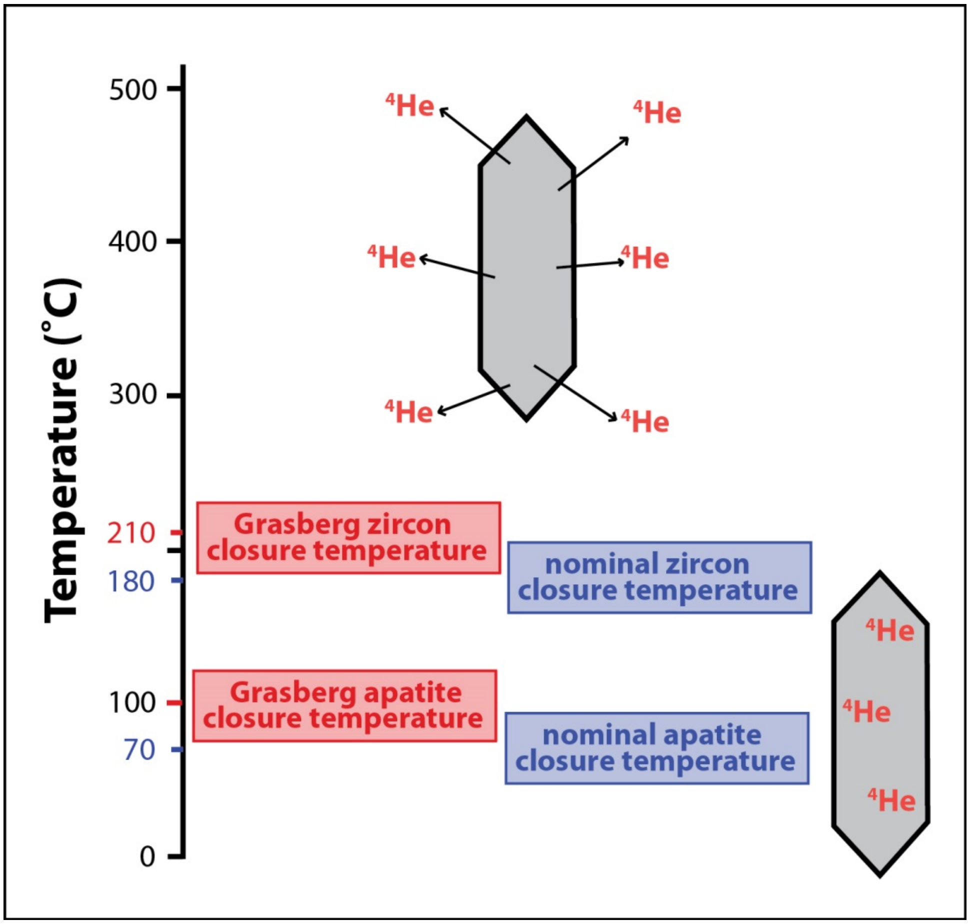

Figure 5-2. Schematic diagram showing the nominal closure temperatures for the zircon and apatite (U-Th)/He system, which is used to evaluate the erosional cooling histories and cooling rates, and the "effective" closure temperature for magmatic zircons and apatites from the Ertsberg-Grasberg mining district, which are used to evaluate the magmatic cooling rates. The "effective" closure temperature for magmatic zircons was determined using experimentally determined diffusion kinetics for six zircons from the Dalam and MGI. The "effective" closure temperature for magmatic apatite was calculated using the RDAAM (radiation damage accumulation and annealing model) from Flowers et al. (2009).

In order to measure a (U-Th)/He age euhedral, inclusion-free apatites and zircons are packed into platinum packets and heated by a diode laser to ~1300°C for 10 minutes (5 minutes for apatite). ^{4}He concentrations are measured using a ^{3}He isotopic tracer on an ultra-high vacuum noble gas extraction line. Following sample degassing the mineral grain is removed from the platinum packet, spiked with a ^{230}Th-^{235}U-^{149}Sm isotopic tracer and dissolved in hydrofluoric and nitric acid. Parent nuclide concentrations are measured using an Element2 ICP-MS. Sample ages are reported as the average and standard deviation of six aliquots.

RESULTS

Ertsberg Pluton

Zircon and apatite (U-Th)/He age results for the Ertsberg pluton samples are shown in Table 5-1. ZHe ages from the 2 km tall vertical profile in the Ertsberg pluton show a younging trend with depth (Figure 5-3). Unfortunately, the quality of the apatite in these samples was not sufficient to measure an aHe age. Problems that can cause poor apatite quality include a lack of euhedral crystals, the presence of mineral inclusions, and the presence of abundant fluid inclusions; in this case mineral inclusions were prevalent, and even grains that appeared to be inclusion free under a microscope exhibited behavior consistent with inclusions during degassing (indicated by the observation that multiple helium re-extracts were required to completely degas the grains). Based on the zircon crystallization age (~700°C) and the zHe cooling ages (~210°C) cooling rates were calculated. The cooling rates in the Ertsberg pluton vertical profile show a similar pattern to the vertical profiles obtained in the GIC; however, the near-surface samples in the Ertsberg pluton show slower cooling than the near-surface samples in the GIC (cooling rates of 4°C/ 10 kyr compared to 10-25°C/ 10 kyr). As expected, this indicates that the level of exposure is deeper in the Ertsberg pluton compared to the top of the GIC, perhaps on the order of 1-2 km, however this is not directly constrained.

Table 5-1. Cooling rates for samples from the Ertsberg pluton

Intrusion	Sample	Elevation	U/Pb Age	zHe Age	Cooling rate (750-210°C) °C/ 10 kyr
Ertsberg	TEW08-01 0m	3145	2.84±0.10	2.5±0.2	9
	TEW08-01 280m	2865	-	2.2±0.5	4
	TEW08-01 500m	2645	3.09±0.14	2.1±0.4	4
	TEW08-01 750m	2395	-	2.3±0.7	4
	TEW08-01 1000m	2145	-	2.1±0.2	5
	TEW08-01 1275m	1870	2.95±0.13	1.6±0.5	3
	TEW-01-01 76m	3960	3.03±0.10	3±0.1	4
	VZW-74S 70m	3840	-	2.2±0.1	-
	VZW-74S 276m	3840	-	2.6±0.4	-
	GB23-02 56m	3791	3.06±0.12	2.5±0.1	1
	DMLZC05-01 248m	2912	3.00±0.11	2.2±0.1	1
	ABE-01-01 143m	2511	2.91±0.14	2.6±0.6	1

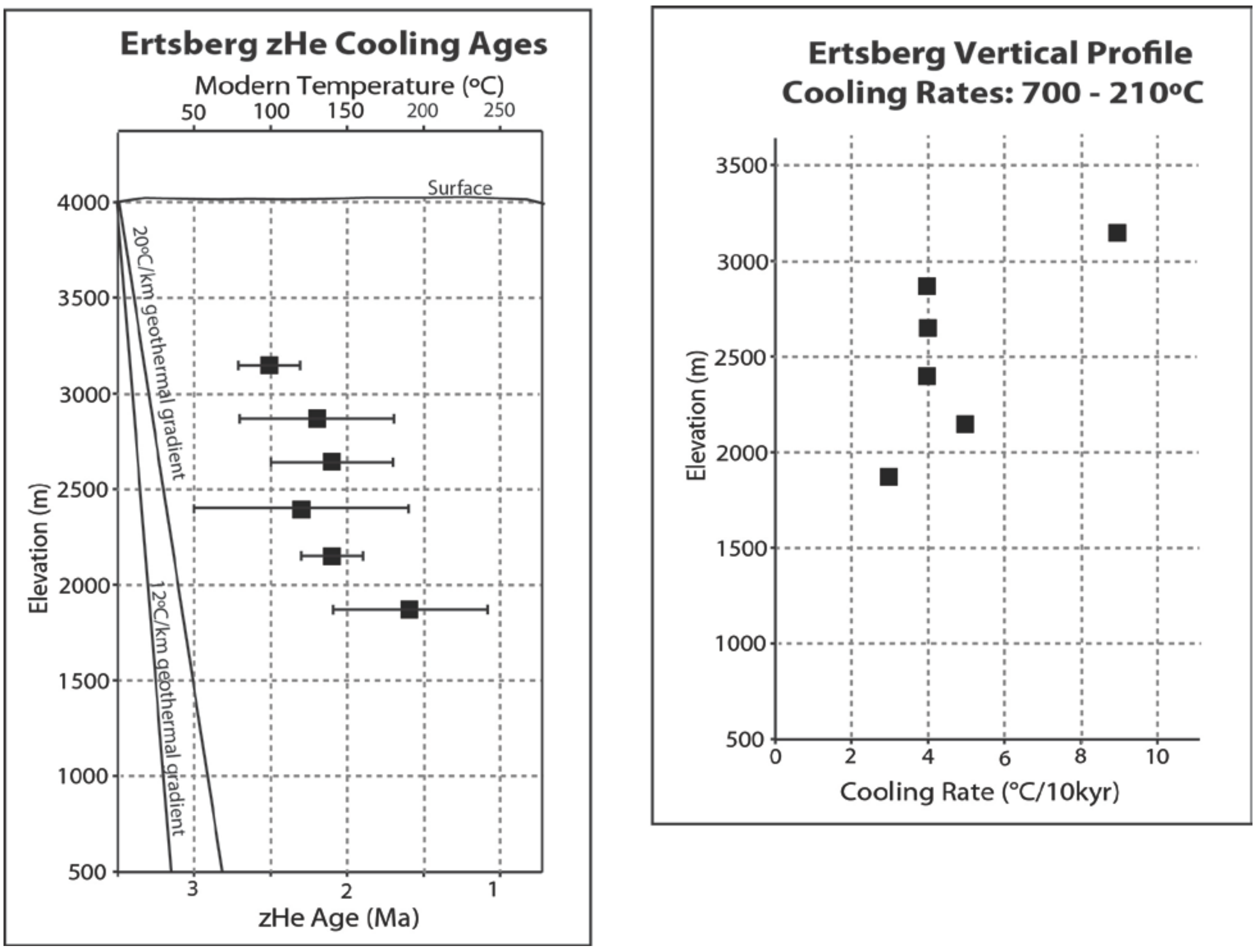

Figure 5-3. Plots showing the zHe ages vs. depth (left) and the cooling rate from 700°C to 210°C vs. depth (right) for the TEW-08-01 vertical profile in the Ertsberg pluton. Present day geothermal gradient is approximately 11-13ºC/km.

Multi-chronometer Samples

Five samples from the suite sent to Brad Hacker (Stanford, 1994) for biotite $^{40}Ar/^{39}Ar$ dating were selected for zHe and aHe dating. Two of the samples (1001 is from the Ertsberg pluton and 3001 is from the North Grasberg plug, which is a small intrusion located to the northwest of the GIC) had also been dated using the apatite fission track technique (Weiland and Cloos, 1996). By dating the same sample using multiple geochronometers and thermochronometers it is possible to construct a refined thermal history (e.g., Stockli, 2005).

Zircon U/Pb crystallization ages were measured for each of the multi-chronometer samples. In each case the zircon crystallization age was older than the cooling ages. Biotite $^{40}Ar/^{39}Ar$ and AFT ages for each of the five samples are shown in Table 5-2. ZHe and aHe samples were collected for four of the five samples; the 2001 sample lacked sufficiently large, euhedral zircons (the sample was re-processed three times however no dateable grains were recovered). Similarly, aHe ages were collected for four of the five samples, as euhedral, inclusion free apatites were also not present in the 2001 sample.

Cooling profiles for each of the multi-chronometer samples are shown in Figure 5-4. For the Ertsberg (1001) and Kali (2004) samples, the cooling profiles show rapid cooling from zircon crystallization at ~700°C to the zircon and apatite closure temperatures, even at depths of 2.9 km. These samples are in agreement with cooling rates reported for the GIC in Chapter 2, on the order of 5-10°C/10 kyr. The North Grasberg (3001) sample also shows very rapid cooling from zircon crystallization to the zircon and apatite cooling, which is expected due to its small volume and its emplacement to shallow depths below an intermontane basin at the crest of the mountain range.

The only sample that shows more prolonged cooling between zircon crystallization and zircon and apatite cooling is the Wanagon Intrusion (4001) (sample elevation of 3.4 km). However; the appearance of prolonged cooling may be a function of the large uncertainty on the aHe age (2.6 ± 0.6 Ma). Prolonged cooling to the ~100°C apatite closure temperature is most likely a function of the depth of the 4001 sample at the time of emplacement. The map patterns show that the GIC, Ertsberg pluton, and the North Grasberg Intrusion were emplaced near the hinge of the Yellow Valley Syncline, which show the shallowest erosion levels in the district. In contrast, the Wanagon Intrusion was emplaced into the steeply dipping southern limb of the Yellow Valley Syncline, where as much as 3 km of overburden may have been eroded off since 3 Ma (Figure 5-6). Therefore, the observed change in the topology of the cooling profile is thought to be a function of the depth of sample emplacement, showing the cooling history of a sample located at ~3 km depth at 3 Ma.

Carstenszweide Valley

The AB1-10-01 core is collared in the Ertsberg pluton. There is a sharp contact at 122 m with a Kali Dike, and then a series of intrusive contacts between the "Plag Dike" and the Karume intrusion. The Plag Dike was named by the Freeport geologists based on the cm-scale plagioclase phenocrysts which float in a finer grained matrix. The plagioclase crystals are typically rounded and show resorption textures. In some cases the Plag Dikes include xenoliths of Karume, indicating that the dikes are younger than the Karume. Six samples from the AB1-10-01 core were selected for analysis, and have been dated using the zircon U/Pb, zHe, and aHe techniques (Figure 5-5). The results show that the zHe ages consistently overlap with the crystallization ages of the intrusions, indicating that the zircons were not reheated and reset during subsequent intrusion of young stocks and plugs (Table 5-3). The exception is the AB1-10-01 500m sample; however, the zircon He age may have been reset due to reheating caused by local flow of hot hydrothermal fluids.

AHe ages from the AB1-10-01 2m, AB1-10-01 382m, and AB1-10-01 578m samples all overlap with the zircon U/Pb crystallization ages. Given that the apatites record magmatic cooling ages, and the fact that the sample locations are near the center of the Yellow Valley Syncline, these samples were most likely never buried deeper than 3 to 4 km.

Table 5-2. Multichronometer cooling ages for the McDowell et al. (1996) sample suite.

Sample ID	Intrusion	Zircon U/Pb	Ar/Ar	zHe	AFT	aHe
1001	**Ertsberg**	2.89±0.09	2.81±0.02	2.4±0.4	2.0±0.4	2.8±0.5
2001	**Ring Dike/ MGI**	3.31±0.10	3.07±0.10	-	-	-
2004	**Kali**	3.06±0.08	2.94±0.02	2.8±0.2	-	2.9±0.4
3001	**North Grasberg**	3.40±0.17	3.06±0.02	3.1±0.2	3.4±0.8	3.2±0.6
4001	**Wanagon Sill**	3.54±0.10	3.7±0.10	3.1±0.2	-	2.6±0.6

Table 5-3. Cooling ages for the AB1-10-01, HEAT Road, and Ridge Camp samples.

Sample Suite	**Sample ID**	**Elevation (m)**	**Zircon U/Pb**	**zHe (Ma)**	**aHe (Ma)**
Horizontal Profile	AB1-10-01 2m	2528	2.96±0.09	2.8±0.3	2.4±0.7
	AB1-10-01 205m	2528	2.99±0.07	2.9±0.2	-
	AB1-10-01 382m	2528	2.95±0.10	3.2±0.2	2.8±0.1
	AB1-10-01 500m	2528	3.24±0.06	2.7±0.1	-
	AB1-10-01 574m	2528	3.28±0.05	3.2±0.3	-
	AB1-10-01 578m	2528	3.19±0.05	2.9±0.6	2.8±0.3
HEAT Road	95-MC-HR4	3725	3.36±0.09	3.3±0.3	3.0±0.3
	93-MC-HR5	3450	3.41±0.11	3.1±0.3	2.7±0.3
	94-MC-HR6	3190	3.61±0.15	2.6±0.4	2.6±0.1
	93-MC-HR8	3060	-	3.0±0.4	2.4±0.2
	93-MC-HR2	2980	-	2.9±0.3	2.3±0.9
	93-MC-HR3a	2650	3.36±0.04	2.6±0.1	2.2±0.6
Ridge Camp	94-MC-RC2	2160	3.73±0.10	2.1±0.3	-

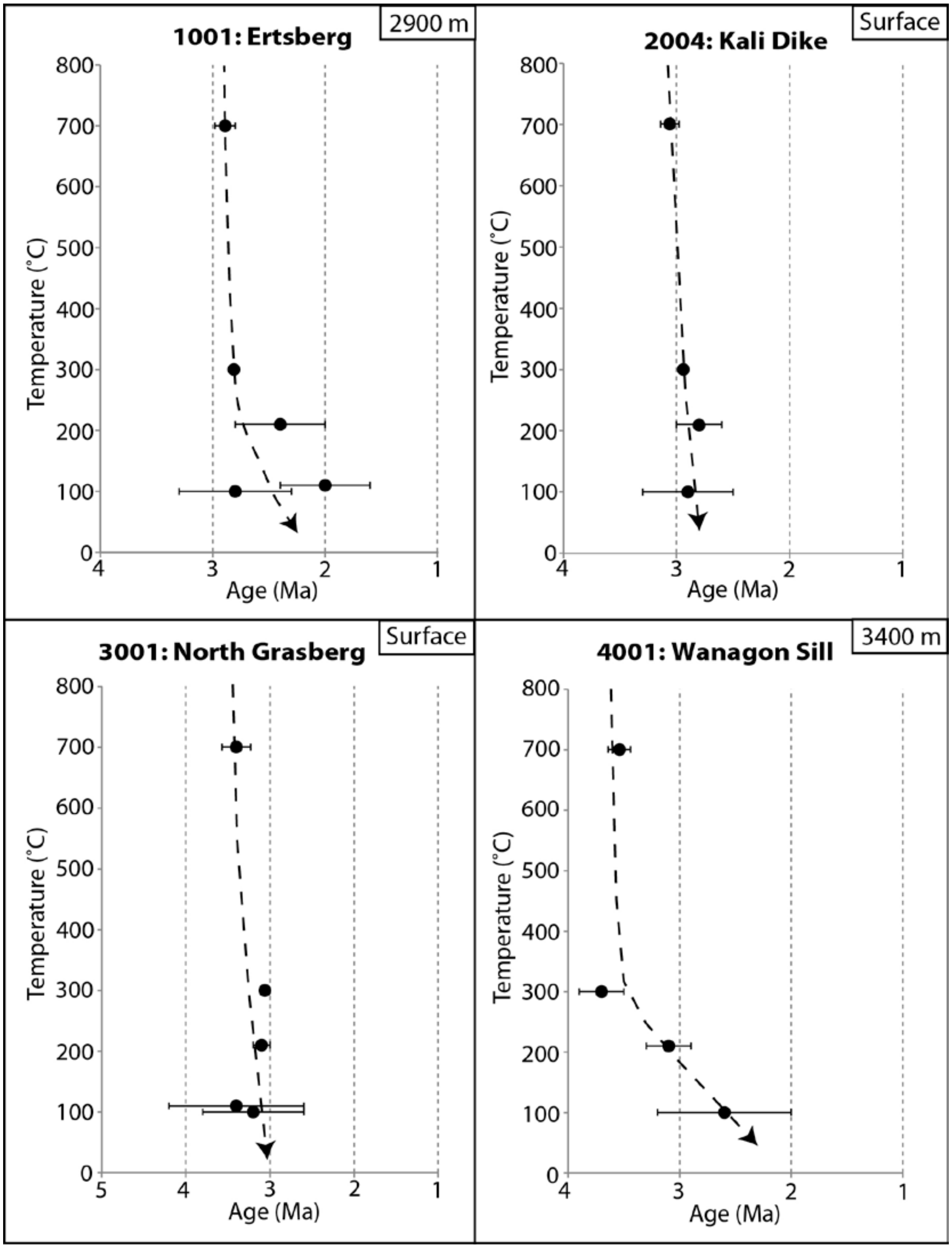

Figure 5-4. Cooling histories for samples that have been dated using multiple geo- and thermochronometers. Dashed line shows cooling path. Cooling profiles for samples 1001, 2004, and 3001 show very rapid cooling for magmatic to low temperature conditions. In contrast, the 4001 sample from the Wanagon Sill shows prolonged cooling from magmatic temperatures to ambient conditions. This is most likely attributed to the depth of emplacement of the samples, where the AFT and aHe chronometers are recording prolonged heating from erosion and unroofing in the southern limb of the Yellow Valley Syncline.

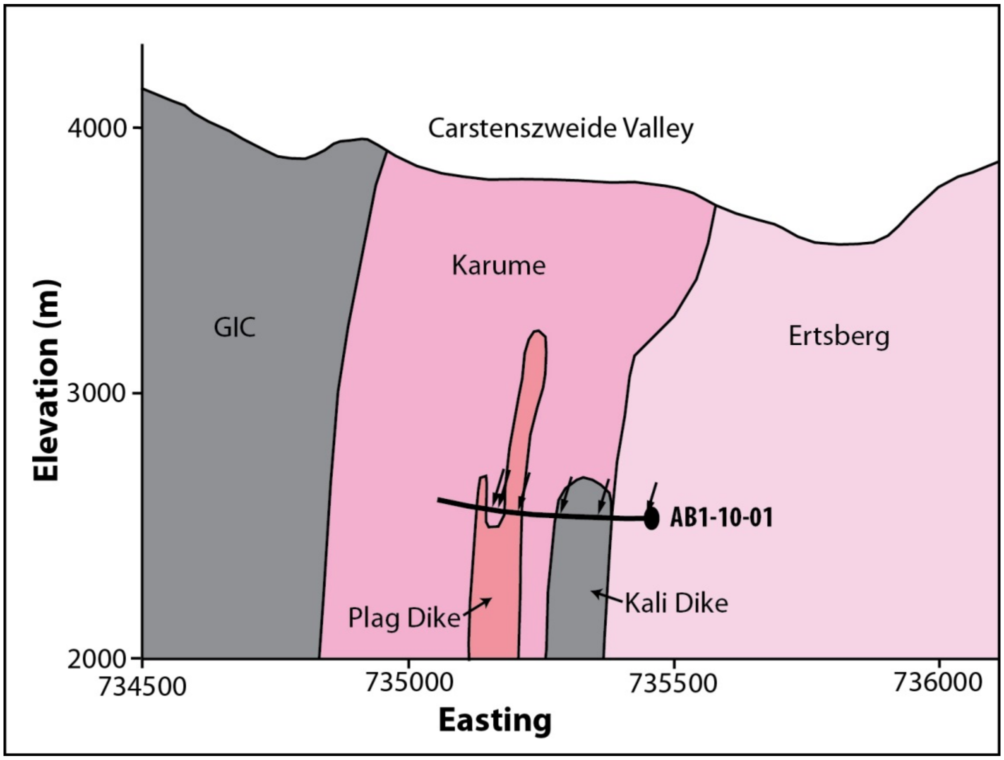

Figure 5-5. Diagram showing the location of the AB1-10-01 drill core beneath the Cartsenszweide valley in the mining district. Black arrows show sample locations.

HEAT Road Samples

The Heavy Equipment Access Trail (HEAT Road) provides access to the Grasberg open pit along a road that was created in a steeply incised West Agahwagon Valley, along the upper flank of the Central Range. Samples of magmatic dikes encountered along the HEAT Road were collected by Mark Cloos during the 1993-1995 field seasons, and although samples were collected less than three km apart, they cover nearly 1100 m of elevation change. Taking into account the Ridge Camp sample, the elevation difference between all of the samples is nearly 1600 m (Figure 5-6).

The age results show that two samples collected nearest to the Grasberg open pit, 95-MC-HR4 and 93-MC-HR5, have magmatic cooling ages, as the zHe ages overlap with the zircon U/Pb crystallization ages (Table 5-3). The first sample that shows prolonged cooling, most likely due to denudation during valley incision, from a depth below the apatite helium partial retention zone, is 94-MC-HR6. The aHe age is well constrained at 2.6 ± 0.1 Ma. Assuming a geothermal gradient of 15 - 20°C/km, the aHe cooling age indicates that prior to ~2.6 Ma the 94-MC-HR6 sample was buried by 3.5 – 5 km of overburden.

For the 93-MC-HR8 and 93-MC-HR2 samples the youngest band of zircon growth was too thin to be well resolved using the LA-ICPMS depth profiling technique. Given the resolution of the depth-profiling technique, if a young zircon growth zone was present, it must have been less than 1-2 µm. The zHe cooling ages provide a constraint on the youngest possible age for zircon crystallization. The spread between the zHe and aHe ages for both samples suggests that both experienced slow unroofing, starting from a depth below 3.5 – 5 km (below the partial retention zone for apatite) to depths less than
3.5 – 5 km.

The Ridge Camp sample is from the lowest elevation (~2160 m) in the profile. The crystallization age of the sample is 3.73 ± 0.10 Ma, whereas the zHe age is 2.1 ± 0.3 Ma. Apatites from this sample were too small and anhedral to obtain a good aHe age. It is unclear whether the cooling ages for the Ridge Camp sample are due to unroofing (assuming a geothermal gradient of 15 – 20°C/km, these results would indicate that the Ridge Camp sample was deeper than 9 – 12 km) or due to proximity to the southern arm of the Ertsberg pluton at depth. Country rock in close proximity to the pluton will experience heating, such that the zHe chronometer records the age of resetting and subsequent cooling to ambient conditions. Given that 9-12 km of erosion in ~2 myr at the Ridge Camp location seems unusually high, the Ridge Camp sample is interpreted to have been reset between dike crystallization and unroofing most likely due to intrusion of the southern limb of the Ertsberg pluton.

Sirga Sandstone

Three samples from the Sirga sandstone unit, 15-SW-16, 91-RW-A, and 91-RW-E', were dated using the zHe thermochronometer (see Figure 5-1 for sample locations). ZHe ages for eight grains from the 15-SW-6 sample vary between 18 and 270 Ma, whereas zHe ages for three grains from the 91-RW-A samples range from 100 to 350 Ma, and zHe ages for six grains from the RW- sample range from 3 to 22 Ma (Table 5-4). Four samples from the Sirga collected by Quarles van Ufford (1996) have biostratigraphic ages in the Early Oligocene, therefore the degree of resetting varies between each sample. The 91-RW-A sample has three zHe ages that are older than the depositional age, indicating that it is not reset. The 15-SW-16 sample has ages that are younger than the depositional age, and there is a positive correlation between the age and equivalent spherical radius (ESR) of the zircon grains, which suggests that the sample has experienced partial resetting (Figure 5-7). Similarly, the 91-RW-E' sample has ages that are all younger than the depositional age of the sandstone, but still older than the intrusion age of the GIC, indicating that it has also been partially reset, but to a larger degree than the 15-SW-16 sample. Overall there is a strong relationship between proximity to the GIC (or Ertsberg pluton in the case of sample 91-RW-A) and the degree of partial resetting

Table 5-4. Sirga Sandstone zHe ages.

Sample	Unit	Elevation	Age, Ma	err., Ma	U (ppm)	Th (ppm)	147Sm (ppm)	[U]e	Th/U	He (nmol/g)	mass (ug)	Ft	ESR
zRWV-2	Sirga	3175	8.3	0.67	71.1	53.0	1.7	83.3	0.75	3.0	9.67	0.81	63.63
zRWV-3	Sirga	3175	13.1	1.05	217.3	116.8	2.9	244.2	0.54	12.7	3.83	0.73	42.91
zRWV-4	Sirga	3175	3.6	0.29	168.1	273.9	331.2	232.8	1.63	3.5	7.61	0.77	53.73
zRWV-5	Sirga	3175	21.6	1.73	226.9	109.8	4.3	252.2	0.48	23.6	8.56	0.80	59.89
zRWV-6	Sirga	3175	5.0	0.40	38.4	41.7	2.4	48.0	1.09	1.1	17.98	0.84	75.20
zSW16-2	Sirga	4200	18.1	1.45	45.4	46.2	1.4	56.0	1.02	3.9	2.54	0.70	39.70
zSW16-3	Sirga	4200	185.3	14.82	202.6	68.6	5.2	218.4	0.34	174.0	7.21	0.79	54.83
zSW16-4	Sirga	4200	102.1	8.17	206.7	78.5	3.1	224.8	0.38	99.5	9.38	0.80	58.30
zSW16-5	Sirga	4200	370.0	29.60	59.4	83.7	1.1	78.7	1.41	135.8	17.47	0.84	76.75
zSW16-6	Sirga	4200	213.0	17.04	41.4	97.4	8.9	63.9	2.35	60.6	10.76	0.81	64.78
zSW16-7	Sirga	4200	68.9	5.51	107.6	54.7	1.0	120.2	0.51	35.4	7.43	0.79	55.99
zSW16-8	Sirga	4200	71.4	5.71	145.4	136.6	2.6	176.9	0.94	54.4	8.63	0.79	58.02
zSW16-9	Sirga	4200	50.9	4.07	86.3	48.6	1.8	97.5	0.56	22.9	25.17	0.85	81.97

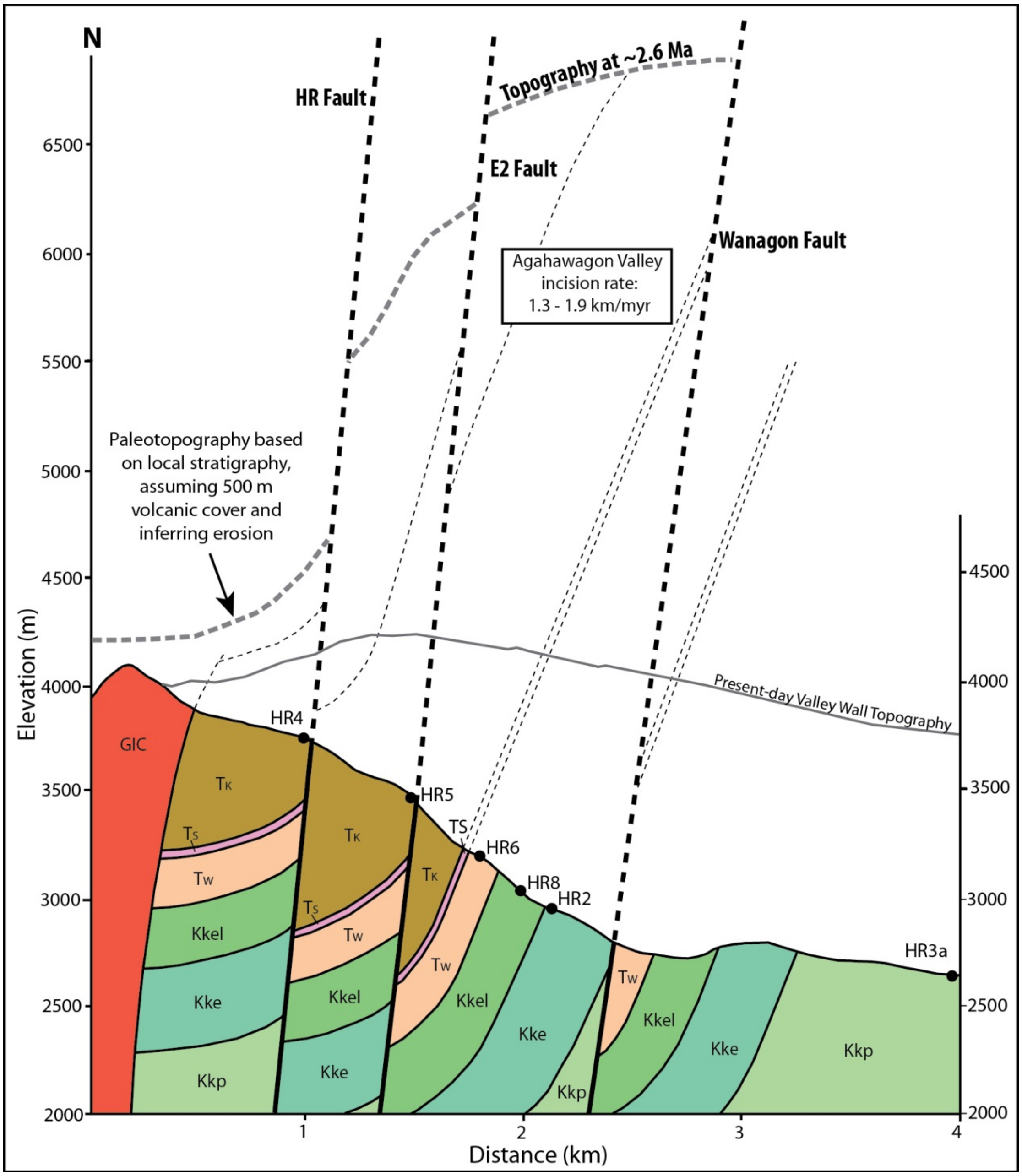

Figure 5-6. Cross section from N-S showing the location of the HEAT Rd Samples. Inset figure shows the paleotopgraphy of the section at approximately 3 Ma. The HEAT Rd samples were collected by M. Cloos during the 1993-1995 field seasons. Zircon U/Pb, zHe, and aHe ages for each sample are shown in Table 4. Erosion rates were calculated assuming a geothermal gradient between 20 - 25°C/km.

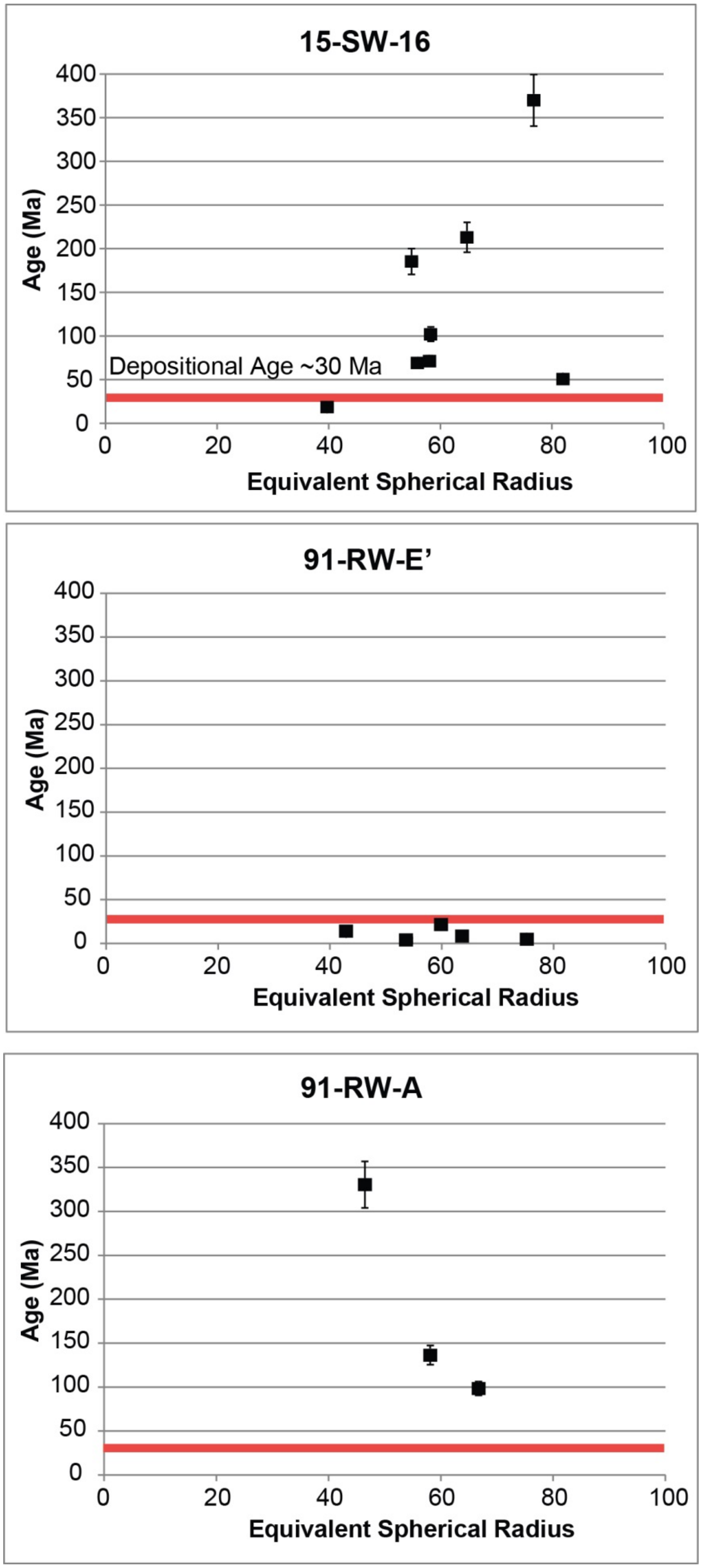

Figure 5-7. Plots showing the zircon (U-Th)/He age (Ma) vs. equivalent spherical radius (ESR) for zircon grains from the 15-SW-16, 91-RW-E’, and 91 RW-A samples of the Sirga sandstone. Red bar indicates the depositional age of the Sirga sandstone. The positive correlation between age and ESR for the 15-SW-16 sample indicates that the zircon grains have been partially reset. In contrast, the 91-RW-E’ sample has been almost completely reset, and the 91-RW-A sample, which located more distal from the intrusions is not reset.

DISCUSSION

Thermal Footprints

There is strong field evidence that intrusions in the Ertsberg-Grasberg mining district have narrow thermal aureoles, described herein as footprints. The marblization front surrounding the GIC is less than 100 m thick, and in some places less than 50 m (MacDonald and Arnold, 1994; Pennington and Kavalieris, 1997). The marblization front surrounding the ~10+ km^3 Ertsberg intrusion is ~200 m wide (Mertig, 1994). In order to quantitatively evaluate the width and age of the thermal halos, samples were selected from the AB1-10-01 core, which was drilled between the two plutons.

The results of this study confirm that the thermal footprints surrounding the intrusions in the Ertsberg-Grasberg district are narrow; a sample from a magmatic dike within 200 m of the Ertsberg pluton shows a magmatic cooling age (zHe chronometer was not reset by reheating during intrusion of the Ertsberg pluton). The samples from the Sirga sandstone that are within 300 m of the GIC are only partially reset (which is in agreement with the observation that the marblization front extends ~ 100 m around the GIC). Based on these observations lateral thermal gradients were on the order of ~150°C/100 m. This discovery supports the interpretation presented in Chapter 2, that the intrusions were emplaced into cold country rock and cooled rapidly.

Cold Country Rock

The cooling rates measured in the Ertsberg vertical profile and the multi-chronometer samples all show rapid cooling, similar to the observations in the GIC. Rapid cooling rates throughout the mining district indicate that the country rock was cold prior to intrusive activity. Steep lateral and thermal gradients, on the order of ~150°C/100 m, are detected and inferred to be a significant contributing factor to ore formation, by governing the efficiency of copper-rich hydrothermal fluid generation and restricting the volume of sulfide deposition.

The observation that cooling rates are rapid throughout the district, and that even the barren plutons show rapid cooling rates, indicates that there must be additional factors that generate ore. Cloos (2001) proposed that, in addition to the steady generation of magmatic-hydrothermal fluids by volatile exsolution due to sidewall crystallization of anhydrous mineral phases, the expansion of bubbles in mobile magma rising along the sidewalls of the stock results in vigorous convection. The convective overturn allows the volatiles and metals to be stripped from a large volume of magma as it circulates through the stock and down into the parental batholith.

Based on this model, limiting factors for ore formation are the size of the stock/ batholith and the duration that mobile magma is present. If a stock intrudes warm country rock (>50°C/km) sidewall crystallization is slow and a vigorous convective system that can strip copper from the magma may never develop. Moreover, in warm country rock the stock may solidify before the bubbling front reaches sufficient depths that copper-rich magmatic-hydrothermal fluids are generated. Steady and passive fluid exsolution must occur at sufficient depths for the chlorine to partition strongly into the fluid phase (~2 kbar or 6 km depth according to experiments by Candela and Holland, 1984; Shinohara et al., 1989). Therefore, the stock must form fast enough and be large enough to maintain mobile magma for sufficient time for a convective system to be established, and fluid exsolution must take place at sufficient depths for the magmatic-hydrothermal fluids to become copper-rich. The overall picture is that rapid strike-slip pull-apart extension creates space for the stocks that extend from the parental batholith.

River Incision Rates in the West Agahwagon Valley

In contrast to the magmatic cooling ages recorded in the GIC and the Ertsberg pluton, the small dikes along the HEAT Road record cooling associated with erosion and unroofing. These ages make it possible to estimate the depth of burial and the river incision rates along the HEAT Road in the West Agahwagon Valley. The rates calculated here are compared to the results of Weiland and Cloos (1996) below.

The HEAT Road dike samples showing different zircon and apatite cooling ages as a function of elevation in the valley, where shallow samples closest to the GIC have magmatic cooling ages, and deeper samples from further down the road have erosion and unroofing related cooling ages. The 95-MC-HR4 and 93-MC-HR5 samples show magmatic zHe and aHe cooling ages, therefore both dikes intruded and cooled at depths less than 3.5 – 5 km (assuming a geothermal gradient of 15 – 20°C/km). In contrast, the 94-MC-HR6 sample has a magmatic crystallization age of 3.61 ± 0.15 Ma and an aHe cooling age of 2.6 ± 0.1 Ma. Assuming a geothermal gradient of 15 – 20°C/km, the river incision rate at 3.2 km elevation is 1 – 2 km/myr. Additionally, the 93-MC-HR8 sample has a zHe age, 3.0 ± 0.4 Ma, and an aHe age, 2.4 ± 0.2 Ma, that are resolvably different (they do not overlap within error), indicating that the aHe age records cooling due to erosion and unroofing. The erosion rate calculated for the 93-MC-HR8 sample at 3.1 km elevation along the HEAT Road is also between 1 – 2 km/myr.

The denudation rates calculated in this study are comparable to those reported by Weiland and Cloos (1996), who measured apatite fission track (AFT) ages from samples along the access road and the Ertsberg-Grasberg mining district. The results of their study show that erosion rates were ~1.7 km/myr along the south flank of the range, and <0.7 km/myr at the crest of the mountain range. They attribute the difference in erosion rates to the orographic precipitation effect: rainfall decreases from 11 m/yr along the flank of the mountain to 3 m/yr at the crest of the mountain. A major difference between the Weiland and Cloos (1996) study and this study is sample location: the HEAT road samples come from a valley in the highlands, whereas the access road samples come from a ridge along the southern flank of the mountain range.

CONCLUSIONS

1. Thermochronology results from throughout the Ertsberg-Grasberg mining district indicate that intrusions experienced rapid cooling, even at depths of greater than 2 km. A vertical profile between 3.9 and 1.8 km elevation in the Ertsberg pluton

records cooling rates between 4 – 1 °C/10kyr, which are similar to those recorded in the deeper parts of the GIC.

2. Rapid cooling rates observed throughout the mining district, including in the GIC (3 km^3) and Ertsberg pluton (10-20 km^3) and in the smaller volume North Grasberg plug and Wanagon Sill (<<1 km^3), indicate geothermal gradients in the country rock was cold prior to intrusive activity. Steep lateral thermal gradients, on the order of ~150°C/100 m, are inferred to be a significant contributing factors to ore formation, as they govern the efficiency of copper-rich hydrothermal fluid generation and restrict the volume of sulfide deposition.
3. An additional advantage of thermochronologic dating in a young mining district is the possibility of differentiating between magmatic cooling and cooling associated with unroofing of the mountain belt. In the Carstenszweide valley, the AB1-10-01 samples record magmatic aHe cooling ages, suggesting they have not been deeply buried. In contrast, the HEAT road dikes record cooling associated with valley incision. Based on the zHe and aHe ages, the incision rate in the West Agahwagon valley is 1 – 2 km/myr.

Chapter 6: Garnet U/Pb Geochronology of the Dom and Kucing Liar Skarns

INTRODUCTION AND MOTIVATION

One of the questions in the refinement of genetic models for hydrothermal skarn ore systems concerns the timing and duration of hydrothermal activity. Traditional approaches to dating skarn systems include zircon U/Pb dating of associated intrusions (e.g. Park et al., 2013), biotite and adularia K-Ar dating (e.g. Theodore et al., 1978; Hastings and Harold, 1988), and muscovite and phlogopite Ar/Ar dating (e.g. Park et al., 2013). Another approach is to directly date the ore minerals; examples include molybdenite Re-Os dating (e.g. Jingwen et al., 1999; Peng et al., 2006) and scheelite Sm-Nd dating (e.g. Yang et al., 2014). Recent studies have also focused on dating hydrothermal zircons (Dong-Deng et al., 2015; Zhao et al., 2016), and hydrothermal titanite (Hu et al., 2014; Chelle-Michou et al., 2015) using the LA-ICPMS U/Pb method. While these technique place constraints on the time of skarn formation, they provide little information on the duration of hydrothermal activity. As the skarn mineral assemblage is the primary controlling factor for which isotopic dating system can be applied to a deposit, and garnet is a ubiquitous mineral in calc-silicate skarns, the garnet U/Pb ICP-MS dating technique may provide a new opportunity to date skarn formation.

The newly developed LA-ICP-MS garnet U/Pb dating technique is discussed in Chapter 3, where robust and precise ages are reported for eight Big Gossan andradite garnets. Duplicate samples gave reproducible ages, and eight samples were in excellent agreement with external age constraints. This chapter presents the results of a reconnaissance study to date the other skarns in the district. J. Richard Kyle selected one sample from the Ertsberg skarn, Ertsberg East Skarn System, and Kucing Liar skarn, and two samples from the Dom skarn (sample locations shown in Figure 6-1). Ages were successfully measured for Dom and Kucing Liar, but results for the Ertsberg and the Ertsberg East skarn were unsuccessful. Uranium concentration appears to be the critical factor: U concentrations for the Dom and Kucing Liar samples are between 1 to 30 ppm, and for the Ertsberg and Ertsberg East Skarn samples are between 0.1 to 2 ppm. In comparison, the U concentrations measured in the Big Gossan garnets were between 20 to 100 ppm. Overall, the age results show that the garnet U/Pb chronometer can be a useful tool for dating skarn garnets.

Rare earth element (REE) patterns were analyzed for each of the garnet samples in order to better understand the characteristics of garnets with measurable U/Pb ages. Additionally, an attempt was made to distinguish between mineralized contact skarns (local exchange) and hydrothermal skarns (injection of fluids from unseen sources): a hydrothermal skarn forms as magmatic-hydrothermal fluids move through carbonate rocks, resulting in reaction of carbonate and production of calc-silicate skarn minerals (Einaudi et al., 1981; Meinert et al., 2003). Dissolution and vug formation are common in hydrothermal skarns. A contact skarn forms as a result of metasomatic exchange at the contact between an intrusion and the sedimentary wall rock. In contact skarns, alteration in the intrusion is termed endoskarn, whereas alteration of the wallrock is termed exoskarn.

The results of the REE analysis show that each skarn garnet has a different REE pattern. These variations may be attributed to differences in the REE contents of the sedimentary host rocks or differences in the REE contents of the hydrothermal fluids. Hantsche (2013) found that REE patterns in anhydrite record a chemical evolution during hydrothermal fluid flow along a single pathway, which may also explain the observed spatial variations in U concentration between garnet samples. Based on the results of the dating and the REE analysis, the best predictors of success for garnet U/Pb dating are andradite composition and high U concentration.

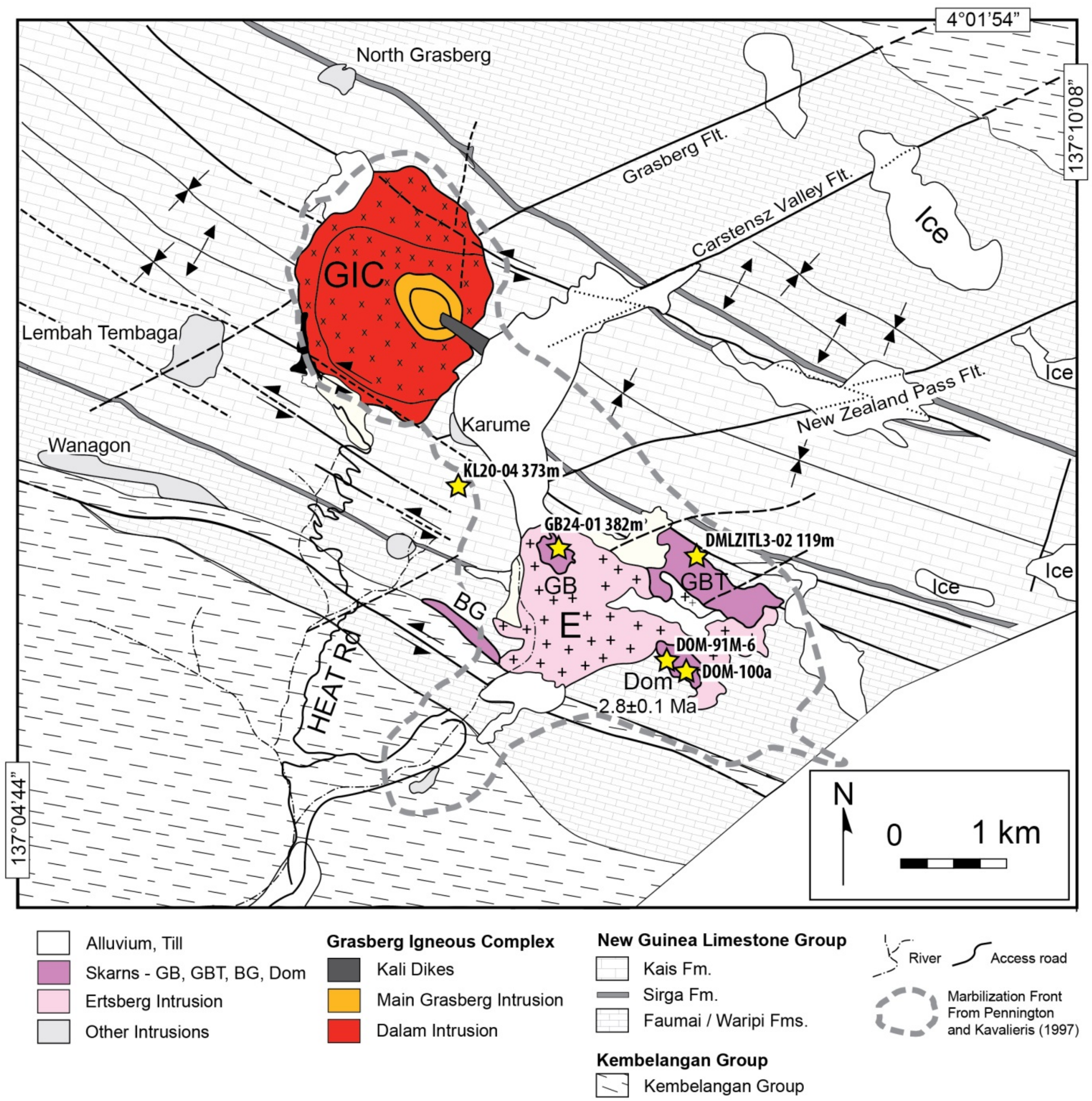

Figure 6-1. Simplified geologic map of the Ertsberg-Grasberg mining district showing drill hole collars/ outcrop locations for five garnet samples. Modified from Paterson and Cloos (2005). Skarns: GB - Gunung Bijih (Ertsberg), GBT - Gunung Bijih Timur (Ertsberg East), BG - Big Gossan.

ANALYTICAL TECHNIQUES

Large garnets (0.1-0.5 cm in size) were separated from the samples using a chisel and the fragments were inspected to avoid inclusions. Five to 12 grains were selected from each sample, mounted in epoxy, and polished to expose a clean face of the garnet rim. BSE images were collected in order to characterize the chemical composition and zoning in the garnet rims.

Garnet U/Pb analyses were completed at the University of Texas at Austin, using a single collector ThermoFisher Element2 ICP-MS with an attached PhotonMachine Analyte G.2 193 nm ArF Excimer Laser and large-volume Helex sample. The method of Seman et al. (in review) was used to acquire data: garnets were ablated for 10 s (10 Hz repetition rate, 6 mJ energy, 17% beam attenuation, resulting in a fluence rate of 1.67 J/cm^2) using a large 110 μm spot size in order to maximize count rates. The instrument was tuned in order to maximize ^{238}U counts and minimize the interferences from oxide masses (UO <0.5%).

As discussed in Chapter 3, standardization protocols for LA-ICPMS garnet U/Pb dating are still being fine-tuned, therefore data reduction was completed twice: once using a Mali andradite garnet primary standard (Seman et al., in review) and once using GJ1, a Sri Lankan zircon primary standard. Even though zircon is not a matrix-matched standard, the use of wide laser pits (which minimize the effects of downhole fractionation) and the uniform U distribution seem to make GJ1 a better standard for Ertsberg-Grasberg district garnet samples at present. As such, the ages reported here were reduced using GJ1 as a primary standard.

Data was reduced using the Iolite software package (Paton et al. 2011) and ages are calculated using Isoplot v.4 (Ludwig, 1998). Ages were calculated using a linear regression in Tera-Wasserburg space, where the lower intercept and its uncertainty are reported as the sample age (Tera and Wasserburg, 1972).

RESULTS

Garnet U/Pb Geochronology

Five samples from Dom (n=2), Ertsberg (n=1), Ertsberg East (n=1), and Kucing Liar (n=1) were tested for U/Pb dating, and ages were successfully measured for samples from Dom and Kucing Liar sample (Figure 6-2). For each garnet sample, 50 laser spot analyses were distributed across three to six of the mounted garnets (wherever crystals were sufficiently large, spots were placed on three garnets; for samples with smaller crystals (<1 mm) the spots had to be distributed over a larger number of garnets). Reported ages and errors are lower intercept ages from Tera-Wasserburg Concordia diagrams. For the Dom and Kucing Liar samples, all of the data points fall along a single mixing line, indicating that at the 1-5 mm scale all of the spots are recording a single growth event.

Dom Skarn

The Dom skarn outcrops between 4100 – 4300 m elevation in the Ertsberg-Grasberg Mining District, approximately 1 km southeast of the original Ertsberg discovery, and 500 m south of the Ertsberg East Skarn System (Mertig et al., 1994). The ore body contains 5.2 million tonnes at 0.66% Cu and 0.56 ppm Au (assuming a 0.5% Cu cutoff grade; Leys et al., 2012), and is elliptical in map view. The Dom skarn is hosted in the Faumai and Lower Kais Formations. The formations of the New Guinea Limestone Group are metamorphosed to marble in the area proximal to the Ertsberg pluton (the width of the marble zone varies between 500 m to 1 km around the pluton). The ore body is bounded on the east, west, and south sides by faults, which Mertig (1995) interpreted as syn- to post-mineralization. The mineralogy of the Dom skarn includes a monticellite-rich, high temperature zone closest to the Ertsberg intrusion, and a garnet – magnetite ± chalcopyrite zone further to the south.

Two samples from garnet – magnetite ± chalcopyrite zone of the Dom skarn were dated: DOM-91M-6 contains greenish-orange massive garnets, with chalcopyrite filling vuggy space, from the Faumai Formation, and DOM-100a contains greenish-orange garnets that occur replacing a platy foram from the lower Kais Formation. The Tera-Wasserburg lower intercept ages are 2.8 ± 0.1 Ma (x=3 garnets, n=50 spots,) for DOM-91M-6 and 3.3 ± 0.5 Ma (x= 6 garnets, n=50 spots) for DOM-100a (see Table 6-1 and Figure 6-3).

The two ages measured for the Dom skarn overlap within error, however the precision for sample DOM-91M-6 is much better than for sample DOM-100a. The DOM-91M-6 sample has a Tera-Wasserburg diagram with small error ellipses and a good spread in the data points, whereas the DOM-100a sample has larger and more erratic error ellipses. The range of U concentrations in the DOM-91M-6 sample is between 8 to 49 ppm, with an average of 18 ppm. The range of U concentrations for the DOM-100a sample is between 0.5 and 5 ppm, with an average of 2 ppm. Backscattered electron (BSE) images also show that the DOM-91M-6 sample is relatively inclusion free (with the exception of a sulfide inclusion that was easily spotted in reflected light and avoided during laser ablation), whereas the DOM-100a sample has many dark inclusions of pyroxene (based on qualitative EDS analysis) (Figure 6-4). Based on these observations, the age from the sample with the higher U concentration and the smaller error ellipses in Tera-Wasserburg space, DOM-91M-6, is taken as the age of formation for the Dom skarn.

Table 6-1. Garnet U/Pb Samples from Dom, Kucing Liar, Ertsberg, and Ertsberg East

Ore Zone	**Sample**	**Description**	**Easting**	**Northing**	**Elevation**	**Unit**	**Age (Ma)**	**[U] (ppm)**	**[Th] (ppm)**	**Garnet Color**
DOM	DOM-91M-6	mass Grd garnet with 25% cp in pores + minor qz, he	737,052	9,547,977	4,006	Faumai?	2.8±0.1	10-30	1-4	Greenish-Orange
DOM	DOM-100a	platy foram replacement Grd garnet with pore-fill cp, qz, and he	736,992	9,547,991	3,988	lower Kais	3.3±0.5	1-5	0.1-2	Greenish-Orange
Kucing Liar	KL20-04-373	massive Grd garnet	734,623	9,549,888	2,792	Kke	4.1±1.0	5-10	1-15	Green
Ertsberg	GB24-01-382	mass And garnet within fine-grained endoskarn in Te with epidote alteration-garnet overgrown by pale lavender coarse anhydrite	735,837	9,549,185	3,481	Ertsberg Diorite	NA	0.1-0.8	<1	Light and Dark Yellow
Ertsberg East	DMLZITL3-02-119	2-4 mm Grd garnet with pore-fill sulfides, he, minor qz	737,575	9,549,315	2,566	Waripi	NA	0.1-2	<1	Greenish-Yellow

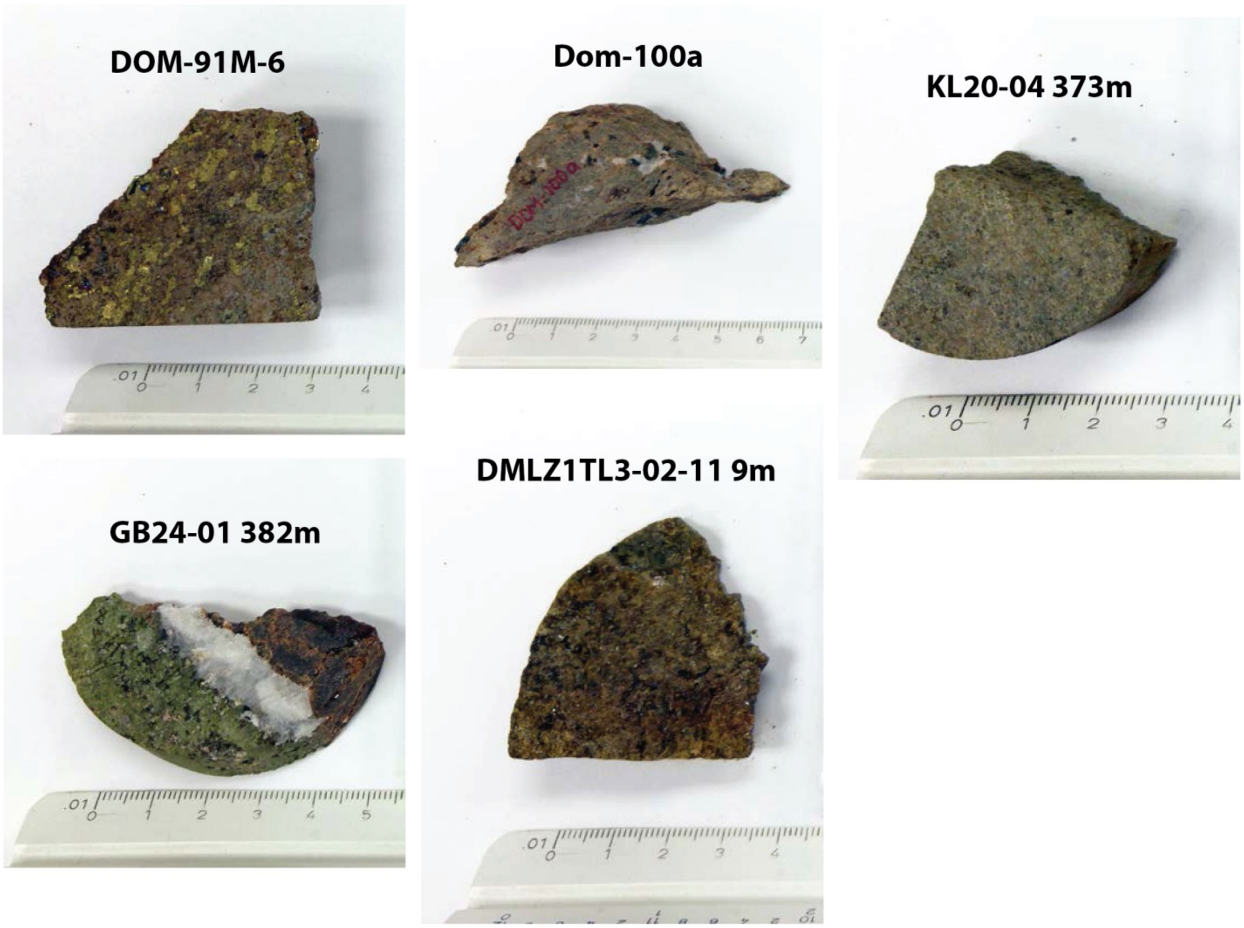

Figure 6-2. Photos showing the garnet samples dated using the LA-ICP-MS U/Pb method. Garnets were separated from each sample using a chisel, mounted in epoxy, and polished. Scale bar is in cm.

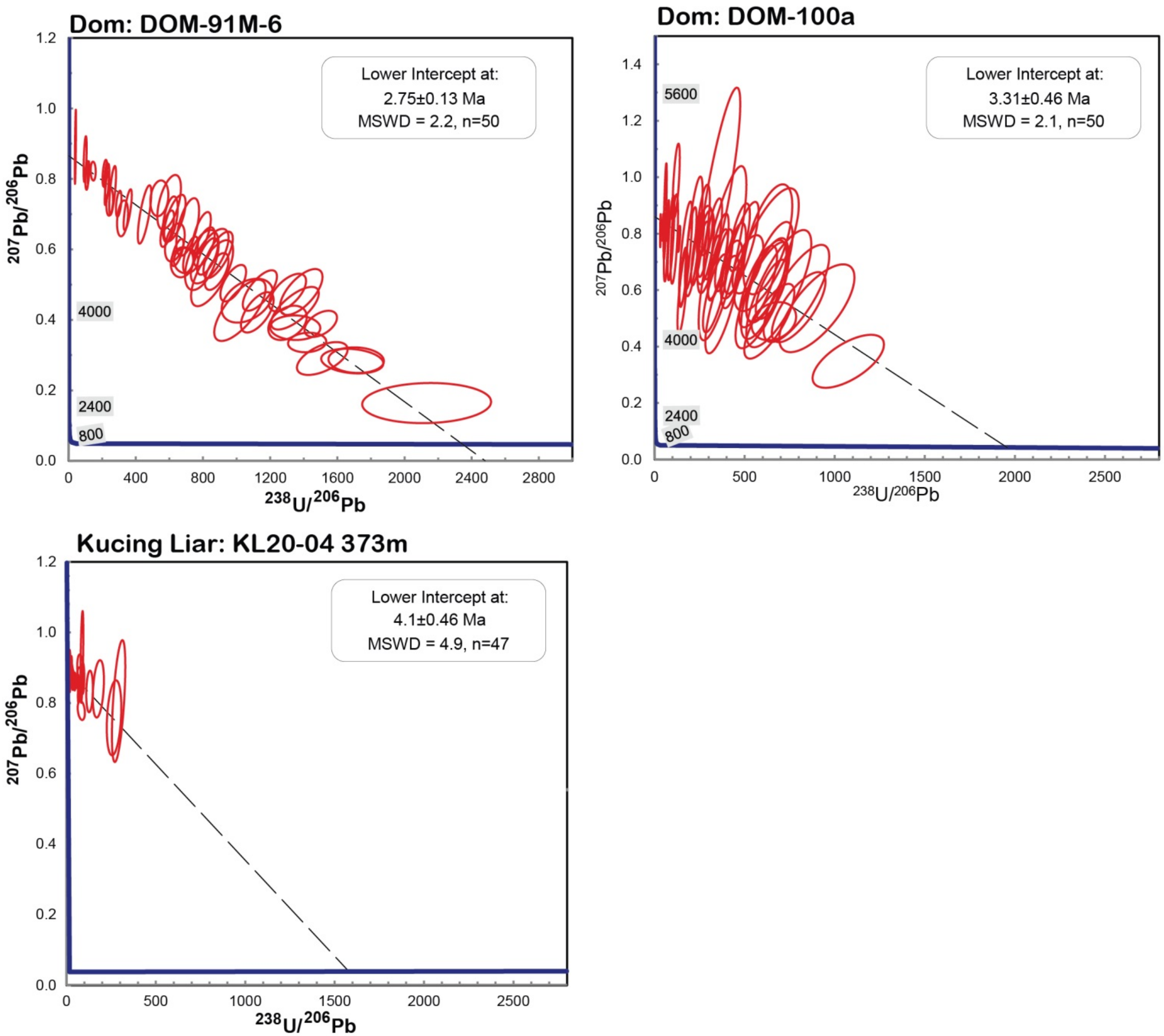

Figure 6-3. Tera Wasserburg plots for the three garnet U/Pb samples that produced successful ages. The two ages for the Dom skarn overlap within error, however given that the DOM-100a sample has significantly lower U concentrations, the DOM-91M-6 is taken as a better age for the Dom skarn. Data-point error ellipses are 2σ.

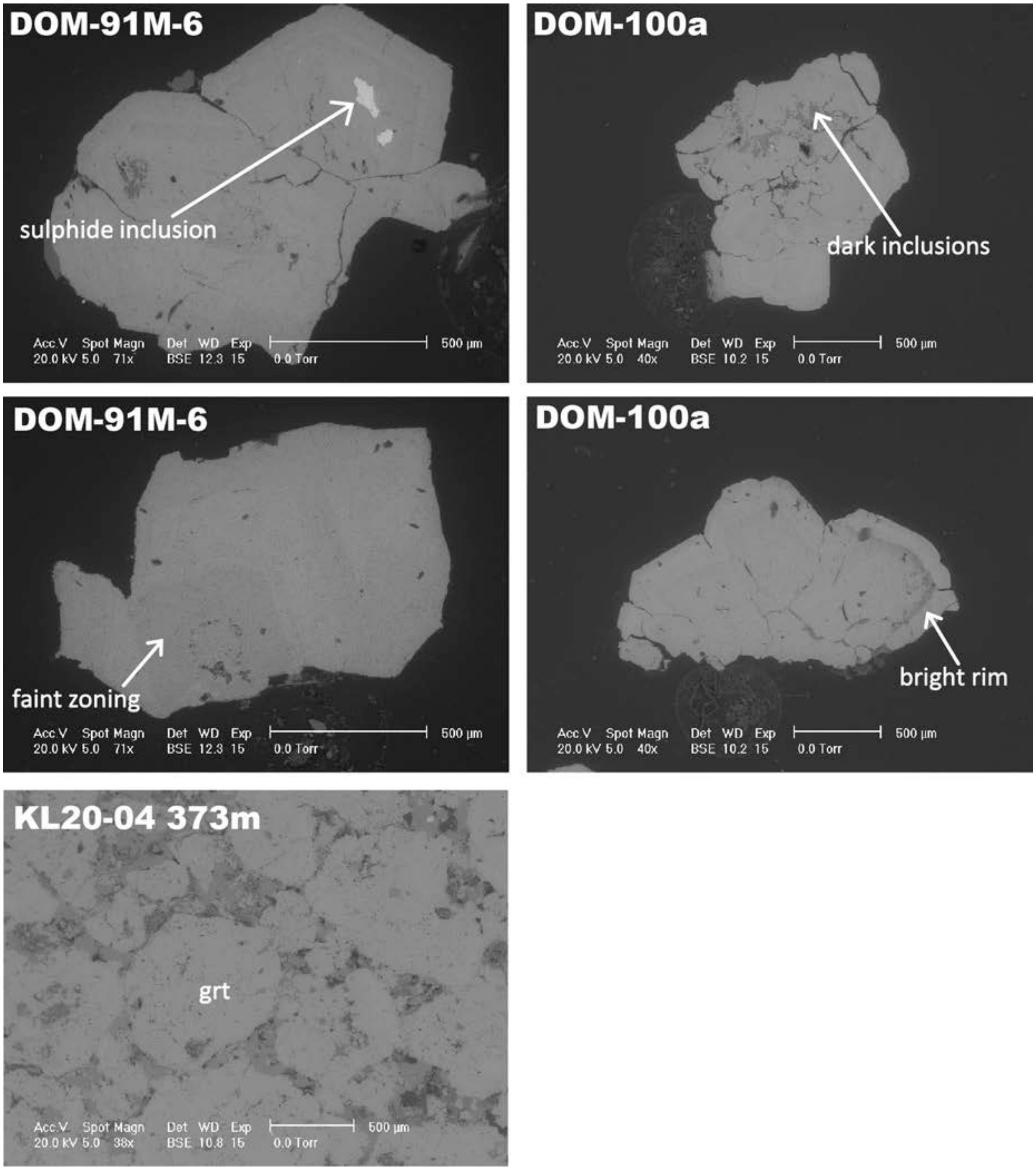

Figure 6-4. Backscattered Electron Images (BSE) of dated garnets.

Kucing Liar Skarn

The Kucing Liar skarn occurs to the southwest of the Grasberg Igneous Complex, and contains 1.7 billion tonnes of ore at 0.97% Cu and 0.82 ppm Au (assuming a 0.5% Cu cutoff grade; Leys et al., 2012). The ore body extends for 1.6 km along strike, ~800 m down-dip, and between 50 to 700 m thick. New (2006) reported phlogopite $^{40}Ar/^{39}Ar$ ages (3.41 ± 0.04 Ma and 3.27 ± 0.03 Ma), biotite $^{40}Ar/^{39}Ar$ ages (3.34 ± 0.02 Ma, 3.23 ± 0.04 Ma, and 3.18 ± 0.02 Ma), and muscovite $^{40}Ar/^{39}Ar$ ages (3.18 ± 0.02 Ma and 3.45 ± 0.06 Ma) for Kucing Liar skarn samples. This works indicates that Kucing Liar is the oldest hydrothermal ore system in the Ertsberg-Grasberg mining district. Garnet U/Pb age results for sample KL20-04 373m has a garnet U/Pb age of 4.1 ± 1.0 Ma (n=49, garnets=4), which is consistent with the early timing of the skarn. The large uncertainty on the garnet U/Pb age is due to the low U concentration (1 ppm) and the high relative proportion of common lead (see Tera-Wasserburg diagram in Figure 6-3). Given the large uncertainty of the garnet U/Pb age, the Ar/Ar ages better constrain the timing of the Kucing Liar skarn at ~3.4 to 3.2 Ma.

Ertsberg Skarn and Ertsberg East Skarn System

The Ertsberg skarn was the first to be mined in the district, and contained 60 million tonnes of ore at 1.68 % Cu and 0.57 ppm Au (assuming a cutoff grade of 0.1% Cu; Leys et al., 2012). The Ertsberg skarn has been interpreted as a roof pendant skarn body in the Ertsberg pluton (e.g. Pollard et al., 2005). As such, it is unknown whether the Ertsberg skarn pre-dates the Ertsberg pluton, or formed coeval with the intrusion.

Garnets from sample GB24-01 382m are massive, and occur within fine-grained endoskarn with epidote and anhydrite. In all cases the garnets (x=3 garnets, n=40 spots) had a range of U concentrations between of 0.1 to 1 ppm, with an average U concentration of 0.4 ppm. The low U concentrations are exacerbated by the prevalence of inclusions in the garnet, as shown in the BSE images in Figure 6-5. As there is little to no radiogenic lead in the garnets (see Figure 6-5), no age was obtained.

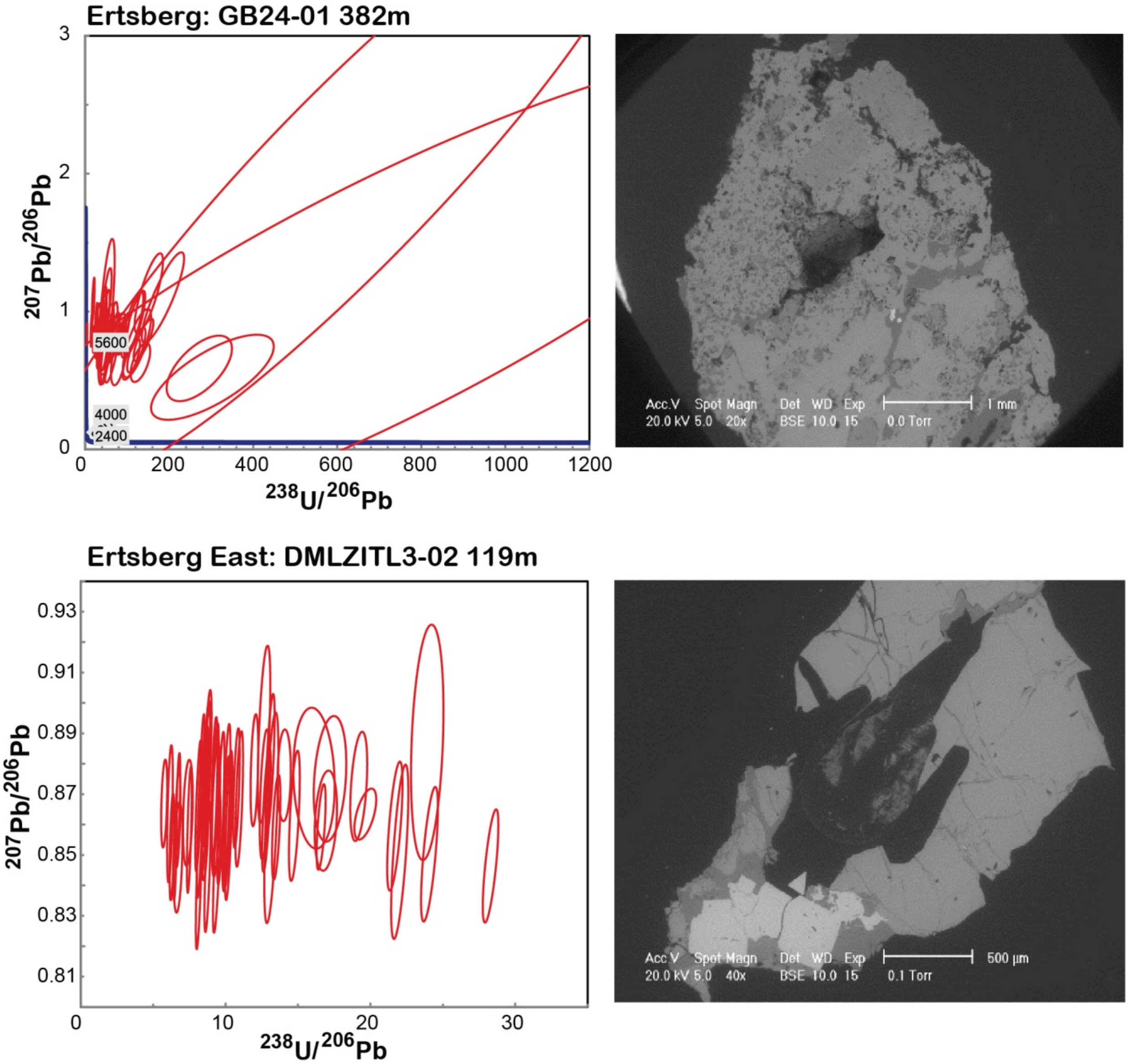

Figure 6-5. Tera-Wasserburg diagrams for the garnet U/Pb samples that were not suitable for dating. Note that the scale is different from figure 6-2. Data-point error ellipses are 2σ. The majority of the data points show that the lead composition is entirely common lead. Backscattered electron images of dated garnets are shown on the right.

The Ertsberg East Skarn System is the largest ore body associated with the Ertsberg pluton, consisting of four vertically stacked ore zones; Gunung Bijih Timur (Ertsberg East) proper, Intermediate Ore Zone (IOZ), Deep Ore Zone (DOZ) and Deep Mill Level Zone (DMLZ). Collectively, the GMT complex is one of the largest economic Mg-rich skarns in the world (Rubin and Kyle, 1998): mineralization is 1.5 km long, ~600 m wide, and at least 1.5 km in vertical extent. Using a cutoff grade of 0.5% Cu, the ore body contains ~1 billion tonnes of ore at 1.17% Cu and 0.76 ppm Au (Leys et al., 2012). For the 3 garnets analyzed (n=40 spots) the U concentrations range between 0.1 – 4 ppm, with an average U concentration of 2 ppm. A representative Tera-Wasserburg diagram for the Ertsberg East skarn samples is shown in Figure 6-5. As the error ellipses are focused at or near the common lead value of 0.86, there is little to no radiogenic lead in the garnet and no age was obtained.

Garnet Rare Earth Element Analysis

Rare earth element (REE) concentrations were measured for each of the dated garnet samples, and the REE patterns are normalized to chondrite (Figure 6-6; see Appendix M for garnet rare earth element results). The results show that the garnets have higher LREE concentrations relative to the HREE. This is unusual compared to most metamorphic garnets, which typically concentrate the HREE (e.g. Dziggel et al., 2009; Jedlicka et al., 2015), but similar to REE patterns measured in andraditic skarn garnets from the Crown Jewel gold deposit (Gaspar et al., 2008) and from the Beinn an Dubhaich skarn aureole (Smith et al., 2004). For example, the Kucing Liar garnets show that the LREE are 100 times chondrite, whereas the HREE are 10 times chrondrite. The Kucing Liar patterns show lower La, but otherwise there are no anomalies. This is in contrast to the Big Gossan REE patterns, which show a distinct positive Eu anomaly, although the LREE are still high relative to the HREE. The Dom shows a similar pattern, although there is only a small positive Eu anomaly in some of the spots, and an overall rounded pattern. The Ertsberg and Ertsberg East skarn garnet contain very low concentrations of

REE: the LREE are only slightly enriched relative to chondrite and the HREE are near detection limits.

DISCUSSION

Skarn Garnet REE Patterns

In order to explain the origin of the REE patterns measured in the skarn garnets, the garnet REE patterns are compared to analyses of the sedimentary host rocks, including the Kais and Waripi, and the Ertsberg pluton (Figure 6-7). The sedimentary wall rock and the magmatic REE patterns all show La/Yb ratios ≥ 10 (with the exception of the Ertsberg garnets). The positive Eu anomaly measured in the garnets suggests that magmatic-hydrothermal fluids may be the dominant source of REE for the skarn garnets. This inference is supported by experimental work done to determine the partition coefficients for Ce, Eu, Gd, Yb between an aqueous phase and a water-saturated silicate melt (2 kbar, 800°C) (Flynn and Burnham, 1978). The results show that, while the REE generally behave similarly, the fluid will be enriched in LREE relative to HREE (hydrothermal fluid La/Yb ~ 2.5 relative to the melt) and have a large positive Eu anomaly.

The skarn garnet REE patterns also differ from the sedimentary host rocks and magmatic REE patterns with respect to La. The garnet patterns show a negative La anomaly relative to the other LREE elements. This anomaly can be explained by the presence of primary epidote in the skarns (Gière and Sorensen, 2004). Epidote group minerals have monoclinic or orthorhombic crystal symmetry, with a general chemical formula of $X_2Y_3Z_3(O,OH,F)_{13}$, where X=Ca, **La**, Ce, Y, Th, Fe^{2+}, Mn^{2+}, Y=Al, Fe^{3+}, Mn^{2+}, Fe^{2+}, Ti, and Z=Si, Be. REE are accommodated into the epidote structure through the reaction:

(1) $Ca^{2+} + Fe^{3+} \leftrightarrow REE^{3+} + Fe^{2+}$

The co-existence of garnet and epidote can explain the negative La anomaly in garnet, given its preference for epidote.

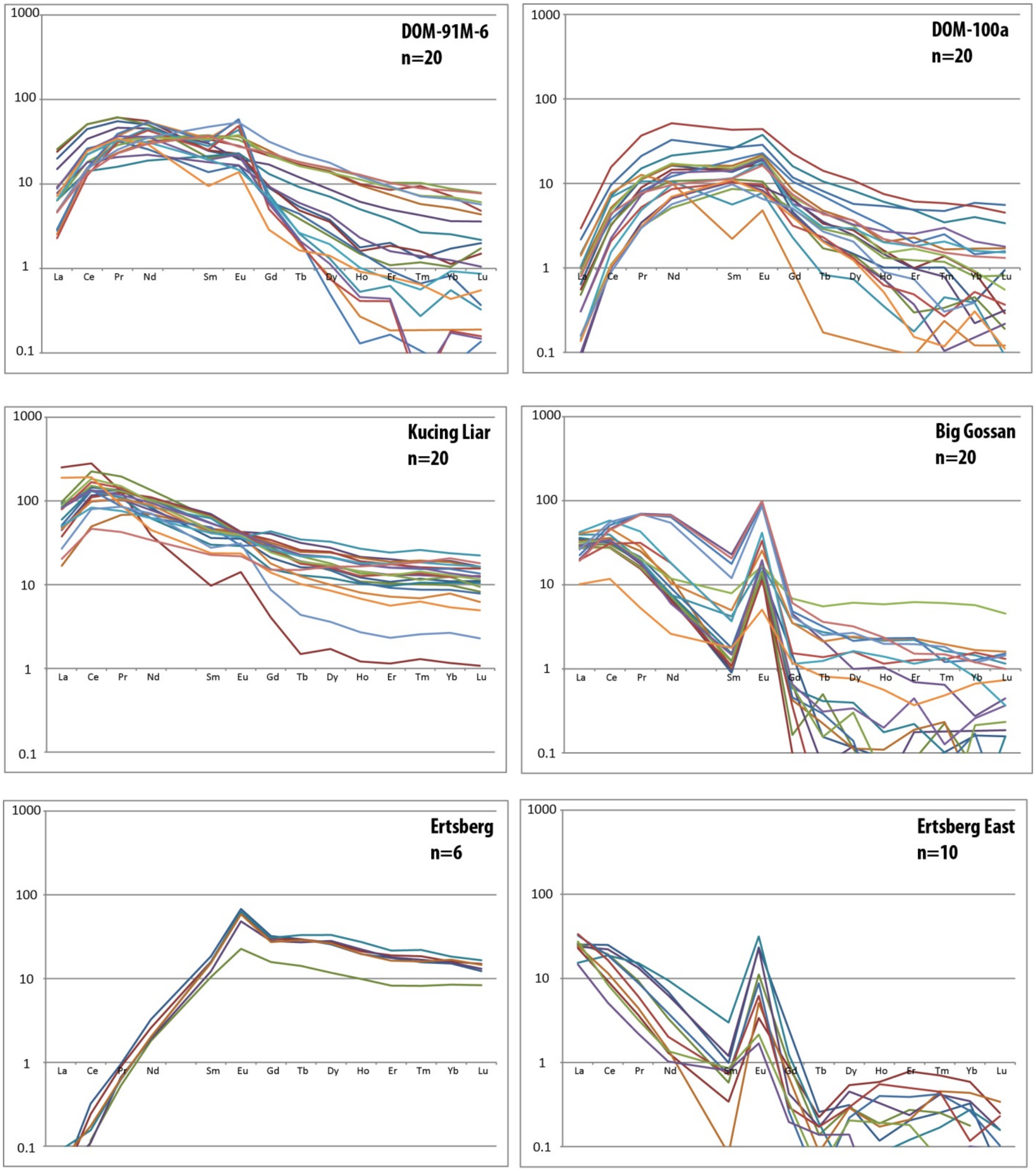

Figure 6-6. REE patterns for the six skarn garnet samples tested for LA-ICPMS U/Pb dating. The results show that with the exception of Ertsberg, the garnets have a La/Yb ratio >1. Dom, Kucing Liar, and Big Gossan show a negative La anomaly, and Dom, Big Gossan, and Ertsberg East show a large positive Eu anomaly.

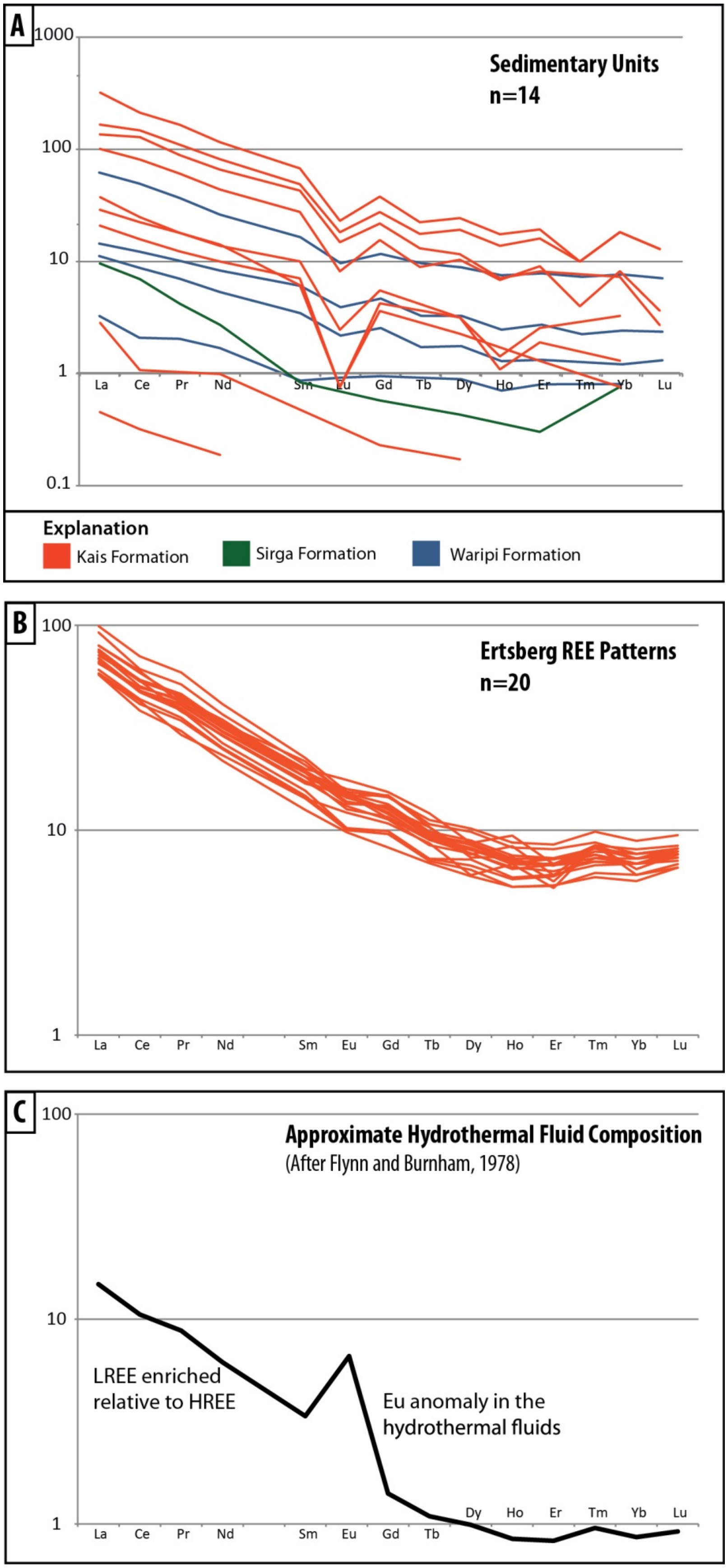

Figure 6-7. (A) REE patterns for the sedimentary units in the district (Cloos, unpublished data), (B) REE patterns for the Ertsberg pluton, (C) estimated composition of the hydrothermal fluids exsolved from a magma similar to the Ertsberg pluton. The partition coefficients, positive europium anomaly, and La/Yb ratio for the hydrothermal fluids from Flynn and Burnham (1978).

Skarn Garnet U Concentrations

The main question that arises from the garnet U/Pb dating results is why do some of the skarn garnets in the district contain high U concentrations, whereas other skarn garnets have low U concentrations. There are two potential sources of U available during the growth of a hydrothermal skarn garnet: the sedimentary host rock and/ or the hydrothermal fluids. Given that U^{6+} is a fluid mobile element in oxidizing fluids, if U is present in the magma it can strongly partition into the hydrothermal fluids (Kessel et al., 2005; Bali et al., 2011**)**.

Based on 14 geochemical analyses of the Kais (n=9) and Waripi (n=5) Formations, and 20 geochemical analyses of the Ertsberg intrusion, the average U concentrations in the sedimentary units are 2 – 3 ppm and the average U concentration in the Ertsberg intrusion is 3 ppm (Cloos, unpublished data). Given that the average U concentrations in garnets range from 20 – 100 ppm for the Big Gossan skarn (see Chapter 3), to 10 – 30 ppm in the Dom skarn, and 5 – 10 ppm in the Kucing Liar skarn, the U must be concentrated in the garnet phase relative to other skarn minerals. However, based on the results of this study there is also evidence that the garnet U concentration varies between skarn systems, and internally within the skarn body; therefore there must be variations in the U budget of the hydrothermal fluids. Potential factors that may impact the availability of U in the hydrothermal fluid include: (1) variations in the U concentration of the parental magma through time, or (2) variations in the U concentrations in the hydrothermal fluid as it moves along a flow path (e.g. Hantsche, 2013) (see Figure 6-8).

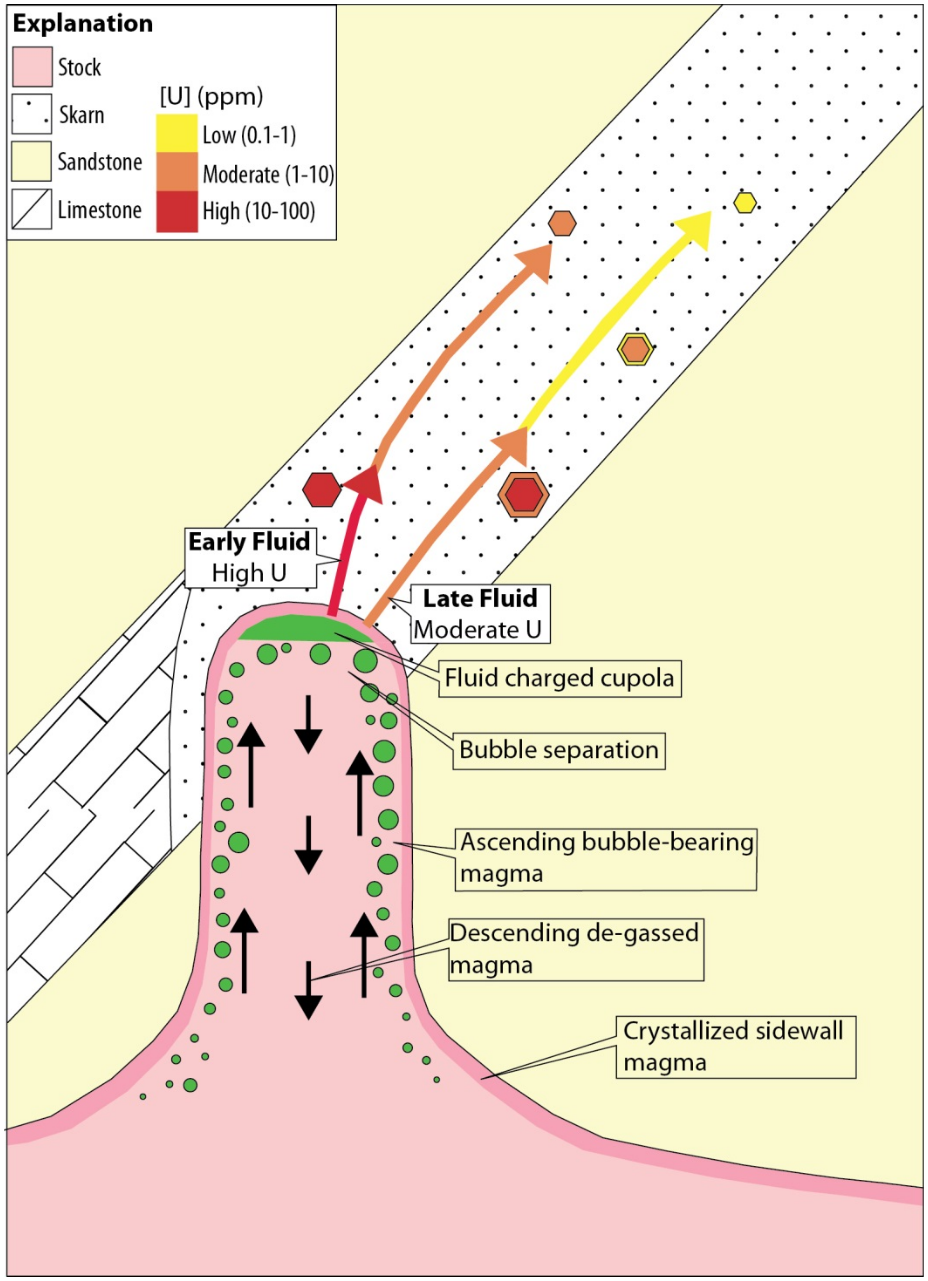

Figure 6-8. Schematic diagram illustrating the mechanisms responsible for variable U concentrations in skarn garnets. Copper-rich, bubble-bearing magma ascends along the sides of a stock until reaching a point where the bubbles separate and collect in the cupola at the top of the stock and degassed magma descends. Copper-rich fluids may rise, either through infiltration fluid flow, or during vein forming events. In the case where the fluids encounter carbonate units, a self-generating karstic-style permeability may develop, and calc-silicate skarn formation occurs. U concentration will vary between batches of hydrothermal fluids, as a function of distance along a flow path, and as a function of crystallization temperature. After Cloos (2001).

Prospective Garnets

Based on the results of this study, the most promising garnets for U/Pb dating are those that have sufficiently high U concentrations to produce measurable amounts of radiogenic lead. For the dated garnet samples from the Ertsberg-Grasberg mining district, the threshold U concentration for obtaining a measurable garnet $^{206}Pb/^{238}U$ ages is ~1-5 ppm. The average garnet compositions for each skarn composition were estimated based on EMPA studies by Mertig (1995, Meinert (1997), and New (2006), and the results suggest that andradite-rich composition garnets ($Ca_3Fe_2Si_3O_{12}$) (e.g. Big Gossan garnets) are the most promising for high U concentrations. Grandite composition garnet, which is a solid solution between andradite and grossular (e.g. Dom and Kucing Liar), can also have sufficiently high U concentrations to measure a garnet U/Pb age. When selecting samples for geochronology, the most promising garnets are dark red to black; however garnets that are greenish orange should also be tested. There was no success dating yellow garnets from Ertsberg or Ertsberg East.

CONCLUSIONS

Five samples from the Dom, Kucing Liar, Ertsberg, and Ertsberg East skarns provided by J. R. Kyle were tested for garnet U/Pb dating. Ages were successfully measured for Dom (2.8 ± 0.1 Ma) and Kucing Liar (4.1 ± 1.0 Ma). The results show that U concentrations from ~1 – 5 ppm are required in order to measure a garnet U/Pb age, otherwise the measured lead is nearly end-member common lead. The age obtained for the Dom skarn (2.8 ± 0.1 Ma) indicates that it formed concurrently with emplacement and cooling of the Ertsberg pluton, from 3.1 to 2.8 Ma.

Chapter 7: Volume of Magma and Hydrothermal Fluids Required to form the Ore Deposits in the Ertsberg-Grasberg Mining District

INTRODUCTION AND APPROACH

There are few well-constrained estimates of the duration of magmatic-hydrothermal activity responsible for porphyry copper ore formation: the best examples are from Bajo de la Alumbrera (Harris et al., 2008) and El Teniente (Maksaev et al., 2004), where zircon U/Pb crystallization ages of intrusions and biotite $^{40}Ar/^{39}Ar$ cooling ages of hydrothermal alteration constrain the maximum duration of the system, and from Chuquicamata (Ballard et al., 2001), where zircon U/Pb dating of intrusions indicates that the magmatic-hydrothermal systems were active episodically (as indicated by overprinting relationships) over time spans of 1 to 2 million years. However, in most cases the duration of a single episode of magmatic-hydrothermal fluid flow is not well resolved, and the duration of ore formation is rarely constrained by well-defined cross-cutting relationships, as is the case for the Grasberg porphyry copper deposit (see Chapter 1).

Duration estimates for the major ore deposits in the Ertsberg-Grasberg mining district, evaluated in conjunction with the tonnage and grade information reported by Leys et al. (2012), make it possible to constrain the volume of magma required to exsolve the flux of hydrothermal fluids required to transport metals for each of the ore deposits in the district (Table 7-1). Furthermore, assuming a half-sphere geometry for a fluid-charged cupola (Cloos, 2001) as the optimal configuration for efficient concentration of copper-rich hydrothermal fluids, it is possible to estimate the number of times a cupola must be charged with hydrothermal fluid (Table 7-2). To the extent that draining occurs as a result of extension fracturing in the cupola driven by earthquake related fault slip, the number and recurrence rate of earthquake events can also be estimated. Ore-forming veins form when hydrothermal fluids jet into the overlying rock, expand, and cool. Some deposits have little veining, whereas others have substantial amounts of vein-hosted copper. The Grasberg ore body is estimated to have a 50/50 ratio of disseminated to vein-hosted copper sulfide (Cloos, pers. comm.). Geometries and dimensions for the cupola, stock, and batholith are shown in Figure 7-1.

The best age constraints for the maximum duration of magmatic-hydrothermal fluid flow are in the Grasberg porphyry copper deposit, where the pre-mineralization MGI is cross-cut by the post-mineralization Late Kali Dike (maximum duration of ~100 to 220 kyr, see Chapter 1). Garnets from the Big Gossan skarn record a duration of approximately 200 kyr (see Chapter 3). As such, the discussion below will focus on the Grasberg and Big Gossan ore bodies. Age constraints for Kucing Liar, the Ertsberg porphyry copper deposit, the Ertsberg skarn, and the East Skarn System include zircon U/Pb crystallization ages of nearby intrusions (see Chapter 4), and in the case of Kucing Liar, biotite $^{40}Ar/^{39}Ar$ ages from New (2006). Based on these ages, it is estimated that ore formation occurred in four distinct pulses, each less than approximately 200 kyr.

Calculations for the amount of copper and gold in each ore body, the volume of hydrothermal fluids required to transport the metals, the volume of magma required to exsolve the magmatic-hydrothermal fluid, and the number of cupola refilling events were based off of the tonnage and grade information reported by Leys et al. (2012). It was assumed that all fluid generation and mineral precipitation reactions are 100% efficiency. In order to account for all of the Cu sulfide and Au mineralization within the ore system, and not just the part of the ore body that would be considered economic to mine, this discussion will use the tonnage and grade values calculated using a 0.1 wt.% Cu cutoff grade (See Table 7-1).

Table 7-1. Volumes of magma and hydrothermal fluid required to form the ore bodies in the Ertsberg-Grasberg Mining District.

Total tonnage (0.1% Cu cutoff grade)									L fluid required to deposit Cu*			L fluid required to deposit Au*		
Grade Information from Leys et al. (2012)									25	3000	11000	0.1	2.5	8
Deposit	million tonnes	Cu (%)	Au (ppm)	Au (%)		Cu (kg)	Au (kg)	**Relative Size (%)**	min	mean	max	min	mean	max
Ertsberg East	3027.9	0.59	0.49	4.9E-05		1.79E+10	1.48E+06	**19**	6.50E+14	5.41E+12	1.48E+12	1.35E+13	5.40E+11	1.69E+11
Ertsberg	134.3	0.83	0.3	0.00003		1.11E+09	4.03E+04	**1**	4.05E+13	3.38E+11	9.21E+10	3.66E+11	1.47E+10	4.58E+09
Dom	157.6	0.2	0.25	2.5E-05		3.15E+08	3.94E+04	**0.3**	1.15E+13	9.55E+10	2.60E+10	3.58E+11	1.43E+10	4.48E+09
Big Gossan	272.3	0.83	0.46	4.6E-05		2.26E+09	1.25E+05	**2**	8.22E+13	6.85E+11	1.87E+11	1.14E+12	4.55E+10	1.42E+10
Ertsberg Intrusion	3591.1	0.6	0.47	4.7E-05		2.15E+10	1.69E+06	**23**	7.84E+14	6.53E+12	1.78E+12	1.53E+13	6.14E+11	1.92E+11
Kucing Liar	3316.4	0.62	0.57	5.7E-05		2.06E+10	1.89E+06	**22**	7.48E+14	6.23E+12	1.70E+12	1.72E+13	6.87E+11	2.15E+11
Grasberg	4216.4	0.75	0.69	6.9E-05		3.16E+10	2.91E+06	**33**	1.15E+15	9.58E+12	2.61E+12	2.64E+13	1.06E+12	3.31E+11

*Assumptions:

1.1 kg/L fluid

3000 ppm Cu in fluid inclusions (Kouzmanov and Pokrovski, 2012)

2.5 ppm Au in fluid inclusions

Table 7-1. Continued.

	Mean Fluid/Rock Ratio		**Flow Rate (mean Cu)**	**Flow Rate (mean Au)**		**km_3 magma required***		
Deposit	Cu	Au	kg/yr	kg/yr	km^3 Fluid	1wt% H_2O	2wt% H_2O	3wt% H_2O
Ertsberg East	1.8	0.2	2.98E+07	2.97E+06	5.4	541	271	180
Ertsberg	2.5	0.1	1.86E+06	8.06E+04	0.3	34	17	11
Dom	0.6	0.1	5.25E+05	7.88E+04	0.1	10	5	3
Big Gossan	2.5	0.2	3.77E+06	2.51E+05	0.7	68	34	23
Ertsberg Intrusion	1.8	0.2	3.59E+07	3.38E+06	6.5	653	326	218
Kucing Liar	1.9	0.2	3.43E+07	3.78E+06	6.2	623	312	208
Grasberg	2.3	0.3	4.79E+07	5.29E+06	9.6	958	479	319

*calculated assuming mean Cu values (3000 ppm)

Table 7-2. Fluid flow rates and earthquake recurrence rates required to form the ore bodies in the Ertsberg-Grasberg Mining District.

Grade Information from Leys et al. (2012)								**# Cupola Refill events**			**Earthquakes/X Years***		
Deposit	million tonnes	Cu (%)	Au (ppm)	Au (%)		Cu (kg)	Au (kg)	r= 50m	r= 100m	r= 300m	r= 50m	r= 100m	r= 300m
Ertsberg East	3027.9	0.59	0.49	4.9E-05		1.79E+10	1.48E+06	20678	2585	96	10	77	2089
Ertsberg	134.3	0.83	0.3	0.00003		1.11E+09	4.03E+04	1290	161	6	155	1240	33482
Dom	157.6	0.2	0.25	2.5E-05		3.15E+08	3.94E+04	365	46	2	548	4385	118408
Big Gossan	272.3	0.83	0.46	4.6E-05		2.26E+09	1.25E+05	2616	327	12	76	612	16514
Ertsberg Intrusion	3591.1	0.6	0.47	4.7E-05		2.15E+10	1.69E+06	24940	3117	115	8	64	1732
Kucing Liar	3316.4	0.62	0.57	5.7E-05		2.06E+10	1.89E+06	23800	2975	110	8	67	1815
Grasberg	4216.4	0.75	0.69	6.9E-05		3.16E+10	2.91E+06	36603	4575	169	6	48	1298

Volume of Cupola (km3)		
r= 50m	r= 100m	r= 300m
0.0003	0.00209	0.05655

*assuming all fluid flow occurs through fractures

Table 7-2. Continued.

	L fluid required to deposit Cu			**kg fluid**			**Years required***			**Years required***			**kg fluid/Year****	
	25 ppm	**3000 ppm**	**11000 ppm**	**25**	**3000**	**11000**	**7x108 kg/yr rate**			**1.5X109 kg/yr rate**				
Deposit	min	mean	max	min	mean	max	min	mean	max	min	mean	max	mean	max
Ertsberg East	6.50E+14	5.41E+12	1.48E+12	7.15E+14	5.95E+12	1.62E+12	~~1020835~~	8507	2320	~~476390~~	3970	1083	29774350	8120277
Ertsberg	4.05E+13	3.38E+11	9.21E+10	4.46E+13	3.72E+11	1.01E+11	~~63697~~	531	145	~~29725~~	248	68	1857817	506677
Dom	1.15E+13	9.55E+10	2.60E+10	1.26E+13	1.05E+11	2.87E+10	~~18011~~	150	41	~~8405.3~~	70	19	525333	143273
Big Gossan	8.22E+13	6.85E+11	1.87E+11	9.04E+13	7.53E+11	2.05E+11	~~129148~~	1076	294	~~60269~~	502	137	3766817	1027314
Ertsberg Intrusion	7.84E+14	6.53E+12	1.78E+12	8.62E+14	7.18E+12	1.96E+12	~~1231234~~	10260	2798	~~574576~~	4788	1306	35911000	9793909
Kucing Liar	7.48E+14	6.23E+12	1.70E+12	8.22E+14	6.85E+12	1.87E+12	~~1174953~~	9791	2670	~~548311~~	4569	1246	34269467	9346218
Grasberg	1.15E+15	9.58E+12	2.61E+12	1.26E+15	1.05E+13	2.87E+12	~~1807029~~	15059	4107	~~843280~~	7027	1917	52705000	14374091

*2000 to 4000 ton/day (7×10^8 to 1.5×10^9 kg/year

Shinohara and Hedenquist (1997)

**assuming 200 kyr for Grasberg

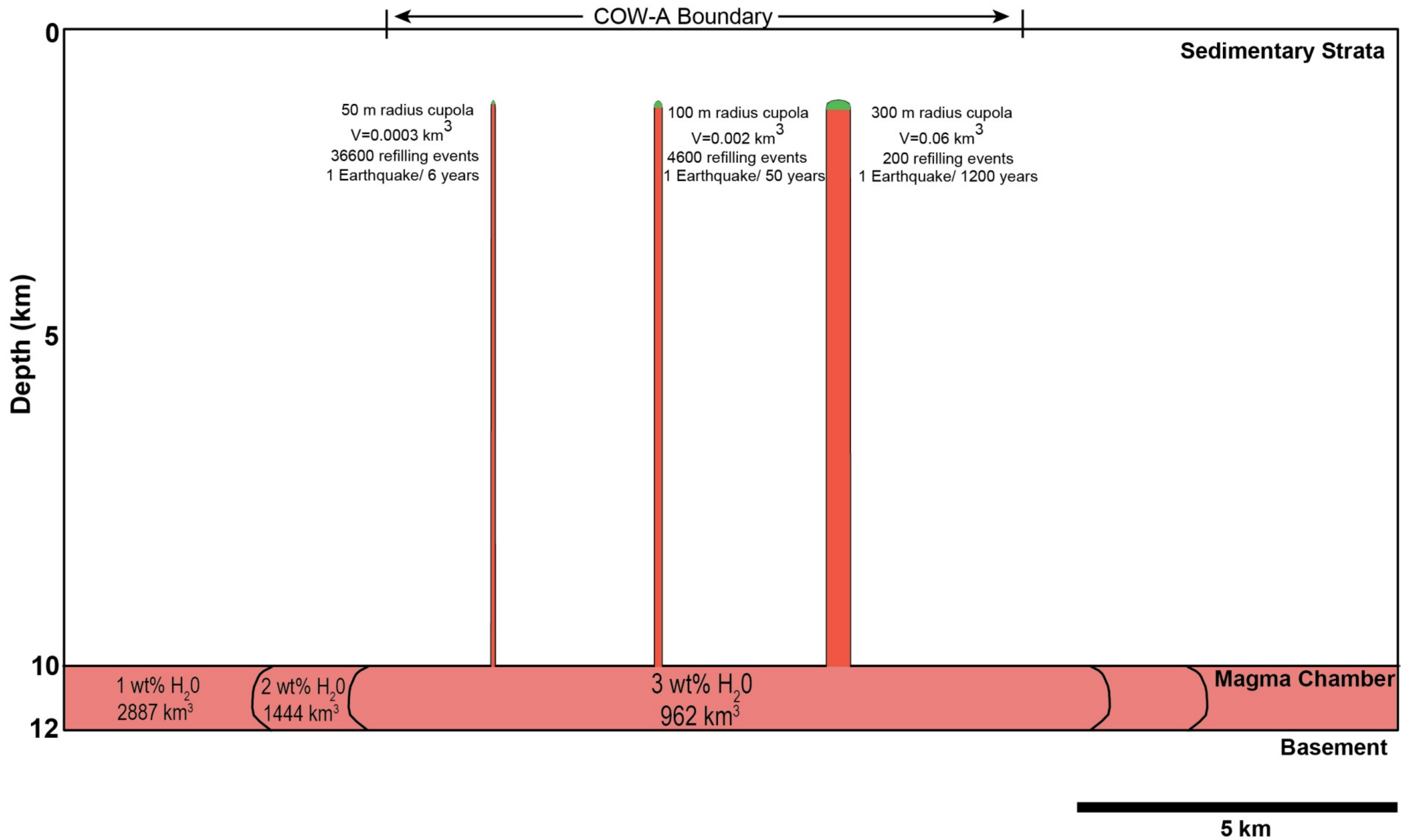

Figure 7-1. Schematic diagram showing a cross-section of a disk-shaped magma chamber and the volume of magma required to exsolve the hydrothermal fluids necessary for ore deposition. The size of the magma chamber depends on the water content of the magma. A disk-shaped, sill-geometry is assumed. Furthermore, the size of the fluid-charged cupola will govern the number of refilling events and the earthquake recurrence rates.

RESULTS

Grasberg Porphyry Copper Deposit

Leys et al. (2012) report that the supergiant Grasberg porphyry copper deposit contains 4216 million tonnes of mineralized rock, using a 0.1 wt. % Cu cutoff grade, with an overall grade of 0.75 wt.% Cu and 0.69 ppm Au. The entire mineralized system therefore contains $3.16 \cdot 10^{10}$ kg of Cu and 2.9 million kg of Au.

Ulrich et al. (1999) report the Cu and Au concentrations for 41 single fluid inclusions in quartz from the Grasberg system, measured using the LA-ICP-MS technique. The results show that the 28 brine inclusions contained 3000 ± 10000 ppm Cu and 0.26 ± 0.18 ppm Au, whereas 13 vapor inclusions contained 12000 ± 13000 ppm and 10.17±6.20 ppm Au. Kouzmanov and Pokrovski (2012) compiled a global compilation of fluid inclusion data, including alkali and metal concentration measured in single-phase, hypersaline, vapor-rich, and low salinity aqueous inclusions from 45 porphyry copper deposits. Their compilation shows that the average Cu concentration in a single-phase fluid inclusion is 3000 ppm, with a minimum of 25 ppm and a maximum of 11000 ppm. As the fluid inclusion data from Ulrich et al. (1999) and the compilation from Kouzmanov and Pokrovski (2012) are in agreement, the average value of 3000 ppm Cu is used for this discussion.

Therefore, assuming the hydrothermal fluids responsible for ore formation have a density of ~1.1 kg/L and contain 3000 ppm Cu, and Cu deposition is 100% efficient, $9.6 \cdot 10^{12}$ L of hydrothermal fluid are required to form an ore body with $3.16 \cdot 10^{10}$ kg of Cu. This is equivalent to 9.6 km^3 of hydrothermal fluid. Kouzmanov and Pokrovski (2012) report 25 ppm and 11,000 ppm as the minimum and maximum Cu concentrations observed in fluid inclusions; taking these end member values into account the volume of hydrothermal fluid may range between 2.6 and 1150 km^3. The latter is an unreasonably large volume of fluid, therefore we can rule out that the Grasberg deposit formed from hydrothermal fluids that contained 25 ppm Cu.

Forming 4216 million tonnes of ore in the Grasberg porphyry copper deposit from 3000 ppm Cu fluids required $9.6 \cdot 10^{12}$ L of hydrothermal fluid. This corresponds to a fluid/rock ratio in the Grasberg ore body was ~2 L/kg. Taking the 220 kyr maximum duration of hydrothermal fluid flow, the maximum flow rates are $4.8 \cdot 10^{7}$ kg of fluid/yr. Taking into account our preferred duration of hydrothermal fluid flow of 100 kyr, the flow rates are $1.1 \cdot 10^{8}$ kg of fluid/yr. The amount of magma required to exsolve 9.6 km^3 of hydrothermal fluid depends on the amount of dissolved volatiles in the magma: assuming that the water concentration in ore-forming magmas is 1-3 wt.% H_2O (Cloos, 2001), and the amount consumed by the growth of biotite and hornblende is negligible, then the amount of magma required to form the Grasberg porphyry copper deposit ranges from 320 to 960 km^3. It is important to note we have assumed 100% efficiency of volatile stripping from the magma and 100% efficiency for metal deposition, therefore these values are minimums.

These results are comparable to Shinohara and Hedenquist (1997), who evaluated magma degassing beneath the Far Southeast porphyry Cu-Au deposit by numerically modeling the evolution of magmatic fluid composition using a magma crystallization model. They assume a 2 km thick magma chamber at 6 km depth (150 MPa) with an initial temperature of 800°C (saturated melt composition at 30 vol. % crystals, 5 wt % H_2O and 0.2 wt % Cl) with homogeneous crystallization during early stage convection, followed by stagnation and crystallization from rim to core once 50 vol% crystals is achieved. Based on their modeling results, the rate of fluid exsolution from the intrusion while active convection occurred was between $7 \cdot 10^{5}$ to $1.5 \cdot 10^{6}$ tonnes of fluid/year. These rates are consistent with the upper range of high temperature fluid discharge for passively degassing volcanoes reported by Hedenquist (1995), between $1 \cdot 10^{8}$ to $5 \cdot 10^{9}$ kg of fluid/year. Based on the rates of Shinohara and Hedenquist (1997) it would take between 4,100 and 15,100 years to exsolve the required volume of fluid to form the Grasberg deposit. Working the problem backwards, given 9.6 km^3 of hydrothermal fluid is required to transport the metals during a maximum time period of 100 to 220 kyr, the rate of fluid exsolution from the magma was between $4.8 \cdot 10^{7}$ and $1.1 \cdot 10^{8}$ tonnes of fluid/year, which is an order of magnitude less than the rates of magma degassing reported by Shinohara and Hedenquist (1997) and Hedenquist (1995).

Big Gossan Skarn

Garnet U/Pb ages suggest a maximum duration of 200 kyr for prograde skarn formation, and therefore hydrothermal fluid flow, in the Big Gossan skarn (see Chapter 3 for discussion). Leys et al. (2012) report that the Big Gossan skarn ore body contains 272 million tonnes of ore at 0.83 wt.% Cu and 0.46 ppm Au, assuming a 0.1 wt.% Cu cutoff grade. Based on the ore grades the Big Gossan skarn contains $2.26 \cdot 10^9$ kg of Cu and $1.25 \cdot 10^5$ kg Au.

Using the same assumptions as stated for the Grasberg porphyry deposit, namely that the hydrothermal fluids have a density of ~1.1 kg/L, contain 3000 ppm Cu (Kouzmanov and Pokrovski, 2012)**,** and Cu deposition is 100% efficient, $6.9 \cdot 10^{11}$ L of hydrothermal fluid are required to form the ore body. This is equivalent to 0.7 km^3 of hydrothermal fluid. Based on these values the fluid/rock ratio in the Big Gossan skarn was 2.5 L/kg. Given the maximum duration of ~200 kyr the flow rates are $3.8 \cdot 10^6$ kg fluid/ yr.

The amount of magma required to exsolve 0.7 km^3 of hydrothermal fluid, assuming the magma contained between 1-3 wt.% H_2O (Cloos, 2001), ranges from 23 to 68 km^3. Again, it is important to note we have assumed 100% efficiency of volatile stripping from the magma and 100% efficiency for metal deposition, therefore these values are approximately minimums. Given the exsolution rates modeled by Shinohara and Hedenquist (1997) it would take between 300 and 1080 years to exsolve the required volume of fluids from magma.

Ertsberg-Grasberg Mining District

The total metal endowment in the Ertsberg-Grasberg mining district is approximately $9.53 \cdot 10^{10}$ kg Cu and $8.18 \cdot 10^6$ kg Au. The total volume of hydrothermal fluid required to transport these metals, assuming the fluids contained on average 3000 ppm Cu, is $2.89 \cdot 10^{13}$ L, which is equivalent to 28.9 km^3 of fluid. This is approximately the volume of water that is held in the Hoover Dam Reservoir (Holdren and Turner, 2010). The total volume of magma required to exsolve the fluids in between 962 and 2887 km^3. Based on these magma volumes a batholithic size magmatic system is apparent.

Copper-Charged Cupola

A cupola, as defined by Cloos (2001), is the domical region at the upper boundary between solidified and mobile magma. In this context, the cupola is where magmatic-hydrothermal fluids that have separated from the magma rise and collect prior to ascending into the overlying rock. Fluid will accumulate if the rate of fluid generation is faster than the rate of discharge. Pervasive infiltration flow creates the characteristic alteration halos observed in many porphyry copper deposits. Most of the time the differential stresses in the cupola must be low, as the roof of the cupola is only slightly below magmatic temperatures. Although the fluid pressure in the cavity beneath the cupola must be at lithostatic values, self-induced hydraulic fracturing in this environment is unlikely, as there is a tensile strength for the overlying rock that must be overcome. Cloos (2001) proposed that earthquake induced extension fracturing could rupture the cupola, allowing the hydrothermal fluids to rise from the cupola, decompress, and cool, causing mineralization in the overlying rock. Buoyant ascent of a fluid pocket beneath a cupola is probably a common trigger for explosive detonation (as was the case at Mt Pinatubo; Pasteris, 1996), therefore the "throttling action" is critical to prevent eruption. Based on the plausible volume of the cupola, and the volume of hydrothermal fluids that must be exsolved, it is possible to calculate the number of times that the cupola must be charged in order to form each of the ore deposits in the district. Note that the discussion below assumes that all of the fluid flow is taking place through fracture flow, however, in the case of the Grasberg porphyry copper deposit, potentially half of the fluid flow may have been due to pervasive infiltration flow, which is responsible for the characteristic alteration halos (see Cloos, 2001; Paterson and Cloos, 2005b; Cloos and Sapiie, 2013). When this is the case, the calculated rupture rates would need to be halved.

A half-sphere geometry is assumed for the cupola. Using the dimensions of the MGI stockwork and alteration zone as an upper boundary, radii of 50 m, 100 m, and 300 m were tested (note that a 300 m radius is an upper limit based on the width of the MGI stock) (see Figure 7-1). For each of these cases the volume of the half-sphere cupola is $2.6 \cdot 10^{-4}$ km^3, 0.0021 km^3, and 0.057 km^3 respectively. A cupola with a radius of 50 m would need to be filled 2600 times to form the Big Gossan deposit and 36,600 times to form the supergiant Grasberg porphyry deposit (see Table 7-2 for all deposit calculations). Assuming a 220 kyr lifespan for the Grasberg porphyry deposit, the cupola would need to be refilled 36,600 times, which equates to a rupture once every ~6 years (assuming that half of the fluid flow occurs as pervasive infiltration flow, the earthquake rate would be once every ~12 years). On the other hand, a cupola with a radius of 100 m or 300 m would need to be emptied and filled 330 to 10 times to collect the volume of fluid required to form the Big Gossan skarn, and 4600 to 170 times to collect the volume of fluid required to form the Grasberg porphyry deposit. Taking the Grasberg deposit as an example, there must have been a cupola rupturing event once every ~50 years (assuming a 100 m radius) or 1300 years (assuming a 300 m radius). Note that these timespans will be doubled if 50% of the fluid flow is through pervasive infiltration.

Based on the number of times a cupola must be filled (defined as filling the half-sphere top of the cupola) in order to account for the volume of hydrothermal fluids required for ore deposition, it is also possible to estimate the magnitude to the earthquakes responsible for extension fracturing in the cupola, resulting in fracture fluid flow, and ultimately, vein formation (throttling cupola theory; Cloos and Sapiie, 2013). Taking the Grasberg porphyry copper deposit as the case example, it seems most likely that the cupola had a radius of approximately 100 m (based on the geometry of the MGI, the size of the alteration halos (Paterson and Cloos, 2005a), and the number of cupola filling events required for a cupola of that size (~4600)). Assuming that approximately half of the fluid flow responsible for ore formation occurred as pervasive infiltration fluid flow and the other half occurred as fracture fluid flow, there must have been ~2300 earthquake events that caused extension fracturing of the cupola, allowing the cupola to drain as the accumulated hydrothermal fluids jet upwards into the fractures. Analysis of earthquake ruptures suggests that the average rupture during a magnitude 7 event is ~1m, whereas the rupture for a magnitude 6 event is ~20 cm, a magnitude 5 event is ~ 10 cm, and a magnitude 4 event is ~4 cm (Sibson, 1989). With magnitude 5 earthquakes, 2300 events would result in approximately 230 meters of extension, and with magnitude 4 earthquakes, 2300 events would result in approximately 90 m of extension. These extension magnitudes are broadly in agreement with the estimates from Sapiie (1998) of 40 m of extension based on vein width measurements outside of the stockwork zone (as such, there is an inherently large uncertainty on this number). Overall, it seems as though more numerous, smaller earthquake events may be responsible for mineralizing fluid flow in the Grasberg deposit.

CONCLUSIONS

The total metal endowment in the Ertsberg-Grasberg mining district is approximately $9.5 \cdot 10^{10}$ kg Cu and $8.2 \cdot 10^{6}$ kg Au, and the total volume of hydrothermal fluid required to transport these metals is approximately 30 km^3, which is roughly equivalent to the volume of water held in the Hoover Dam Reservoir. Between 960 and 2900 km^3 of magma is needed to exsolve the volume of magmatic-hydrothermal fluids required for ore formation. For the supergiant Grasberg porphyry copper deposit, $3.16 \cdot 10^{10}$ kg of Cu and 2.9 million kg of Au were transported by 9.6 km^3 of magmatic-hydrothermal fluids. Assuming a 100 m radius, half-sphere charged cupola, and that 50% of fluid flow occurs as pervasive infiltration flow and the other 50% occurs as fracture fluid flow, the cupola would need to be filled and drained of fluid ~4600 times, with ~2300 earthquake events, one every ~ 20 years, resulting in extension fracturing and vein formation. Fault slip consistent with magnitude 4 or 5 earthquakes, occurring once every couple decades, for the duration of ore formation in the Grasberg deposit should be sufficient to create the extension observed in the deposit while also allowing for sufficient cupola throttling to form the supergiant ore body.

Appendix A: Estimates for the Duration of Ore-Forming Magmatic-Hydrothermal Systems

Ore Deposit	Location	Ore Type	Resource	Dating Techniques	Duration	References	Notes
Cross-Cutting Relationships							
Cerro Rico de Potosi (polymetalic vein deposit)	Bolivia	Epithermal-Ag, Sn	Ag, Sn	40Ar/39Ar sanidine and biotite, K-Ar supergene alunite (compared with older sericite Ar/Ar)	min 0.2 m.y. (dome intrusion to start of supergene alt.)	Rice et al. (2005)	Dated oldest Cerro Rico dome (pre-dates mineralization) and Huakajchi ignimbrite, which contains clasts of mineralized rocks (must post-date mineralization). Independent check by dating a dome that intrudes the ignimbrite. Presence of sanidine rather than perthite indicates rapid cooling
Far Southeast (FSE)	Philippines	Porphyry Cu-Au	Cu, Au	K/Ar magmatic hornblende and biotite, hydrothermal biotite and illite	~300 k.y.	Arribas et al. (1995)	dated pre-mineralization and post-mineralization volcanics. Not clear that these fully constrain the duration of hydrothermal activity
Cerro de Pasco	Peru	Epithermal Polymetallic	Base Metals (Zn, Pb, Cu ± Ag, Au, Bi)	Single grain zircon U/Pb, sericite and alunite Ar/Ar	Magmatic-hydrothermal activity ~1 m.y.; magmatic activity 350 k.y.; stage 2 mineralization 100 k.y.	Baumgartner et al. (2009)	Well constrained cross-cutting relationships. Dating the magmatic phases using single grain zircon U/Pb and the hydrothermal veins using Ar/Ar. All ages overlap within error, therefore the estimates are based on the errors. Really nice compilation of previous estimates
Bajo de la Alumbrera	Argentina	Porphyry Cu-Au	Cu, Au	ID-TIMS zircon (single grain analysis from two cross-cutting porphyry intrusions)	90 ± 34 k.y. (or more conservatively 124 k.y.)	von Quadt et al. (2011)	Agreement that the volcanic complex had a long lifetime, at least 2.7 m.y., *Taking individual zircon ages; however both porphyries have concordant zircons that are older and interpreted as antecrysts
Bingham Canyon	Utah, USA	Porphyry Cu-Au-Mo	Cu, Au, Mo	ID-TIMS zircon (single grain analysis from pre-, syn-, and post-ore intrusions)	0.32 m.y. (two mineralization pulses)	von Quadt et al. (2011)	
Direct Dating of Mineralization							
La Caridad	Mexico	Porphyry	Cu	Zircon U/Pb and molybdenite Re-Os	"Short lived"	Valencia et al. (2005)	Ages for the host quartz monzonite and the molybedenite overal witihin error
Dating Multiple Intrusions							
Chuquicamata	Chile	Porphyry	Cu	ELA-ICP-MS and SHRIMP zircon U/Pb	East Porphyry <0.5 m.y.; intrusions 1 m.y. apart	Ballard et al. (2001)	Argue that anomalously large size is due to protracted igneous history and superposition of two magmatic-hydrothermal systems *SHRIMP AGES 1.5-2.5% OLDER THAN ICP-MS AGES **1000°C/m.y. cooling rate
Chuquicamata	Chile	Porphyry	Cu	ELA-ICP-MS zircon U/Pb	5.5 m.y.	Campbell et al. (2006)	Dated 22 intrusions from the composite Los Picos-Fortuna-Pajonal El Abra igneous complex
Dating Crystallization and Cooling							
El Teniente	Chile	Porphyry Cu-Mo	Cu, Mo	zircon U/Pb, biotite and sericite Ar/Ar, molybdenite Re-Os	System active for at least 1.5 m.y., principal hydrothermal stage ~100 k.y.	Maksaev et al. (2004); Cannell et al. (2005)	Largest known porphyry deposit, multiple intrusions, active over 1.5 to 2 m.y.
Toki Cluster, Chuquicamata District	Chile	Porphyry	Cu	Re-Os molybdenite, 40Ar/39Ar biotite, muscovite and k-spar, zircon U/Pb	2 m.y.	Barra et al. (2013)	No map showing the location of samples. No cross-cutting relationships noted
Rio Blanco	Chile	Porphyry	Cu, Mo	ID-TIMS and SHRIMP zircon U/Pb, 40Ar/39Ar biotite and orthoclase veins	~1.5 m.y.	Deckart et al. (2005)	Not clear whether mineralization was continuous or episodic. Dated magmatic biotite and unequivocally hydrothermal biotite. Need better cross-cutting relationships
Zaldivar Deposit, Escondida District	Chile	Porphyry	Cu	40Ar/39Ar igneous and hydrothermal biotite, zircon U/Pb, ZFT	~1.5 m.y.	Campos et al. (2009)	~300°C/m.y. cooling rate. ZFT ages constrain district wide thermal relaxation. No clear cross-cutting relationships
Bajo de la Alumbrera	Argentina	Porphyry Cu-Au	Cu, Au	ELA-ICP-MS zircon U/Pb, Ar/Ar k-spar and biotite, aHe and zHe	episodic over 1-2 m.y.	Harris et al. (2008)	Emplaced during two episodes. System underwent protracted cooling after initial collapse of the magmatic system (rapidly to <300°C)
Bingham Canyon	Utah, USA	Porphyry Cu-Au-Mo	Cu, Au, Mo	K-Ar compilation for all intrusions	2.2 m.y. for several pulses of hydrothermal activity	Warnaars et al. (1978)	Based on field relationships - assumed that mineralization started after intrusion of the equigranular monzonite and culminated before emplacement of the quartz latite plug
Chuquicamata	Chile	Porphyry	Cu	K-spar and biotite Ar/Ar from samples in the quartz-sericite and potassic alteration zones	~2-3 m.y.	Reynolds et al. (1998)	Selected samples from each alteration zone. Timing is poorly constrained and data are not convincing. Suggest cooling rate of 60-80°C/M.y.
Corbre, Potrerillos District	Chile	Porphyry Cu-Mo-(Au)	Cu, Mo, Au	Ar/Ar hornblende and sericite	230 ± 210 k.y.	Marsh et al. (1997)	Dated magmatic hornblende for minimum intrusion age and sericite from a late Au-bearing vein for mineralization age

Ore Deposit	Location	Ore Type	Resource	Dating Techniques	Duration	References	Notes
Porgera	PNG	Porphyry Au	Au	roscoelite, biotite and hornblende Ar/Ar	"Short lived"	Ronacher et al. (2001)	Dated magmatic and hydrothermal biotite to contrain the duration - ages overlap in error
OK Tedi	PNG	Porphyry Cu-Au	Cu, Au	SHRIMP zircon U/Pb, K-Ar	< 0.5 m.y.	van Dongen et al. (2010)	
Morococha District	Peru	Porphyry and Polymetallic vein	Cu-Mo and base metals	Zircon and Titanite U/Pb, Ar/Ar, and Re-Os	Codiciada - 200 k.y., Ticlio - 300 k.y., Tormocho - 1.3 m.y.	Catchpole et al. (2015)	Polymettalic veins post-date the youngest recorded porphyry mineralization at Toromocho by 0.5 m.y.
Flux Measurements/ Diffusion Profiles/ Modern Analogues							
Ladolam	PNG	Epithermal (Active)	Au	Gold flux measurements	~55,000	Simmons and Brown (2006)	Titanium down-hole sampler used to measure gold content in deep geothermal brines. 15 ppb Au, current flux of 24 kg/yr, deposit required 55,000 yr to form *assuming constant aqueous gold concentration and fluid flow, and 100% deposition
Kuroko Ores	Japan	VMS	Cu, Zn	Fe depletion profiles	210 k.y.	Mizuta and Scott (1997)	Based on Fe diffusion experiments by Mizuta
Waiotapu,	New Zealand	Active Geothermal	Au	100,000 oz gold precipitated in 900 yr	900 yr	Hedenquist and Brown (1989)	A deposit the size of Round Mountain could form in as little as 10 k.y.
Overlapping Errors							
Nambija	Ecuador	Au-skarn	Au (minor Cu)	U/Pb zircon, U/Pb titanite (prograde skarn), Re-Os molybdenite (retrograde skarn)	<~0.7 m.y.	Chiaradia et al. (2009)	All ages are indistinguisable within the error of the analytical techniques. Approximation is based on the errors of the ages
Norte Porphyry, Potrerillos District	Chile	Porphyry Cu-Mo-(Au)	Cu, Mo, Au	Ar/Ar hornblende, biotite, and plagioclase	120 ± 220 k.y.	Marsh et al. (1997)	All ages are indistinguisable. Best estimate is taken as the age difference between the hornblende and plagioclase
Numerical Modeling							
				Numerical Modeling	10's k.y.-800 k.y.	Cathles et al. (1997)	Modeling of conductive and convective cooling - would a single intrusion can maintain a geothermal system for up to 800 k.y. under optimal permeability and heat loss conditions. In the models strong convective cells develop along the edge of the sill (main intrusion)
Butte	MT, USA	Porphyry	Cu, Mo	Numerical Modeling	900 yr	Cathles and Shannon (2007)	Uses the volume of potassically altered rocks to estimate the rate of fluid expulsion and the duration
Round Mountain	NV, USA	Epithermal Au, Ag	Au, Ag	Ar/Ar sanidine and adularia	0.1 m.y. indicated by thermal modeling, no more than 0.5 m.y.	Henry et al. (1997)	Dated the host ash flow (related to caldera collapse) and a post-mineral ash tuff to constrain system to 0.5m.y. Dated mineralization with adularia - thermal modeling indicates rapid cooling and 0.1 m.y duration

Appendix B: Age Corrections for U/Pb dating of young zircons

<u>Age Adjustments</u>

Due to the fact that the Grasberg district zircons are less than 10 Ma, it is necessary to correct for any common (non-radiogenic) lead that is incorporated into the zircon crystal structure, and for the time it takes for the radioactive decay to reach secular equilibrium. The two procedures used to "correct" young zircon ages are described below.

(1) Common Lead Correction

In most zircons any lead found in the crystal is radiogenic (produced by radioactive decay); however in some cases common (non-radiogenic) lead (typically less than 3%, but can be as much as 15%) may be incorporated into the zircon crystal structure (either as it grows or as a result of later alteration). A Concordia line on a Tera-Wasserburg diagram, which plots the $^{238}U/^{206}Pb$ ratio on the x-axis and the $^{207}Pb/^{206}Pb$ ratio on the y-axis, is a line that shows all of the points where the decay of ^{238}U to ^{206}Pb gives the same age as the constantly evolving $^{207}Pb/^{206}Pb$ age for bulk Earth U to Pb decay (Tera and Wasserburg, 1972).

A zircon that has common lead will not fall on the Concordia because the $^{207}Pb/^{206}Pb$ age will differ from the ^{238}U to ^{206}Pb age. In order to correct for this phenomenon the common lead $^{207}Pb/^{206}Pb$ ratio was measured in K-feldspar from the Karume intrusion, which has near-zero U and Th, and in whole rock samples of the igneous rocks in the district. In the Ertsberg district the whole rock and the feldspar common lead ratio is ~0.86. This common lead ratio was used to pin the y-axis intercept of the Discordia regression line on the Tera-Wasserburg plot. Most analyses have errors that overlap with the Concordia line; however, knowing the y-intercept of the Discordia regression line improves the precision of the Concordia intercept for those samples that are slightly discordant.

In order to evaluate the magnitude of the common lead correction the "y-axis pinned" ages were compared with the unpinned ages. Histogram A in Figure A4-1 shows the magnitude of the correction: the correction is typically on the order of 0.1 myr; however, the correction can be as great as 0.5 myr and as small as 0 myr.

(2) ^{230}Th Disequilibrium Correction

The young age of the Ertsberg-Grasberg mining district zircons makes it necessary to correct for the time it takes for the uranium decay chain to reach secular equilibrium. A ^{230}Th correction is important for zircons less than ~10 Ma.

In most zircons the Th/U ratio of the zircon is less than the Th/U ratio of the magma, which results in the near exclusion of Th from the zircon crystal structure. The initial scarcity of ^{230}Th in the zircon causes disequilibrium in the ^{238}U radioactive decay chain, which ultimately results in a deficit in radiogenic ^{206}Pb. In order to correct for this deficit it is assumed that the Th/U ratio of a fresh, whole rock sample reflects the Th/U of the magma. The correction is calculated using the equations in Scharer (1983):

(1) $t_{deficit} = \frac{1}{\lambda_{238}} \ln(1 + (f - 1)(\frac{\lambda_{238}}{\lambda_{230}})$

Where,

(2) $f = \frac{Th/U_{mineral}}{Th/U_{liquid}}$

The final age is calculated by adding the common lead corrected age with the amount of time lost to the Th disequilibrium ($t_{deficit}$). This correction is typically on the order of 0.08 to 0.10 m.y; the range in the magnitude of the Th disequilibrium correction is shown in Figure A4-2.

(3) $t_{final} = t_{common\ lead\ corrected} + t_{deficit}$

The main assumption for this correction is that the whole rock Th/U ratio reflects the Th/U ratio of the parental magma that is co-genetic with the zircons. The Th/U ratio of the rock was calculated using the whole rock geochemistry database for rocks in the Ertsberg-Grasberg district. These samples were originally selected due to their lack of hydrothermal alteration or rock geochemistry. For these samples the Th/U ratio of the whole rock is assumed to be the Th/U_{liquid}. For the remaining samples the Th/U ratio was estimated based on the average Th/U ratio for the intrusion. In the case where an intrusion has no geochemical data, then the district-wide average of 3 was used to approximate the Th/U_{liquid}. The range of zircon Th/U ratios and whole rock Th/U ratios are shown in Figure A4-2. Note that varying the magma Th/U ratio by 1 only changes the final age by 0.01 M.y., therefore using the district wide Th/U average for samples with an unknown Th/U ratio is a safe assumption.

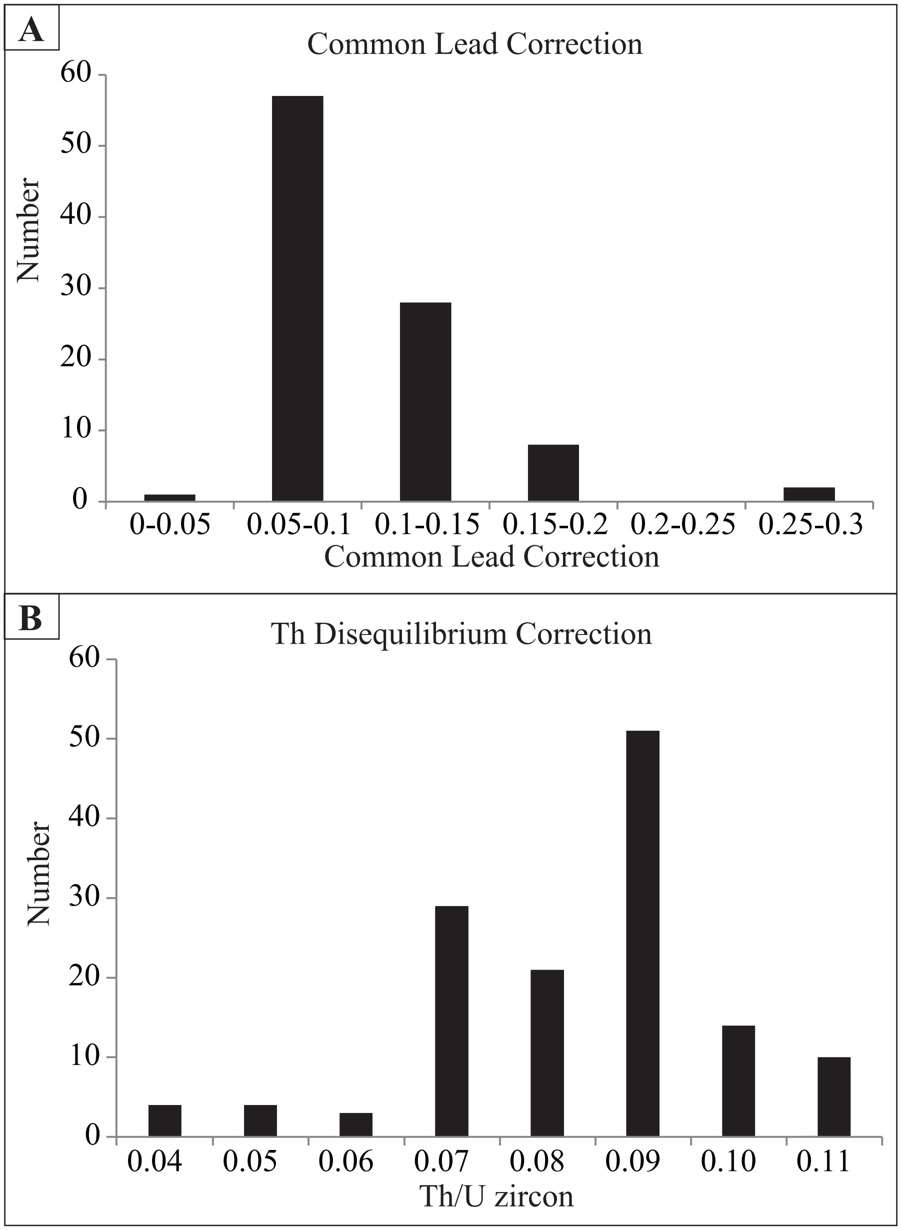

Figure B-1: Histograms showing the magnitude of the common lead and Th disequilibrium corrections. Each histogram shows the m.yr. difference between the uncorrected age and the corrected age.

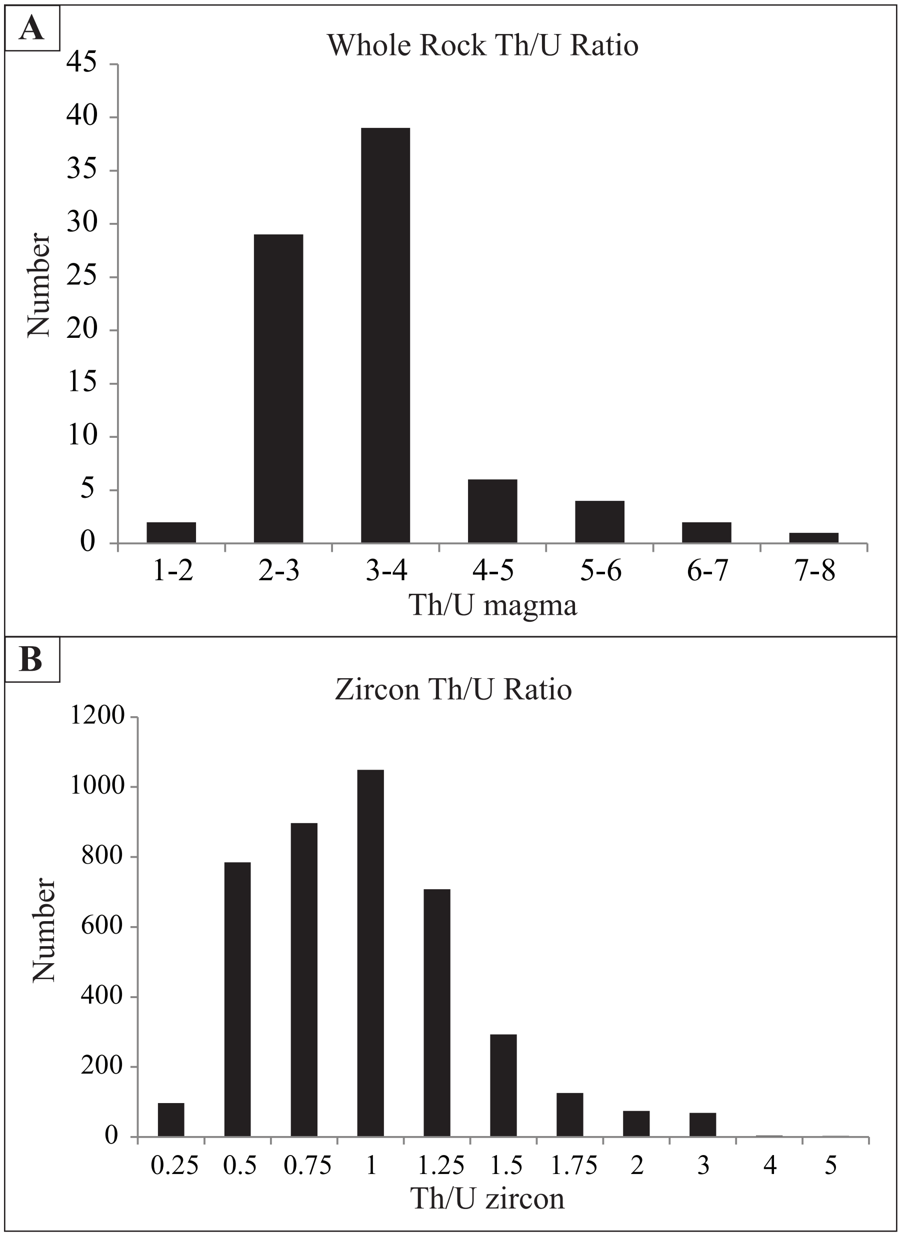

Figure B-2: Histograms showing the range of whole rock Th/U ratio (top) and the range of zircon Th/U ratio (bottom).

Appendix C: Zircon U/Pb Sample Locations

Sample Type	Sample Number	UTM Easting	UTM Northing	Elevation (m)	DDH ID	Depth	Rock Type
Core	GRD32-06-279	734642	9550848	3039	GRD32-06	279	Post-Kali Dike
Core	GBC6-01-01-74	735206	9550642	2828	GBC6-01-01	74	Post-Kali Dike
Core	GBC6-01-01-95.7	735206	9550642	2828	GBC6-01-01	95.7	Post-Kali Dike
Outcrop	M1996: 2004	735180	9550920	3785			LKI
Outcrop	M1996: 2005	734660	9551120	3600			LKI
Core	AM96-40-09-148m	18774	22118	2955	AM96-40-09	148	LKI
Core	KL98-10-21-1693	734101	9550741	3063	KL98-10-21	1693	LKI*
Outcrop	M1996: 2003	734590	9551060	3950			EKI*
Core	GRD32-06-258	734642	9550848	3039	GRD32-06	258	EKI
Outcrop	M1996: 2006	734840	9551005	3680			EKI
Core	GRD41-01-59	734505	9551369	3044	GRD41-01	59	EKI
Outcrop	M1996: 2002	734535	9551330	3950			EKI
Outcrop	M1996: 2007	734720	9551210	3785			EKI
Core	KL98-10-21-1315	734101	9550741	3063	KL98-10-21	1315	EKI*
Outcrop	95-MC-RD1	734380	9551680	4030			Ring Dike
Outcrop	95-MC-RD2	734400	9551355	4015			Ring Dike
Outcrop	M1996: 2001	734460	9551620	3985			Ring Dike
Core	INF42-01-200	734480	9551489	3052	INF42-01	200	MGI*
Amole Drift	02-UT-AM-J	734495	9551380	3045			MGI
Core	90-TM-GRS-3	735605	9549890	2528			MGI
Outcrop	94-MC-MGI2-3	734625	9551180	3995			MGI
Core	GRD41-01-273.5	734505	9551369	3044	GRD41-01	273.5	MGI
Core	GRD42-06-389.2	734479	9551487	3046	GRD42-06	389.2	MGI
Core	GRS-93A-0m	18439	22503	4112	GRS-93A	0	MGI
Core	INF42-01-32	734480	9551489	3052	INF42-01	32	Xenolith in MGI
Core	AB1-10-01-578m	735605	9549890	2528	AB1-10-01	578	Plag Dike
Core	AB1-10-01-500m	735605	9549890	2528	AB1-10-01	500	Plag Dike
Core	GRD41-01-322.5	734505	9551369	3044	GRD41-01	322.5	Plag Dike
Core	AM96-50-36-12.5	734168	9551407	3056	AM96-50-36	12.5	Plag Dike
Outcrop	94-TH3-DA	734530	9552585	4270			Dalam Andesite
Outcrop	90-TM-GRS-1	734600	9552370	4265			Dalam Andesite
Core	NSC-09-02-246	734334	9552357	4225	NSC-09-02	246	Tvs
Core	GCZ-41-01-59.1	734278	9552475	4078	GCZ-41-01	59.1	Tvs

Sample Type	Sample Number	UTM Easting	UTM Northing	Elevation (m)	DDH ID	Depth	Rock Type
Core	GT-INC-023-22	734184	9552463	4032	GT-INC-023	22	Tvs
Core	NSC-09-02-290	734334	9552357	4225	NSC-09-02	290	Tvs
Core	GCZ-50-02-105	734297	9552353	4061	GCZ-50-02	105	Tvs
Core	GRS-123-0m	18015	22427	4053	GRS-123	0	Dalam Volcanic
Outcrop	14-SW-07	734030	9551246	3580			Dalam Volcanic
Outcrop	14-SW-06	734128	9551593	3570			Dalam Fragmental
Core	GRD32-06-46	734642	9550848	3039	GRD32-06	46	Dalam Diorite
Core	GRD41-01-348	734505	9551369	3044	GRD41-01	348	Dalam Diorite
Core	GRD42-06-523.4	734479	9551487	3046	GRD42-06	523.4	Dalam Diorite
Core	KL40-06-416m	18018	21502	2978	KL40-60	416	Dalam Diorite
Core	KL40-06-516m	18018	21502	2978	KL40-61	516	Dalam Diorite
Core	KL40-06-762m	18018	21502	2978	KL40-62	762	Dalam Diorite
Core	GBC3-01-01-1033	735179	9550388	2819	GBC3-01-01	1033	Ertsberg Dike
Core	TE07-29	737254	9548960	2593	TE07-29	5	Ertsberg
Core	SEID-MLZ-05-297	736648	9549142	3112	SEIDMLZ-05	297	Ertsberg
Core	TEW11-10	736524	9549414	3149	TEW11-10	690	Ertsberg
Outcrop	M1996: 1001	735650	9549175	3580			Ertsberg
Outcrop	M1996: 1004	736140	9548340	2890			Ertsberg
Outcrop	M1996: 1002	736625	9548175	3650			Ertsberg
Core	ABE-01-01	735735	9548227	2511	ABE-01-01	143	Ertsberg
Core	D5-15	737108	9547938	3968	D5-15	244.5	Ertsberg
Core	AB1-10-01-2.2m	735605	9549890	2528	AB1-10-01	2.2	Ertsberg
Outcrop	M1996: 1009	737125	9548250	3940			Ertsberg
Core	GBC3-01-01-902	735179	9550388	2819	GBC3-01-01	902	Ertsberg
Core	DMLZC05-01	736233	9547349	2912	DMLZC05-01	248	Ertsberg
Core	TEW01-01	736483	9548606	3960	TEW01-01	75.5	Ertsberg
Outcrop	M1996: 1008	734535	9546810	2750			Ertsberg
Core	GB23-02	736008	9549327	3791	GB23-02	56	Ertsberg
Core	KL12-02	735259	9550046	2849	KL12-02	82.8	Ertsberg
Core	TEW 08-01-0m	736633	9549336	3145	TEW 08-01	0	Ertsberg
Core	TEW 08-01-500m	736633	9549336	3145	TEW 08-01	500	Ertsberg
Core	TEW 08-01-1275m	736633	9549336	3145	TEW 08-01	1275	Ertsberg
Outcrop	M1996: 1003	735110	9548875	4125			Ertsberg

Sample Type	Sample Number	UTM Easting	UTM Northing	Elevation (m)	DDH ID	Depth	Rock Type
Core	DOW-53-01	736760	9548707	3151	DOW-53-01	458.4	Ertsberg
Core	GBC3-01-01-37	735179	9550388	2819	GBC3-01-01	37	Karume
Core	GBC6-01-01-50	735206	9550642	2828	GBC6-01-01	50	Karume
Core	KL20-10	735024	9550482	2804	KL20-10	3	Karume
Core	AB1-10-01-574.2m	735605	9549890	2528	AB1-10-01	574.2	Karume
Outcrop	M1996: 5002	735325	9550220	3560			Karume
Outcrop	M1996: 5003	734960	9550280	3850			Karume
Core	KL98-10-22-1505	734099	9550739	3063	KL98-10-22	1505	Tpi
Core	KL98-10-22-1544	734099	9550739	3063	KL98-10-22	1544	Tpi
Core	KL98-10-22-1460	734099	9550739	3063	KL98-10-22	1460	Tpi
Core	KL98-10-21 727	734101	9550741	3062	KL98-10-21	727	Tigt
Core	KL98-10-21 841	734101	9550741	3062	KL98-10-21	841	Tigt
Core	KL98-10-21 922	734101	9550741	3062	KL98-10-21	922	Tigt
Core	KL98-10-21 948	734101	9550741	3062	KL98-10-21	948	Tigt
Core	KL98-10-21 982	734101	9550741	3062	KL98-10-21	982	Tigt
Core	KL98-10-21 1132	734101	9550741	3062	KL98-10-21	1132	Tigt*
Core	KL98-10-21 1192	734101	9550741	3062	KL98-10-21	1192	Tigt
Core	KL98-10-22-1254	734099	9550739	3063	KL98-10-22	1254	Tigt
Core	KL98-10-22-1344	734099	9550739	3063	KL98-10-22	1344	Tigt
Core	KL98-10-22-1386	734099	9550739	3063	KL98-10-22	1386	Tigt
Outcrop	ID41E-02-645m	731725	9551429	4166	ID41E-01	645	Idenberg
Core	BG-WSH-04 237m	734726	9548458	3184	BG-WGH-04	237	Big Gossan
Core	BG-WSH-04 241.6.m	734726	9548458	3184	BG-WGH-04	241.6	Big Gossan
Outcrop	K4-197-91-6001	734420	9549105	3610			Kay
Outcrop	M1996: 3001	733820	9553445	4125			North Grasberg
Core	WDDPZ-05-209	732482	9550480	3698	WDDPZ-05	209.6	Lembah Tembaga
Core	WDDPZ-05-211	732482	9550480	3698	WDDPZ-05	211.6	Lembah Tembaga
Outcrop	M1996: 4001	732310	9549690	4025			Wanagon
Core	WD17-05-19	732238	9549568	3901	WD17-05	18.7	Wanagon
Outcrop	M1996: 7001	733185	9547880	2725			Heat Road Intrusion
Outcrop	93-MC-HR1	733630	9550720	4030			Heat Road Intrusion
Outcrop	93-MC-HR3a	733450	9547180	2760			Heat Road Intrusion
Outcrop	93-MC-HR3b	733450	9547180	2760			Heat Road Intrusion

Sample Type	Sample Number	UTM Easting	UTM Northing	Elevation (m)	DDH ID	Depth	Rock Type
Outcrop	95-MC-HR4	734020	9550000	3790			Heat Road Intrusion
Outcrop	93-MC-HR5	733850	9549560	3535			Heat Road Intrusion
Outcrop	94-MC-HR6	733690	9549270	3335			Heat Road Intrusion
Outcrop	94-MC-HR7	733590	9549300	3315			Heat Road Intrusion
Outcrop	95-MC-UR3	733095	9541355	2129			Utiki River Sample
Outcrop	M1996: 7002	733075	9544120	2865			Scappert Falls
Outcrop	M1996: 6002	733535	9549205	3235			Big Gossan
Core	KL20-10	735024	9550482	2804	KL20-10	601.9	Tpi
Outcrop	94-MC-RC2	732240	9544980	2160			Ridge Camp
Core	SE02-01	737662	9544065	2687	SE02-01	117.4	Southeast Intrusion

Appendix D: Polished Slab Photos

Post-Kali Dike

GRD32-06 (278.8m) | PPL & XPL

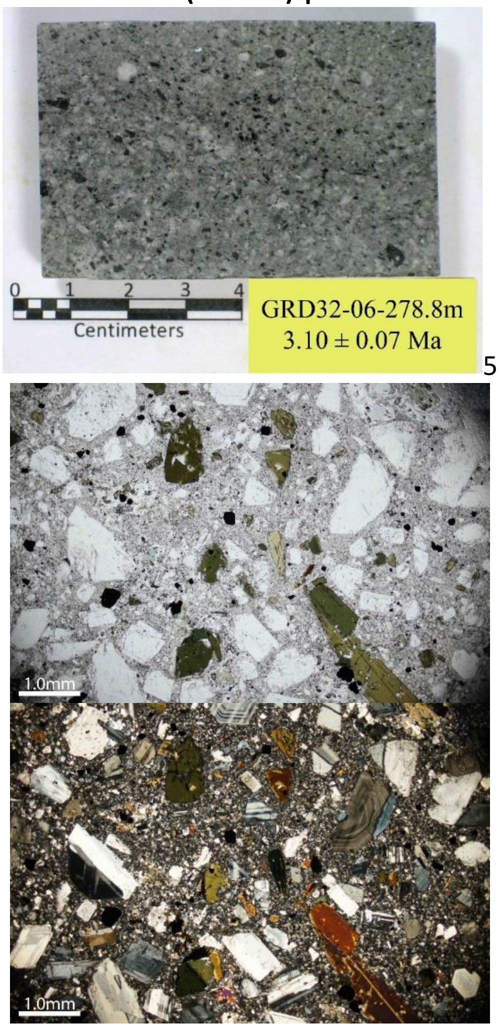

5

GBC6-01-01 (95.7m) | PPL & XPL

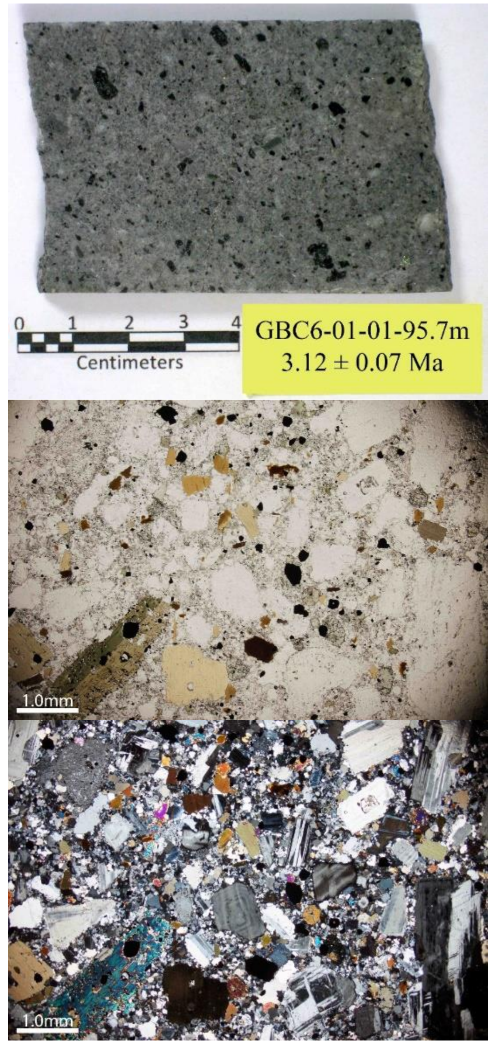

GBC6-01-01 (74m) | PPL & XPL

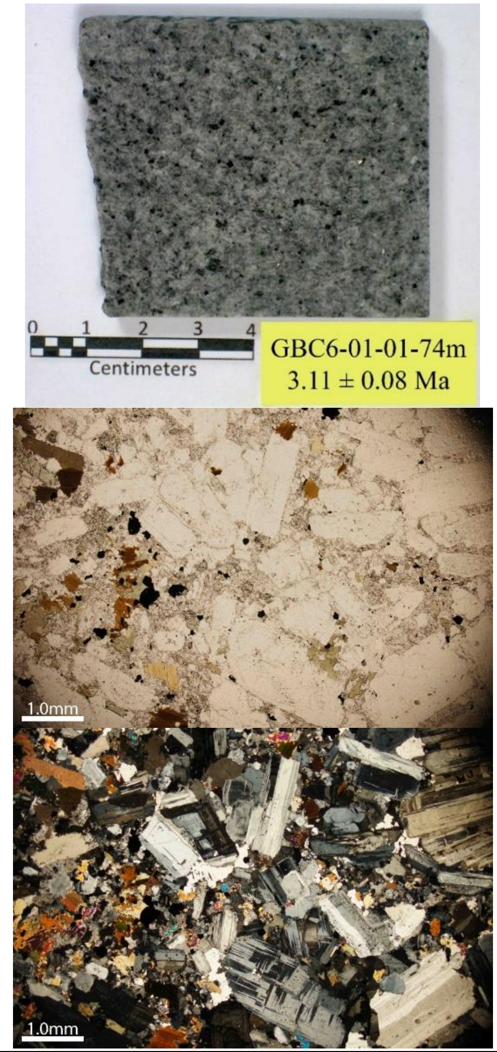

Undifferentiated Kali

90-TM-CST-1 (5001) | PPL & XPL

90-TM-CST-1 (5001)
Collected by Timothy McMahon as Karume but ages and other work provides evidence that it is Kali
Additional Ages:
K-Ar Age: 3.13 ± 0.09 Ma

AB1-10-01 (204.7m) | PPL & XPL

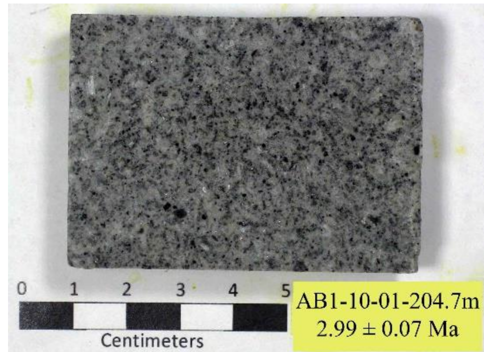

AB1-10-01 (381.6m) | PPL & XPL

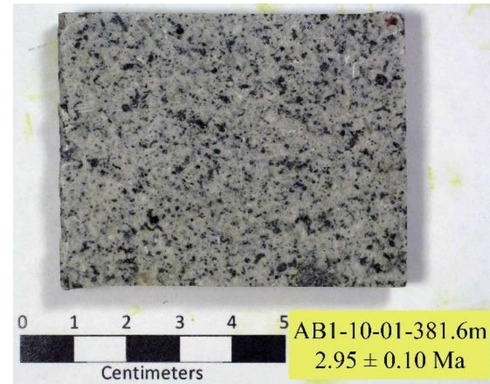

Undifferentiated Kali

Late Kali Dike

89-TM-SK1 (2004) | PPL & XPL

89-TM-SK1 (2004) Additional Ages:
Ar-Ar Age: 2.94 ± 0.02 Ma
K-Ar Age: 3.14 ± 0.08 Ma

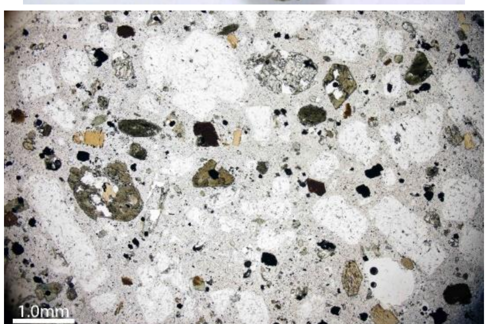

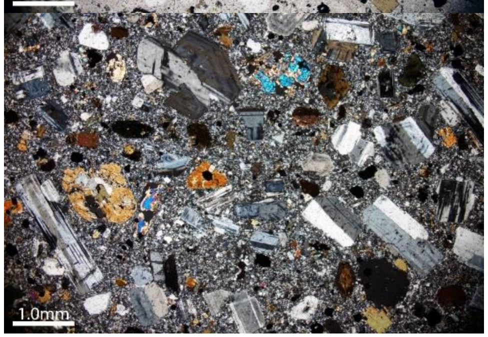

GRD32-05 (250m) | PPL & XPL

AM96-40-09 (148m) | PPL & XPL

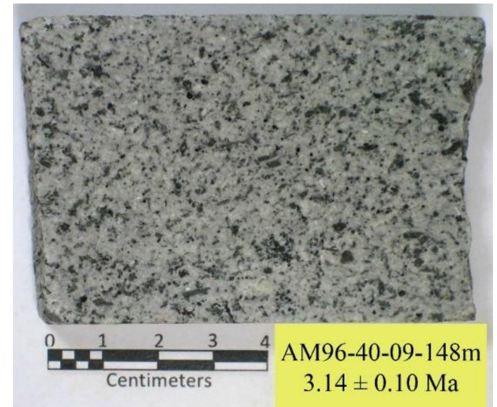

Late Kali Dike

90-TM-CORDI-1 (2005) | PPL & XPL

90-TM-CORDI-1 (2005) Additional Ages:
K-Ar Age: 3.13 ± 0.15 Ma
Apatite Fission Track Age: 2.4 ± 0.6 Ma

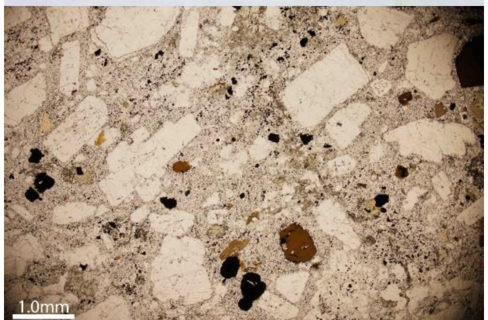

AM96-40-09 (344.7) | PPL & XPL

AM96-40-09 (344.7) | PPL & XPL

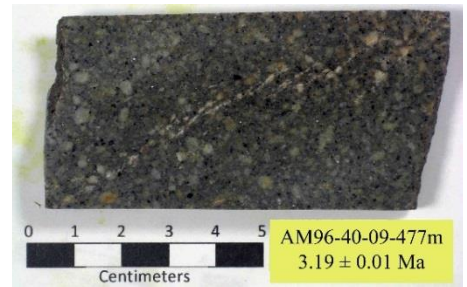

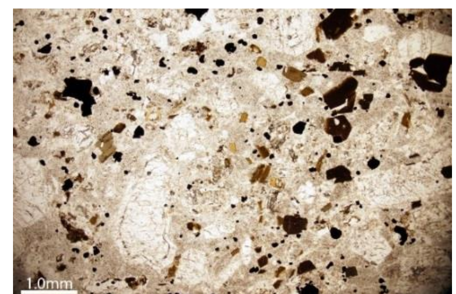

Late Kali Dike

15-SW-05 | PPL & XPL

GBCPA-01-06 (500m) | PPL & XPL

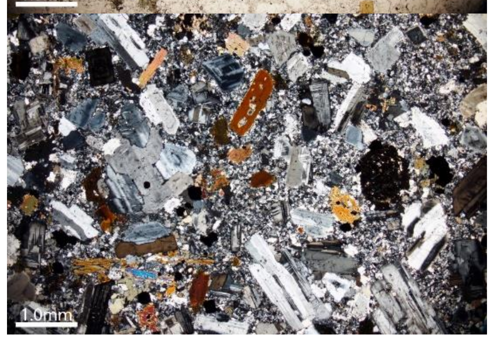

Early Kali Dike

GRD41-01 (59m) | PPL & XPL

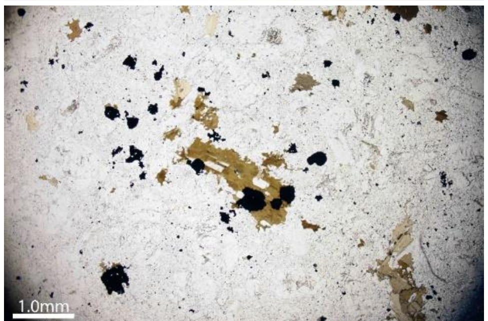

89-TM-PIR-1 (2002) | PPL & XPL

89-TM-PIR-1 (2002) Additional Ages:
K-Ar Age: 2.77 ± 0.34 Ma

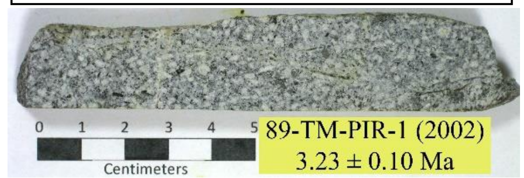

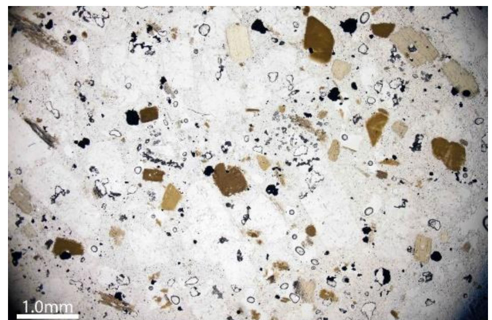

GRD32-06 (258m) | PPL & XPL

Early Kali Dike

90-TM-QD-3 (2003) | PPL & XPL

90-TM-QD-3 (2003) Additional Ages:
K-Ar Age: 3.01 ± 0.23 Ma

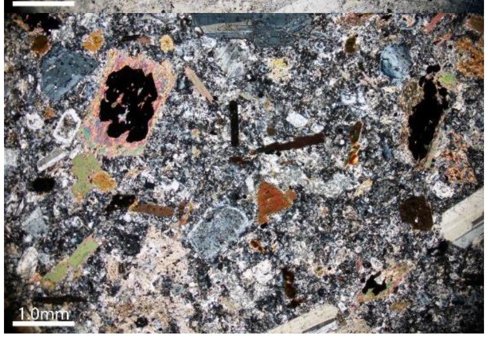

90-TM-QD-2 (2006) | PPL & XPL

90-TM-QD-2 (2006) Additional Ages:
K-Ar Age: 3.23 ± 0.32 Ma

INF37-02 (75m) | PPL & XPL

MGI Ring Dike Samples

95-MC-RD1 | PPL & XPL

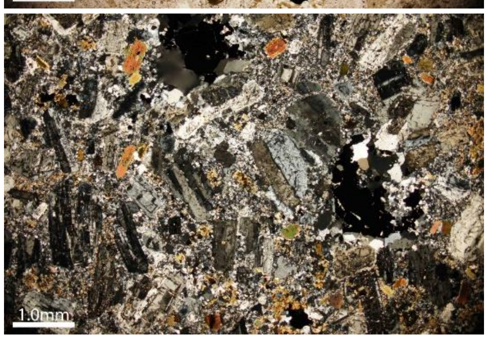

95-MC-RD2 | PPL & XPL

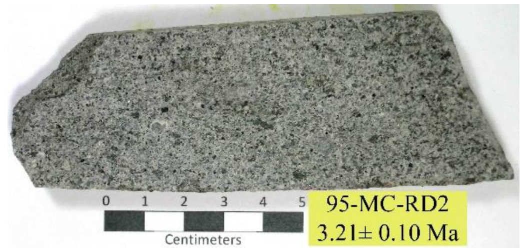

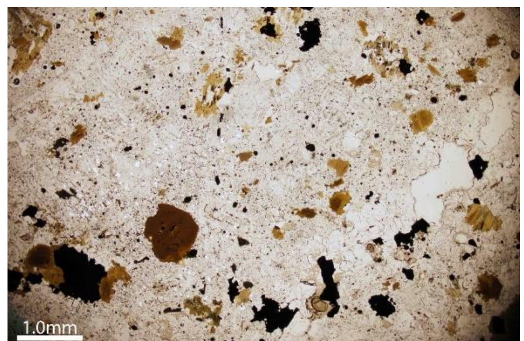

89-TM-GRS-1 (2001) | PPL & XPL

89-TM-GRS-1 (2001) Additional Ages:
Ar-Ar Age: 3.07 ± 0.10 Ma
K-Ar Age: 2.83 ± 0.07 Ma

INF42-01 (200m) | PPL & XPL

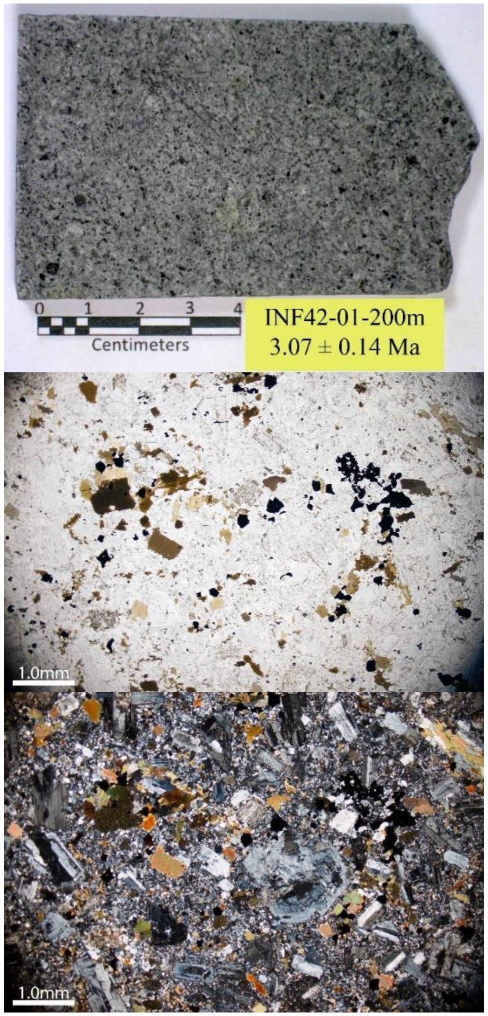

GRD42-06 (389m) | PPL & XPL

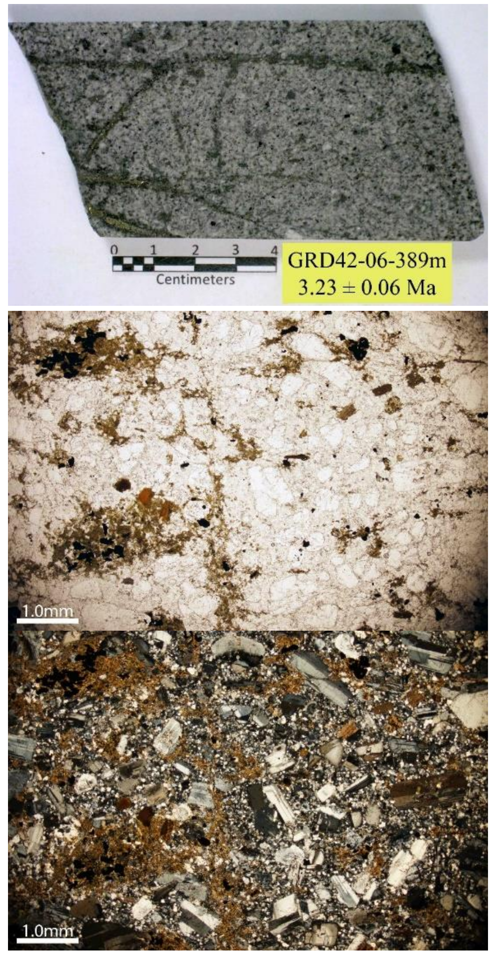

GRD41-01 (273.4m) | PPL & XPL

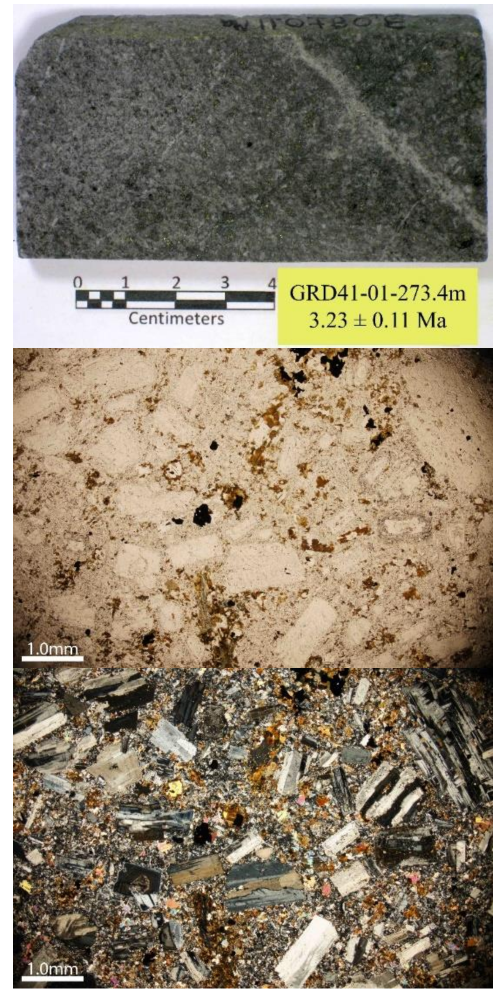

02-UT-AM-J | PPL & XPL

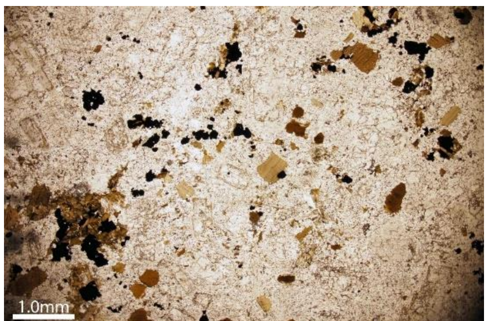

94-MC-MGI2-3 | PPL & XPL

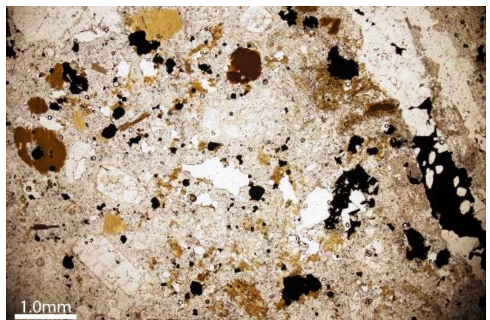

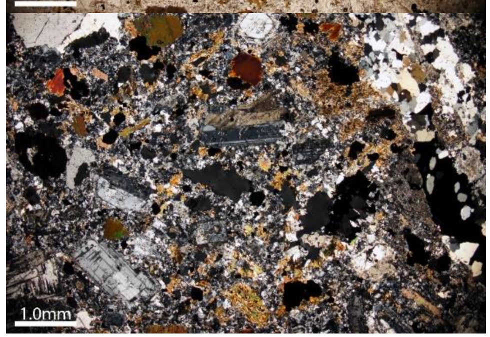

89-GA-GRS-2 (2007) | PPL & XPL

GRS-93A (0m) | PPL & XPL

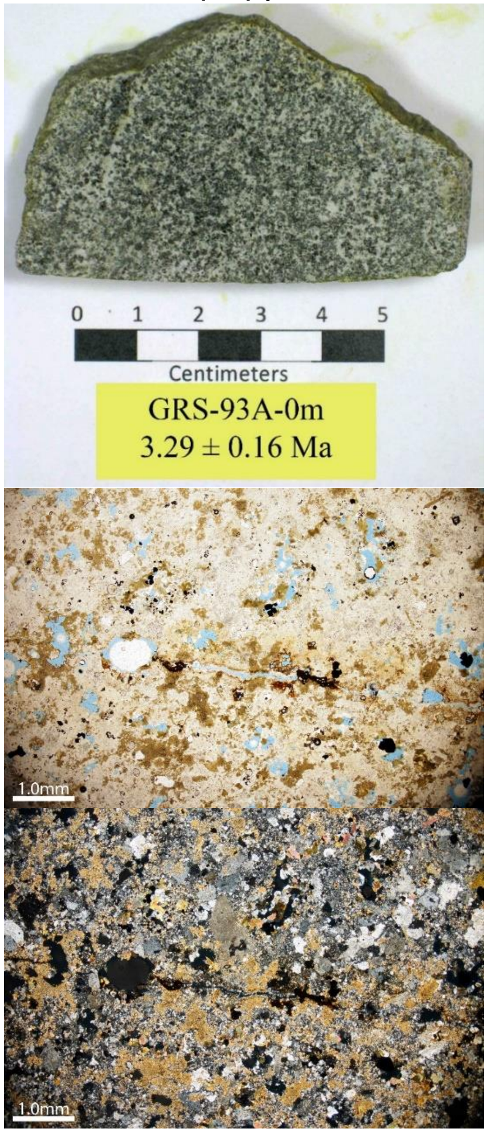

GBCPA-01-05 (505m) | PPL & XPL

GBCPA-01-06 (525m) | PPL & XPL

Xenolith in MGI?

INF42-01 (32m) | PPL & XPL

Age relationship – older than MGI – may suggest that it is a xenolith

Plag Dike

GRD41-01 (322.5m) | PPL & XPL

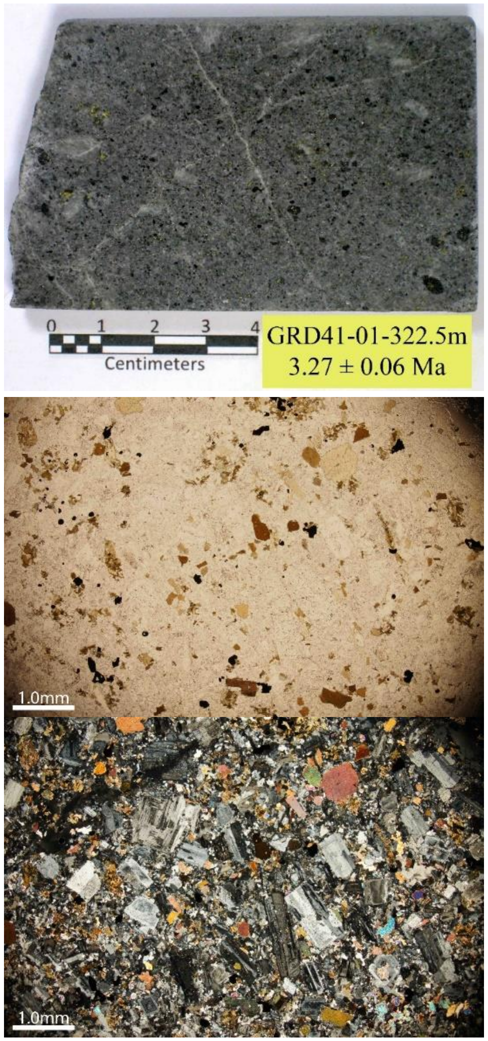

AM96-50-36 (12.5m) | PPL & XPL

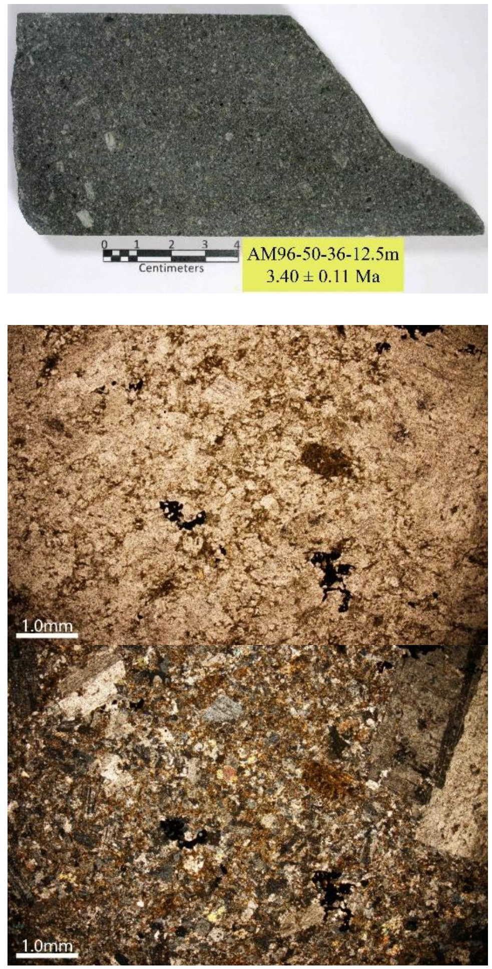

AB1-01-10 (578.3m) | PPL & XPL

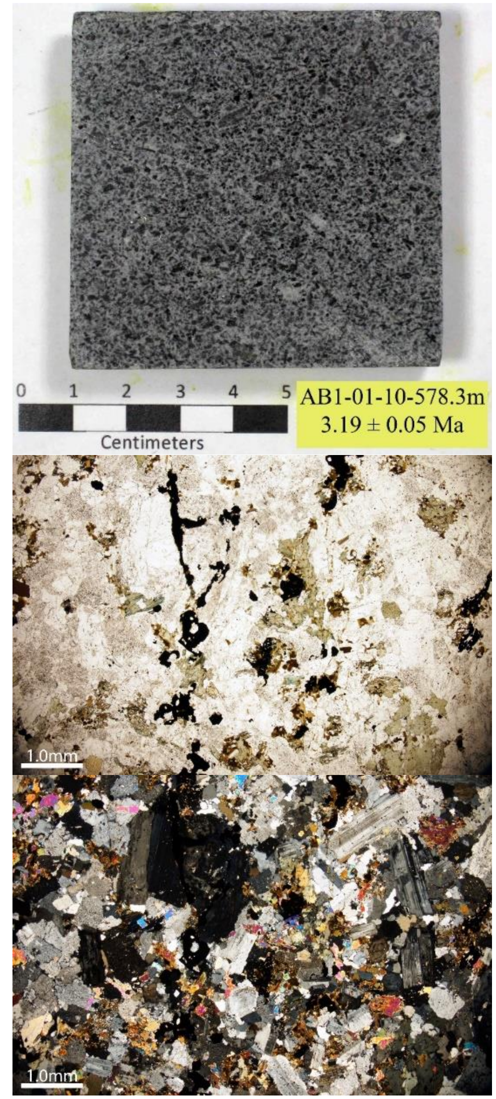

Plag Dike

AB1-01-10 (499.3m) | PPL & XPL

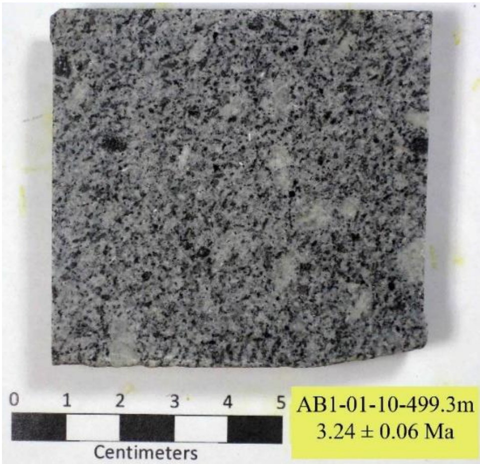

Dalam Andesite

90-TM-GRS-1 | PPL & XPL

94-TH3-DA | PPL & XPL

NSC-09-02 (246m) | PPL & XPL

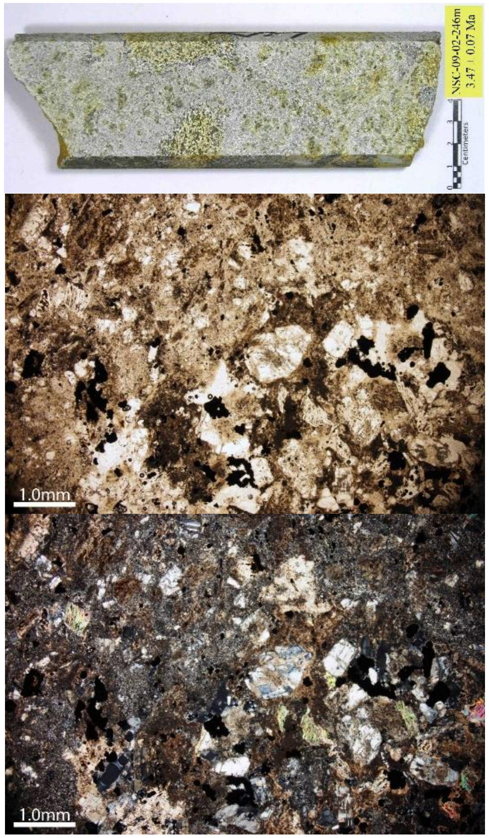

GCZ-50-02 (105m) | PPL & XPL

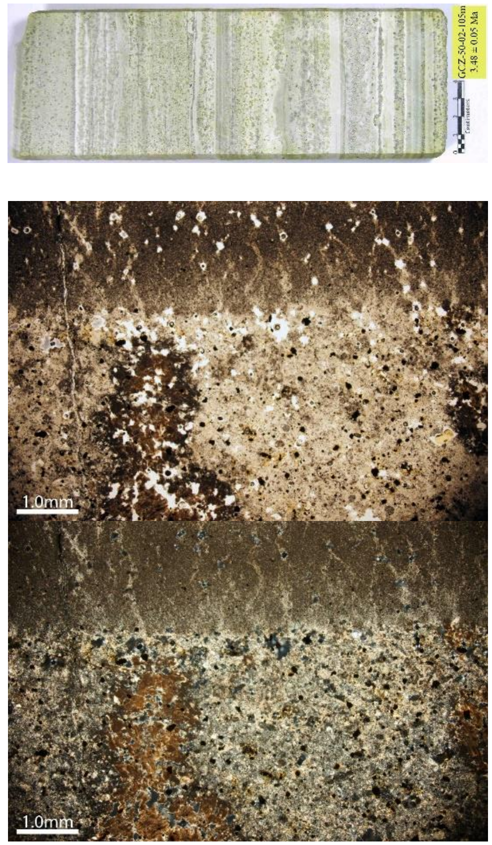

GCZ-41-01 (59.1m) | PPL & XPL

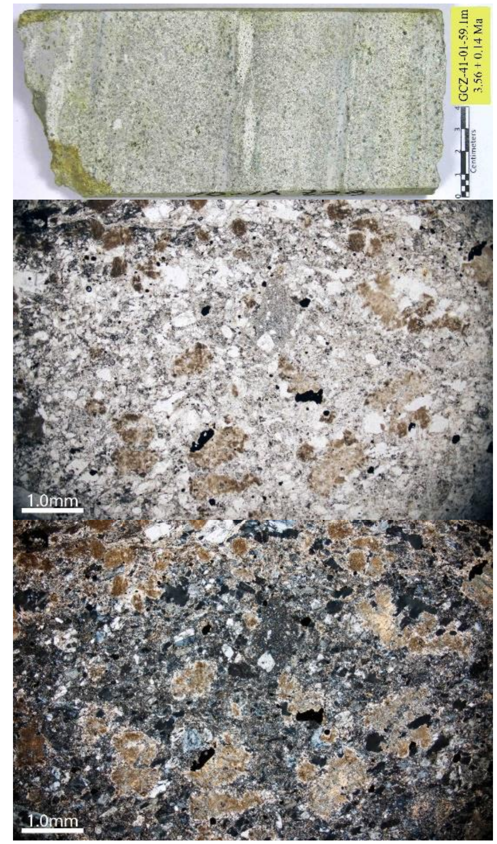

GT-INC-023 (22m) | PPL & XPL

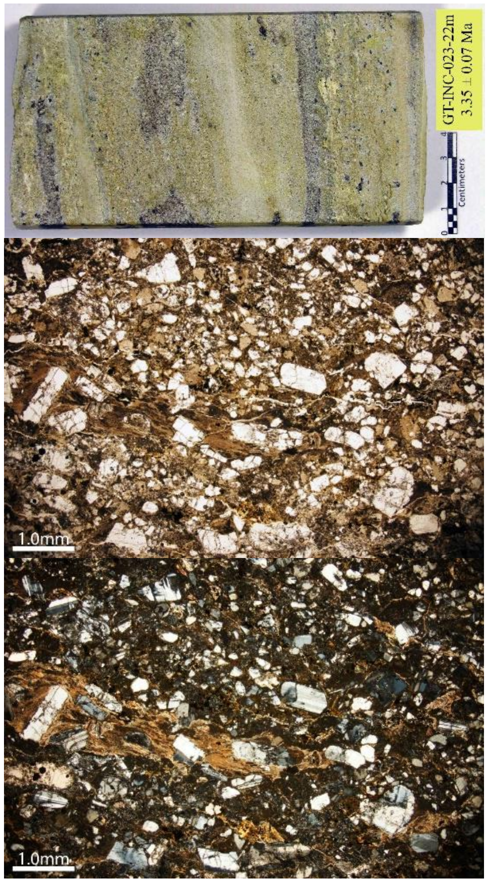

NSC-09-02 (290m)

Dalam Volcanic

Dalam Fragmental

14-SW-07 | PPL & XPL

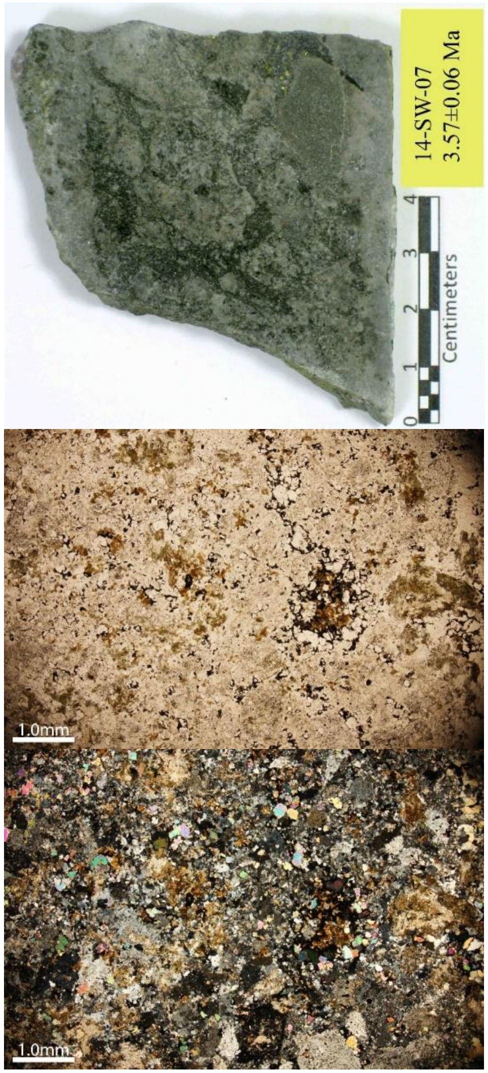

GRS-123 (0m) | PPL & XPL

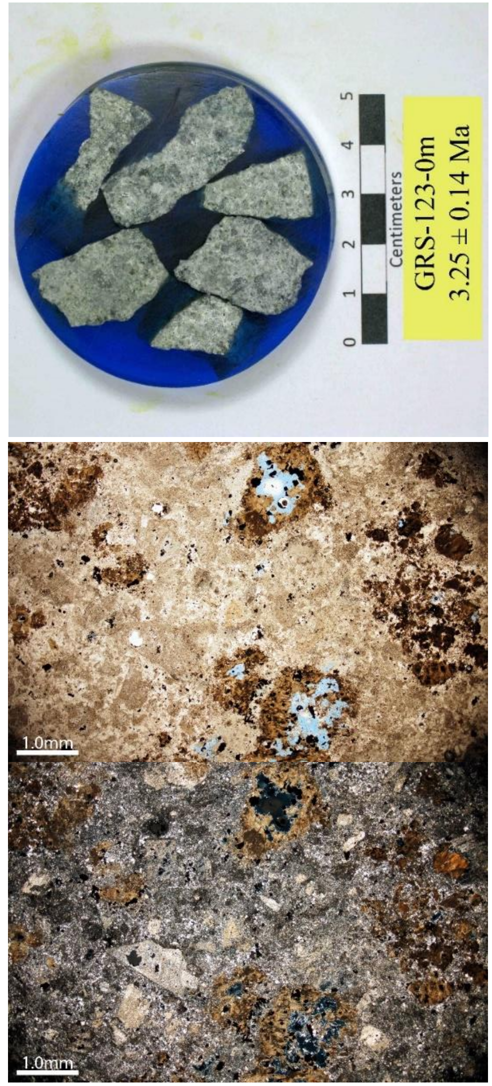

14-SW-06

Dalam Diorite

GRD41-01 (348m) | PPL & XPL

GRD42-06 (523.4m) | PPL & XPL

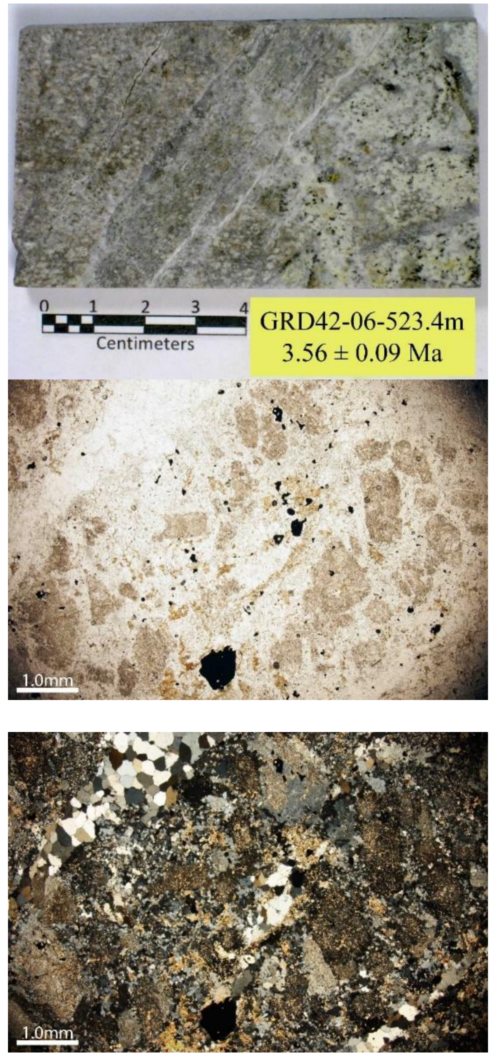

GRD32-06 (46m) | PPL & XPL

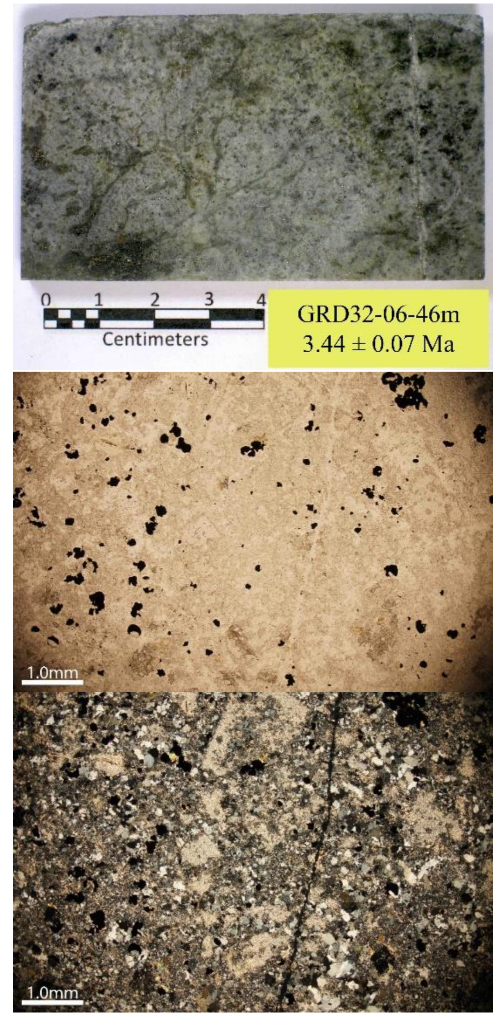

Dalam Diorite

GRD36-14 (308m) | PPL & XPL

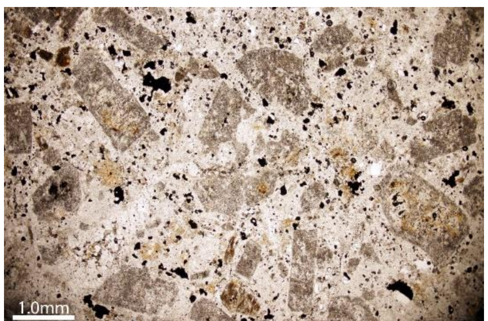

GRD36-15 (328m) | PPL & XPL

KL98-10-21 (1192m) | PPL & XPL

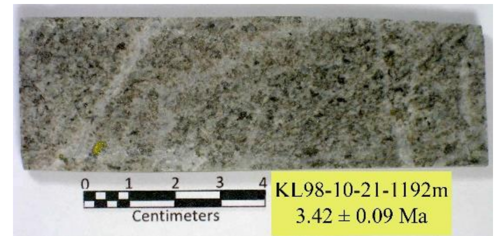

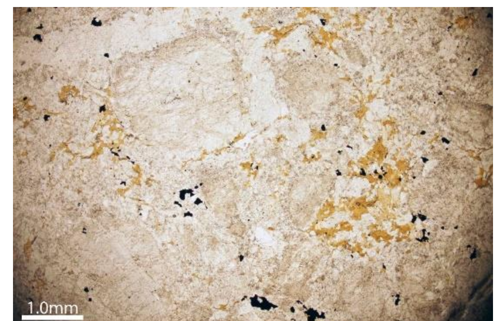

Dalam Diorite

KL98-10-21 (1243m) | PPL & XPL

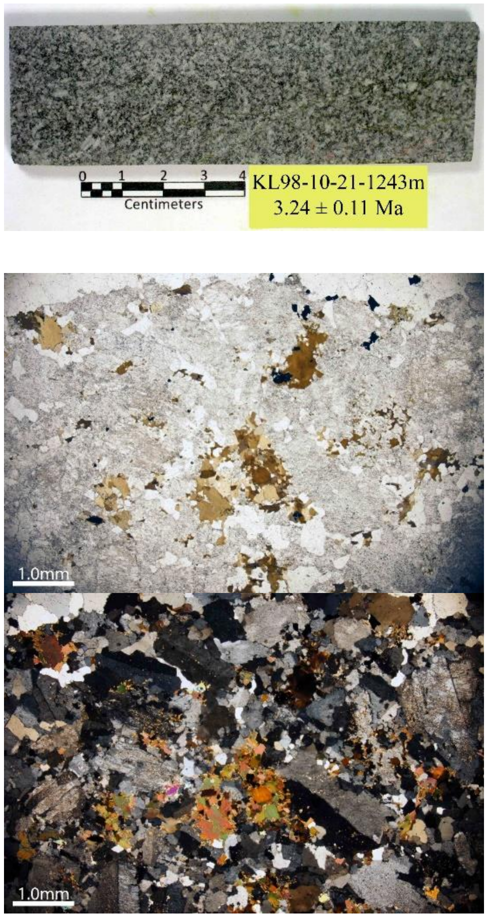

KL98-10-21 (1266m) | PPL & XPL

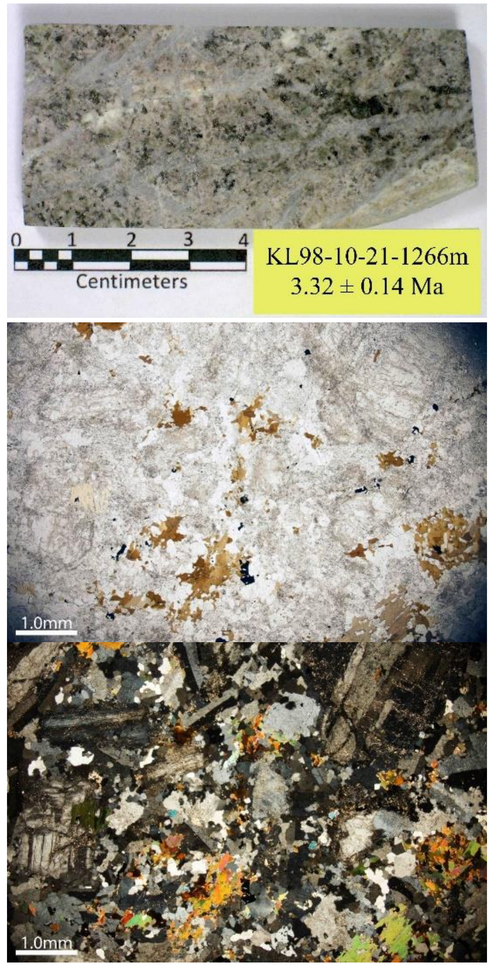

Dalam Diorite - Samples Collected by Reza Al Furqan

KL40-06 (416m) | PPL & XPL

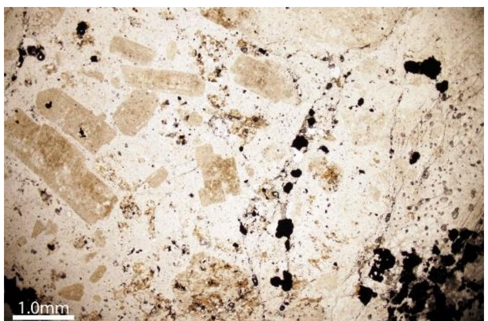

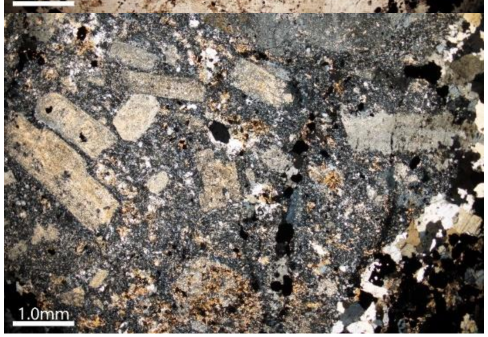

KL40-06 (516m) | PPL & XPL

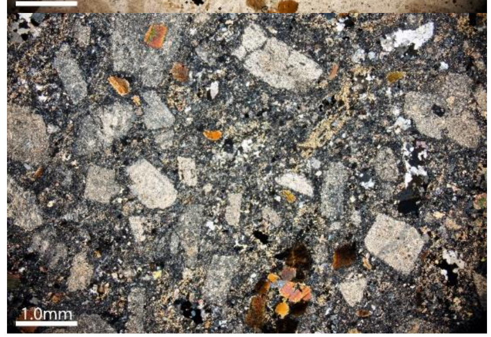

KL40-06 (762m) | PPL & XPL

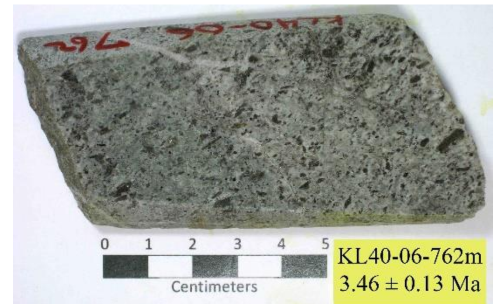

Ertsberg

TE 07-29-5m | PPL & XPL

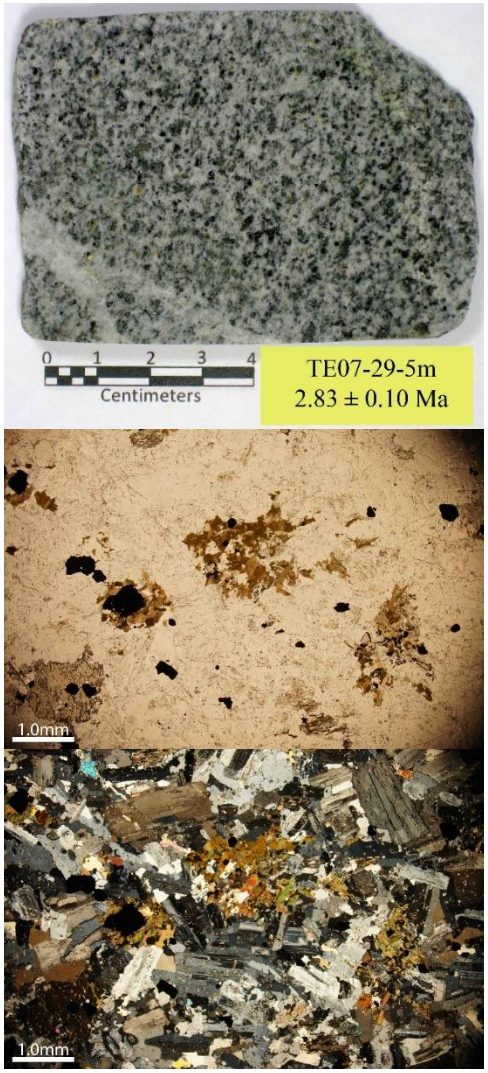

D5-15 (244.5m) | PPL & XPL

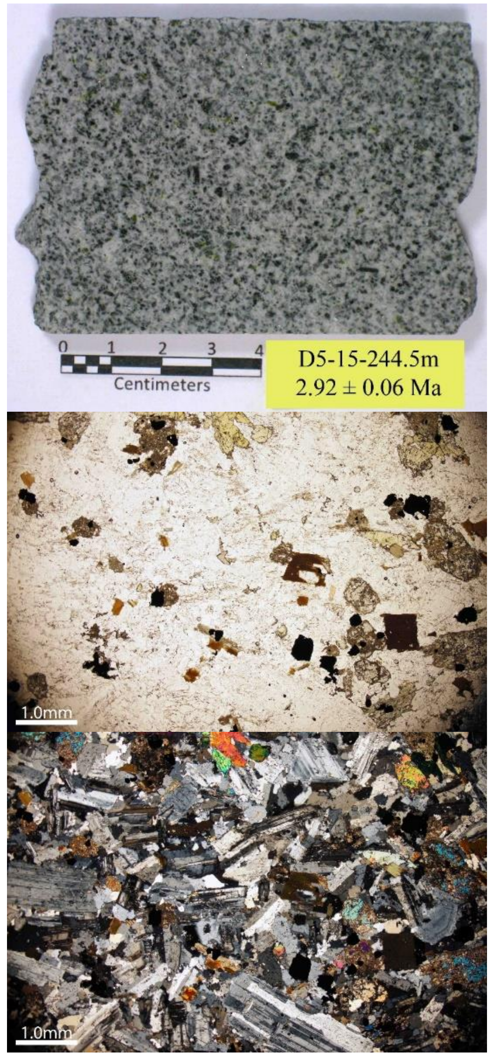

DMLZC-05-01 (248m) | PPL & XPL

TEW01-01 (75.5m) | PPL & XPL

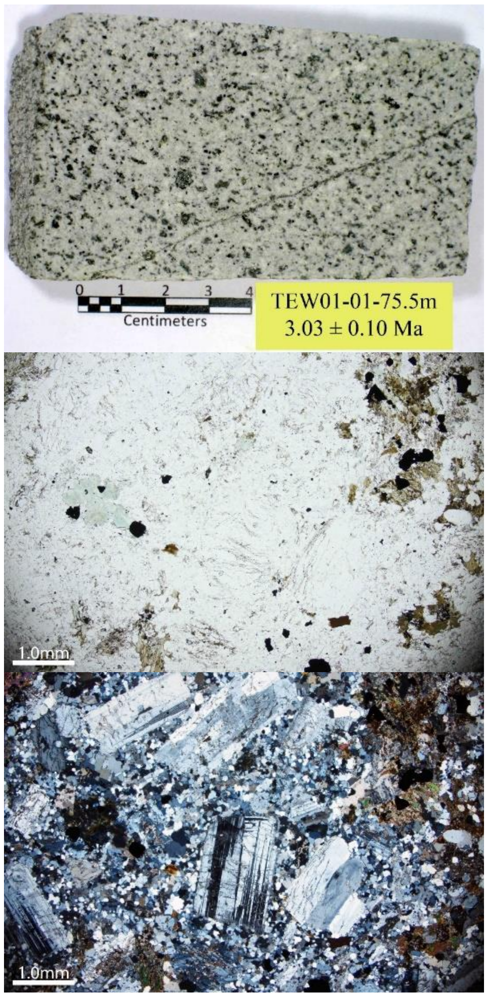

GB23-02 (56m) | PPL & XPL

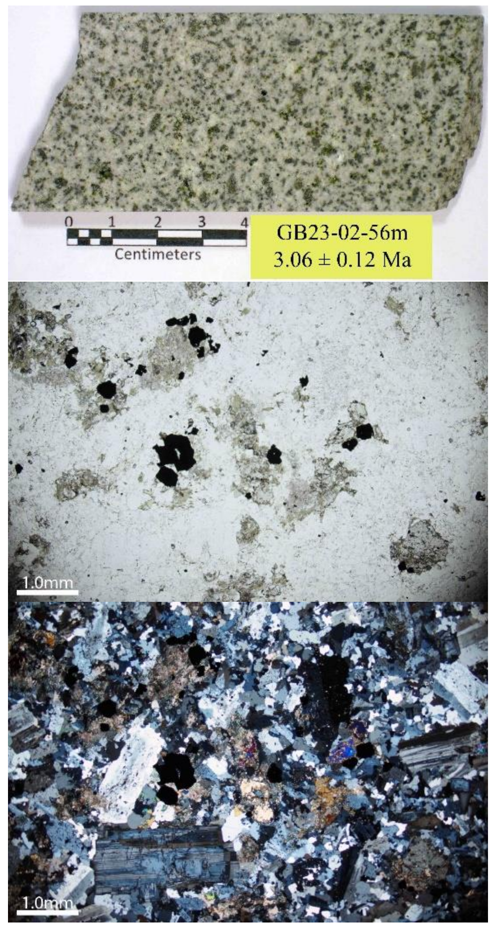

GBC3-01-01 (902m) | PPL & XPL

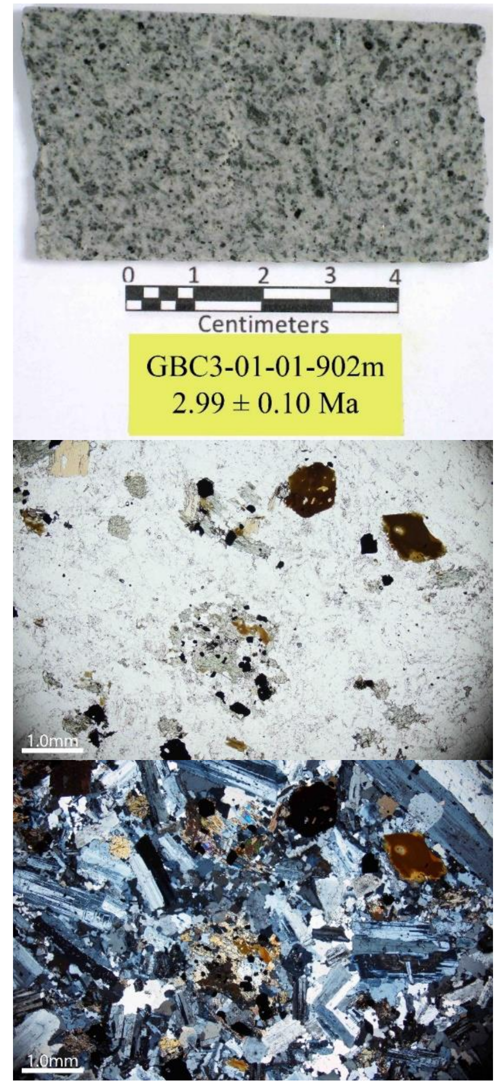

Ertsberg

KL12-02 (82m) | PPL & XPL

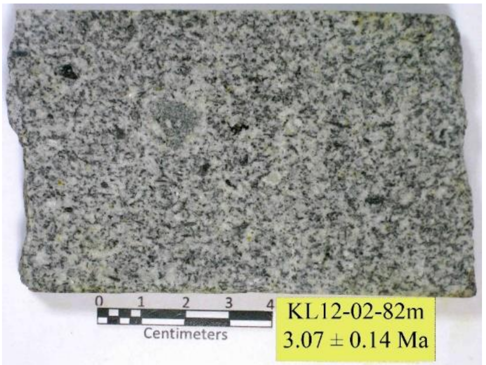

89-GA-GB-1 (1001) | PPL & XPL

89-GA-GB-1 (1001) Additional Ages:
K-Ar Age: 3.00 ± 0.09 Ma
Ar-Ar Age: 2.81 ± 0.02 Ma

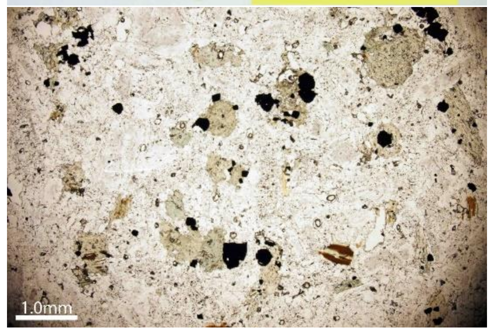

DOW-53-01 (458.4) | PPL & XPL

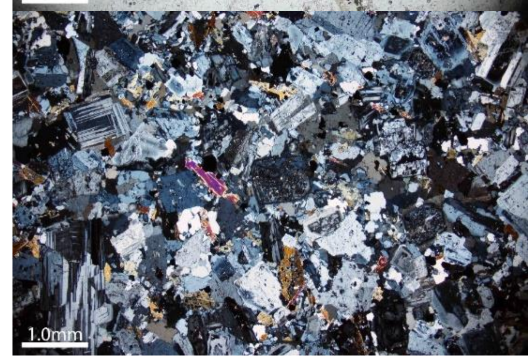

Ertsberg

SEID-MLZ-05 (297m) | PPL & XPL

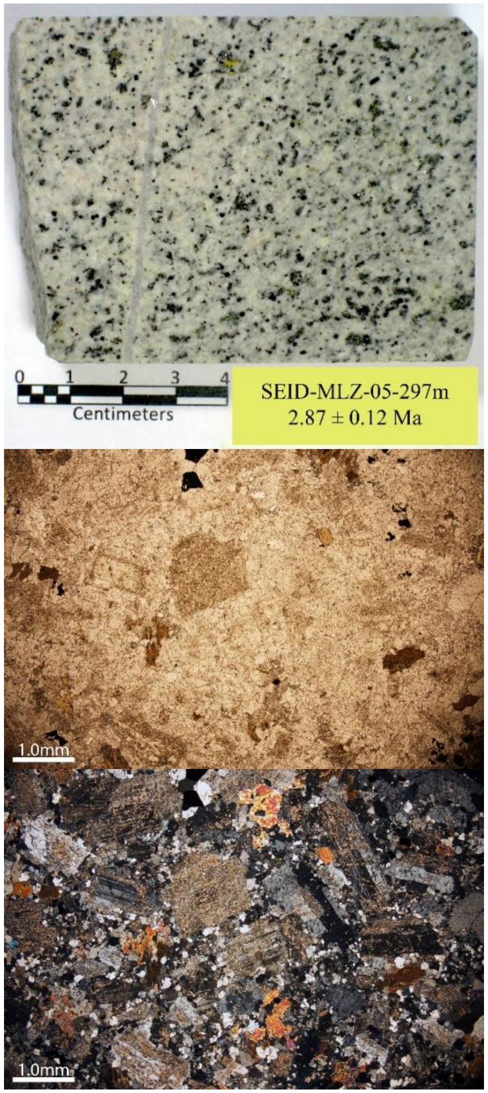

90-TM-MLA-1 (1004) | PPL & XPL

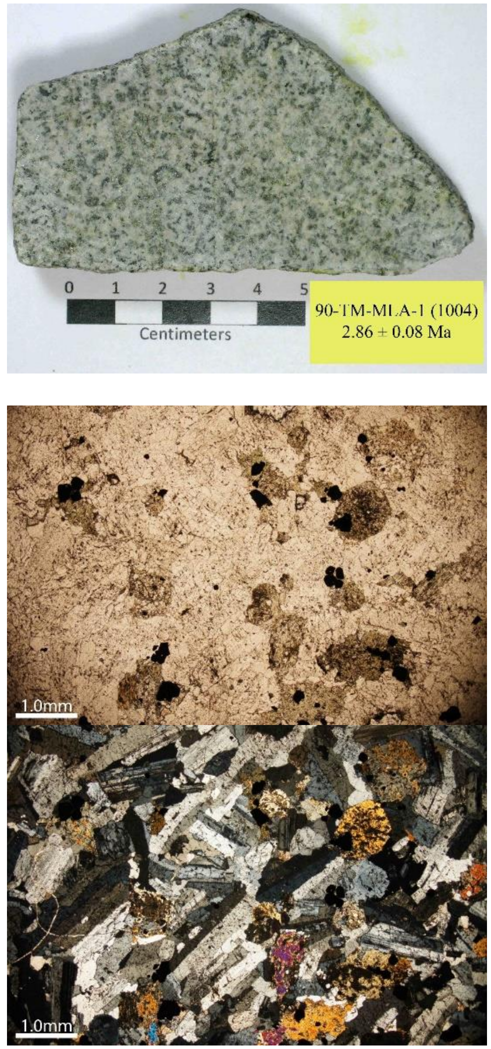

ABE-01-01 (143m) | PPL & XPL

Ertsberg

AB1-10-01 (2.2m) | PPL & XPL

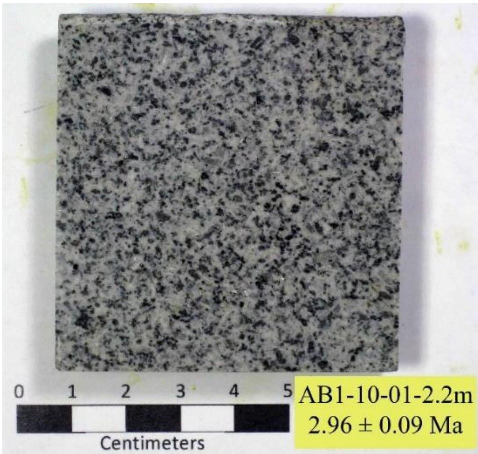

73.1-91 (1008) | PPL & XPL

ET 69/70-91 (1003) | PPL & XPL

ET69/70-91 (1003) Additional Ages:
K-Ar Age: 3.09 ± 0.25 Ma
Apatite Fission Track Age: 3.3 ± 0.8 Ma

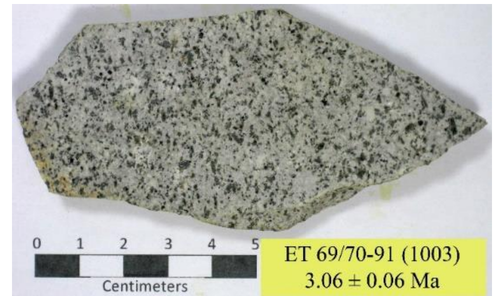

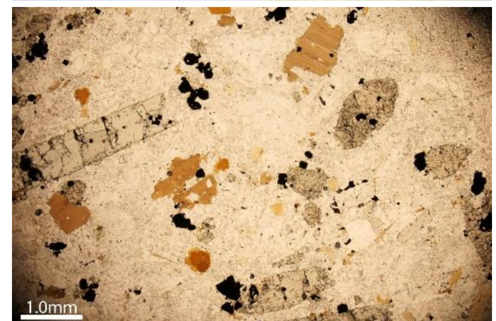

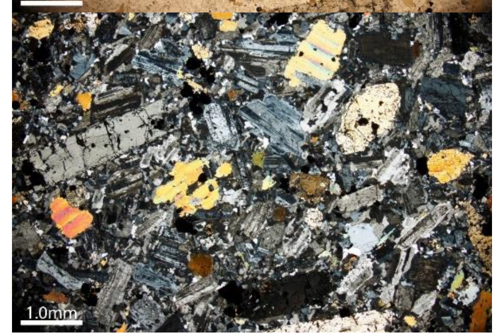

Ertsberg

TEW-11-01 (690m)

Ertsberg Vertical Core

TEW08-01 (0m) | PPL & XPL

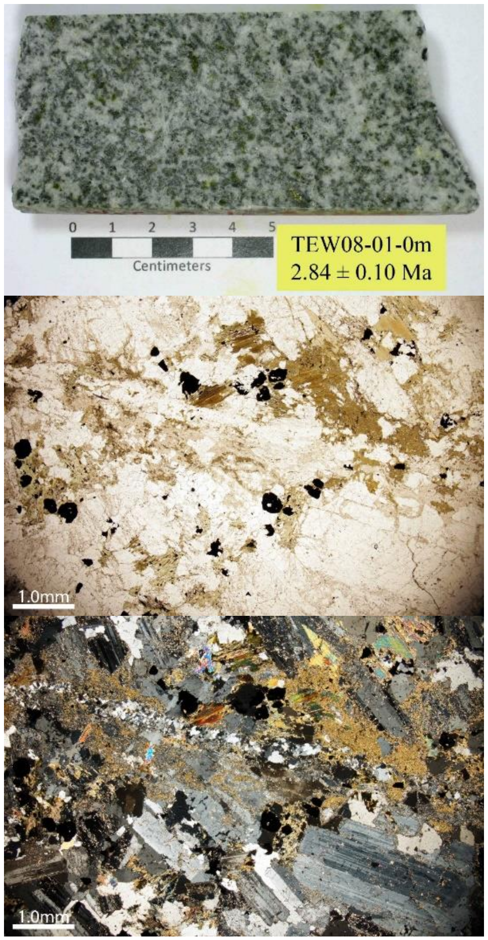

TEW08-01 (500m) | PPL & XPL

TEW08-01 (1275m) | PPL & XPL

Dike in Ertsberg

GBC3-01-01 (1033m) | PPL & XPL

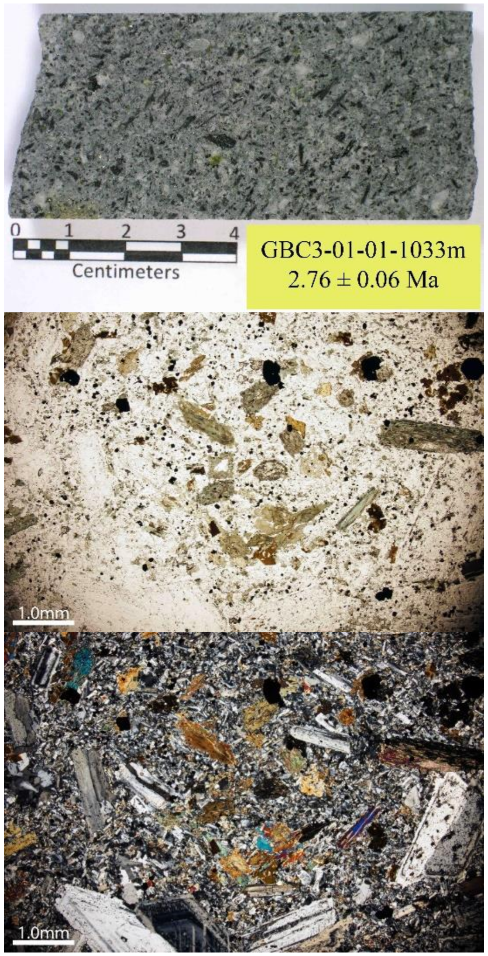

Karume

GBC6-01-01 (50.9m) | PPL & XPL

GBC3-01-01 (37.7m) | PPL & XPL

KL20-10 (3m) | PPL & XPL

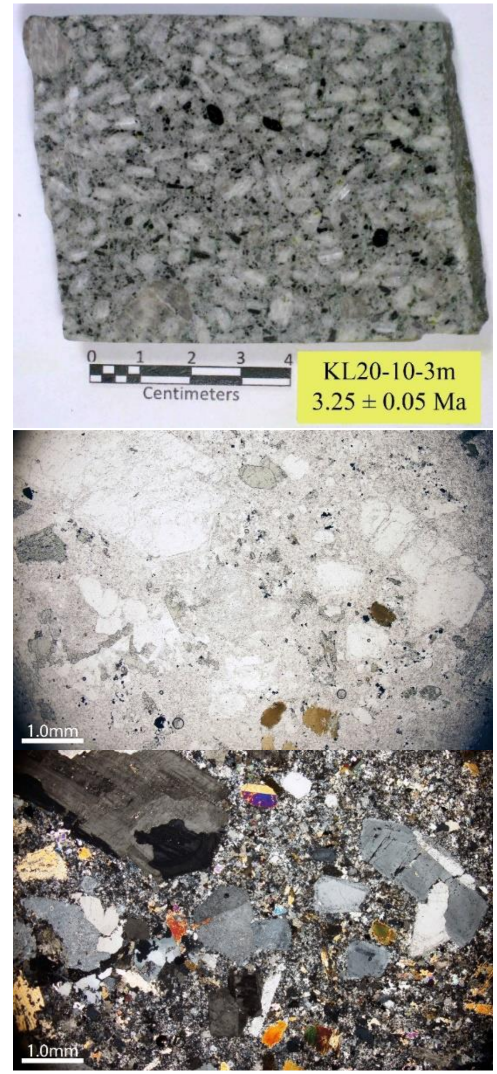

AB1-10-01 (573.2m) | PPL & XPL

90-TM-KP-1 (5003) | PPL & XPL

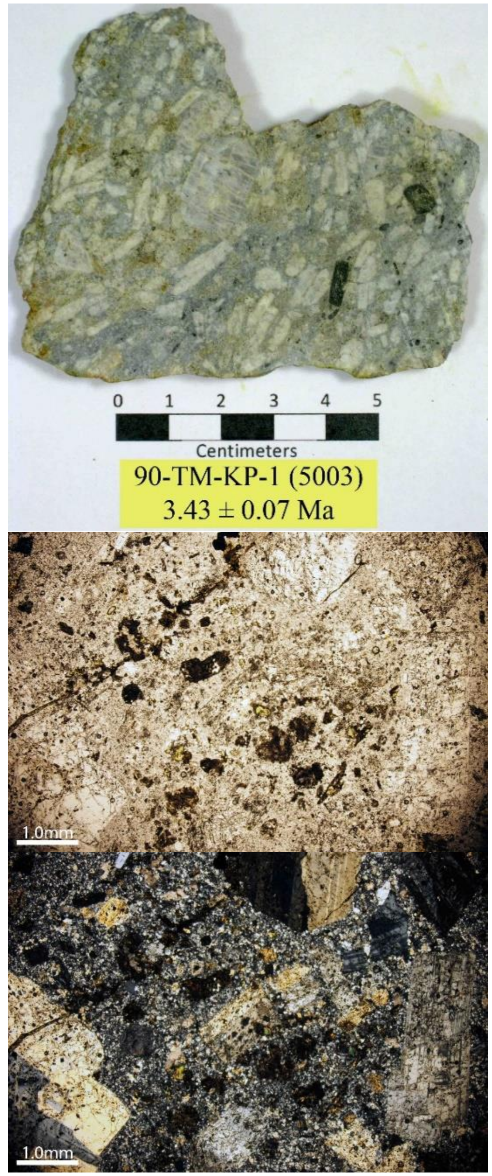

Kucing Liar Area

Tpi

KL98-10-22 (1460m) | PPL & XPL

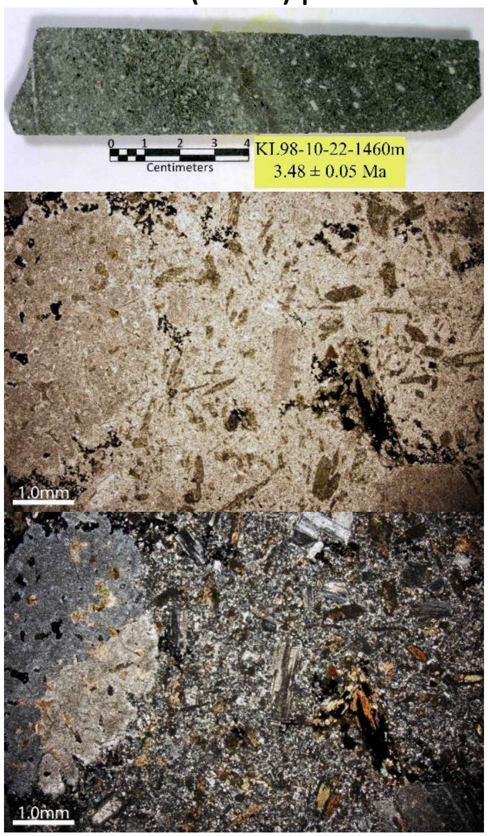

KL98-10-22 (1505m) | PPL & XPL

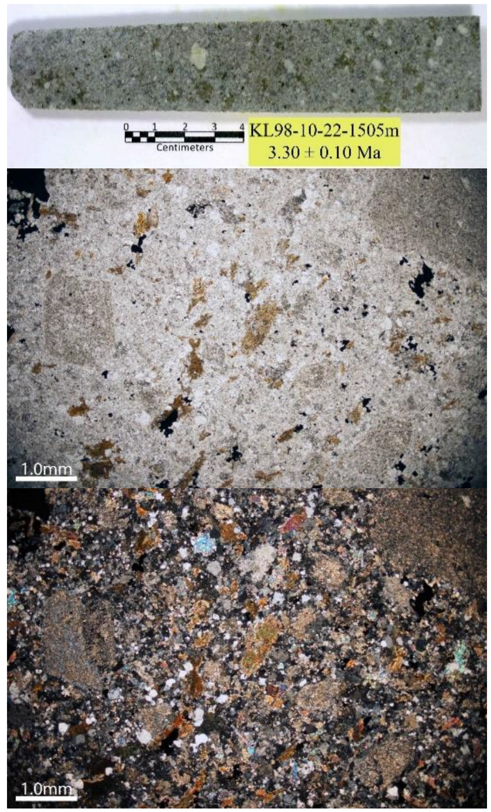

KL98-10-22 (1544m) | PPL & XPL

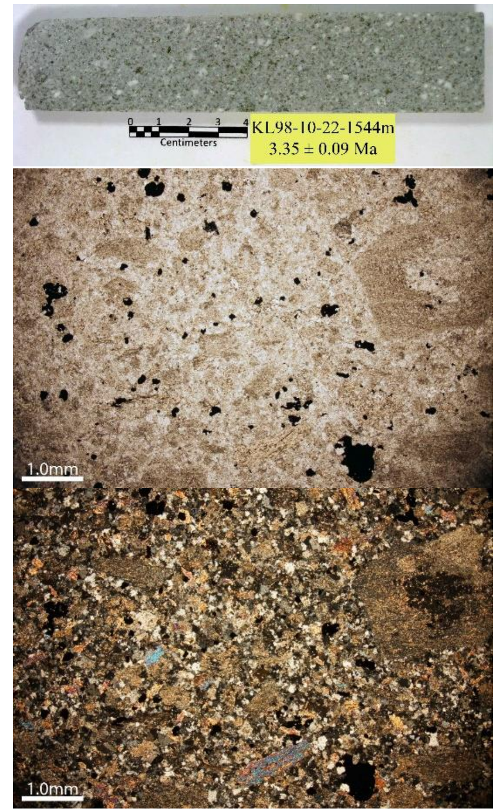

KL98-10-21 (727m) | PPL & XPL

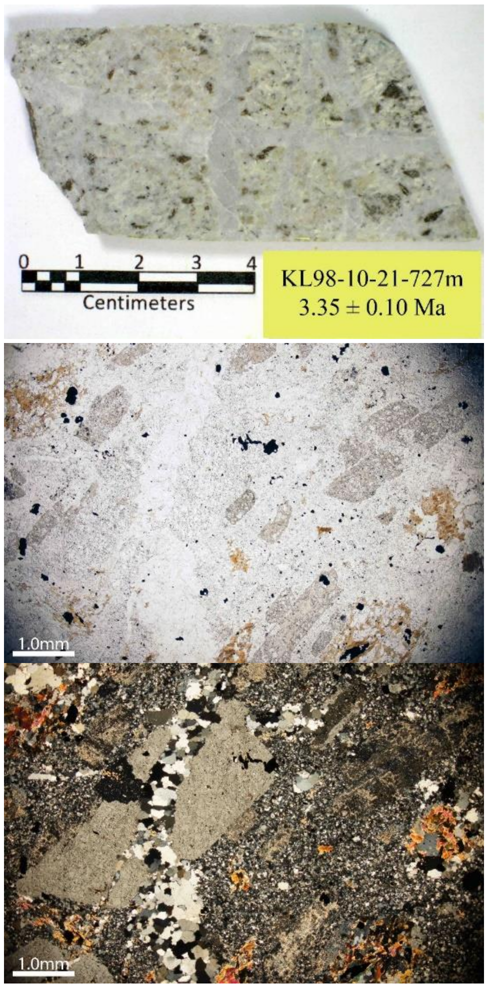

KL98-10-21 (841m) | PPL & XPL

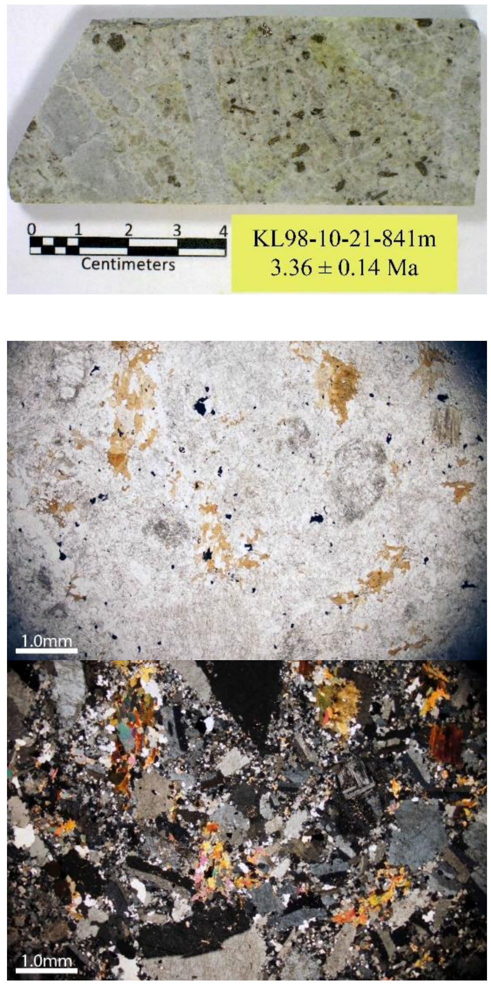

KL98-10-21 (922m) | PPL & XPL

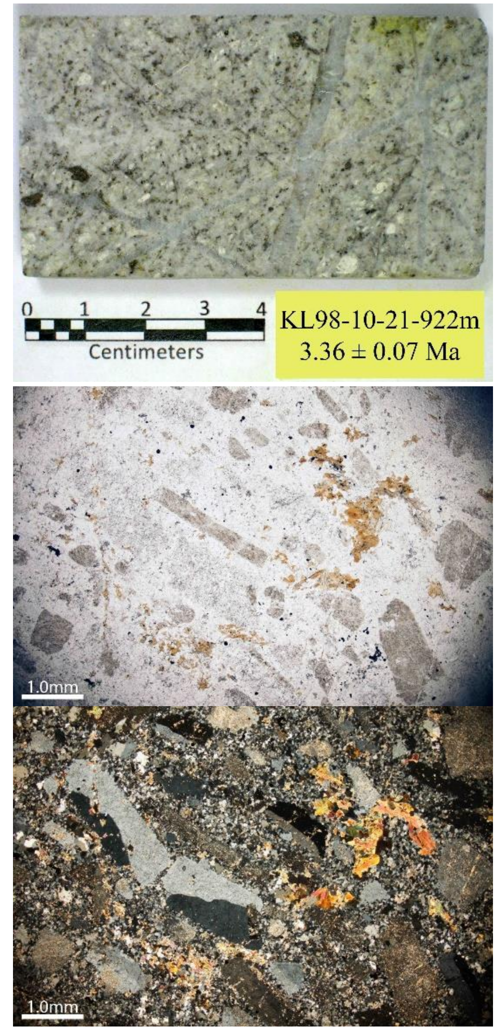

Tigt

KL98-10-21 (948m) | PPL & XPL

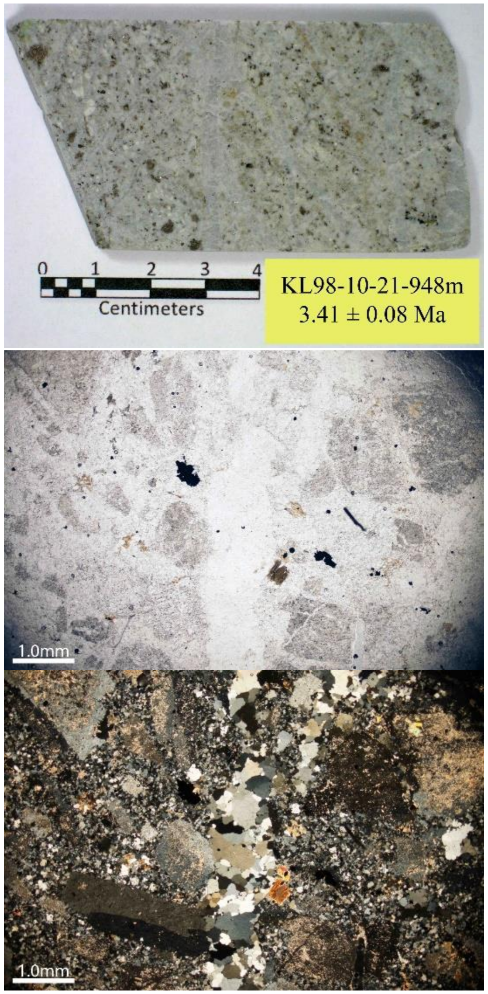

KL98-10-21 (982m) | PPL & XPL

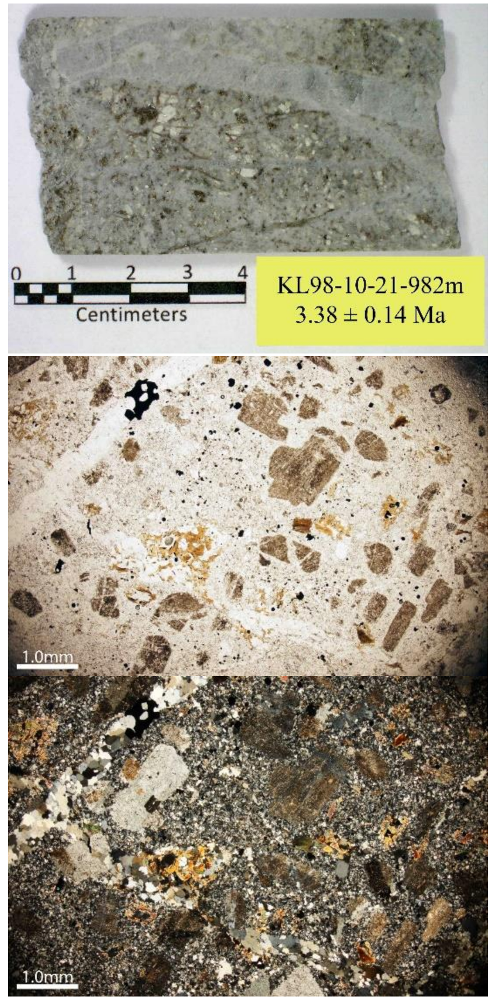

KL98-10-21 (1132m) | PPL & XPL

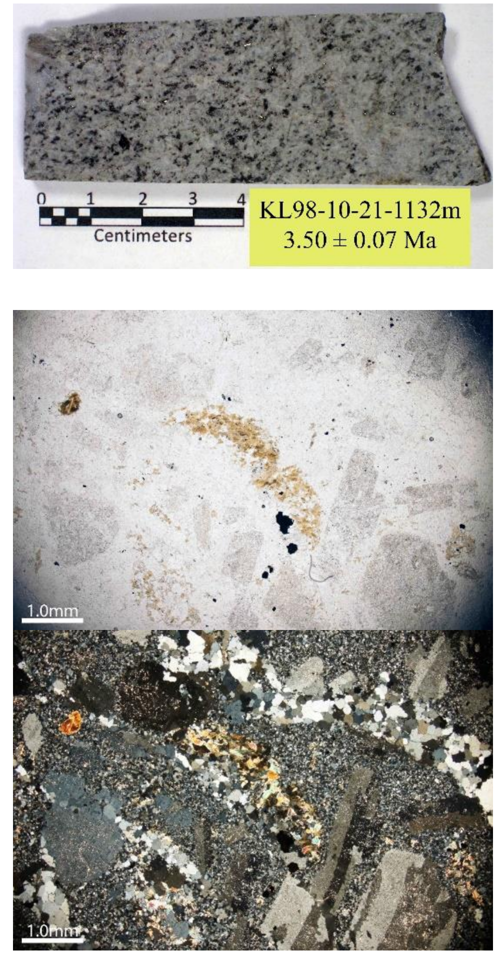

KL98-10-22 (1254m) | PPL & XPL

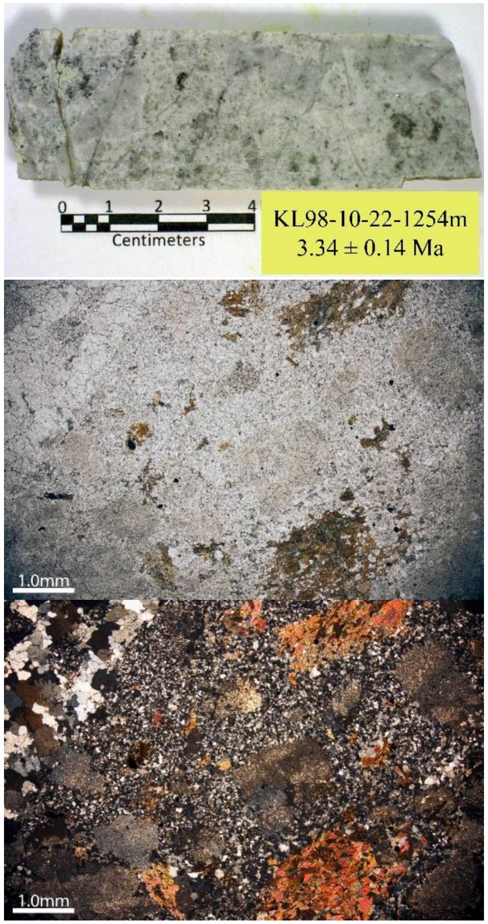

KL98-10-22 (1344m) | PPL & XPL

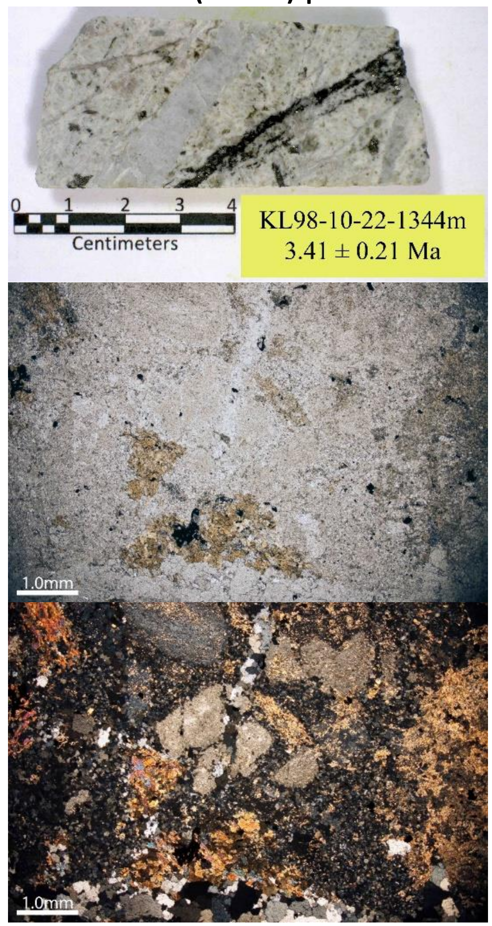

KL98-10-22 (1389m) | PPL & XPL

Other Samples

Idenberg

ID41E-02 (645m) | PPL & XPL

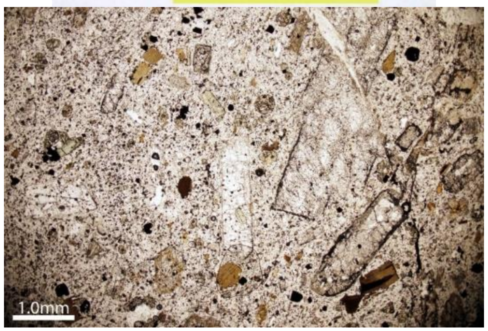

Kay

K4-197-91 (6001) | PPL & XPL

K4-197-91 (6001) Additional Ages:
K-Ar Age: 4.44 ± 0.10 Ma
Apatite Fission Track Age: 3.0 ± 0.9 Ma

North Grasberg

89-TM-NG-1 (3001) | PPL & XPL

89-TM-NG-1 (3001) Additional Ages:
Ar-Ar Age: 3.06 ± 0.02 Ma
K-Ar Age: 3.50 ± 0.23 Ma

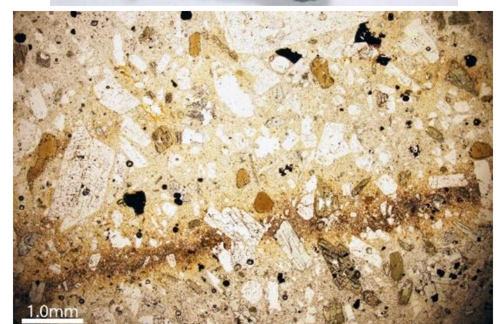

WDDPZ-05 (211.6m) | PPL & XPL

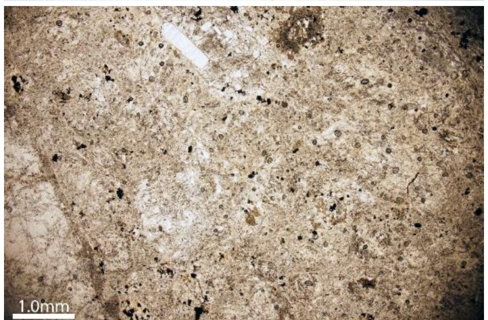

WDDPZ-05 (211.6m) | PPL & XPL

Wanagon Area

WD17-05 (18.7m) | PPL & XPL

89-TM-WAN-1 (4001) | PPL & XPL

89-TM-WAN-1 (4001) Additional Ages:
Ar-Ar Age: 3.7 ± 0.1 Ma
K-Ar Age: 3.81 ± 0.06 Ma

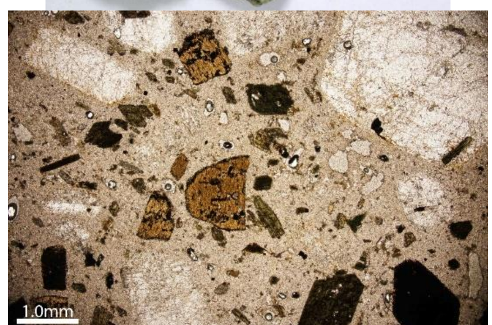

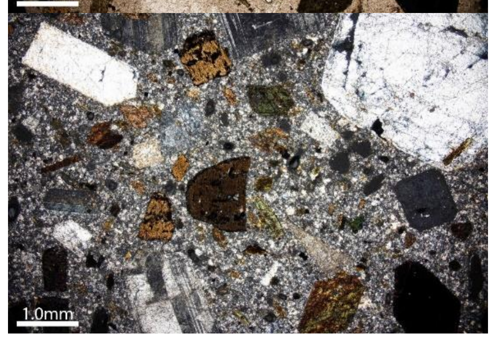

WA1-91 (7001) | PPL & XPL

93-MC-HR3a | PPL & XPL

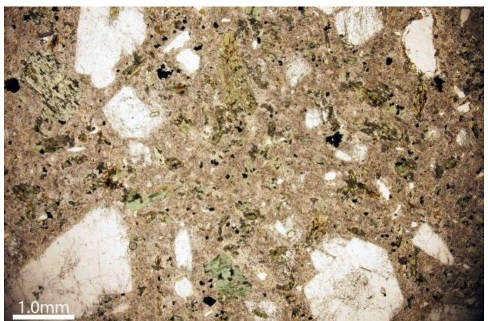

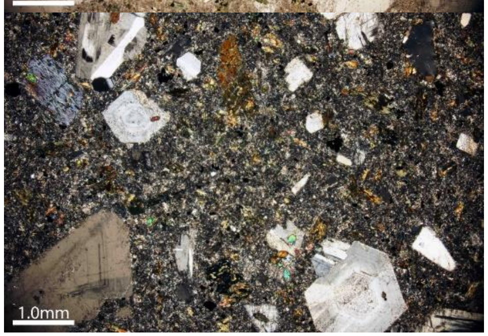

93-MC-HR3b | PPL & XPL

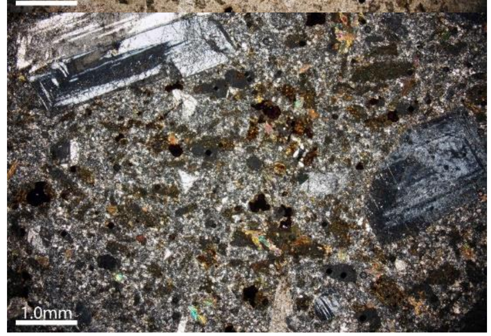

93-MC-HR5 | PPL & XPL

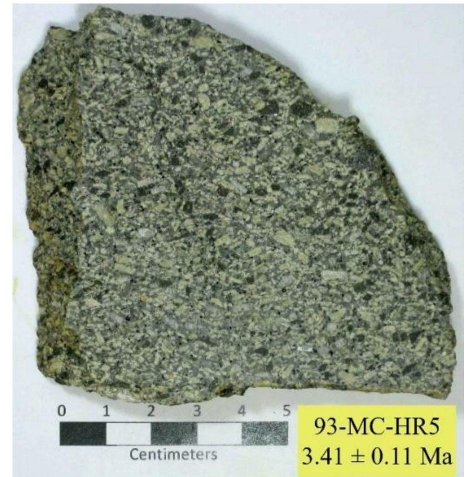

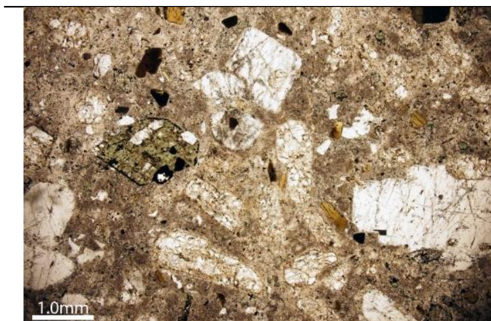

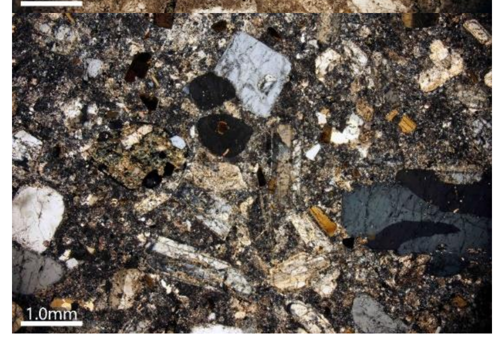

Heat Road Intrusions

94-MC-HR6 | PPL & XPL

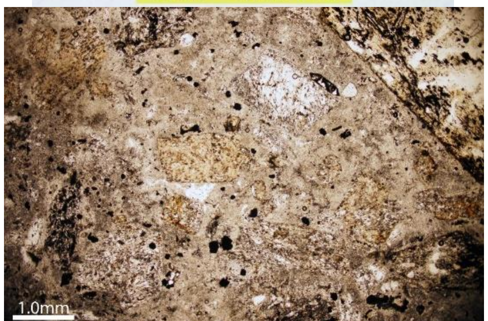

94-MC-HR7 | PPL & XPL

Utikinogen | Schappert Falls | Tpi 2

95-MC-UR3 | PPL & XPL

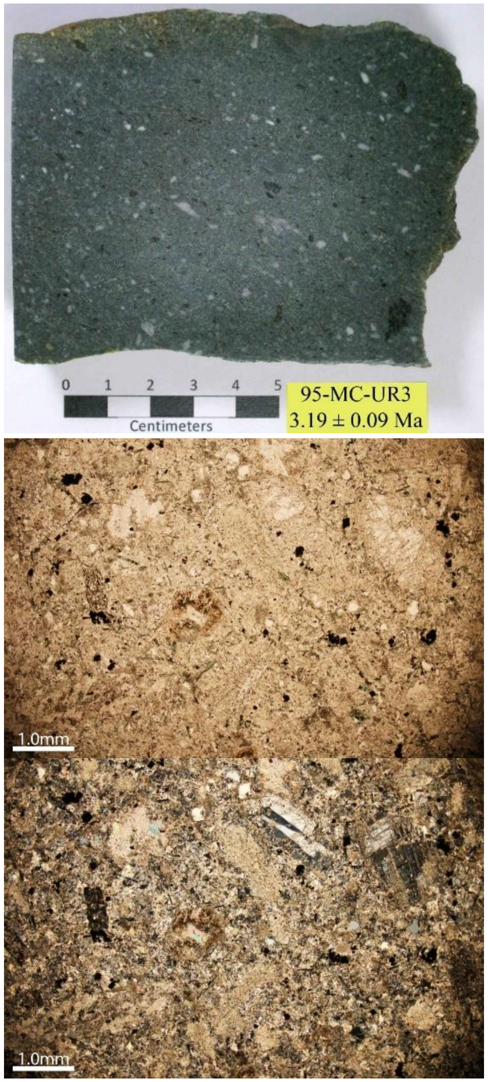

I1-91 (7002) | PPL & XPL

KL20-10 (601.9m) | PPL & XPL

Big Gossan Dike

KL20-10 (601.9m) | PPL & XPL

Ridge Camp

94-MC-RC2 | PPL & XPL

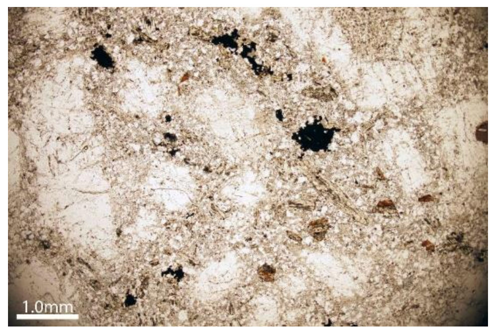

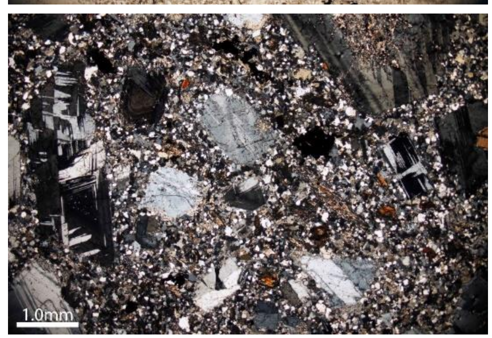

Southeast Intrusion

SE02-01 (117.4m) | PPL & XPL

Appendix E: Zircon U/Pb Age Results

	207Pb/235U	207Pb/235U error	206Pb/238U	206Pb/238U Error	Error Correlation 206/238 vs. 207/235	Final Age (Ma)	Error (Ma)	Approx U (ppm)	Approx Th (ppm)
GRD32-06-279m_1	0.0035	0.0021	0.000481	0.000079	-0.013126	3.1	0.51	110	103
GRD32-06-279m_2	0.0033	0.0013	0.000476	0.000044	0.038971	3.07	0.29	169	168
GRD32-06-279m_3	0.0043	0.0013	0.000523	0.00004	0.0026672	3.37	0.25	196	162
GRD32-06-279m_4	0.0043	0.0014	0.000464	0.000055	-0.017047	2.99	0.35	203	217
GRD32-06-279m_5	0.0058	0.0012	0.000471	0.000051	0.035985	3.04	0.33	245.1	220
GRD32-06-279m_6	0.00548	0.00086	0.000504	0.000043	-0.097618	3.25	0.27	350.9	331.1
GRD32-06-279m_7	0.00401	0.00069	0.000472	0.000046	-0.080786	3.04	0.3	248	268
GRD32-06-279m_8	0.0075	0.0027	0.000557	0.000092	-0.047261	3.59	0.59	120.5	108.5
GRD32-06-279m_9	0.0066	0.001	0.000449	0.000044	0.26886	2.9	0.28	332	210
GRD32-06-279m_10	0.006	0.0012	0.000515	0.000068	-0.059177	3.32	0.44	169.4	108.1
GRD32-06-279m_11	0.0084	0.0022	0.000529	0.00005	0.16836	3.41	0.32	166.3	135.5
GRD32-06-279m_12	0.0078	0.001	0.000489	0.00006	0.094909	3.15	0.39	189.7	137.9
GRD32-06-279m_13	0.0073	0.0018	0.000535	0.000053	0.29007	3.45	0.34	236	189
GRD32-06-279m_14	0.0041	0.0013	0.000544	0.000053	0.16548	3.51	0.34	170	132
GRD32-06-279m_15	0.0074	0.0011	0.000476	0.000044	0.076302	3.07	0.28	249	253
GRD32-06-279m_16	0.00288	0.00099	0.00044	0.00005	0.55333	2.83	0.32	355.5	458
GRD32-06-279m_17	0.0085	0.0022	0.000504	0.000077	0.1518	3.25	0.5	173	145
GRD32-06-279m_18	0.0084	0.0016	0.000453	0.00005	0.076366	2.92	0.32	322	286
GRD32-06-279m_19	0.00494	0.00095	0.000481	0.000037	0.079841	3.1	0.24	297	197
GRD32-06-279m_20	0.0252	0.0032	0.000656	0.000094	0.30147	4.23	0.6	195.9	140.8
GRD32-06-279m_21	0.0044	0.0011	0.000454	0.000051	-0.12318	2.93	0.33	283	232
GRD32-06-279m_22	0.0089	0.0032	0.000404	0.000083	0.0017715	2.61	0.54	149	122
GRD32-06-279m_23	0.0048	0.0019	0.000474	0.000092	-0.13915	3.06	0.59	198.1	112.5
GRD32-06-279m_24	0.00669	0.00092	0.000493	0.000047	-0.10287	3.18	0.3	307	310
GRD32-06-279m_25	0.00462	0.00085	0.000474	0.000044	0.19035	3.06	0.28	271.7	215
GRD32-06-279m_26	0.0061	0.001	0.00054	0.000064	-0.1279	3.48	0.41	313	461
GRD32-06-279m_27	0.0098	0.0018	0.000549	0.000094	-0.16116	3.54	0.61	185.9	147.1
GBC6-01-01-74m_1	0.0066	0.0014	0.000482	0.000047	0.0022376	3.11	0.31	160	151
GBC6-01-01-74m_2	0.00431	0.00098	0.00051	0.000055	0.041467	3.29	0.35	158.9	138.6
GBC6-01-01-74m_3	0.0066	0.0013	0.000547	0.000075	0.67542	3.53	0.48	170	170
GBC6-01-01-74m_4	0.0043	0.001	0.000498	0.000052	0.011913	3.21	0.34	167	158
GBC6-01-01-74m_5	0.0051	0.0011	0.000457	0.000048	0.085164	2.95	0.31	177	175
GBC6-01-01-74m_6	0.0059	0.001	0.000495	0.000046	0.14238	3.19	0.3	160.4	126.3
GBC6-01-01-74m_7	0.006	0.0015	0.000488	0.000047	0.043578	3.14	0.3	170.7	128
GBC6-01-01-74m_8	0.0053	0.0012	0.000488	0.000057	0.18276	3.14	0.37	120.4	102
GBC6-01-01-74m_9	0.0051	0.0012	0.000476	0.000054	0.16336	3.07	0.34	135.1	74.8
GBC6-01-01-74m_10	0.00576	0.00097	0.000489	0.000051	0.28962	3.15	0.33	201.8	204
GBC6-01-01-74m_11	0.00362	0.00083	0.000416	0.000044	0.0053107	2.68	0.28	150.9	106.4
GBC6-01-01-74m_12	0.0038	0.001	0.000458	0.000044	0.19902	2.95	0.28	145	112
GBC6-01-01-74m_13	0.00388	0.00079	0.000446	0.000041	0.23141	2.87	0.26	189.4	180.2
GBC6-01-01-74m_14	0.0062	0.0012	0.000501	0.000048	0.12881	3.23	0.31	166	159
GBC6-01-01-74m_15	0.0058	0.0013	0.000464	0.000047	0.17956	2.99	0.3	165	117.7
GBC6-01-01-74m_16	0.00568	0.00093	0.000507	0.000045	0.28804	3.27	0.29	205	191
GBC6-01-01-74m_17	0.0033	0.001	0.00056	0.000056	0.019504	3.61	0.36	150.5	139.3
GBC6-01-01-74m_18	0.005	0.001	0.000478	0.000036	0.18135	3.08	0.23	295	282
GBC6-01-01-74m_19	0.0065	0.0013	0.000502	0.000051	0.33572	3.23	0.33	219	203
GBC6-01-01-74m_20	0.00432	0.00096	0.000473	0.000053	0.17069	3.05	0.34	155.9	139
GBC6-01-01-74m_21	0.0054	0.0014	0.000467	0.000049	0.19204	3.01	0.32	179	151
GBC6-01-01-74m_22	0.00357	0.00077	0.000511	0.000046	0.056407	3.29	0.3	193	149
GBC6-01-01-74m_23	0.00428	0.00093	0.00051	0.000046	0.11634	3.29	0.3	149	108.3
GBC6-01-01-74m_24	0.00399	0.00073	0.00043	0.000038	0.045122	2.77	0.25	303	274
GBC6-01-01-74m_25	0.0056	0.001	0.000472	0.000041	0.069531	3.04	0.26	188	121.2
GBC6-01-01-74m_26	0.0052	0.0012	0.000542	0.000056	0.16402	3.49	0.36	166	92.3
GBC6-01-01-74m_27	0.00404	0.00079	0.000427	0.000038	0.020127	2.75	0.24	161.7	132.3
GBC6-01-01-74m_28	0.00502	0.00085	0.000461	0.000037	0.13574	2.97	0.24	221	149.5
GBC6-01-01-74m_29	0.00438	0.0009	0.000463	0.000048	0.22884	2.98	0.31	172	141
GBC6-01-01-74m_30	0.00402	0.00096	0.000512	0.000056	0.11827	3.3	0.36	192	157
GBC6-01-01-74m_31	0.00342	0.00065	0.000452	0.000053	0.036075	2.91	0.34	190	169
GBC6-01-01-74m_32	0.3044	0.008	0.04142	0.00088	0.23916	261.6	5.5	439.3	424
GBC6-01-01-74m_33	0.384	0.018	0.0517	0.0012	0.78952	325	7.2	600	797
GBC6-01-01-96m_1	0.0043	0.0009	0.00044	0.000048	0.0042881	2.84	0.31	168.3	150
GBC6-01-01-96m_2	0.0033	0.0011	0.000406	0.000052	0.13708	2.62	0.34	134	109
GBC6-01-01-96m_3	0.0055	0.001	0.00047	0.000047	0.19336	3.03	0.3	147.4	91.7
GBC6-01-01-96m_4	0.0045	0.00074	0.000492	0.000045	0.08419	3.17	0.29	190	157
GBC6-01-01-96m_5	0.0299	0.0038	0.000715	0.000095	0.050091	4.61	0.61	80.2	43
GBC6-01-01-96m_6	0.0044	0.001	0.000487	0.000048	0.025567	3.14	0.31	151	97
GBC6-01-01-96m_7	0.004	0.0014	0.000448	0.000066	0.12481	2.89	0.42	203	181

	207Pb/235U	207Pb/235U error	206Pb/238U	206Pb/238U Error	Error Correlation 206/238 vs. 207/235	Final Age (Ma)	Error (Ma)	Approx U (ppm)	Approx Th (ppm)
GBC6-01-01-96m_8	0.00302	0.00081	0.000472	0.000045	0.038932	3.04	0.29	176	164
GBC6-01-01-96m_9	0.0037	0.001	0.000416	0.000049	0.26039	2.68	0.31	138.6	141.3
GBC6-01-01-96m_10	0.024	0.0038	0.00067	0.00007	0.15812	4.32	0.45	194.2	156.3
GBC6-01-01-96m_11	0.0055	0.001	0.000475	0.000051	0.50851	3.06	0.33	208	209
GBC6-01-01-96m_12	0.0051	0.0014	0.000454	0.000052	0.025941	2.92	0.33	139	129
GBC6-01-01-96m_13	0.0039	0.0014	0.00055	0.00013	0.057096	3.53	0.83	315	314
GBC6-01-01-96m_14	0.00339	0.00088	0.000479	0.000059	0.02568	3.09	0.38	171	163
GBC6-01-01-96m_15	0.0045	0.0014	0.0005	0.000063	0.14454	3.22	0.41	108	81
GBC6-01-01-96m_16	0.00394	0.00068	0.000479	0.000035	0.15392	3.09	0.23	267.6	383
GBC6-01-01-96m_17	0.0062	0.0022	0.000498	0.000091	0.003737	3.21	0.59	82.3	74.8
GBC6-01-01-96m_18	0.0057	0.001	0.000519	0.000039	0.3234	3.35	0.25	222	262
GBC6-01-01-96m_19	0.0054	0.0012	0.000483	0.00005	0.096848	3.11	0.32	143	120
GBC6-01-01-96m_20	0.0048	0.0011	0.000482	0.000054	0.00097429	3.11	0.35	138.2	118.5
GBC6-01-01-96m_21	0.00416	0.00072	0.000498	0.000044	0.08892	3.21	0.28	242.9	149.1
GBC6-01-01-96m_22	0.00453	0.00087	0.000532	0.000049	0.14321	3.43	0.31	164.4	122.4
GBC6-01-01-96m_23	0.00356	0.00065	0.000473	0.00004	0.061943	3.05	0.26	200	136.1
GBC6-01-01-96m_24	0.00426	0.00075	0.000457	0.000046	0.033547	2.95	0.3	167	152.6
GBC6-01-01-96m_25	0.00271	0.00065	0.000443	0.000049	0.024658	2.85	0.31	178	149.8
GBC6-01-01-96m_26	0.00452	0.0009	0.000484	0.000059	0.055818	3.12	0.38	152.7	86.6
GBC6-01-01-96m_27	0.0055	0.0011	0.000497	0.000061	0.091048	3.21	0.39	197	142.7
GBC6-01-01-96m_28	4.32	0.067	0.2835	0.0059	0.73784	1608	30	327	29
2004_1	0.0033	0.0013	0.000468	0.000072	0.0070353	3.01	0.46	129.6	80.4
2004_2	0.0036	0.0012	0.000466	0.000073	0.038472	3	0.47	138	126
2004_3	0.0061	0.0016	0.000449	0.000076	0.064396	2.89	0.49	106.3	87
2004_4	0.0051	0.0023	0.000444	0.000087	0.30895	2.86	0.56	146.7	95.1
2004_5	0.003	0.002	0.00051	0.00011	0.15356	3.26	0.71	78	58
2004_6	0.004	0.0015	0.000383	0.000068	0.21544	2.47	0.44	95.7	78.1
2004_7	0.0056	0.0013	0.000479	0.000063	0.037238	3.09	0.4	228	157
2004_8	0.00317	0.00093	0.000467	0.000059	0.055567	3.01	0.38	173.9	137
2004_9	0.0042	0.0012	0.000457	0.000053	0.060463	2.95	0.34	180	153
2004_10	0.0037	0.0013	0.000464	0.000066	0.25539	2.99	0.43	123.5	92.2
2004_11	0.0041	0.001	0.000473	0.000054	0.13621	3.05	0.35	225	239
2004_12	0.0037	0.00095	0.000446	0.000057	0.029321	2.88	0.37	218.3	192
2004_13	0.005	0.0017	0.000516	0.000077	0.37923	3.32	0.5	170	163
2004_14	0.0053	0.0014	0.000471	0.000066	0.19784	3.03	0.43	147.5	138
2004_15	0.00385	0.00081	0.000499	0.000058	0.020476	3.22	0.37	207	200
2004_16	0.0054	0.0014	0.000455	0.000057	0.060493	2.93	0.36	204	181
2004_17	0.0058	0.0015	0.000465	0.000055	0.021706	2.99	0.35	166	135
2004_18	0.0049	0.0012	0.000476	0.000066	0.18206	3.07	0.42	170	139
2004_19	0.0044	0.001	0.000494	0.000054	0.070997	3.19	0.35	252	138.8
2004_20	0.0073	0.0024	0.000543	0.000096	0.11456	3.5	0.62	193	174
2004_21	0.0055	0.0014	0.000514	0.000056	0.090036	3.31	0.36	275	124.6
2004_22	0.0063	0.0013	0.000446	0.000062	0.013857	2.87	0.4	136	131
2004_23	0.0109	0.0053	0.00054	0.00011	0.030256	3.5	0.68	203.7	143.4
2004_24	0.0048	0.0013	0.000441	0.000057	0.03209	2.84	0.37	165	140
2004_25	0.0021	0.00094	0.000407	0.000056	0.11608	2.63	0.36	205	171.9
2004_26	0.0053	0.0013	0.000489	0.000072	0.085562	3.15	0.46	228.4	177.1
2004_27	0.00428	0.00096	0.000454	0.000054	0.066674	2.92	0.35	232	235
2004_28	0.0037	0.0011	0.000517	0.000071	0.069065	3.33	0.46	176	149
2004_29	0.0045	0.0011	0.000503	0.000067	0.017185	3.24	0.43	163.5	111.4
2004_30	0.0062	0.0013	0.000474	0.000062	0.031332	3.06	0.4	234	203
2004_31	0.0028	0.00087	0.000503	0.000061	0.22762	3.24	0.39	173	143.6
2005_1	0.0031	0.0012	0.00042	0.000068	0.016546	2.71	0.44	131.6	120.5
2005_2	0.00367	0.00063	0.000477	0.000038	0.10768	3.08	0.24	391.5	185.4
2005_3	0.0039	0.0012	0.000446	0.000064	0.0057675	2.88	0.41	147.8	121.4
2005_4	0.0034	0.0011	0.000481	0.00007	0.075647	3.1	0.45	145	69.1
2005_5	0.0041	0.001	0.000461	0.000068	0.39981	2.97	0.44	217.1	130.8
2005_6	0.0069	0.0015	0.00048	0.000062	0.057077	3.09	0.4	181.2	147.1
2005_7	0.0047	0.0022	0.00046	0.0001	0.029168	2.96	0.67	65.8	47.8
2005_8	0.0056	0.0021	0.000498	0.000089	0.050614	3.21	0.57	122	117
2005_9	0.00569	0.00093	0.000553	0.000055	0.19572	3.56	0.36	287	260
2005_10	0.004	0.00088	0.000432	0.000042	0.12653	2.78	0.27	243	258
2005_11	0.0042	0.0014	0.000429	0.000069	0.18154	2.76	0.44	116.3	104.8
2005_12	0.004	0.0013	0.000518	0.000081	0.089267	3.34	0.52	142.7	68.8
2005_13	0.0053	0.0018	0.000442	0.000075	0.011862	2.85	0.48	91.1	73
2005_14	0.0048	0.0012	0.000443	0.000056	0.083696	2.85	0.36	185	175
2005_15	0.0039	0.0011	0.000431	0.000057	0.0081518	2.77	0.37	166	131.2
2005_16	0.0061	0.0013	0.000483	0.000071	0.024698	3.12	0.46	169	157
2005_17	0.0041	0.0012	0.000451	0.000068	0.060352	2.91	0.44	151.5	111.8

	207Pb/235U	207Pb/235U error	206Pb/238U	206Pb/238U Error	Error Correlation 206/238 vs. 207/235	Final Age (Ma)	Error (Ma)	Approx U (ppm)	Approx Th (ppm)
2005_18	0.005	0.0016	0.000357	0.000074	0.034837	2.3	0.47	99.7	89.7
2005_19	0.0045	0.00093	0.000484	0.000055	0.0056611	3.12	0.35	228.4	263
2005_20	0.0044	0.0015	0.000439	0.000069	0.04543	2.83	0.44	119.3	101
2005_21	0.0078	0.0022	0.000512	0.000059	0.15152	3.3	0.38	236	244
2005_22	0.0041	0.0011	0.000453	0.000058	0.17518	2.92	0.37	196	194
2005_23	0.00372	0.00086	0.000449	0.000053	0.19247	2.89	0.34	280	183
2005_24	0.0045	0.0011	0.000467	0.000057	0.05158	3.01	0.37	279	288
2005_25	0.0039	0.0012	0.000424	0.000063	0.13433	2.73	0.41	140.6	86.6
2005_26	0.0038	0.0013	0.000454	0.000069	0.021317	2.92	0.44	137	127
2005_27	0.0045	0.0012	0.000554	0.000075	0.077816	3.57	0.49	143	118
2005_28	0.0045	0.0014	0.000511	0.000087	0.029358	3.29	0.56	136	115
2005_29	0.0045	0.0011	0.000484	0.000065	0.17785	3.12	0.42	144.9	128.8
2005_30	0.315	0.015	0.03868	0.00078	0.22444	244.6	4.8	204	210
AM9640-09-148m_1	0.0046	0.0015	0.000499	0.000068	0.039346	3.21	0.44	143.5	115.1
AM9640-09-148m_2	0.0044	0.0015	0.000532	0.00008	0.2502	3.43	0.51	129.7	122.3
AM9640-09-148m_3	0.0132	0.0035	0.000506	0.000085	0.59585	3.26	0.55	150	136
AM9640-09-148m_4	0.0077	0.002	0.000489	0.000072	0.31856	3.15	0.46	226	232
AM9640-09-148m_5	0.0058	0.0014	0.000564	0.000056	0.28978	3.64	0.36	271	181
AM9640-09-148m_6	0.0071	0.0019	0.000534	0.000079	0.045453	3.44	0.51	145	126
AM9640-09-148m_7	0.0195	0.0022	0.000604	0.000068	0.038798	3.89	0.44	280	121
AM9640-09-148m_8	0.0112	0.0023	0.000499	0.000059	0.13837	3.22	0.38	245	169
AM9640-09-148m_9	0.0074	0.0018	0.000558	0.00007	0.19973	3.6	0.45	152.5	151.1
AM9640-09-148m_10	0.0108	0.004	0.00061	0.00013	0.24402	3.93	0.83	153	140
AM9640-09-148m_11	0.0052	0.0014	0.000477	0.000063	0.020096	3.07	0.41	195	198
AM9640-09-148m_12	0.0165	0.0024	0.000551	0.000067	0.0021252	3.55	0.43	170	167.2
AM9640-09-148m_13	0.0054	0.001	0.000483	0.000046	0.054157	3.11	0.29	315.1	236
AM9640-09-148m_14	0.0082	0.0015	0.000523	0.000062	0.013958	3.37	0.4	212	200
AM9640-09-148m_15	0.00654	0.00068	0.000498	0.000029	0.0094099	3.21	0.18	816	398
AM9640-09-148m_16	0.0055	0.0013	0.000441	0.000047	0.38286	2.84	0.31	228	230
AM9640-09-148m_17	0.0078	0.0019	0.000494	0.000071	0.25146	3.18	0.46	168	144
AM9640-09-148m_18	0.0083	0.0022	0.000457	0.000069	0.1261	2.95	0.45	179.9	177.4
AM9640-09-148m_19	0.0044	0.0012	0.000464	0.000054	0.077262	2.99	0.35	169.4	178.8
AM9640-09-148m_20	0.0133	0.0025	0.000581	0.00007	0.072325	3.74	0.45	184.2	119.6
AM9640-09-148m_21	0.0157	0.0022	0.000613	0.000069	0.19642	3.95	0.45	254	267
AM9640-09-148m_22	0.0054	0.002	0.000514	0.000094	0.0088713	3.31	0.6	303	302
AM9640-09-148m_23	0.0069	0.0017	0.000519	0.000069	0.0089887	3.34	0.44	165	160
AM9640-09-148m_24	0.0167	0.0036	0.00056	0.00011	0.087849	3.6	0.73	128.6	123.1
AM9640-09-148m_25	0.0074	0.0016	0.000471	0.000048	0.13023	3.03	0.31	211.6	218
AM9640-09-148m_26	0.0049	0.0013	0.000467	0.00005	0.23912	3.01	0.32	227.4	275.4
AM9640-09-148m_27	0.00453	0.00088	0.000539	0.000048	0.080454	3.47	0.31	379	143.2
AM9640-09-148m_28	0.0167	0.004	0.000506	0.000083	0.087665	3.26	0.54	111	97
AM9640-09-148m_29	0.2484	0.0094	0.0343	0.0012	0.73514	217.5	7.6	328	242.8
AM9640-09-148m_30	3.763	0.055	0.2767	0.0046	0.5466	1574	23	285.4	327.8
AM9640-09-148m_31	0.395	0.019	0.0534	0.002	0.39384	335	12	163.8	113.7
KL98-10-21-1693m_1	0.00394	0.00047	0.00047	0.000032	0.056779	3.03	0.2	374	165
KL98-10-21-1693m_2	0.00337	0.00043	0.000464	0.000028	0.026876	2.99	0.18	414	198
KL98-10-21-1693m_3	0.0062	0.0011	0.000468	0.000043	-0.13766	3.01	0.27	158	149
KL98-10-21-1693m_4	0.0095	0.0031	0.000541	0.000041	0.74236	3.49	0.26	358	430
KL98-10-21-1693m_5	0.0076	0.0027	0.00045	0.000099	0.2423	2.9	0.64	220	140
KL98-10-21-1693m_6	0.00411	0.00066	0.000513	0.000042	-0.02572	3.3	0.27	289	292
KL98-10-21-1693m_7	0.0059	0.001	0.000499	0.000052	-0.35852	3.22	0.34	205	326
KL98-10-21-1693m_8	0.00437	0.00076	0.000452	0.000037	-0.024182	2.92	0.24	197.3	252
KL98-10-21-1693m_9	0.0052	0.001	0.000519	0.000052	-0.048505	3.34	0.33	232	217
KL98-10-21-1693m_10	0.0063	0.0013	0.000521	0.000053	-0.10016	3.36	0.34	205	172
KL98-10-21-1693m_11	0.00419	0.00063	0.000475	0.000031	-0.075259	3.06	0.2	290	330
KL98-10-21-1693m_12	0.00514	0.00086	0.000456	0.000046	0.16432	2.94	0.29	234	174
KL98-10-21-1693m_13	0.00442	0.0006	0.000481	0.00003	0.032673	3.1	0.19	610	1440
KL98-10-21-1693m_14	0.00314	0.00034	0.000438	0.000031	0.18258	2.82	0.2	509	169
KL98-10-21-1693m_15	0.00403	0.00043	0.000474	0.000021	0.11091	3.05	0.14	750	470
KL98-10-21-1693m_16	0.00535	0.00092	0.00046	0.000049	-0.014759	2.96	0.32	203.6	208
KL98-10-21-1693m_17	0.0041	0.00098	0.000467	0.000038	-0.0060459	3.01	0.25	174	153
KL98-10-21-1693m_18	0.004	0.00052	0.000447	0.000025	0.21697	2.88	0.16	690	1020
KL98-10-21-1693m_19	0.00569	0.00099	0.000546	0.000044	0.085656	3.52	0.29	182	146.4
KL98-10-21-1693m_20	0.0045	0.0011	0.000502	0.000048	-0.058982	3.24	0.31	187	175
KL98-10-21-1693m_21	0.019	0.006	0.000652	0.000094	0.4769	4.2	0.61	202	145
KL98-10-21-1693m_22	0.0039	0.00052	0.000466	0.000034	0.070023	3	0.22	399	697
KL98-10-21-1693m_23	0.00554	0.00093	0.000527	0.000038	-0.11284	3.4	0.25	207.9	201.2
KL98-10-21-1693m_24	0.0035	0.00073	0.000518	0.000042	-0.076482	3.34	0.27	204.6	226.1
KL98-10-21-1693m_25	0.00478	0.00091	0.000527	0.000038	0.11809	3.4	0.24	199	175

	207Pb/235U	207Pb/235U error	206Pb/238U	206Pb/238U Error	Error Correlation 206/238 vs. 207/235	Final Age (Ma)	Error (Ma)	Approx U (ppm)	Approx Th (ppm)
KL98-10-21-1693m_26	0.0045	0.0011	0.000476	0.000048	-0.11712	3.07	0.31	125.5	106.4
KL98-10-21-1693m_27	0.0037	0.0008	0.000544	0.000048	0.13994	3.5	0.31	179	129
KL98-10-21-1693m_28	0.319	0.015	0.03974	0.00064	0.46304	251.2	3.9	290.7	121.9
2003_1	0.0097	0.0024	0.000528	0.00008	0.33892	3.4	0.52	176	176
2003_2	0.00375	0.00097	0.000513	0.000061	0.055948	3.3	0.39	154.4	125.4
2003_3	0.00407	0.00094	0.000464	0.000057	0.084784	2.99	0.37	176.6	143
2003_4	0.0033	0.0017	0.0006	0.0001	0.17331	3.88	0.68	148.7	116
2003_5	0.0045	0.0013	0.000468	0.00006	0.029421	3.02	0.38	174	160
2003_6	0.0059	0.0025	0.00049	0.00011	0.097315	3.14	0.68	184	154
2003_7	0.0061	0.0014	0.000475	0.000049	0.034104	3.06	0.31	441	190.3
2003_8	0.0056	0.0013	0.000514	0.000057	0.1802	3.31	0.37	232	126
2003_9	0.015	0.011	0.00048	0.00011	0.025218	3.09	0.69	87.2	55.5
2003_10	0.0045	0.00095	0.000469	0.00005	0.0050747	3.02	0.32	335	381
2003_11	0.0058	0.0018	0.000418	0.000065	0.045363	2.69	0.42	114.9	109.1
2003_12	0.0149	0.0045	0.00069	0.00012	0.3071	4.46	0.76	121	113
2003_13	0.0057	0.0016	0.000493	0.000067	0.062709	3.18	0.43	153	130
2003_14	0.0043	0.0012	0.000405	0.000054	0.106	2.61	0.35	156	139
2003_15	0.0065	0.0018	0.000508	0.000075	0.26562	3.27	0.48	126.8	94
2003_16	0.0064	0.0014	0.000423	0.000063	0.12716	2.73	0.41	239	216
2003_17	0.0069	0.0018	0.000517	0.000076	0.16715	3.33	0.49	166.4	159
2003_18	0.0107	0.0023	0.000508	0.000082	0.011482	3.27	0.53	116.1	85.8
2003_19	0.00565	0.00093	0.000483	0.000055	0.15238		0.35	199.4	164.4
2003_20	0.0213	0.0031	0.000552	0.000077	0.30133	3.56	0.49	166.5	137.7
2003_21	0.0068	0.0017	0.000528	0.000064	0.063312	3.4	0.41	152	126
2003_22	0.0072	0.0018	0.000475	0.000073	0.25826	3.06	0.47	143.2	114
2003_23	0.00464	0.00099	0.000487	0.000059	0.0036719	3.14	0.38	203.3	143.4
2003_24	0.003	0.0013	0.000478	0.000077	0.20541	3.08	0.5	108	90
2003_25	0.0061	0.0014	0.000521	0.000055	0.070014	3.36	0.36	267	236
2003_26	0.0052	0.0015	0.000461	0.000066	0.0079133	2.97	0.43	122	116.8
2003_27	0.0043	0.0012	0.000489	0.000062	0.14057	3.15	0.4	156.6	122.4
2003_28	0.0048	0.0011	0.000514	0.000064	0.0096441	3.31	0.41	294	53.7
2003_29	1.32	0.02	0.1401	0.0019	0.64575	847	11	309	166.2
GRD32-06-258m_1	0.00425	0.00068	0.000526	0.000051	-0.018886	3.39	0.33	549	203
GRD32-06-258m_2	0.0038	0.0011	0.000495	0.000058	0.096185	3.19	0.37	218	192
GRD32-06-258m_3	0.0053	0.0021	0.000527	0.000054	0.33498	3.4	0.35	200	188
GRD32-06-258m_4	0.005	0.0015	0.000494	0.00005	-0.1915	3.18	0.32	158.2	92.5
GRD32-06-258m_5	0.00368	0.00077	0.00051	0.000046	-0.047203	3.29	0.29	235	161
GRD32-06-258m_6	0.00425	0.00098	0.000488	0.000043	-0.056804	3.14	0.27	265	129.9
GRD32-06-258m_7	0.00412	0.00093	0.000438	0.000037	0.029224	2.82	0.24	270	279
GRD32-06-258m_8	0.00349	0.00096	0.000458	0.000046	0.11816	2.95	0.3	241.5	210.6
GRD32-06-258m_9	0.0037	0.0013	0.000483	0.000059	-0.18969	3.11	0.38	194	191
GRD32-06-258m_10	0.0039	0.0012	0.000485	0.000055	-0.10975	3.13	0.35	216	219.5
GRD32-06-258m_11	0.0055	0.002	0.000527	0.000065	0.12614	3.4	0.42	147.2	129
GRD32-06-258m_12	0.0045	0.0017	0.00047	0.000059	0.039351	3.03	0.38	160	149
GRD32-06-258m_13	0.0052	0.0016	0.00049	0.000055	-0.03032	3.16	0.35	261	259
GRD32-06-258m_14	0.00481	0.00097	0.000521	0.000047	0.13192	3.36	0.3	236	235
GRD32-06-258m_15	0.0046	0.0013	0.000446	0.000058	-0.15775	2.87	0.37	161.8	124
GRD32-06-258m_16	0.005	0.0013	0.000524	0.000059	0.063306	3.38	0.38	165.8	126
GRD32-06-258m_17	0.0056	0.0012	0.000504	0.000041	-0.17507	3.25	0.26	215	231
GRD32-06-258m_18	0.0067	0.0018	0.000504	0.000052	0.24458	3.25	0.34	205	212
GRD32-06-258m_19	0.0053	0.0013	0.000503	0.000054	0.034998	3.24	0.34	208.5	167.7
GRD32-06-258m_20	0.0069	0.0015	0.000579	0.000074	0.034553	3.73	0.47	139.3	116
GRD32-06-258m_21	0.00409	0.00074	0.000449	0.000041	0.088692	2.9	0.27	261	213
GRD32-06-258m_22	0.00328	0.00099	0.000416	0.00005	0.11224	2.68	0.32	205.3	156.1
GRD32-06-258m_23	0.0054	0.0012	0.000472	0.000046	-0.047649	3.04	0.3	226	245
GRD32-06-258m_24	0.0047	0.0019	0.000498	0.000065	-0.055744	3.21	0.42	162	164
GRD32-06-258m_25	0.0041	0.0013	0.000516	0.000057	0.26991	3.33	0.37	168	160
GRD32-06-258m_26	0.0041	0.0013	0.000471	0.000053	-0.01906	3.04	0.34	166.4	135
GRD32-06-258m_27	5.12	0.26	0.322	0.018	0.9939	1792	90	339	177
2006_1	0.0041	0.0011	0.000479	0.000058	0.10962	3.09	0.37	202	160
2006_2	0.0043	0.0014	0.00051	0.000082	0.12917	3.29	0.53	135.5	124
2006_3	0.003	0.0014	0.000439	0.000073	0.11362	2.83	0.47	136	135
2006_4	0.0047	0.0012	0.000388	0.000051	0.076563	2.5	0.33	201.2	222.8
2006_5	0.0074	0.0018	0.000485	0.000059	0.048567	3.13	0.38	164.4	162
2006_6	0.0037	0.0013	0.000488	0.000078	0.14455	3.14	0.5	125.6	133
2006_7	0.0037	0.0017	0.00046	0.00011	0.28451	2.94	0.69	174	137
2006_8	0.0037	0.0018	0.00054	0.0001	0.38737	3.47	0.65	209	190
2006_9	0.00468	0.00093	0.000529	0.000051	0.21098	3.41	0.33	202	208
2006_10	0.0036	0.0014	0.000443	0.000072	0.0097301	2.85	0.46	123.5	122.5

	207Pb/235U	207Pb/235U error	206Pb/238U	206Pb/238U Error	Error Correlation 206/238 vs. 207/235	Final Age (Ma)	Error (Ma)	Approx U (ppm)	Approx Th (ppm)
2006_11	0.0042	0.0013	0.000488	0.000072	0.1311	3.14	0.46	203	166.8
2006_12	0.0033	0.0014	0.000561	0.000094	0.028967	3.62	0.61	94.5	70.2
2006_13	0.0044	0.0012	0.000491	0.000064	0.011062	3.16	0.41	161	153.7
2006_14	0.0072	0.0027	0.00059	0.00012	0.11458	3.82	0.8	74.5	56.8
2006_15	0.0072	0.0024	0.00053	0.00011	0.22857	3.39	0.69	67.1	51.8
2006_16	0.0053	0.0011	0.000463	0.000045	0.16458	2.98	0.29	245.4	231.3
2006_17	0.0048	0.0015	0.000465	0.000067	0.15869	2.99	0.43	254	267
2006_18	0.00338	0.00097	0.000523	0.000053	0.01137	3.37	0.34	251	286
2006_19	0.0039	0.0017	0.00051	0.0001	0.3005	3.28	0.65	110.5	80.5
2006_20	0.0069	0.0019	0.00049	0.000075	0.2482	3.16	0.48	117.7	73.1
2006_21	0.0046	0.0012	0.000523	0.00007	0.010595	3.37	0.45	157.8	108.7
2006_22	0.0037	0.0013	0.000546	0.000068	0.062842	3.52	0.44	160	139
2006_23	0.005	0.0012	0.000465	0.000058	0.19385	3	0.37	172	157
2006_24	0.0037	0.0014	0.000515	0.00008	0.1026	3.32	0.52	123.9	95.1
2006_25	0.00472	0.00095	0.000469	0.000055	0.011283	3.02	0.36	207	182
2006_26	0.0047	0.001	0.00047	0.000059	0.075482	3.03	0.38	168.6	137.4
2006_27	0.0045	0.0014	0.000488	0.000066	0.13333	3.15	0.43	124.3	96.4
2006_28	0.0045	0.0013	0.000438	0.000072	0.072816	2.82	0.46	145.8	113.7
2006_29	0.0037	0.0016	0.00047	0.00012	0.18724	3.01	0.79	213	192
2006_30	0.00425	0.00097	0.000531	0.000069	0.0048385	3.42	0.44	199.1	173.6
2006_31	0.0038	0.0011	0.00049	0.00005	0.025152	3.16	0.32	207	174.4
GRD41-01-59m_1	0.0075	0.002	0.000553	0.00008	0.065339	3.56	0.52	90.1	46.4
GRD41-01-59m_2	0.0026	0.0019	0.000468	0.000072	0.14111	3.02	0.46	136	142
GRD41-01-59m_3	0.0044	0.0011	0.00054	0.000046	0.06996	3.48	0.3	330	111.9
GRD41-01-59m_4	0.0033	0.0023	0.000531	0.000098	0.23032	3.42	0.63	67	56
GRD41-01-59m_5	0.0062	0.0033	0.000422	0.000076	0.08988	2.72	0.49	76.6	53.9
GRD41-01-59m_6	0.00403	0.00099	0.000496	0.000043	0.10491	3.2	0.28	264	163
GRD41-01-59m_7	0.0051	0.0026	0.000385	0.000077	0.40009	2.48	0.5	158	80
GRD41-01-59m_8	0.0036	0.0033	0.0004	0.0001	0.091765	2.57	0.67	60.3	33.7
GRD41-01-59m_9	0.0061	0.0031	0.00061	0.00012	0.23342	3.93	0.79	128	112
GRD41-01-59m_10	0.0033	0.0012	0.000481	0.000062	0.082202	3.1	0.4	157	168
GRD41-01-59m_11	0.0026	0.0019	0.000489	0.000069	0.046153	3.15	0.45	156.1	94.8
GRD41-01-59m_12	0.0059	0.0012	0.000509	0.000039	0.0828	3.28	0.25	279.7	172.4
GRD41-01-59m_13	0.00336	0.00072	0.00051	0.000032	0.12627	3.29	0.21	337	182.6
GRD41-01-59m_14	0.0045	0.0016	0.000477	0.000052	0.22631	3.08	0.33	154.5	112
GRD41-01-59m_15	0.0159	0.0044	0.000606	0.000083	0.0042063	3.91	0.53	110	68
GRD41-01-59m_16	0.0047	0.0012	0.000453	0.000053	0.015511	2.92	0.34	146.9	153.2
GRD41-01-59m_17	0.0061	0.0018	0.000437	0.000054	0.12709	2.82	0.35	115	90.6
GRD41-01-59m_18	0.0043	0.0021	0.000453	0.000068	0.11159	2.92	0.44	108	91
GRD41-01-59m_19	0.00369	0.00062	0.000504	0.000039	0.048355	3.25	0.25	371	139.1
GRD41-01-59m_20	0.0055	0.002	0.000416	0.000072	0.15326	2.68	0.47	164	188
GRD41-01-59m_21	0.0051	0.0018	0.000471	0.000064	0.013169	3.03	0.41	124.5	148.3
GRD41-01-59m_22	0.0039	0.001	0.000439	0.000047	0.16099	2.83	0.3	183.9	231.2
GRD41-01-59m_23	0.00527	0.00092	0.000464	0.000038	0.31438	2.99	0.24	328	173.8
GRD41-01-59m_24	0.0039	0.0011	0.000487	0.000062	0.19412	3.14	0.4	173.1	222
GRD41-01-59m_25	0.0041	0.00073	0.00049	0.000038	0.116	3.16	0.24	305	124.5
GRD41-01-59m_26	0.00332	0.00068	0.000496	0.000038	0.020333	3.2	0.24	361	133.5
GRD41-01-59m_27	0.0038	0.0021	0.000426	0.000076	0.0050123	2.74	0.49	87.5	54.6
GRD41-01-59m_28	0.0097	0.0019	0.000482	0.000049	0.2048	3.11	0.32	150.6	100.5
GRD41-01-59m_29	0.242	0.013	0.03377	0.00097	0.20928	214.1	6	180.6	83.7
GRD41-01-59m_30	0.351	0.024	0.0494	0.002	0.39984	311	12	136.2	81.1
GRD41-01-59m_31	2.839	0.038	0.2268	0.0031	0.88435	1317	17	731	251
GRD41-01-59m_32	0.3344	0.0099	0.0475	0.001	0.44236	299.8	6.6	178.8	143.9
2002_1	0.0047	0.0012	0.000468	0.000063	0.086748	3.01	0.41	177	261
2002_2	0.0041	0.001	0.000475	0.000057	0.19027	3.06	0.36	249	250
2002_3	0.0053	0.0015	0.000468	0.000076	0.19292	3.02	0.49	187	181
2002_4	0.00371	0.00025	0.000524	0.000017	0.16095	3.38	0.11	3800	2420
2002_5	0.00398	0.00096	0.000521	0.000042	0.0363	3.36	0.27	223	223.4
2002_6	0.0051	0.001	0.00045	0.000058	0.058341	2.9	0.37	204.4	158.6
2002_7	0.0044	0.0013	0.000399	0.000061	0.091159	2.57	0.39	176	120
2002_8	0.0039	0.0032	0.00044	0.00012	0.089087	2.86	0.75	62.6	63
2002_9	0.0044	0.0014	0.000469	0.000062	0.17737	3.02	0.4	157	159
2002_10	0.0049	0.0012	0.000459	0.000049	0.046132	2.96	0.32	180	124.1
2002_11	0.0035	0.0016	0.000459	0.000079	0.18292	2.96	0.51	130	71.2
2002_12	0.0047	0.0013	0.000495	0.000071	0.016361	3.19	0.46	178	155
2002_13	0.0068	0.0026	0.000519	0.000091	0.14324	3.35	0.59	120	95.2
2002_14	0.0049	0.0011	0.000476	0.000066	0.18505	3.07	0.42	165	172
2002_15	0.004	0.002	0.00049	0.000091	0.075987	3.16	0.59	111	88
2002_16	0.0028	0.0011	0.000436	0.000066	0.12445	2.81	0.43	168	174

	207Pb/235U	207Pb/235U error	206Pb/238U	206Pb/238U Error	Error Correlation 206/238 vs. 207/235	Final Age (Ma)	Error (Ma)	Approx U (ppm)	Approx Th (ppm)
2002_17	0.0055	0.0013	0.000476	0.000056	0.097875	3.07	0.36	186.7	230
2002_18	0.0034	0.0013	0.000435	0.000063	0.054194	2.8	0.4	196	187
2002_19	0.00445	0.00072	0.000511	0.000046	0.061762	3.29	0.29	372	147.4
2002_20	0.0057	0.0019	0.00042	0.000066	0.029747	2.71	0.42	103.3	83.1
2002_21	0.0048	0.0023	0.00046	0.0001	0.080913	2.97	0.64	77.4	52.8
2002_22	0.0027	0.0016	0.000428	0.000085	0.2554	2.76	0.55	83.1	77.4
2002_23	0.0034	0.0011	0.000492	0.000054	0.11388	3.17	0.35	170.1	200
2002_24	0.0043	0.0017	0.000462	0.000081	0.22456	2.98	0.52	73.7	53.9
2002_25	0.007	0.0016	0.000507	0.000062	0.11099	3.27	0.4	187	176
2002_26	0.0044	0.0015	0.000447	0.00008	0.029784	2.88	0.51	109.5	88.6
2002_27	0.00416	0.00095	0.000468	0.000053	0.1754	3.02	0.34	196	163
2002_28	0.0047	0.0019	0.000457	0.000068	0.24049	2.95	0.44	110	97
2002_29	0.0063	0.0019	0.000465	0.000077	0.22809	3	0.5	108.6	69.4
2007_1	0.0074	0.0024	0.000509	0.000078	0.30102	3.28	0.5	102	114.4
2007_2	0.0142	0.0034	0.000729	0.000097	0.15131	4.7	0.63	153.8	93.1
2007_3	0.0107	0.0029	0.00063	0.000099	0.11687	4.06	0.64	101	77
2007_4	0.013	0.0021	0.000629	0.000076	0.16524	4.06	0.49	284	254
2007_5	0.0087	0.0033	0.000514	0.000091	0.19223	3.32	0.58	137	162
2007_6	0.0064	0.0022	0.000464	0.000058	0.10502	2.99	0.37	164	143
2007_7	0.00338	0.00077	0.000487	0.000049	0.12277	3.14	0.32	346	434
2007_8	0.0031	0.0024	0.00035	0.00014	0.048898	2.29	0.88	226	199
2007_9	0.0078	0.0016	0.000563	0.000079	0.29065	3.63	0.51	363	327
2007_10	0.0045	0.0015	0.000465	0.000053	0.05694	2.99	0.34	249	261
2007_11	0.0083	0.0019	0.000498	0.000063	0.10757	3.21	0.4	170.8	90.8
2007_12	0.0039	0.0014	0.000485	0.000071	0.020317	3.12	0.46	128.3	62.4
2007_13	0.0041	0.0023	0.00061	0.00011	0.10052	3.92	0.68	142	107
2007_14	0.0034	0.001	0.00047	0.000057	0.19237	3.03	0.36	266	194
2007_15	0.0049	0.0014	0.000488	0.000064	0.0031232	3.14	0.41	202.9	159.6
2007_16	0.0045	0.0018	0.000453	0.000062	0.42691	2.92	0.4	313	298
2007_17	0.0089	0.0017	0.000501	0.000062	0.20453	3.23	0.4	221.4	122.4
2007_18	0.0058	0.0015	0.000479	0.000062	0.1664	3.09	0.4	166.4	86.9
2007_19	0.0025	0.0011	0.0004	0.000064	0.037262	2.57	0.41	238	193
2007_20	0.0043	0.0034	0.00049	0.00013	0.19297	3.14	0.82	346	255
2007_21	0.0066	0.0019	0.000502	0.000062	0.1106	3.24	0.4	149.5	158
2007_22	0.0056	0.0013	0.000536	0.000071	0.06172	3.45	0.46	204	176
2007_23	0.0048	0.0012	0.000516	0.000055	0.08732	3.32	0.35	221	151
2007_24	0.0073	0.0028	0.00055	0.00012	0.12693	3.56	0.75	91.6	97.9
2007_25	0.00286	0.00085	0.000452	0.000054	0.18751	2.91	0.35	276	172
2007_26	0.0058	0.0022	0.000583	0.000097	0.067376	3.76	0.63	256	284
2007_27	0.0067	0.0015	0.000475	0.000057	0.1041	3.06	0.36	222.7	115.9
2007_28	0.0055	0.0012	0.000524	0.000062	0.17922	3.38	0.4	256	258
2007_29	0.271	0.019	0.0383	0.0021	0.53512	242	13	72.7	68.8
2007_30	5.415	0.085	0.3422	0.0059	0.60955	1897	28	148.9	60.4
KL98-10-21-1315m_1	0.00668	0.00082	0.000582	0.000038	0.23122	3.75	0.24	419	193
KL98-10-21-1315m_2	0.0034	0.0011	0.000508	0.00005	0.13249	3.27	0.32	330	450
KL98-10-21-1315m_3	0.0045	0.002	0.000402	0.000064	-0.055121	2.59	0.41	85	72.5
KL98-10-21-1315m_4	0.0038	0.0017	0.000422	0.000063	-0.20065	2.72	0.41	112.2	135.5
KL98-10-21-1315m_5	0.0042	0.0015	0.000528	0.000053	-0.056446	3.4	0.34	134.7	123
KL98-10-21-1315m_6	0.00371	0.00068	0.00052	0.000033	-0.091429	3.35	0.21	433	244.7
KL98-10-21-1315m_7	0.0045	0.0013	0.000508	0.000051	0.20904	3.28	0.33	203	314
KL98-10-21-1315m_8	0.0123	0.0049	0.00051	0.0001	-0.095444	3.27	0.67	237	174
KL98-10-21-1315m_9	0.00397	0.00061	0.00047	0.000037	0.12652	3.03	0.24	434	194.7
KL98-10-21-1315m_10	0.00385	0.00051	0.000546	0.00004	-0.02806	3.52	0.26	436	194
KL98-10-21-1315m_11	0.00499	0.00081	0.000469	0.000041	-0.045832	3.02	0.27	315	265
KL98-10-21-1315m_12	0.00396	0.00094	0.000479	0.000043	-0.008592	3.09	0.28	232	181
KL98-10-21-1315m_13	0.0098	0.0024	0.000557	0.000065	-0.0023128	3.59	0.42	113.5	92.4
KL98-10-21-1315m_14	0.0084	0.0015	0.000572	0.000037	0.30911	3.69	0.24	522	296
KL98-10-21-1315m_15	0.0046	0.0014	0.000469	0.000069	0.062002	3.02	0.44	114.9	108
KL98-10-21-1315m_16	0.0096	0.0029	0.000503	0.000037	0.075152	3.24	0.24	347	293
KL98-10-21-1315m_17	0.0077	0.0023	0.000502	0.00005	0.17391	3.24	0.32	228	212
KL98-10-21-1315m_18	0.00355	0.00057	0.000502	0.000044	-0.022482	3.24	0.28	434	306
KL98-10-21-1315m_19	0.0058	0.00068	0.000519	0.000038	0.11048	3.35	0.24	439	194.3
KL98-10-21-1315m_20	0.00357	0.00067	0.000496	0.000042	0.091678	3.19	0.27	280	284
KL98-10-21-1315m_21	0.00388	0.00049	0.000493	0.000031	-0.077078	3.18	0.2	526	243.3
KL98-10-21-1315m_22	0.059	0.015	0.00095	0.00011	0.92015	6.09	0.69	329.2	185.6
KL98-10-21-1315m_23	0.0051	0.0015	0.000552	0.000054	0.0068952	3.56	0.35	237	207
KL98-10-21-1315m_24	0.0073	0.0012	0.000518	0.000032	0.48062	3.34	0.21	881	388
KL98-10-21-1315m_25	0.00343	0.00044	0.000517	0.000027	0.19787	3.33	0.18	600	315
KL98-10-21-1315m_26	0.00358	0.00048	0.000483	0.000032	0.027225	3.11	0.2	604	218

	207Pb/235U	207Pb/235U error	206Pb/238U	206Pb/238U Error	Error Correlation 206/238 vs. 207/235	Final Age (Ma)	Error (Ma)	Approx U (ppm)	Approx Th (ppm)
KL98-10-21-1315m_27	0.0103	0.0016	0.000576	0.000045	0.22133	3.71	0.29	222	208
KL98-10-21-1315m_28	5.152	0.086	0.3261	0.0069	0.73298	1818	33	320.4	230.6
95-MC-RD1_1	0.0074	0.0027	0.00049	0.000061	0.40638	3.16	0.39	364	165
95-MC-RD1_2	0.0047	0.0012	0.000483	0.000056	-0.03757	3.11	0.36	302	173
95-MC-RD1_3	0.0082	0.0038	0.00073	0.00014	0.61269	4.67	0.88	63.3	45.4
95-MC-RD1_4	0.0071	0.0026	0.000495	0.000089	0.058381	3.19	0.57	80.6	66.9
95-MC-RD1_5	0.00413	0.0007	0.000504	0.000049	-0.22809	3.25	0.31	461	180.1
95-MC-RD1_6	0.0089	0.0027	0.000444	0.000093	0.17143	2.86	0.6	82.6	52.11
95-MC-RD1_7	0.0043	0.0019	0.000448	0.000072	0.16749	2.89	0.47	116.5	134.8
95-MC-RD1_8	0.0045	0.0013	0.00042	0.000053	0.10525	2.71	0.34	158.5	195.5
95-MC-RD1_9	0.0049	0.0017	0.000462	0.000068	-0.036822	2.98	0.44	135.1	161.5
95-MC-RD1_10	0.0042	0.0017	0.000442	0.000061	0.025604	2.85	0.39	128.7	135.4
95-MC-RD1_11	0.0033	0.0017	0.000485	0.00008	0.17615	3.13	0.51	121.1	129.8
95-MC-RD1_12	0.0061	0.0022	0.0006	0.0001	-0.088337	3.85	0.67	84.2	73.4
95-MC-RD1_13	0.0053	0.0021	0.0005	0.00008	0.17782	3.22	0.52	203	174
95-MC-RD1_14	0.00377	0.0009	0.000521	0.000052	0.19521	3.4	0.33	333	119.1
95-MC-RD1_15	0.0139	0.0026	0.000606	0.000072	0.15585	3.9	0.46	118	65.6
95-MC-RD1_16	0.0042	0.0014	0.000423	0.000064	-0.18781	2.73	0.41	194	218
95-MC-RD1_17	0.0049	0.0035	0.00037	0.00013	0.18283	2.41	0.86	80.3	48.2
95-MC-RD1_18	0.00423	0.00083	0.000479	0.000043	0.097819	3.09	0.28	374	126.7
95-MC-RD1_19	0.0088	0.0017	0.000492	0.000054	0.36982	3.17	0.35	210.8	287.4
95-MC-RD1_20	0.0034	0.0012	0.000403	0.000064	-0.060922	2.6	0.41	186.9	165.6
95-MC-RD1_21	0.00459	0.00099	0.000469	0.000048	-0.042041	3.02	0.31	330	473
95-MC-RD1_22	0.0068	0.0022	0.00053	0.0001	0.041421	3.44	0.67	88.6	60.7
95-MC-RD1_23	0.0079	0.0019	0.000508	0.000075	-0.055161	3.27	0.48	111.5	81.9
95-MC-RD1_24	0.00427	0.00081	0.000461	0.000045	-0.10813	2.97	0.29	389.2	168.1
95-MC-RD1_25	0.0042	0.0015	0.000389	0.000053	0.33431	2.51	0.34	193.3	216
95-MC-RD1_26	0.346	0.019	0.04235	0.0007	0.61122	267.3	4.3	250.2	215
95-MC-RD1_27	0.216	0.018	0.0294	0.0025	0.86794	187	16	265	119.4
95-MC-RD1_28	0.288	0.012	0.0397	0.0012	0.28731	251.2	7.7	128.7	121.6
95-MC-RD1_29	0.213	0.01	0.0306	0.0012	0.63282	194.4	7.4	189.4	142.3
95-MC-RD1_30	0.3335	0.0081	0.0465	0.0012	0.80973	293	7.5	771	510
95-MC-RD2_1	0.00537	0.00071	0.000459	0.000036	0.24908	2.96	0.24	470	240
95-MC-RD2_2	0.0026	0.0016	0.000563	0.000089	0.056834	3.63	0.57	87.1	63.1
95-MC-RD2_3	0.0037	0.00061	0.000465	0.000034	0.035578	3	0.22	571	251
95-MC-RD2_4	0.0035	0.0013	0.000509	0.000068	-0.13058	3.28	0.44	148	72.7
95-MC-RD2_5	0.00318	0.00089	0.000471	0.000056	-0.20643	3.03	0.36	215.1	197.4
95-MC-RD2_6	0.0072	0.0025	0.00046	0.000089	0.010283	2.97	0.57	85	67.8
95-MC-RD2_7	0.0041	0.0014	0.00044	0.000064	-0.013314	2.84	0.41	145.7	152.8
95-MC-RD2_8	0.0021	0.0037	0.000471	0.000085	0.83655	3.04	0.55	171	171
95-MC-RD2_9	0.0037	0.00067	0.000481	0.000045	-0.10488	3.1	0.29	344	123.3
95-MC-RD2_10	0.00395	0.00077	0.000531	0.000047	0.15371	3.42	0.3	346	160.1
95-MC-RD2_11	0.0057	0.002	0.000566	0.000069	0.35147	3.65	0.45	159.9	140.1
95-MC-RD2_12	0.0041	0.002	0.000524	0.000097	-0.10137	3.38	0.63	81.9	62.2
95-MC-RD2_13	0.0031	0.0011	0.000491	0.000067	-0.088377	3.16	0.43	197	198
95-MC-RD2_14	0.00427	0.00071	0.000501	0.000046	0.24117	3.23	0.3	362	133
95-MC-RD2_15	0.00431	0.00082	0.000512	0.000042	0.16836	3.3	0.27	478.1	219
95-MC-RD2_16	0.0089	0.002	0.000526	0.000065	0.10185	3.39	0.42	131.6	96.8
95-MC-RD2_17	0.00536	0.00099	0.000432	0.000049	-0.1384	2.78	0.32	290.1	326
95-MC-RD2_18	0.0079	0.0014	0.000528	0.000036	0.086684	3.4	0.24	537	162.3
95-MC-RD2_19	0.0065	0.0012	0.000534	0.000063	-0.15908	3.44	0.41	273.5	156.8
95-MC-RD2_20	0.0041	0.002	0.000495	0.000069	-0.22622	3.19	0.45	98.3	80.5
95-MC-RD2_21	0.0049	0.0015	0.000468	0.000068	0.039133	3.02	0.44	143.8	122.6
95-MC-RD2_22	0.0041	0.0015	0.000459	0.000065	-0.012682	2.96	0.42	157.6	151.4
95-MC-RD2_23	0.0051	0.002	0.000488	0.000096	0.1388	3.15	0.62	84.9	61.1
95-MC-RD2_24	0.005	0.0016	0.000468	0.000072	-0.24804	3.02	0.46	154	105
95-MC-RD2_25	0.0039	0.001	0.000482	0.000046	-0.15518	3.11	0.3	279.7	231.8
95-MC-RD2_26	0.0055	0.001	0.000569	0.000061	0.058098	3.67	0.39	403	198
95-MC-RD2_27	0.3093	0.0077	0.0429	0.00088	0.44124	270.7	5.5	385	288
95-MC-RD2_28	0.3713	0.0088	0.0502	0.0011	0.26887	315.6	6.8	181.3	125.5
95-MC-RD2_29	0.356	0.013	0.0486	0.001	0.061322	305.9	6.1	128.2	105
95-MC-RD2_30	0.248	0.023	0.0312	0.0015	-0.29667	198	9.1	161.3	90.6
95-MC-RD2_31	0.309	0.012	0.0446	0.0011	0.21213	281.2	6.7	291	334
2001_1	0.00437	0.00056	0.000495	0.00003	0.065279	3.19	0.19	463	188
2001_2	0.00398	0.00051	0.000539	0.000031	0.0056094	3.47	0.2	502	226
2001_3	0.0237	0.0039	0.000644	0.000081	0.26004	4.15	0.52	170.6	198.1
2001_4	0.0091	0.0015	0.000527	0.000047	0.027081	3.4	0.3	160.5	190
2001_5	0.00278	0.0007	0.000444	0.000039	0.097804	2.86	0.25	252	270
2001_6	0.0049	0.0015	0.000519	0.000077	0.13481	3.35	0.49	98	93

	207Pb/235U	207Pb/235U error	206Pb/238U	206Pb/238U Error	Error Correlation 206/238 vs. 207/235	Final Age (Ma)	Error (Ma)	Approx U (ppm)	Approx Th (ppm)
2001_7	0.0045	0.00074	0.000498	0.00004	0.020142	3.21	0.26	394	154.7
2001_8	0.0091	0.0012	0.000519	0.000041	0.10026	3.34	0.26	523	269.7
2001_9	0.0071	0.0019	0.000566	0.000073	0.00021822	3.65	0.47	159	184.8
2001_10	0.0045	0.0013	0.000471	0.00006	0.088135	3.03	0.39	158	133.3
2001_11	0.0037	0.0015	0.000522	0.000069	0.079164	3.36	0.44	129.5	95.2
2001_12	0.0064	0.0013	0.000461	0.000061	0.11982	2.97	0.39	277.8	328.8
2001_13	0.0164	0.0043	0.000592	0.000081	0.64345	3.82	0.52	245	186
2001_14	0.0165	0.0057	0.0006	0.00013	0.58223	3.89	0.81	215	238
2001_15	0.0041	0.0012	0.000474	0.000061	0.12	3.06	0.39	159.8	141.8
2001_16	0.00481	0.0005	0.00055	0.000034	0.21084	3.55	0.22	831	358
2001_17	0.0038	0.00043	0.000539	0.000029	0.052768	3.47	0.19	809	406
2001_18	0.00468	0.00066	0.000471	0.000039	0.089301	3.03	0.25	547	1200
2001_19	0.0083	0.0024	0.000479	0.000074	0.025922	3.09	0.48	110.9	61.5
2001_20	0.0051	0.0025	0.000481	0.000096	0.050961	3.1	0.62	79.7	65.8
2001_21	0.0082	0.0011	0.00057	0.000049	0.11179	3.67	0.32	299.6	152.9
2001_22	0.0085	0.0013	0.000497	0.000059	0.0093875	3.2	0.38	225	222
2001_23	0.005	0.0013	0.000496	0.000052	0.089649	3.19	0.33	252	324
2001_24	0.009	0.0027	0.000446	0.000071	0.043676	2.87	0.46	88.2	77.7
2001_25	0.0059	0.0011	0.000472	0.000049	0.019748	3.04	0.32	372	137.6
2001_26	0.00508	0.00099	0.000536	0.000086	0.14319	3.45	0.55	512	205
2001_27	0.00559	0.00096	0.000552	0.000049	0.20901	3.56	0.32	360.9	170.1
2001_28	0.363	0.0098	0.04911	0.00086	0.39585	309	5.3	197.6	171.1
INF42-01-200m_1	0.0035	0.00099	0.000462	0.000053	-0.11141	2.98	0.34	121.2	139
INF42-01-200m_2	0.0048	0.0013	0.000394	0.000067	0.43085	2.54	0.43	182	62.1
INF42-01-200m_3	0.00353	0.0004	0.000442	0.000034	-0.0045797	2.85	0.22	481	159.7
INF42-01-200m_4	0.00388	0.00057	0.000498	0.000041	-0.17984	3.21	0.26	588	148.5
INF42-01-200m_5	0.0049	0.0014	0.000384	0.000053	0.16065	2.47	0.34	109.5	82.4
INF42-01-200m_6	0.0046	0.0011	0.000461	0.00006	0.069498	2.97	0.39	155.4	179.4
INF42-01-200m_7	0.0046	0.0011	0.000445	0.00006	0.51766	2.87	0.38	342	116
INF42-01-200m_8	0.0043	0.0011	0.00045	0.000064	-0.098745	2.9	0.41	136	70.5
INF42-01-200m_9	0.0057	0.0011	0.000439	0.000057	0.021563	2.83	0.37	134	99.2
INF42-01-200m_10	0.00281	0.00025	0.000526	0.000024	0.17451	3.39	0.15	8.70E+03	2.75E+05
INF42-01-200m_11	0.0049	0.0011	0.000435	0.00006	0.13474	2.8	0.39	134.9	99.6
INF42-01-200m_12	0.0043	0.0012	0.000448	0.000054	0.055725	2.89	0.35	110.7	71
INF42-01-200m_13	0.0046	0.0015	0.000408	0.000067	0.10239	2.63	0.43	73.2	50.5
INF42-01-200m_14	0.006	0.0016	0.000426	0.000062	0.15392	2.75	0.4	132	82.7
INF42-01-200m_15	0.0176	0.0048	0.000579	0.000066	0.63117	3.73	0.42	335	162.3
INF42-01-200m_16	0.0036	0.0022	0.00046	0.00011	-0.096667	2.96	0.7	109	90
INF42-01-200m_17	0.00487	0.00096	0.000464	0.000068	0.41931	2.99	0.44	568	87.7
INF42-01-200m_18	0.00335	0.00068	0.000405	0.000042	-0.22114	2.61	0.27	252	237.6
INF42-01-200m_19	0.004	0.00055	0.000507	0.000042	0.2541	3.27	0.27	499	198.2
INF42-01-200m_20	0.00437	0.00052	0.000471	0.00003	-0.037274	3.04	0.19	377	133
INF42-01-200m_21	0.00423	0.00092	0.000468	0.000049	-0.09962	3.02	0.32	181.7	178.7
INF42-01-200m_22	0.0052	0.001	0.000465	0.000044	0.21573	3	0.28	191	158.7
INF42-01-200m_23	0.0034	0.0014	0.000432	0.000079	-0.0043076	2.78	0.51	107.2	105
INF42-01-200m_24	4.737	0.045	0.2993	0.003	0.81324	1687	15	698	293
INF42-01-200m_25	4.062	0.056	0.2482	0.0034	0.92563	1429	18	668	303
02-UT-AM-J_1	0.023	0.0037	0.000662	0.000058	0.70229	4.26	0.38	260	318
02-UT-AM-J_2	0.0062	0.0012	0.000467	0.000047	0.0089535	3.01	0.3	285	338
02-UT-AM-J_3	0.0105	0.0017	0.000528	0.000046	0.28084	3.4	0.3	306	467
02-UT-AM-J_4	0.0045	0.0011	0.000519	0.000058	0.10346	3.34	0.37	194	291
02-UT-AM-J_5	0.0629	0.0059	0.000954	0.000097	0.27707	6.15	0.62	302	494
02-UT-AM-J_6	0.0095	0.0045	0.000512	0.000061	0.38049	3.3	0.39	369	206
02-UT-AM-J_7	0.00442	0.00088	0.000493	0.00004	0.4487	3.17	0.26	349	192
02-UT-AM-J_8	0.0348	0.0086	0.000734	0.000088	0.44118	4.73	0.57	314	182.7
02-UT-AM-J_9	0.00675	0.00097	0.000494	0.000035	0.010919	3.18	0.22	431	229.2
02-UT-AM-J_10	0.008	0.0016	0.000488	0.000061	0.16527	3.14	0.39	144.4	176.3
02-UT-AM-J_11	0.0448	0.0056	0.00077	0.00011	0.39726	4.99	0.69	96.5	71.5
02-UT-AM-J_13	0.00443	0.00051	0.000503	0.000035	0.014795	3.24	0.22	437	256
02-UT-AM-J_14	0.0113	0.0035	0.000464	0.000068	-0.11867	2.99	0.44	134.3	133.9
02-UT-AM-J_21	0.0088	0.0028	0.000553	0.000071	0.046379	3.56	0.46	114.9	134.8
02-UT-AM-J_25	0.0067	0.0012	0.000505	0.000037	0.13283	3.26	0.24	334	251.1
02-UT-AM-J_26	0.0088	0.0031	0.000622	0.000089	0.082456	4.01	0.58	110	63
02-UT-AM-J_27	0.0033	0.0014	0.000465	0.000058	-0.13446	3	0.38	140.8	168.8
02-UT-AM-J_12	5.208	0.096	0.3287	0.0068	0.70714	1831	33	181.6	155.9
90-TM-GRS-3_1	0.0047	0.0012	0.00051	0.000069	0.0036296	3.28	0.44	135.2	164.4
90-TM-GRS-3_2	0.071	0.006	0.001069	0.000086	0.45437	6.89	0.55	145.1	160.4
90-TM-GRS-3_3	0.0079	0.0023	0.000478	0.000074	0.26746	3.08	0.48	110.6	147.5
90-TM-GRS-3_4	0.0049	0.00093	0.000436	0.00004	0.0082242	2.81	0.26	218	214

	207Pb/235U	207Pb/235U error	206Pb/238U	206Pb/238U Error	Error Correlation 206/238 vs. 207/235	Final Age (Ma)	Error (Ma)	Approx U (ppm)	Approx Th (ppm)
90-TM-GRS-3_5	0.0059	0.0016	0.000528	0.000059	0.083181	3.4	0.38	155.1	194.7
90-TM-GRS-3_6	0.00431	0.00058	0.000514	0.00003	0.12181	3.31	0.2	522	206.9
90-TM-GRS-3_7	0.0073	0.0023	0.000578	0.000078	0.14779	3.72	0.5	80.9	71.9
90-TM-GRS-3_8	0.0049	0.001	0.000436	0.000046	0.27616	2.81	0.3	214	175
90-TM-GRS-3_9	0.0056	0.0011	0.000508	0.000055	0.0033832	3.27	0.36	160.4	160.4
90-TM-GRS-3_10	0.0605	0.0097	0.001	0.00012	0.74714	6.46	0.77	86.4	105.3
90-TM-GRS-3_11	0.0082	0.0024	0.00055	0.000036	0.0038422	3.55	0.23	514	185
90-TM-GRS-3_12	0.0292	0.0041	0.000689	0.000082	0.071717	4.44	0.53	83.5	102
90-TM-GRS-3_13	0.00453	0.0005	0.000494	0.000029	0.013272	3.18	0.18	605	326
90-TM-GRS-3_14	0.0041	0.0021	0.000435	0.000091	0.2005	2.8	0.58	76.8	69.6
90-TM-GRS-3_15	0.0057	0.0023	0.000554	0.000073	0.013787	3.57	0.47	142.5	123.7
90-TM-GRS-3_16	0.0263	0.007	0.000626	0.000081	0.031981	4.03	0.52	191	230
90-TM-GRS-3_17	0.0059	0.0014	0.000519	0.000071	0.3239	3.34	0.46	209	300
90-TM-GRS-3_18	0.0059	0.0022	0.000466	0.000077	0.18502	3	0.49	110.7	93.6
90-TM-GRS-3_19	0.006	0.0024	0.000531	0.000074	0.04305	3.42	0.47	112.9	111.2
90-TM-GRS-3_20	0.0046	0.0015	0.000456	0.000049	0.045256	2.94	0.32	192.4	207
90-TM-GRS-3_21	0.00453	0.00062	0.000493	0.000028	0.16333	3.18	0.18	715	563
90-TM-GRS-3_22	0.0276	0.0033	0.000695	0.000068	0.50261	4.48	0.44	181.6	158.6
90-TM-GRS-3_23	0.0173	0.0035	0.000594	0.000081	0.24565	3.82	0.52	114	112
90-TM-GRS-3_24	0.0073	0.0016	0.000549	0.000074	0.027036	3.54	0.48	109.9	142.6
90-TM-GRS-3_25	0.0141	0.0029	0.000547	0.00005	0.18044	3.52	0.32	303.8	172
90-TM-GRS-3_26	0.57	0.011	0.0716	0.0014	0.50059	445.7	8.3	277	73
90-TM-GRS-3_27	0.3675	0.0097	0.049	0.0011	0.58281	308.6	6.6	263	198
94-MC-MGI2_1	0.004	0.0012	0.000425	0.00006	-0.17387	2.74	0.39	164	184
94-MC-MGI2_2	0.00398	0.00073	0.000463	0.000034	0.12095	2.99	0.22	381	502
94-MC-MGI2_3	0.00367	0.00074	0.000455	0.000034	-0.10466	2.93	0.22	404	507
94-MC-MGI2_4	0.0048	0.0013	0.000441	0.000042	0.072095	2.84	0.27	194	166
94-MC-MGI2_5	0.0165	0.0036	0.000596	0.000068	0.51166	3.84	0.44	335	313
94-MC-MGI2_6	0.0038	0.0018	0.00043	0.00015	0.25774	2.79	0.98	221	174
94-MC-MGI2_7	0.00912	0.00092	0.000576	0.000027	0.26567	3.71	0.18	1080	387
94-MC-MGI2_8	0.0054	0.0022	0.000461	0.000053	0.23921	2.97	0.34	157.2	102.9
94-MC-MGI2_9	0.00429	0.00085	0.000522	0.000046	-0.10198	3.36	0.3	247	225
94-MC-MGI2_10	0.00382	0.00034	0.000516	0.00002	-0.017249	3.33	0.13	1610	492
94-MC-MGI2_11	0.0057	0.002	0.00045	0.00006	0.24789	2.9	0.38	130.2	107.3
94-MC-MGI2_12	0.00435	0.00061	0.000529	0.000038	-0.1203	3.41	0.25	380	293
94-MC-MGI2_13	0.0046	0.0013	0.00048	0.000056	-0.060735	3.09	0.36	141.8	120.4
94-MC-MGI2_14	0.0076	0.0022	0.0005	0.000073	-0.022109	3.22	0.47	115	108
94-MC-MGI2_15	0.00425	0.00065	0.000528	0.000035	-0.043332	3.41	0.23	390	440
94-MC-MGI2_16	0.0053	0.0018	0.000476	0.00006	-0.1175	3.07	0.39	145	112
94-MC-MGI2_17	0.0034	0.0017	0.000418	0.000075	-0.05859	2.69	0.48	90.7	66.4
94-MC-MGI2_18	0.00394	0.00075	0.000447	0.00004	-0.017774	2.88	0.26	372	319
94-MC-MGI2_19	0.00371	0.00085	0.000476	0.00005	-0.12227	3.06	0.32	236	220
94-MC-MGI2_20	0.0051	0.0013	0.000465	0.000053	0.053988	3.04	0.33	175.1	110.2
94-MC-MGI2_21	0.0043	0.0013	0.000428	0.000061	-0.38237	2.76	0.39	276	263
94-MC-MGI2_22	0.00397	0.00084	0.000448	0.000044	0.12895	2.89	0.28	266	276
94-MC-MGI2_23	0.0127	0.0039	0.00055	0.000073	0.45286	3.55	0.47	128.3	93.1
94-MC-MGI2_24	0.0047	0.0014	0.000429	0.000051	-0.064951	2.77	0.33	120.4	82.2
94-MC-MGI2_25	0.106	0.01	0.00137	0.00015	0.49887	8.84	0.96	111.3	114.2
94-MC-MGI2_26	0.00368	0.00072	0.000485	0.000039	0.067409	3.13	0.25	381	180
94-MC-MGI2_27	0.00413	0.00077	0.000445	0.000038	-0.12891	2.87	0.24	411	245
94-MC-MGI2_28	0.0048	0.002	0.000527	0.00006	-0.14984	3.4	0.39	141	112
94-MC-MGI2_29	0.0056	0.0023	0.000504	0.000085	0.077819	3.25	0.54	96.2	70.4
94-MC-MGI2_30	0.00341	0.00068	0.00051	0.000051	0.34216	3.29	0.33	324	368
94-MC-MGI2_31	0.0029	0.0023	0.000431	0.000078	-0.02281	2.78	0.5	96	90
94-MC-MGI2_32	0.0039	0.0017	0.000494	0.00007	-0.13354	3.18	0.45	370	290
94-MC-MGI2_33	0.0048	0.0025	0.00054	0.0001	-0.18236	3.45	0.65	244	205
94-MC-MGI2_34	0.0062	0.0014	0.000542	0.000056	0.21465	3.49	0.36	200	160.6
94-MC-MGI2_35	0.0081	0.0018	0.000444	0.000067	-0.2191	2.86	0.43	221	127
94-MC-MGI2_36	4.301	0.078	0.2714	0.0054	0.67187	1550	28	881	830
GRD41-01-273m_1	0.0045	0.00063	0.000519	0.000037	-0.17877	3.35	0.24	450	334
GRD41-01-273m_2	0.00453	0.00076	0.000457	0.000036	0.030028	2.94	0.23	326	579
GRD41-01-273m_3	0.0066	0.0012	0.000581	0.000047	0.15194	3.74	0.3	494	179
GRD41-01-273m_4	0.00914	0.00094	0.000582	0.000036	0.32912	3.75	0.23	574	264
GRD41-01-273m_5	0.00399	0.00053	0.000509	0.000039	-0.0090151	3.28	0.25	450	128
GRD41-01-273m_6	0.0058	0.0013	0.000495	0.000047	0.064237	3.19	0.3	197	197
GRD41-01-273m_7	0.00546	0.00098	0.000497	0.000038	0.033927	3.2	0.24	417	114.8
GRD41-01-273m_8	0.00383	0.00057	0.000446	0.000028	-0.027018	2.88	0.18	536	281
GRD41-01-273m_9	0.0049	0.0016	0.000413	0.000052	-0.061992	2.66	0.33	149.8	132
GRD41-01-273m_10	0.0031	0.0011	0.000488	0.000046	-0.075375	3.15	0.3	171.1	167.5

	207Pb/235U	207Pb/235U error	206Pb/238U	206Pb/238U Error	Error Correlation 206/238 vs. 207/235	Final Age (Ma)	Error (Ma)	Approx U (ppm)	Approx Th (ppm)
GRD41-01-273m_11	0.0046	0.0015	0.000469	0.000068	-0.20883	3.02	0.44	135	126.2
GRD41-01-273m_12	0.00488	0.00065	0.000499	0.000031	0.0068584	3.21	0.2	579	302.4
GRD41-01-273m_13	0.0045	0.0012	0.000559	0.000049	-0.083137	3.6	0.32	274	169
GRD41-01-273m_14	0.00501	0.00068	0.000536	0.000028	0.002902	3.45	0.18	519	230
GRD41-01-273m_15	0.00413	0.00048	0.00051	0.000032	-0.02052	3.29	0.2	595	277
GRD41-01-273m_16	0.00439	0.00062	0.000475	0.000031	0.063891	3.06	0.2	445	179
GRD41-01-273m_17	0.00405	0.00055	0.000508	0.000045	-0.15128	3.27	0.29	806	905
GRD41-01-273m_18	0.00703	0.00095	0.000502	0.000031	0.053745	3.24	0.2	333	194
GRD41-01-273m_19	0.00635	0.00067	0.000522	0.000036	0.0069793	3.37	0.23	375	181.1
GRD41-01-273m_20	0.00419	0.00071	0.000438	0.000026	0.066971	2.83	0.16	827	1206
GRD41-01-273m_21	0.0053	0.0014	0.000478	0.00005	-0.13004	3.08	0.32	205	236
GRD41-01-273m_22	0.006	0.0012	0.000516	0.000039	0.1061	3.33	0.25	240.4	376.8
GRD41-01-273m_23	0.0184	0.0034	0.000528	0.000071	-0.17402	3.4	0.45	172.7	126
GRD42-06-389m_1	0.0082	0.002	0.000547	0.000067	0.1987	3.52	0.43	173	94.2
GRD42-06-389m_2	0.0045	0.0014	0.000458	0.000068	0.25098	2.95	0.44	140	99.3
GRD42-06-389m_3	0.0176	0.0023	0.000626	0.000061	-0.0022468	4.03	0.39	158.9	126.8
GRD42-06-389m_4	0.0273	0.0028	0.000562	0.000065	0.061034	3.62	0.42	104.5	87.2
GRD42-06-389m_5	0.0052	0.001	0.00053	0.00004	0.037795	3.42	0.26	305	129.8
GRD42-06-389m_6	0.00366	0.00093	0.000501	0.000061	-0.09185	3.23	0.39	152.9	117.2
GRD42-06-389m_7	0.0046	0.0016	0.000519	0.000074	-0.0060698	3.34	0.47	105.5	118.9
GRD42-06-389m_8	0.00315	0.00091	0.000483	0.000045	0.061645	3.11	0.29	146.9	161.3
GRD42-06-389m_9	0.00429	0.00072	0.000524	0.000048	-0.11705	3.37	0.31	360	112
GRD42-06-389m_10	0.00493	0.00061	0.000504	0.000042	0.16943	3.25	0.27	393	142.7
GRD42-06-389m_11	0.0077	0.0012	0.000546	0.000039	-0.0084209	3.52	0.25	184	191
GRD42-06-389m_12	0.0225	0.0085	0.00062	0.00012	0.1407	4	0.75	150	156.8
GRD42-06-389m_13	0.0029	0.0016	0.000497	0.000093	0.11516	3.21	0.6	78.3	55.7
GRD42-06-389m_14	0.0044	0.0013	0.000484	0.000057	0.034027	3.12	0.37	417	130.3
GRD42-06-389m_15	0.0061	0.0012	0.000548	0.000037	0.21425	3.53	0.24	426	218
GRD42-06-389m_16	0.00462	0.00061	0.000473	0.000027	-0.0048729	3.05	0.18	407.1	162.1
GRD42-06-389m_17	0.00487	0.00065	0.000519	0.000038	-0.24469	3.34	0.24	373.1	158.2
GRD42-06-389m_18	0.0075	0.0014	0.000482	0.000053	0.031512	3.11	0.34	355.2	158.9
GRD42-06-389m_19	0.00411	0.00085	0.000472	0.000048	-0.09533	3.04	0.31	197.8	196.5
GRD42-06-389m_20	0.0067	0.003	0.00073	0.00021	0.32856	4.7	1.3	117	89
GRD42-06-389m_21	0.00479	0.00086	0.00051	0.000039	0.28133	3.29	0.25	443	371
GRD42-06-389m_22	0.0092	0.0019	0.000481	0.000088	0.22103	3.1	0.56	171.8	131.6
GRD42-06-389m_23	0.0066	0.0025	0.000535	0.000098	0.35036	3.45	0.63	131.4	108.4
GRD42-06-389m_24	0.0057	0.0012	0.000483	0.000053	-0.055047	3.11	0.34	153.6	116
GRD42-06-389m_25	0.00364	0.00054	0.000466	0.000034	-0.15372	3	0.22	370	358
GRD42-06-389m_26	0.00473	0.00059	0.000485	0.000036	0.041046	3.13	0.23	404	178
GRD42-06-389m_27	0.0039	0.001	0.000523	0.000063	0.013789	3.37	0.41	145.9	131.7
GRD42-06-389m_28	0.2253	0.0057	0.0319	0.00045	0.42842	202.4	2.8	350	644
GRD42-06-389m_29	0.3544	0.0061	0.04951	0.0005	0.17987	311.5	3	268	171.8
GRD42-06-389m_30	0.412	0.012	0.05133	0.00083	0.21857	322.7	5.1	616	389
GRD42-06-389m_31	0.3578	0.0079	0.04891	0.00074	0.37598	307.8	4.5	283	345
GRD42-06-389m_32	0.3648	0.0072	0.05105	0.00062	0.13195	320.9	3.8	216.3	111.8
GRS-93A_1	0.00422	0.00078	0.000534	0.000038	0.19014	3.44	0.25	375	172
GRS-93A_2	0.006	0.0013	0.000553	0.000058	0.025336	3.56	0.37	227	107.9
GRS-93A_3	0.0041	0.0011	0.000534	0.00006	0.093211	3.44	0.38	543	320
GRS-93A_4	0.00389	0.00083	0.000514	0.000043	0.11513	3.31	0.28	390	142
GRS-93A_5	0.008	0.0021	0.000533	0.00008	0.091204	3.44	0.51	134.1	82.4
GRS-93A_6	0.0044	0.0019	0.000573	0.00008	0.13551	3.69	0.52	104.9	45.5
GRS-93A_7	0.0042	0.0017	0.00056	0.000082	0.18679	3.61	0.53	128	49.2
GRS-93A_8	0.0042	0.0021	0.00062	0.00016	0.42654	4	1	194	96.1
GRS-93A_9	0.006	0.0014	0.000446	0.000051	0.0071695	2.87	0.33	199	79
GRS-93A_10	0.00412	0.00088	0.000597	0.000058	0.24562	3.85	0.38	498	271
GRS-93A_11	0.0047	0.0015	0.000464	0.000079	0.06533	2.99	0.51	106.7	65.1
GRS-93A_12	0.0041	0.0014	0.000436	0.000068	0.013043	2.81	0.44	233.6	132
GRS-93A_13	0.0085	0.0029	0.00059	0.00011	0.275	3.8	0.73	149.1	117.5
GRS-93A_14	0.0028	0.001	0.000399	0.000057	0.046205	2.57	0.36	266	106.8
GRS-93A_15	0.0065	0.002	0.000414	0.000054	0.53065	2.67	0.35	542	406
GRS-93A_16	0.0033	0.0015	0.000408	0.000072	0.070517	2.63	0.46	116.2	74.4
GRS-93A_17	0.0055	0.0016	0.000441	0.000058	0.1884	2.84	0.37	132.4	123
GRS-93A_18	0.0085	0.0026	0.00058	0.00015	0.089146	3.75	0.94	140	103.1
GRS-93A_19	0.0112	0.0032	0.00062	0.00011	0.13084	3.98	0.72	83.4	50.2
GRS-93A_20	0.0057	0.0017	0.000483	0.000077	0.39289	3.12	0.49	220	132
GRS-93A_21	0.0113	0.0016	0.000461	0.000055	0.059396	2.97	0.36	204	149.5
GRS-93A_22	0.0063	0.0012	0.000536	0.00005	0.073406	3.46	0.32	406	210
GRS-93A_23	0.006	0.0019	0.000448	0.000066	0.0086455	2.89	0.43	122.2	71

	207Pb/235U	207Pb/235U error	206Pb/238U	206Pb/238U Error	Error Correlation 206/238 vs. 207/235	Final Age (Ma)	Error (Ma)	Approx U (ppm)	Approx Th (ppm)
GRS-93A_24	0.0048	0.0017	0.000451	0.000083	0.077758	2.9	0.54	97.6	62.1
GRS-93A_25	0.0044	0.0015	0.000452	0.000071	0.088034	2.91	0.46	137	127.6
GRS-93A_26	0.00464	0.00092	0.000504	0.000052	0.031265	3.25	0.33	373	243
GRS-93A_27	0.0056	0.0015	0.000474	0.000057	0.19529	3.05	0.37	164.3	183
GRS-93A_28	0.0058	0.0019	0.000503	0.000077	0.20925	3.24	0.49	130.4	74.2
GRS-93A_29	0.327	0.012	0.0456	0.0013	0.66435	287.3	8.2	977	670
GRS-93A_30	5.121	0.096	0.3154	0.0058	0.75457	1767	29	256	286
INF42-01-32m_1	0.00707	0.00079	0.000504	0.000033	-0.10396	3.25	0.21	409.5	151.3
INF42-01-32m_2	0.00418	0.00041	0.00046	0.00003	-0.11804	2.97	0.2	423	221.6
INF42-01-32m_3	0.0181	0.0031	0.000598	0.000084	0.053578	3.85	0.54	98	71.9
INF42-01-32m_4	0.00627	0.00075	0.000524	0.000032	0.27028	3.38	0.21	419	242
INF42-01-32m_5	0.0089	0.0015	0.000573	0.000065	0.2962	3.7	0.42	309	117
INF42-01-32m_6	0.0115	0.0031	0.00054	0.000061	0.10653	3.48	0.39	117.6	118.5
INF42-01-32m_7	0.00434	0.00044	0.000492	0.000025	0.12188	3.17	0.16	673	163
INF42-01-32m_8	0.0087	0.0014	0.000531	0.000047	-0.0042356	3.42	0.3	301	218
INF42-01-32m_9	0.0119	0.0022	0.000526	0.000058	0.080255	3.56	0.35	93.9	108.9
INF42-01-32m_10	0.00515	0.00063	0.000504	0.000038	0.053734	3.25	0.25	508.5	449
INF42-01-32m_11	0.00562	0.00078	0.000562	0.000033	0.10841	3.62	0.21	481	344
INF42-01-32m_12	0.00704	0.00079	0.000538	0.000044	0.089558	3.47	0.28	382	463
INF42-01-32m_13	0.00552	0.00048	0.000519	0.00003	0.026093	3.34	0.2	777	232
INF42-01-32m_14	0.0109	0.0023	0.00053	0.000035	0.69897	3.42	0.23	602	251.1
INF42-01-32m_15	0.0109	0.0016	0.000555	0.000053	0.23708	3.58	0.34	429	422
INF42-01-32m_16	0.0079	0.0018	0.000555	0.000054	-0.061907	3.57	0.35	361	306
INF42-01-32m_17	0.0258	0.0029	0.000639	0.000059	0.24005	4.12	0.38	148.2	120.6
INF42-01-32m_18	0.00778	0.00089	0.000521	0.000035	0.17281	3.36	0.23	489	279.3
INF42-01-32m_19	0.00493	0.00061	0.000516	0.000034	0.10136	3.33	0.22	463	212.9
INF42-01-32m_20	0.00335	0.0003	0.000494	0.00003	-0.055965	3.19	0.19	783	324
INF42-01-32m_21	0.0278	0.0064	0.00062	0.00011	0.15582	4.02	0.71	48.6	34.21
INF42-01-32m_22	0.00555	0.00065	0.000505	0.000029	0.23427	3.25	0.19	496	194.7
INF42-01-32m_23	0.0227	0.0022	0.001034	0.000065	-0.023147	6.66	0.42	499	30.6
INF42-01-32m_24	0.336	0.0044	0.0467	0.00051	0.16873	294.2	3.2	511	605
INF42-01-32m_25	0.3649	0.0078	0.05037	0.00091	0.21363	316.8	5.6	220	130.6
INF42-01-32m_26	7.33	0.29	0.3592	0.0099	0.58891	1975	47	9.83	12.93
INF42-01-32m_27	5	0.045	0.318	0.0028	0.75395	1780	13	329	227
INF42-01-32m_28	0.3236	0.0049	0.04442	0.00044	0.31532	280.2	2.7	420	469
AB1-10-01-578m_1	0.00393	0.00064	0.000454	0.000032	0.080267	2.93	0.2	271	104.3
AB1-10-01-578m_2	0.00388	0.00057	0.000481	0.000032	0.061442	3.1	0.21	310.5	127.7
AB1-10-01-578m_3	0.00495	0.00073	0.000487	0.000038	0.0086763	3.14	0.25	246.3	103.8
AB1-10-01-578m_4	0.00397	0.00065	0.000538	0.00004	0.13998	3.47	0.26	274.5	92.8
AB1-10-01-578m_5	0.00378	0.00044	0.000509	0.000028	0.15768	3.28	0.18	446	167.7
AB1-10-01-578m_6	0.00375	0.0004	0.000504	0.00003	0.11298	3.25	0.2	539	209.6
AB1-10-01-578m_7	0.00341	0.00046	0.000444	0.00003	0.022205	2.86	0.2	446	197
AB1-10-01-578m_8	0.00389	0.00049	0.000485	0.000029	0.13189	3.13	0.19	433.2	174.7
AB1-10-01-578m_9	0.00359	0.0005	0.0005	0.00003	0.13695	3.23	0.2	347	173
AB1-10-01-578m_10	0.00317	0.00042	0.000459	0.000028	0.23632	2.96	0.18	397	194
AB1-10-01-578m_11	0.00435	0.00043	0.000516	0.000027	0.026351	3.33	0.17	410	161.6
AB1-10-01-578m_12	0.00325	0.00041	0.000486	0.000028	0.042244	3.13	0.18	413	121.9
AB1-10-01-578m_13	0.00348	0.00061	0.000481	0.000033	0.012692	3.1	0.21	349	106.2
AB1-10-01-578m_14	0.00432	0.00044	0.000474	0.000031	0.039989	3.06	0.2	477	171
AB1-10-01-578m_15	0.00692	0.00094	0.000503	0.000032	0.2315	3.24	0.21	340	326
AB1-10-01-578m_16	0.00491	0.0008	0.000458	0.000033	0.26427	2.95	0.21	299	201
AB1-10-01-578m_17	0.0031	0.0016	0.000464	0.000066	0.029676	2.99	0.43	161	98
AB1-10-01-578m_18	0.00335	0.00075	0.0005	0.000042	0.027048	3.22	0.27	215.1	90
AB1-10-01-578m_19	0.00402	0.00036	0.000492	0.000027	0.18954	3.17	0.17	455	139
AB1-10-01-578m_20	0.00491	0.00064	0.0005	0.000032	0.20981	3.22	0.21	371	99.3
AB1-10-01-578m_21	0.0039	0.00046	0.000459	0.000028	0.044538	2.96	0.18	474	128.7
AB1-10-01-578m_22	0.00339	0.00043	0.000487	0.00003	0.018717	3.14	0.19	428	147
AB1-10-01-578m_23	0.00412	0.00061	0.000524	0.000038	0.12907	3.38	0.24	260.5	88.5
AB1-10-01-578m_24	0.0038	0.00055	0.00049	0.000038	0.15444	3.16	0.25	312	118.1
AB1-10-01-578m_25	0.00451	0.00071	0.000505	0.000036	0.046653	3.26	0.23	298	67.6
AB1-10-01-578m_26	0.00438	0.00046	0.000491	0.000027	0.11075	3.17	0.17	424	166.2
AB1-10-01-578m_27	0.00393	0.00053	0.000496	0.000035	0.19493	3.2	0.22	428	169
AB1-10-01-578m_28	0.00358	0.00049	0.000458	0.000039	0.12721	2.95	0.25	307	114.2
AB1-10-01-578m_29	0.00355	0.00053	0.000476	0.000028	0.18297	3.07	0.18	392	108.8
AB1-10-01-500m_1	0.00367	0.00058	0.00047	0.000031	0.54119	3.03	0.2	414	760
AB1-10-01-500m_2	0.0041	0.0017	0.00045	0.0001	0.038222	2.88	0.65	178.2	129.6
AB1-10-01-500m_3	0.00399	0.00024	0.000512	0.000018	0.026713	3.3	0.12	1388	2438
AB1-10-01-500m_4	0.00427	0.00051	0.000529	0.000028	0.17377	3.41	0.18	510	578
AB1-10-01-500m_5	0.00388	0.00034	0.000526	0.000024	0.14921	3.39	0.15	774	1813

	207Pb/235U	207Pb/235U error	206Pb/238U	206Pb/238U Error	Error Correlation 206/238 vs. 207/235	Final Age (Ma)	Error (Ma)	Approx U (ppm)	Approx Th (ppm)
AB1-10-01-500m_6	0.00395	0.00035	0.000485	0.000022	0.035257	3.12	0.14	674	1324
AB1-10-01-500m_7	0.00421	0.00046	0.000547	0.00002	0.30821	3.52	0.13	880	1160
AB1-10-01-500m_8	0.00491	0.00064	0.000511	0.000027	0.087277	3.3	0.17	761	1590
AB1-10-01-500m_9	0.00437	0.00056	0.000508	0.000028	0.15734	3.27	0.18	1075	905
AB1-10-01-500m_10	0.00342	0.00031	0.000513	0.000018	0.20146	3.31	0.12	925	1929
AB1-10-01-500m_11	0.00417	0.00052	0.000488	0.000033	0.32932	3.14	0.21	536	914
AB1-10-01-500m_12	0.00489	0.00056	0.000485	0.000038	0.12421	3.13	0.24	580	344.7
AB1-10-01-500m_13	0.00381	0.0003	0.00052	0.000023	0.07959	3.35	0.15	731	1387
AB1-10-01-500m_14	0.00845	0.00093	0.000544	0.000028	0.29598	3.51	0.18	674	1180
AB1-10-01-500m_15	0.00396	0.00032	0.000497	0.000018	0.012901	3.2	0.11	934	870
AB1-10-01-500m_16	0.00423	0.00049	0.000502	0.000028	0.25678	3.24	0.18	673.7	1525
AB1-10-01-500m_17	0.00345	0.00032	0.000517	0.000022	0.1904	3.33	0.14	1090	1430
AB1-10-01-500m_18	0.0089	0.0012	0.000497	0.000032	0.43992	3.2	0.21	401	644
AB1-10-01-500m_19	0.00341	0.00074	0.000464	0.000039	0.025679	2.99	0.25	308	444
AB1-10-01-500m_20	0.00464	0.00056	0.000492	0.000028	0.0625	3.17	0.18	668	941
AB1-10-01-500m_21	0.00402	0.00054	0.000506	0.000034	0.28232	3.26	0.22	788	1125
AB1-10-01-500m_22	0.00401	0.00042	0.00049	0.000023	0.33135	3.16	0.15	674	1335
AB1-10-01-500m_23	0.00497	0.00064	0.000522	0.000031	0.31747	3.37	0.2	823	1320
AB1-10-01-500m_24	0.00552	0.00072	0.000494	0.000029	0.35816	3.18	0.19	826	1269
AB1-10-01-500m_25	0.00327	0.00032	0.000432	0.000026	0.042702	2.78	0.17	516	754
AB1-10-01-500m_26	0.00378	0.00041	0.000478	0.000021	0.24753	3.08	0.13	696	1293
AB1-10-01-500m_27	0.00505	0.00046	0.00051	0.000023	0.11807	3.29	0.15	818	1480
AB1-10-01-500m_28	0.00437	0.00047	0.000479	0.000026	0.13703	3.09	0.17	1460	2020
AB1-10-01-500m_29	0.00305	0.0004	0.000503	0.000023	0.13304	3.24	0.15	722	1538
GRD41-01-322.5m_1	0.00412	0.00064	0.000506	0.000038	0.044937	3.26	0.24	360	123.1
GRD41-01-322.5m_2	0.00437	0.00088	0.000513	0.000039	0.15931	3.3	0.25	304	70.3
GRD41-01-322.5m_3	0.00462	0.00073	0.000526	0.000041	0.026452	3.39	0.26	360	99.2
GRD41-01-322.5m_4	0.0069	0.0015	0.0005	0.000052	-0.16253	3.22	0.34	186	149
GRD41-01-322.5m_5	0.023	0.0038	0.000577	0.000079	0.12215	3.72	0.51	113.7	81.3
GRD41-01-322.5m_6	0.0062	0.0014	0.000558	0.000049	0.42284	3.6	0.31	621	229.6
GRD41-01-322.5m_7	0.00439	0.00074	0.000506	0.00004	-0.30907	3.26	0.26	409	175
GRD41-01-322.5m_8	0.00445	0.00061	0.000472	0.000028	-0.16739	3.04	0.18	592	257
GRD41-01-322.5m_9	0.00442	0.00074	0.000502	0.000036	-0.15125	3.23	0.23	427	149
GRD41-01-322.5m_10	0.0056	0.0019	0.000539	0.000029	0.1142	3.48	0.19	726	440
GRD41-01-322.5m_11	0.0068	0.0013	0.000553	0.000047	0.57155	3.57	0.3	434	98
GRD41-01-322.5m_12	0.0081	0.0015	0.000561	0.000048	0.61884	3.62	0.31	362	87.9
GRD41-01-322.5m_13	0.00363	0.00088	0.000488	0.000038	0.047962	3.14	0.24	364	175.8
GRD41-01-322.5m_14	0.0032	0.00036	0.000461	0.000026	0.048086	2.97	0.17	911	1547
GRD41-01-322.5m_15	0.0111	0.0012	0.000549	0.00004	-0.015701	3.54	0.26	510	190
GRD41-01-322.5m_16	0.00381	0.00034	0.000493	0.000028	-0.026336	3.18	0.18	910	383
GRD41-01-322.5m_17	0.00457	0.00083	0.000495	0.000033	-0.055169	3.19	0.22	439	169
GRD41-01-322.5m_18	0.0057	0.00087	0.000519	0.00005	0.18621	3.35	0.32	381	304.2
GRD41-01-322.5m_19	0.0061	0.001	0.00054	0.000043	0.23923	3.48	0.28	436	170
GRD41-01-322.5m_20	0.00559	0.00076	0.000522	0.000035	0.036051	3.36	0.22	626	248
GRD41-01-322.5m_21	0.00329	0.00053	0.000483	0.000032	0.18008	3.11	0.21	630	285
GRD41-01-322.5m_22	0.00406	0.00078	0.00052	0.000036	0.040847	3.35	0.23	335	129.5
GRD41-01-322.5m_23	0.0042	0.001	0.000469	0.000041	-0.069122	3.02	0.27	199.1	218.9
GRD41-01-322.5m_24	0.0034	0.0012	0.000471	0.000062	-0.0611	3.03	0.4	153	156
GRD41-01-322.5m_25	0.0063	0.0016	0.0005	0.000058	0.14505	3.22	0.37	135.8	135.6
GRD41-01-322.5m_26	0.0058	0.0019	0.000459	0.000065	0.067004	2.96	0.42	96.4	60.95
GRD41-01-322.5m_27	0.00459	0.00059	0.00054	0.000033	-0.098837	3.48	0.21	507	164.7
GRD41-01-322.5m_28	0.00525	0.00077	0.000501	0.000046	0.020443	3.23	0.3	421.3	186
GRD41-01-322.5m_29	0.00528	0.00098	0.000464	0.000047	-0.24378	2.99	0.3	834	455
AM96-50-36m_1	0.0034	0.001	0.000488	0.000056	-0.031314	3.14	0.36	171.8	118.4
AM96-50-36m_2	0.00415	0.00059	0.000472	0.000027	-0.10222	3.04	0.18	483	275
AM96-50-36m_3	0.00532	0.00055	0.000539	0.000027	0.17375	3.47	0.17	768	386
AM96-50-36m_4	0.00383	0.00049	0.000506	0.000032	0.13467	3.26	0.21	559	233
AM96-50-36m_5	0.0037	0.0015	0.000423	0.000075	0.42416	2.73	0.49	403	148
AM96-50-36m_6	0.0247	0.0021	0.000666	0.000039	0.4007	4.29	0.25	621	209
AM96-50-36m_7	0.00464	0.00063	0.000535	0.000036	-0.14785	3.45	0.23	385	256
AM96-50-36m_8	0.00345	0.00048	0.000518	0.000032	-0.054694	3.34	0.21	643	352
AM96-50-36m_9	0.0055	0.0012	0.000531	0.000047	0.14906	3.42	0.3	318	291
AM96-50-36m_10	0.00418	0.00042	0.000494	0.00003	0.019853	3.18	0.19	680	245.9
AM96-50-36m_11	0.00436	0.00059	0.000483	0.000037	-0.020981	3.11	0.24	477.4	138
AM96-50-36m_12	0.00299	0.0003	0.00046	0.000027	-0.0026539	2.97	0.17	905	395
AM96-50-36m_13	0.00347	0.00053	0.000552	0.000033	0.14043	3.56	0.22	458	203.3
AM96-50-36m_14	0.003	0.00063	0.000507	0.000044	0.27687	3.27	0.28	460	167
AM96-50-36m_15	0.0072	0.0015	0.00058	0.000075	0.015875	3.73	0.48	392	215
AM96-50-36m_16	0.00339	0.00044	0.000486	0.000029	-0.053778	3.13	0.19	626	241.7

	207Pb/235U	207Pb/235U error	206Pb/238U	206Pb/238U Error	Error Correlation 206/238 vs. 207/235	Final Age (Ma)	Error (Ma)	Approx U (ppm)	Approx Th (ppm)
AM96-50-36m_17	0.0122	0.0013	0.000616	0.000043	0.23894	3.97	0.28	802	1725
AM96-50-36m_18	0.0151	0.0026	0.000625	0.000077	0.22202	4.03	0.5	89.9	64.2
AM96-50-36m_19	0.0053	0.0016	0.000563	0.000059	-0.070537	3.63	0.38	127.2	162.1
AM96-50-36m_20	0.0063	0.00081	0.000619	0.000048	0.10586	3.99	0.31	479	200
AM96-50-36m_21	0.00534	0.00071	0.00057	0.000041	-0.050244	3.67	0.26	420	268
AM96-50-36m_22	0.0057	0.0013	0.000634	0.000063	0.098081	4.08	0.4	260.1	126.4
AM96-50-36m_23	0.00328	0.00046	0.000512	0.000032	0.0036299	3.3	0.21	538.8	171.4
AM96-50-36m_24	0.813	0.015	0.0968	0.0017	0.090989	595.4	9.7	384	8.19
94_TH3_DA_1	0.00436	0.00077	0.000505	0.000035	0.22339	3.25	0.22	163	134.3
94_TH3_DA_2	0.00491	0.00059	0.000543	0.000035	0.08277	3.5	0.22	246	264
94_TH3_DA_3	0.00369	0.00075	0.00058	0.000038	0.08047	3.74	0.24	170	174
94_TH3_DA_4	0.00394	0.0006	0.000534	0.000041	0.0080288	3.44	0.26	189	144
94_TH3_DA_5	0.0046	0.0007	0.000546	0.000043	0.12042	3.52	0.27	169.7	156
94_TH3_DA_6	0.00471	0.00063	0.000516	0.000035	0.010779	3.32	0.23	242	246
94_TH3_DA_7	0.00454	0.00059	0.000518	0.000036	0.022345	3.34	0.23	190	194
94_TH3_DA_8	0.0063	0.0011	0.000529	0.00006	0.046357	3.41	0.39	222.5	209
94_TH3_DA_9	0.0049	0.0007	0.000508	0.000036	0.014071	3.27	0.23	167.9	147
94_TH3_DA_10	0.0054	0.0011	0.000537	0.000048	0.23791	3.46	0.31	208.8	173.6
94_TH3_DA_11	0.0063	0.0011	0.000585	0.000057	0.034928	3.77	0.37	145	93
94_TH3_DA_12	0.00398	0.0003	0.000571	0.000023	0.026686	3.68	0.15	848	510
94_TH3_DA_13	0.00521	0.00085	0.000516	0.00004	0.063595	3.33	0.26	231.7	204.5
94_TH3_DA_14	0.00483	0.00066	0.000563	0.000043	0.12864	3.63	0.28	222.7	166.7
94_TH3_DA_15	0.0056	0.00099	0.000534	0.000034	0.0075809	3.44	0.22	167	137.3
94_TH3_DA_16	0.00395	0.00078	0.000563	0.000039	0.030823	3.63	0.25	189.6	169.6
94_TH3_DA_17	0.00454	0.00063	0.000533	0.000039	0.039247	3.44	0.25	173	129
94_TH3_DA_18	0.00471	0.0006	0.000511	0.000039	0.075671	3.29	0.25	184.6	142.5
94_TH3_DA_19	0.00532	0.00063	0.000508	0.000044	0.0081969	3.27	0.28	165.4	123.6
94_TH3_DA_20	0.00446	0.00052	0.000517	0.000043	0.14909	3.33	0.28	368.6	219.6
94_TH3_DA_21	0.0059	0.001	0.000512	0.00005	0.34209	3.3	0.32	192	167
94_TH3_DA_22	0.00456	0.00072	0.000563	0.000046	0.1351	3.63	0.3	141.3	111
94_TH3_DA_23	0.00543	0.00056	0.000631	0.000031	0.25132	4.07	0.2	431	277
94_TH3_DA_24	0.0082	0.0017	0.000616	0.00006	0.41575	3.97	0.39	147.6	110.6
94_TH3_DA_25	0.0043	0.00052	0.000536	0.000036	0.046877	3.45	0.23	245	196
94_TH3_DA_26	0.00419	0.0007	0.000517	0.00004	0.051601	3.33	0.26	191.4	131.2
94_TH3_DA_27	0.00516	0.00057	0.000554	0.000039	0.1026	3.57	0.25	242.9	171.9
90-TM-GRS-1_1	0.00392	0.00085	0.000594	0.000061	-0.021387	3.83	0.39	247	220
90-TM-GRS-1_2	0.00404	0.00083	0.000555	0.000041	-0.02631	3.58	0.26	246	245
90-TM-GRS-1_3	0.0061	0.0011	0.000551	0.00005	0.10709	3.55	0.32	256	245
90-TM-GRS-1_4	0.0062	0.0017	0.000514	0.000083	0.31766	3.31	0.53	136.9	116
90-TM-GRS-1_5	0.00432	0.00054	0.000566	0.000031	0.21081	3.65	0.2	394	440
90-TM-GRS-1_6	0.0067	0.0016	0.000537	0.000057	0.005697	3.46	0.37	99.8	60.9
90-TM-GRS-1_7	0.0088	0.0015	0.000602	0.000071	0.085572	3.88	0.46	141.1	99
90-TM-GRS-1_8	0.00377	0.00042	0.000491	0.000024	0.062458	3.16	0.16	543	229
90-TM-GRS-1_9	0.0087	0.0015	0.000569	0.000066	-0.016427	3.67	0.42	166	136
90-TM-GRS-1_10	0.0116	0.0027	0.000737	0.000085	0.17085	4.75	0.55	90.8	74
90-TM-GRS-1_11	0.0119	0.0015	0.000592	0.000032	0.23351	3.81	0.21	439	800
90-TM-GRS-1_12	0.00463	0.00047	0.000547	0.000036	0.022546	3.53	0.23	394	185
90-TM-GRS-1_13	0.00435	0.00045	0.000534	0.00003	0.14783	3.44	0.2	433	202
90-TM-GRS-1_14	0.0072	0.0014	0.00053	0.000056	0.083597	3.42	0.36	157	132
90-TM-GRS-1_15	0.00527	0.00084	0.000531	0.000044	0.07829	3.42	0.29	198.1	158.1
90-TM-GRS-1_16	0.0118	0.0079	0.000489	0.000088	-0.17198	3.15	0.57	243.2	225
90-TM-GRS-1_17	0.00497	0.0009	0.000577	0.000043	0.17559	3.72	0.28	338	426
90-TM-GRS-1_18	0.0049	0.00095	0.000551	0.000048	0.27125	3.55	0.31	203	231
90-TM-GRS-1_19	0.00615	0.00091	0.000491	0.000042	-0.13426	3.16	0.27	183	192
90-TM-GRS-1_20	0.00553	0.00099	0.000569	0.000046	-0.0007881	3.67	0.29	210.4	216.3
90-TM-GRS-1_21	0.0052	0.0013	0.000534	0.00006	-0.038891	3.44	0.39	129	89.5
90-TM-GRS-1_22	0.00375	0.00034	0.000556	0.000023	0.18526	3.58	0.15	959	1400
90-TM-GRS-1_23	0.00509	0.00085	0.000516	0.000045	-0.094663	3.32	0.29	264	305
90-TM-GRS-1_25	0.0052	0.00072	0.00046	0.000043	0.09156	2.96	0.28	248	263
90-TM-GRS-1_26	0.00418	0.00057	0.00049	0.000036	-0.17937	3.16	0.23	263.8	271
90-TM-GRS-1_27	0.00331	0.00063	0.00051	0.00004	0.079285	3.28	0.26	355	273
90-TM-GRS-1_28	0.0055	0.0017	0.000493	0.000051	-0.022229	3.18	0.33	136.3	86.4
90-TM-GRS-1_29	0.0065	0.0011	0.000486	0.000052	0.017833	3.13	0.34	163.1	120.6
90-TM-GRS-1_30	9.78	0.13	0.4319	0.0038	0.60461	2314	17	143.9	131.5
90-TM-GRS-1_24	0.256	0.011	0.03603	0.00076	0.31874	228.2	4.8	126.9	142.1
NSC-09-02-246m_1	0.0072	0.0014	0.000581	0.00007	-0.028619	3.74	0.45	164	59.5
NSC-09-02-246m_2	0.00581	0.00096	0.000575	0.000057	0.077142	3.71	0.37	246	128
NSC-09-02-246m_3	0.00409	0.00093	0.000513	0.000043	0.13755	3.31	0.28	283	104.7
NSC-09-02-246m_4	0.00552	0.00096	0.00052	0.000048	0.12017	3.35	0.31	328	123
NSC-09-02-246m_5	0.00433	0.0006	0.000497	0.000028	-0.31366	3.21	0.18	964	537
NSC-09-02-246m_6	0.00465	0.00075	0.000536	0.000039	-0.069373	3.45	0.25	513	415

	207Pb/235U	207Pb/235U error	206Pb/238U	206Pb/238U Error	Error Correlation 206/238 vs. 207/235	Final Age (Ma)	Error (Ma)	Approx U (ppm)	Approx Th (ppm)
NSC-09-02-246m_7	0.00507	0.00089	0.000548	0.000052	-0.019263	3.53	0.34	222.8	119.7
NSC-09-02-246m_8	0.00502	0.00074	0.000541	0.000041	-0.11412	3.49	0.27	384	149
NSC-09-02-246m_9	0.0044	0.00099	0.000525	0.000047	0.22253	3.39	0.3	317	128.3
NSC-09-02-246m_10	0.0051	0.0013	0.000546	0.000051	0.15627	3.52	0.33	258	156
NSC-09-02-246m_11	0.00462	0.0005	0.000531	0.000033	-0.0082764	3.42	0.22	545	266
NSC-09-02-246m_12	0.00493	0.00055	0.000546	0.000031	0.35428	3.52	0.2	633	375
NSC-09-02-246m_13	0.00567	0.00046	0.000502	0.000026	0.0024441	3.23	0.17	795	421
NSC-09-02-246m_14	0.006	0.0016	0.000617	0.00006	-0.061026	3.97	0.38	186.7	97.2
NSC-09-02-246m_15	0.0071	0.0016	0.000534	0.00007	-0.076618	3.44	0.45	189	74
NSC-09-02-246m_16	0.0043	0.001	0.000537	0.000041	0.089882	3.46	0.26	351	152
NSC-09-02-246m_17	0.00616	0.00089	0.000583	0.000044	0.025532	3.76	0.29	391	253
NSC-09-02-246m_18	0.0047	0.001	0.000529	0.000054	-0.13624	3.41	0.35	338	158
NSC-09-02-246m_19	0.00468	0.00077	0.000574	0.000057	0.16581	3.7	0.37	343	252
NSC-09-02-246m_20	0.0198	0.0048	0.00073	0.0001	0.44535	4.71	0.68	319	126
NSC-09-02-246m_21	0.00426	0.0004	0.000516	0.000023	-0.13386	3.32	0.15	1228	883
NSC-09-02-246m_22	0.00496	0.00063	0.000564	0.000037	-0.16341	3.64	0.24	560	436
NSC-09-02-246m_23	0.00839	0.00094	0.000603	0.000046	-0.053117	3.88	0.29	364	208
NSC-09-02-246m_24	0.00498	0.00061	0.000521	0.00003	-0.12803	3.36	0.19	661	390
NSC-09-02-246m_25	0.0072	0.0022	0.000583	0.000041	0.24328	3.76	0.27	423	174
NSC-09-02-246m_26	0.00506	0.00077	0.000556	0.000034	-0.096219	3.58	0.22	487	198
GCZ-41-01-59m_1	0.005	0.001	0.000467	0.000044	0.092071	3.01	0.28	305	129.1
GCZ-41-01-59m_2	0.0086	0.0011	0.000531	0.000034	-0.12459	3.42	0.22	744	500
GCZ-41-01-59m_3	0.0085	0.0015	0.00057	0.00006	0.25758	3.68	0.39	257	133
GCZ-41-01-59m_4	0.0037	0.00093	0.000474	0.000042	0.033037	3.05	0.27	291	124.7
GCZ-41-01-59m_5	0.0056	0.0012	0.000563	0.000067	0.37602	3.63	0.43	226	93.8
GCZ-41-01-59m_6	0.0039	0.0018	0.00061	0.000068	0.34862	3.93	0.44	225	120
GCZ-41-01-59m_7	0.00627	0.00087	0.000595	0.000057	0.093275	3.84	0.37	361	164
GCZ-41-01-59m_8	0.0037	0.00068	0.000466	0.000037	-0.19656	3	0.24	429	259
GCZ-41-01-59m_9	0.0094	0.0027	0.000578	0.000084	0.09325	3.72	0.54	229	145
GCZ-41-01-59m_11	0.00381	0.00089	0.000569	0.00006	-0.036756	3.67	0.39	423	132
GCZ-41-01-59m_13	0.00508	0.00082	0.000632	0.000054	0.066155	4.07	0.35	354	275
GCZ-41-01-59m_14	0.00415	0.00054	0.000522	0.000034	-0.017434	3.37	0.22	665	412
GCZ-41-01-59m_15	0.0051	0.0014	0.000588	0.000053	0.18848	3.79	0.34	221	93.6
GCZ-41-01-59m_16	0.0042	0.00093	0.000487	0.00006	0.068311	3.14	0.39	311	153
GCZ-41-01-59m_17	0.0069	0.0015	0.000564	0.000047	0.24135	3.63	0.3	348	409
GCZ-41-01-59m_18	0.0057	0.001	0.000605	0.000058	-0.038488	3.9	0.38	262	176
GCZ-41-01-59m_19	0.00473	0.0009	0.000664	0.000061	0.12165	4.28	0.39	338	263
GCZ-41-01-59m_20	0.00388	0.00066	0.000503	0.000046	-0.19679	3.24	0.29	613	335
GCZ-41-01-59m_22	0.0074	0.002	0.000599	0.000076	0.32168	3.86	0.49	394	224
GCZ-41-01-59m_23	0.0066	0.0011	0.000648	0.000065	-0.015436	4.18	0.42	272	97.4
GCZ-41-01-59m_24	0.00421	0.0006	0.000597	0.000043	0.14672	3.85	0.28	505	321
GCZ-41-01-59m_25	0.00348	0.0009	0.000559	0.000057	0.047148	3.6	0.36	329	142
GCZ-41-01-59m_26	0.00365	0.00049	0.000482	0.000033	-0.13353	3.1	0.21	743	721
GCZ-41-01-59m_27	0.0087	0.0023	0.000535	0.000078	-0.07309	3.45	0.51	197	93.2
GCZ-41-01-59m_28	0.00437	0.0007	0.000534	0.000037	-0.33382	3.44	0.24	406	209
GCZ-41-01-59m_29	0.00503	0.0007	0.000539	0.000033	0.037415	3.47	0.21	447	259
GCZ-41-01-59m_31	0.00461	0.00081	0.00058	0.000041	-0.066188	3.74	0.27	388	174
GCZ-41-01-59m_32	0.00494	0.00072	0.000547	0.000034	0.0049427	3.53	0.22	687	450
GCZ-41-01-59m_12	5.029	0.046	0.3346	0.0052	0.38164	1860	25	452	40.1
GCZ-41-01-59m_21	1.29	0.12	0.1287	0.007	0.45429	787	42	9.7	8.23
GCZ-41-01-59m_30	4.76	0.066	0.3205	0.0064	0.25718	1792	31	123	152
GT-INC-023-22m_1	0.00427	0.0009	0.000519	0.000051	-0.098274	3.34	0.33	249	193.1
GT-INC-023-22m_2	0.00383	0.00072	0.000553	0.000043	-0.091146	3.56	0.27	456	187
GT-INC-023-22m_3	0.00415	0.00043	0.000537	0.000025	-0.18685	3.46	0.16	692	390
GT-INC-023-22m_4	0.00382	0.00047	0.000524	0.000034	-0.12435	3.38	0.22	520	232
GT-INC-023-22m_5	0.00391	0.00057	0.000496	0.000033	-0.18417	3.19	0.21	537	261
GT-INC-023-22m_6	0.0048	0.0015	0.000517	0.000058	0.13506	3.33	0.38	164	73.1
GT-INC-023-22m_7	0.00451	0.00058	0.000502	0.000041	0.011731	3.23	0.26	495	216
GT-INC-023-22m_8	0.00407	0.00076	0.000505	0.000046	-0.021341	3.26	0.3	504	270
GT-INC-023-22m_9	0.00445	0.00065	0.000512	0.000041	0.32238	3.3	0.26	466	196
GT-INC-023-22m_10	0.00351	0.00037	0.000508	0.000028	-0.03764	3.27	0.18	790	386
GT-INC-023-22m_11	0.00377	0.00071	0.000527	0.000034	-0.20166	3.39	0.22	450	189
GT-INC-023-22m_12	0.00421	0.00063	0.000536	0.000045	0.17736	3.46	0.29	456	186
GT-INC-023-22m_13	0.00356	0.00057	0.000498	0.00004	0.012038	3.21	0.26	508	204
GT-INC-023-22m_14	0.0045	0.001	0.00056	0.000047	-0.11594	3.61	0.31	538	181
GT-INC-023-22m_15	0.00518	0.00082	0.000508	0.000044	0.278	3.27	0.28	251	99.7
GT-INC-023-22m_16	0.005	0.0011	0.000508	0.000047	-0.058883	3.27	0.3	271	139
GT-INC-023-22m_17	0.00401	0.00039	0.000537	0.000028	-0.10403	3.46	0.18	905	526

	207Pb/235U	207Pb/235U error	206Pb/238U	206Pb/238U Error	Error Correlation 206/238 vs. 207/235	Final Age (Ma)	Error (Ma)	Approx U (ppm)	Approx Th (ppm)
GT-INC-023-22m_18	0.00544	0.00063	0.000495	0.000035	-0.14073	3.19	0.22	530	364
GT-INC-023-22m_19	0.0063	0.00097	0.000503	0.000046	0.22609	3.24	0.3	396.8	102.7
GT-INC-023-22m_20	0.0063	0.0012	0.000504	0.000062	0.3685	3.25	0.4	207	82.8
GT-INC-023-22m_21	0.00397	0.00048	0.000514	0.000032	-0.28884	3.31	0.21	595	618
GT-INC-023-22m_22	0.00449	0.00065	0.000466	0.000036	0.023417	3	0.23	450	204
GT-INC-023-22m_23	0.0157	0.0026	0.000525	0.000055	0.37189	3.38	0.35	250	96.6
GT-INC-023-22m_24	0.00482	0.00098	0.000486	0.000052	-0.17373	3.13	0.34	460	344.8
GT-INC-023-22m_25	0.00571	0.00067	0.000481	0.000032	-0.2543	3.1	0.21	702	454
GT-INC-023-22m_26	0.00428	0.00097	0.000528	0.000066	0.049278	3.4	0.43	285	139.5
GT-INC-023-22m_27	0.00479	0.00065	0.000526	0.000041	0.017756	3.39	0.27	568	244.6
GT-INC-023-22m_28	0.00529	0.00099	0.000491	0.000054	-0.0067943	3.17	0.35	341	228.2
NSC-09-02-290m_1	0.00735	0.00084	0.000535	0.000039	0.047138	3.45	0.25	479	343
NSC-09-02-290m_2	0.0074	0.0017	0.000559	0.000059	-0.27133	3.6	0.38	361	178
NSC-09-02-290m_3	0.0076	0.0018	0.000521	0.00006	0.30341	3.36	0.39	391	97
NSC-09-02-290m_4	0.00252	0.00072	0.00043	0.00004	-0.20187	2.77	0.26	347	147
NSC-09-02-290m_5	0.0371	0.0047	0.000813	0.000065	0.54369	5.24	0.42	391	231
NSC-09-02-290m_6	0.00534	0.00073	0.000546	0.000044	0.20658	3.52	0.28	481	357
NSC-09-02-290m_7	0.00433	0.00055	0.000519	0.000047	0.053411	3.34	0.3	752	341
NSC-09-02-290m_8	0.00604	0.00096	0.000654	0.000071	0.34408	4.21	0.46	670	308
NSC-09-02-290m_9	0.0076	0.0017	0.000543	0.000058	-0.16942	3.5	0.37	383	176
NSC-09-02-290m_10	0.0074	0.0016	0.000568	0.000056	-0.078929	3.66	0.36	271	132
NSC-09-02-290m_11	0.0059	0.0011	0.000506	0.000053	0.23297	3.26	0.34	293	119
NSC-09-02-290m_12	0.0104	0.001	0.000583	0.00004	0.12758	3.76	0.26	559	249
NSC-09-02-290m_13	0.00393	0.00063	0.000536	0.000039	-0.38908	3.46	0.25	550	298
NSC-09-02-290m_14	0.00366	0.00054	0.000472	0.000034	0.064256	3.04	0.22	592	302
NSC-09-02-290m_15	0.00454	0.00059	0.000492	0.00003	0.094227	3.17	0.2	661	379
NSC-09-02-290m_16	0.00526	0.00097	0.000497	0.000046	-0.15382	3.21	0.29	348	208
NSC-09-02-290m_17	0.00425	0.00062	0.00049	0.00003	0.09051	3.16	0.19	556	374
NSC-09-02-290m_18	0.0076	0.002	0.000569	0.000071	0.24656	3.67	0.46	583	214
NSC-09-02-290m_19	0.0119	0.0014	0.000611	0.000041	0.04243	3.94	0.26	521	293
NSC-09-02-290m_20	0.00424	0.00083	0.000572	0.000032	-0.072776	3.69	0.21	556	261
NSC-09-02-290m_21	0.00348	0.00052	0.000478	0.000046	0.18652	3.08	0.3	707	489
NSC-09-02-290m_22	0.00397	0.00062	0.000475	0.000029	-0.032752	3.06	0.19	640	291
NSC-09-02-290m_23	0.0056	0.0013	0.000538	0.000058	0.05195	3.46	0.38	446	232
NSC-09-02-290m_24	0.0075	0.0016	0.00052	0.0001	0.13528	3.37	0.67	632	226
NSC-09-02-290m_25	4.63	0.1	0.2977	0.0048	0.88207	1680	24	787	16.9
NSC-09-02-290m_26	6.34	0.21	0.3249	0.0055	0.76433	1813	27	135.7	65
GCZ-50-02-105m_1	0.0053	0.001	0.00055	0.000059	-0.19251	3.54	0.38	321	180.2
GCZ-50-02-105m_2	0.00415	0.00097	0.000524	0.000054	-0.066371	3.37	0.34	267	182
GCZ-50-02-105m_3	0.0041	0.00045	0.000562	0.000037	0.7151	3.62	0.24	1630	820
GCZ-50-02-105m_4	0.00578	0.00081	0.000568	0.000042	-0.13794	3.66	0.27	463	306
GCZ-50-02-105m_5	0.0045	0.0012	0.00053	0.000042	0.25689	3.42	0.27	289	136
GCZ-50-02-105m_6	0.00405	0.00092	0.000505	0.000055	0.14389	3.26	0.36	877	599
GCZ-50-02-105m_8	0.00452	0.00086	0.000542	0.000048	0.1112	3.49	0.31	319	134
GCZ-50-02-105m_9	0.0043	0.00066	0.000492	0.000032	-0.10739	3.17	0.21	635	319
GCZ-50-02-105m_10	0.00385	0.00049	0.000518	0.000032	-0.2688	3.34	0.2	480	226
GCZ-50-02-105m_11	0.00355	0.00058	0.000553	0.000039	0.14802	3.56	0.25	491	255
GCZ-50-02-105m_12	0.0044	0.00063	0.000522	0.000037	-0.2122	3.36	0.24	435	352
GCZ-50-02-105m_13	0.00431	0.00063	0.000543	0.000034	0.45145	3.5	0.22	488	285
GCZ-50-02-105m_14	0.00416	0.0006	0.000564	0.000032	-0.17264	3.63	0.21	571	733
GCZ-50-02-105m_15	0.00439	0.00052	0.000537	0.000028	0.0082658	3.46	0.18	2170	2371
GCZ-50-02-105m_16	0.00383	0.00057	0.000527	0.000043	0.37258	3.4	0.28	404	193
GCZ-50-02-105m_17	0.00479	0.00087	0.000516	0.000042	-0.0094791	3.33	0.27	671	433
GCZ-50-02-105m_18	0.00443	0.00086	0.000509	0.000046	-0.095499	3.28	0.3	277	106.4
GCZ-50-02-105m_19	0.00512	0.0009	0.000541	0.000051	-0.1286	3.49	0.33	310	133
GCZ-50-02-105m_20	0.00508	0.00083	0.000527	0.000034	-0.029155	3.4	0.22	519	322
GCZ-50-02-105m_21	0.00406	0.00048	0.000543	0.000039	0.083824	3.5	0.25	615	350
GCZ-50-02-105m_22	0.00506	0.00094	0.000533	0.000043	-0.085825	3.44	0.28	1110	780
GCZ-50-02-105m_23	0.0183	0.004	0.000772	0.000089	0.86336	4.97	0.57	467	197
GCZ-50-02-105m_24	0.004	0.0011	0.000562	0.000058	-0.25059	3.62	0.37	501	183
GCZ-50-02-105m_25	0.0041	0.00064	0.000516	0.000042	0.22208	3.32	0.27	890	425
GCZ-50-02-105m_26	0.00387	0.00075	0.000552	0.000045	0.10603	3.55	0.29	319	204.6
GCZ-50-02-105m_27	0.007	0.0013	0.000604	0.000052	0.26809	3.89	0.33	420	328
GCZ-50-02-105m_28	0.00398	0.00069	0.000486	0.000037	-0.14895	3.13	0.24	362	189
GCZ-50-02-105m_29	0.00458	0.00047	0.000542	0.000025	0.11721	3.49	0.16	927	1260
GCZ-50-02-105m_30	0.00415	0.00043	0.000521	0.000025	0.19027	3.36	0.16	1060	713
GCZ-50-02-105m_31	0.00348	0.00054	0.000505	0.000031	0.086805	3.25	0.2	714	394
GCZ-50-02-105m_7	4.846	0.076	0.3154	0.0047	0.54782	1767	23	62.7	21.53

	207Pb/235U	207Pb/235U error	206Pb/238U	206Pb/238U Error	Error Correlation 206/238 vs. 207/235	Final Age (Ma)	Error (Ma)	Approx U (ppm)	Approx Th (ppm)
GRS123_0_1	0.0056	0.0013	0.000551	0.00006	0.061782	3.55	0.39	164.4	86.9
GRS123_0_2	0.00457	0.00043	0.000547	0.000035	0.035217	3.52	0.22	712	355.3
GRS123_0_3	0.0049	0.0012	0.000579	0.000053	0.043494	3.73	0.34	184.5	202
GRS123_0_4	0.0065	0.0028	0.000448	0.000092	0.016935	2.89	0.59	87.7	41.9
GRS123_0_5	0.0067	0.0014	0.000511	0.000062	0.012898	3.29	0.4	162	128.8
GRS123_0_6	0.0081	0.0025	0.00045	0.000075	0.16688	2.9	0.48	91.3	91.1
GRS123_0_7	0.00303	0.00065	0.000397	0.000039	0.060588	2.56	0.25	289	216.1
GRS123_0_8	0.0075	0.0032	0.00048	0.00011	0.11112	3.07	0.73	71.2	38.3
GRS123_0_9	0.0069	0.0022	0.000571	0.000085	0.035456	3.68	0.55	107.6	99.8
GRS123_0_10	0.00339	0.00081	0.000464	0.000052	0.028911	2.99	0.33	302.1	147.5
GRS123_0_11	0.0051	0.0022	0.000419	0.000075	0.055684	2.7	0.49	86	60.5
GRS123_0_12	0.0044	0.001	0.000519	0.00007	0.043711	3.34	0.45	311	125.8
GRS123_0_13	0.0049	0.0016	0.000469	0.00007	0.038009	3.02	0.45	107.5	82.7
GRS123_0_15	0.0041	0.0014	0.00051	0.000063	0.11955	3.28	0.4	148.2	96.9
GRS123_0_16	0.0052	0.0017	0.000501	0.000081	0.19187	3.23	0.52	109	132.6
GRS123_0_17	0.0047	0.0013	0.000484	0.000059	0.19212	3.12	0.38	296	190
GRS123_0_18	0.0123	0.0039	0.000567	0.000096	0.28817	3.66	0.62	91.7	53.1
GRS123_0_20	0.0055	0.0016	0.000536	0.00007	0.11217	3.45	0.45	122.6	77.4
GRS123_0_22	0.00545	0.00095	0.000548	0.000057	0.27188	3.53	0.37	751	532
GRS123_0_23	0.0064	0.002	0.000527	0.00008	0.029612	3.4	0.51	124.2	123.3
GRS123_0_24	0.0051	0.0016	0.000395	0.000054	0.069451	2.54	0.35	135.2	82.4
GRS123_0_25	0.00446	0.00068	0.000487	0.000038	0.02057	3.14	0.25	525	334
GRS123_0_26	0.0044	0.0012	0.000447	0.000053	0.11823	2.88	0.34	368	276
GRS123_0_28	0.0069	0.0013	0.000474	0.000054	0.17259	3.05	0.35	262	152
GRS123_0_30	0.0046	0.0014	0.00048	0.000059	0.099504	3.1	0.38	161	90
GRS123_0_14	0.1121	0.0089	0.00128	0.00014	0.32852	8.24	0.91	186	99
GRS123_0_21	0.122	0.021	0.0014	0.00018	0.45641	9	1.2	165.8	99.3
GRS123_0_19	10.99	0.38	0.3927	0.0094	0.85863	2132	43	117.9	81.8
GRS123_0_29	7.51	0.25	0.368	0.016	0.81969	2020	74	312.4	107.1
14-SW-07_1	0.00501	0.0008	0.000537	0.000047	0.073855	3.46	0.3	483	180.7
14-SW-07_2	0.00539	0.0009	0.000574	0.000053	-0.15238	3.7	0.34	314	170
14-SW-07_3	0.00527	0.00066	0.000571	0.000045	0.092801	3.68	0.29	424	331
14-SW-07_4	0.0089	0.0025	0.000616	0.00006	0.42082	3.97	0.38	826	424
14-SW-07_5	0.00382	0.00048	0.000523	0.000038	0.20712	3.37	0.24	464	255
14-SW-07_6	0.0147	0.0031	0.000588	0.000085	0.063799	3.79	0.55	156	132
14-SW-07_7	0.0055	0.0011	0.000531	0.000066	-0.098134	3.42	0.42	189	90.6
14-SW-07_8	0.0085	0.0024	0.000585	0.000096	0.36518	3.77	0.62	166	86.3
14-SW-07_9	0.00398	0.00072	0.000496	0.000048	-0.20445	3.2	0.31	312	126.6
14-SW-07_10	0.00434	0.00068	0.000507	0.00004	0.037595	3.27	0.25	377	272
14-SW-07_11	0.0064	0.001	0.000606	0.000058	-0.021641	3.91	0.37	277	145
14-SW-07_12	0.00494	0.00069	0.000566	0.000037	0.15414	3.65	0.24	524	270
14-SW-07_13	0.00499	0.00087	0.000567	0.000049	-0.045908	3.65	0.31	730	460
14-SW-07_14	0.00536	0.00053	0.000596	0.000036	-0.069223	3.84	0.23	511	312
14-SW-07_15	0.004	0.00064	0.00056	0.00004	0.057083	3.61	0.26	456	240
14-SW-07_16	0.007	0.0015	0.000539	0.000051	-0.078892	3.47	0.33	204	116.4
14-SW-07_17	0.00451	0.00036	0.000551	0.000026	0.30148	3.55	0.17	1434	1153
14-SW-07_18	0.00406	0.00064	0.000517	0.000042	-0.11899	3.33	0.27	436	166.1
14-SW-07_19	0.007	0.0014	0.00056	0.000056	-0.031344	3.61	0.36	221	163.3
14-SW-07_20	0.0069	0.0017	0.000578	0.000054	0.71246	3.73	0.35	268	140
14-SW-07_21	0.0044	0.00076	0.000527	0.000051	-0.030944	3.4	0.33	264	179
14-SW-07_22	0.0076	0.0015	0.000613	0.000048	0.033926	3.95	0.31	305	211.9
14-SW-07_23	0.00472	0.00071	0.000506	0.000039	-0.15873	3.26	0.25	353	159.5
14-SW-07_24	0.0068	0.0013	0.000589	0.000051	0.035269	3.79	0.33	269	156.3
14-SW-07_25	0.0135	0.0021	0.000572	0.000053	0.33663	3.68	0.34	759	430
14-SW-07_26	0.00596	0.00088	0.000574	0.000038	0.14533	3.7	0.25	354	166
14-SW-07_27	0.0079	0.0017	0.000554	0.000072	0.069006	3.57	0.46	137.4	133.6
14-SW-06_1	0.00544	0.0007	0.000548	0.000036	0.29396	3.53	0.23	535	200
14-SW-06_2	0.0364	0.005	0.00077	0.00011	0.37816	4.96	0.7	122.7	79.5
14-SW-06_3	0.0061	0.00099	0.000548	0.000054	-0.17258	3.53	0.35	357	145
14-SW-06_4	0.00523	0.00072	0.000518	0.000039	-0.15043	3.34	0.25	434	328
14-SW-06_5	0.0084	0.0011	0.000535	0.000045	0.013431	3.45	0.29	303.3	217
14-SW-06_6	0.00536	0.00074	0.000528	0.00004	0.16266	3.4	0.26	330	189.3
14-SW-06_7	0.0074	0.0012	0.000557	0.00004	0.036502	3.59	0.26	389	193
14-SW-06_8	0.0079	0.0012	0.000555	0.000051	-0.093923	3.57	0.33	241.1	124.5
14-SW-06_9	0.0077	0.0011	0.000558	0.000049	0.054502	3.59	0.32	197	131.3
14-SW-06_10	0.00476	0.00056	0.000527	0.000036	0.15769	3.4	0.23	555	220.8
14-SW-06_11	0.00567	0.00097	0.000553	0.000048	0.026836	3.56	0.31	297	132
14-SW-06_12	0.00492	0.00064	0.000502	0.000026	0.29805	3.24	0.17	823	628
14-SW-06_13	0.0138	0.0035	0.000581	0.000065	-0.19206	3.74	0.42	378	264

	207Pb/235U	207Pb/235U error	206Pb/238U	206Pb/238U Error	Error Correlation 206/238 vs. 207/235	Final Age (Ma)	Error (Ma)	Approx U (ppm)	Approx Th (ppm)
14-SW-06_14	0.00394	0.00049	0.000537	0.000029	0.13772	3.46	0.18	553	346
14-SW-06_15	0.0096	0.0014	0.00057	0.000047	0.183	3.67	0.3	345	158.4
14-SW-06_16	0.01	0.0011	0.000687	0.00007	-0.013698	4.43	0.45	584	291
14-SW-06_17	0.009	0.0015	0.000536	0.000047	0.054764	3.46	0.3	344	166
14-SW-06_18	0.0103	0.0018	0.00055	0.00007	0.37085	3.54	0.45	145	76.2
14-SW-06_19	0.0091	0.0013	0.000604	0.000054	0.34384	3.89	0.35	298	210
14-SW-06_20	0.051	0.012	0.00097	0.00015	0.72442	6.26	0.98	173	92
14-SW-06_21	0.008	0.0015	0.000603	0.000049	0.15948	3.89	0.32	264	133.8
14-SW-06_22	0.0177	0.0042	0.000634	0.000064	0.64526	4.09	0.41	332	234
14-SW-06_23	0.00498	0.00059	0.000571	0.000038	0.24064	3.68	0.25	309	162
14-SW-06_24	0.0107	0.002	0.000485	0.000032	0.46831	3.12	0.2	1280	770
14-SW-06_25	0.0186	0.0021	0.00069	0.00005	0.22609	4.45	0.32	360.8	217.3
14-SW-06_26	0.0073	0.001	0.000577	0.000045	0.1559	3.72	0.29	366	175
14-SW-06_27	0.00833	0.00099	0.000528	0.000053	0.0075671	3.4	0.34	349	174
GRD32-06-46m_1	0.0065	0.0012	0.00055	0.00004	0.35371	3.54	0.26	756	414
GRD32-06-46m_2	0.00536	0.00067	0.000559	0.00004	-0.011576	3.6	0.26	476	301
GRD32-06-46m_3	0.0268	0.0049	0.000677	0.000057	0.59559	4.36	0.37	960	860
GRD32-06-46m_4	0.00499	0.00075	0.000468	0.000047	-0.080382	3.02	0.3	331	179
GRD32-06-46m_5	0.00578	0.00096	0.000489	0.000048	-0.14165	3.15	0.31	289	101
GRD32-06-46m_6	0.00462	0.00062	0.000482	0.000038	0.077455	3.11	0.24	599	308
GRD32-06-46m_7	0.0071	0.0016	0.000544	0.000042	0.092393	3.51	0.27	440	183
GRD32-06-46m_8	0.00429	0.0005	0.000519	0.000036	0.10699	3.34	0.23	538	429
GRD32-06-46m_9	0.0104	0.0019	0.000586	0.000051	0.22276	3.78	0.33	480	730
GRD32-06-46m_10	0.0092	0.002	0.000565	0.000044	0.088821	3.64	0.29	718	340
GRD32-06-46m_11	0.00398	0.00069	0.000505	0.000038	0.3167	3.26	0.24	929	385
GRD32-06-46m_12	0.0093	0.0014	0.000572	0.000048	0.19894	3.69	0.31	436	205
GRD32-06-46m_13	0.0055	0.0011	0.000517	0.000036	0.37864	3.33	0.23	530	423
GRD32-06-46m_14	0.0066	0.0014	0.000537	0.000038	0.074182	3.46	0.25	610	257
GRD32-06-46m_15	0.00753	0.00084	0.000545	0.000036	-0.014601	3.51	0.23	512	339
GRD32-06-46m_16	0.0088	0.002	0.000523	0.000061	-0.0775	3.37	0.39	307	173
GRD32-06-46m_17	0.0121	0.0014	0.000648	0.000043	0.27319	4.18	0.28	350	180
GRD32-06-46m_18	0.0149	0.0022	0.000617	0.000034	0.55175	3.97	0.22	1130	1020
GRD32-06-46m_19	0.00404	0.00057	0.000516	0.000035	0.015932	3.33	0.23	447	204
GRD32-06-46m_20	0.00448	0.00049	0.00051	0.000033	0.36087	3.28	0.22	628	357
GRD32-06-46m_21	0.0091	0.004	0.000519	0.000069	0.56593	3.35	0.45	554	217
GRD32-06-46m_22	0.00473	0.00061	0.000537	0.000042	0.033871	3.46	0.27	327	175
GRD32-06-46m_23	0.00419	0.00067	0.000547	0.000042	-0.018599	3.53	0.27	331	196
GRD32-06-46m_24	0.00562	0.00079	0.00054	0.000036	-0.04051	3.48	0.23	358	208
GRD32-06-46m_25	0.0331	0.0064	0.000751	0.000075	0.82642	4.84	0.48	437	215.3
GRD32-06-46m_26	0.0076	0.0017	0.000608	0.000054	0.49752	3.92	0.35	284	123
GRD32-06-46m_27	0.0127	0.0022	0.000669	0.000059	0.16331	4.31	0.38	773	469
GRD32-06-46m_28	0.012	0.0014	0.000651	0.000049	0.28358	4.19	0.32	496	284.5
GRD32-06-46m_29	0.0104	0.00093	0.000582	0.000028	0.11923	3.75	0.18	1040	599
GRD32-06-46m_30	0.00501	0.00076	0.000563	0.000041	0.16278	3.63	0.27	299	144.2
GRD32-06-46m_31	0.32	0.018	0.04232	0.00097	0.44528	267.2	6	127.4	113.3
GRD41-01-348m_1	0.0093	0.0025	0.000523	0.000086	0.046234	3.37	0.55	137	157
GRD41-01-348m_2	0.0073	0.0017	0.00045	0.000056	0.041177	2.9	0.36	141.4	106
GRD41-01-348m_3	0.0055	0.001	0.000512	0.000049	0.057917	3.3	0.32	233.7	228.5
GRD41-01-348m_4	0.0106	0.0022	0.000523	0.000065	0.14487	3.37	0.42	145	85.7
GRD41-01-348m_5	0.005	0.0014	0.000575	0.000064	0.28051	3.71	0.41	305	285
GRD41-01-348m_6	0.0065	0.0015	0.000586	0.000055	0.044836	3.78	0.35	173	165
GRD41-01-348m_7	0.0046	0.001	0.000485	0.000048	0.12311	3.13	0.31	256	266
GRD41-01-348m_8	0.0055	0.0015	0.000633	0.000068	0.11953	4.08	0.44	157.4	134.3
GRD41-01-348m_9	0.0049	0.0014	0.00058	0.000057	0.0047434	3.74	0.37	172	179
GRD41-01-348m_10	0.0049	0.0012	0.000538	0.000056	0.10084	3.46	0.36	218	217
GRD41-01-348m_11	0.0078	0.002	0.000596	0.000064	0.15345	3.84	0.41	219.7	247
GRD41-01-348m_12	0.0072	0.0024	0.000561	0.000086	0.20557	3.61	0.55	127.5	87.5
GRD41-01-348m_13	0.0062	0.0014	0.000583	0.00006	0.15156	3.76	0.39	210	187
GRD41-01-348m_14	0.0082	0.003	0.000593	0.000082	0.039689	3.82	0.53	87.4	78.7
GRD41-01-348m_15	0.0111	0.0018	0.000632	0.000046	0.039898	4.07	0.3	216.4	203
GRD41-01-348m_16	0.0062	0.001	0.000571	0.000054	0.0073208	3.68	0.35	251	240
GRD41-01-348m_17	0.0069	0.0014	0.00057	0.000049	0.24278	3.67	0.32	237	210
GRD41-01-348m_18	0.0072	0.0013	0.000572	0.000056	0.25179	3.69	0.36	235.1	271.9
GRD41-01-348m_19	0.0076	0.0017	0.000538	0.000059	0.059148	3.47	0.38	152.4	109.4
GRD41-01-348m_20	0.0046	0.0012	0.000523	0.000059	0.06376	3.37	0.38	210	208
GRD41-01-348m_21	0.0083	0.0039	0.00066	0.00013	0.099699	4.24	0.84	57.9	37.6
GRD41-01-348m_22	0.0066	0.0015	0.000608	0.000062	0.049117	3.92	0.4	148.6	117.6
GRD41-01-348m_23	0.0139	0.0025	0.000663	0.000056	0.31175	4.27	0.36	184.7	146.6
GRD41-01-348m_24	0.023	0.0038	0.000724	0.000067	0.48	4.67	0.43	176.2	143.5
GRD41-01-348m_25	0.0044	0.0012	0.00053	0.000063	0.064953	3.42	0.4	207	211
GRD41-01-348m_26	0.00552	0.00088	0.000548	0.000043	0.11574	3.53	0.28	368	211

	207Pb/235U	207Pb/235U error	206Pb/238U	206Pb/238U Error	Error Correlation 206/238 vs. 207/235	Final Age (Ma)	Error (Ma)	Approx U (ppm)	Approx Th (ppm)
GRD41-01-348m_27	0.0047	0.0014	0.000522	0.000049	0.16895	3.37	0.32	198	142
GRD41-01-348m_28	0.0048	0.0015	0.000546	0.000056	0.14739	3.52	0.36	221	272
GRD41-01-348m_29	0.005	0.0015	0.000501	0.000054	0.32224	3.23	0.35	176	149.1
GRD41-01-348m_30	4.966	0.081	0.3232	0.0041	0.53991	1805	20	305	122.3
GRD42-06-523m_1	0.0048	0.0012	0.000524	0.000056	-0.099596	3.37	0.36	154	83
GRD42-06-523m_2	0.00461	0.00071	0.000492	0.000044	-0.16406	3.17	0.28	221	103.9
GRD42-06-523m_3	0.0053	0.0014	0.000538	0.000062	-0.027986	3.47	0.4	138	64.8
GRD42-06-523m_4	0.0072	0.0014	0.000551	0.000079	0.12913	3.55	0.51	207	150
GRD42-06-523m_5	0.0053	0.001	0.000512	0.000057	0.11978	3.3	0.37	178	123.4
GRD42-06-523m_6	0.00474	0.00086	0.000541	0.000044	0.025562	3.49	0.29	304	282
GRD42-06-523m_7	0.0045	0.0011	0.000509	0.000058	-0.17341	3.28	0.37	125.9	66.8
GRD42-06-523m_8	0.00466	0.00078	0.000498	0.000038	-0.045031	3.21	0.24	256	130.9
GRD42-06-523m_9	0.00444	0.00088	0.000507	0.000047	-0.10818	3.27	0.31	200	115
GRD42-06-523m_10	0.0097	0.0013	0.000568	0.000045	0.22351	3.66	0.29	245	124.9
GRD42-06-523m_11	0.00524	0.00096	0.000545	0.000042	0.19662	3.51	0.27	218	93.6
GRD42-06-523m_12	0.00452	0.0006	0.000517	0.000037	0.10528	3.33	0.24	340	218
GRD42-06-523m_13	0.00551	0.00099	0.000585	0.00005	0.11761	3.77	0.32	205	134
GRD42-06-523m_14	0.00484	0.00069	0.000581	0.000044	0.05566	3.75	0.28	329	190
GRD42-06-523m_15	0.00556	0.00074	0.00056	0.000035	0.046468	3.61	0.23	494	416
GRD42-06-523m_16	0.0064	0.0015	0.000543	0.000071	0.044607	3.5	0.46	99.5	51
GRD42-06-523m_17	0.00458	0.00095	0.00055	0.000058	0.0025236	3.54	0.37	151.1	76.1
GRD42-06-523m_18	0.00508	0.0007	0.000567	0.000036	-0.22196	3.65	0.23	299	209
GRD42-06-523m_19	0.0064	0.0017	0.000542	0.000063	0.062633	3.49	0.41	213	94
GRD42-06-523m_20	0.0151	0.0036	0.000668	0.000083	0.47277	4.3	0.53	318	286
GRD42-06-523m_21	0.005	0.001	0.000513	0.000055	-0.22073	3.3	0.35	141.2	97.1
GRD42-06-523m_22	0.0071	0.0012	0.000527	0.000056	-0.079606	3.4	0.36	165.9	112.3
GRD42-06-523m_23	0.0169	0.0055	0.00069	0.00014	0.36535	4.44	0.89	171	102
GRD42-06-523m_24	0.0126	0.0026	0.000703	0.000072	0.59462	4.53	0.46	204	167
GRD42-06-523m_25	0.0047	0.001	0.000628	0.000061	-0.059228	4.05	0.4	182	93.4
GRD42-06-523m_26	0.00434	0.00066	0.000578	0.000044	-0.028998	3.73	0.28	359	325
GRD42-06-523m_27	0.0054	0.0012	0.000525	0.000057	-0.029162	3.38	0.37	158	80.1
GRD42-06-523m_28	0.0044	0.0017	0.000498	0.000073	0.14594	3.21	0.47	207	136
GRD42-06-523m_29	0.004	0.0011	0.000509	0.000058	-0.10182	3.28	0.38	208	108.6
GRD42-06-523m_30	0.0056	0.0011	0.000599	0.00006	0.045865	3.86	0.39	185	108
GRD42-06-523m_31	0.0048	0.0013	0.000598	0.000051	0.014745	3.85	0.33	206	135
GRD42-06-523m_32	0.0076	0.0019	0.000602	0.000092	-0.10556	3.88	0.59	219	113.8
GRD42-06-523m_33	0.0294	0.0044	0.000752	0.000069	0.29057	4.85	0.45	213.5	168
KL40-06-416m_1	0.007	0.0031	0.00057	0.00018	0.034733	3.7	1.1	119.2	111.8
KL40-06-416m_2	0.0061	0.0018	0.000567	0.000079	0.12348	3.65	0.51	138	141.6
KL40-06-416m_3	0.007	0.0017	0.000561	0.000072	0.028373	3.61	0.47	137.4	80.6
KL40-06-416m_4	0.006	0.0015	0.000574	0.000067	0.28983	3.7	0.43	168	160
KL40-06-416m_5	0.0055	0.0013	0.000545	0.00007	0.070177	3.51	0.45	193.1	135.3
KL40-06-416m_6	0.0053	0.0017	0.00065	0.0001	0.19017	4.2	0.67	226	218
KL40-06-416m_7	0.0054	0.0013	0.000575	0.000059	0.15699	3.7	0.38	250	260
KL40-06-416m_8	0.008	0.0019	0.000566	0.000097	0.07576	3.65	0.63	187.9	170.9
KL40-06-416m_9	0.0154	0.0025	0.000627	0.000085	0.080931	4.04	0.55	277	208
KL40-06-416m_10	0.005	0.0014	0.0005	0.000059	0.074121	3.22	0.38	372	246
KL40-06-416m_11	0.00528	0.00089	0.00054	0.000043	0.015796	3.48	0.28	399	324
KL40-06-416m_12	0.0059	0.0015	0.000552	0.000062	0.20789	3.56	0.4	224	225
KL40-06-416m_13	0.0065	0.0016	0.000522	0.000084	0.10997	3.36	0.54	160.7	128.2
KL40-06-416m_14	0.0258	0.0047	0.000661	0.000083	0.19837	4.26	0.53	163	184
KL40-06-416m_15	0.0083	0.0021	0.000457	0.000085	0.14493	2.94	0.55	180.2	197
KL40-06-416m_16	0.0067	0.0018	0.000419	0.000066	0.027032	2.7	0.43	146.3	135.2
KL40-06-416m_17	0.0068	0.0022	0.000522	0.000089	0.016761	3.36	0.57	108	93
KL40-06-416m_18	0.0081	0.0021	0.000516	0.000087	0.13335	3.33	0.56	146.7	141.7
KL40-06-416m_19	0.0082	0.0025	0.00053	0.0001	0.21229	3.44	0.64	134.8	126.3
KL40-06-416m_20	0.018	0.003	0.00062	0.000079	0.49967	4	0.51	491	670
KL40-06-416m_21	0.0091	0.0023	0.000567	0.000096	0.2986	3.65	0.62	130	154.8
KL40-06-416m_22	0.0044	0.0012	0.000438	0.000052	0.082496	2.82	0.34	254	261
KL40-06-416m_23	0.0113	0.0047	0.00053	0.00015	0.22304	3.44	0.94	131	129
KL40-06-416m_24	0.0248	0.0034	0.000631	0.000088	0.050957	4.07	0.57	170.1	155.6
KL40-06-416m_25	0.0071	0.0016	0.00054	0.000065	0.14684	3.48	0.42	240.7	186.2
KL40-06-416m_26	0.007	0.0014	0.000514	0.00007	0.31697	3.31	0.45	386.6	369
KL40-06-416m_27	0.008	0.0024	0.00065	0.00011	0.19267	4.17	0.69	159	150
KL40-06-416m_28	6.87	0.28	0.369	0.014	0.77345	2026	63	80.3	40.9
KL40-06-416m_29	0.3043	0.0098	0.04264	0.0008	0.31989	269.1	4.9	158	174
KL40-06-516m_1	0.0069	0.0016	0.000594	0.000065	0.0080206	3.83	0.42	227	245.5
KL40-06-516m_2	0.0079	0.0028	0.00063	0.00014	0.023912	4.05	0.88	172	142
KL40-06-516m_3	0.0059	0.0024	0.000553	0.000087	0.064388	3.56	0.56	140	151.1
KL40-06-516m_4	0.0062	0.0022	0.0006	0.0001	0.04165	3.86	0.65	163	133
KL40-06-516m_5	0.0093	0.0029	0.00049	0.00011	0.054967	3.18	0.69	369	349

	207Pb/235U	207Pb/235U error	206Pb/238U	206Pb/238U Error	Error Correlation 206/238 vs. 207/235	Final Age (Ma)	Error (Ma)	Approx U (ppm)	Approx Th (ppm)
KL40-06-516m_6	0.018	0.0038	0.000584	0.000081	0.25682	3.77	0.52	152	93.8
KL40-06-516m_7	0.0092	0.0028	0.000577	0.000074	0.062118	3.72	0.48	247	271
KL40-06-516m_8	0.0187	0.0033	0.00062	0.00011	0.10989	4.01	0.72	153	114.5
KL40-06-516m_9	0.0208	0.0041	0.000594	0.000078	0.15499	3.83	0.5	169.8	157.8
KL40-06-516m_10	0.0073	0.0017	0.000555	0.000078	0.07506	3.57	0.5	300	133
KL40-06-516m_11	0.0084	0.0017	0.000573	0.000098	0.074342	3.69	0.63	257.5	264.7
KL40-06-516m_12	0.0325	0.0041	0.00071	0.00013	0.18813	4.6	0.81	153.9	116.5
KL40-06-516m_13	0.0071	0.0018	0.000545	0.00008	0.0276	3.51	0.51	215.7	249
KL40-06-516m_14	0.0233	0.0048	0.00063	0.00012	0.12423	4.08	0.77	120.1	119
KL40-06-516m_15	0.0083	0.0029	0.000542	0.000096	0.27803	3.49	0.62	182	200
KL40-06-516m_16	0.0076	0.0026	0.00054	0.00013	0.19193	3.5	0.81	380	590
KL40-06-516m_17	0.0259	0.0042	0.00072	0.00011	0.008298	4.63	0.68	195	208
KL40-06-516m_18	0.0145	0.0021	0.000574	0.000089	0.27836	3.7	0.57	249	217
KL40-06-516m_19	0.0177	0.0076	0.00061	0.00017	0.38192	3.9	1.1	175	169
KL40-06-516m_20	0.0118	0.0029	0.000539	0.000085	0.1159	3.47	0.55	314	341
KL40-06-516m_21	0.0086	0.0019	0.000611	0.000083	0.23878	3.93	0.54	312	182
KL40-06-516m_22	0.0082	0.0021	0.00049	0.000071	0.06766	3.16	0.46	246	207
KL40-06-516m_23	0.0097	0.0028	0.000486	0.000096	0.014143	3.13	0.62	196	181
KL40-06-516m_24	0.008	0.0022	0.000504	0.000074	0.1606	3.25	0.47	157.4	181
KL40-06-516m_25	0.223	0.03	0.0335	0.0021	0.11232	212	13	55.8	60
KL40-06-762m_1	0.0099	0.0038	0.00059	0.00013	0.097908	3.78	0.83	88.6	48.5
KL40-06-762m_2	0.0107	0.0036	0.00062	0.00012	0.023195	3.99	0.8	84.2	50.7
KL40-06-762m_3	0.0063	0.0029	0.00052	0.00012	0.24559	3.32	0.76	94.6	57.5
KL40-06-762m_4	0.00553	0.00095	0.000618	0.000057	0.060974	3.98	0.37	1015	1063
KL40-06-762m_5	0.0075	0.0014	0.000585	0.000084	0.0501	3.77	0.54	473	428
KL40-06-762m_6	0.0074	0.0017	0.000523	0.00007	0.016921	3.37	0.45	290	278
KL40-06-762m_7	0.057	0.005	0.00092	0.00011	0.16537	5.95	0.68	181.6	150.7
KL40-06-762m_8	0.0113	0.0033	0.00066	0.00013	0.11262	4.26	0.83	161.4	149.3
KL40-06-762m_9	0.0096	0.0026	0.000492	0.00009	0.046909	3.17	0.58	146.7	117.8
KL40-06-762m_10	0.0097	0.0026	0.00057	0.00011	0.16341	3.69	0.71	154.6	152
KL40-06-762m_11	0.0078	0.0018	0.000492	0.000084	0.062279	3.17	0.54	334	470
KL40-06-762m_12	0.0063	0.001	0.000556	0.000066	0.011511	3.58	0.42	365.3	204.5
KL40-06-762m_13	0.0216	0.0036	0.000681	0.000097	0.069656	4.39	0.63	152.8	115.4
KL40-06-762m_14	0.0227	0.0035	0.00066	0.00012	0.18885	4.26	0.8	111.8	75
KL40-06-762m_15	0.023	0.0043	0.00068	0.00014	0.062115	4.4	0.92	325	550
KL40-06-762m_16	0.0532	0.0091	0.00101	0.00017	0.015867	6.5	1.1	75.1	47.6
KL40-06-762m_17	0.0078	0.002	0.000486	0.000079	0.09889	3.13	0.51	232	200
KL40-06-762m_18	0.009	0.0029	0.00054	0.0001	0.0072718	3.47	0.64	189.5	171
KL40-06-762m_19	0.0092	0.003	0.000625	0.000096	0.12099	4.03	0.62	153.3	123.2
KL40-06-762m_20	0.006	0.0012	0.000499	0.000062	0.36756	3.21	0.4	579	378
KL40-06-762m_21	0.0194	0.0027	0.000621	0.000083	0.16407	4	0.54	177.9	137.8
KL40-06-762m_22	0.0161	0.0033	0.000594	0.000098	0.22601	3.83	0.63	170	209
KL40-06-762m_23	0.227	0.057	0.00241	0.00049	0.94939	15.5	3.1	339	283
KL40-06-762m_24	4.899	0.046	0.3239	0.0037	0.61638	1808	18	568	58.4
KL40-06-762m_25	0.361	0.016	0.0493	0.0012	0.071484	310.2	7.2	127.9	123.6
KL40-06-762m_26	0.383	0.014	0.049	0.0011	0.086753	308	6.5	101.8	74.6
GBC3-01-01-1033m_1	0.00324	0.00038	0.000441	0.000022	0.096083	2.84	0.14	898	1610
GBC3-01-01-1033m_2	0.00326	0.00047	0.000396	0.000029	0.16693	2.55	0.19	551	828
GBC3-01-01-1033m_3	0.00321	0.00048	0.000394	0.000028	0.0077274	2.54	0.18	736	1025
GBC3-01-01-1033m_4	0.0064	0.0014	0.000473	0.000048	-0.1377	3.05	0.31	574	996
GBC3-01-01-1033m_5	0.00338	0.00034	0.000445	0.000024	-0.0187	2.87	0.15	751	1242
GBC3-01-01-1033m_6	0.00354	0.00039	0.000446	0.000023	0.068196	2.87	0.15	969	1440
GBC3-01-01-1033m_7	0.0105	0.0028	0.000536	0.000046	0.11878	3.45	0.3	593	1070
GBC3-01-01-1033m_8	0.00415	0.00076	0.000472	0.000027	0.18561	3.04	0.17	570	1020
GBC3-01-01-1033m_9	0.00244	0.00086	0.000463	0.000056	-0.16613	2.99	0.36	460.5	548
GBC3-01-01-1033m_10	0.003	0.00029	0.000408	0.000019	0.034223	2.63	0.12	1330	1150
GBC3-01-01-1033m_11	0.00752	0.00087	0.000447	0.000035	-0.11886	2.88	0.22	575	738
GBC3-01-01-1033m_12	0.00392	0.00061	0.000386	0.000028	0.0038256	2.49	0.18	474	660
GBC3-01-01-1033m_13	0.00381	0.00036	0.000451	0.000024	-0.014037	2.91	0.16	1046	1891
GBC3-01-01-1033m_14	0.00282	0.0004	0.000451	0.000029	-0.082366	2.9	0.19	571	531
GBC3-01-01-1033m_15	0.00297	0.00028	0.000431	0.000021	0.003136	2.78	0.14	1458	3570
GBC3-01-01-1033m_16	0.00398	0.00044	0.000438	0.000024	-0.1386	2.82	0.15	865	1770
GBC3-01-01-1033m_17	0.00387	0.00047	0.000398	0.000029	-0.18791	2.56	0.19	967	1947
GBC3-01-01-1033m_18	0.0058	0.0024	0.00051	0.000092	-0.1357	3.29	0.59	77.6	46.1
GBC3-01-01-1033m_19	0.00388	0.00042	0.000436	0.000025	-0.14275	2.81	0.16	802	455
GBC3-01-01-1033m_20	0.0037	0.00042	0.0004	0.000022	0.079143	2.58	0.14	943	1668
GBC3-01-01-1033m_21	0.0036	0.00041	0.000403	0.000022	-0.072331	2.6	0.14	834	1472
GBC3-01-01-1033m_22	0.00344	0.00037	0.000437	0.000019	-0.082741	2.81	0.12	1005	1656
GBC3-01-01-1033m_23	0.0058	0.0012	0.000468	0.000045	-0.042172	3.01	0.29	447	744

	207Pb/235U	207Pb/235U error	206Pb/238U	206Pb/238U Error	Error Correlation 206/238 vs. 207/235	Final Age (Ma)	Error (Ma)	Approx U (ppm)	Approx Th (ppm)
GBC3-01-01-1033m_24	0.0061	0.0014	0.000472	0.00006	0.32308	3.04	0.39	957	660
GBC3-01-01-1033m_25	0.00316	0.00031	0.000437	0.00002	0.30611	2.82	0.13	1633	4408
GBC3-01-01-1033m_26	0.00294	0.00024	0.000415	0.000016	0.047551	2.68	0.1	1970	4970
GBC3-01-01-1033m_27	0.0097	0.0014	0.000413	0.000037	-0.09485	2.66	0.24	524	1500
TE07-29-5m_1	0.0005	0.0029	0.000376	0.000068	0.077022	2.42	0.44	76.9	97
TE07-29-5m_2	0.0021	0.0012	0.000398	0.000046	0.032636	2.56	0.3	228	379
TE07-29-5m_3	0.0022	0.0019	0.00041	0.000071	0.14171	2.64	0.46	118.4	146.4
TE07-29-5m_4	0.00321	0.00066	0.000461	0.000038	0.20338	2.97	0.24	357	104.4
TE07-29-5m_5	0.0036	0.0015	0.000383	0.000049	0.053615	2.47	0.31	194	238
TE07-29-5m_6	0.0043	0.0023	0.00037	0.000068	0.037232	2.39	0.44	116.8	123.7
TE07-29-5m_7	0.00375	0.00056	0.000488	0.000028	0.10114	3.14	0.18	614	216
TE07-29-5m_8	0.0038	0.0017	0.000375	0.00006	0.30224	2.42	0.39	108.8	139.5
TE07-29-5m_9	0.0041	0.0015	0.000447	0.000046	0.18929	2.88	0.3	160	225
TE07-29-5m_10	0.00264	0.00067	0.000385	0.000038	0.14073	2.51	0.25	327	418.2
TE07-29-5m_11	0.0028	0.0018	0.000379	0.000056	0.13487	2.44	0.36	120.5	180.8
TE07-29-5m_12	0.0036	0.0013	0.000467	0.000047	0.042741	3.01	0.3	177	273
TE07-29-5m_13	0.005	0.0027	0.000505	0.000077	0.26074	3.26	0.49	83.5	47.8
TE07-29-5m_14	0.004	0.0011	0.000445	0.000064	0.11785	2.87	0.42	168	167
TE07-29-5m_15	0.0041	0.0012	0.000427	0.000043	0.049281	2.75	0.28	182	194
TE07-29-5m_16	0.0066	0.0023	0.000446	0.000059	0.33864	2.87	0.38	163	178
TE07-29-5m_17	0.0042	0.0015	0.000457	0.000057	0.013465	2.94	0.37	155.4	227
TE07-29-5m_18	0.0035	0.0011	0.000423	0.000073	0.086157	2.72	0.47	206	319
TE07-29-5m_19	0.0041	0.0017	0.000412	0.000061	0.19183	2.66	0.4	153	140
TE07-29-5m_20	0.0036	0.0025	0.000421	0.000088	0.032591	2.71	0.57	77.3	90
TE07-29-5m_21	0.0041	0.0018	0.000411	0.000068	0.18133	2.65	0.44	102.1	143.8
TE07-29-5m_22	0.00331	0.00063	0.000433	0.000027	0.15267	2.79	0.17	387	628
TE07-29-5m_23	0.0033	0.0011	0.000375	0.000037	0.093478	2.42	0.24	219	278
TE07-29-5m_24	0.0271	0.0073	0.00061	0.00015	0.1299	3.92	0.99	47.2	35.7
TE07-29-5m_25	0.0026	0.003	0.00046	0.000098	0.17092	2.96	0.63	59.4	49.1
TE07-29-5m_26	0.4079	0.0087	0.0547	0.0011	0.75244	343.6	6.7	456	279
TE07-29-5m_27	0.3386	0.0095	0.04732	0.00092	0.34353	298	5.7	188.6	125.1
TE07-29-5m_28	0.273	0.012	0.03847	0.00079	0.034087	243.3	4.9	84.3	85
TE07-29-5m_29	0.3139	0.0076	0.04346	0.00078	0.62326	274.2	4.8	407	212.3
TE07-29-5m_30	0.3155	0.0058	0.04383	0.00076	0.41406	276.5	4.7	220.3	243
SEID-MLZ-05-297m_1	0.0047	0.0012	0.00045	0.000066	-0.15077	2.9	0.43	132.7	172.3
SEID-MLZ-05-297m_2	0.0093	0.0069	0.000416	0.000078	-0.040541	2.68	0.5	64.2	54.4
SEID-MLZ-05-297m_3	0.0052	0.0019	0.000395	0.000067	0.11597	2.55	0.43	82.8	81.7
SEID-MLZ-05-297m_4	0.0036	0.0013	0.000417	0.000056	-0.065659	2.69	0.36	99.9	137.3
SEID-MLZ-05-297m_5	0.0025	0.0015	0.00042	0.000062	-0.10568	2.71	0.4	79	89.4
SEID-MLZ-05-297m_6	0.0048	0.0014	0.000435	0.000061	-0.10707	2.8	0.4	89.3	111.7
SEID-MLZ-05-297m_7	0.0101	0.002	0.000437	0.000069	-0.13835	2.81	0.45	87.2	74.9
SEID-MLZ-05-297m_8	0.00385	0.00099	0.00047	0.00004	0.14988	3.03	0.26	189	237
SEID-MLZ-05-297m_9	0.0116	0.0031	0.000586	0.00005	0.51427	3.77	0.32	228	254
SEID-MLZ-05-297m_10	0.00305	0.00041	0.000434	0.000027	0.0056434	2.8	0.17	591	987
SEID-MLZ-05-297m_11	0.0028	0.00025	0.000374	0.000016	-0.20971	2.41	0.11	1110	2950
SEID-MLZ-05-297m_12	0.00403	0.00095	0.000402	0.000045	-0.19563	2.59	0.29	167	268.6
SEID-MLZ-05-297m_13	0.00216	0.00015	0.000324	0.000011	-0.026204	2.089	0.068	3540	368
SEID-MLZ-05-297m_14	0.00344	0.00098	0.000475	0.000047	0.062549	3.06	0.3	191	77.4
SEID-MLZ-05-297m_15	0.00281	0.0006	0.000411	0.000036	0.015004	2.65	0.23	239.9	305.8
SEID-MLZ-05-297m_16	0.0055	0.002	0.000406	0.000063	-0.13116	2.62	0.41	92.5	91
SEID-MLZ-05-297m_17	0.0027	0.0012	0.000521	0.000049	-0.051983	3.36	0.31	104.8	112.1
SEID-MLZ-05-297m_18	0.00383	0.00055	0.000474	0.000039	-0.057968	3.05	0.25	416	221
SEID-MLZ-05-297m_19	0.00325	0.00064	0.000408	0.000034	0.050834	2.63	0.22	226	240
SEID-MLZ-05-297m_20	0.004	0.0014	0.000424	0.000061	0.1762	2.73	0.39	107.1	76.5
SEID-MLZ-05-297m_21	0.0042	0.0011	0.000408	0.000045	0.12153	2.63	0.29	137.5	218.2
SEID-MLZ-05-297m_22	0.0041	0.0018	0.00044	0.000069	-0.19184	2.83	0.45	69.1	65.5
SEID-MLZ-05-297m_23	0.0037	0.0014	0.000451	0.00008	0.14264	2.91	0.51	240	190
SEID-MLZ-05-297m_24	0.00512	0.00077	0.000525	0.000034	-0.033825	3.38	0.22	438	199.4
SEID-MLZ-05-297m_25	0.00339	0.00032	0.000423	0.000021	-0.034834	2.73	0.14	1150	1480
SEID-MLZ-05-297m_26	0.0051	0.002	0.000508	0.000063	0.09451	3.27	0.41	100.6	125.1
SEID-MLZ-05-297m_27	0.003	0.0018	0.0005	0.000069	0.21565	3.22	0.45	107	107
SEID-MLZ-05-297m_28	0.0033	0.001	0.000432	0.000042	-0.012371	2.78	0.27	134.2	154.5
SEID-MLZ-05-297m_29	0.0044	0.0011	0.000437	0.000042	-0.13792	2.82	0.27	137.5	163.6
SEID-MLZ-05-297m_30	0.0037	0.00055	0.00043	0.000033	0.032084	2.77	0.21	364	484
SEID-MLZ-05-297m_31	0.2	0.01	0.02878	0.00068	0.0052073	182.9	4.2	219.5	162.5
TEW11-10-690m_1	0.0044	0.00069	0.000436	0.000033	0.046586	2.81	0.21	602	1020
TEW11-10-690m_2	0.0076	0.0011	0.00047	0.000036	0.17919	3.03	0.23	276.1	70
TEW11-10-690m_3	0.00331	0.00069	0.000441	0.000039	0.05334	2.84	0.25	255.8	269
TEW11-10-690m_4	0.00441	0.00063	0.000422	0.000035	0.11585	2.72	0.23	253.2	215.2

	207Pb/235U	207Pb/235U error	206Pb/238U	206Pb/238U Error	Error Correlation 206/238 vs. 207/235	Final Age (Ma)	Error (Ma)	Approx U (ppm)	Approx Th (ppm)
TEW11-10-690m_5	0.00511	0.0009	0.000467	0.000041	0.013649	3.01	0.27	239.4	232.8
TEW11-10-690m_6	0.00306	0.00047	0.000426	0.000033	0.032151	2.74	0.21	329.2	446.3
TEW11-10-690m_7	0.0068	0.0015	0.000458	0.000063	0.043474	2.95	0.4	97.6	127.4
TEW11-10-690m_8	0.00327	0.00063	0.000437	0.000035	0.0084413	2.81	0.22	244	187
TEW11-10-690m_9	0.0105	0.0031	0.000561	0.000049	0.21819	3.62	0.32	568	1310
TEW11-10-690m_10	0.00403	0.00071	0.000461	0.000035	0.1487	2.97	0.23	223.1	209.3
TEW11-10-690m_11	0.00433	0.00059	0.000426	0.000032	0.087409	2.75	0.2	617	762
TEW11-10-690m_12	0.00329	0.00037	0.000449	0.000029	0.065424	2.89	0.19	728	1451
TEW11-10-690m_13	0.00363	0.00058	0.000412	0.000035	0.091065	2.66	0.22	344.5	444.7
TEW11-10-690m_14	0.00289	0.00059	0.000448	0.000046	0.058916	2.89	0.29	215.3	177.9
TEW11-10-690m_15	0.00449	0.00072	0.00044	0.000038	0.033329	2.84	0.25	203.5	180
TEW11-10-690m_16	0.00394	0.00049	0.00045	0.000027	0.24544	2.9	0.17	403	520
TEW11-10-690m_17	0.00435	0.00068	0.00044	0.000043	0.22055	2.84	0.28	199.6	155.7
TEW11-10-690m_18	0.00391	0.00047	0.000452	0.000025	0.21402	2.91	0.16	632	298
TEW11-10-690m_19	0.00319	0.00036	0.000451	0.000026	0.023825	2.91	0.17	498.1	792
TEW11-10-690m_20	0.00865	0.00096	0.000496	0.000033	0.044648	3.19	0.21	405	409
TEW11-10-690m_21	0.00409	0.00066	0.000452	0.000034	0.0085866	2.91	0.22	279	264
TEW11-10-690m_22	0.0093	0.0016	0.000491	0.00005	0.21272	3.16	0.32	201.2	253
TEW11-10-690m_23	0.004	0.00042	0.000442	0.000025	0.052796	2.85	0.16	593.3	1114
TEW11-10-690m_24	0.00398	0.00055	0.000445	0.000037	0.11984	2.87	0.24	274.4	334
TEW11-10-690m_25	0.00308	0.00033	0.000443	0.000028	0.13169	2.85	0.18	922	1465
TEW11-10-690m_26	0.00403	0.00052	0.000464	0.000028	0.093912	2.99	0.18	458	743
TEW11-10-690m_27	0.00339	0.00044	0.000433	0.000027	0.052325	2.79	0.17	353	481
TEW11-10-690m_28	0.00444	0.00056	0.000462	0.000032	0.031425	2.98	0.21	447	456
TEW11-10-690m_29	0.00385	0.00057	0.000431	0.000031	0.13598	2.78	0.2	320	401
1001_1	0.00282	0.00069	0.0004	0.000045	0.0429	2.58	0.29	198	187
1001_2	0.00261	0.00058	0.000363	0.00004	0.10842	2.34	0.26	137.1	170
1001_3	0.0052	0.0016	0.00039	0.000042	0.064705	2.52	0.27	108.8	126.2
1001_4	0.0071	0.0016	0.000466	0.000022	0.028357	3.01	0.14	466	816
1001_5	0.00412	0.00034	0.000483	0.000021	0.17385	3.11	0.13	617	1267
1001_6	0.00405	0.00068	0.000406	0.000031	0.25359	2.62	0.2	206	147.2
1001_7	0.00389	0.00039	0.000466	0.000024	0.12549	3	0.15	463	866
1001_8	0.00347	0.00041	0.000449	0.00003	0.0055746	2.9	0.19	429	731
1001_9	0.00351	0.00061	0.000371	0.000028	0.033506	2.39	0.18	257	450
1001_10	0.009	0.001	0.000426	0.000041	0.14984	2.74	0.26	286	455
1001_11	0.00301	0.00032	0.00043	0.000023	0.10245	2.77	0.15	433	834
1001_12	0.00291	0.00035	0.000447	0.000023	0.053998	2.88	0.15	462	817
1001_13	0.005	0.0017	0.000373	0.000076	0.10563	2.4	0.49	54.1	57.6
1001_14	0.00355	0.00036	0.000448	0.000026	0.11119	2.89	0.16	505	747
1001_15	0.0047	0.0013	0.000335	0.00005	0.017454	2.16	0.32	69.1	82.9
1001_16	0.00317	0.00045	0.000434	0.000024	0.0067609	2.8	0.15	351	594
1001_17	0.00334	0.00039	0.000448	0.000025	0.12402	2.89	0.16	531	796
1001_18	0.0055	0.0012	0.000471	0.000026	0.062201	3.04	0.16	413	711
1001_19	0.00364	0.00044	0.000442	0.000026	0.18587	2.85	0.17	430.8	842
1001_20	0.00353	0.00042	0.000459	0.000031	0.017578	2.96	0.2	357	645
1001_21	0.00371	0.00055	0.000434	0.000029	0.18217	2.79	0.19	375	689
1001_22	0.0032	0.00046	0.000463	0.00003	0.069968	2.98	0.19	392	706
1001_23	0.0034	0.0011	0.000418	0.000058	0.2367	2.7	0.37	248	249
1001_24	0.00364	0.00048	0.000439	0.00003	0.0014668	2.83	0.19	382	678
1001_25	0.00389	0.00036	0.000495	0.000021	0.13158	3.19	0.14	634	1078
1001_26	0.0109	0.0017	0.000473	0.000034	0.6994	3.05	0.22	408	893
1001_27	0.00379	0.00095	0.000345	0.000038	0.20828	2.23	0.24	156.2	226.8
1001_28	0.0058	0.0015	0.000335	0.000058	0.040213	2.16	0.37	69.9	80.2
1001_29	0.299	0.025	0.0406	0.0023	0.52833	257	14	122.3	131.7
1001_30	0.0429	0.0057	0.000772	0.000054	0.59796	4.97	0.35	429	748
1004_1	0.0083	0.0023	0.000536	0.000063	0.3114	3.46	0.41	177	148.3
1004_2	0.00367	0.0006	0.000405	0.000041	0.05366	2.61	0.26	182.8	275.5
1004_3	0.00395	0.00043	0.000449	0.000025	0.082092	2.9	0.16	461	454
1004_4	0.0029	0.0015	0.000385	0.000045	0.13059	2.48	0.29	121	129.3
1004_5	0.00296	0.00088	0.000455	0.000052	0.024511	2.93	0.34	90.5	121
1004_6	0.0047	0.0012	0.000464	0.000049	0.095411	2.99	0.31	118	153
1004_7	0.00384	0.00073	0.000425	0.000045	0.0059208	2.74	0.29	129	116
1004_8	0.00516	0.00088	0.000475	0.000037	0.48254	3.06	0.24	565	490
1004_9	0.0056	0.0011	0.000448	0.000059	0.054054	2.89	0.38	342	332
1004_10	0.0041	0.0012	0.000434	0.000051	0.010252	2.8	0.33	90	122
1004_11	0.0055	0.0014	0.000423	0.000045	0.079399	2.72	0.29	220.1	285
1004_12	0.00428	0.00086	0.000442	0.000046	0.15684	2.85	0.3	99	119
1004_13	0.00327	0.00047	0.000431	0.00003	0.18745	2.78	0.19	335	347
1004_14	0.00469	0.00067	0.000464	0.00003	0.020728	2.99	0.19	265	95.4
1004_15	0.0045	0.0018	0.000404	0.000065	0.12661	2.6	0.42	47.4	41.8
1004_16	0.00332	0.00053	0.000434	0.000032	0.01028	2.79	0.2	209	155.6

	207Pb/235U	207Pb/235U error	206Pb/238U	206Pb/238U Error	Error Correlation 206/238 vs. 207/235	Final Age (Ma)	Error (Ma)	Approx U (ppm)	Approx Th (ppm)
1004_17	0.00377	0.00066	0.000429	0.000026	0.092654	2.77	0.17	289	358
1004_18	0.0042	0.001	0.000413	0.000045	0.077657	2.66	0.29	87.6	98.1
1004_19	0.00348	0.00046	0.000424	0.00003	0.090148	2.73	0.19	267	271.4
1004_20	0.0037	0.0012	0.000478	0.000055	0.019212	3.08	0.35	63	65.7
1004_21	0.00543	0.00076	0.000522	0.000048	0.11522	3.37	0.31	338	206
1004_22	0.00311	0.00054	0.000407	0.000036	0.11442	2.62	0.23	329	608
1004_23	0.00348	0.00028	0.000467	0.000021	0.059861	3.01	0.14	452	525
1004_24	0.0072	0.0019	0.000445	0.000053	0.11376	2.87	0.34	472	138.7
1002_1	0.2737	0.0064	0.03783	0.00088	0.6761	239.3	5.5	303.2	218.7
1002_2	0.00288	0.0009	0.000433	0.000046	0.026918	2.79	0.29	111.1	98.2
1002_3	0.0041	0.0011	0.000394	0.000051	0.0051614	2.54	0.33	104.6	154.8
1002_4	0.0035	0.0014	0.000435	0.00006	0.051728	2.8	0.39	82.8	123
1002_5	0.0039	0.0014	0.000448	0.00006	0.013828	2.88	0.39	77.3	116.1
1002_6	0.00303	0.00098	0.000455	0.00004	0.030316	2.93	0.25	197	169
1002_7	0.00324	0.00099	0.000456	0.00004	0.077691	2.94	0.26	324	106
1002_8	0.003	0.0012	0.000538	0.000076	0.025347	3.47	0.49	123	152
1002_9	0.0039	0.00056	0.000432	0.000036	0.011312	2.78	0.23	415	611
1002_10	0.0029	0.0016	0.000476	0.000084	0.13224	3.07	0.54	63.8	77.6
1002_11	0.0048	0.001	0.000521	0.000059	0.012896	3.36	0.38	201.7	155.6
1002_12	0.0046	0.0013	0.000442	0.000059	0.052676	2.85	0.38	101.9	147
1002_13	0.0027	0.0018	0.000401	0.000083	0.067533	2.58	0.54	103	132
1002_14	0.00407	0.00081	0.000412	0.000038	0.19108	2.65	0.24	230.5	290
1002_15	0.0111	0.002	0.000509	0.000051	0.14436	3.28	0.33	126.8	216
1002_16	0.0054	0.0013	0.000507	0.000075	0.04925	3.27	0.48	139.4	166
1002_17	0.0039	0.0012	0.00043	0.000051	0.13193	2.77	0.33	119.9	126
1002_18	0.00355	0.00063	0.00041	0.000031	0.11872	2.65	0.2	282	413
1002_19	0.00359	0.0008	0.000423	0.000039	0.091379	2.73	0.25	173	178
1002_20	0.0057	0.0017	0.000476	0.000057	0.091815	3.06	0.37	95.9	115.2
1002_21	0.00418	0.0009	0.000448	0.00004	0.056819	2.88	0.25	178	269
1002_22	0.0057	0.0017	0.00048	0.000064	0.092143	3.1	0.41	81.1	119
1002_23	0.00293	0.00039	0.000453	0.000028	0.18465	2.92	0.18	414	750
1002_24	0.0191	0.0029	0.000503	0.000066	0.32569	3.24	0.43	125	126.9
1002_25	0.0039	0.0011	0.000464	0.000058	0.17655	2.99	0.38	113.1	131
1002_26	0.0041	0.0012	0.000428	0.000055	0.087298	2.76	0.35	105.7	127.6
1002_27	0.0041	0.0013	0.000457	0.000065	0.16655	2.95	0.42	188	300
1002_28	0.0048	0.0014	0.000472	0.000076	0.083911	3.04	0.49	95.8	116
1002_29	0.0346	0.0089	0.00076	0.00013	0.54093	4.88	0.81	84	91
1002_30	0.0046	0.0024	0.000422	0.000083	0.06996	2.72	0.53	46.4	48.4
ABE01-01-143m_1	0.01	0.0017	0.000506	0.00007	0.34517	3.26	0.45	284.1	212.3
ABE01-01-143m_2	0.00505	0.00089	0.00044	0.000049	0.15686	2.84	0.32	260.5	391
ABE01-01-143m_3	0.00408	0.00088	0.000464	0.000056	0.16744	2.99	0.36	220.9	282.7
ABE01-01-143m_4	0.00496	0.00095	0.000363	0.000047	0.11995	2.34	0.3	316.6	373
ABE01-01-143m_5	0.0051	0.0011	0.000419	0.000054	0.023179	2.7	0.35	338	399
ABE01-01-143m_6	0.00314	0.00056	0.000391	0.000037	0.28622	2.52	0.24	673	139.8
ABE01-01-143m_7	0.0057	0.0019	0.000497	0.000075	0.48568	3.2	0.48	385.2	549
ABE01-01-143m_8	0.0053	0.0011	0.000447	0.000052	0.078558	2.92	0.34	245	303
ABE01-01-143m_9	0.00562	0.00093	0.000474	0.000059	0.022741	3.06	0.38	427	417
ABE01-01-143m_10	0.0069	0.0012	0.000534	0.000035	0.19123	3.44	0.23	626	700
ABE01-01-143m_11	0.00411	0.00059	0.000453	0.00004	0.16608	2.92	0.26	610	580
ABE01-01-143m_12	0.00427	0.00078	0.000422	0.000047	0.038029	2.72	0.3	306	406
ABE01-01-143m_13	0.0066	0.0016	0.000522	0.000049	0.14202	3.36	0.31	273	218
ABE01-01-143m_14	0.0046	0.0016	0.000586	0.000074	0.0093334	3.77	0.48	166	303.9
ABE01-01-143m_15	0.0062	0.0012	0.000456	0.000039	0.34929	2.94	0.25	530	525
ABE01-01-143m_16	0.0051	0.0016	0.00045	0.000094	0.30546	2.9	0.61	158	222
ABE01-01-143m_17	0.00376	0.00096	0.000458	0.000058	0.017646	2.95	0.38	188	262
ABE01-01-143m_18	0.0055	0.0012	0.000356	0.000052	0.010913	2.3	0.33	239	203.8
ABE01-01-143m_19	0.0211	0.0099	0.000441	0.000067	0.98004	2.84	0.43	584	233.1
ABE01-01-143m_20	0.00459	0.00075	0.000493	0.000039	0.0062384	3.17	0.25	345	402
ABE01-01-143m_21	0.00409	0.00081	0.000498	0.000047	0.01292	3.21	0.3	324	406
ABE01-01-143m_22	0.0058	0.0018	0.000461	0.000087	0.23609	2.97	0.56	157	245
ABE01-01-143m_23	0.0056	0.0019	0.00052	0.0001	0.016387	3.34	0.65	138	216
ABE01-01-143m_24	0.0051	0.0011	0.000356	0.000047	0.075701	2.29	0.3	216.3	332.8
ABE01-01-143m_25	0.0037	0.0011	0.000406	0.000048	0.15084	2.62	0.31	272	506
ABE01-01-143m_26	0.0046	0.0011	0.000465	0.000059	0.07581	3	0.38	277	620
ABE01-01-143m_27	0.00404	0.00077	0.00046	0.000038	0.019618	2.96	0.25	345	529.3
ABE01-01-143m_28	0.00292	0.00046	0.000357	0.000028	0.089503	2.3	0.18	1040	240
ABE01-01-143m_29	0.0042	0.0013	0.000431	0.00008	0.12301	2.78	0.51	127.2	130
ABE01-01-143m_30	0.0044	0.0011	0.000418	0.000048	0.1508	2.69	0.31	241.4	317
D5-15-244m_1	0.00304	0.0007	0.000414	0.000033	0.022485	2.67	0.21	388	757
D5-15-244m_2	0.00381	0.00068	0.000421	0.000034	0.062785	2.71	0.22	441	667
D5-15-244m_3	0.0054	0.0025	0.000519	0.000087	0.010144	3.34	0.56	82.1	82.7

	207Pb/235U	207Pb/235U error	206Pb/238U	206Pb/238U Error	Error Correlation 206/238 vs. 207/235	Final Age (Ma)	Error (Ma)	Approx U (ppm)	Approx Th (ppm)
D5-15-244m_4	0.00384	0.00072	0.0005	0.000036	-0.080903	3.22	0.23	477	807
D5-15-244m_5	0.00397	0.00087	0.000464	0.000051	0.0089069	2.99	0.33	342.9	519.4
D5-15-244m_6	0.00435	0.00065	0.000429	0.000035	0.12144	2.77	0.23	503	807
D5-15-244m_7	0.0039	0.00072	0.000456	0.000041	0.30397	2.94	0.27	393	560
D5-15-244m_8	0.00318	0.00065	0.000424	0.000039	0.11821	2.73	0.25	369	659
D5-15-244m_9	0.00346	0.00047	0.000472	0.000033	0.081892	3.04	0.22	586	949
D5-15-244m_10	0.0064	0.0017	0.000409	0.000044	-0.036818	2.64	0.28	327.1	574
D5-15-244m_11	0.00381	0.00061	0.000453	0.000034	0.10333	2.92	0.22	459	513
D5-15-244m_12	0.0044	0.00063	0.000417	0.000038	-0.032595	2.69	0.25	343	362
D5-15-244m_13	0.00318	0.00056	0.000436	0.000027	0.16202	2.81	0.17	548	768
D5-15-244m_14	0.00432	0.00059	0.000443	0.000026	0.010752	2.86	0.17	559	720
D5-15-244m_15	0.00314	0.00059	0.000421	0.000035	-0.020014	2.71	0.23	505	770
D5-15-244m_16	0.00412	0.00066	0.000436	0.000032	-0.10686	2.81	0.2	492	876
D5-15-244m_17	0.00357	0.00055	0.000453	0.00004	0.10592	2.92	0.26	310	410
D5-15-244m_18	0.00519	0.00088	0.000446	0.000045	-0.04683	2.87	0.29	607	447
D5-15-244m_19	0.0038	0.0012	0.000474	0.000037	0.14676	3.06	0.24	359	580
D5-15-244m_20	0.00338	0.00054	0.000478	0.000029	0.067608	3.08	0.19	521	904
D5-15-244m_21	0.00435	0.00063	0.000449	0.000039	-0.14521	2.9	0.25	425	679
D5-15-244m_22	0.00334	0.00071	0.000422	0.000039	-0.0033527	2.72	0.25	352	464
D5-15-244m_23	0.00389	0.00067	0.000465	0.000039	0.15624	3	0.25	470	398
D5-15-244m_24	0.00383	0.00055	0.000443	0.000032	-0.030808	2.86	0.21	444	614
D5-15-244m_25	0.00362	0.00057	0.000426	0.000035	0.08256	2.74	0.22	400	371
D5-15-244m_26	0.0065	0.0018	0.000412	0.00007	0.11856	2.65	0.45	265	591
D5-15-244m_27	0.00319	0.00036	0.000431	0.000028	0.18895	2.78	0.18	835	1230
D5-15-244m_28	0.00337	0.00063	0.000452	0.000037	0.19497	2.92	0.24	397	669
D5-15-244m_29	0.00338	0.00049	0.000464	0.000028	0.13579	2.99	0.18	514	861
D5-15-244m_30	0.00364	0.00045	0.00047	0.000028	-0.0052675	3.03	0.18	593	787
D5-15-244m_31	0.0076	0.0034	0.000511	0.000057	0.42539	3.29	0.37	433	632
AB1-10-01-2m_1	0.013	0.0056	0.00052	0.00012	0.25224	3.35	0.76	116.2	93.6
AB1-10-01-2m_2	0.0066	0.0017	0.000418	0.000065	0.03941	2.7	0.42	103.5	96.7
AB1-10-01-2m_3	0.00437	0.00069	0.000467	0.000033	0.13343	3.01	0.21	236	192
AB1-10-01-2m_4	0.0092	0.0029	0.000469	0.000067	0.2437	3.02	0.43	69.4	55.3
AB1-10-01-2m_5	0.0096	0.0039	0.00051	0.000066	0.11112	3.28	0.43	227	282
AB1-10-01-2m_6	0.0081	0.0024	0.000524	0.000086	0.059567	3.38	0.55	62.8	63.3
AB1-10-01-2m_7	0.0099	0.0015	0.000515	0.000065	0.062311	3.32	0.42	156	241
AB1-10-01-2m_8	0.0054	0.0014	0.000481	0.000053	0.11068	3.1	0.34	128	125.4
AB1-10-01-2m_9	0.0041	0.0021	0.000566	0.000074	0.09141	3.65	0.47	81	106
AB1-10-01-2m_10	0.0056	0.0014	0.00051	0.000047	0.2832	3.29	0.3	134.6	111.9
AB1-10-01-2m_11	0.0246	0.0027	0.000607	0.000059	0.010986	3.91	0.38	187.3	161.2
AB1-10-01-2m_12	0.0063	0.0014	0.000443	0.000065	0.30863	2.85	0.42	164	203
AB1-10-01-2m_13	0.0054	0.0013	0.000522	0.000055	0.046639	3.37	0.36	122.2	122.4
AB1-10-01-2m_14	0.0074	0.0023	0.000488	0.00005	0.005641	3.15	0.32	150.7	123
AB1-10-01-2m_15	0.0081	0.0016	0.000487	0.000046	0.079133	3.14	0.3	186	268
AB1-10-01-2m_16	0.00444	0.00088	0.000407	0.000034	0.26481	2.63	0.22	381	351
AB1-10-01-2m_17	0.0063	0.0016	0.000446	0.000061	0.10039	2.88	0.39	131.6	113.2
AB1-10-01-2m_18	0.0055	0.0012	0.000444	0.00004	0.07833	2.86	0.26	217	141.7
AB1-10-01-2m_19	0.0045	0.0017	0.000416	0.000065	0.084295	2.68	0.42	181	182
AB1-10-01-2m_20	0.0077	0.0021	0.000477	0.000059	0.28954	3.07	0.38	220	174
AB1-10-01-2m_21	0.00343	0.00043	0.00046	0.000025	0.0005253	2.96	0.16	586	639
AB1-10-01-2m_22	0.006	0.0013	0.000461	0.000046	0.41936	2.97	0.3	215.9	332
AB1-10-01-2m_23	0.0141	0.0024	0.000572	0.000061	0.21739	3.68	0.39	185	234
AB1-10-01-2m_24	0.0057	0.0014	0.000451	0.000042	0.12724	2.91	0.27	196	203.6
AB1-10-01-2m_25	0.0061	0.0016	0.000476	0.000056	0.23898	3.07	0.36	124.5	128
AB1-10-01-2m_26	0.00499	0.00081	0.000458	0.000045	0.034596	2.95	0.29	224	277
AB1-10-01-2m_27	0.0136	0.0042	0.00053	0.0001	0.18204	3.43	0.67	78.4	79.3
AB1-10-01-2m_28	2.444	0.062	0.1861	0.0054	0.79282	1100	29	368	205
AB1-10-01-2m_29	0.4761	0.0095	0.0624	0.001	0.52868	390.2	6.3	174.1	208.2
1009_1	0.00339	0.00033	0.000466	0.000019	0.04467	3.01	0.12	508	786
1009_2	0.00327	0.00031	0.000466	0.000024	0.2648	3.01	0.15	488	940
1009_3	0.00341	0.00035	0.000462	0.000023	0.059375	2.98	0.15	442	886
1009_4	0.00332	0.00033	0.000441	0.000025	0.00063628	2.84	0.16	441	719
1009_5	0.00323	0.0004	0.0004	0.000025	0.099525	2.58	0.16	335	651
1009_6	0.0032	0.00024	0.000475	0.000021	0.10875	3.06	0.14	604	775
1009_7	0.00393	0.00041	0.000464	0.000024	0.0060475	2.99	0.15	474	827
1009_8	0.00303	0.00031	0.000467	0.000022	0.21211	3.01	0.14	477	853
1009_9	0.00334	0.00032	0.000446	0.000025	0.069602	2.89	0.16	516	641
1009_10	0.00313	0.00034	0.000459	0.000024	0.064665	2.96	0.15	418	571
1009_11	0.00374	0.00046	0.000458	0.000026	0.020031	2.95	0.16	273	294
1009_12	0.00278	0.00032	0.000451	0.000024	0.09929	2.9	0.16	483	561
1009_13	0.00321	0.00038	0.000461	0.000022	0.17667	2.97	0.14	305.2	497

	207Pb/235U	207Pb/235U error	206Pb/238U	206Pb/238U Error	Error Correlation 206/238 vs. 207/235	Final Age (Ma)	Error (Ma)	Approx U (ppm)	Approx Th (ppm)
1009_14	0.00353	0.00028	0.000468	0.00002	0.16343	3.02	0.13	434	787
1009_15	0.00323	0.00028	0.000468	0.000021	0.098327	3.02	0.14	509	971
1009_16	0.00344	0.00045	0.000446	0.000027	0.17611	2.88	0.17	328	541
1009_17	0.00389	0.00041	0.00047	0.000022	0.091968	3.03	0.14	469	677
1009_18	0.00337	0.00036	0.00046	0.000023	0.063247	2.96	0.15	398	684
1009_19	0.00321	0.0003	0.000425	0.000024	0.062987	2.74	0.15	410	677
1009_20	0.00299	0.00028	0.000427	0.000019	0.17826	2.75	0.12	512	922
1009_21	0.00462	0.00051	0.000455	0.000025	0.08848	2.93	0.16	449	486
1009_22	0.00332	0.00038	0.000441	0.000029	0.069573	2.84	0.19	386	463
1009_23	0.00387	0.00035	0.000458	0.000023	0.22218	2.95	0.15	799	154
1009_24	0.00295	0.00029	0.000471	0.00002	0.0043861	3.03	0.13	473.4	1011
1009_25	0.00333	0.00022	0.000466	0.000016	0.062092	3	0.1	1087	1760
1009_26	0.00363	0.00042	0.000428	0.000024	0.17579	2.76	0.15	436	924
1009_27	0.00319	0.00042	0.00042	0.000022	0.13471	2.71	0.14	330	353
1009_28	0.00325	0.0003	0.000461	0.000015	0.19099	2.972	0.095	444	757
1009_29	0.00334	0.00026	0.000466	0.000018	0.31985	3	0.11	696	1389
1009_30	0.00284	0.00035	0.000404	0.000023	0.032556	2.6	0.15	349	580
1009_31	0.00338	0.00041	0.00046	0.000026	0.016532	2.97	0.17	365	678
GBC3-01-01-902m_1	0.0039	0.0013	0.000425	0.000055	-0.20523	2.74	0.36	145	177
GBC3-01-01-902m_2	0.0038	0.0033	0.00039	0.00013	0.23721	2.53	0.84	111	71
GBC3-01-01-902m_3	0.003	0.0012	0.00047	0.000061	0.098765	3.03	0.39	158	172
GBC3-01-01-902m_4	0.0043	0.0021	0.000475	0.000069	0.22375	3.06	0.44	107	111
GBC3-01-01-902m_5	0.006	0.0019	0.00045	0.000068	0.016885	2.9	0.44	97.17	70.19
GBC3-01-01-902m_6	0.0054	0.0019	0.000466	0.000073	-0.071861	3	0.47	86.7	64.4
GBC3-01-01-902m_7	0.0041	0.0011	0.000413	0.000049	0.10782	2.66	0.31	188	122.5
GBC3-01-01-902m_8	0.0035	0.0014	0.000461	0.00006	0.053559	2.97	0.39	141.6	114
GBC3-01-01-902m_9	0.00362	0.00094	0.000449	0.000051	0.052378	2.89	0.33	187	156
GBC3-01-01-902m_10	0.0036	0.0014	0.000484	0.00006	-0.020796	3.12	0.39	146	95.3
GBC3-01-01-902m_11	0.0062	0.0021	0.000418	0.000075	0.03626	2.7	0.48	86	68.6
GBC3-01-01-902m_12	-0.0004	0.0024	0.000374	0.000087	-0.052141	2.41	0.56	62.8	65.4
GBC3-01-01-902m_13	0.00353	0.00098	0.00052	0.000044	0.15497	3.35	0.28	311	680
GBC3-01-01-902m_14	0.0029	0.001	0.00047	0.000046	0.034152	3.03	0.3	193	183
GBC3-01-01-902m_15	0.0057	0.0019	0.000352	0.000049	0.0005743	2.27	0.31	660	790
GBC3-01-01-902m_16	0.005	0.002	0.00045	0.000062	-0.037512	2.9	0.4	130	135
GBC3-01-01-902m_17	0.00345	0.00088	0.000458	0.000053	0.11737	2.95	0.34	240	248
GBC3-01-01-902m_18	0.0024	0.0017	0.000406	0.000072	0.036818	2.62	0.46	98	75
GBC3-01-01-902m_19	0.0036	0.0012	0.00042	0.000049	-0.1504	2.71	0.31	174	104
GBC3-01-01-902m_20	0.0036	0.0011	0.000476	0.00005	0.24618	3.07	0.32	162	175
GBC3-01-01-902m_21	0.0049	0.0015	0.000424	0.000063	0.10883	2.73	0.4	141	117.4
GBC3-01-01-902m_22	0.0059	0.0026	0.000488	0.000085	-0.15933	3.15	0.55	78	79
GBC3-01-01-902m_23	0.0056	0.0018	0.000476	0.000057	0.0050373	3.07	0.36	180	159
GBC3-01-01-902m_24	0.0038	0.0013	0.000451	0.000057	-0.021618	2.91	0.37	136.7	152.8
GBC3-01-01-902m_25	0.0042	0.0015	0.000468	0.000052	-0.11609	3.01	0.33	138	159
GBC3-01-01-902m_26	0.0034	0.0011	0.000436	0.000037	0.11028	2.81	0.24	510	560
GBC3-01-01-902m_27	0.0027	0.0016	0.000408	0.000081	-0.059374	2.63	0.52	98	97
GBC3-01-01-902m_28	0.0031	0.0011	0.000487	0.000059	0.061174	3.14	0.38	159.7	146.1
GBC3-01-01-902m_29	0.3565	0.0089	0.04876	0.00085	0.30876	306.9	5.2	358	320
GBC3-01-01-902m_30	0.0238	0.0014	0.00312	0.00012	0.278	20.05	0.76	496	100.7
DMLZC05-01-248m_1	0.0033	0.0017	0.000432	0.000061	-0.12652	2.78	0.39	133.9	193
DMLZC05-01-248m_2	0.0021	0.0013	0.000445	0.000062	0.093547	2.86	0.4	151	205
DMLZC05-01-248m_3	0.0014	0.0016	0.000456	0.000061	-0.13814	2.94	0.39	97.3	132.4
DMLZC05-01-248m_4	0.0032	0.0019	0.000489	0.000066	0.069877	3.15	0.42	107.6	127.8
DMLZC05-01-248m_5	0.0027	0.0017	0.000473	0.00006	-0.00055555	3.05	0.38	115	110
DMLZC05-01-248m_6	0.0023	0.0015	0.000492	0.000064	-0.25691	3.17	0.42	104.6	140.1
DMLZC05-01-248m_7	0.0042	0.0025	0.000445	0.00008	0.087533	2.87	0.52	91	132
DMLZC05-01-248m_8	0.0032	0.0018	0.000388	0.000067	0.10292	2.5	0.43	181	84.8
DMLZC05-01-248m_9	0.0039	0.0016	0.000437	0.000061	-0.015999	2.82	0.39	114.8	130.7
DMLZC05-01-248m_10	0.0059	0.0027	0.00048	0.000088	-0.11661	3.1	0.57	63.2	63.4
DMLZC05-01-248m_11	0.0041	0.0018	0.000542	0.000075	0.27924	3.49	0.48	131	173
DMLZC05-01-248m_12	0.0055	0.0017	0.000421	0.000059	0.047456	2.71	0.38	139.1	138
DMLZC05-01-248m_13	0.002	0.0016	0.000455	0.000074	0.03398	2.93	0.48	99.7	137.9
DMLZC05-01-248m_14	0.0047	0.0021	0.000454	0.000064	-0.14376	2.93	0.41	99.3	137
DMLZC05-01-248m_15	0.00359	0.00057	0.000432	0.00003	0.025959	2.78	0.2	553	229
DMLZC05-01-248m_16	0.0039	0.0019	0.000463	0.000065	0.16201	2.98	0.42	89.5	109.6
DMLZC05-01-248m_17	0.0024	0.0019	0.000471	0.000072	0.022356	3.03	0.46	96	108.2
DMLZC05-01-248m_18	0.0022	0.0026	0.000382	0.000089	-0.048832	2.46	0.58	76	72
DMLZC05-01-248m_19	0.0027	0.0012	0.000463	0.000057	-0.10516	2.98	0.37	217	225
DMLZC05-01-248m_20	0.0034	0.0012	0.000464	0.000057	0.066347	2.99	0.37	153.5	203.9
DMLZC05-01-248m_21	0.001	0.0024	0.00052	0.00013	-0.12319	3.34	0.83	115	137
DMLZC05-01-248m_22	0.0024	0.0021	0.000431	0.00006	0.035366	2.78	0.39	108	130

	207Pb/235U	207Pb/235U error	206Pb/238U	206Pb/238U Error	Error Correlation 206/238 vs. 207/235	Final Age (Ma)	Error (Ma)	Approx U (ppm)	Approx Th (ppm)
DMLZC05-01-248m_23	0.0047	0.0016	0.000483	0.000042	0.044632	3.11	0.27	281	206
DMLZC05-01-248m_24	0.0037	0.001	0.000484	0.000067	0.03397	3.12	0.43	408	343
DMLZC05-01-248m_25	0.0022	0.0021	0.000472	0.000076	-0.14517	3.04	0.49	121	84
DMLZC05-01-248m_26	0.0045	0.0023	0.000547	0.000074	0.050253	3.52	0.47	135	81.9
DMLZC05-01-248m_27	0.0037	0.0013	0.000441	0.00007	0.10435	2.84	0.45	205	261
DMLZC05-01-248m_28	0.0047	0.0013	0.000444	0.000055	0.15124	2.86	0.36	330	475
DMLZC05-01-248m_29	0.0034	0.0014	0.000443	0.000052	0.077365	2.86	0.34	253	233
DMLZC05-01-248m_30	0.00333	0.00045	0.000395	0.000025	0.009203	2.55	0.16	616	727
TEW01-01-75m_1	0.0045	0.0017	0.000494	0.000085	0.14577	3.18	0.55	99.8	77.6
TEW01-01-75m_2	0.0043	0.0018	0.000398	0.000097	-0.1219	2.57	0.62	72.7	48.2
TEW01-01-75m_3	0.0069	0.0016	0.000484	0.000078	0.12027	3.12	0.5	184	153
TEW01-01-75m_4	0.0043	0.0018	0.00044	0.0001	0.12842	2.8	0.64	73.4	80
TEW01-01-75m_5	0.0045	0.0011	0.000422	0.00006	-0.18443	2.72	0.38	191.9	248.3
TEW01-01-75m_6	0.00341	0.0007	0.000481	0.000034	-0.053278	3.1	0.22	590	335
TEW01-01-75m_7	0.0051	0.0013	0.000484	0.000058	-0.0078282	3.12	0.38	260	306
TEW01-01-75m_8	0.00387	0.00092	0.000481	0.00006	0.072249	3.1	0.39	183.7	119.5
TEW01-01-75m_9	0.007	0.0021	0.000519	0.000092	0.090886	3.34	0.59	122.4	134
TEW01-01-75m_10	0.00557	0.00086	0.000497	0.000048	-0.033952	3.2	0.31	350	163.9
TEW01-01-75m_11	0.0031	0.0013	0.000453	0.000078	0.23991	2.92	0.5	115.6	94.2
TEW01-01-75m_12	0.0033	0.001	0.000426	0.000065	0.052824	2.74	0.42	225	237
TEW01-01-75m_13	0.0041	0.0012	0.000439	0.000075	-0.096296	2.83	0.48	151	129
TEW01-01-75m_14	0.0053	0.0011	0.000531	0.000051	0.21963	3.42	0.33	263	276
TEW01-01-75m_15	0.0048	0.0012	0.00044	0.000058	0.16273	2.83	0.38	207	218
TEW01-01-75m_16	0.00281	0.00096	0.000437	0.000066	-0.072474	2.82	0.42	173	120
TEW01-01-75m_17	0.00412	0.00091	0.00047	0.000053	0.11602	3.03	0.34	245	245
TEW01-01-75m_18	0.0054	0.0011	0.00042	0.00006	0.094947	2.71	0.39	200.1	169
TEW01-01-75m_19	0.005	0.0017	0.000398	0.000087	-0.27788	2.56	0.56	222	204
TEW01-01-75m_20	0.00438	0.00096	0.000457	0.000057	0.046785	2.94	0.37	227	261
TEW01-01-75m_21	0.00462	0.00096	0.000432	0.000058	-0.070453	2.78	0.38	224	136
TEW01-01-75m_22	0.00403	0.00082	0.000466	0.000055	0.19714	3	0.36	248	241
TEW01-01-75m_23	0.00358	0.00089	0.000416	0.000061	-0.033665	2.68	0.39	1260	550
TEW01-01-75m_24	0.279	0.011	0.0392	0.0012	-0.034005	248	7.1	135.7	190.5
TEW01-01-75m_25	0.0034	0.0012	0.000479	0.000075	-0.061541	3.09	0.49	142	138.3
TEW01-01-75m_26	0.00308	0.00089	0.000453	0.000049	0.093579	2.92	0.32	257	290
TEW01-01-75m_27	0.00332	0.0008	0.000451	0.000041	0.082646	2.91	0.27	295	273
TEW01-01-75m_28	0.0036	0.0013	0.000349	0.000062	-0.042949	2.25	0.4	157	176
TEW01-01-75m_29	0.0127	0.0025	0.000454	0.000069	0.04212	2.93	0.44	216	210
TEW01-01-75m_30	0.0034	0.001	0.000499	0.000065	0.091362	3.22	0.42	212	178
TEW01-01-75m_31	0.00427	0.00087	0.000533	0.000064	-0.027674	3.44	0.41	233	202
1008_1	0.0045	0.0013	0.000538	0.00007	0.13323	3.46	0.45	149.8	103.5
1008_2	0.00354	0.0005	0.000448	0.000029	0.050281	2.89	0.19	768	1201
1008_3	0.0062	0.0017	0.000468	0.000079	0.099359	3.01	0.51	120.4	123.3
1008_4	0.0052	0.0024	0.000425	0.000084	0.056422	2.74	0.54	86.1	79.2
1008_5	0.0047	0.0015	0.000483	0.000069	0.11313	3.11	0.44	162	130
1008_6	0.009	0.0026	0.000533	0.000095	0.33076	3.44	0.61	159	188
1008_7	0.0102	0.0033	0.00052	0.00012	0.11258	3.35	0.75	123	174.6
1008_8	0.0045	0.0019	0.000456	0.000074	0.062187	2.94	0.47	99.8	84.2
1008_9	0.0053	0.0016	0.000516	0.000062	0.082415	3.33	0.4	136.2	120.8
1008_10	0.0045	0.0019	0.000445	0.000073	0.065923	2.87	0.47	101	109
1008_11	0.0051	0.0013	0.000467	0.000052	0.040311	3.01	0.33	234	245
1008_12	0.004	0.0015	0.000408	0.000058	0.099127	2.63	0.37	137	147
1008_13	0.0059	0.0018	0.000498	0.000081	0.005236	3.21	0.52	100.1	89.8
1008_14	0.00391	0.0008	0.000471	0.000044	0.19661	3.04	0.29	271	428
1008_15	0.0025	0.0011	0.000474	0.00006	0.20631	3.06	0.38	159	140
1008_16	0.0051	0.0019	0.000437	0.00007	0.069158	2.81	0.45	116	93.9
1008_17	0.0044	0.0016	0.000516	0.000082	0.045072	3.33	0.53	132	155
1008_18	0.0042	0.0014	0.000493	0.000083	0.032839	3.18	0.53	104.2	93.6
1008_19	0.0046	0.0013	0.000496	0.00005	0.11275	3.19	0.32	265	191
1008_20	0.007	0.0019	0.000464	0.000068	0.1665	2.99	0.43	119.4	100.5
1008_21	0.0053	0.0017	0.000447	0.000072	0.072897	2.88	0.46	122.3	106.3
1008_22	0.0069	0.0029	0.000374	0.000085	0.017384	2.41	0.55	79	55
1008_23	0.0069	0.0021	0.000535	0.000083	0.0059951	3.44	0.54	148.6	113.3
1008_24	0.0059	0.002	0.000496	0.000072	0.024001	3.2	0.46	136.4	131.9
1008_25	0.0048	0.0016	0.0005	0.000058	0.064869	3.22	0.38	210	192
1008_26	0.0036	0.0012	0.00053	0.000067	0.055581	3.41	0.43	162	168
1008_27	0.006	0.0015	0.000436	0.000063	0.14893	2.81	0.41	154.8	114.8
1008_28	0.0058	0.0016	0.000453	0.000069	0.030656	2.92	0.45	161.1	119.1
GB23-02-56m_1	0.0042	0.0013	0.000464	0.000057	0.077128	2.99	0.37	165	148
GB23-02-56m_2	0.0033	0.0014	0.000489	0.000075	-0.012196	3.15	0.49	156.7	129.5
GB23-02-56m_3	0.0051	0.0021	0.000406	0.000095	0.051651	2.62	0.61	96.9	77

	207Pb/235U	207Pb/235U error	206Pb/238U	206Pb/238U Error	Error Correlation 206/238 vs. 207/235	Final Age (Ma)	Error (Ma)	Approx U (ppm)	Approx Th (ppm)
GB23-02-56m_4	0.0055	0.0011	0.000556	0.00006	0.13631	3.58	0.39	203	298
GB23-02-56m_5	0.0033	0.0015	0.00046	0.000075	0.084047	2.97	0.48	89.5	146.8
GB23-02-56m_6	0.00366	0.00098	0.000465	0.000062	-0.17219	3	0.4	203	230.3
GB23-02-56m_7	0.00395	0.00085	0.000494	0.000046	-0.24581	3.18	0.3	282	298
GB23-02-56m_8	0.0032	0.0011	0.000446	0.000059	-0.23618	2.87	0.38	181.7	131.3
GB23-02-56m_9	0.0059	0.0019	0.00056	0.00006	0.081074	3.61	0.39	187	147.4
GB23-02-56m_10	0.0168	0.004	0.00063	0.00011	0.41901	4.04	0.73	305	293
GB23-02-56m_11	0.0094	0.0028	0.00057	0.00013	0.17885	3.66	0.87	115.9	107
GB23-02-56m_12	0.0072	0.0027	0.00047	0.00012	-0.083612	3.04	0.76	89	115
GB23-02-56m_13	0.0047	0.0016	0.000397	0.000068	-0.14262	2.56	0.44	124	153.4
GB23-02-56m_14	0.0048	0.0014	0.000446	0.000069	-0.0133	2.88	0.45	132	188
GB23-02-56m_15	0.0047	0.0018	0.000428	0.00009	-0.19815	2.76	0.58	105.8	150.3
GB23-02-56m_16	0.00401	0.00093	0.000472	0.000064	-0.00088388	3.04	0.41	218	227
GB23-02-56m_17	0.0043	0.001	0.000518	0.00006	-0.093433	3.34	0.39	229.4	220
GB23-02-56m_18	0.0039	0.0014	0.000461	0.000072	-0.014853	2.97	0.46	155	131
GB23-02-56m_19	0.0048	0.0011	0.000489	0.000054	-0.15754	3.15	0.35	256	296
GB23-02-56m_20	0.0111	0.0022	0.000441	0.000078	0.089957	2.84	0.51	103	95.4
GB23-02-56m_21	0.0064	0.0019	0.000501	0.000094	-0.10843	3.23	0.61	87.5	130.3
GB23-02-56m_22	0.0061	0.0018	0.000419	0.000067	0.062097	2.7	0.43	149	193
GB23-02-56m_23	0.0053	0.0018	0.000465	0.000073	-0.10621	2.99	0.47	132	133.1
GB23-02-56m_24	0.0057	0.0018	0.000433	0.000068	0.089872	2.79	0.44	172	148
GB23-02-56m_25	0.004	0.0011	0.00038	0.000049	0.0025752	2.45	0.32	214	231
GB23-02-56m_26	0.0043	0.0013	0.000473	0.000072	0.063879	3.05	0.47	167.4	134
GB23-02-56m_27	0.0051	0.0018	0.000422	0.000077	0.24393	2.72	0.5	97.2	98.5
GB23-02-56m_28	0.0061	0.0017	0.000509	0.000073	-0.084957	3.28	0.47	185	207
GB23-02-56m_29	0.005	0.0014	0.000454	0.000076	-0.097876	2.92	0.49	152.8	136.3
GB23-02-56m_30	0.0046	0.0013	0.0005	0.000087	-0.039702	3.22	0.56	168.7	131.6
GB23-02-56m_31	0.0064	0.0015	0.00044	0.000063	0.090849	2.84	0.4	169.1	177
KL12-02-82.8m_1	0.0063	0.0011	0.000399	0.000054	0.11543	2.57	0.35	216	227
KL12-02-82.8m_2	0.0053	0.0015	0.000459	0.000064	0.018553	2.96	0.41	157	144
KL12-02-82.8m_3	0.0085	0.0022	0.000475	0.000074	0.13129	3.06	0.48	114	94.4
KL12-02-82.8m_4	0.0056	0.0014	0.000437	0.000067	0.2827	2.81	0.43	133.4	137.2
KL12-02-82.8m_5	0.0156	0.0023	0.00059	0.0001	0.48686	3.82	0.67	300	240
KL12-02-82.8m_6	0.0043	0.0014	0.000497	0.000078	0.18595	3.2	0.5	131	117
KL12-02-82.8m_7	0.0063	0.0019	0.000451	0.000064	0.10465	2.9	0.41	181	197
KL12-02-82.8m_8	0.0073	0.0018	0.000548	0.000075	0.29919	3.53	0.48	117.4	100.3
KL12-02-82.8m_9	0.0117	0.0028	0.000471	0.000075	0.11297	3.04	0.49	112.3	81.6
KL12-02-82.8m_10	0.0061	0.0014	0.000456	0.000059	0.051997	2.94	0.38	174.2	133.4
KL12-02-82.8m_11	0.0075	0.002	0.000494	0.000075	0.067816	3.19	0.48	186	170
KL12-02-82.8m_12	0.0438	0.008	0.00077	0.00015	0.010498	4.96	0.94	125.3	135.6
KL12-02-82.8m_13	0.0084	0.0026	0.000517	0.000092	0.11895	3.33	0.59	79.9	57.6
KL12-02-82.8m_14	0.0096	0.004	0.000463	0.000069	0.098361	2.99	0.44	130	133
KL12-02-82.8m_15	0.022	0.019	0.000568	0.000093	0.077512	3.66	0.6	120.1	91.4
KL12-02-82.8m_16	0.0046	0.001	0.000449	0.000054	0.073682	2.89	0.35	235	259
KL12-02-82.8m_17	0.0044	0.0011	0.000438	0.000049	0.028209	2.82	0.32	246	279
KL12-02-82.8m_18	0.0166	0.0056	0.000588	0.000086	0.49235	3.79	0.55	119.3	94.6
KL12-02-82.8m_19	0.0041	0.0014	0.000591	0.000074	0.081956	3.81	0.47	193	161
KL12-02-82.8m_20	0.0061	0.0014	0.000394	0.00007	0.083131	2.54	0.45	144.3	111.5
KL12-02-82.8m_21	0.0089	0.0028	0.000448	0.000098	0.31048	2.89	0.63	92.6	72.1
KL12-02-82.8m_22	0.0071	0.0017	0.000449	0.000068	0.10509	2.89	0.44	133.5	110.2
KL12-02-82.8m_23	0.0047	0.0019	0.000504	0.000081	0.035858	3.25	0.52	97.4	72.6
KL12-02-82.8m_24	0.0058	0.0016	0.00052	0.000071	0.18091	3.35	0.46	132.5	85.5
KL12-02-82.8m_25	0.0094	0.0012	0.000598	0.000061	0.1088	3.86	0.39	415.9	114.9
KL12-02-82.8m_26	0.0056	0.0012	0.000526	0.000064	0.1374	3.39	0.41	185.9	143.1
KL12-02-82.8m_27	0.0226	0.0072	0.00064	0.00012	0.43933	4.1	0.8	144	130.4
KL12-02-82.8m_28	0.008	0.002	0.000517	0.000064	0.29279	3.33	0.41	177	106.5
KL12-02-82.8m_29	0.0066	0.0017	0.000449	0.000079	0.054447	2.89	0.51	103.8	78.8
KL12-02-82.8m_30	0.0063	0.0013	0.000491	0.00006	0.0068143	3.16	0.39	236	224
KL12-02-82.8m_31	0.352	0.02	0.0254	0.0015	0.77031	161.6	9.3	356	180.1
KL12-02-82.8m_32	0.318	0.014	0.04303	0.00095	0.31609	271.6	5.9	153.7	143.9
TEW08-01-0m_1	0.0056	0.0019	0.000416	0.000059	0.0098488	2.68	0.38	108.8	124
TEW08-01-0m_2	0.007	0.0023	0.000474	0.000072	0.068918	3.06	0.46	91.9	114.4
TEW08-01-0m_3	0.005	0.0019	0.000408	0.000068	0.0081428	2.63	0.44	106.9	144.6
TEW08-01-0m_4	0.0084	0.0014	0.000395	0.000051	0.084977	2.55	0.33	192	205.7
TEW08-01-0m_5	0.0054	0.0021	0.000432	0.000079	0.034872	2.78	0.51	102.8	114.7
TEW08-01-0m_6	0.0057	0.0021	0.000467	0.000082	0.018591	3.01	0.53	127	152.6
TEW08-01-0m_7	0.0037	0.0017	0.000451	0.000058	0.11805	2.91	0.38	165	203
TEW08-01-0m_8	0.0047	0.0018	0.000436	0.000072	0.11495	2.81	0.46	128	158
TEW08-01-0m_9	0.0057	0.0014	0.000449	0.000035	0.24457	2.89	0.23	903	376
TEW08-01-0m_10	0.0041	0.0016	0.000377	0.000066	0.0048793	2.43	0.42	124.5	143

	207Pb/235U	207Pb/235U error	206Pb/238U	206Pb/238U Error	Error Correlation 206/238 vs. 207/235	Final Age (Ma)	Error (Ma)	Approx U (ppm)	Approx Th (ppm)
TEW08-01-0m_11	0.0046	0.0025	0.000431	0.000084	0.036119	2.78	0.54	71.4	93.5
TEW08-01-0m_12	0.0053	0.0015	0.000415	0.000052	0.18292	2.67	0.34	179	188
TEW08-01-0m_13	0.0069	0.0022	0.000443	0.000088	0.01874	2.86	0.57	95	103
TEW08-01-0m_14	0.0046	0.0017	0.000367	0.000074	0.19154	2.36	0.48	97	126.4
TEW08-01-0m_15	0.0042	0.0015	0.000487	0.00008	0.099498	3.14	0.51	115	122
TEW08-01-0m_16	0.0057	0.0012	0.000468	0.000055	0.04076	3.02	0.36	300	223
TEW08-01-0m_17	0.0067	0.002	0.00043	0.000062	0.0078182	2.77	0.4	127	76.5
TEW08-01-0m_18	0.0043	0.0012	0.000492	0.000061	0.18435	3.17	0.39	245	273
TEW08-01-0m_19	0.0073	0.002	0.00048	0.000065	0.14489	3.1	0.42	169	235
TEW08-01-0m_20	0.0088	0.0025	0.000488	0.000065	0.23666	3.14	0.42	174	220
TEW08-01-0m_21	0.0034	0.0012	0.000412	0.000059	0.26944	2.66	0.38	161	194
TEW08-01-0m_22	0.0049	0.0015	0.000495	0.000072	0.17767	3.19	0.47	145.6	169.5
TEW08-01-0m_23	0.0039	0.0016	0.00049	0.000073	0.17146	3.15	0.47	135	159
TEW08-01-0m_24	0.0057	0.0021	0.000457	0.000081	0.022585	2.95	0.52	79.8	64.9
TEW08-01-0m_25	0.0062	0.0015	0.000445	0.000062	0.026506	2.87	0.4	165.3	191.3
TEW08-01-0m_26	0.0052	0.0012	0.000443	0.000053	0.24936	2.86	0.34	214	238
TEW08-01-0m_27	0.0046	0.0018	0.000529	0.000081	0.029058	3.41	0.52	149	158
TEW08-01-0m_28	0.0026	0.0013	0.000501	0.000077	0.054651	3.23	0.5	114.4	153
TEW08-01-500m_1	0.0059	0.0021	0.000496	0.000077	0.0035856	3.19	0.49	93.9	111
TEW08-01-500m_2	0.00345	0.00072	0.000535	0.00004	0.17187	3.45	0.26	416	457
TEW08-01-500m_3	0.0061	0.0022	0.00048	0.000073	0.1141	3.09	0.47	116.3	142.2
TEW08-01-500m_4	0.0044	0.0022	0.000377	0.000078	0.031522	2.43	0.5	80.5	88.1
TEW08-01-500m_5	0.0039	0.0025	0.000432	0.000093	0.16539	2.78	0.6	64.1	60.4
TEW08-01-500m_6	0.003	0.0023	0.000422	0.000085	0.085548	2.72	0.55	71.9	78.5
TEW08-01-500m_7	0.0034	0.0026	0.000444	0.000085	0.073241	2.86	0.55	73.4	60
TEW08-01-500m_8	0.0029	0.0023	0.000376	0.000074	0.084582	2.42	0.48	84.2	125.3
TEW08-01-500m_9	0.0039	0.0016	0.000505	0.000071	0.15877	3.25	0.46	123.1	156.5
TEW08-01-500m_10	0.0048	0.0024	0.000416	0.000093	0.096223	2.68	0.6	106	110
TEW08-01-500m_11	0.0048	0.0022	0.000428	0.000078	0.00048805	2.76	0.51	92.6	117.6
TEW08-01-500m_12	0.0045	0.0018	0.000424	0.000068	0.04487	2.73	0.44	125.2	133.4
TEW08-01-500m_13	0.0031	0.0013	0.000452	0.000064	0.097014	2.91	0.41	135.2	162.5
TEW08-01-500m_14	0.0034	0.001	0.000459	0.00006	0.0059397	2.96	0.38	204	309
TEW08-01-500m_15	0.0032	0.0019	0.000481	0.000098	0.057773	3.1	0.63	87.9	82.5
TEW08-01-500m_16	0.0051	0.0024	0.000418	0.000082	0.20948	2.69	0.53	81.6	80.8
TEW08-01-500m_17	0.0041	0.0023	0.00048	0.0001	0.014473	3.12	0.65	73.7	62.3
TEW08-01-500m_18	0.00317	0.00093	0.000445	0.00005	0.22818	2.86	0.32	244	237
TEW08-01-500m_19	0.0039	0.0022	0.00054	0.000083	0.30651	3.48	0.53	108	93
TEW08-01-500m_20	0.006	0.0014	0.00041	0.000058	0.15328	2.64	0.38	158.7	215.2
TEW08-01-500m_21	0.0084	0.0027	0.00058	0.0001	0.32554	3.74	0.68	104	75.4
TEW08-01-500m_22	0.0058	0.0012	0.000476	0.000053	0.087661	3.07	0.34	229	220
TEW08-01-500m_23	0.0069	0.0024	0.00054	0.0001	0.1404	3.46	0.67	97.3	63.6
TEW08-01-500m_24	0.0023	0.0022	0.000572	0.000089	0.14123	3.68	0.58	93.1	136.1
TEW08-01-500m_25	0.0043	0.0015	0.000425	0.000062	0.070974	2.74	0.4	132.4	157.8
TEW08-01-500m_26	0.0038	0.0016	0.000449	0.000067	0.21617	2.89	0.43	109.5	93.1
TEW08-01-500m_27	0.0037	0.00094	0.000427	0.000047	0.052139	2.75	0.3	321	182
TEW08-01-500m_28	0.008	0.0042	0.00056	0.00013	0.14125	3.58	0.83	46.8	21.19
TEW08-01-500m_29	0.0052	0.0029	0.00049	0.00011	0.51945	3.13	0.72	82	62.3
TEW08-01-1275m_1	0.0081	0.003	0.00053	0.0001	0.061399	3.42	0.66	63	59
TEW08-01-1275m_2	0.008	0.0026	0.000441	0.000091	0.31273	2.84	0.58	460	71.4
TEW08-01-1275m_3	0.0062	0.0022	0.000498	0.000092	0.40451	3.21	0.59	103.3	132
TEW08-01-1275m_4	0.007	0.0023	0.000488	0.000073	0.18888	3.15	0.47	92.7	112.5
TEW08-01-1275m_5	0.0055	0.0025	0.0005	0.0001	0.088465	3.21	0.65	73.1	59.8
TEW08-01-1275m_6	0.0034	0.001	0.000448	0.000052	0.19633	2.89	0.34	179.6	234
TEW08-01-1275m_7	0.0094	0.0026	0.000491	0.000088	0.091891	3.16	0.57	158	102.5
TEW08-01-1275m_8	0.0085	0.0025	0.000438	0.000073	0.061877	2.82	0.47	102.2	79.6
TEW08-01-1275m_9	0.0068	0.0017	0.00048	0.000068	0.021227	3.09	0.44	168	149
TEW08-01-1275m_10	0.0054	0.0013	0.000499	0.000063	0.036602	3.21	0.41	396	236
TEW08-01-1275m_11	0.00485	0.00097	0.000391	0.000048	0.13453	2.52	0.31	744	221.1
TEW08-01-1275m_12	0.0043	0.0017	0.000476	0.000074	0.096566	3.07	0.48	118.4	126.5
TEW08-01-1275m_13	0.0038	0.0013	0.000357	0.000048	0.20813	2.3	0.31	167	226
TEW08-01-1275m_14	0.0036	0.0023	0.000407	0.000081	0.07301	2.62	0.52	78.6	100.7
TEW08-01-1275m_15	0.0091	0.0028	0.000542	0.000097	0.070925	3.5	0.63	94	59.9
TEW08-01-1275m_16	0.0056	0.0011	0.000392	0.000059	0.1586	2.53	0.38	304.8	409.6
TEW08-01-1275m_17	0.0043	0.00082	0.000518	0.00004	0.077118	3.34	0.26	360	343
TEW08-01-1275m_18	0.0083	0.0022	0.000485	0.000065	0.049446	3.13	0.42	211	329
TEW08-01-1275m_19	0.00465	0.00077	0.000467	0.000044	0.19427	3.01	0.28	503	407
TEW08-01-1275m_20	0.0059	0.0019	0.000415	0.000065	0.30017	2.67	0.42	293	449
TEW08-01-1275m_21	0.00486	0.00099	0.000405	0.000048	0.079532	2.61	0.31	271	241
TEW08-01-1275m_22	0.0062	0.002	0.000506	0.000086	0.0066343	3.26	0.55	97.6	100.8
TEW08-01-1275m_23	0.00525	0.00094	0.000446	0.000047	0.3341	2.87	0.3	394	464
TEW08-01-1275m_24	0.0039	0.0031	0.0006	0.00013	0.093722	3.89	0.85	57.3	32.7

	207Pb/235U	207Pb/235U error	206Pb/238U	206Pb/238U Error	Error Correlation 206/238 vs. 207/235	Final Age (Ma)	Error (Ma)	Approx U (ppm)	Approx Th (ppm)
TEW08-01-1275m_25	0.0037	0.0014	0.000474	0.000066	0.076688	3.05	0.43	145	136
TEW08-01-1275m_26	0.006	0.0019	0.000392	0.000062	0.0076598	2.53	0.4	99.6	93.3
TEW08-01-1275m_27	0.0066	0.0022	0.000404	0.000077	0.088198	2.6	0.5	98.1	117.2
TEW08-01-1275m_28	0.0054	0.0013	0.000487	0.00005	0.1341	3.14	0.32	261	243
TEW08-01-1275m_29	0.0056	0.0018	0.000425	0.000079	0.072415	2.74	0.51	101.4	133.6
1003_1	0.00315	0.00069	0.000418	0.000035	0.057187	2.69	0.23	445	837
1003_2	0.00369	0.00039	0.000506	0.000022	0.14636	3.26	0.14	1133	2860
1003_3	0.00362	0.00041	0.000477	0.000032	0.071181	3.07	0.21	704	1530
1003_4	0.0057	0.0027	0.000512	0.000088	0.24595	3.3	0.57	73.6	71.7
1003_5	0.0052	0.0014	0.000491	0.00002	0.01684	3.17	0.13	1453	3650
1003_6	0.00341	0.00022	0.00049	0.000017	0.08142	3.16	0.11	1993	5840
1003_7	0.00326	0.00034	0.000471	0.000025	0.14537	3.03	0.16	1000	2410
1003_8	0.004	0.0017	0.000448	0.000064	0.26815	2.88	0.41	113	138
1003_9	0.00323	0.00044	0.000429	0.000024	0.18222	2.76	0.15	627	1192
1003_10	0.00429	0.00055	0.000483	0.000028	0.078927	3.11	0.18	764	1970
1003_11	0.00518	0.0008	0.000472	0.000044	0.02873	3.04	0.28	542	1413
1003_12	0.0059	0.0012	0.000502	0.00003	0.47325	3.24	0.19	1629	3506
1003_13	0.00334	0.00057	0.000439	0.000025	0.11766	2.83	0.16	1120	2350
1003_14	0.00384	0.00049	0.000484	0.000023	0.079983	3.12	0.15	721	1667
1003_15	0.0059	0.0017	0.000511	0.000052	0.035168	3.29	0.33	139.1	123.7
1003_16	0.00344	0.0004	0.000468	0.000026	0.18229	3.02	0.17	800	1960
1003_17	0.008	0.0022	0.000506	0.000063	0.049716	3.26	0.41	142.8	158.4
1003_18	0.00331	0.00073	0.000486	0.000037	0.1543	3.13	0.24	569	1210
1003_19	0.00396	0.00039	0.000472	0.000033	0.057257	3.04	0.22	822	1657
1003_20	0.00512	0.00076	0.000485	0.000046	0.14999	3.12	0.3	1090	2920
1003_21	0.00361	0.00056	0.000435	0.000031	0.080046	2.81	0.2	669	1520
1003_22	0.00406	0.00054	0.000463	0.000029	0.036094	2.98	0.19	877	2530
1003_23	0.00405	0.00057	0.000455	0.000035	0.1636	2.93	0.23	841	1957
1003_24	0.006	0.0017	0.000468	0.000057	0.069412	3.01	0.37	836	2641
1003_25	0.0074	0.0018	0.000476	0.000068	0.10341	3.07	0.44	158.3	226.5
1003_26	0.00422	0.00043	0.000491	0.000029	0.13349	3.16	0.19	1079	2913
1003_27	0.00332	0.0004	0.000475	0.000023	0.028917	3.06	0.15	718	1555
1003_28	0.00499	0.00086	0.000452	0.000033	0.32129	2.92	0.21	680	1663
1003_29	0.00458	0.00068	0.000453	0.000027	0.12793	2.92	0.17	968	2613
DOW53-01-458m_1	0.0053	0.0022	0.000389	0.000065	-0.014943	2.5	0.42	101.6	138.1
DOW53-01-458m_2	0.00407	0.00076	0.000494	0.000038	-0.13305	3.18	0.25	301	130
DOW53-01-458m_3	0.0044	0.002	0.000426	0.000056	0.040624	2.74	0.36	123.5	152.8
DOW53-01-458m_4	0.0057	0.0023	0.000425	0.000063	-0.051059	2.74	0.4	91.6	73.5
DOW53-01-458m_5	0.0029	0.0029	0.000406	0.000093	0.021646	2.62	0.6	57.2	47.8
DOW53-01-458m_6	0.00479	0.00085	0.000557	0.000028	0.19184	3.59	0.18	354	248.7
DOW53-01-458m_7	0.003	0.0022	0.000492	0.000078	0.008023	3.17	0.5	90.3	107.6
DOW53-01-458m_8	0.0052	0.0015	0.000428	0.000054	-0.13789	2.76	0.35	143.5	113.3
DOW53-01-458m_9	0.0015	0.0023	0.000424	0.00006	-0.10187	2.73	0.39	96.4	109.7
DOW53-01-458m_10	0.0096	0.004	0.00046	0.00011	-0.0068849	2.95	0.69	88.5	81.5
DOW53-01-458m_11	0.0061	0.0028	0.000359	0.000067	0.047112	2.31	0.43	90.8	85.5
DOW53-01-458m_12	0.0025	0.0021	0.000576	0.000077	0.10742	3.71	0.5	108.3	137
DOW53-01-458m_13	0.00423	0.00088	0.000462	0.000045	0.075476	2.97	0.29	302	238
DOW53-01-458m_14	0.0048	0.0032	0.000514	0.000084	0.1431	3.31	0.54	92.1	78.1
DOW53-01-458m_15	0.003	0.0018	0.000423	0.000055	0.11362	2.72	0.35	178.2	214
DOW53-01-458m_16	0.0024	0.0021	0.000405	0.000069	-0.047727	2.61	0.44	111.1	133.3
DOW53-01-458m_17	0.004	0.002	0.00041	0.00007	0.17726	2.64	0.45	107.3	145.5
DOW53-01-458m_18	0.0025	0.0011	0.000505	0.000054	0.38959	3.25	0.35	202	187
DOW53-01-458m_19	0.0027	0.002	0.000381	0.000055	0.082781	2.46	0.35	94.6	116.7
DOW53-01-458m_20	0.0043	0.0014	0.000377	0.000052	0.0845	2.43	0.34	194	236
DOW53-01-458m_21	0.0033	0.0015	0.000381	0.000048	-0.16143	2.46	0.31	165.2	208.5
DOW53-01-458m_22	0.0037	0.003	0.000437	0.000083	-0.0033461	2.81	0.53	92.4	111
DOW53-01-458m_23	0.0019	0.0033	0.000574	0.000094	0.018154	3.7	0.61	90.5	117
DOW53-01-458m_24	0.0016	0.0021	0.000367	0.000068	0.099334	2.36	0.44	114	132
DOW53-01-458m_25	0.3165	0.0067	0.0436	0.001	0.60043	275.1	6.3	335	310
DOW53-01-458m_26	0.3097	0.0074	0.04296	0.00072	0.54444	271.1	4.4	324	338
DOW53-01-458m_27	0.2828	0.0049	0.04012	0.00055	0.55577	253.5	3.4	668	592
DOW53-01-458m_28	0.3172	0.0069	0.04375	0.00067	0.38464	276	4.2	274	182.8
DOW53-01-458m_29	0.2976	0.0064	0.04137	0.00071	0.54665	261.3	4.4	221.9	148.1
GBC3-01-01-37m_1	0.00499	0.00095	0.000511	0.000043	0.33859	3.3	0.28	367	204
GBC3-01-01-37m_2	0.0056	0.0014	0.000544	0.000056	0.27658	3.51	0.36	264	76.9
GBC3-01-01-37m_3	0.00394	0.00088	0.000451	0.000041	-0.070061	2.91	0.26	320	124.2
GBC3-01-01-37m_5	0.00398	0.00059	0.000449	0.000036	-0.096281	2.89	0.23	385	113.8
GBC3-01-01-37m_6	0.0053	0.0012	0.000493	0.00005	0.10546	3.17	0.32	273.9	90.9
GBC3-01-01-37m_7	0.00333	0.00071	0.000465	0.000032	0.044008	3	0.2	374	106.9
GBC3-01-01-37m_10	0.00378	0.00065	0.000519	0.000039	-0.13741	3.34	0.25	375	107.3
GBC3-01-01-37m_11	0.00422	0.00085	0.000453	0.000044	0.2305	2.92	0.28	296.8	91.8

	207Pb/235U	207Pb/235U error	206Pb/238U	206Pb/238U Error	Error Correlation 206/238 vs. 207/235	Final Age (Ma)	Error (Ma)	Approx U (ppm)	Approx Th (ppm)
GBC3-01-01-37m_12	0.0036	0.00056	0.000451	0.000036	-0.13245	2.91	0.23	388	149
GBC3-01-01-37m_13	0.00458	0.00094	0.000519	0.000043	0.25757	3.35	0.28	367	131.2
GBC3-01-01-37m_14	0.00509	0.00089	0.000488	0.000043	-0.032555	3.15	0.28	270	89.2
GBC3-01-01-37m_15	0.007	0.0018	0.000464	0.000053	0.18661	2.99	0.34	250	102
GBC3-01-01-37m_16	0.0041	0.00053	0.00046	0.00004	-0.10975	2.97	0.26	381	135
GBC3-01-01-37m_17	0.0094	0.0021	0.000474	0.000043	0.27914	3.05	0.28	363.7	174.9
GBC3-01-01-37m_18	0.00391	0.00083	0.000495	0.00004	0.028155	3.19	0.26	336	105.1
GBC3-01-01-37m_19	0.00441	0.00099	0.00048	0.000054	0.25077	3.1	0.34	297	106.2
GBC3-01-01-37m_20	0.0049	0.0014	0.000468	0.000046	0.077753	3.01	0.3	158.2	81.9
GBC3-01-01-37m_21	0.00353	0.00057	0.000493	0.000033	0.035124	3.18	0.21	386	168
GBC3-01-01-37m_22	0.0043	0.0016	0.000573	0.000064	0.075718	3.69	0.41	120.7	41.5
GBC3-01-01-37m_23	0.0038	0.00054	0.00048	0.000038	-0.018798	3.09	0.24	347	130
GBC3-01-01-37m_25	0.00457	0.00073	0.00051	0.000036	0.25964	3.29	0.23	372	88.1
GBC3-01-01-37m_26	0.005	0.00071	0.000508	0.000036	-0.092262	3.27	0.23	434	128
GBC3-01-01-37m_27	0.00371	0.00058	0.00043	0.000036	0.021772	2.77	0.23	384	106.7
GBC3-01-01-37m_30	0.00497	0.0007	0.000504	0.000041	-0.017356	3.25	0.26	422	195.1
GBC3-01-01-37m_31	0.0059	0.001	0.000527	0.000041	0.046104	3.4	0.26	514.3	234
GBC3-01-01-37m_32	0.00449	0.00057	0.00047	0.000039	0.098235	3.03	0.25	427	173.8
GBC3-01-01-37m_33	0.00433	0.00062	0.0005	0.000037	0.15709	3.22	0.24	381	139
GBC3-01-01-37m_4	0.8108	0.0096	0.09747	0.00062	0.25372	599.6	3.6	381	8.26
GBC6-01-01-50m_1	0.00381	0.00049	0.000465	0.000025	0.086182	3	0.16	833	1626
GBC6-01-01-50m_2	0.00439	0.00079	0.000446	0.000037	-0.092019	2.87	0.24	295.1	92.8
GBC6-01-01-50m_3	0.00355	0.00056	0.000481	0.000036	0.018208	3.1	0.23	461	125.4
GBC6-01-01-50m_4	0.00427	0.00056	0.000448	0.000044	-0.1816	2.89	0.28	421	156.5
GBC6-01-01-50m_5	0.00406	0.00059	0.000496	0.000043	0.085776	3.2	0.28	388	104.7
GBC6-01-01-50m_6	0.00392	0.00066	0.000523	0.000043	-0.046337	3.37	0.28	414	145.8
GBC6-01-01-50m_7	0.0059	0.0016	0.000506	0.00006	0.090481	3.26	0.39	404	153
GBC6-01-01-50m_8	0.00422	0.00074	0.0005	0.000042	0.13697	3.22	0.27	368	94.2
GBC6-01-01-50m_9	0.00539	0.00091	0.000487	0.000035	-0.069482	3.14	0.23	454	186
GBC6-01-01-50m_10	0.006	0.0013	0.000479	0.00004	0.30533	3.09	0.26	392	207.9
GBC6-01-01-50m_11	0.00493	0.00079	0.000498	0.000038	-0.032904	3.21	0.25	341.1	128
GBC6-01-01-50m_12	0.0047	0.0012	0.000519	0.000062	-0.15653	3.34	0.4	554	102
GBC6-01-01-50m_13	0.00455	0.00057	0.000484	0.000033	0.092724	3.12	0.21	577	277
GBC6-01-01-50m_14	0.00366	0.00098	0.000404	0.000039	-0.024745	2.6	0.25	233	81.6
GBC6-01-01-50m_15	0.005	0.00081	0.000496	0.000041	0.058604	3.19	0.26	344	139
GBC6-01-01-50m_16	0.00556	0.00093	0.000555	0.000038	-0.023894	3.58	0.25	360	149.8
GBC6-01-01-50m_17	0.00376	0.00091	0.000512	0.000057	-0.14346	3.3	0.37	388	107
GBC6-01-01-50m_18	0.00358	0.0007	0.0005	0.000041	0.11945	3.22	0.27	371	139.2
GBC6-01-01-50m_19	0.00465	0.00087	0.000501	0.000045	0.028539	3.23	0.29	362	157
GBC6-01-01-50m_20	0.00357	0.00061	0.000535	0.000047	-0.067571	3.45	0.3	351	149.5
GBC6-01-01-50m_21	0.00381	0.00059	0.000509	0.000035	-0.1338	3.28	0.22	459	212
GBC6-01-01-50m_22	0.00447	0.00084	0.000499	0.000041	-0.055154	3.22	0.26	401	186.1
GBC6-01-01-50m_23	0.00375	0.00057	0.000452	0.00004	-0.089569	2.91	0.26	435	210.7
GBC6-01-01-50m_24	0.00346	0.0007	0.00047	0.000039	-0.085015	3.03	0.25	356	132.1
GBC6-01-01-50m_25	0.00562	0.00086	0.000517	0.000044	0.1204	3.33	0.28	384	135.6
GBC6-01-01-50m_26	0.004	0.00069	0.000475	0.000041	-0.011811	3.06	0.27	366	167.2
GBC6-01-01-50m_27	0.00344	0.00054	0.000461	0.00003	0.032498	2.97	0.19	436	141.5
GBC6-01-01-50m_28	0.0048	0.00054	0.000512	0.000029	0.082739	3.3	0.19	2210	191
GBC6-01-01-50m_29	0.00407	0.0007	0.000508	0.00005	0.073822	3.27	0.32	397	194
GBC6-01-01-50m_30	0.00356	0.00058	0.000474	0.000032	-0.12151	3.06	0.21	409	148.4
GBC6-01-01-50m_31	0.00461	0.00064	0.000475	0.000038	0.041013	3.06	0.24	551	206.9
GBC6-01-01-50m_32	0.2899	0.0081	0.03983	0.00076	0.081155	251.7	4.7	176.1	166.1
KL20-10-3m_1	0.006	0.0016	0.000539	0.000064	0.033125	3.48	0.41	164.5	214.2
KL20-10-3m_2	0.0044	0.0015	0.000487	0.000061	0.04487	3.14	0.4	141.4	174
KL20-10-3m_3	0.0183	0.0051	0.00075	0.00013	0.031628	4.86	0.86	141.5	138
KL20-10-3m_4	0.0056	0.0018	0.000487	0.000088	0.13058	3.14	0.56	137	127
KL20-10-3m_5	0.0083	0.0028	0.00056	0.0001	0.1198	3.58	0.65	80	51.9
KL20-10-3m_6	0.0038	0.0012	0.000522	0.00007	0.14765	3.36	0.45	155.8	149
KL20-10-3m_7	0.0052	0.0016	0.000531	0.000059	0.2491	3.42	0.38	224	247
KL20-10-3m_8	0.0064	0.0017	0.000622	0.000086	0.36821	4.01	0.55	145.4	164
KL20-10-3m_9	0.004	0.0015	0.000522	0.000073	0.070849	3.36	0.47	135	164.5
KL20-10-3m_10	0.0259	0.0042	0.00068	0.000066	0.013449	4.38	0.43	142.6	151.4
KL20-10-3m_11	0.00605	0.00086	0.000561	0.000057	0.13466	3.62	0.37	524	1243
KL20-10-3m_12	0.0043	0.0012	0.000608	0.00007	0.22031	3.92	0.45	270	277
KL20-10-3m_13	0.0092	0.0022	0.000553	0.000087	0.1025	3.56	0.56	89.4	79.8
KL20-10-3m_14	0.0061	0.0021	0.000459	0.000068	0.078977	2.96	0.44	116.4	94.3
KL20-10-3m_15	0.006	0.0017	0.000586	0.000081	0.17043	3.77	0.52	99.3	109.3
KL20-10-3m_16	0.00458	0.00082	0.000502	0.000043	0.12214	3.23	0.28	251.2	337
KL20-10-3m_17	0.0057	0.0017	0.000494	0.000082	0.046487	3.19	0.53	153	191.5
KL20-10-3m_18	0.0056	0.0019	0.000591	0.000096	0.058	3.81	0.62	91.2	64.5
KL20-10-3m_19	0.0043	0.0011	0.000518	0.000058	0.26742	3.34	0.37	211	232

	207Pb/235U	207Pb/235U error	206Pb/238U	206Pb/238U Error	Error Correlation 206/238 vs. 207/235	Final Age (Ma)	Error (Ma)	Approx U (ppm)	Approx Th (ppm)
KL20-10-3m_20	0.0104	0.0039	0.0005	0.00015	0.31817	3.21	0.94	114.9	143.3
KL20-10-3m_21	0.0048	0.002	0.000666	0.000096	0.16128	4.29	0.62	86.8	85.5
KL20-10-3m_22	0.006	0.0014	0.000525	0.000069	0.0045015	3.39	0.44	138.9	126.3
KL20-10-3m_23	0.0032	0.0023	0.00066	0.00011	0.10617	4.23	0.7	64.2	47.1
KL20-10-3m_24	0.0055	0.002	0.000537	0.000078	0.01896	3.46	0.5	103.7	107
KL20-10-3m_25	0.2827	0.0075	0.03928	0.00064	0.16057	248.4	4	334	376
KL20-10-3m_26	4.68	0.056	0.2992	0.0044	0.85676	1686	22	443	114.9
KL20-10-3m_27	0.3755	0.0089	0.04943	0.00071	0.22918	311	4.4	155.9	103.9
KL20-10-3m_28	0.296	0.018	0.0408	0.0011	0.007849	257.9	6.7	109.3	120.1
KL20-10-3m_29	3.481	0.027	0.2617	0.0024	0.67093	1499	12	950	1203
KL20-10-3m_30	4.969	0.04	0.3135	0.0024	0.61832	1758	12	285.9	183.6
AB1-10-01-574m_1	0.00472	0.00077	0.00055	0.00003	0.38272	3.55	0.19	802	1702
AB1-10-01-574m_2	0.00397	0.0004	0.000519	0.00002	0.26944	3.35	0.13	989	1492
AB1-10-01-574m_3	0.00749	0.00051	0.000536	0.000025	0.16424	3.45	0.16	711	1233
AB1-10-01-574m_4	0.0075	0.0011	0.000527	0.000033	0.18787	3.4	0.21	368	335
AB1-10-01-574m_5	0.00344	0.00041	0.000464	0.000029	0.17497	2.99	0.19	538	703
AB1-10-01-574m_6	0.00411	0.00027	0.000521	0.000023	0.189	3.36	0.15	1061	1964
AB1-10-01-574m_7	0.00347	0.00058	0.000483	0.000037	0.16436	3.11	0.24	265.8	276
AB1-10-01-574m_8	0.00347	0.00023	0.000507	0.000018	0.10086	3.27	0.12	908	2490
AB1-10-01-574m_9	0.00412	0.00032	0.000525	0.000021	0.32582	3.39	0.14	1408	2825
AB1-10-01-574m_10	0.00342	0.00023	0.000517	0.000023	0.19515	3.33	0.15	886	1468
AB1-10-01-574m_11	0.0037	0.00055	0.000477	0.00003	0.023069	3.08	0.19	360	430
AB1-10-01-574m_12	0.00343	0.00028	0.0005	0.000022	0.071892	3.22	0.14	1060	2060
AB1-10-01-574m_13	0.00441	0.00045	0.000517	0.000023	0.41282	3.33	0.15	4960	6.00E+04
AB1-10-01-574m_14	0.00317	0.00033	0.000468	0.00002	0.065148	3.02	0.13	679	1567
AB1-10-01-574m_15	0.0036	0.00038	0.000475	0.000027	0.081258	3.06	0.17	570	768
AB1-10-01-574m_16	0.00386	0.00034	0.000486	0.000022	0.27567	3.13	0.14	834	1542
AB1-10-01-574m_17	0.00376	0.00035	0.000466	0.000019	0.045804	3	0.12	946	2099
AB1-10-01-574m_18	0.00323	0.0003	0.000472	0.000023	0.060973	3.04	0.15	702	1477
AB1-10-01-574m_19	0.00387	0.00035	0.000503	0.000022	0.20921	3.24	0.14	1810	2720
AB1-10-01-574m_20	0.00428	0.00034	0.000506	0.000025	0.20097	3.26	0.16	923	1240
AB1-10-01-574m_21	0.00365	0.00027	0.000525	0.000023	0.091664	3.38	0.15	1201	2131
AB1-10-01-574m_22	0.00438	0.00056	0.000489	0.000034	0.1648	3.15	0.22	534	866
AB1-10-01-574m_23	0.00326	0.00029	0.000504	0.000022	0.087898	3.25	0.14	774	1460
AB1-10-01-574m_24	0.0038	0.00027	0.000512	0.000022	0.25352	3.3	0.14	924	1501
AB1-10-01-574m_25	0.00394	0.0003	0.000535	0.000016	0.1508	3.45	0.1	1780	4020
AB1-10-01-574m_26	0.00357	0.00023	0.000509	0.000018	0.21832	3.28	0.12	1220	2958
AB1-10-01-574m_27	0.0036	0.00035	0.000517	0.000022	0.20623	3.33	0.14	767	1408
AB1-10-01-574m_28	0.00352	0.0002	0.000516	0.000013	0.053725	3.324	0.082	2280	3900
AB1-10-01-574m_29	0.00363	0.00026	0.000505	0.000019	0.06132	3.25	0.12	884	1620
AB1-10-01-574m_30	0.00378	0.00066	0.000459	0.00004	0.011332	2.96	0.26	207.9	132.7
AB1-10-01-574m_31	0.00357	0.00038	0.000534	0.000026	0.23063	3.44	0.17	850	1662
AB1-10-01-574m_32	0.00348	0.00038	0.000464	0.000021	0.15373	2.99	0.14	584	1448
5002_1	0.00341	0.00045	0.000475	0.000024	0.24314	3.06	0.16	338.7	95.3
5002_2	0.00362	0.00038	0.000485	0.000024	0.082172	3.13	0.16	311	98.6
5002_3	0.00459	0.00051	0.000503	0.000027	0.1585	3.24	0.17	371	127.9
5002_4	0.00493	0.00068	0.000505	0.000035	0.33099	3.26	0.22	324	95.8
5002_5	0.00451	0.0005	0.000504	0.000027	0.2048	3.25	0.17	350.7	118.6
5002_6	0.00471	0.0005	0.000524	0.000028	0.059341	3.38	0.18	427	171
5002_7	0.00426	0.00057	0.000511	0.000025	0.096299	3.29	0.16	478	180
5002_8	0.00479	0.00072	0.000554	0.000041	0.07823	3.57	0.26	615	150.9
5002_9	0.00398	0.00041	0.000516	0.000029	0.19714	3.33	0.19	389	195.6
5002_10	0.0044	0.00043	0.000527	0.000024	0.09205	3.39	0.15	443	196
5002_11	0.0045	0.00056	0.00053	0.000036	0.10453	3.41	0.23	259	117.3
5002_12	0.00486	0.00043	0.000564	0.000021	0.067508	3.63	0.14	596	350
5002_13	0.00417	0.00047	0.000487	0.000025	0.024236	3.14	0.16	548	338
5002_14	0.00421	0.00032	0.000518	0.000032	0.064366	3.34	0.21	420	144
5002_15	0.00397	0.00033	0.000508	0.000024	0.14096	3.28	0.16	494	201
5002_16	0.00478	0.00058	0.000516	0.000029	0.17379	3.32	0.19	405	163.5
5002_17	0.00445	0.00044	0.000535	0.000031	0.33641	3.45	0.2	540	150.6
5002_18	0.00388	0.00035	0.000524	0.000025	0.2373	3.37	0.16	440	144.7
5002_19	0.00411	0.00044	0.000509	0.000026	0.11507	3.28	0.17	344.3	153
5002_20	0.00451	0.00031	0.000548	0.000023	0.19351	3.53	0.15	610	216
5002_21	0.00426	0.00048	0.000558	0.000036	0.09582	3.59	0.23	278	123.9
5002_22	0.00472	0.00048	0.00052	0.000026	0.030417	3.35	0.17	485	148.8
5002_23	0.00411	0.00038	0.000508	0.000025	0.082441	3.27	0.16	452.3	122.4
5002_24	0.00532	0.00083	0.000533	0.000038	0.1674	3.43	0.25	426.3	141.5
5002_25	0.00447	0.00051	0.000537	0.000032	0.09165	3.46	0.21	388	150.2
5002_26	0.00419	0.00037	0.000501	0.000023	0.26444	3.23	0.15	473	241
5002_27	0.00399	0.00034	0.000524	0.000024	0.015835	3.38	0.15	478	199
5002_28	0.00427	0.00042	0.000515	0.000029	0.02676	3.32	0.19	338	70.2

	207Pb/235U	207Pb/235U error	206Pb/238U	206Pb/238U Error	Error Correlation 206/238 vs. 207/235	Final Age (Ma)	Error (Ma)	Approx U (ppm)	Approx Th (ppm)
5002_29	5.236	0.079	0.3235	0.0058	0.79254	1810	29	1189	99.3
5003_1	0.00391	0.00041	0.000506	0.000023	0.20656	3.26	0.15	413	122.8
5003_2	0.00387	0.00037	0.000507	0.000021	0.037213	3.27	0.14	473.6	160
5003_3	0.00479	0.0005	0.000504	0.000045	0.094508	3.25	0.29	394.4	163.2
5003_4	0.00386	0.00031	0.000494	0.000023	0.03165	3.18	0.15	470.2	109.4
5003_5	0.00411	0.00049	0.000523	0.00002	0.13105	3.37	0.13	489	184
5003_6	0.00361	0.00032	0.000555	0.00003	0.068414	3.58	0.19	451	215
5003_7	0.00442	0.00027	0.000548	0.000025	0.045957	3.53	0.16	661	383
5003_8	0.0036	0.00043	0.000504	0.000029	0.029321	3.25	0.19	414	111
5003_9	0.00443	0.00057	0.000542	0.00003	0.076501	3.49	0.19	377	147
5003_10	0.00459	0.00042	0.000545	0.00003	0.057713	3.51	0.19	403	110.9
5003_11	0.00368	0.00034	0.000497	0.000025	0.1858	3.2	0.16	455	126.8
5003_12	0.00552	0.00075	0.000542	0.000049	0.24376	3.49	0.32	483	163.7
5003_13	0.0055	0.001	0.000504	0.000041	0.4244	3.25	0.26	508	82
5003_14	0.00374	0.00036	0.000538	0.000022	0.00028698	3.47	0.14	446	134.4
5003_15	0.00449	0.00052	0.000494	0.000027	0.19542	3.18	0.17	403	154.2
5003_16	0.00452	0.00061	0.00047	0.000027	0.020124	3.03	0.18	367	104.1
5003_17	0.00401	0.00033	0.000547	0.000027	0.10697	3.52	0.18	486	201.5
5003_18	0.00527	0.00095	0.000522	0.000039	0.20284	3.36	0.25	245.9	125
5003_19	0.00439	0.00047	0.000485	0.000032	0.069983	3.12	0.21	284	83.7
5003_20	0.0046	0.00036	0.000516	0.000017	0.12151	3.32	0.11	550	210.8
5003_21	0.00327	0.00049	0.000546	0.000036	0.087013	3.52	0.23	395	156.7
5003_22	0.00374	0.00034	0.000495	0.000024	0.043051	3.19	0.15	451.1	145.9
5003_23	0.00523	0.0006	0.000536	0.000041	0.14306	3.46	0.26	432	109.3
5003_24	0.00431	0.00039	0.000562	0.000027	0.066536	3.62	0.17	563	344
5003_25	0.00416	0.00037	0.000526	0.000027	0.015268	3.39	0.17	583	122
5003_26	0.00494	0.00043	0.000578	0.000028	0.015919	3.72	0.18	495	185
5003_27	0.00478	0.00056	0.000544	0.000034	0.23502	3.51	0.22	623	246
KL98-10-22-1505m_1	0.004	0.0006	0.000539	0.000037	0.0020522	3.47	0.24	281	240.9
KL98-10-22-1505m_2	0.00425	0.00079	0.000554	0.000039	-0.04935	3.57	0.25	226	226
KL98-10-22-1505m_3	0.0044	0.0011	0.000555	0.000057	0.12124	3.58	0.36	121.2	106.3
KL98-10-22-1505m_4	0.00539	0.00069	0.000515	0.000033	-0.02799	3.32	0.21	374	414
KL98-10-22-1505m_5	0.0058	0.0012	0.000575	0.000035	0.28078	3.7	0.23	443	552
KL98-10-22-1505m_6	0.00365	0.00045	0.000484	0.000027	-0.039196	3.12	0.17	426	179
KL98-10-22-1505m_7	0.00396	0.00029	0.00051	0.000017	0.011833	3.29	0.11	1120	610
KL98-10-22-1505m_8	0.00357	0.00041	0.000565	0.000028	-0.1154	3.64	0.18	472	198
KL98-10-22-1505m_9	0.00356	0.00036	0.0005	0.000026	-0.07149	3.22	0.17	497	178.7
KL98-10-22-1505m_10	0.00351	0.00035	0.000501	0.000027	0.13597	3.23	0.18	483	207
KL98-10-22-1505m_11	0.00392	0.00045	0.000461	0.000021	0.17811	2.97	0.14	548	226
KL98-10-22-1505m_12	0.00367	0.00027	0.00047	0.000017	0.35704	3.03	0.11	2250	242
KL98-10-22-1505m_13	0.00303	0.00088	0.000451	0.000048	0.22074	2.95	0.3	132.8	77.5
KL98-10-22-1505m_14	0.00383	0.00076	0.000455	0.00004	0.045785	2.93	0.26	191	189
KL98-10-22-1505m_15	0.0039	0.0011	0.000457	0.00005	0.077856	2.95	0.32	130.9	75.7
KL98-10-22-1505m_16	0.00413	0.00045	0.000534	0.000026	0.0016013	3.44	0.16	414	257
KL98-10-22-1505m_17	0.00504	0.00055	0.000499	0.00003	0.10181	3.21	0.19	564	340
KL98-10-22-1505m_18	0.00396	0.00049	0.000494	0.000033	0.13864	3.18	0.21	381	314.1
KL98-10-22-1505m_19	0.00445	0.00053	0.000524	0.000034	0.024638	3.38	0.22	341	284
KL98-10-22-1505m_20	0.1249	0.0048	0.01782	0.00032	0.31667	113.9	2	146	145
KL98-10-22-1505m_21	1.265	0.013	0.132	0.0011	0.54521	799.1	6.2	394	76.1
KL98-10-22-1505m_22	0.1147	0.004	0.01698	0.00035	-0.0071128	108.5	2.2	168.5	159
KL98-10-22-1505m_23	0.6289	0.0063	0.07941	0.00065	0.37242	492.6	3.9	328	262
KL98-10-22-1505m_24	0.3418	0.0042	0.04691	0.00049	0.43867	295.5	3	413	325
KL98-10-22-1505m_25	0.3364	0.0043	0.0474	0.00037	0.21882	298.5	2.3	384	291
KL98-10-22-1505m_26	0.686	0.01	0.08628	0.00072	0.24703	533.4	4.3	136.3	325
KL98-10-22-1505m_27	0.336	0.017	0.0404	0.00047	0.61536	255.3	2.9	258	160
KL98-10-22-1505m_28	0.372	0.011	0.04764	0.00063	-0.19938	300	3.9	167	80.1
KL98-10-22-1505m_29	0.756	0.016	0.0914	0.0013	0.25371	564.7	7.4	92.2	73.9
KL98-10-22-1505m_30	0.1173	0.0039	0.0175	0.00034	-0.087984	111.8	2.1	179	189
KL98-10-22-1544m_1	0.00426	0.00078	0.000521	0.000045	0.3466	3.36	0.29	291	184
KL98-10-22-1544m_2	0.102	0.003	0.01508	0.00037	-0.15221	96.5	2.3	342	263
KL98-10-22-1544m_3	0.0074	0.0012	0.000617	0.000044	0.11279	3.97	0.28	341	182
KL98-10-22-1544m_4	0.00504	0.00064	0.000509	0.000036	0.090247	3.28	0.23	432	235.4
KL98-10-22-1544m_5	0.00409	0.00049	0.000502	0.000028	0.22888	3.24	0.18	744	374
KL98-10-22-1544m_6	0.00369	0.00054	0.000523	0.000029	-0.0009338	3.37	0.18	550	271
KL98-10-22-1544m_7	0.00458	0.00053	0.000518	0.00003	-0.0036533	3.34	0.19	521	275
KL98-10-22-1544m_8	0.00447	0.00058	0.000535	0.000036	-0.063675	3.45	0.23	408	231
KL98-10-22-1544m_9	0.00379	0.00069	0.000485	0.00004	-0.042158	3.13	0.25	308	276
KL98-10-22-1544m_10	0.0056	0.0015	0.000493	0.000055	0.034694	3.18	0.36	154	98.3
KL98-10-22-1544m_11	0.00398	0.0004	0.000508	0.000026	0.10771	3.27	0.16	728	328
KL98-10-22-1544m_12	0.00492	0.00082	0.00052	0.000036	0.010188	3.35	0.24	1300	987
KL98-10-22-1544m_13	0.00552	0.00066	0.000533	0.000031	0.1326	3.43	0.2	697	296

	207Pb/235U	207Pb/235U error	206Pb/238U	206Pb/238U Error	Error Correlation 206/238 vs. 207/235	Final Age (Ma)	Error (Ma)	Approx U (ppm)	Approx Th (ppm)
KL98-10-22-1544m_14	0.00406	0.00049	0.000536	0.000032	0.020366	3.45	0.2	619	230
KL98-10-22-1544m_15	0.00491	0.00058	0.000528	0.000028	-0.18271	3.4	0.18	671	430
KL98-10-22-1544m_16	0.00447	0.00066	0.000505	0.000026	0.00026673	3.25	0.16	680	334
KL98-10-22-1544m_17	0.00412	0.00064	0.000448	0.000037	0.047488	2.88	0.24	353	269.1
KL98-10-22-1544m_18	0.00384	0.00048	0.000491	0.000042	-0.14644	3.16	0.27	576	228
KL98-10-22-1544m_19	0.458	0.012	0.06	0.0013	0.21419	375.8	8.2	401	318
KL98-10-22-1544m_20	0.1383	0.0095	0.01738	0.00033	0.35292	111.1	2.1	789	459
KL98-10-22-1544m_21	0.3056	0.0077	0.04257	0.0009	0.28547	268.7	5.6	367	298
KL98-10-22-1544m_22	0.2631	0.006	0.03791	0.00088	0.27087	239.8	5.5	179	156
KL98-10-22-1544m_23	0.2976	0.0058	0.04132	0.00072	0.33033	261	4.5	471	521
KL98-10-22-1544m_24	0.1168	0.0045	0.01613	0.00039	0.24627	103.1	2.5	482	727
KL98-10-22-1544m_25	0.1167	0.0044	0.01595	0.00034	0.4527	102	2.2	993	1010
KL98-10-22-1544m_26	0.3347	0.0064	0.04697	0.00096	0.25335	295.9	5.9	267	181.2
KL98-10-22-1544m_27	0.2244	0.0082	0.03154	0.00093	0.37588	200.1	5.8	209.2	228.8
KL98-10-22-1544m_28	0.1091	0.0029	0.01631	0.00041	0.20459	104.3	2.6	301.2	365.2
KL98-10-22-1544m_29	0.1292	0.004	0.01883	0.00044	0.14094	120.2	2.8	808	816
KL98-10-22-1544m_30	0.2622	0.0087	0.0355	0.0011	0.30903	225	6.8	187.2	181.4
KL98-10-22-1460m_1	0.0056	0.002	0.000512	0.000064	-0.0054138	3.3	0.41	116.2	101.8
KL98-10-22-1460m_2	0.0035	0.0015	0.00054	0.000064	-0.067569	3.48	0.41	126.4	146.7
KL98-10-22-1460m_3	0.0034	0.0016	0.000416	0.000053	0.032457	2.68	0.34	134.3	141.2
KL98-10-22-1460m_4	0.00486	0.00074	0.000575	0.000041	0.41245	3.71	0.27	439	526
KL98-10-22-1460m_5	0.0039	0.00073	0.000534	0.000036	0.028989	3.44	0.23	399	505
KL98-10-22-1460m_6	0.00432	0.0007	0.000563	0.000045	-0.084681	3.63	0.29	464	351.3
KL98-10-22-1460m_7	0.00439	0.00043	0.000524	0.000023	-0.013691	3.38	0.15	704	344
KL98-10-22-1460m_8	0.00475	0.00044	0.000555	0.000029	0.13666	3.58	0.19	1300	450
KL98-10-22-1460m_9	0.00419	0.00045	0.000522	0.000026	-0.098068	3.37	0.17	693	343.5
KL98-10-22-1460m_10	0.00363	0.00035	0.000538	0.000026	0.023116	3.47	0.17	942	480
KL98-10-22-1460m_11	0.00443	0.0006	0.000506	0.00003	0.1288	3.26	0.2	525	231.6
KL98-10-22-1460m_12	0.0082	0.0013	0.000568	0.000039	0.57412	3.66	0.25	568	270
KL98-10-22-1460m_13	0.00458	0.00083	0.000462	0.000045	0.090723	2.98	0.29	360	384
KL98-10-22-1460m_14	0.072	0.011	0.00109	0.0001	0.71529	7.02	0.67	506	638
KL98-10-22-1460m_15	0.00415	0.00091	0.000558	0.00004	-0.035052	3.59	0.26	415	243
KL98-10-22-1460m_16	0.00484	0.00098	0.000518	0.000039	0.086554	3.34	0.25	398.8	217.2
KL98-10-22-1460m_17	0.00386	0.00059	0.000534	0.000043	-0.027561	3.44	0.28	578	437
KL98-10-22-1460m_18	0.00438	0.00085	0.000547	0.00005	-0.020834	3.53	0.32	340	368
KL98-10-22-1460m_19	0.00414	0.00067	0.000526	0.000028	-0.059578	3.39	0.18	428	236.6
KL98-10-22-1460m_20	0.00403	0.0004	0.000526	0.000032	0.087702	3.39	0.2	588	311
KL98-10-22-1460m_21	0.00382	0.00054	0.000536	0.00004	-0.066547	3.45	0.26	411	320
KL98-10-22-1460m_22	0.00421	0.00057	0.000556	0.000032	0.14338	3.58	0.21	489	510
KL98-10-22-1460m_23	0.357	0.014	0.0456	0.001	0.23635	287.7	6.2	456	246.4
KL98-10-22-1460m_24	0.126	0.0053	0.01731	0.00037	0.16054	110.6	2.4	238.2	228.4
KL98-10-22-1460m_25	0.3177	0.0077	0.04552	0.00096	0.36664	286.9	5.9	315	283
KL98-10-22-1460m_26	0.3328	0.0091	0.04631	0.00081	0.31425	291.8	5	263.3	212.5
KL98-10-22-1460m_27	0.3118	0.0088	0.0446	0.0012	0.51872	281.1	7.6	319	348
KL98-10-21-727m_1	0.00546	0.00098	0.000516	0.000044	-0.26726	3.32	0.28	335	293
KL98-10-21-727m_2	0.0094	0.0019	0.000604	0.000055	0.71101	3.89	0.36	321.9	289
KL98-10-21-727m_3	0.042	0.0045	0.000819	0.00007	0.58116	5.28	0.45	156	155
KL98-10-21-727m_4	0.1134	0.0075	0.00139	0.00012	0.16875	8.95	0.77	62.9	114
KL98-10-21-727m_5	0.0544	0.007	0.000841	0.000089	0.14769	5.42	0.57	81.1	49.5
KL98-10-21-727m_6	0.0175	0.0029	0.000648	0.000054	0.47655	4.18	0.35	226	221
KL98-10-21-727m_7	0.0396	0.0027	0.00071	0.000052	0.31866	4.58	0.34	245.2	299
KL98-10-21-727m_8	0.017	0.0027	0.000625	0.000059	0.23803	4.03	0.38	124	168
KL98-10-21-727m_9	0.00997	0.00095	0.000517	0.000043	-0.10885	3.33	0.28	370	404
KL98-10-21-727m_10	0.0164	0.0019	0.000634	0.000053	0.096185	4.09	0.34	128.4	101.1
KL98-10-21-727m_11	0.00639	0.00051	0.000461	0.000022	0.24031	2.97	0.14	734	873
KL98-10-21-727m_12	0.00683	0.00088	0.000538	0.000033	0.33187	3.47	0.21	316	321
KL98-10-21-727m_13	0.0092	0.0012	0.000557	0.000046	-0.12318	3.59	0.29	247	236
KL98-10-21-727m_14	0.0108	0.0025	0.000553	0.000072	0.020216	3.56	0.46	56	53.9
KL98-10-21-727m_15	0.0238	0.0036	0.000764	0.000084	0.23695	4.92	0.54	110	121.5
KL98-10-21-727m_16	0.0278	0.0026	0.000689	0.000074	0.62588	4.44	0.48	162	126.3
KL98-10-21-727m_17	0.00411	0.00046	0.000501	0.000023	0.042469	3.23	0.15	487	552
KL98-10-21-727m_18	0.0046	0.0011	0.000606	0.000063	0.15545	3.91	0.41	318.2	280
KL98-10-21-727m_19	0.00473	0.00066	0.000493	0.000032	0.052795	3.18	0.2	310	360
KL98-10-21-727m_20	0.032	0.0087	0.0007	0.00011	0.60276	4.49	0.69	369	294
KL98-10-21-727m_21	0.0073	0.0016	0.000506	0.000064	0.14421	3.26	0.41	117.7	135
KL98-10-21-727m_22	0.00645	0.00083	0.000546	0.000047	-0.015964	3.52	0.31	172	119
KL98-10-21-727m_23	0.00396	0.00048	0.000493	0.000034	0.0055376	3.18	0.22	357.7	389.8
KL98-10-21-727m_24	0.0048	0.0012	0.000531	0.000052	-0.18074	3.42	0.33	124	135.6
KL98-10-21-727m_25	0.00422	0.00054	0.000491	0.000029	0.26983	3.16	0.19	325	233
KL98-10-21-727m_26	0.00562	0.00076	0.000576	0.000035	0.26475	3.71	0.23	317	366
KL98-10-21-841m_1	0.0053	0.0013	0.000542	0.000044	0.056617	3.49	0.29	253	251

	207Pb/235U	207Pb/235U error	206Pb/238U	206Pb/238U Error	Error Correlation 206/238 vs. 207/235	Final Age (Ma)	Error (Ma)	Approx U (ppm)	Approx Th (ppm)
KL98-10-21-841m_2	0.0074	0.0012	0.000495	0.000039	0.15289	3.19	0.25	206	210
KL98-10-21-841m_3	0.0094	0.0012	0.000541	0.000041	-0.067255	3.49	0.27	291	279
KL98-10-21-841m_4	0.0209	0.0042	0.000664	0.000079	0.32154	4.28	0.51	161	135
KL98-10-21-841m_5	0.0527	0.0049	0.00091	0.0001	0.43472	5.85	0.65	86.5	96.2
KL98-10-21-841m_6	0.083	0.014	0.00103	0.00024	0.0023808	6.6	1.5	22.05	22.11
KL98-10-21-841m_7	0.00498	0.00093	0.000474	0.000043	0.067853	3.06	0.28	315	264
KL98-10-21-841m_8	0.0102	0.0014	0.000577	0.00005	0.24761	3.72	0.32	393	395
KL98-10-21-841m_9	0.0584	0.0075	0.000934	0.000069	0.76541	6.02	0.45	182	168
KL98-10-21-841m_10	0.0202	0.0027	0.000672	0.000059	0.21643	4.33	0.38	130	112
KL98-10-21-841m_11	0.1056	0.0079	0.00144	0.00015	0.28963	9.25	0.96	52.5	32
KL98-10-21-841m_12	0.0582	0.0067	0.00113	0.00011	0.19477	7.25	0.73	118.2	77.2
KL98-10-21-841m_13	0.924	0.021	0.0769	0.0017	0.56106	477	10	275	53.9
KL98-10-21-841m_14	0.0262	0.0052	0.00072	0.00012	0.038246	4.63	0.78	41	37.3
KL98-10-21-841m_15	0.018	0.0017	0.000665	0.000047	0.21184	4.28	0.3	193	178.4
KL98-10-21-841m_16	0.0215	0.0029	0.000624	0.000043	0.80414	4.02	0.27	350	409
KL98-10-21-841m_17	0.012	0.0016	0.000537	0.000051	-0.17414	3.46	0.33	176.6	185.6
KL98-10-21-841m_18	0.0173	0.0025	0.000647	0.000038	0.40969	4.17	0.25	262	551
KL98-10-21-841m_19	0.015	0.003	0.000553	0.000093	0.32599	3.56	0.6	298	204
KL98-10-21-841m_20	0.00516	0.00094	0.000491	0.000049	0.26315	3.16	0.32	188.5	223
KL98-10-21-841m_21	0.0169	0.0015	0.000613	0.000042	0.15318	3.95	0.27	290	284
KL98-10-21-841m_22	0.00371	0.00096	0.00051	0.000042	-0.093223	3.29	0.27	168	174
KL98-10-21-841m_23	0.00401	0.00047	0.000481	0.000026	-0.21181	3.1	0.17	439	444
KL98-10-21-841m_24	0.00385	0.00035	0.000493	0.000027	0.13706	3.17	0.17	578	319.3
KL98-10-21-922m_1	0.00417	0.00089	0.000514	0.000042	-0.091496	3.31	0.27	280.9	131.6
KL98-10-21-922m_2	0.00339	0.00038	0.000491	0.000031	0.074866	3.16	0.2	1610	810
KL98-10-21-922m_3	0.0043	0.0013	0.000502	0.000055	-0.049885	3.23	0.36	213	249
KL98-10-21-922m_4	0.0038	0.0012	0.000511	0.000058	0.059602	3.3	0.38	232	107
KL98-10-21-922m_5	0.0047	0.0011	0.000559	0.000048	-0.042842	3.6	0.31	201	124.5
KL98-10-21-922m_6	0.00379	0.00087	0.000525	0.000045	-0.029258	3.39	0.29	202	198
KL98-10-21-922m_7	0.00553	0.00087	0.000533	0.000041	-0.16911	3.43	0.26	340	381
KL98-10-21-922m_8	0.0139	0.0012	0.000576	0.000047	0.068589	3.71	0.3	307	328
KL98-10-21-922m_9	0.0045	0.0012	0.000504	0.000058	-0.039829	3.25	0.37	313	299
KL98-10-21-922m_10	0.0093	0.0014	0.000523	0.000044	0.27929	3.37	0.28	254	273
KL98-10-21-922m_11	0.0077	0.0014	0.000544	0.000052	0.069389	3.51	0.34	157	186
KL98-10-21-922m_12	0.0066	0.0015	0.000564	0.000077	0.19823	3.63	0.5	218	220
KL98-10-21-922m_13	0.0056	0.002	0.000476	0.000075	-0.22943	3.07	0.48	277	290
KL98-10-21-922m_14	0.0043	0.001	0.000552	0.000052	-0.04959	3.56	0.34	339	365
KL98-10-21-922m_15	0.005	0.0013	0.000547	0.000051	-0.22415	3.53	0.33	158	164
KL98-10-21-922m_16	0.00471	0.00053	0.000495	0.000034	-0.090545	3.19	0.22	345	362
KL98-10-21-922m_17	0.0202	0.0027	0.000655	0.000049	0.55746	4.22	0.32	383.8	296.2
KL98-10-21-922m_18	0.00524	0.00067	0.000549	0.000044	-0.23159	3.54	0.29	314	392
KL98-10-21-922m_19	0.0053	0.0011	0.000511	0.000047	-0.071441	3.3	0.3	220.7	299.9
KL98-10-21-922m_20	0.00414	0.00075	0.000508	0.000058	-0.21074	3.27	0.37	345	250
KL98-10-21-922m_21	0.458	0.028	0.06	0.0034	0.78092	375	21	189.1	160.2
KL98-10-21-922m_22	0.0049	0.0012	0.00052	0.000069	-0.12476	3.35	0.44	151.8	118.8
KL98-10-21-922m_23	0.0056	0.0016	0.00052	0.000076	0.15825	3.35	0.49	187	210
KL98-10-21-922m_24	0.00549	0.00096	0.000512	0.000038	0.22671	3.3	0.24	422	406
KL98-10-21-922m_25	0.0138	0.0025	0.000613	0.00009	0.18761	3.95	0.58	86.2	66.6
KL98-10-21-922m_26	4.73	0.17	0.297	0.01	0.94599	1673	52	105.1	33.8
KL98-10-21-948m_1	0.0079	0.0019	0.000518	0.000066	0.028507	3.34	0.43	128	122.2
KL98-10-21-948m_2	0.0051	0.0019	0.000598	0.000074	0.1922	3.85	0.48	126	138
KL98-10-21-948m_3	0.0048	0.0014	0.000513	0.000056	-0.070943	3.3	0.36	145	148
KL98-10-21-948m_4	0.0087	0.0025	0.000523	0.00008	-0.11061	3.37	0.52	83.8	65.8
KL98-10-21-948m_5	0.0039	0.0012	0.000501	0.000046	-0.047152	3.23	0.3	224	184
KL98-10-21-948m_6	0.0034	0.0015	0.000524	0.000075	0.063293	3.38	0.48	379.4	290.5
KL98-10-21-948m_7	0.0029	0.0013	0.000494	0.00008	-0.21346	3.18	0.51	119.5	128.9
KL98-10-21-948m_8	0.0039	0.0012	0.00056	0.000072	-0.10531	3.61	0.46	151	98
KL98-10-21-948m_9	0.00337	0.0008	0.000544	0.000047	-0.17225	3.5	0.3	224.1	181.6
KL98-10-21-948m_10	0.0142	0.0021	0.000581	0.000059	-0.10921	3.74	0.38	148	120
KL98-10-21-948m_11	0.0073	0.0013	0.00061	0.000067	-0.14963	3.93	0.43	378	369
KL98-10-21-948m_12	0.00379	0.00047	0.000502	0.000034	-0.015795	3.24	0.22	717	521
KL98-10-21-948m_13	0.0156	0.0031	0.000689	0.000088	0.071527	4.44	0.57	130	130
KL98-10-21-948m_14	0.00413	0.00084	0.000529	0.000043	0.063471	3.41	0.28	279	331
KL98-10-21-948m_15	0.0047	0.00066	0.00049	0.000036	0.019124	3.16	0.23	490	211
KL98-10-21-948m_16	0.00408	0.00081	0.000517	0.000059	0.10771	3.33	0.38	401	429
KL98-10-21-948m_17	0.0059	0.0019	0.000567	0.000079	0.11414	3.65	0.51	128	98.6
KL98-10-21-948m_18	0.0046	0.002	0.000606	0.000083	-0.03721	3.9	0.53	93.4	53.6
KL98-10-21-948m_19	0.0078	0.0017	0.000535	0.000074	-0.094232	3.45	0.48	133.6	94.5
KL98-10-21-948m_20	0.0108	0.003	0.00061	0.00011	0.28378	3.94	0.72	100.6	81.5
KL98-10-21-948m_21	0.0041	0.001	0.000554	0.000054	0.16522	3.57	0.35	228	238
KL98-10-21-948m_22	0.0042	0.0011	0.00053	0.000055	-0.059734	3.41	0.36	371	423

	207Pb/235U	207Pb/235U error	206Pb/238U	206Pb/238U Error	Error Correlation 206/238 vs. 207/235	Final Age (Ma)	Error (Ma)	Approx U (ppm)	Approx Th (ppm)
KL98-10-21-948m_23	0.00492	0.00097	0.000525	0.000053	-0.11102	3.39	0.34	212	224
KL98-10-21-948m_24	0.0114	0.0034	0.000503	0.000099	-0.06931	3.24	0.64	78.7	56.81
KL98-10-21-948m_25	0.00468	0.00091	0.000528	0.000046	-0.090882	3.4	0.3	333.7	264.5
KL98-10-21-948m_26	0.315	0.011	0.04393	0.00089	0.32691	277.1	5.5	136	80
KL98-10-21-948m_27	4.66	0.042	0.3004	0.0034	0.72511	1693	17	446	239.9
KL98-10-21-948m_28	0.3139	0.0054	0.04415	0.00057	0.24482	278.5	3.5	367	222
KL98-10-21-948m_29	11.085	0.072	0.4746	0.0035	0.53049	2503	15	124.5	179
KL98-10-21-982m_1	0.00618	0.00097	0.00056	0.000058	-0.011445	3.61	0.37	148	187
KL98-10-21-982m_2	0.00805	0.00075	0.000548	0.000038	-0.093402	3.53	0.24	305	261
KL98-10-21-982m_3	0.0057	0.0011	0.000502	0.000047	-0.2802	3.24	0.31	169.4	185
KL98-10-21-982m_4	0.0048	0.0011	0.000537	0.000051	0.1388	3.46	0.33	177	171
KL98-10-21-982m_5	0.00469	0.00065	0.00047	0.000041	-0.1576	3.03	0.26	317	389
KL98-10-21-982m_6	0.0137	0.0016	0.000484	0.00005	0.18799	3.12	0.32	112.6	101
KL98-10-21-982m_7	0.0219	0.0022	0.00065	0.000072	0.10061	4.19	0.46	122.3	101.1
KL98-10-21-982m_8	0.0272	0.0025	0.000806	0.000062	0.29188	5.19	0.4	137.3	151.4
KL98-10-21-982m_9	0.0417	0.0035	0.000828	0.00008	0.22312	5.33	0.52	109	114
KL98-10-21-982m_10	0.0345	0.0054	0.00082	0.00017	-0.1754	5.3	1.1	100	147
KL98-10-21-982m_11	0.0291	0.0032	0.000788	0.000097	-0.24289	5.08	0.63	189	236
KL98-10-21-982m_12	0.0176	0.0019	0.000696	0.000077	0.29267	4.48	0.49	104.3	136
KL98-10-21-982m_13	0.01	0.0013	0.000635	0.000051	-0.048637	4.09	0.33	203	237
KL98-10-21-982m_14	0.023	0.0028	0.000694	0.000089	0.20642	4.47	0.57	85.6	138.5
KL98-10-21-982m_15	0.0653	0.0052	0.001044	0.00009	0.3169	6.72	0.58	103	65
KL98-10-21-982m_16	0.0045	0.00056	0.000511	0.000033	0.071372	3.29	0.21	455	610
KL98-10-21-982m_17	0.006	0.0014	0.000516	0.000059	0.078673	3.32	0.38	113	119
KL98-10-21-982m_18	0.00538	0.00096	0.000504	0.000039	0.08247	3.25	0.25	251	286
KL98-10-21-982m_19	0.0077	0.0012	0.00048	0.000043	-0.11202	3.09	0.28	196	203
KL98-10-21-982m_20	0.052	0.011	0.00083	0.0001	0.75471	5.38	0.65	155	375
KL98-10-21-982m_21	0.278	0.011	0.03642	0.00099	0.17041	230.6	6.1	88.3	51.1
KL98-10-21-1132m_1	0.0074	0.001	0.000494	0.000051	0.12275	3.18	0.33	297	403
KL98-10-21-1132m_2	0.0079	0.0022	0.00058	0.0001	0.23383	3.73	0.66	470	312
KL98-10-21-1132m_3	0.0038	0.0011	0.000525	0.000058	0.0027994	3.38	0.38	167.4	139.7
KL98-10-21-1132m_4	0.00356	0.00092	0.000494	0.000052	-0.00050874	3.18	0.33	170.4	216.3
KL98-10-21-1132m_5	0.0046	0.0015	0.000562	0.00007	-0.14705	3.62	0.45	136	140.2
KL98-10-21-1132m_6	0.0064	0.0021	0.000511	0.000072	0.047464	3.3	0.46	133.3	118.9
KL98-10-21-1132m_7	0.0059	0.0014	0.000557	0.000052	0.030752	3.59	0.34	166	158
KL98-10-21-1132m_8	0.0041	0.0014	0.000487	0.000068	0.30427	3.14	0.44	591	523
KL98-10-21-1132m_9	0.0046	0.0044	0.00041	0.00013	0.77632	2.62	0.83	210	174
KL98-10-21-1132m_10	0.0061	0.0024	0.00057	0.0001	-0.393	3.67	0.65	117.3	111
KL98-10-21-1132m_11	0.0039	0.0012	0.000473	0.00007	0.10059	3.05	0.45	147.5	133
KL98-10-21-1132m_12	0.0058	0.0015	0.000522	0.000069	-0.06433	3.37	0.45	141.1	194
KL98-10-21-1132m_13	0.048	0.0074	0.000897	0.000096	0.50273	5.78	0.62	318	278
KL98-10-21-1132m_14	0.0036	0.0021	0.00054	0.00013	-0.0069962	3.49	0.86	134.3	153.8
KL98-10-21-1132m_15	0.0035	0.0015	0.000566	0.000077	0.27139	3.65	0.49	122	142
KL98-10-21-1132m_16	0.005	0.0012	0.000553	0.00007	-0.059112	3.56	0.45	136	166
KL98-10-21-1132m_17	0.007	0.0017	0.000597	0.000064	-0.078716	3.85	0.41	141.6	118
KL98-10-21-1132m_18	0.004	0.001	0.000559	0.000053	0.13739	3.6	0.34	164.8	145.9
KL98-10-21-1132m_19	0.007	0.002	0.000548	0.000068	-0.21983	3.53	0.44	99	114.5
KL98-10-21-1132m_20	0.0041	0.0014	0.000587	0.000055	0.24219	3.79	0.35	125.5	152.6
KL98-10-21-1132m_21	0.0176	0.0022	0.000651	0.000075	0.22347	4.19	0.48	144	87.8
KL98-10-21-1132m_22	0.00518	0.00064	0.000535	0.000021	0.41668	3.45	0.14	1667	1094
KL98-10-21-1132m_23	0.021	0.0037	0.000819	0.000096	-0.031361	5.27	0.62	94.4	78.4
KL98-10-21-1132m_24	0.0046	0.0012	0.000543	0.000053	0.052704	3.5	0.34	153	115
KL98-10-21-1132m_25	0.00443	0.00072	0.000575	0.000041	0.03721	3.71	0.26	361	188
KL98-10-21-1132m_26	24.63	0.41	0.6305	0.0077	0.78283	3151	31	108.8	63.8
KL98-10-21-1132m_27	0.3688	0.0091	0.04918	0.00058	0.065321	309.5	3.5	273	140.4
KL98-10-21-1132m_28	5.151	0.076	0.3288	0.0092	0.79638	1832	45	420	46.1
KL98-10-21-1132m_29	11.22	0.14	0.48	0.0051	0.47178	2527	22	136.7	49.6
KL98-10-21-1132m_30	0.444	0.015	0.04991	0.00088	0.28605	313.9	5.4	117.3	110
KL98-10-21-1132m_31	2.514	0.056	0.2146	0.0038	0.41379	1253	20	68.4	67.16
KL98-10-21-1132m_32	0.3504	0.0065	0.04688	0.00056	0.33048	295.3	3.5	345	314
KL98-10-21-1132m_33	9.59	0.11	0.4443	0.0037	0.65337	2370	17	168	141
KL98-10-21-1132m_34	3.333	0.033	0.2538	0.0023	0.85287	1458	12	730	301
KL98-10-21-1132m_35	0.3635	0.0084	0.0496	0.00085	0.79308	312	5.2	470	379
KL98-10-21-1192m_1	0.0104	0.0012	0.000554	0.000041	0.094435	3.57	0.26	196	170
KL98-10-21-1192m_2	0.0045	0.0011	0.000523	0.00005	-0.038688	3.37	0.32	111.5	103.6
KL98-10-21-1192m_3	0.00426	0.00049	0.000519	0.000023	0.47546	3.34	0.15	794	1250
KL98-10-21-1192m_4	0.00523	0.00074	0.000521	0.000038	-0.076728	3.36	0.24	276	394
KL98-10-21-1192m_5	0.0076	0.0023	0.00063	0.00012	0.15344	4.04	0.75	271	222
KL98-10-21-1192m_6	0.009	0.0022	0.000555	0.000041	0.54831	3.58	0.27	710	940
KL98-10-21-1192m_7	0.0088	0.0024	0.000609	0.000071	0.066253	3.92	0.46	139.8	144.1
KL98-10-21-1192m_8	0.00438	0.00094	0.000581	0.000064	-0.13244	3.75	0.41	182	215

	207Pb/235U	207Pb/235U error	206Pb/238U	206Pb/238U Error	Error Correlation 206/238 vs. 207/235	Final Age (Ma)	Error (Ma)	Approx U (ppm)	Approx Th (ppm)
KL98-10-21-1192m_9	0.0095	0.001	0.0005	0.000041	-0.063077	3.22	0.26	176	101.6
KL98-10-21-1192m_10	0.0043	0.0016	0.000623	0.000082	-0.11582	4.02	0.53	158	161
KL98-10-21-1192m_11	0.0049	0.0011	0.000541	0.00005	0.091983	3.49	0.32	139.5	97.9
KL98-10-21-1192m_12	0.0077	0.0014	0.000612	0.000071	0.24398	3.94	0.46	114.3	130.8
KL98-10-21-1192m_13	0.00561	0.00086	0.000526	0.000042	0.062945	3.39	0.27	192	192
KL98-10-21-1192m_14	0.00442	0.00093	0.000533	0.000048	0.0019684	3.44	0.31	144	131.4
KL98-10-21-1192m_15	0.00438	0.00067	0.000483	0.000037	-0.088059	3.11	0.24	175	141
KL98-10-21-1192m_16	0.0058	0.0012	0.000505	0.000045	-0.057409	3.26	0.29	372	415
KL98-10-21-1192m_17	0.0075	0.0019	0.000478	0.000079	0.13537	3.08	0.51	94	81
KL98-10-21-1192m_18	0.0274	0.006	0.000756	0.000079	0.42369	4.87	0.51	213	211.8
KL98-10-21-1192m_19	0.0058	0.0014	0.000554	0.000068	-0.014222	3.57	0.44	121.6	98.3
KL98-10-21-1192m_20	0.0057	0.0011	0.000494	0.000042	0.12278	3.18	0.27	151	148
KL98-10-21-1192m_21	0.0077	0.0017	0.000534	0.000057	0.37478	3.44	0.36	212	184
KL98-10-21-1192m_22	0.00374	0.00068	0.000535	0.000041	-0.072568	3.45	0.27	205	250
KL98-10-21-1192m_23	0.036	0.0064	0.00084	0.00011	0.46666	5.41	0.69	121.7	152
KL98-10-21-1192m_24	0.0036	0.00089	0.000561	0.000052	0.21967	3.62	0.34	116	104
KL98-10-21-1192m_25	0.0212	0.006	0.00066	0.000092	0.30004	4.25	0.6	90	59.5
KL98-10-21-1192m_26	0.0071	0.0014	0.000546	0.000063	0.063291	3.52	0.41	112	119
KL98-10-21-1192m_27	0.00373	0.00066	0.000531	0.000035	0.11878	3.42	0.22	251	224
KL98-10-21-1192m_28	0.2414	0.0062	0.0331	0.00065	0.17678	209.9	4	343	368
KL98-10-22-1254m_1	0.00847	0.00089	0.000633	0.000044	0.18612	4.08	0.28	361.8	267.3
KL98-10-22-1254m_2	0.00655	0.00096	0.000556	0.000036	0.049375	3.58	0.23	302	266.7
KL98-10-22-1254m_3	0.0155	0.0034	0.000571	0.000051	0.71755	3.68	0.33	380	381
KL98-10-22-1254m_4	0.00553	0.00075	0.000516	0.000039	-0.089956	3.33	0.25	292	242
KL98-10-22-1254m_5	0.0365	0.0039	0.000853	0.000075	0.41204	5.5	0.48	153	119
KL98-10-22-1254m_6	0.005	0.001	0.000512	0.000058	0.26894	3.3	0.37	336	234
KL98-10-22-1254m_7	0.0113	0.0018	0.000524	0.000057	-0.069065	3.38	0.37	119	122
KL98-10-22-1254m_8	0.0089	0.0018	0.000473	0.000066	0.046674	3.05	0.42	107	93
KL98-10-22-1254m_9	0.00589	0.00067	0.000486	0.000035	0.03257	3.13	0.22	610	365
KL98-10-22-1254m_10	0.0092	0.0018	0.000612	0.000047	-0.05092	3.95	0.3	278	258
KL98-10-22-1254m_11	0.0198	0.0036	0.000628	0.000058	0.4906	4.05	0.37	374	323
KL98-10-22-1254m_12	0.00708	0.00099	0.000508	0.000037	0.080786	3.27	0.24	337	308
KL98-10-22-1254m_13	0.00509	0.00069	0.0005	0.000041	0.18069	3.22	0.26	341	554
KL98-10-22-1254m_14	0.00671	0.00069	0.000525	0.00003	0.041964	3.38	0.19	360	360
KL98-10-22-1254m_15	0.00482	0.00055	0.000497	0.000025	0.0528	3.21	0.16	509	760
KL98-10-22-1254m_16	0.00602	0.00088	0.000583	0.000035	-0.10565	3.76	0.23	407	424
KL98-10-22-1254m_17	0.0069	0.0014	0.000492	0.000038	-0.0015838	3.17	0.25	191	129.5
KL98-10-22-1254m_18	0.00659	0.00096	0.000527	0.000033	0.31622	3.4	0.21	374.3	350
KL98-10-22-1254m_19	0.00542	0.0008	0.000522	0.000038	-0.013598	3.36	0.25	364	370
KL98-10-22-1254m_20	0.00548	0.00068	0.000579	0.000054	-0.1691	3.73	0.35	740	650
KL98-10-22-1254m_21	0.0122	0.0027	0.000566	0.000068	0.38747	3.65	0.44	362	241
KL98-10-22-1254m_22	0.0054	0.0011	0.000543	0.000057	-0.082521	3.5	0.36	147	105.1
KL98-10-22-1254m_23	0.0058	0.0012	0.000484	0.000043	0.050274	3.12	0.28	144.9	109.5
KL98-10-22-1254m_24	0.00476	0.00046	0.000518	0.000031	0.21064	3.34	0.2	429	435
KL98-10-22-1254m_25	0.0102	0.0015	0.000613	0.000051	0.088189	3.95	0.33	155	103
KL98-10-22-1254m_26	0.00506	0.00049	0.00051	0.000025	-0.19752	3.29	0.16	553	738
KL98-10-22-1254m_27	4.541	0.067	0.296	0.0032	0.78106	1671	16	566	139
KL98-10-22-1254m_28	0.3262	0.0068	0.04453	0.00052	0.35146	280.8	3.2	242	184.9
KL98-10-22-1254m_29	0.3054	0.0051	0.04346	0.00041	0.25039	274.2	2.5	350	345
KL98-10-22-1254m_30	0.405	0.011	0.054	0.001	0.29537	339.3	6.3	180.8	233
KL98-10-22-1344m_1	0.0077	0.0015	0.000508	0.00005	0.33723	3.27	0.32	887.9	2037
KL98-10-22-1344m_2	0.0072	0.0016	0.000596	0.000079	0.153	3.84	0.51	369	286
KL98-10-22-1344m_3	0.00392	0.00077	0.000497	0.000048	-0.17332	3.28	0.29	515	535
KL98-10-22-1344m_4	0.0043	0.002	0.0006	0.0001	-0.043508	3.85	0.66	131.8	134.7
KL98-10-22-1344m_5	0.012	0.0019	0.000654	0.000065	-0.12088	4.21	0.42	417	349.8
KL98-10-22-1344m_6	0.0047	0.0012	0.000489	0.000071	-0.18385	3.15	0.45	313.5	276.7
KL98-10-22-1344m_7	0.0051	0.0026	0.00049	0.0001	0.027993	3.17	0.65	102.9	104
KL98-10-22-1344m_8	0.0071	0.0025	0.00043	0.0001	0.12865	2.77	0.65	134.3	115.8
KL98-10-22-1344m_9	0.0073	0.003	0.00053	0.00014	0.20988	3.43	0.92	159.5	133
KL98-10-22-1344m_10	0.0135	0.0046	0.00045	0.00013	0.12997	2.9	0.85	103	87.7
KL98-10-22-1344m_11	0.00374	0.00061	0.000427	0.000033	0.1637	2.75	0.21	889	1170
KL98-10-22-1344m_12	0.0591	0.0086	0.000959	0.000097	0.79334	6.18	0.63	553	460
KL98-10-22-1344m_13	0.0057	0.0016	0.000473	0.000058	-0.16207	3.05	0.37	535	560
KL98-10-22-1344m_14	0.0079	0.0011	0.000516	0.000042	0.35818	3.32	0.27	1110	197
KL98-10-22-1344m_15	0.0056	0.0014	0.000536	0.000071	-0.0074458	3.45	0.46	321	255
KL98-10-22-1344m_16	0.085	0.017	0.00108	0.00015	0.70871	6.94	0.98	178.7	204
KL98-10-22-1344m_17	0.006	0.0014	0.000578	0.000071	-0.19092	3.72	0.46	409	334
KL98-10-22-1344m_18	0.0046	0.0014	0.000553	0.000078	0.083552	3.56	0.5	254.1	230.1
KL98-10-22-1344m_19	0.0022	0.002	0.00046	0.00011	0.055	2.99	0.72	108.3	139
KL98-10-22-1344m_20	0.0063	0.0018	0.000663	0.000077	0.084313	4.27	0.5	226	149.3
KL98-10-22-1344m_21	5.011	0.046	0.3272	0.0033	0.55725	1824	16	401	315.3

	207Pb/235U	207Pb/235U error	206Pb/238U	206Pb/238U Error	Error Correlation 206/238 vs. 207/235	Final Age (Ma)	Error (Ma)	Approx U (ppm)	Approx Th (ppm)
KL98-10-22-1344m_22	8.055	0.087	0.397	0.0041	0.43491	2155	19	180.2	112
KL98-10-22-1344m_23	0.433	0.025	0.0401	0.0011	-0.10873	253.1	6.9	64.5	70.2
KL98-10-22-1344m_24	0.305	0.023	0.0401	0.0014	-0.01805	253.5	8.4	75.6	52.6
KL98-10-22-1344m_25	8.74	0.14	0.4159	0.005	0.85122	2241	23	513.1	188
KL98-10-22-1344m_26	7.098	0.081	0.3726	0.0049	0.60951	2041	23	1195	327
KL98-10-22-1344m_27	0.251	0.011	0.03333	0.0008	0.080537	211.3	5	233	123
KL98-10-22-1344m_28	0.1654	0.0052	0.02304	0.00047	0.25263	146.8	3	327	187.8
KL98-10-22-1344m_29	4.315	0.049	0.2779	0.0031	0.66946	1581	16	1533	222.4
KL98-10-22-1344m_30	1.528	0.018	0.1001	0.0021	0.045232	615	12	562	492.6
KL98-10-22-1386m_1	0.004	0.0011	0.00057	0.000071	0.0098477	3.67	0.46	249	209
KL98-10-22-1386m_2	0.0078	0.0032	0.000564	0.000038	0.10894	3.63	0.24	310	300
KL98-10-22-1386m_3	0.0046	0.00093	0.000516	0.000036	-0.046734	3.33	0.24	299	295
KL98-10-22-1386m_4	0.00441	0.00057	0.000563	0.000032	0.17987	3.63	0.21	379	401
KL98-10-22-1386m_5	0.00425	0.00069	0.000518	0.000039	-0.075101	3.34	0.25	254	225
KL98-10-22-1386m_6	0.0075	0.0014	0.000584	0.00004	0.35196	3.77	0.26	277	269
KL98-10-22-1386m_7	0.00404	0.00085	0.000554	0.000035	0.083649	3.57	0.23	269	271
KL98-10-22-1386m_8	0.00457	0.00054	0.00054	0.000034	0.039567	3.48	0.22	404	455
KL98-10-22-1386m_9	0.0083	0.0019	0.00061	0.00007	-0.0815	3.93	0.45	166	153.1
KL98-10-22-1386m_10	0.0068	0.0012	0.000574	0.000029	0.41637	3.7	0.19	493	448
KL98-10-22-1386m_11	0.0054	0.0011	0.000498	0.000057	0.12214	3.21	0.37	187	141
KL98-10-22-1386m_12	0.0038	0.0013	0.000531	0.000064	-0.072699	3.42	0.41	273	288
KL98-10-22-1386m_13	0.0098	0.001	0.000599	0.000053	0.11522	3.86	0.34	240	228
KL98-10-22-1386m_14	0.0134	0.0042	0.000603	0.000047	0.11408	3.88	0.3	257	235
KL98-10-22-1386m_15	0.00782	0.00084	0.000573	0.000031	0.041815	3.69	0.2	481	781
KL98-10-22-1386m_16	0.00485	0.00097	0.000542	0.000049	0.0094408	3.49	0.32	251	235
KL98-10-22-1386m_17	0.0062	0.003	0.00046	0.00012	-0.33246	3	0.78	308	179
KL98-10-22-1386m_18	0.00399	0.00059	0.000516	0.000025	0.065346	3.32	0.16	531	650
KL98-10-22-1386m_19	0.0071	0.0015	0.000517	0.000056	0.53232	3.33	0.36	441	419
KL98-10-22-1386m_20	0.006	0.0014	0.000526	0.000051	-0.051125	3.39	0.33	228	254
KL98-10-22-1386m_21	0.0061	0.0011	0.000517	0.000045	-0.032285	3.33	0.29	289	282
KL98-10-22-1386m_22	0.0076	0.0019	0.000554	0.000071	0.51174	3.57	0.45	418	454
KL98-10-22-1386m_23	0.0057	0.0011	0.00056	0.000049	0.2127	3.61	0.32	222	263
KL98-10-22-1386m_24	0.00384	0.00092	0.000529	0.00005	-0.025502	3.41	0.32	191.3	196.3
KL98-10-22-1386m_25	0.0054	0.0013	0.000563	0.000066	-0.016009	3.63	0.42	189	194.6
KL98-10-22-1386m_26	0.0098	0.0018	0.000534	0.00005	0.31522	3.44	0.32	278	363
KL98-10-22-1386m_27	0.00588	0.00094	0.000537	0.000049	-0.078356	3.46	0.31	228	218
KL98-10-22-1386m_28	0.00671	0.00096	0.000546	0.000035	0.43862	3.52	0.23	411	454
KL98-10-22-1386m_29	0.00499	0.00079	0.000546	0.000043	0.19118	3.52	0.28	363	379
KL98-10-22-1386m_30	0.0052	0.00096	0.000511	0.000047	-0.054283	3.29	0.3	281	297
KL98-10-22-1386m_31	2.394	0.04	0.218	0.0056	0.74682	1276	28	127.1	78.9
ID41E-02-645m_1	0.00513	0.00077	0.000497	0.000044	0.12897	3.2	0.28	395.6	106.4
ID41E-02-645m_2	0.0074	0.0013	0.000408	0.000036	0.48667	2.63	0.23	422	216
ID41E-02-645m_3	0.0067	0.0016	0.000597	0.000092	0.35163	3.85	0.59	236.4	72.3
ID41E-02-645m_4	0.0035	0.0007	0.00044	0.000044	0.17848	2.84	0.28	402	226
ID41E-02-645m_5	0.00403	0.00097	0.000468	0.000056	0.077177	3.02	0.36	335	153
ID41E-02-645m_6	0.0058	0.0013	0.000482	0.000055	0.1046	3.1	0.36	323	140
ID41E-02-645m_7	0.0032	0.002	0.000364	0.000082	0.2222	2.35	0.53	100.7	66.9
ID41E-02-645m_8	0.0071	0.002	0.00049	0.00011	0.12741	3.17	0.7	201	79.3
ID41E-02-645m_9	0.0043	0.0014	0.000488	0.000074	0.16239	3.14	0.48	193	126
ID41E-02-645m_10	0.00526	0.00099	0.000408	0.000047	0.22306	2.63	0.3	492	208
ID41E-02-645m_11	0.0053	0.0012	0.0005	0.00006	0.12417	3.22	0.38	293	107.8
ID41E-02-645m_12	0.0034	0.001	0.000453	0.000051	0.15048	2.92	0.33	338	97.7
ID41E-02-645m_13	0.0046	0.0021	0.000475	0.000077	0.034291	3.06	0.49	136.6	140
ID41E-02-645m_14	0.0044	0.001	0.000427	0.000038	0.012946	2.75	0.25	401	219
ID41E-02-645m_15	0.0051	0.0018	0.00045	0.000075	0.25036	2.9	0.48	216	67.1
ID41E-02-645m_16	0.0035	0.001	0.000551	0.000066	0.020666	3.55	0.43	401	188
ID41E-02-645m_17	0.0078	0.0019	0.000491	0.000073	0.049662	3.17	0.47	157.9	127
ID41E-02-645m_18	0.0052	0.0013	0.000465	0.000051	0.31532	2.99	0.33	344.4	150.5
ID41E-02-645m_19	0.00353	0.0007	0.000462	0.00004	0.14716	2.98	0.26	401.4	217
ID41E-02-645m_20	0.00307	0.00059	0.000381	0.000038	0.06197	2.45	0.24	390	180.1
ID41E-02-645m_21	0.00443	0.00079	0.000395	0.000037	0.00080291	2.55	0.24	403	180.5
ID41E-02-645m_22	0.00369	0.00069	0.000406	0.000043	0.057586	2.62	0.28	380	174.2
ID41E-02-645m_23	0.0032	0.0013	0.000382	0.000059	0.07941	2.46	0.38	327	190
ID41E-02-645m_24	0.00387	0.00062	0.000431	0.000045	0.1807	2.78	0.29	481	230.3
ID41E-02-645m_25	0.00384	0.00057	0.000465	0.00004	0.14569	3	0.25	514.4	254
ID41E-02-645m_26	0.00417	0.00066	0.000471	0.000032	0.028866	3.03	0.2	548	219
ID41E-02-645m_27	0.00522	0.00073	0.000508	0.000037	0.00010993	3.27	0.24	398	119.6
ID41E-02-645m_28	0.0071	0.0021	0.000526	0.000072	0.077559	3.39	0.46	118.1	83.2
BG-WSH-04-237m_1	0.0182	0.0024	0.000702	0.000069	0.1479	4.52	0.44	237	303
BG-WSH-04-237m_2	0.0266	0.0093	0.000668	0.000094	0.039477	4.3	0.6	216.4	226.5
BG-WSH-04-237m_3	0.0303	0.0054	0.0008	0.00011	0.49356	5.18	0.71	161.7	134

	207Pb/235U	207Pb/235U error	206Pb/238U	206Pb/238U Error	Error Correlation 206/238 vs. 207/235	Final Age (Ma)	Error (Ma)	Approx U (ppm)	Approx Th (ppm)
BG-WSH-04-237m_4	0.0125	0.003	0.000606	0.000084	0.10444	3.9	0.54	155.2	188
BG-WSH-04-237m_5	0.022	0.0033	0.000625	0.000082	0.023002	4.03	0.53	146	107.4
BG-WSH-04-237m_6	0.0774	0.0068	0.00119	0.00014	0.21277	7.64	0.88	87.1	90.6
BG-WSH-04-237m_7	0.093	0.052	0.00073	0.0001	0.22621	4.69	0.68	74.7	86.7
BG-WSH-04-237m_8	0.006	0.0013	0.000507	0.000057	0.043909	3.27	0.37	327	535
BG-WSH-04-237m_9	0.0739	0.0085	0.00101	0.00012	0.49289	6.48	0.79	72	81.7
BG-WSH-04-237m_10	0.0157	0.0023	0.000558	0.000064	0.09398	3.6	0.41	153.4	116.4
BG-WSH-04-237m_11	0.0183	0.0031	0.000572	0.000086	0.23372	3.68	0.56	88.6	123.7
BG-WSH-04-237m_12	0.024	0.013	0.000489	0.000046	0.0026179	3.15	0.3	230.3	336.2
BG-WSH-04-237m_13	0.016	0.0048	0.00052	0.000091	0.13469	3.35	0.58	70.7	73.8
BG-WSH-04-237m_14	0.0136	0.0032	0.000462	0.00008	0.088465	2.97	0.51	64.1	76.2
BG-WSH-04-237m_15	0.0156	0.0048	0.000538	0.000095	0.063795	3.46	0.61	60.4	89.1
BG-WSH-04-237m_16	0.0167	0.0038	0.00048	0.00011	0.22938	3.07	0.69	102.3	111
BG-WSH-04-237m_17	0.0191	0.003	0.000487	0.000068	0.11578	3.14	0.44	80.3	120.4
BG-WSH-04-237m_18	0.0103	0.0023	0.000497	0.000066	0.22262	3.2	0.42	96.9	106.1
BG-WSH-04-237m_19	0.0159	0.0043	0.000533	0.000082	0.002183	3.43	0.53	74.3	111
BG-WSH-04-237m_20	0.023	0.01	0.000554	0.000075	0.0024464	3.57	0.48	103.5	103.9
BG-WSH-04-237m_21	0.046	0.023	0.000659	0.000079	0.18427	4.25	0.51	86.5	102.4
BG-WSH-04-237m_22	0.01	0.0032	0.000506	0.000078	0.29551	3.26	0.5	117.2	199.8
BG-WSH-04-237m_23	0.0145	0.0054	0.000481	0.000098	0.057664	3.1	0.63	69.1	113
BG-WSH-04-237m_24	0.0165	0.004	0.000558	0.000089	0.40794	3.6	0.57	100.9	147.8
BG-WSH-04-237m_25	0.021	0.018	0.000578	0.000094	0.094777	3.72	0.6	107.3	117.5
BG-WSH-04-237m_26	0.0086	0.0027	0.000476	0.000073	0.16132	3.07	0.47	100.1	122.8
BG-WSH-04-237m_27	0.181	0.015	0.0021	0.00021	0.42797	13.5	1.4	55	53.5
BG-WSH-04-237m_28	0.087	0.0078	0.001269	0.00009	0.14933	8.18	0.58	101.6	150.9
BG-WSH-04-241.6m_1	0.0136	0.0068	0.000541	0.000056	0.072771	3.49	0.36	114.5	98.5
BG-WSH-04-241.6m_2	0.0043	0.0017	0.000433	0.000062	0.024868	2.79	0.4	90.4	128.8
BG-WSH-04-241.6m_3	0.0034	0.0015	0.00045	0.000061	0.2515	2.9	0.39	109.2	140.5
BG-WSH-04-241.6m_4	0.0019	0.0016	0.000403	0.000074	0.0072285	2.6	0.48	81.9	108.1
BG-WSH-04-241.6m_5	0.0076	0.0044	0.000519	0.000065	0.088681	3.34	0.42	97.9	99.3
BG-WSH-04-241.6m_6	0.0034	0.0019	0.000438	0.000069	0.058148	2.83	0.44	89.4	115.8
BG-WSH-04-241.6m_7	0.013	0.008	0.000501	0.000086	0.0088618	3.23	0.56	63.2	64.3
BG-WSH-04-241.6m_8	0.0094	0.0057	0.000445	0.000081	0.04139	2.87	0.52	79.4	77.8
BG-WSH-04-241.6m_9	0.0042	0.003	0.000456	0.000085	0.070512	2.94	0.55	62.8	58.2
BG-WSH-04-241.6m_10	0.0036	0.0021	0.000473	0.000083	0.084741	3.05	0.53	92.7	138.1
BG-WSH-04-241.6m_11	0.008	0.0043	0.00056	0.00015	0.034154	3.58	0.94	101.1	106.6
BG-WSH-04-241.6m_12	0.0067	0.0021	0.000428	0.000063	0.11951	2.76	0.41	92.3	129.8
BG-WSH-04-241.6m_13	0.0037	0.0016	0.000476	0.000053	0.071981	3.07	0.34	158	158
BG-WSH-04-241.6m_14	0.0054	0.0029	0.000452	0.000087	0.036779	2.91	0.56	52.83	56.6
BG-WSH-04-241.6m_15	0.0037	0.0017	0.00053	0.000078	0.04153	3.41	0.5	96.1	144.7
BG-WSH-04-241.6m_16	0.0047	0.0022	0.000473	0.000081	0.061885	3.05	0.52	74.7	75.7
BG-WSH-04-241.6m_17	0.0042	0.0012	0.000396	0.000042	0.10007	2.55	0.27	154.7	213
BG-WSH-04-241.6m_18	0.004	0.0018	0.000493	0.000068	0.028899	3.18	0.43	89.7	78
BG-WSH-04-241.6m_19	0.0044	0.0028	0.00059	0.000076	0.1074	3.8	0.49	63.3	36
BG-WSH-04-241.6m_20	0.0046	0.0022	0.00043	0.000067	0.06559	2.77	0.43	85.1	65.5
BG-WSH-04-241.6m_21	0.0028	0.0016	0.000404	0.000063	0.15006	2.6	0.4	89.7	119.7
BG-WSH-04-241.6m_22	0.0064	0.0029	0.000439	0.000086	0.20719	2.83	0.55	72.3	91
BG-WSH-04-241.6m_23	0.0053	0.0027	0.000496	0.00007	0.17339	3.19	0.45	184.9	186.6
BG-WSH-04-241.6m_24	0.0063	0.0028	0.00051	0.00011	0.019525	3.26	0.69	62.4	81.6
BG-WSH-04-241.6m_25	0.0119	0.004	0.000468	0.000063	0.054206	3.02	0.41	115.8	88.9
BG-WSH-04-241.6m_26	0.0036	0.0025	0.000482	0.000089	0.10056	3.1	0.57	63.3	65.4
BG-WSH-04-241.6m_27	0.231	0.024	0.02906	0.00087	0.0017492	184.6	5.5	115.3	68.1
BG-WSH-04-241.6m_28	0.305	0.018	0.0433	0.0014	0.22067	275	8.8	74.8	64.92
BG-WSH-04-241.6m_29	0.3002	0.0038	0.04144	0.00052	0.44732	261.7	3.2	533	318
BG-WSH-04-241.6m_30	0.2728	0.0045	0.03827	0.00048	0.11342	242.1	3	293	228
BG-WSH-04-241.6m_31	0.3634	0.0066	0.04909	0.00062	0.16345	308.9	3.8	354	24.8
6001_1	0.00352	0.00037	0.000491	0.000023	0.14649	3.16	0.15	606	219
6001_2	0.00357	0.00039	0.000475	0.000028	0.069548	3.06	0.18	532	208.7
6001_3	0.00358	0.00052	0.000505	0.000029	-0.14195	3.25	0.18	398	141.1
6001_4	0.00407	0.0005	0.000477	0.000026	0.021449	3.07	0.17	450	168.4
6001_5	0.00371	0.00052	0.000505	0.000034	-0.12022	3.25	0.22	427	154.1
6001_6	0.00358	0.00042	0.000527	0.000028	-0.080551	3.4	0.18	449	156.8
6001_7	0.00402	0.00036	0.000515	0.00003	0.13039	3.32	0.19	474	166
6001_8	0.00381	0.00038	0.000543	0.00003	0.10327	3.5	0.2	687	507
6001_9	0.00745	0.00077	0.00056	0.000032	0.25061	3.61	0.21	426	212.6
6001_10	0.00344	0.00038	0.000491	0.000026	0.16791	3.16	0.17	467	178.8
6001_11	0.00433	0.00048	0.000508	0.000035	-0.01462	3.28	0.22	442	179.3
6001_12	0.00417	0.00051	0.000544	0.000033	0.19828	3.51	0.21	451	195
6001_13	0.00459	0.00076	0.000506	0.000031	0.32822	3.26	0.2	538	256
6001_14	0.00537	0.00067	0.000553	0.000032	0.062765	3.56	0.21	494	256.5
6001_15	0.00373	0.00049	0.000502	0.000028	0.1463	3.23	0.18	477	215

	207Pb/235U	207Pb/235U error	206Pb/238U	206Pb/238U Error	Error Correlation 206/238 vs. 207/235	Final Age (Ma)	Error (Ma)	Approx U (ppm)	Approx Th (ppm)
6001_16	0.00391	0.0005	0.000525	0.000037	0.1498	3.38	0.24	476	239
6001_17	0.00451	0.00044	0.000495	0.000025	-0.17781	3.19	0.16	524	245
6001_18	0.00385	0.00037	0.000524	0.00003	-0.10237	3.37	0.19	570	311
6001_19	0.00403	0.00049	0.000506	0.000032	-0.050194	3.26	0.21	433	221
6001_20	0.00447	0.00067	0.000517	0.000034	-0.014256	3.33	0.22	386	168.2
6001_21	0.0044	0.00052	0.000503	0.000027	-0.05292	3.24	0.18	445	184.4
6001_22	0.00424	0.00045	0.000518	0.000029	-0.043713	3.34	0.19	481	299
6001_23	0.00399	0.00043	0.000515	0.000027	0.054718	3.32	0.17	550	238
6001_24	0.00358	0.0004	0.000507	0.000024	0.22872	3.27	0.16	740	441
6001_25	0.00377	0.00045	0.000508	0.00003	0.21	3.28	0.19	588	810
6001_26	0.00397	0.00061	0.000519	0.000034	0.034609	3.34	0.22	342	157.5
6001_27	0.0039	0.00045	0.000521	0.000035	-0.068536	3.36	0.22	404	155
6001_28	0.00356	0.00051	0.000497	0.000031	-0.081254	3.2	0.2	353	224
6001_29	0.00354	0.00027	0.000493	0.000028	-0.31423	3.18	0.18	711	387
6001_30	0.00435	0.00046	0.000534	0.000034	-0.089159	3.44	0.22	487	215
6001_31	0.0471	0.0033	0.00404	0.0002	0.58835	26	1.3	615.1	385
6001_32	4.032	0.074	0.2743	0.0047	0.86028	1562	24	185.1	31.6
3001_1	0.00536	0.00091	0.000587	0.000053	0.10278	3.78	0.34	322.4	132.2
3001_2	0.00556	0.00087	0.000497	0.000046	0.13288	3.2	0.3	306	120.4
3001_3	0.0052	0.001	0.00058	0.000071	0.005744	3.74	0.45	399	327
3001_4	0.008	0.0018	0.000633	0.000058	0.043601	4.08	0.38	246	294
3001_5	0.00386	0.00056	0.0005	0.000039	0.14999	3.22	0.25	469	220.5
3001_6	0.0043	0.0012	0.000484	0.000062	0.032503	3.12	0.4	201	158
3001_7	0.0058	0.0015	0.000433	0.000068	0.21211	2.79	0.44	132.3	77.88
3001_8	0.00415	0.00071	0.000477	0.000048	0.026977	3.07	0.31	318	287
3001_9	0.0042	0.00066	0.00052	0.000042	0.018054	3.35	0.27	665	388
3001_10	0.0081	0.0042	0.00059	0.00014	0.19995	3.8	0.91	100	65
3001_11	0.00394	0.00058	0.000501	0.000036	0.08601	3.23	0.23	472.9	213.7
3001_12	0.00454	0.00081	0.000553	0.000044	0.065914	3.56	0.28	411	210
3001_13	0.00395	0.00056	0.00049	0.000043	0.081226	3.16	0.28	518	172.9
3001_14	0.0054	0.0016	0.000509	0.000072	0.15168	3.28	0.46	363.1	171.3
3001_15	0.0814	0.0072	0.0059	0.00034	0.40435	37.9	2.2	403.6	224.9
3001_16	0.489	0.011	0.0651	0.0011	0.054411	406.3	6.8	119.7	100.5
3001_17	0.3328	0.0072	0.04425	0.00052	0.19679	279.1	3.2	546	114.9
3001_18	5.65	0.26	0.0468	0.0031	0.040631	295	19	7.37	31.8
3001_19	0.361	0.0076	0.0493	0.00076	0.089484	310.2	4.7	186	159.4
3001_20	0.374	0.011	0.05143	0.00072	0.16198	323.3	4.4	167	91.2
WDDPZ-05-209m_1	0.0222	0.0031	0.000649	0.000061	0.56678	4.18	0.39	398	238
WDDPZ-05-209m_2	0.0062	0.0011	0.000601	0.000055	0.028557	3.87	0.35	590	133
WDDPZ-05-209m_3	0.00593	0.00089	0.000547	0.000056	-0.02984	3.52	0.36	326	123.9
WDDPZ-05-209m_4	0.0126	0.003	0.00061	0.000078	0.4146	3.93	0.5	332	101.4
WDDPZ-05-209m_5	0.00492	0.00077	0.000504	0.000044	-0.10506	3.25	0.28	377	195
WDDPZ-05-209m_6	0.00618	0.00099	0.000569	0.000052	-0.092675	3.67	0.33	382	146.4
WDDPZ-05-209m_7	0.0074	0.0015	0.000548	0.000049	0.21554	3.53	0.31	541	405
WDDPZ-05-209m_8	0.007	0.0013	0.000597	0.000066	-0.18269	3.85	0.43	496	136.5
WDDPZ-05-209m_9	0.00657	0.00095	0.000638	0.000044	0.13101	4.11	0.28	689	675
WDDPZ-05-209m_10	0.00538	0.00076	0.000531	0.000043	-0.16855	3.42	0.28	538	470
WDDPZ-05-209m_11	0.00431	0.00081	0.00052	0.00005	-0.17359	3.35	0.32	514	227
WDDPZ-05-209m_12	0.00528	0.00051	0.000513	0.000033	-0.21586	3.31	0.21	605	291
WDDPZ-05-209m_13	0.00577	0.00098	0.000567	0.000043	0.19397	3.65	0.28	369.8	130.1
WDDPZ-05-209m_14	0.0051	0.0013	0.000586	0.000055	0.025209	3.77	0.36	438	235.5
WDDPZ-05-209m_15	0.00583	0.00092	0.000542	0.000047	-0.21145	3.49	0.3	561	247
WDDPZ-05-209m_16	0.00504	0.00082	0.000579	0.000049	0.012987	3.73	0.32	333	154.7
WDDPZ-05-209m_17	0.0158	0.0071	0.000577	0.000041	0.0086939	3.72	0.26	598	567
WDDPZ-05-209m_18	0.0069	0.0024	0.00059	0.00005	0.15934	3.8	0.33	351	218
WDDPZ-05-209m_19	0.0042	0.0013	0.000425	0.000025	0.043899	2.74	0.16	986	1290
WDDPZ-05-209m_20	0.00434	0.00078	0.000548	0.000043	-0.16111	3.53	0.27	369	261
WDDPZ-05-209m_21	0.00486	0.00068	0.000594	0.000051	-0.028422	3.83	0.33	423	238
WDDPZ-05-209m_22	0.0046	0.0012	0.000498	0.000081	0.52631	3.21	0.52	518	305
WDDPZ-05-209m_23	0.00562	0.00093	0.00063	0.00005	0.067098	4.06	0.32	469	256
WDDPZ-05-209m_24	0.0061	0.0016	0.000555	0.000038	-0.016781	3.58	0.24	622	701
WDDPZ-05-209m_25	0.00445	0.00087	0.000541	0.000068	-0.16439	3.49	0.44	658	535
WDDPZ-05-211m_1	0.00572	0.00096	0.000586	0.000038	-0.19503	3.77	0.25	522	264
WDDPZ-05-211m_2	0.00421	0.00043	0.000556	0.000033	-0.082505	3.58	0.21	700	685
WDDPZ-05-211m_3	0.00324	0.00065	0.000469	0.000039	-0.066652	3.02	0.25	558	416
WDDPZ-05-211m_4	0.00419	0.00049	0.000507	0.000036	0.08826	3.27	0.23	568	420
WDDPZ-05-211m_5	0.00433	0.0007	0.000574	0.000041	-0.19687	3.7	0.27	517	217
WDDPZ-05-211m_6	0.0061	0.00089	0.00055	0.000033	0.14282	3.54	0.21	563	432
WDDPZ-05-211m_7	0.00495	0.00071	0.000522	0.000039	-0.080328	3.36	0.25	438	116.7
WDDPZ-05-211m_8	0.00451	0.00057	0.000541	0.000036	0.063028	3.49	0.23	592	426
WDDPZ-05-211m_9	0.00453	0.00042	0.00055	0.000027	0.021197	3.54	0.17	712	714

	207Pb/235U	207Pb/235U error	206Pb/238U	206Pb/238U Error	Error Correlation 206/238 vs. 207/235	Final Age (Ma)	Error (Ma)	Approx U (ppm)	Approx Th (ppm)
WDDPZ-05-211m_10	0.00429	0.00067	0.000566	0.000041	0.10392	3.64	0.26	378	128.1
WDDPZ-05-211m_11	0.0071	0.0015	0.000548	0.000048	0.2082	3.53	0.31	347	193
WDDPZ-05-211m_12	0.0037	0.0011	0.000495	0.000062	-0.1114	3.19	0.4	548	219
WDDPZ-05-211m_13	0.00414	0.00046	0.000526	0.000034	-0.19126	3.39	0.22	619	597
WDDPZ-05-211m_14	0.00526	0.00071	0.000511	0.000035	0.10849	3.29	0.23	532	401
WDDPZ-05-211m_15	0.0046	0.0013	0.000523	0.000051	-0.38174	3.37	0.33	1002	356.1
WDDPZ-05-211m_16	0.00437	0.00072	0.000549	0.000036	-0.17182	3.54	0.23	404	197
WDDPZ-05-211m_17	0.024	0.0023	0.000683	0.000044	0.20376	4.4	0.29	444	217.4
WDDPZ-05-211m_18	0.00375	0.00048	0.000442	0.000031	-0.076637	2.85	0.2	535	321
WDDPZ-05-211m_19	0.00528	0.00076	0.000577	0.000044	0.25861	3.72	0.28	424	276
WDDPZ-05-211m_20	0.0042	0.00059	0.000544	0.00003	-0.25157	3.51	0.19	579	438
WDDPZ-05-211m_21	0.00496	0.00054	0.000532	0.000032	-0.030951	3.43	0.21	610	540
WDDPZ-05-211m_22	0.0047	0.00074	0.000534	0.000034	0.042748	3.44	0.22	533	367
WDDPZ-05-211m_23	0.0044	0.00074	0.000456	0.000037	0.05988	2.94	0.24	509	314
WDDPZ-05-211m_24	0.00469	0.00051	0.000519	0.000033	-0.051783	3.35	0.21	650	533
WDDPZ-05-211m_25	0.00415	0.00056	0.000501	0.000038	0.10777	3.23	0.24	651	565
WDDPZ-05-211m_26	0.00467	0.0008	0.000551	0.000047	0.21522	3.55	0.31	400	246
WDDPZ-05-211m_27	0.00371	0.00053	0.000526	0.00004	-0.023217	3.39	0.26	573	352
WDDPZ-05-211m_28	4.906	0.055	0.3215	0.0038	0.54855	1797	18	244.1	143.9
WDDPZ-05-211m_29	4.25	0.051	0.2811	0.0045	0.74023	1597	23	563	138
WDDPZ-05-211m_30	9.524	0.096	0.4323	0.0038	0.61249	2316	17	142.7	139.6
4001_1	0.0041	0.00061	0.000541	0.000038	0.093195	3.49	0.25	325	90.5
4001_2	0.00428	0.00082	0.000534	0.000042	0.25504	3.44	0.27	376	85.8
4001_3	0.00494	0.00072	0.000591	0.000038	0.053541	3.81	0.24	352	102.5
4001_4	0.00475	0.00072	0.000493	0.000034	0.092668	3.17	0.22	346	99.9
4001_5	0.00408	0.00067	0.000572	0.000051	0.16674	3.69	0.33	388	102.6
4001_6	0.00497	0.00068	0.000498	0.000036	0.06725	3.21	0.23	420	149.9
4001_7	0.00576	0.00084	0.000581	0.000044	0.11468	3.74	0.29	308	93.1
4001_8	0.00445	0.00059	0.000561	0.000044	0.07892	3.62	0.28	357	103.6
4001_9	0.00451	0.0008	0.000586	0.000071	0.75068	3.77	0.46	418	222
4001_10	0.00385	0.00089	0.000519	0.000051	0.046921	3.35	0.33	450	138
4001_11	0.0046	0.0011	0.000518	0.000049	0.0062225	3.34	0.32	454	116.3
4001_12	0.0059	0.0023	0.00065	0.00018	0.29971	4.2	1.2	578	96
4001_13	0.00375	0.0005	0.000507	0.000035	0.15453	3.27	0.23	392	103.5
4001_14	0.00403	0.00057	0.000473	0.000039	0.10428	3.05	0.25	414	111.3
4001_15	0.0041	0.0011	0.000568	0.00005	0.16296	3.66	0.32	391	113.7
4001_16	0.0043	0.0013	0.000509	0.000067	0.16069	3.28	0.43	446	144
4001_17	0.0039	0.001	0.0006	0.000084	0.16159	3.86	0.54	387	106.3
4001_18	0.00546	0.00084	0.000509	0.000037	0.14258	3.28	0.24	444	110.5
4001_19	0.00487	0.00069	0.000524	0.000034	0.018736	3.37	0.22	321	116.1
4001_20	0.00368	0.00057	0.000519	0.000038	0.064183	3.34	0.24	352	98.7
4001_21	0.00634	0.0008	0.000596	0.000044	0.12919	3.84	0.28	415	135.3
4001_22	0.00422	0.00087	0.00058	0.000087	0.0050256	3.74	0.56	467	171
4001_23	0.0033	0.0013	0.000491	0.000094	0.12603	3.17	0.61	476	161
4001_24	0.00616	0.00068	0.000626	0.000059	0.16296	4.03	0.38	384.7	78.8
4001_25	0.00443	0.00076	0.000596	0.00005	0.24148	3.84	0.32	306.2	71.1
4001_26	0.00493	0.00059	0.000529	0.000041	0.089303	3.41	0.26	415	117.1
4001_27	0.00362	0.0006	0.000535	0.000038	0.038605	3.45	0.24	352	89.3
4001_28	5.578	0.084	0.3552	0.0072	0.73496	1958	34	500	173.1
4001_29	6.01	0.1	0.4042	0.0061	0.55721	2188	28	870	71.2
4001_30	4.81	0.22	0.317	0.012	0.9198	1770	59	80.5	32.7
4001_31	0.349	0.017	0.0462	0.0018	0.46986	291	11	92.4	108
4001_32	5.3	0.13	0.371	0.01	0.86598	2034	47	681	3.78
WD17-05-19m_1	0.0051	0.001	0.000603	0.00005	-0.066079	3.89	0.32	296	91
WD17-05-19m_2	0.0051	0.001	0.000555	0.000063	-0.014786	3.57	0.4	345	125
WD17-05-19m_3	0.0059	0.0016	0.000517	0.000057	-0.067251	3.33	0.37	386	127.3
WD17-05-19m_4	0.0048	0.0014	0.000552	0.000058	0.06427	3.56	0.37	272	57.5
WD17-05-19m_5	0.0044	0.0017	0.00055	0.00007	0.71834	3.54	0.45	419	166
WD17-05-19m_6	0.0073	0.001	0.000559	0.000057	0.15712	3.6	0.37	315	110.2
WD17-05-19m_7	0.0063	0.0028	0.00058	0.00014	0.26517	3.72	0.9	450	158.2
WD17-05-19m_8	0.0055	0.0011	0.000589	0.000053	0.06681	3.8	0.34	393	128.2
WD17-05-19m_9	0.0044	0.0014	0.000479	0.000074	0.023673	3.09	0.48	630	336
WD17-05-19m_10	0.0055	0.0014	0.000563	0.000052	0.06029	3.63	0.33	399	110.9
WD17-05-19m_11	0.0041	0.00062	0.000539	0.00006	-0.071509	3.47	0.39	437	130.5
WD17-05-19m_12	0.006	0.0013	0.000632	0.000095	0.62447	4.07	0.61	329	87.8
WD17-05-19m_13	0.00481	0.00083	0.000514	0.000048	-0.032073	3.32	0.31	541	302
WD17-05-19m_14	0.0051	0.0013	0.000595	0.00006	0.068855	3.84	0.39	402.1	98.2
WD17-05-19m_15	0.0069	0.0015	0.00062	0.00013	-0.068601	3.97	0.84	432	160
WD17-05-19m_16	0.00514	0.00066	0.000597	0.000042	-0.23417	3.85	0.27	508	178.1
WD17-05-19m_17	0.0054	0.001	0.000514	0.000072	-0.087566	3.31	0.46	451	184
WD17-05-19m_18	0.0054	0.0014	0.000545	0.000094	0.028668	3.51	0.61	547	170.6

	207Pb/235U	207Pb/235U error	206Pb/238U	206Pb/238U Error	Error Correlation 206/238 vs. 207/235	Final Age (Ma)	Error (Ma)	Approx U (ppm)	Approx Th (ppm)
WD17-05-19m_19	0.0043	0.00086	0.000526	0.00005	-0.023888	3.39	0.32	457	141.9
WD17-05-19m_20	0.00475	0.00072	0.000502	0.000047	0.062938	3.23	0.3	416	152.6
WD17-05-19m_21	0.00423	0.00068	0.000538	0.000048	-0.044705	3.47	0.31	560	135.7
WD17-05-19m_22	0.0048	0.0011	0.000529	0.000046	-0.27181	3.41	0.3	636	372
WD17-05-19m_23	0.0095	0.0012	0.000606	0.000042	0.29496	3.9	0.27	419.2	119.8
WD17-05-19m_24	0.0051	0.0013	0.000581	0.00006	0.23263	3.74	0.38	461	156.7
WD17-05-19m_25	0.00436	0.00063	0.000543	0.000042	0.13672	3.5	0.27	335	96.6
WD17-05-19m_26	0.0057	0.001	0.000568	0.000058	0.090471	3.66	0.38	426	183
WD17-05-19m_27	0.0059	0.0028	0.00052	0.00011	0.19105	3.33	0.7	440	288
WD17-05-19m_28	0.00546	0.00093	0.000506	0.000046	0.15631	3.26	0.29	391	108.9
WD17-05-19m_29	0.0049	0.0016	0.000414	0.000081	0.15174	2.67	0.52	466	255
WD17-05-19m_30	11.07	0.13	0.4827	0.0048	0.52434	2539	21	93.9	366
WD17-05-19m_31	0.0156	0.0019	0.001	0.00013	0.64634	6.46	0.81	393	102.3
WD17-05-19m_32	0.356	0.015	0.0474	0.0013	0.17976	298.7	8.3	68.6	49.3
7001_1	0.00456	0.00069	0.000477	0.000036	0.173	3.07	0.23	483	240
7001_2	0.0059	0.0018	0.000599	0.000085	0.38179	3.86	0.55	257	164
7001_3	0.00407	0.00056	0.000475	0.00004	0.019848	3.06	0.26	544	181
7001_4	0.0062	0.0038	0.0008	0.00017	0.30141	5.1	1.1	317	195
7001_5	0.0146	0.0033	0.00122	0.00025	0.44217	7.9	1.6	209	110
7001_6	0.0083	0.0045	0.00066	0.00021	-0.044995	4.3	1.3	302.1	170
7001_7	0.00429	0.00061	0.000507	0.000037	0.14897	3.27	0.24	510	159
7001_8	0.00287	0.00049	0.000503	0.000032	0.14472	3.24	0.2	470	191
7001_9	0.00456	0.00072	0.000486	0.000037	0.010761	3.13	0.24	465	190
7001_10	0.0042	0.0021	0.00064	0.0001	0.43603	4.11	0.66	419	260
7001_11	0.0058	0.0021	0.00056	0.00014	-0.059244	3.58	0.92	218	132
7001_12	0.00407	0.00046	0.000449	0.000029	-0.1067	2.89	0.18	629	257
7001_13	0.00346	0.00037	0.000518	0.000027	-0.086399	3.34	0.17	1021	583
7001_14	0.00364	0.00038	0.000486	0.000031	0.14617	3.13	0.2	852	528
7001_15	0.00538	0.00082	0.000507	0.000061	0.20099	3.27	0.39	516	140
7001_16	0.0124	0.0023	0.000548	0.000051	0.16503	3.53	0.33	425	157
7001_17	0.00357	0.00068	0.000521	0.00006	0.32073	3.36	0.38	543	249
7001_18	0.0052	0.0011	0.000549	0.000055	0.19534	3.54	0.35	683	175
7001_19	0.00435	0.0006	0.000504	0.000044	0.11287	3.25	0.28	569	216
7001_20	3.531	0.04	0.2692	0.0033	0.49259	1538	17	422	179
7001_21	0.414	0.012	0.0546	0.001	0.16332	342.7	6.3	201.2	194.3
7001_22	6.57	0.27	0.378	0.014	0.96912	2063	67	1224	215
7001_23	6.144	0.086	0.3573	0.0052	0.55076	1969	25	192.8	94.8
7001_24	23.19	0.27	0.6434	0.0092	0.63946	3201	36	140.1	210.5
7001_25	4.725	0.079	0.3038	0.0059	0.65985	1709	29	400	219.2
7001_26	9.48	0.22	0.441	0.01	0.5686	2354	46	719	212.2
7001_27	4.82	0.16	0.309	0.0078	0.13244	1735	39	22.21	9.7
7001_28	4.898	0.089	0.3163	0.0064	0.65626	1771	31	89.8	26.19
7001_29	4.828	0.093	0.3103	0.0078	0.78029	1741	38	148.2	40.6
93-MC-HR1_1	0.0226	0.0036	0.000743	0.000085	0.11957	4.79	0.55	211	150
93-MC-HR1_2	0.0045	0.00099	0.000509	0.000047	-0.05549	3.28	0.31	364	441
93-MC-HR1_3	0.0063	0.0011	0.00053	0.000063	-0.24738	3.42	0.41	394	541
93-MC-HR1_4	0.00581	0.00086	0.000545	0.000055	-0.026501	3.52	0.35	408	632
93-MC-HR1_5	0.0032	0.0013	0.000539	0.000065	-0.1826	3.47	0.42	233	255
93-MC-HR1_6	0.00533	0.00077	0.000568	0.000033	0.13429	3.66	0.21	561	447
93-MC-HR1_7	0.00383	0.00052	0.000488	0.000026	0.030667	3.15	0.17	787	940
93-MC-HR1_8	0.00434	0.00085	0.000516	0.000047	-0.14394	3.32	0.3	352	398
93-MC-HR1_9	0.00403	0.00092	0.000529	0.000046	-0.035859	3.41	0.29	326	326
93-MC-HR1_10	0.0083	0.0026	0.00054	0.000062	0.065306	3.48	0.4	427	476
93-MC-HR1_11	0.0055	0.0019	0.000505	0.000097	0.012489	3.26	0.63	186	222
93-MC-HR1_12	0.0059	0.0011	0.0005	0.00006	-0.081291	3.22	0.39	366	454
93-MC-HR1_13	0.0063	0.0015	0.000471	0.000066	-0.10711	3.04	0.42	195	159
93-MC-HR1_14	0.0086	0.0012	0.000551	0.000055	-0.065419	3.55	0.36	328	387
93-MC-HR1_15	0.0063	0.0014	0.000491	0.000055	0.15733	3.17	0.35	313	308
93-MC-HR1_16	0.0071	0.0017	0.000479	0.000054	0.055374	3.09	0.35	446	373
93-MC-HR1_17	0.0041	0.0013	0.000579	0.000079	-0.1829	3.73	0.51	517	598
93-MC-HR1_18	0.0071	0.0011	0.000568	0.00005	-0.015526	3.66	0.32	304	344
93-MC-HR1_19	0.0044	0.0014	0.000532	0.000058	-0.30244	3.43	0.38	215	230
93-MC-HR1_20	0.0052	0.0012	0.000512	0.000051	0.017535	3.3	0.33	271	222.4
93-MC-HR1_21	0.0067	0.0016	0.000564	0.000082	0.12526	3.64	0.53	205	110
93-MC-HR1_22	0.0066	0.0018	0.000591	0.000051	0.40236	3.81	0.33	256	292
93-MC-HR1_23	0.0054	0.0015	0.000568	0.000068	-0.004462	3.66	0.44	236	257
93-MC-HR1_24	0.00367	0.00067	0.000512	0.000051	0.01513	3.3	0.33	333	428
93-MC-HR1_25	0.00495	0.00099	0.000482	0.000051	0.16729	3.1	0.33	348	374
93-MC-HR1_26	0.00421	0.00073	0.000527	0.000054	0.14727	3.4	0.35	340	386
93-MC-HR1_27	0.0043	0.001	0.000567	0.000057	0.083292	3.65	0.37	295	283
93-MC-HR1_28	0.1239	0.0099	0.0158	0.0011	-0.0069741	100.9	7.2	103.8	78.3

	207Pb/235U	207Pb/235U error	206Pb/238U	206Pb/238U Error	Error Correlation 206/238 vs. 207/235	Final Age (Ma)	Error (Ma)	Approx U (ppm)	Approx Th (ppm)
93-MC-HR1_29	0.3274	0.0089	0.04355	0.00088	0.19986	274.7	5.4	250	191
93-MC-HR3a_1	0.00429	0.00038	0.000489	0.000027	0.29402	3.15	0.18	378	94.7
93-MC-HR3a_2	0.00436	0.00037	0.000523	0.000024	-0.1541	3.37	0.15	562	228
93-MC-HR3a_3	0.00416	0.00033	0.000571	0.000024	0.18277	3.68	0.15	523	246
93-MC-HR3a_4	0.0044	0.00034	0.000522	0.000029	-0.21812	3.36	0.19	511	247
93-MC-HR3a_5	0.00592	0.00094	0.000523	0.000049	-0.21845	3.37	0.32	216.4	132.2
93-MC-HR3a_6	0.00453	0.00055	0.000501	0.000028	-0.0081076	3.23	0.18	378	110.3
93-MC-HR3a_7	0.00401	0.00034	0.000516	0.000024	-0.046076	3.32	0.16	491	180
93-MC-HR3a_8	0.00352	0.00036	0.000501	0.000023	-0.024639	3.23	0.15	419	187.1
93-MC-HR3a_9	0.00406	0.00037	0.000508	0.00002	-0.014663	3.28	0.13	503.1	239
93-MC-HR3a_10	0.00396	0.00036	0.000514	0.000021	-0.036934	3.31	0.14	468	168
93-MC-HR3a_11	0.00517	0.00049	0.000606	0.000035	0.45086	3.9	0.22	689	373
93-MC-HR3a_12	0.00393	0.00037	0.000548	0.000025	0.17499	3.53	0.16	464	237
93-MC-HR3a_13	0.0036	0.00033	0.000498	0.000028	0.11217	3.21	0.18	452	198
93-MC-HR3a_14	0.00448	0.00045	0.000502	0.000027	0.13922	3.24	0.17	436	282.5
93-MC-HR3a_15	0.00407	0.00052	0.00049	0.000025	0.018922	3.16	0.16	336	148.8
93-MC-HR3a_16	0.00392	0.00043	0.000512	0.000026	0.22979	3.3	0.16	433	128
93-MC-HR3a_17	0.00423	0.00038	0.000584	0.000023	0.090233	3.77	0.15	975	348
93-MC-HR3a_18	0.00372	0.00036	0.000526	0.000024	0.0023372	3.39	0.16	517	160.9
93-MC-HR3a_19	0.0041	0.00042	0.000509	0.000026	0.083806	3.28	0.17	428	144
93-MC-HR3a_20	0.00358	0.00035	0.000498	0.000023	-0.13828	3.21	0.15	422	112.4
93-MC-HR3a_21	0.00365	0.00035	0.000509	0.000029	0.02795	3.28	0.19	352	123.7
93-MC-HR3a_22	0.00424	0.00033	0.000531	0.000024	0.11331	3.42	0.15	447	117.2
93-MC-HR3a_23	0.00438	0.00052	0.00052	0.000027	-0.086664	3.35	0.17	503	176
93-MC-HR3a_24	0.00318	0.00027	0.000488	0.000024	0.013827	3.14	0.16	496	188
93-MC-HR3a_25	0.0038	0.00046	0.000494	0.000028	-0.0077632	3.18	0.18	356	130.5
93-MC-HR3a_26	0.00523	0.00085	0.000503	0.000048	0.29532	3.24	0.31	457	195
93-MC-HR3a_27	0.00414	0.00035	0.000518	0.000027	-0.16414	3.34	0.18	523.6	234
93-MC-HR3a_28	0.00417	0.00051	0.0005	0.000029	0.031786	3.22	0.19	337	159.5
93-MC-HR3a_29	0.00433	0.00047	0.000529	0.000026	0.071942	3.41	0.17	537	235
93-MC-HR3a_30	0.0037	0.00036	0.000531	0.000023	-0.1766	3.42	0.15	510	165
93-MC-HR3a_31	0.00384	0.00033	0.000548	0.000024	-0.048891	3.53	0.15	576	251
93-MC-HR3b_1	0.00429	0.00038	0.000489	0.000027	0.29402	3.15	0.18	378	94.7
93-MC-HR3b_2	0.00436	0.00037	0.000523	0.000024	0.1541	3.37	0.15	562	228
93-MC-HR3b_3	0.00416	0.00033	0.000571	0.000024	0.18277	3.68	0.15	523	246
93-MC-HR3b_4	0.0044	0.00034	0.000522	0.000029	0.21812	3.36	0.19	511	247
93-MC-HR3b_5	0.00592	0.00094	0.000523	0.000049	0.21845	3.37	0.32	216.4	132.2
93-MC-HR3b_6	0.00453	0.00055	0.000501	0.000028	0.0081076	3.23	0.18	378	110.3
93-MC-HR3b_7	0.00401	0.00034	0.000516	0.000024	0.046076	3.32	0.16	491	180
93-MC-HR3b_8	0.00352	0.00036	0.000501	0.000023	0.024639	3.23	0.15	419	187.1
93-MC-HR3b_9	0.00406	0.00037	0.000508	0.00002	0.014663	3.28	0.13	503.1	239
93-MC-HR3b_10	0.00396	0.00036	0.000514	0.000021	0.036934	3.31	0.14	468	168
93-MC-HR3b_11	0.00517	0.00049	0.000606	0.000035	0.45086	3.9	0.22	689	373
93-MC-HR3b_12	0.00393	0.00037	0.000548	0.000025	0.17499	3.53	0.16	464	237
93-MC-HR3b_13	0.0036	0.00033	0.000498	0.000028	0.11217	3.21	0.18	452	198
93-MC-HR3b_14	0.00448	0.00045	0.000502	0.000027	0.13922	3.24	0.17	436	282.5
93-MC-HR3b_15	0.00407	0.00052	0.00049	0.000025	0.018922	3.16	0.16	336	148.8
93-MC-HR3b_16	0.00392	0.00043	0.000512	0.000026	0.22979	3.3	0.16	433	128
93-MC-HR3b_17	0.00423	0.00038	0.000584	0.000023	0.090233	3.77	0.15	975	348
93-MC-HR3b_18	0.00372	0.00036	0.000526	0.000024	0.0023372	3.39	0.16	517	160.9
93-MC-HR3b_19	0.0041	0.00042	0.000509	0.000026	0.083806	3.28	0.17	428	144
93-MC-HR3b_20	0.00358	0.00035	0.000498	0.000023	0.13828	3.21	0.15	422	112.4
93-MC-HR3b_21	0.00365	0.00035	0.000509	0.000029	0.02795	3.28	0.19	352	123.7
93-MC-HR3b_22	0.00424	0.00033	0.000531	0.000024	0.11331	3.42	0.15	447	117.2
93-MC-HR3b_23	0.00438	0.00052	0.00052	0.000027	0.086664	3.35	0.17	503	176
93-MC-HR3b_24	0.00318	0.00027	0.000488	0.000024	0.013827	3.14	0.16	496	188
93-MC-HR3b_25	0.0038	0.00046	0.000494	0.000028	0.0077632	3.18	0.18	356	130.5
93-MC-HR3b_26	0.00523	0.00085	0.000503	0.000048	0.29532	3.24	0.31	457	195
93-MC-HR3b_27	0.00414	0.00035	0.000518	0.000027	0.16414	3.34	0.18	523.6	234
93-MC-HR3b_28	0.00417	0.00051	0.0005	0.000029	0.031786	3.22	0.19	337	159.5
93-MC-HR3b_29	0.00433	0.00047	0.000529	0.000026	0.071942	3.41	0.17	537	235
93-MC-HR3b_30	0.0037	0.00036	0.000531	0.000023	0.1766	3.42	0.15	510	165
93-MC-HR3b_31	0.00384	0.00033	0.000548	0.000024	0.048891	3.53	0.15	576	251
95-MC-HR4_1	0.0048	0.0013	0.000511	0.000071	0.051106	3.29	0.46	547.5	315.4
95-MC-HR4_2	0.0079	0.0021	0.000566	0.000062	0.025639	3.65	0.4	470	330
95-MC-HR4_3	0.0136	0.0039	0.00067	0.00013	0.29853	4.29	0.81	319	192
95-MC-HR4_4	0.0102	0.0043	0.00059	0.00016	0.2519	3.8	1	768	273
95-MC-HR4_5	0.0059	0.0017	0.000529	0.000069	0.0096477	3.41	0.45	498	288.1
95-MC-HR4_6	0.0084	0.0018	0.000526	0.000056	0.53488	3.39	0.36	452	272.5
95-MC-HR4_7	0.0049	0.0013	0.000558	0.000057	0.0047205	3.6	0.37	452	270
95-MC-HR4_8	0.0073	0.0023	0.000614	0.000086	0.074775	3.96	0.55	245	165.6

	207Pb/235U	207Pb/235U error	206Pb/238U	206Pb/238U Error	Error Correlation 206/238 vs. 207/235	Final Age (Ma)	Error (Ma)	Approx U (ppm)	Approx Th (ppm)
95-MC-HR4_9	0.0085	0.0012	0.000518	0.000046	0.02968	3.34	0.3	910	948
95-MC-HR4_10	0.025	0.012	0.000603	0.000078	0.055454	3.88	0.5	348	236
95-MC-HR4_11	0.0052	0.0014	0.000555	0.000059	0.16336	3.57	0.38	379	213
95-MC-HR4_12	0.0054	0.0019	0.000503	0.000095	0.040089	3.24	0.61	574	238
95-MC-HR4_13	0.006	0.0011	0.000516	0.00005	0.026934	3.33	0.32	1359	981
95-MC-HR4_14	0.0077	0.0019	0.000553	0.000057	0.23944	3.56	0.37	643	319
95-MC-HR4_15	0.0263	0.0084	0.00075	0.0002	0.13456	4.9	1.3	74	93
95-MC-HR4_16	0.0084	0.0011	0.000502	0.000046	0.11447	3.24	0.3	866	478
95-MC-HR4_17	0.0061	0.0013	0.000493	0.000046	0.15488	3.18	0.29	790	357
95-MC-HR4_18	0.0091	0.0023	0.000559	0.000081	0.27472	3.6	0.52	805	373
95-MC-HR4_19	0.0122	0.0032	0.00066	0.00011	0.0047119	4.24	0.73	299.6	153.3
95-MC-HR4_20	0.0052	0.0018	0.000474	0.000065	0.28157	3.05	0.42	261	143.3
95-MC-HR4_21	0.008	0.003	0.000604	0.000081	0.0010497	3.89	0.52	237.2	244
95-MC-HR4_22	0.0049	0.0016	0.000516	0.000064	0.0085551	3.32	0.41	289	199
95-MC-HR4_23	0.0062	0.0016	0.000537	0.000075	0.29428	3.46	0.49	340	178
95-MC-HR4_24	0.0079	0.0027	0.000559	0.000078	0.22946	3.6	0.5	322	174
95-MC-HR4_25	0.0076	0.0032	0.000641	0.000096	0.17891	4.13	0.62	270	128
95-MC-HR4_26	0.0051	0.0018	0.000557	0.000082	0.14191	3.59	0.53	300	234
95-MC-HR4_27	4.31	0.17	0.2963	0.0067	0.70459	1673	33	125.7	60.6
95-MC-HR4_28	0.266	0.011	0.0377	0.00081	0.3005	238.5	5	195.6	232
93-MC-HR5_1	0.0058	0.0024	0.000509	0.000075	0.17418	3.28	0.49	286	267
93-MC-HR5_2	0.006	0.0033	0.00056	0.00011	0.19675	3.6	0.71	138.6	188
93-MC-HR5_3	0.0043	0.0022	0.000476	0.000069	0.16925	3.07	0.44	291	257
93-MC-HR5_4	0.0021	0.002	0.000508	0.00006	0.0033158	3.27	0.39	238	171
93-MC-HR5_5	0.0036	0.0024	0.000594	0.000091	0.0094499	3.83	0.59	217	145.1
93-MC-HR5_6	0.0038	0.002	0.000525	0.000072	0.21167	3.38	0.46	290	305
93-MC-HR5_7	0.0063	0.0028	0.000542	0.000096	0.015279	3.49	0.62	198	119
93-MC-HR5_8	0.0051	0.0015	0.000475	0.000087	0.013955	3.06	0.56	519	397
93-MC-HR5_9	0.0043	0.0025	0.000494	0.000083	0.10887	3.18	0.53	221	231
93-MC-HR5_10	0.0042	0.0016	0.000463	0.000064	0.016622	2.98	0.41	430	504
93-MC-HR5_11	0.0005	0.0034	0.00056	0.00017	0.2183	3.6	1.1	196	130
93-MC-HR5_12	0.0049	0.0022	0.000506	0.000087	0.028123	3.26	0.56	327	312
93-MC-HR5_13	0.0057	0.0019	0.000544	0.000081	0.11511	3.5	0.52	269	141.6
93-MC-HR5_14	0.0031	0.0029	0.00043	0.00011	0.15457	2.74	0.73	331	350
93-MC-HR5_15	0.0029	0.0025	0.000537	0.00009	0.13597	3.46	0.58	220	142
93-MC-HR5_16	0.0028	0.0012	0.000478	0.000059	0.3396	3.08	0.38	410	562
93-MC-HR5_17	0.0045	0.0039	0.00062	0.00014	0.082222	3.98	0.89	151	134
93-MC-HR5_18	0.007	0.0028	0.000511	0.000081	0.13772	3.29	0.53	283	186.4
93-MC-HR5_19	0.0045	0.0017	0.000529	0.000073	0.09532	3.41	0.47	380	521
93-MC-HR5_20	0.0034	0.0026	0.000547	0.000082	0.093637	3.52	0.53	236	218
93-MC-HR5_21	0.0048	0.0017	0.00051	0.000068	0.18293	3.29	0.44	414	373
93-MC-HR5_22	0.0039	0.0021	0.000544	0.000086	0.15043	3.51	0.56	283	299
93-MC-HR5_23	0.0048	0.0041	0.00049	0.00012	0.012923	3.16	0.76	120	110.8
93-MC-HR5_24	0.0018	0.0034	0.00055	0.0001	0.12528	3.53	0.64	254	257
93-MC-HR5_25	0.0063	0.0023	0.000549	0.000087	0.073094	3.54	0.56	244	259
93-MC-HR5_26	0.0041	0.0022	0.000458	0.000089	0.013228	2.95	0.58	367	345
93-MC-HR5_27	0.0039	0.0034	0.00054	0.0001	0.17969	3.45	0.67	243	262
93-MC-HR5_28	0.003	0.0022	0.00055	0.000095	0.092535	3.54	0.61	307	345
93-MC-HR5_29	4.93	0.12	0.3184	0.0055	0.032753	1782	27	81.9	14.9
93-MC-HR5_30	5.48	0.27	0.331	0.016	0.68037	1844	78	89.8	74.1
93-MC-HR5_31	0.359	0.022	0.0521	0.002	0.21782	327	12	94	60
94-MC-HR6_1	0.0065	0.0028	0.000627	0.000097	0.029783	4.04	0.62	255	253
94-MC-HR6_2	0.0055	0.0014	0.000558	0.000061	0.0030917	3.6	0.39	436	498
94-MC-HR6_3	0.0042	0.0016	0.000512	0.000074	0.02419	3.3	0.48	331	187
94-MC-HR6_4	0.0082	0.0028	0.000605	0.000093	0.057961	3.9	0.6	206	140.4
94-MC-HR6_5	0.0087	0.0039	0.00069	0.00012	0.034125	4.42	0.77	171	196
94-MC-HR6_6	0.005	0.0027	0.000588	0.000086	0.04313	3.79	0.56	261	280
94-MC-HR6_7	0.0061	0.0028	0.000436	0.000075	0.196	2.81	0.49	275	270
94-MC-HR6_8	0.0053	0.0022	0.00046	0.000076	0.072181	2.96	0.49	292	168
94-MC-HR6_9	0.0107	0.0035	0.00056	0.00012	0.12	3.62	0.78	238	245
94-MC-HR6_10	0.0044	0.0022	0.000542	0.000081	0.17329	3.49	0.52	180	201
94-MC-HR6_11	0.0042	0.0026	0.000523	0.000077	0.037051	3.37	0.5	223	181.4
94-MC-HR6_12	0.0056	0.0029	0.000654	0.000099	0.17156	4.21	0.64	191	222
94-MC-HR6_13	0.0052	0.0013	0.000618	0.000052	0.0038614	3.98	0.33	464	343
94-MC-HR6_14	0.0026	0.0029	0.00051	0.000096	0.13858	3.29	0.62	160	84.2
94-MC-HR6_15	0.007	0.0018	0.000547	0.000063	0.094048	3.52	0.4	319	226
94-MC-HR6_16	0.009	0.0039	0.00055	0.00012	0.2123	3.57	0.78	181.1	256.3
94-MC-HR6_17	0.005	0.0011	0.000558	0.000058	0.0097539	3.6	0.38	498	601
94-MC-HR6_18	0.0054	0.0024	0.000537	0.000088	0.0078683	3.46	0.57	247	248
94-MC-HR6_19	0.0102	0.0031	0.000529	0.000079	0.14462	3.41	0.51	206	265
94-MC-HR6_20	0.01	0.0049	0.000604	0.000086	0.083502	3.89	0.56	273	228

	207Pb/235U	207Pb/235U error	206Pb/238U	206Pb/238U Error	Error Correlation 206/238 vs. 207/235	Final Age (Ma)	Error (Ma)	Approx U (ppm)	Approx Th (ppm)
94-MC-HR6_21	0.0154	0.005	0.00079	0.00014	0.072282	5.08	0.87	121.1	118.4
94-MC-HR6_22	0.0147	0.0049	0.00065	0.00011	0.19792	4.21	0.71	318	375
94-MC-HR6_23	0.0084	0.0021	0.000576	0.000076	0.03901	3.71	0.49	359	416
94-MC-HR6_24	0.0087	0.0038	0.00051	0.00011	0.1319	3.32	0.7	179	156
94-MC-HR6_25	0.0078	0.0022	0.000612	0.000086	0.082395	3.94	0.56	300	357
94-MC-HR6_26	0.0041	0.0022	0.000571	0.000095	0.13575	3.68	0.61	267	327
94-MC-HR6_27	0.0065	0.0021	0.000528	0.000072	0.1133	3.4	0.46	282.8	235.3
94-MC-HR6_28	0.0067	0.0039	0.00048	0.00012	0.043537	3.07	0.75	91.4	83.3
94-MC-HR6_29	4.52	0.13	0.292	0.0089	0.42525	1651	45	251.5	61.8
94-MC-HR6_30	0.0021	0.0036	0.00036	0.00012	0.2097	2.33	0.77	104	65.8
94-MC-HR7_1	0.006	0.0036	0.00046	0.00011	0.043327	2.96	0.7	94.9	129
94-MC-HR7_2	0.009	0.0049	0.00047	0.00011	0.076354	3.02	0.7	88.1	118.2
94-MC-HR7_3	0.0016	0.0032	0.00053	0.00011	0.0017473	3.44	0.7	100.3	137.9
94-MC-HR7_4	0.0233	0.005	0.000601	0.000089	0.30575	3.87	0.57	283	334
94-MC-HR7_5	0.0171	0.004	0.00059	0.00011	0.12473	3.78	0.72	130.1	165
94-MC-HR7_6	0.0126	0.0034	0.000623	0.000089	0.39638	4.01	0.57	209	299
94-MC-HR7_7	0.0037	0.002	0.000624	0.000098	0.13769	4.02	0.63	200	220.9
94-MC-HR7_8	0.0057	0.0019	0.000431	0.000053	0.095663	2.78	0.34	413	508
94-MC-HR7_9	0.0167	0.0074	0.00057	0.0002	0.096595	3.7	1.3	59.5	48.3
94-MC-HR7_10	0.0077	0.0047	0.00038	0.00012	0.012925	2.46	0.76	72.7	89
94-MC-HR7_11	0.0092	0.0037	0.000443	0.000091	0.24848	2.86	0.58	112.6	157.2
94-MC-HR7_12	0.0067	0.0023	0.000539	0.000086	0.23163	3.47	0.56	237	297
94-MC-HR7_13	0.0078	0.0027	0.000537	0.000074	0.2973	3.46	0.48	172.8	250
94-MC-HR7_14	0.0075	0.0044	0.00066	0.00014	0.073616	4.26	0.9	110.5	123.8
94-MC-HR7_15	0.0044	0.0036	0.00052	0.0001	0.13861	3.33	0.65	108	118.6
94-MC-HR7_16	0.0027	0.0038	0.00043	0.00012	0.10186	2.76	0.75	105	128
95-MC-UR3_1	0.0042	0.0014	0.000509	0.000072	0.028937	3.28	0.47	149.4	140.9
95-MC-UR3_2	0.0057	0.0017	0.000506	0.000076	0.067777	3.26	0.49	166	131
95-MC-UR3_3	0.00331	0.00087	0.000409	0.000048	-0.17044	2.64	0.31	226	205
95-MC-UR3_4	0.0043	0.0012	0.000514	0.000069	0.058271	3.31	0.44	158	148
95-MC-UR3_5	0.0043	0.0012	0.000536	0.000057	-0.17503	3.46	0.37	185	181
95-MC-UR3_6	0.0053	0.0012	0.000441	0.000059	-0.073093	2.84	0.38	193	180
95-MC-UR3_7	0.00335	0.00093	0.000475	0.000058	0.028371	3.06	0.37	228	236
95-MC-UR3_8	0.076	0.013	0.00096	0.00013	0.71243	6.18	0.86	136	115
95-MC-UR3_9	0.0044	0.00099	0.000447	0.000044	0.14897	2.88	0.28	249.2	227.1
95-MC-UR3_10	0.004	0.0012	0.000442	0.000061	-0.0098681	2.85	0.39	193	166.4
95-MC-UR3_11	0.005	0.0011	0.00053	0.000057	0.20681	3.41	0.37	241	211
95-MC-UR3_12	0.0052	0.002	0.000475	0.000085	0.28673	3.06	0.55	195.6	178
95-MC-UR3_13	0.0055	0.0015	0.000495	0.000067	-0.012315	3.19	0.43	182.5	159.8
95-MC-UR3_14	0.0077	0.0017	0.000523	0.000068	0.1951	3.37	0.44	195.9	144.8
95-MC-UR3_15	0.0044	0.0011	0.00047	0.000047	0.035195	3.03	0.3	269	262
95-MC-UR3_16	0.0077	0.0034	0.000584	0.000093	0.21631	3.76	0.6	241	203
95-MC-UR3_17	0.0042	0.0012	0.000481	0.000059	0.074113	3.1	0.38	227	181
95-MC-UR3_18	0.00398	0.00097	0.000472	0.000056	0.19079	3.04	0.36	259	533
95-MC-UR3_19	0.0065	0.0018	0.000526	0.000078	0.18436	3.39	0.5	216	218
95-MC-UR3_20	0.00345	0.00087	0.000533	0.000054	-0.11458	3.43	0.35	242.7	186.9
95-MC-UR3_21	0.0031	0.0016	0.000484	0.00008	0.0099957	3.12	0.52	127	112.9
95-MC-UR3_22	0.3274	0.0075	0.04489	0.00079	0.17445	283	4.9	356	247
95-MC-UR3_23	0.363	0.0089	0.0489	0.001	-0.012039	307.9	6.3	140.3	121.2
95-MC-UR3_24	0.3281	0.0078	0.04585	0.00069	0.38196	289	4.2	237.9	291.1
95-MC-UR3_25	4.8	0.14	0.3005	0.0094	0.7547	1692	47	574	37.5
95-MC-UR3_26	0.3568	0.0063	0.04957	0.00075	0.3652	311.8	4.6	395	161.6
95-MC-UR3_27	0.364	0.012	0.0501	0.001	0.18202	315	6.3	112.4	66
95-MC-UR3_28	0.3006	0.0074	0.04143	0.00078	0.11101	261.6	4.8	302	362
95-MC-UR3_29	0.369	0.01	0.05039	0.00086	0.47028	317.5	5.4	264	217
95-MC-UR3_30	0.369	0.0086	0.05017	0.00086	0.25343	315.5	5.3	231	199
95-MC-UR3_31	0.34	0.01	0.0474	0.0016	0.68928	299	10	479	274.1
7002_1	0.0371	0.0083	0.00085	0.00014	0.5365	5.47	0.9	92.7	46.4
7002_2	0.0113	0.0027	0.000562	0.000069	0.3138	3.62	0.45	185	148
7002_3	0.0055	0.0019	0.000474	0.000081	0.02798	3.05	0.52	122.9	64.7
7002_4	0.0032	0.0017	0.000494	0.000064	0.044998	3.18	0.41	113.9	69.3
7002_5	0.0109	0.0025	0.000396	0.00007	0.14695	2.55	0.45	117	81
7002_6	0.0065	0.0025	0.000468	0.000074	0.23708	3.01	0.48	91.4	71.3
7002_7	0.0346	0.0051	0.000713	0.000081	0.58527	4.59	0.52	166.7	167.1
7002_8	0.0058	0.0029	0.00045	0.0001	0.25337	2.9	0.66	66.5	55.1
7002_9	0.0023	0.0014	0.000375	0.000061	0.093411	2.42	0.39	116.6	100
7002_10	0.0055	0.0019	0.000416	0.000056	0.11084	2.68	0.36	155.2	108.9
7002_11	0.0047	0.0012	0.000501	0.000057	0.1164	3.23	0.37	248	270
7002_12	0.0026	0.0016	0.00049	0.000073	0.19102	3.16	0.47	144	111
7002_13	0.019	0.011	0.00054	0.00017	0.17693	3.5	1.1	60	52.9
7002_14	0.0053	0.0018	0.000496	0.000065	0.21025	3.19	0.42	153	126

	207Pb/235U	207Pb/235U error	206Pb/238U	206Pb/238U Error	Error Correlation 206/238 vs. 207/235	Final Age (Ma)	Error (Ma)	Approx U (ppm)	Approx Th (ppm)
7002_15	0.0048	0.001	0.000494	0.000051	0.038115	3.18	0.33	241	224
7002_16	0.0041	0.0011	0.000434	0.000046	0.077186	2.8	0.3	200.2	165
7002_17	0.006	0.0018	0.000506	0.000054	0.54474	3.26	0.35	209.2	155.5
7002_18	0.00509	0.00097	0.00048	0.000044	0.099406	3.1	0.28	355	273
7002_19	0.0025	0.0013	0.000428	0.00006	0.14068	2.76	0.39	120.6	102.6
7002_20	0.0033	0.0011	0.000501	0.000065	0.10684	3.23	0.42	240	208
7002_21	0.00393	0.00029	0.000566	0.000027	0.035907	3.64	0.17	1422	327
7002_22	0.376	0.012	0.0518	0.001	0.32084	325.4	6.2	85.1	108.2
7002_23	0.3356	0.0066	0.04714	0.00067	0.41213	296.9	4.1	335	255
7002_24	5.186	0.054	0.3265	0.0043	0.68517	1821	21	452	25.2
7002_25	0.3396	0.0049	0.04703	0.00045	0.17782	296.3	2.8	621	304
7002_26	0.4342	0.0091	0.05799	0.00076	0.58119	363.3	4.6	446	431
7002_27	0.3098	0.0064	0.04421	0.00077	0.14756	278.8	4.7	307	312
6002_1	0.01	0.0041	0.0007	0.00027	0.50465	4.5	1.7	275	159
6002_2	0.00424	0.00069	0.000507	0.000043	0.13192	3.26	0.28	379	194
6002_3	0.0045	0.0023	0.0005	0.00018	0.30642	3.2	1.2	161	109
6002_4	0.00377	0.0004	0.000497	0.000026	0.019434	3.2	0.17	655	273
6002_5	0.0078	0.0053	0.00069	0.00014	0.40367	4.47	0.93	327	188
6002_6	0.00467	0.00071	0.000531	0.000034	0.05181	3.42	0.22	436	157.5
6002_7	0.00402	0.00042	0.000512	0.000028	0.10398	3.3	0.18	804	589
6002_8	0.0065	0.0013	0.000567	0.00005	0.11214	3.66	0.32	324.8	232.5
6002_9	0.0039	0.0038	0.00055	0.00019	0.38435	3.5	1.2	122	70.5
6002_10	0.00472	0.0007	0.000524	0.000045	0.11236	3.38	0.29	381	231.4
6002_11	0.00474	0.00082	0.000487	0.000039	0.08869	3.14	0.25	284.9	316.4
6002_12	0.0081	0.0044	0.00062	0.00021	0.46658	4	1.4	180	144
6002_13	0.0094	0.0026	0.00053	0.0001	0.16056	3.4	0.64	172.4	65.2
6002_14	0.00402	0.00049	0.000559	0.000033	0.087788	3.6	0.21	614	260
6002_15	0.0071	0.0023	0.00052	0.00011	0.24042	3.38	0.71	327	144.4
6002_16	11.1	0.16	0.4643	0.0067	0.62921	2458	30	500	365
6002_17	6.232	0.078	0.3735	0.0044	0.6539	2045	21	382	215
6002_18	4.76	0.14	0.311	0.0089	0.3821	1745	44	16.9	22.3
6002_19	12.73	0.2	0.5158	0.006	0.65726	2681	25	76.6	59.12
6002_20	11.49	0.19	0.493	0.013	0.66966	2584	56	761	621
6002_21	5.142	0.073	0.339	0.0074	0.86751	1881	36	1226	87.2
6002_22	11.3	0.15	0.507	0.0072	0.51628	2644	31	1138	557
6002_23	7.78	0.2	0.3834	0.0055	0.60285	2091	26	138.2	149.4
6002_24	6.2	0.1	0.3733	0.0071	0.4458	2045	33	254.1	102
6002_25	4.77	0.1	0.3115	0.0071	0.61225	1753	36	377	105.8
6002_26	8.14	0.24	0.3878	0.0051	0.13705	2112	24	90.4	134
6002_27	7.77	0.11	0.3908	0.0065	0.78887	2126	30	728	97.5
6002_28	0.105	0.037	0.00155	0.00036	0.75823	10	2.3	274	193
6002_29	8.86	0.16	0.4099	0.0064	0.8466	2214	29	235	146
6002_30	10.28	0.11	0.4581	0.0057	0.47473	2431	25	245.1	78.9
6002_31	6.638	0.093	0.3716	0.0063	0.73585	2036	30	588	430
6002_32	7.93	0.13	0.412	0.0098	0.81429	2238	37	581	551
KL20-10-602m_1	0.006	0.0012	0.000508	0.000042	0.13695	3.27	0.27	311.2	108.1
KL20-10-602m_2	0.00517	0.0007	0.000529	0.000033	0.043321	3.41	0.21	504	161
KL20-10-602m_3	0.0077	0.0031	0.000496	0.00004	0.1014	3.19	0.26	347.4	103.7
KL20-10-602m_4	0.00483	0.00094	0.000449	0.00004	0.048454	2.89	0.26	376	105.6
KL20-10-602m_5	0.00446	0.0008	0.000495	0.000043	0.02639	3.19	0.28	380.9	135.4
KL20-10-602m_6	0.00434	0.00063	0.000503	0.000048	0.15899	3.24	0.31	441	135
KL20-10-602m_7	0.00496	0.00096	0.000552	0.000054	0.18627	3.56	0.35	490	156
KL20-10-602m_8	0.0058	0.001	0.000514	0.000051	0.037609	3.31	0.33	346	86.6
KL20-10-602m_9	0.006	0.001	0.000514	0.000048	0.091398	3.31	0.31	310.9	106.2
KL20-10-602m_10	0.0058	0.0011	0.000486	0.000048	0.051061	3.13	0.31	336	98.1
KL20-10-602m_11	0.00445	0.00074	0.000505	0.000041	0.016454	3.26	0.26	408	100.2
KL20-10-602m_12	0.0057	0.002	0.000443	0.000039	0.19172	2.85	0.25	496	168
KL20-10-602m_13	0.0047	0.0011	0.000484	0.000063	0.079088	3.12	0.41	538	151
KL20-10-602m_14	0.00571	0.00085	0.000515	0.000053	0.20586	3.32	0.34	497	197
KL20-10-602m_15	0.0111	0.0021	0.000577	0.000052	0.12372	3.72	0.34	421	128
KL20-10-602m_16	0.00494	0.00084	0.000563	0.000047	0.09938	3.63	0.31	362	82.5
KL20-10-602m_17	0.00465	0.00074	0.000499	0.000051	0.10207	3.21	0.33	347.8	97.2
KL20-10-602m_18	0.0061	0.0012	0.000504	0.000041	0.11038	3.25	0.27	392	115
KL20-10-602m_19	0.00406	0.00063	0.000532	0.000048	0.069596	3.43	0.31	439	177.3
KL20-10-602m_20	0.0073	0.0019	0.000492	0.000066	0.11774	3.17	0.42	328	110.8
KL20-10-602m_21	0.00483	0.00072	0.000502	0.000041	0.18734	3.24	0.27	392	123.3
KL20-10-602m_22	0.00486	0.00058	0.000491	0.000046	0.024794	3.17	0.3	502	220.7
KL20-10-602m_23	0.00428	0.00063	0.000486	0.000047	0.0070239	3.13	0.3	444	186
KL20-10-602m_24	0.00533	0.0009	0.000535	0.000042	0.10887	3.45	0.27	435	161

	207Pb/235U	207Pb/235U error	206Pb/238U	206Pb/238U Error	Error Correlation 206/238 vs. 207/235	Final Age (Ma)	Error (Ma)	Approx U (ppm)	Approx Th (ppm)
KL20-10-602m_25	0.0057	0.0013	0.000481	0.000065	0.004161	3.1	0.42	378	149.3
KL20-10-602m_26	0.007	0.0017	0.000523	0.00007	0.19772	3.37	0.45	562	219
KL20-10-602m_27	0.0057	0.0011	0.000516	0.000045	0.088774	3.33	0.29	284	98.9
KL20-10-602m_28	0.00515	0.00065	0.000504	0.000046	0.11888	3.25	0.3	494	253
KL20-10-602m_29	0.00544	0.00086	0.000512	0.000037	0.090745	3.3	0.24	406.9	139.2
KL20-10-602m_30	0.0057	0.001	0.000499	0.00004	0.16394	3.21	0.26	469	184
KL20-10-602m_31	0.00582	0.00095	0.000542	0.000047	0.18903	3.49	0.3	408	233
KL20-10-602m_32	0.00498	0.00077	0.000474	0.000042	0.15538	3.05	0.27	437	175
94-MC-RC2_1	0.0069	0.0012	0.000606	0.000055	0.074718	3.9	0.35	171.9	118.9
94-MC-RC2_2	0.00493	0.00059	0.000618	0.000043	0.26596	3.98	0.28	700	616
94-MC-RC2_3	0.00538	0.00066	0.000579	0.000034	0.051747	3.73	0.22	240	244
94-MC-RC2_4	0.00486	0.0005	0.000551	0.000028	0.032657	3.55	0.18	362	290
94-MC-RC2_5	0.00552	0.00088	0.000572	0.000043	0.13598	3.69	0.28	218	162.1
94-MC-RC2_6	0.0043	0.00071	0.000521	0.000026	0.099297	3.36	0.17	192.7	156.6
94-MC-RC2_7	0.012	0.0018	0.000631	0.000052	0.19047	4.07	0.34	188	86.1
94-MC-RC2_8	0.00473	0.00057	0.000556	0.000026	0.030896	3.58	0.17	263.4	222.4
94-MC-RC2_9	0.00553	0.00088	0.000571	0.000045	0.14576	3.68	0.29	197	125
94-MC-RC2_10	0.0064	0.001	0.000574	0.000049	0.10531	3.7	0.32	565	340
94-MC-RC2_11	0.00516	0.00067	0.000621	0.000043	0.53067	4	0.28	902	761
94-MC-RC2_12	0.0065	0.0011	0.000606	0.000039	0.2545	3.9	0.25	235.4	201.8
94-MC-RC2_13	0.0056	0.00084	0.000608	0.000032	0.17161	3.92	0.2	188.9	138.7
94-MC-RC2_14	0.00445	0.00035	0.000595	0.000025	0.19753	3.83	0.16	700	274
94-MC-RC2_15	0.0063	0.0022	0.00056	0.00011	0.012025	3.6	0.74	192	128.3
94-MC-RC2_16	0.0072	0.0012	0.000628	0.000093	0.44493	4.05	0.6	657	617
94-MC-RC2_17	0.00636	0.00072	0.000586	0.000037	0.31583	3.78	0.24	253.5	185.3
94-MC-RC2_18	0.00567	0.0009	0.000555	0.000034	0.14421	3.58	0.22	340	415
94-MC-RC2_19	0.00608	0.00068	0.000577	0.000033	0.067459	3.72	0.21	316	277
94-MC-RC2_20	0.0069	0.0012	0.00053	0.000076	0.11056	3.42	0.49	186	119.8
94-MC-RC2_21	0.00538	0.00087	0.000511	0.000038	0.30373	3.29	0.24	211.9	186.3
94-MC-RC2_22	0.00627	0.00098	0.00058	0.000057	0.074915	3.74	0.37	340	263
94-MC-RC2_23	0.00684	0.00083	0.00068	0.000059	0.13456	4.38	0.38	537	591
94-MC-RC2_24	0.0057	0.00093	0.000509	0.000037	0.13387	3.28	0.24	205.9	171.1
94-MC-RC2_25	0.00583	0.00073	0.000587	0.000035	0.064348	3.78	0.23	329	310
94-MC-RC2_26	0.00436	0.00068	0.000659	0.000058	0.66249	4.25	0.37	762	483
94-MC-RC2_27	0.0071	0.0015	0.000564	0.000058	0.11025	3.63	0.37	113.8	61.8
94-MC-RC2_28	0.0078	0.0016	0.000604	0.000071	0.017475	3.89	0.46	137.6	84.5
94-MC-RC2_29	4.592	0.054	0.3002	0.003	0.33634	1692	15	190	110.7
94-MC-RC2_30	0.1652	0.006	0.02196	0.00084	0.34863	140	5.3	309	185.2
94-MC-RC2_31	1.986	0.067	0.1313	0.0034	0.72267	795	19	87.9	65.8
SE02-01-117m_1	0.00465	0.00091	0.00063	0.000059	-0.02589	4.06	0.38	462	102
SE02-01-117m_2	0.0088	0.0026	0.00077	0.00013	-0.0058243	4.94	0.81	204	27.6
SE02-01-117m_3	0.0056	0.001	0.000709	0.000068	0.18204	4.57	0.44	200	59.9
SE02-01-117m_4	0.0061	0.0014	0.000629	0.000071	-0.16102	4.06	0.46	373	78.5
SE02-01-117m_5	0.0037	0.0012	0.000665	0.000088	-0.031267	4.28	0.57	154.8	71.7
SE02-01-117m_6	0.009	0.0027	0.0009	0.00014	0.38308	5.81	0.9	379	68
SE02-01-117m_7	0.0045	0.0016	0.000687	0.000087	-0.18719	4.42	0.56	187	169
SE02-01-117m_8	0.0031	0.0013	0.00061	0.00012	0.33124	3.94	0.79	432	82
SE02-01-117m_9	0.0089	0.0016	0.00069	0.00013	0.40163	4.46	0.82	437	75.2
SE02-01-117m_10	0.0052	0.0011	0.00066	0.000056	0.032739	4.25	0.36	368	49
SE02-01-117m_11	0.00423	0.00066	0.000618	0.000049	-0.053426	3.98	0.31	424	212
SE02-01-117m_12	0.0069	0.0016	0.000564	0.000087	-0.044914	3.63	0.56	344	56.6
SE02-01-117m_13	0.00551	0.00073	0.0007	0.000039	0.032386	4.51	0.25	479	245
SE02-01-117m_14	0.0051	0.0016	0.000671	0.000083	-0.023297	4.33	0.53	324	58.1
SE02-01-117m_15	0.0058	0.0014	0.000652	0.000082	0.029019	4.2	0.53	257	48
SE02-01-117m_16	0.0174	0.0039	0.00075	0.00019	-0.28125	4.8	1.2	81.5	32.98
SE02-01-117m_17	0.0056	0.0012	0.000628	0.000053	-0.14207	4.05	0.34	399	83.7
SE02-01-117m_18	0.0047	0.0034	0.00075	0.00014	-0.18073	4.86	0.92	102	1
SE02-01-117m_19	0.0053	0.0018	0.000688	0.000096	0.036938	4.43	0.62	103.3	68.3
SE02-01-117m_20	0.00606	0.0008	0.00072	0.000051	0.12373	4.64	0.33	428	157
SE02-01-117m_21	0.0039	0.0011	0.00065	0.000079	-0.28184	4.19	0.51	577	116.9
SE02-01-117m_22	0.0195	0.0039	0.00072	0.00011	-0.022579	4.66	0.7	94.1	91
SE02-01-117m_23	0.0033	0.0021	0.00063	0.00016	0.33658	4	1	320	48.9
SE02-01-117m_24	0.0063	0.0013	0.000682	0.000063	0.016957	4.39	0.41	392	84.3
SE02-01-117m_25	4.64	0.13	0.2992	0.0062	0.17956	1698	33	29.8	97
SE02-01-117m_26	3.41	0.15	0.249	0.01	0.71288	1433	52	138.6	135.9
SE02-01-117m_27	6.45	0.16	0.3402	0.008	0.57063	1887	39	139.4	94
SE02-01-117m_28	4.113	0.069	0.3005	0.0049	0.46574	1693	24	118.4	118.7
SE02-01-117m_29	4.78	0.27	0.3056	0.0093	0.97224	1717	45	146	83.8

	207Pb/235U	207Pb/235U error	206Pb/238U	206Pb/238U Error	Error Correlation 206/238 vs. 207/235	Final Age (Ma)	Error (Ma)	Approx U (ppm)	Approx Th (ppm)
SE02-01-117m_30	5.15	0.12	0.3287	0.0055	0.70978	1835	26	77.5	96.5
SE02-01-117m_31	11.11	0.13	0.4693	0.0065	0.60589	2480	29	90.7	114.8
SE02-01-117m_32	9.99	0.26	0.429	0.01	0.64823	2300	46	29.4	111.6
SE02-01-117m_33	10.18	0.42	0.45	0.014	0.83925	2392	64	46.6	50.4
SE02-01-117m_34	7.572	0.083	0.4103	0.0062	0.75912	2216	28	971	451
SE02-01-117m_35	4.112	0.086	0.2793	0.0045	0.85292	1587	23	716	119.1

Appendix F: Tera-Wasserburg Diagrams

Tera-Wasserburg diagrams for each of the zircon U/Pb dated samples are shown in Appendix F. Each plot shows the results of the 32 zircons that were analyzed for that sample, and the plots are in the same order as the samples shown in Figure 1-11, Figure 4-3, and Figure 4-4. The lower intercept between the Concordia line and the regression line through the individual zircon analyses is reported as the age and uncertainty.

Grasberg Igneous Complex

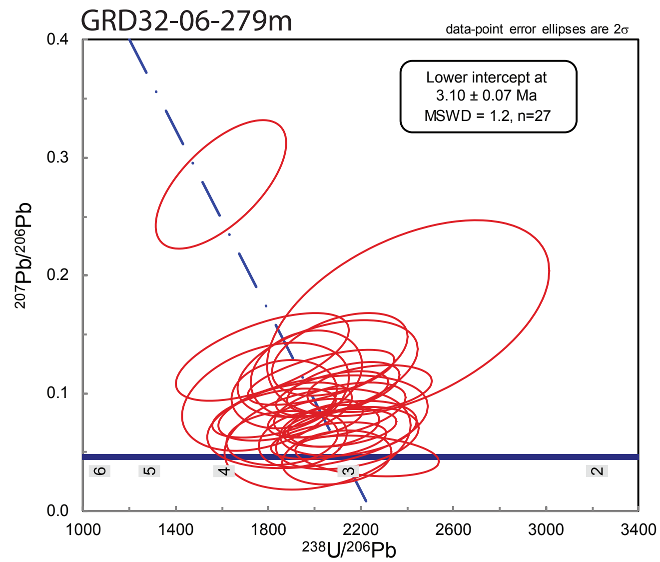

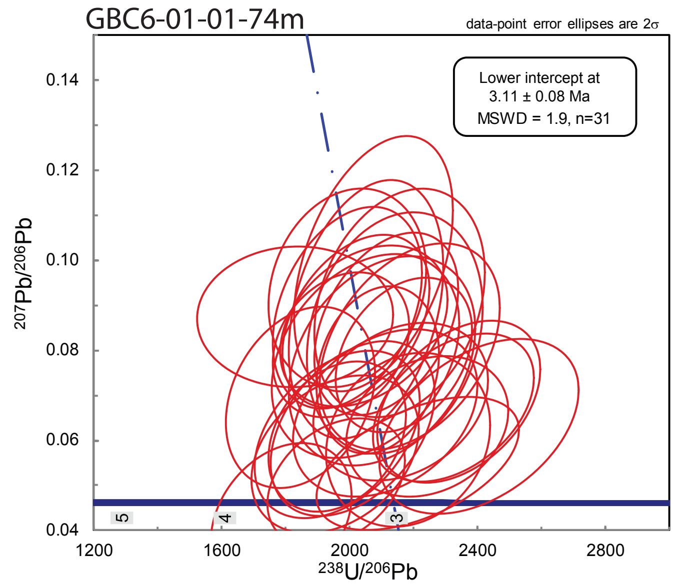

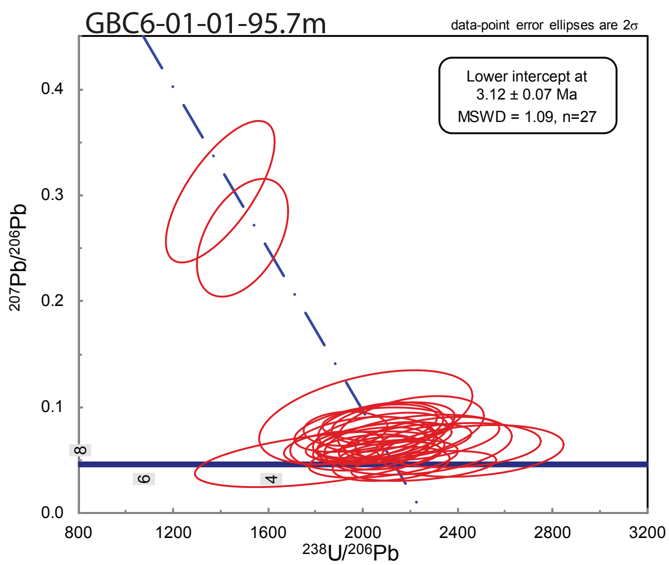

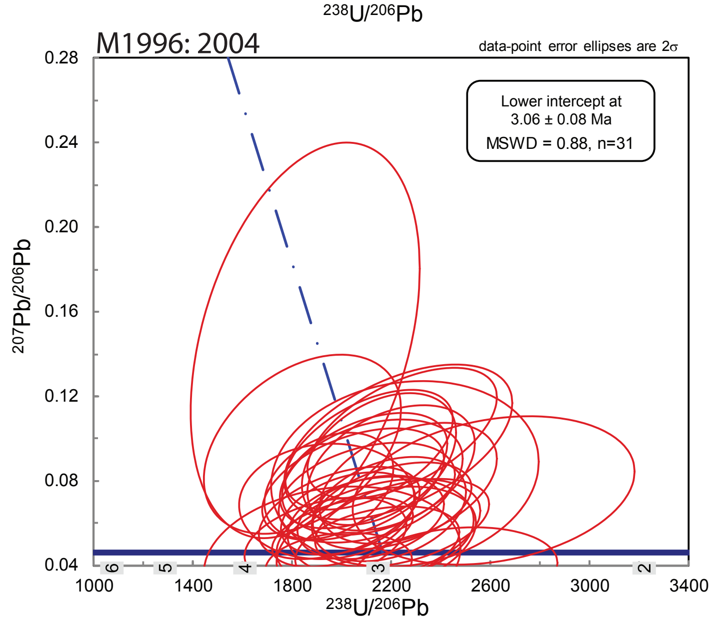

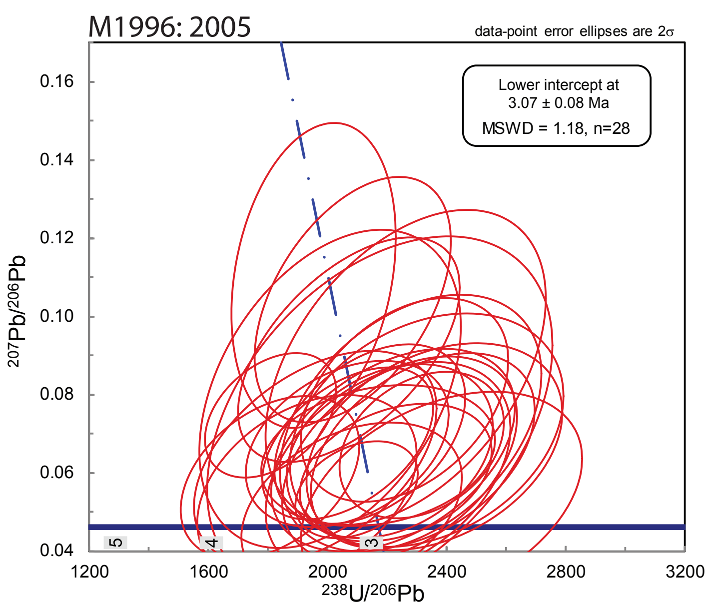

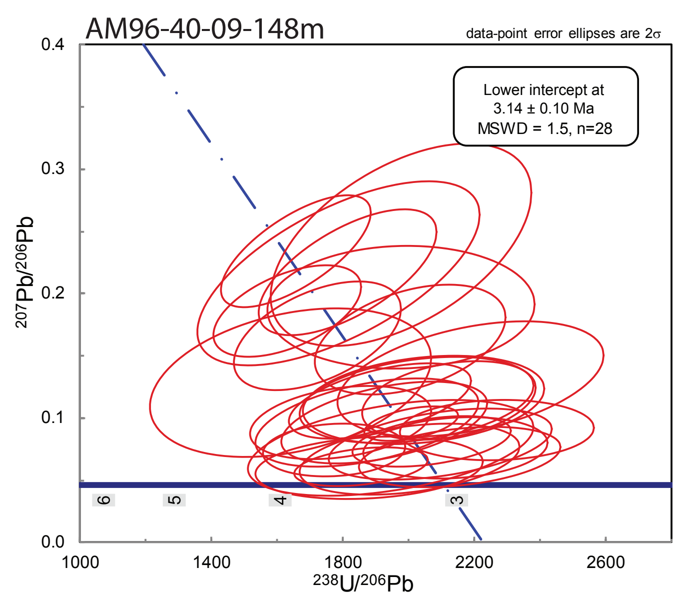

Grasberg Igneous Complex

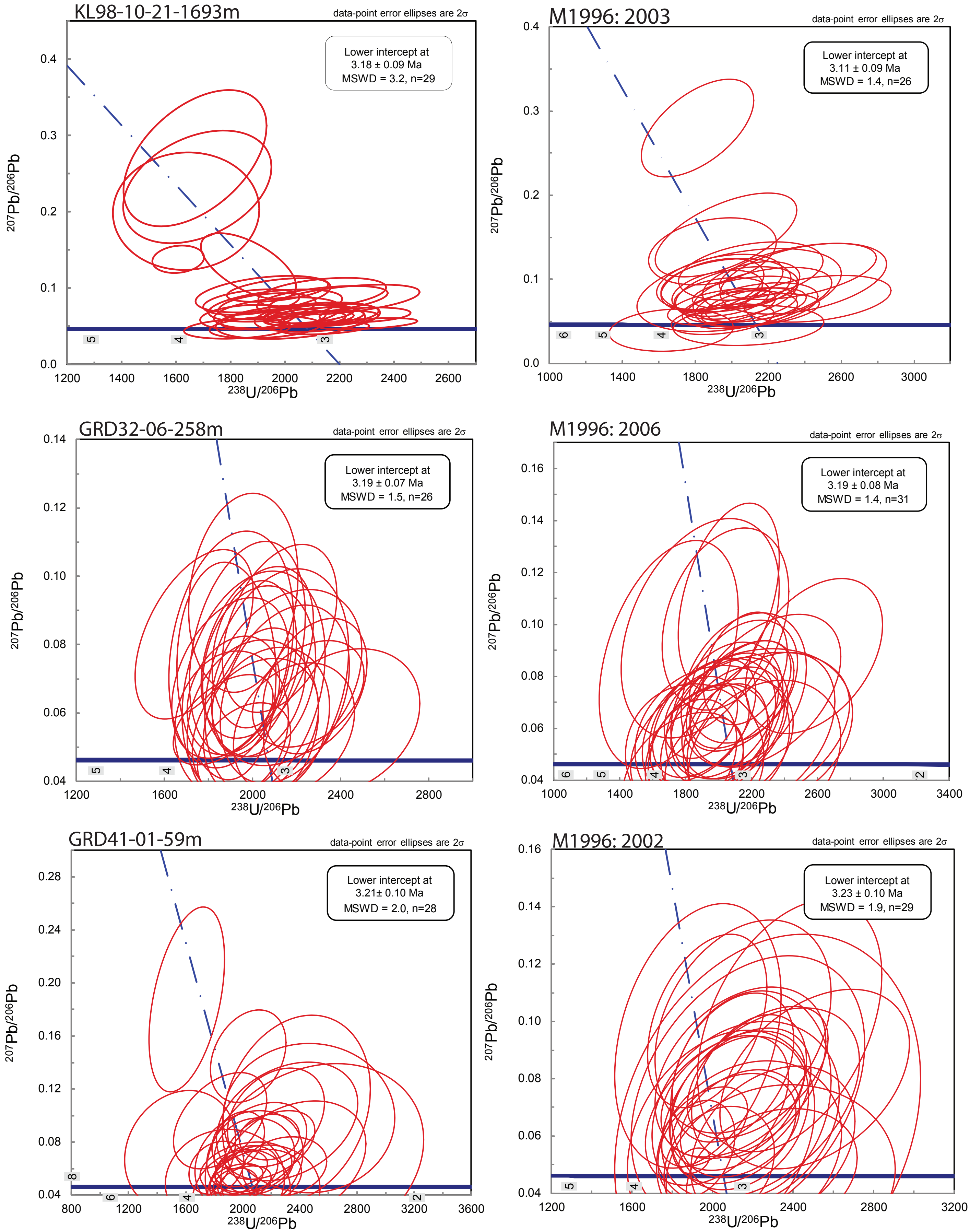

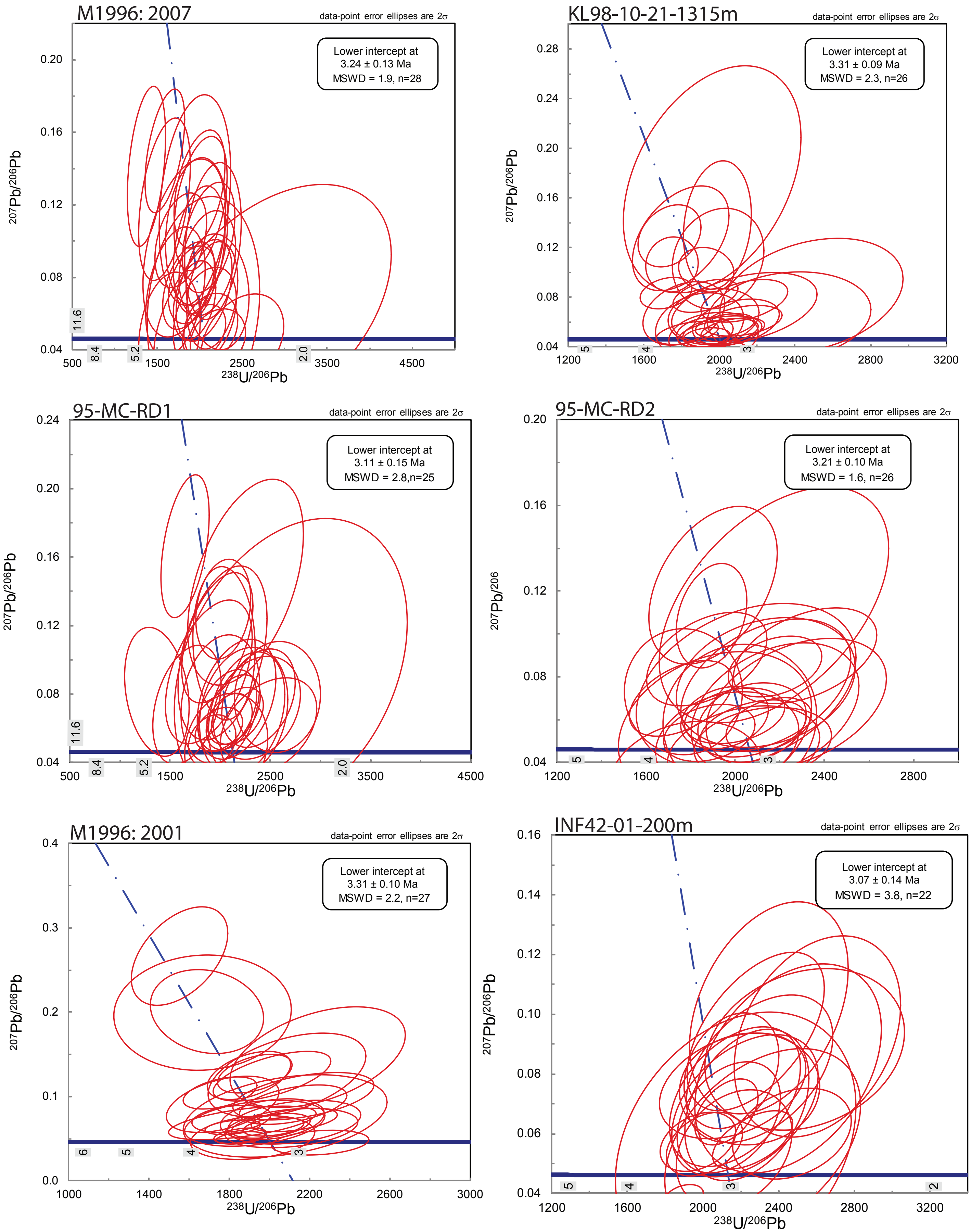
M1996: 2007
data-point error ellipses are 2σ
Lower intercept at
3.24 ± 0.13 Ma
MSWD = 1.9, n=28
207Pb/206Pb
238U/206Pb
KL98-10-21-1315m
data-point error ellipses are 2σ
Lower intercept at
3.31 ± 0.09 Ma
MSWD = 2.3, n=26
207Pb/206Pb
238U/206Pb
95-MC-RD1
data-point error ellipses are 2σ
Lower intercept at
3.11 ± 0.15 Ma
MSWD = 2.8,n=25
207Pb/206Pb
238U/206Pb
95-MC-RD2
data-point error ellipses are 2σ
Lower intercept at
3.21 ± 0.10 Ma
MSWD = 1.6, n=26
207Pb/206
238U/206Pb
M1996: 2001
data-point error ellipses are 2σ
Lower intercept at
3.31 ± 0.10 Ma
MSWD = 2.2, n=27
207Pb/206Pb
238U/206Pb
INF42-01-200m
data-point error ellipses are 2σ
Lower intercept at
3.07 ± 0.14 Ma
MSWD = 3.8, n=22
207Pb/206Pb
238U/206Pb

Grasberg Igneous Complex

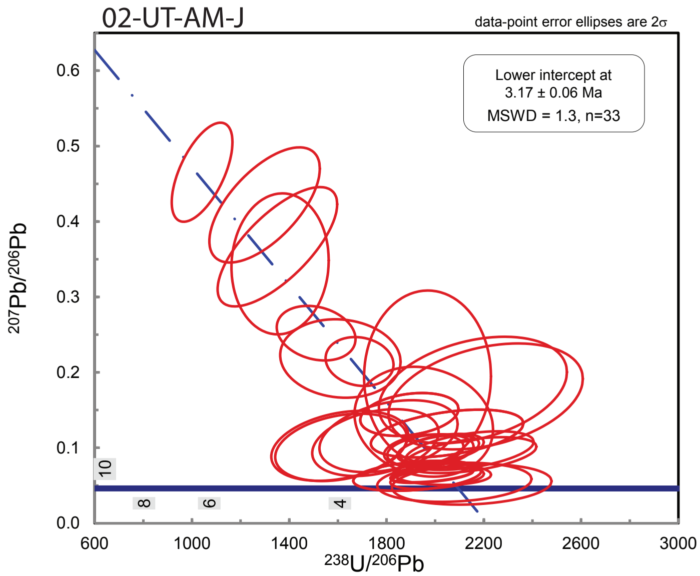

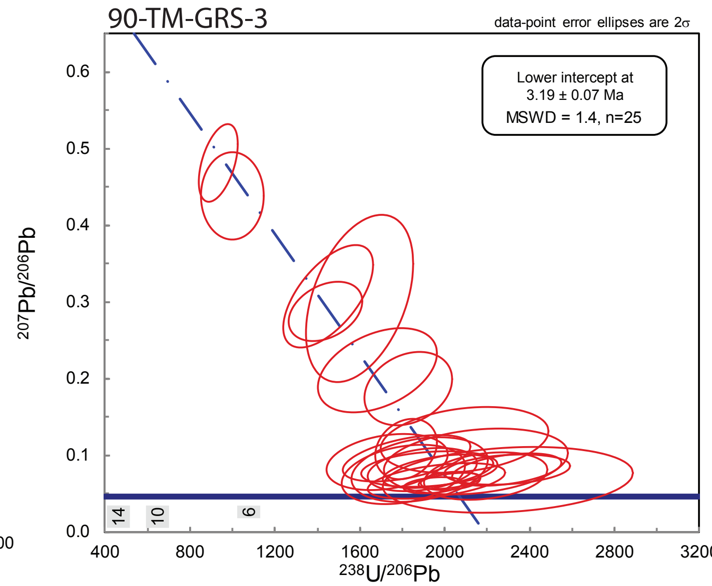

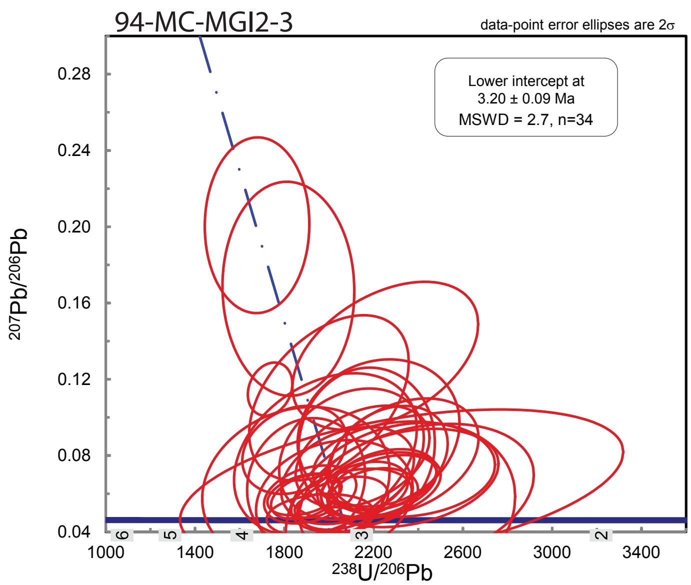

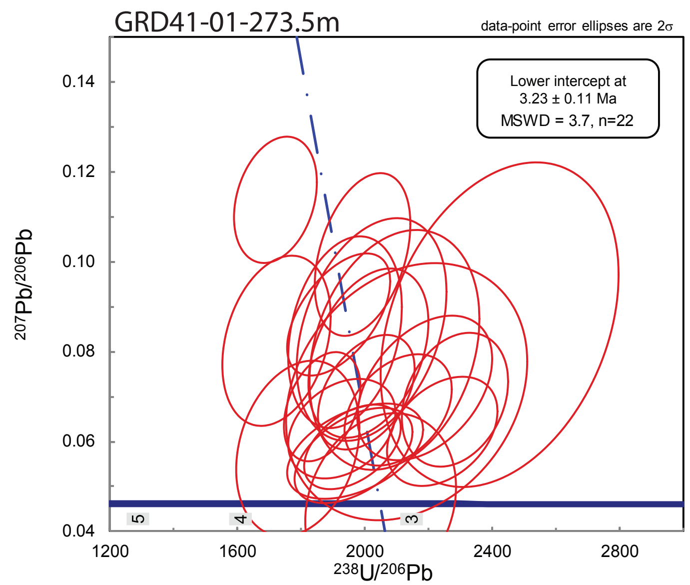

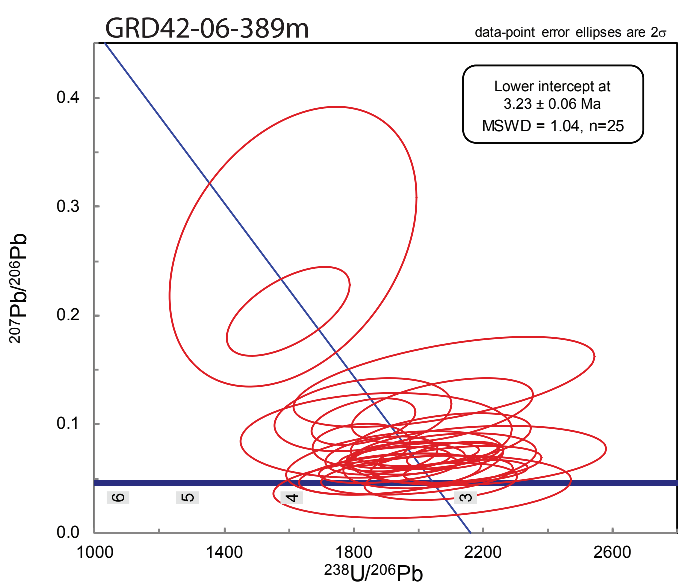

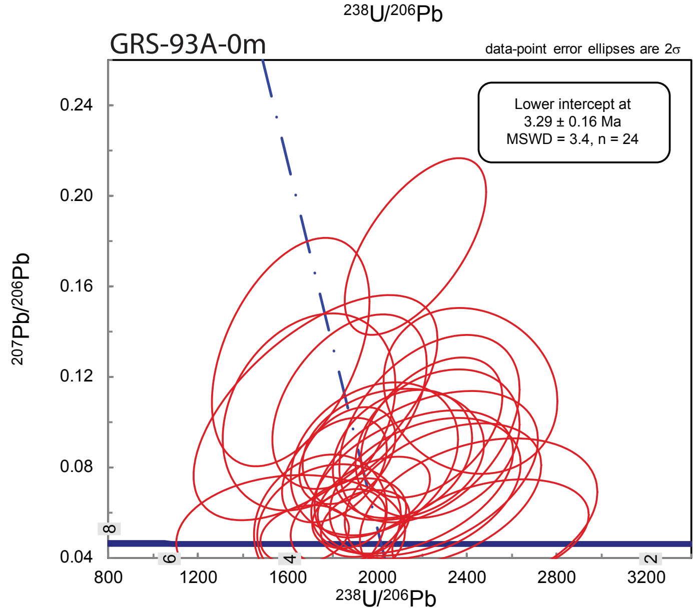

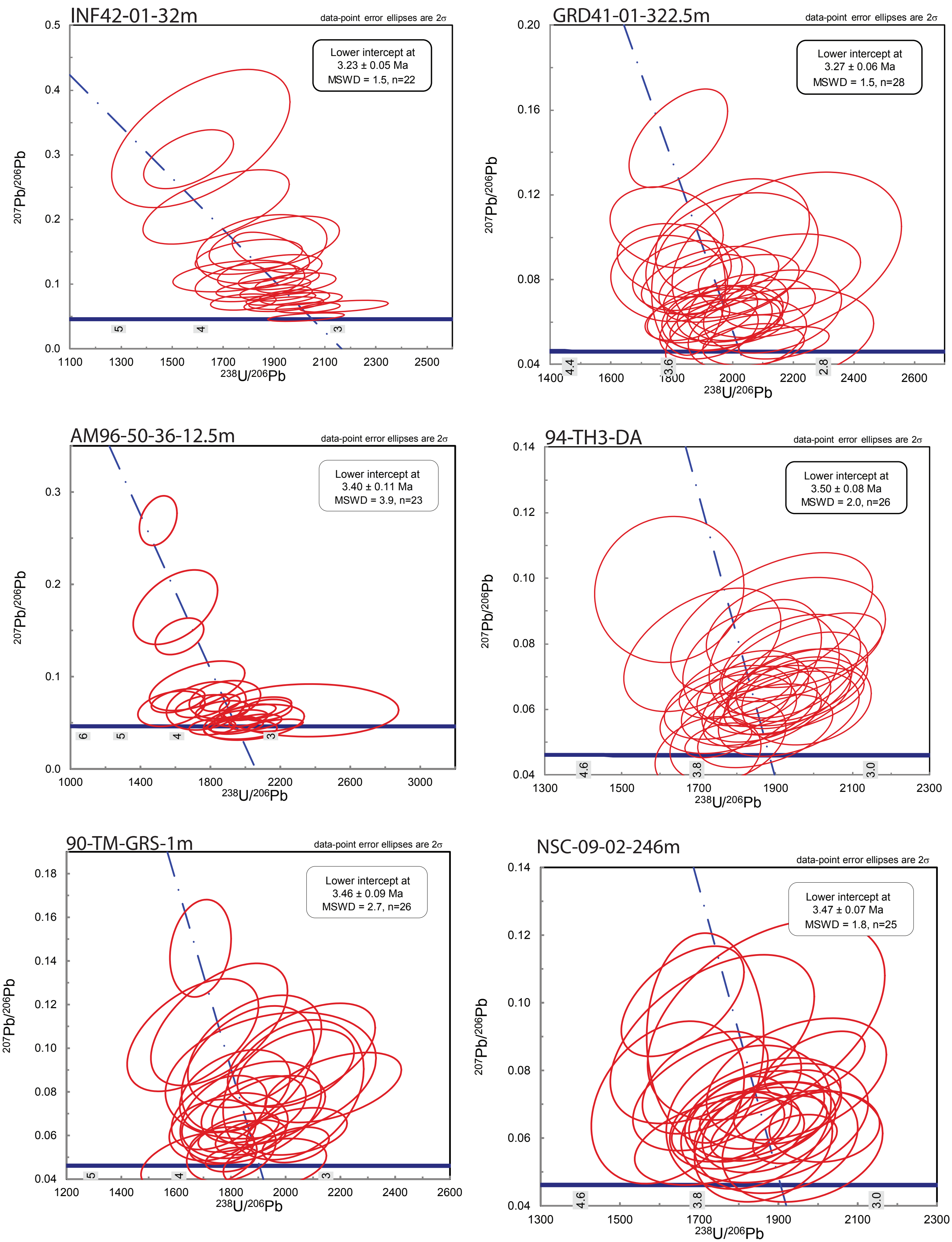
INF42-01-32m
data-point error ellipses are 2σ
Lower intercept at
3.23 ± 0.05 Ma
MSWD = 1.5, n=22
$^{207}Pb/^{206}Pb$
$^{238}U/^{206}Pb$
GRD41-01-322.5m
data-point error ellipses are 2σ
Lower intercept at
3.27 ± 0.06 Ma
MSWD = 1.5, n=28
AM96-50-36-12.5m
data-point error ellipses are 2σ
Lower intercept at
3.40 ± 0.11 Ma
MSWD = 3.9, n=23
94-TH3-DA
data-point error ellipses are 2σ
Lower intercept at
3.50 ± 0.08 Ma
MSWD = 2.0, n=26
90-TM-GRS-1m
data-point error ellipses are 2σ
Lower intercept at
3.46 ± 0.09 Ma
MSWD = 2.7, n=26
NSC-09-02-246m
data-point error ellipses are 2σ
Lower intercept at
3.47 ± 0.07 Ma
MSWD = 1.8, n=25

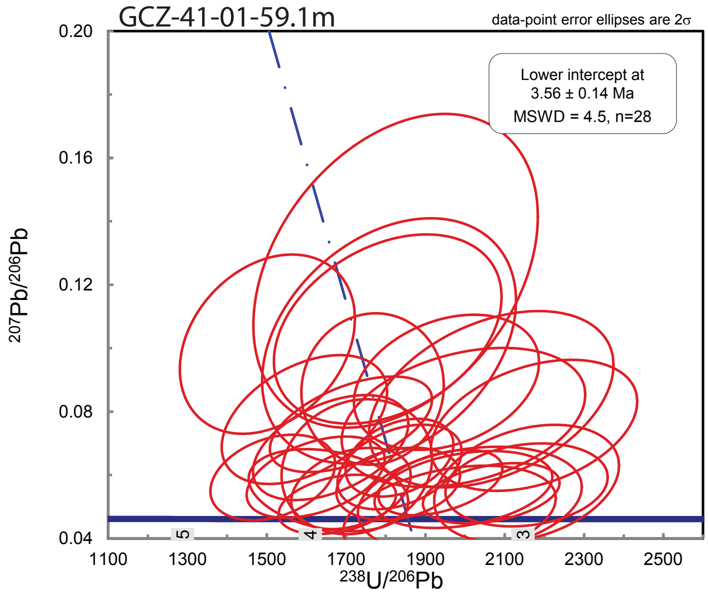
GCZ-41-01-59.1m
data-point error ellipses are 2σ
Lower intercept at
3.56 ± 0.14 Ma
MSWD = 4.5, n=28
207Pb/206Pb
238U/206Pb

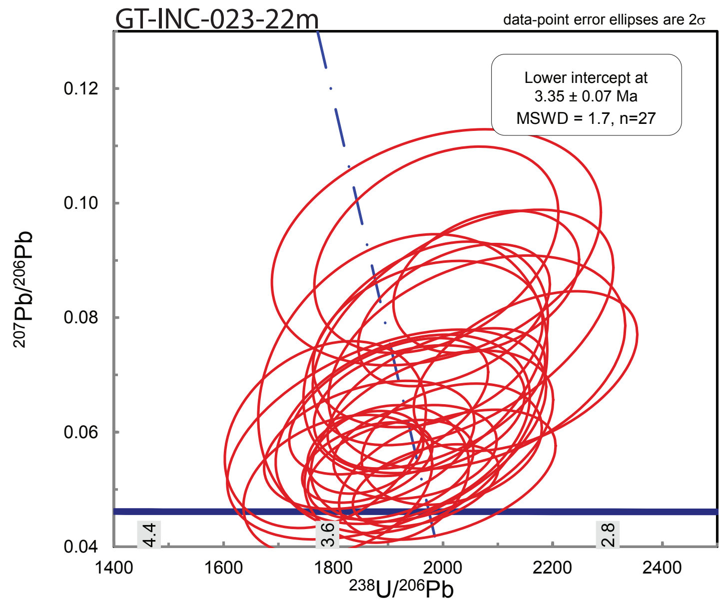
GT-INC-023-22m
data-point error ellipses are 2σ
Lower intercept at
3.35 ± 0.07 Ma
MSWD = 1.7, n=27
207Pb/206Pb
238U/206Pb

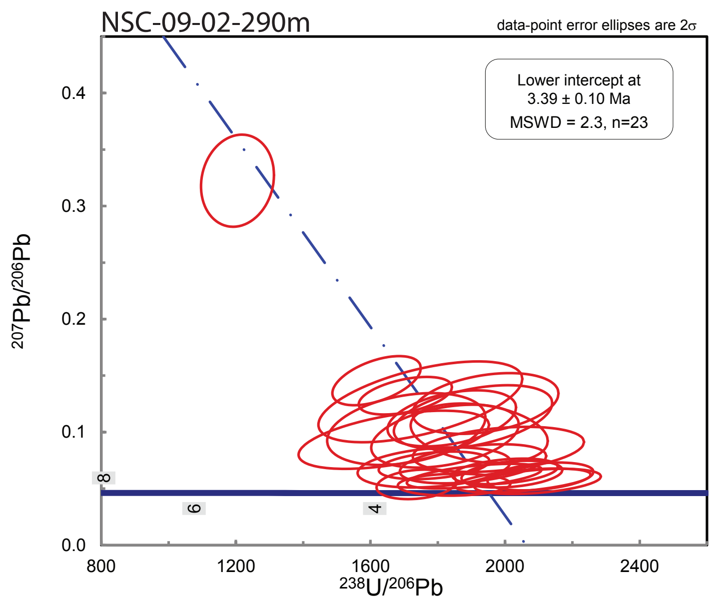
NSC-09-02-290m
data-point error ellipses are 2σ
Lower intercept at
3.39 ± 0.10 Ma
MSWD = 2.3, n=23
207Pb/206Pb
238U/206Pb

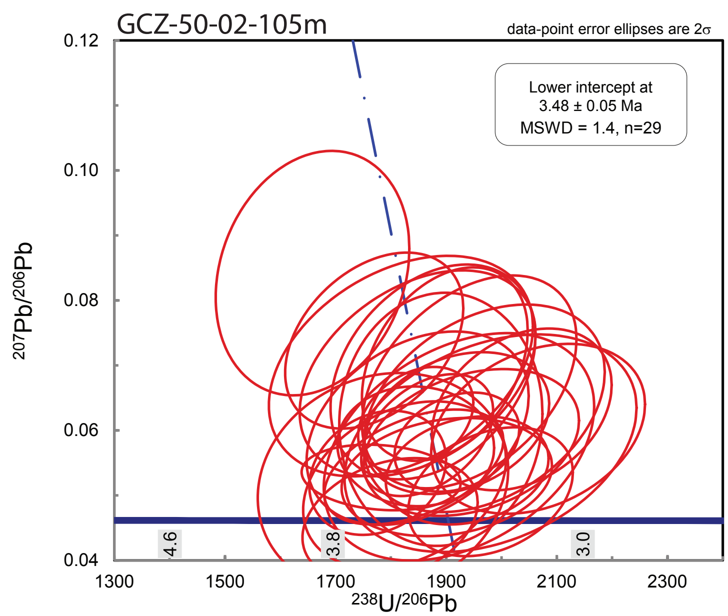
GCZ-50-02-105m
data-point error ellipses are 2σ
Lower intercept at
3.48 ± 0.05 Ma
MSWD = 1.4, n=29
207Pb/206Pb
238U/206Pb

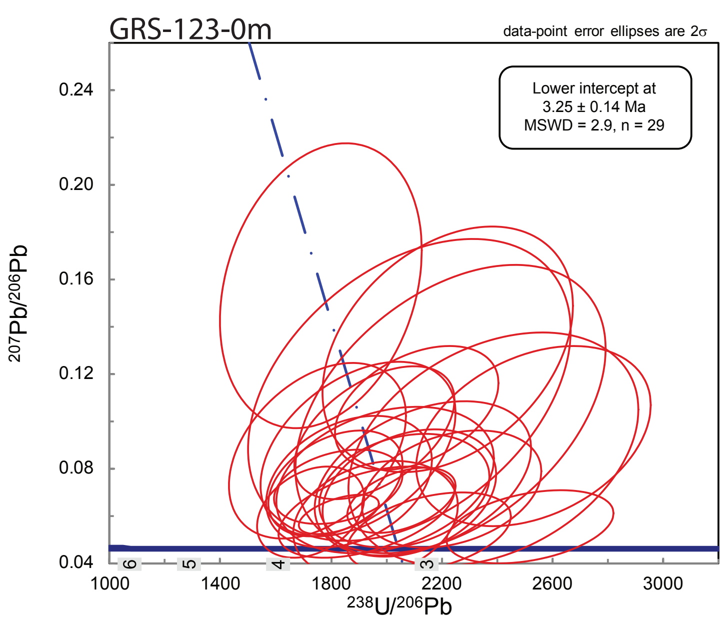
GRS-123-0m
data-point error ellipses are 2σ
Lower intercept at
3.25 ± 0.14 Ma
MSWD = 2.9, n = 29
207Pb/206Pb
238U/206Pb

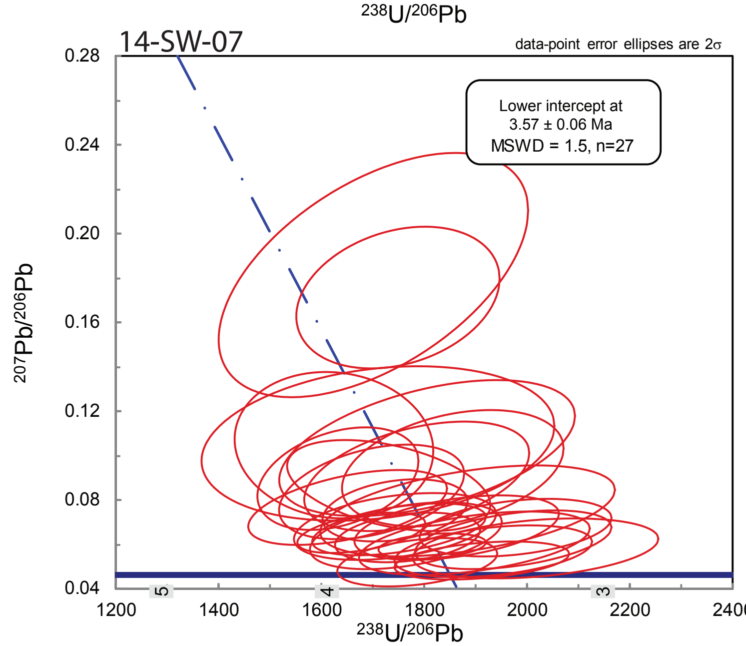
14-SW-07
data-point error ellipses are 2σ
Lower intercept at
3.57 ± 0.06 Ma
MSWD = 1.5, n=27
207Pb/206Pb
238U/206Pb

Grasberg Igneous Complex

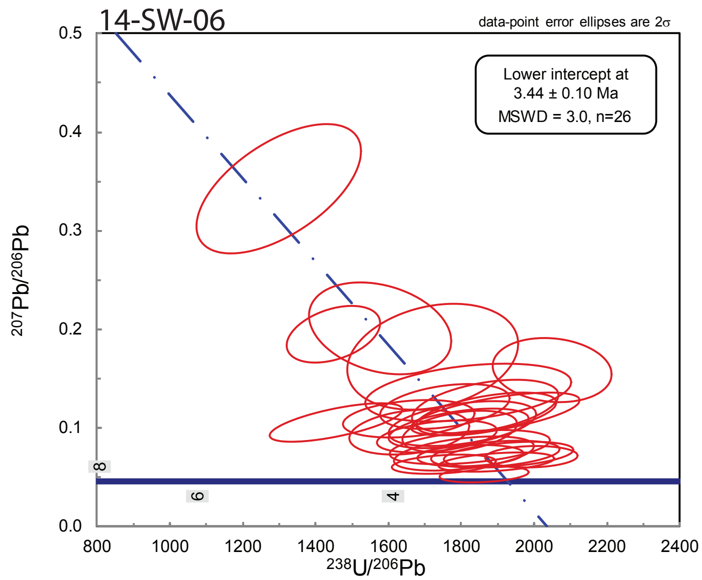

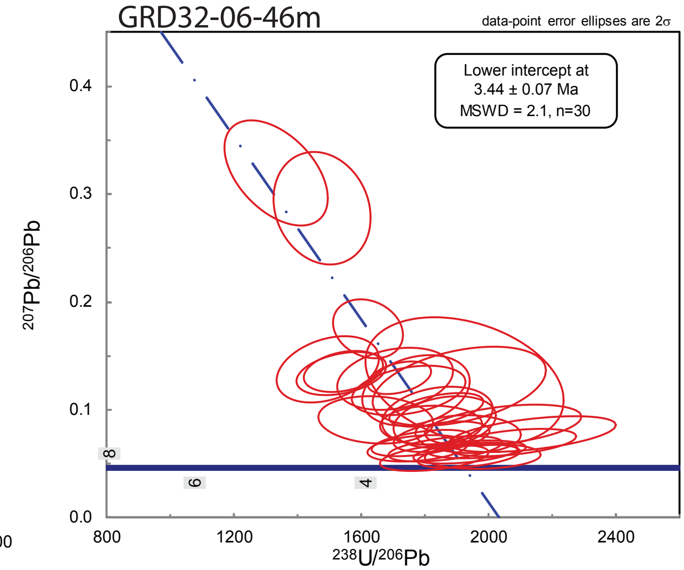

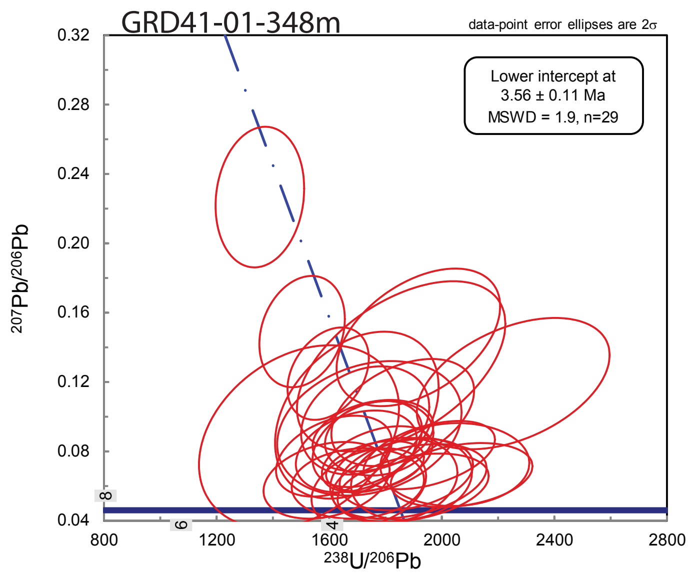

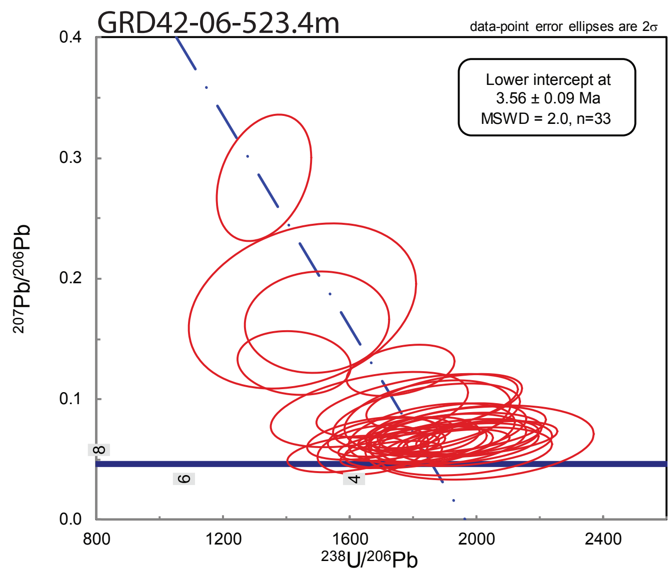

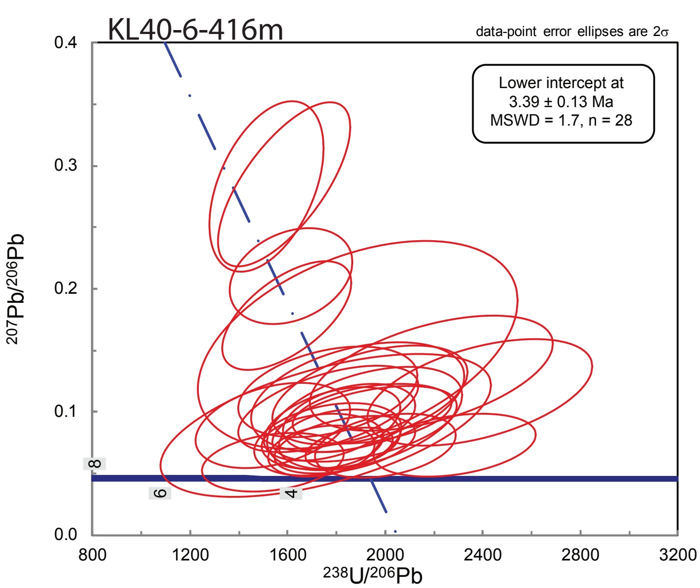

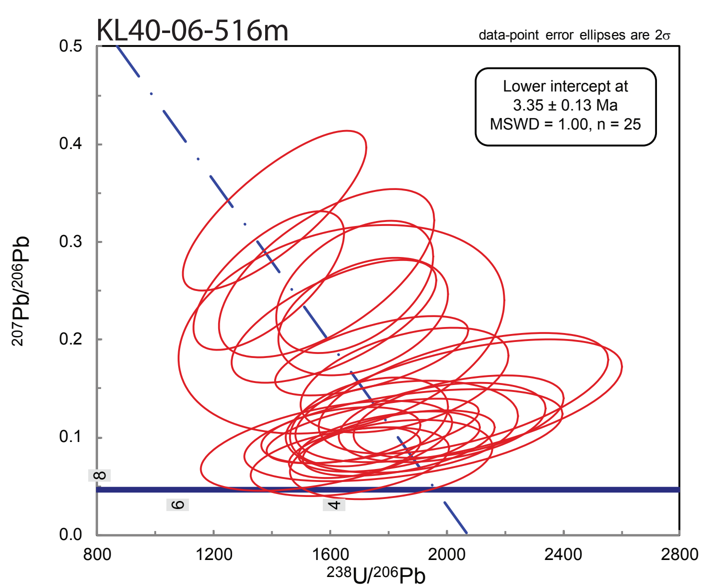

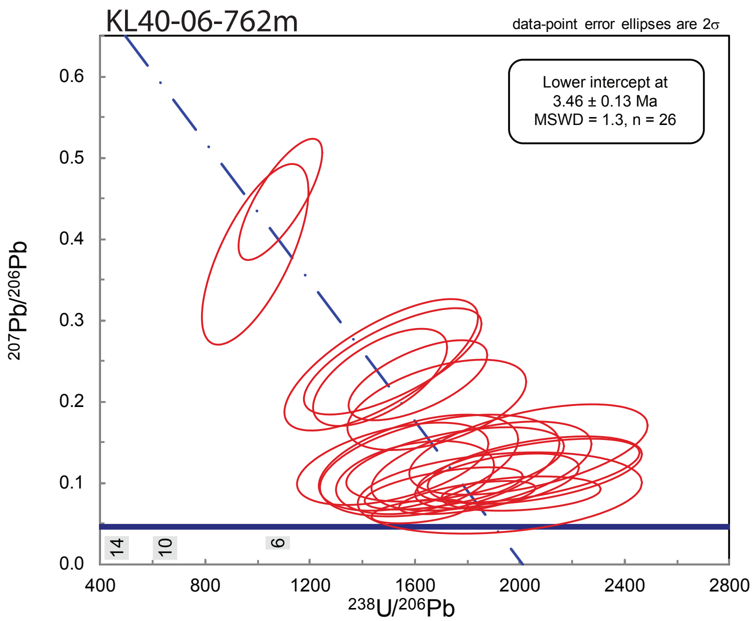

KL40-06-762m
data-point error ellipses are 2σ
Lower intercept at
3.46 ± 0.13 Ma
MSWD = 1.3, n = 26
0.6
0.5
0.4
0.3
0.2
0.1
0.0
14
10
6
400
800
1200
1600
2000
2400
2800
238U/206Pb
207Pb/206Pb

Ertsberg

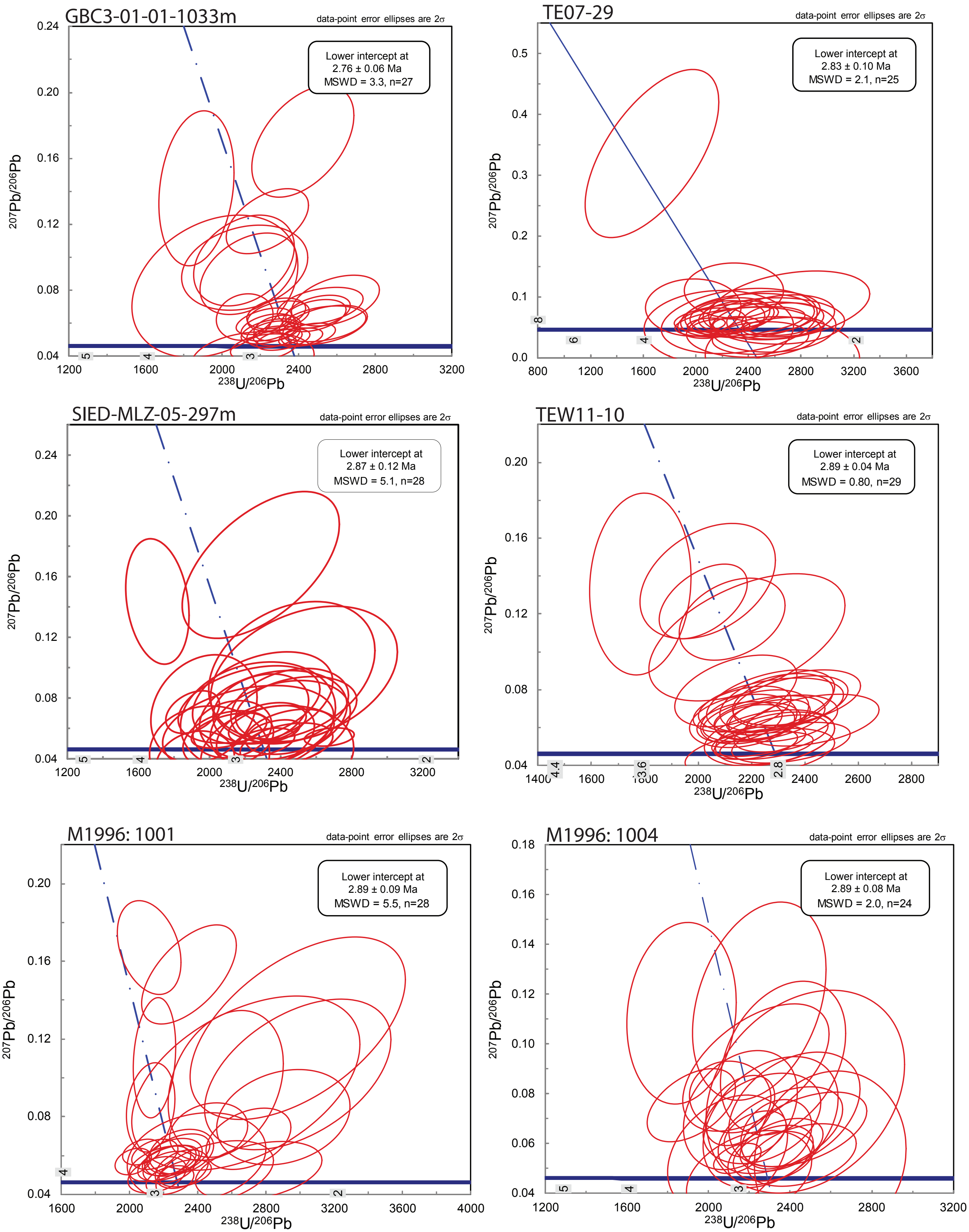

GBC3-01-01-1033m
data-point error ellipses are 2σ
Lower intercept at
2.76 ± 0.06 Ma
MSWD = 3.3, n=27
TE07-29
data-point error ellipses are 2σ
Lower intercept at
2.83 ± 0.10 Ma
MSWD = 2.1, n=25
SIED-MLZ-05-297m
data-point error ellipses are 2σ
Lower intercept at
2.87 ± 0.12 Ma
MSWD = 5.1, n=28
TEW11-10
data-point error ellipses are 2σ
Lower intercept at
2.89 ± 0.04 Ma
MSWD = 0.80, n=29
M1996: 1001
data-point error ellipses are 2σ
Lower intercept at
2.89 ± 0.09 Ma
MSWD = 5.5, n=28
M1996: 1004
data-point error ellipses are 2σ
Lower intercept at
2.89 ± 0.08 Ma
MSWD = 2.0, n=24
$^{207}Pb/^{206}Pb$
$^{238}U/^{206}Pb$

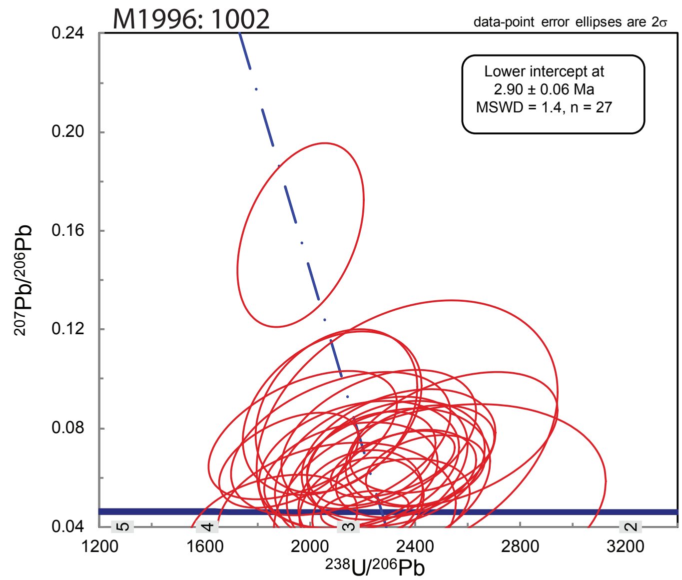
M1996: 1002
data-point error ellipses are 2σ
Lower intercept at
2.90 ± 0.06 Ma
MSWD = 1.4, n = 27
$^{207}Pb/^{206}Pb$
$^{238}U/^{206}Pb$
0.24
0.20
0.16
0.12
0.08
0.04
1200
1600
2000
2400
2800
3200
5
4
3
2

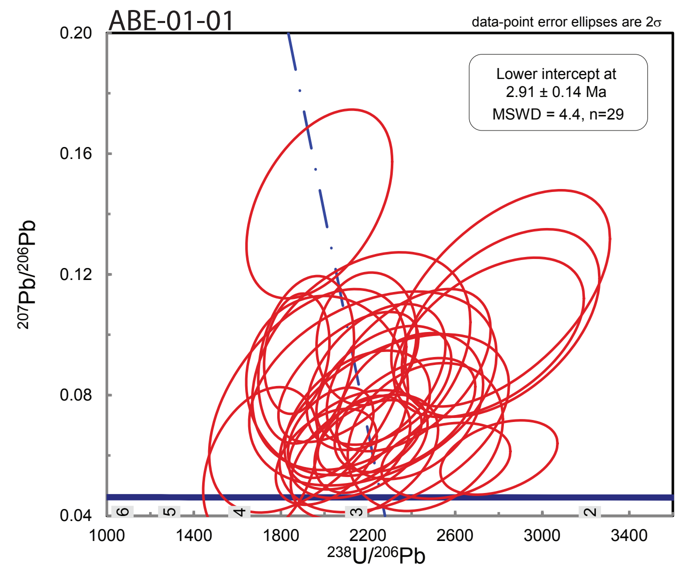
ABE-01-01
data-point error ellipses are 2σ
Lower intercept at
2.91 ± 0.14 Ma
MSWD = 4.4, n=29
$^{207}Pb/^{206}Pb$
$^{238}U/^{206}Pb$
0.20
0.16
0.12
0.08
0.04
1000
1400
1800
2200
2600
3000
3400
6
5
4
3
2

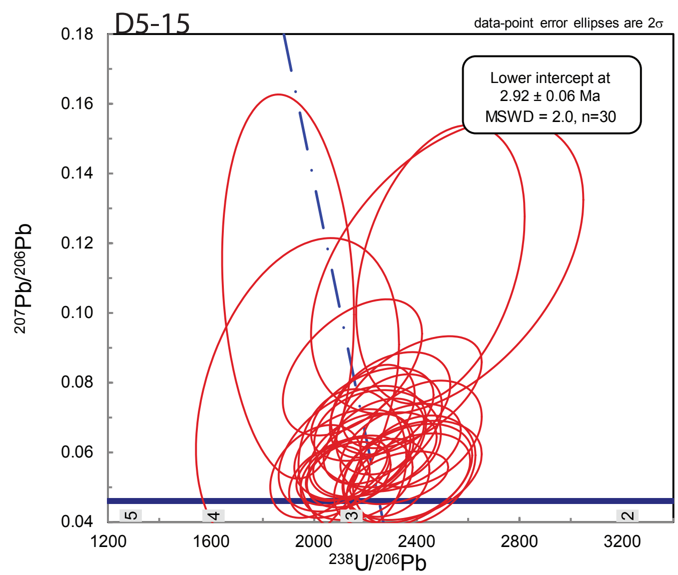
D5-15
data-point error ellipses are 2σ
Lower intercept at
2.92 ± 0.06 Ma
MSWD = 2.0, n=30
$^{207}Pb/^{206}Pb$
$^{238}U/^{206}Pb$
0.18
0.16
0.14
0.12
0.10
0.08
0.06
0.04
1200
1600
2000
2400
2800
3200
5
4
3
2

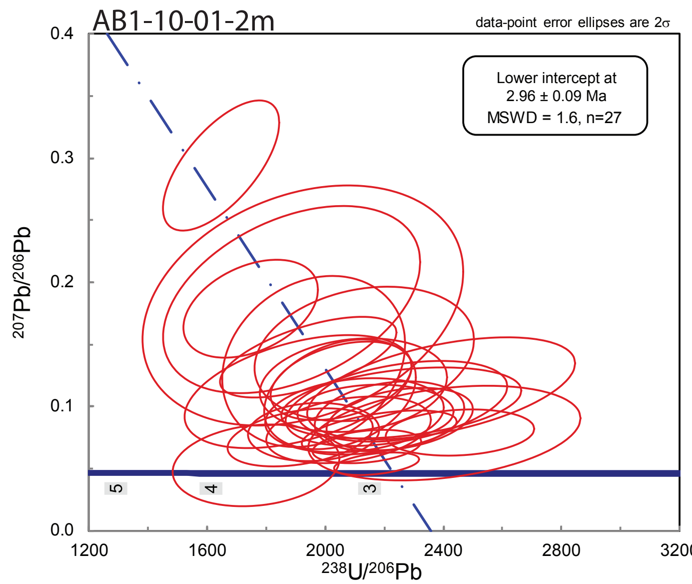
AB1-10-01-2m
data-point error ellipses are 2σ
Lower intercept at
2.96 ± 0.09 Ma
MSWD = 1.6, n=27
$^{207}Pb/^{206}Pb$
$^{238}U/^{206}Pb$
0.4
0.3
0.2
0.1
0.0
1200
1600
2000
2400
2800
3200
5
4
3

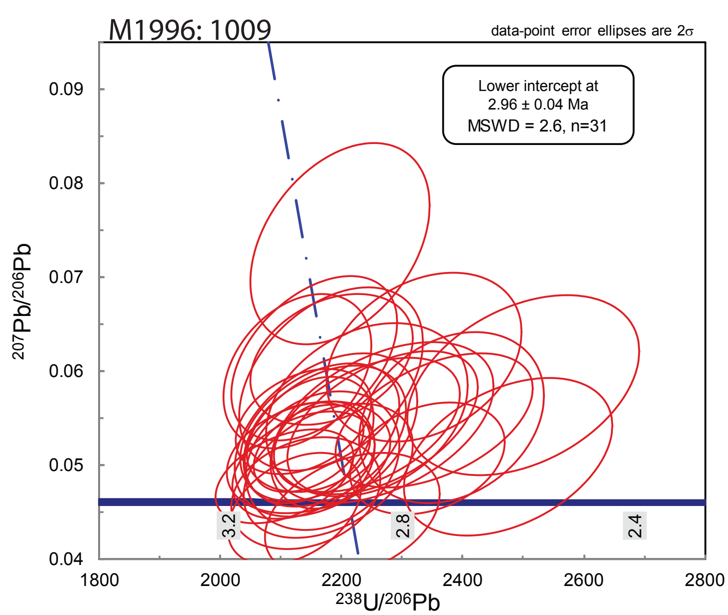
M1996: 1009
data-point error ellipses are 2σ
Lower intercept at
2.96 ± 0.04 Ma
MSWD = 2.6, n=31
$^{207}Pb/^{206}Pb$
$^{238}U/^{206}Pb$
0.09
0.08
0.07
0.06
0.05
0.04
1800
2000
2200
2400
2600
2800
3.2
2.8
2.4

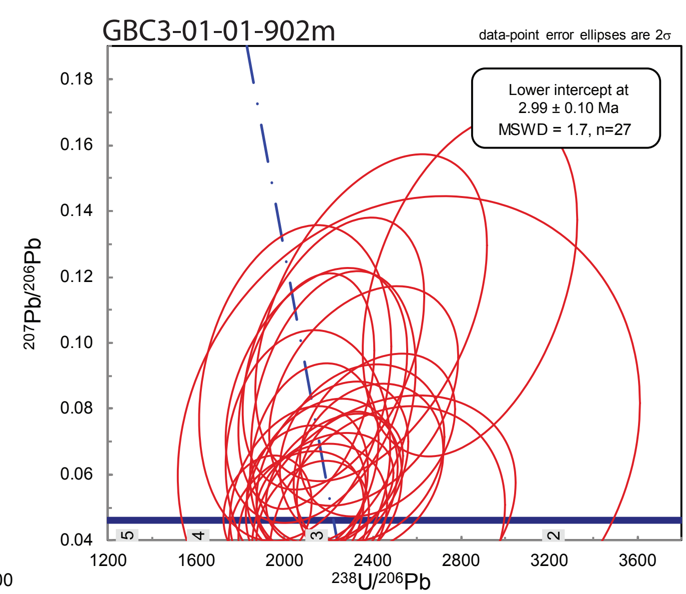
GBC3-01-01-902m
data-point error ellipses are 2σ
Lower intercept at
2.99 ± 0.10 Ma
MSWD = 1.7, n=27
$^{207}Pb/^{206}Pb$
$^{238}U/^{206}Pb$
0.18
0.16
0.14
0.12
0.10
0.08
0.06
0.04
1200
1600
2000
2400
2800
3200
3600
5
4
3
2

Ertsberg

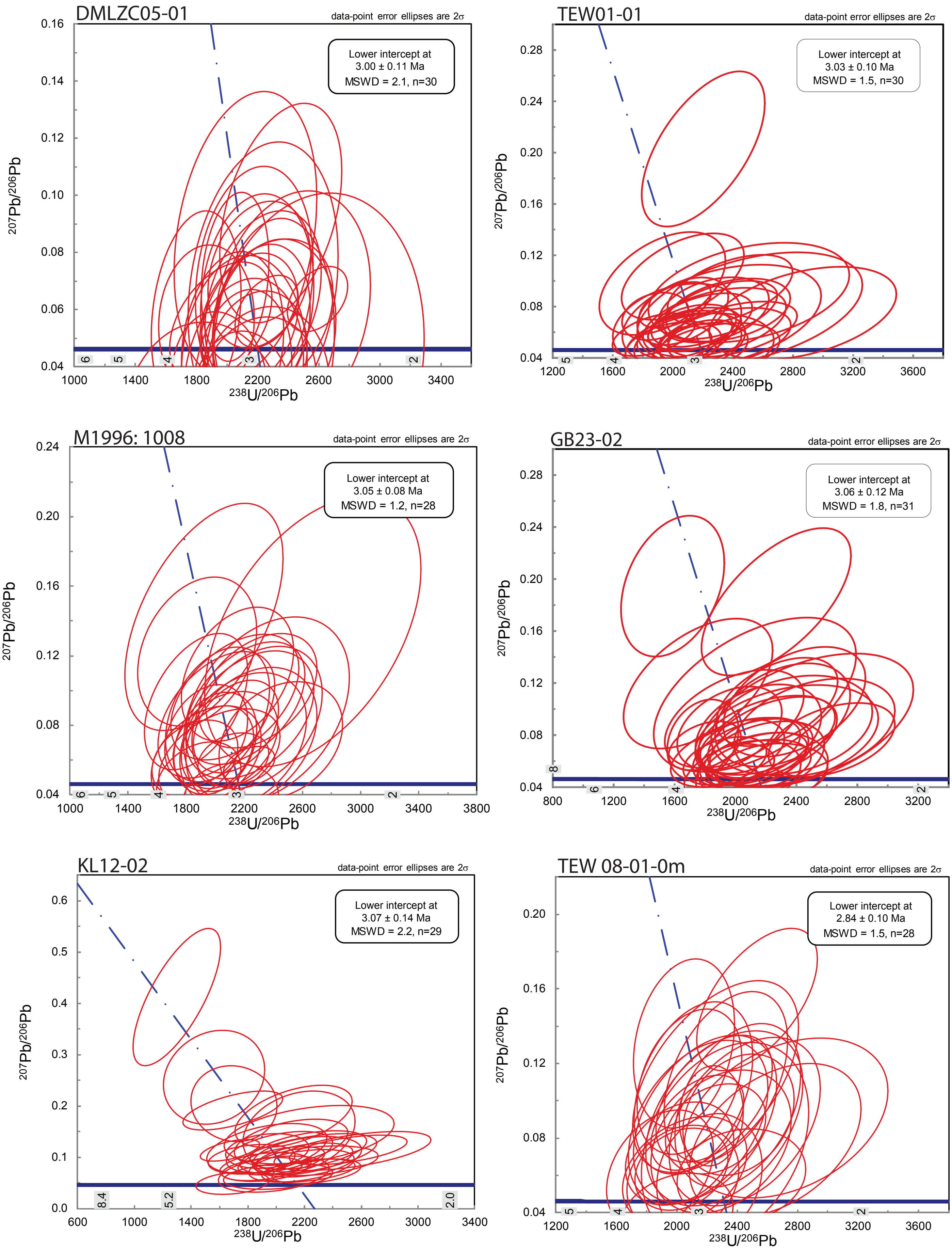

DMLZC05-01
data-point error ellipses are 2σ
Lower intercept at
3.00 ± 0.11 Ma
MSWD = 2.1, n=30
$^{207}Pb/^{206}Pb$
$^{238}U/^{206}Pb$
TEW01-01
data-point error ellipses are 2σ
Lower intercept at
3.03 ± 0.10 Ma
MSWD = 1.5, n=30
$^{207}Pb/^{206}Pb$
$^{238}U/^{206}Pb$
M1996: 1008
data-point error ellipses are 2σ
Lower intercept at
3.05 ± 0.08 Ma
MSWD = 1.2, n=28
$^{207}Pb/^{206}Pb$
$^{238}U/^{206}Pb$
GB23-02
data-point error ellipses are 2σ
Lower intercept at
3.06 ± 0.12 Ma
MSWD = 1.8, n=31
$^{207}Pb/^{206}Pb$
$^{238}U/^{206}Pb$
KL12-02
data-point error ellipses are 2σ
Lower intercept at
3.07 ± 0.14 Ma
MSWD = 2.2, n=29
$^{207}Pb/^{206}Pb$
$^{238}U/^{206}Pb$
TEW 08-01-0m
data-point error ellipses are 2σ
Lower intercept at
2.84 ± 0.10 Ma
MSWD = 1.5, n=28
$^{207}Pb/^{206}Pb$
$^{238}U/^{206}Pb$

Ertsberg

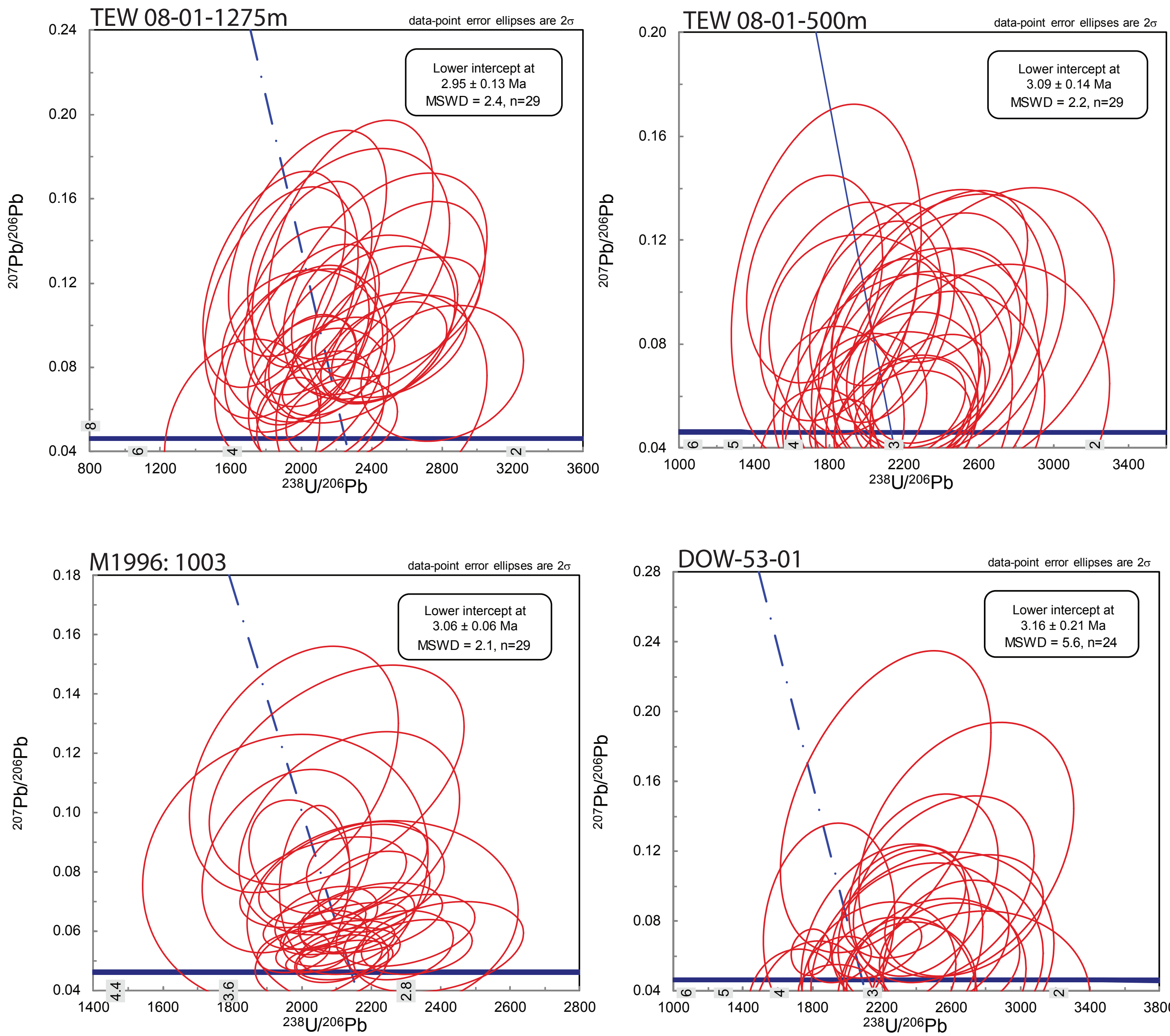
TEW 08-01-1275m
data-point error ellipses are 2σ
Lower intercept at
2.95 ± 0.13 Ma
MSWD = 2.4, n=29
207Pb/206Pb
238U/206Pb
TEW 08-01-500m
data-point error ellipses are 2σ
Lower intercept at
3.09 ± 0.14 Ma
MSWD = 2.2, n=29
207Pb/206Pb
238U/206Pb
M1996: 1003
data-point error ellipses are 2σ
Lower intercept at
3.06 ± 0.06 Ma
MSWD = 2.1, n=29
207Pb/206Pb
238U/206Pb
DOW-53-01
data-point error ellipses are 2σ
Lower intercept at
3.16 ± 0.21 Ma
MSWD = 5.6, n=24
207Pb/206Pb
238U/206Pb

Karume

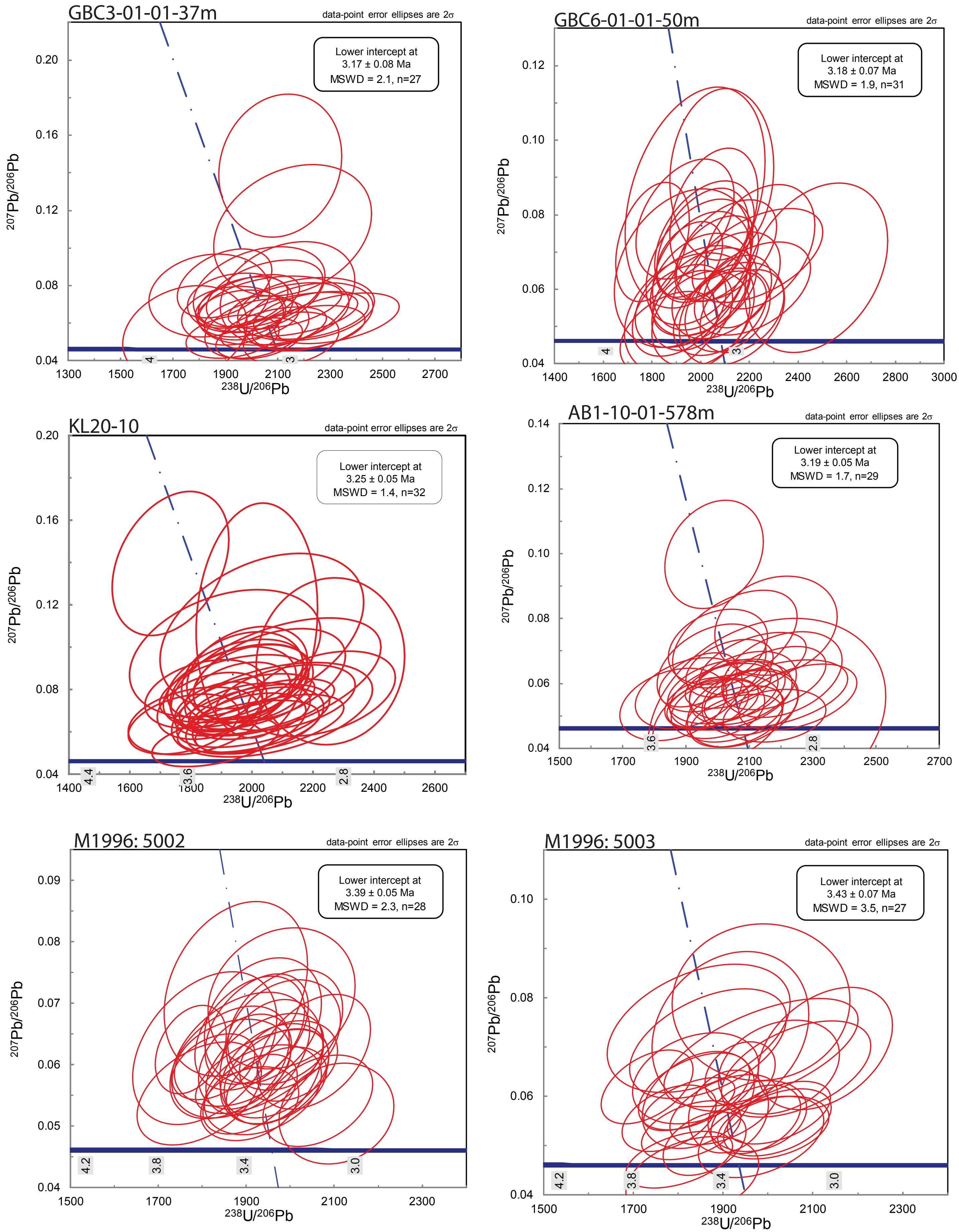
GBC3-01-01-37m
data-point error ellipses are 2σ
Lower intercept at
3.17 ± 0.08 Ma
MSWD = 2.1, n=27
$^{207}Pb/^{206}Pb$
$^{238}U/^{206}Pb$
GBC6-01-01-50m
data-point error ellipses are 2σ
Lower intercept at
3.18 ± 0.07 Ma
MSWD = 1.9, n=31
KL20-10
data-point error ellipses are 2σ
Lower intercept at
3.25 ± 0.05 Ma
MSWD = 1.4, n=32
AB1-10-01-578m
data-point error ellipses are 2σ
Lower intercept at
3.19 ± 0.05 Ma
MSWD = 1.7, n=29
M1996: 5002
data-point error ellipses are 2σ
Lower intercept at
3.39 ± 0.05 Ma
MSWD = 2.3, n=28
M1996: 5003
data-point error ellipses are 2σ
Lower intercept at
3.43 ± 0.07 Ma
MSWD = 3.5, n=27

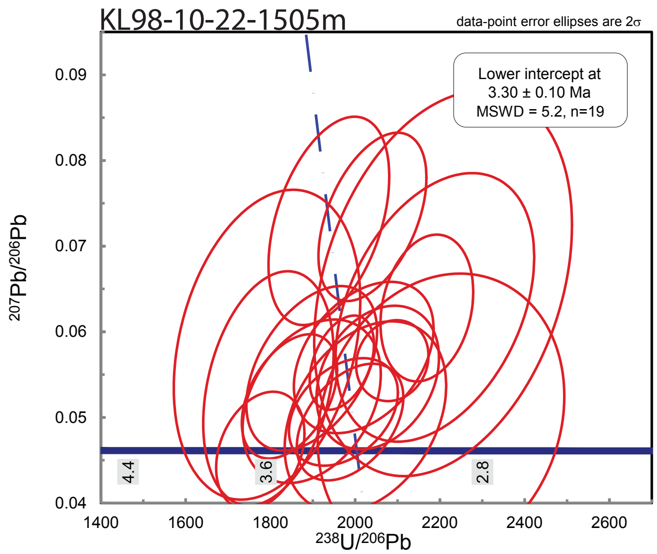
KL98-10-22-1505m
data-point error ellipses are 2σ
Lower intercept at
3.30 ± 0.10 Ma
MSWD = 5.2, n=19
²⁰⁷Pb/²⁰⁶Pb
²³⁸U/²⁰⁶Pb
4.4
3.6
2.8

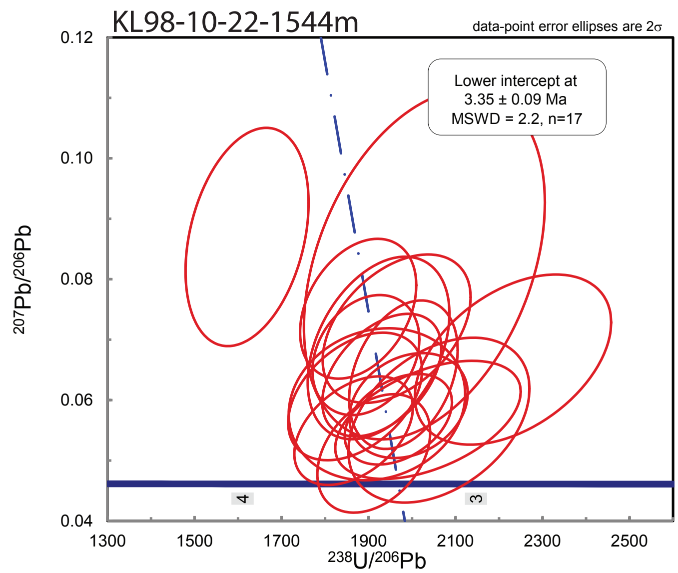
KL98-10-22-1544m
data-point error ellipses are 2σ
Lower intercept at
3.35 ± 0.09 Ma
MSWD = 2.2, n=17
²⁰⁷Pb/²⁰⁶Pb
²³⁸U/²⁰⁶Pb
4
3

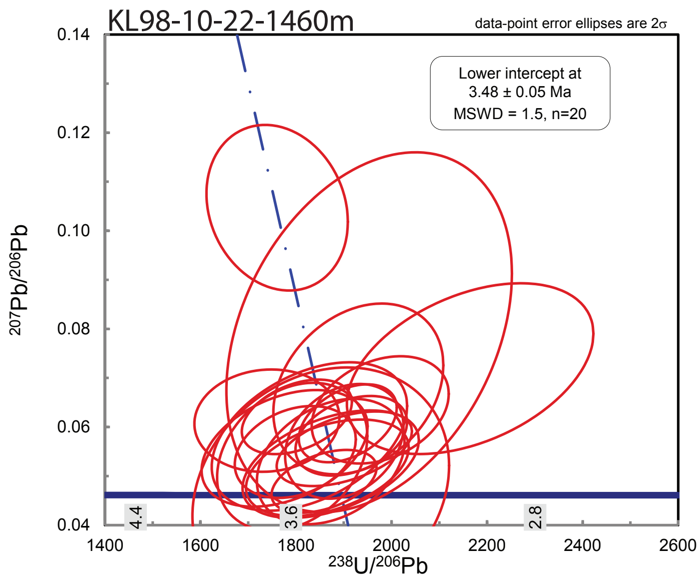
KL98-10-22-1460m
data-point error ellipses are 2σ
Lower intercept at
3.48 ± 0.05 Ma
MSWD = 1.5, n=20
²⁰⁷Pb/²⁰⁶Pb
²³⁸U/²⁰⁶Pb
4.4
3.6
2.8

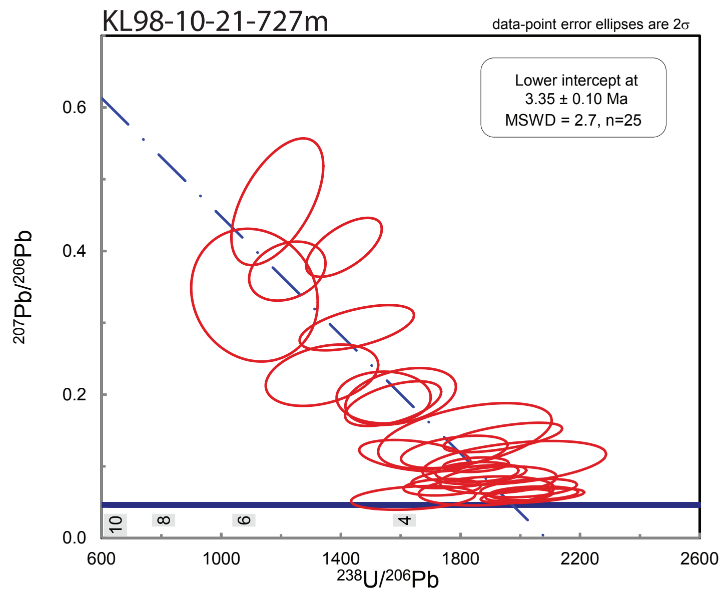
KL98-10-21-727m
data-point error ellipses are 2σ
Lower intercept at
3.35 ± 0.10 Ma
MSWD = 2.7, n=25
²⁰⁷Pb/²⁰⁶Pb
²³⁸U/²⁰⁶Pb
10
8
6
4

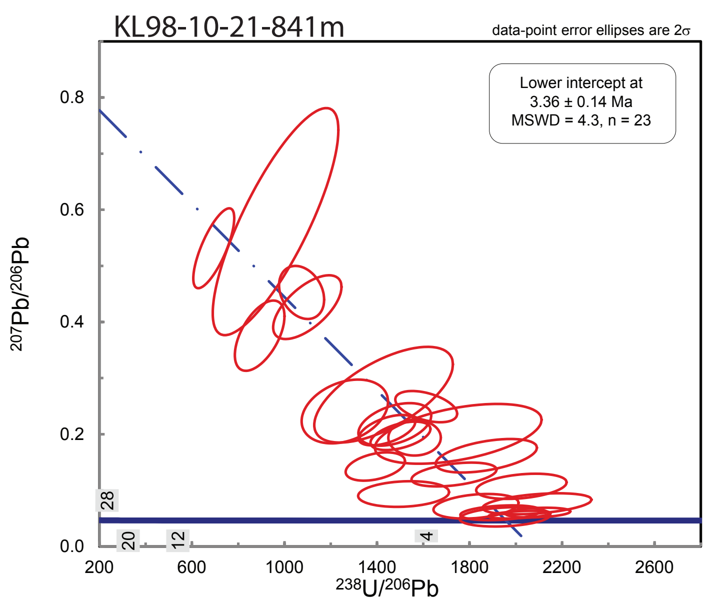
KL98-10-21-841m
data-point error ellipses are 2σ
Lower intercept at
3.36 ± 0.14 Ma
MSWD = 4.3, n = 23
²⁰⁷Pb/²⁰⁶Pb
²³⁸U/²⁰⁶Pb
28
20
12
4

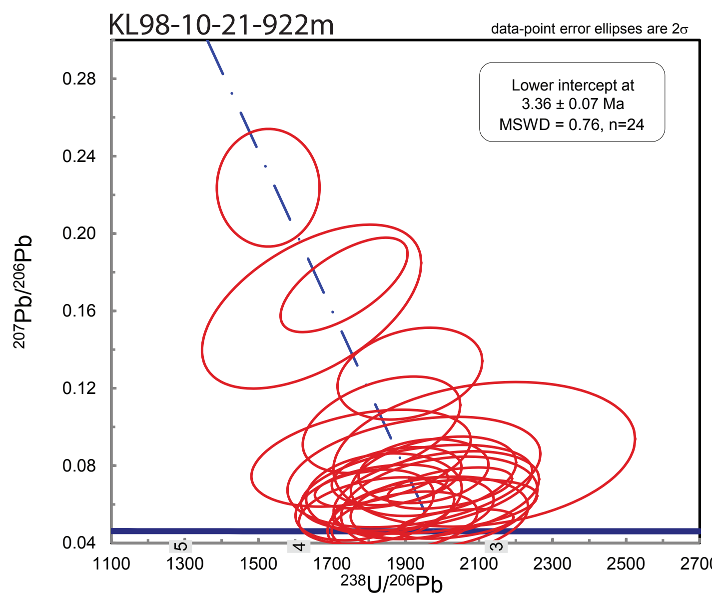
KL98-10-21-922m
data-point error ellipses are 2σ
Lower intercept at
3.36 ± 0.07 Ma
MSWD = 0.76, n=24
²⁰⁷Pb/²⁰⁶Pb
²³⁸U/²⁰⁶Pb
5
4
3

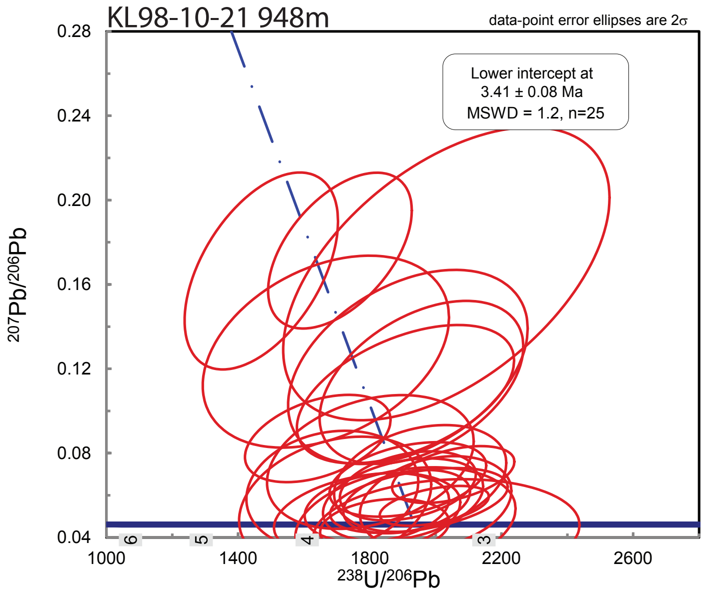
KL98-10-21 948m
data-point error ellipses are 2σ
Lower intercept at
3.41 ± 0.08 Ma
MSWD = 1.2, n=25
207Pb/206Pb
238U/206Pb
0.28
0.24
0.20
0.16
0.12
0.08
0.04
1000
1400
1800
2200
2600
6
5
4
3

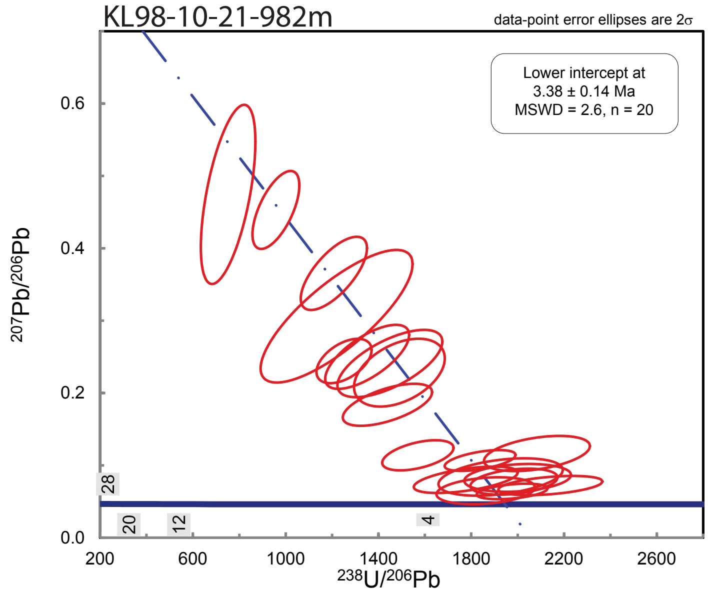
KL98-10-21-982m
data-point error ellipses are 2σ
Lower intercept at
3.38 ± 0.14 Ma
MSWD = 2.6, n = 20
207Pb/206Pb
238U/206Pb
0.6
0.4
0.2
0.0
200
600
1000
1400
1800
2200
2600
28
20
12
4

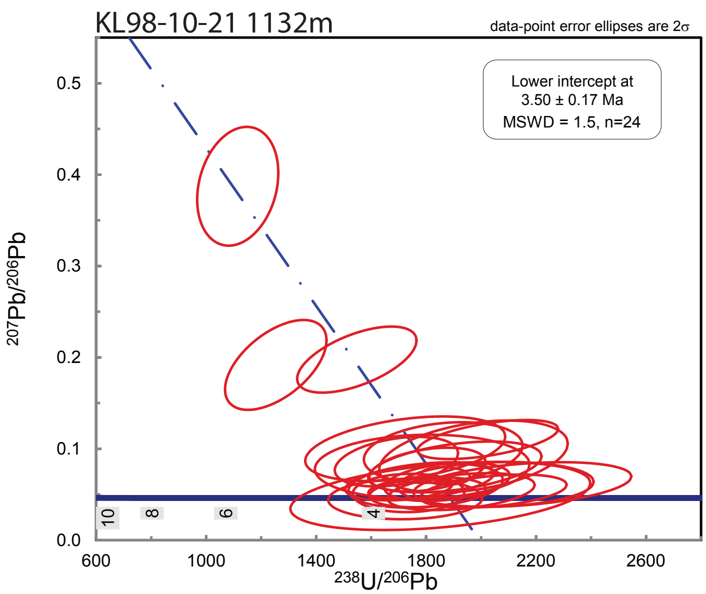
KL98-10-21 1132m
data-point error ellipses are 2σ
Lower intercept at
3.50 ± 0.17 Ma
MSWD = 1.5, n=24
207Pb/206Pb
238U/206Pb
0.5
0.4
0.3
0.2
0.1
0.0
600
1000
1400
1800
2200
2600
10
8
6
4

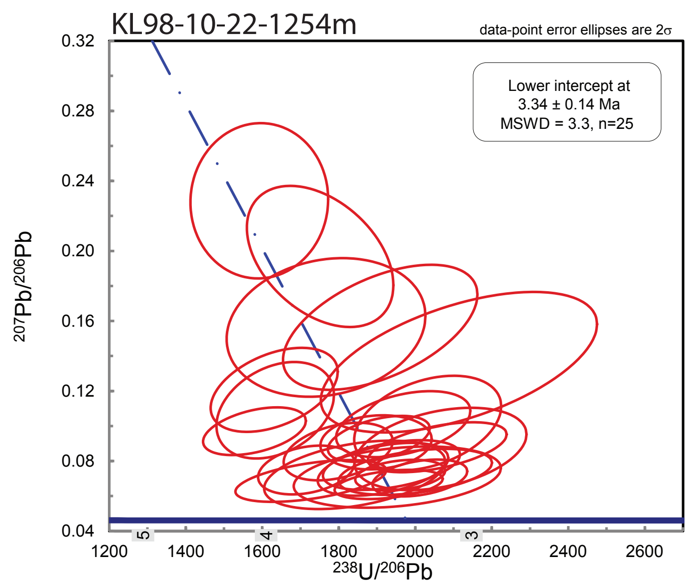
KL98-10-22-1254m
data-point error ellipses are 2σ
Lower intercept at
3.34 ± 0.14 Ma
MSWD = 3.3, n=25
207Pb/206Pb
238U/206Pb
0.32
0.28
0.24
0.20
0.16
0.12
0.08
0.04
1200
1400
1600
1800
2000
2200
2400
2600
5
4
3

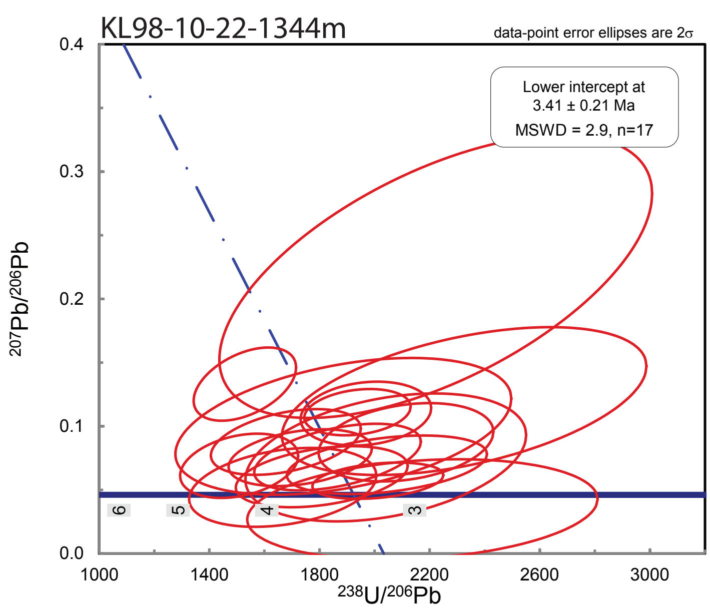
KL98-10-22-1344m
data-point error ellipses are 2σ
Lower intercept at
3.41 ± 0.21 Ma
MSWD = 2.9, n=17
207Pb/206Pb
238U/206Pb
0.4
0.3
0.2
0.1
0.0
1000
1400
1800
2200
2600
3000
6
5
4
3

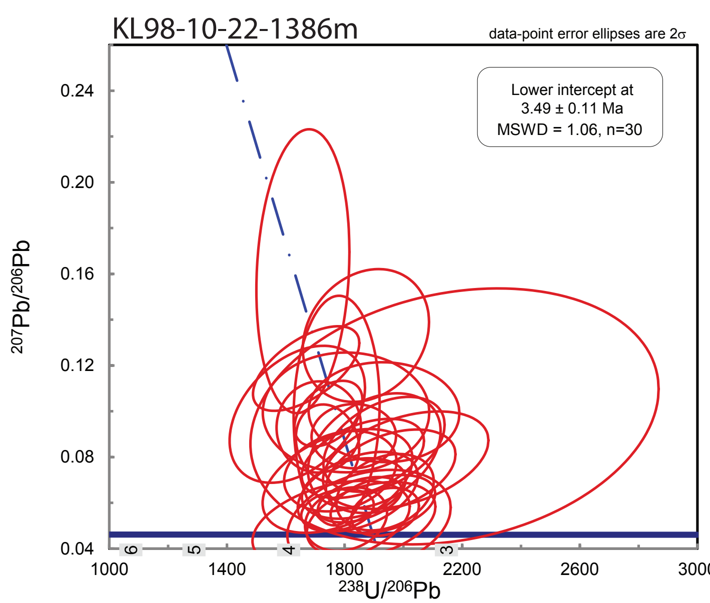
KL98-10-22-1386m
data-point error ellipses are 2σ
Lower intercept at
3.49 ± 0.11 Ma
MSWD = 1.06, n=30
207Pb/206Pb
238U/206Pb
0.24
0.20
0.16
0.12
0.08
0.04
1000
1400
1800
2200
2600
3000
6
5
4
3

Other

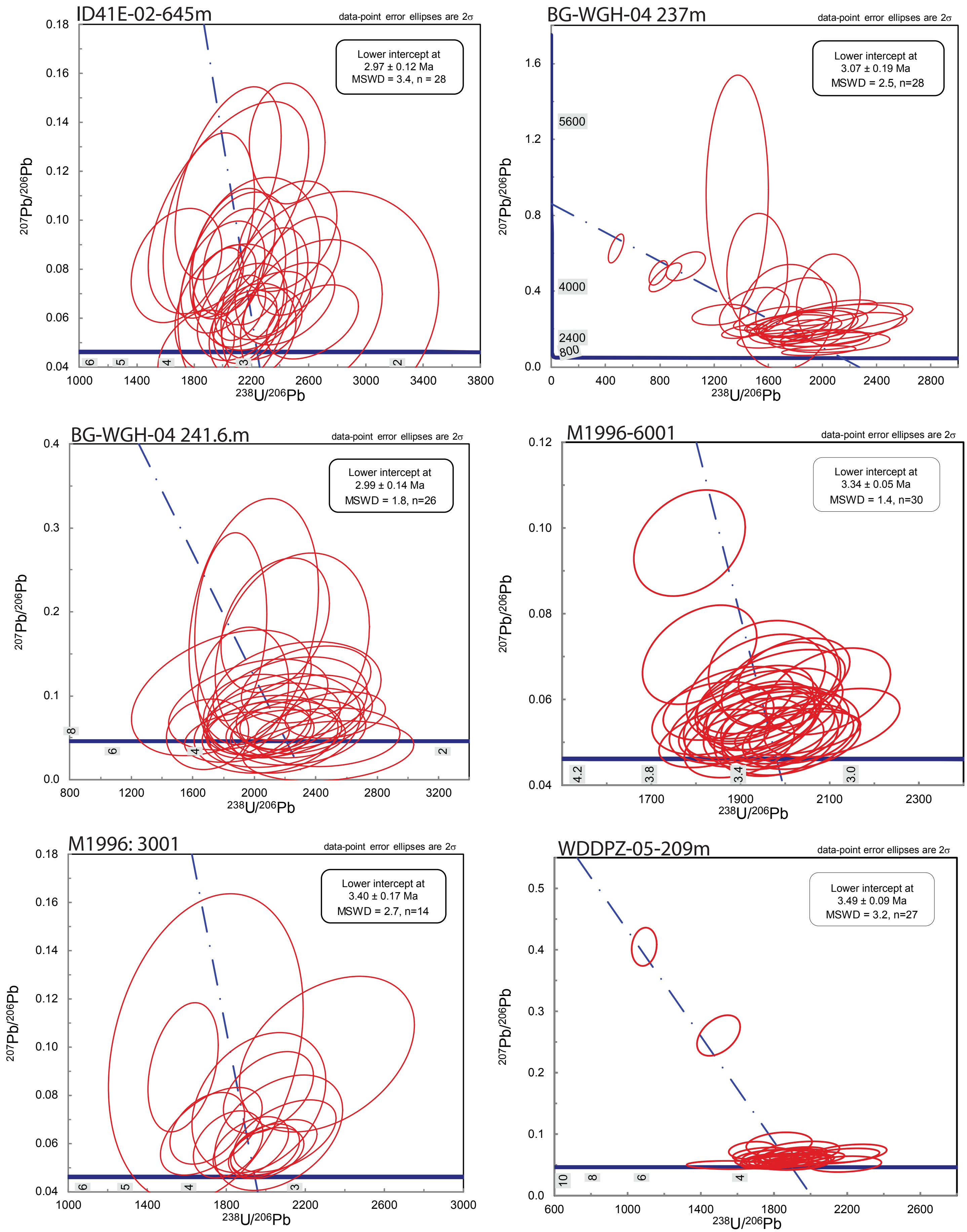
ID41E-02-645m
data-point error ellipses are 2σ
Lower intercept at
2.97 ± 0.12 Ma
MSWD = 3.4, n = 28
0.18
0.16
0.14
0.12
0.10
0.08
0.06
0.04
6
5
4
3
2
1000
1400
1800
2200
2600
3000
3400
3800
207Pb/206Pb
238U/206Pb
BG-WGH-04 237m
data-point error ellipses are 2σ
Lower intercept at
3.07 ± 0.19 Ma
MSWD = 2.5, n=28
1.6
1.2
0.8
0.4
0.0
5600
4000
2400
800
0
400
800
1200
1600
2000
2400
2800
207Pb/206Pb
238U/206Pb
BG-WGH-04 241.6.m
data-point error ellipses are 2σ
Lower intercept at
2.99 ± 0.14 Ma
MSWD = 1.8, n=26
0.4
0.3
0.2
0.1
0.0
8
6
4
2
800
1200
1600
2000
2400
2800
3200
207Pb/206Pb
238U/206Pb
M1996-6001
data-point error ellipses are 2σ
Lower intercept at
3.34 ± 0.05 Ma
MSWD = 1.4, n=30
0.12
0.10
0.08
0.06
0.04
4.2
3.8
3.4
3.0
1700
1900
2100
2300
207Pb/206Pb
238U/206Pb
M1996: 3001
data-point error ellipses are 2σ
Lower intercept at
3.40 ± 0.17 Ma
MSWD = 2.7, n=14
0.18
0.16
0.14
0.12
0.10
0.08
0.06
0.04
6
5
4
3
1000
1400
1800
2200
2600
3000
207Pb/206Pb
238U/206Pb
WDDPZ-05-209m
data-point error ellipses are 2σ
Lower intercept at
3.49 ± 0.09 Ma
MSWD = 3.2, n=27
0.5
0.4
0.3
0.2
0.1
0.0
10
8
6
4
600
1000
1400
1800
2200
2600
207Pb/206Pb
238U/206Pb

Other

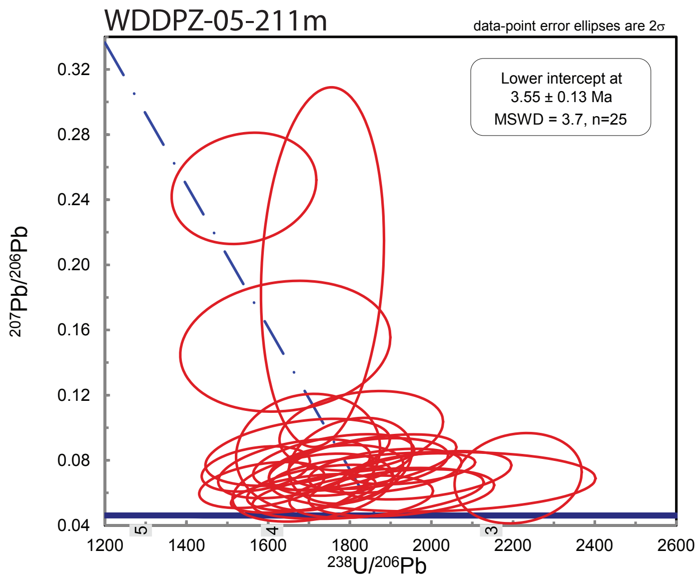
WDDPZ-05-211m
data-point error ellipses are 2σ
Lower intercept at
3.55 ± 0.13 Ma
MSWD = 3.7, n=25
0.32
0.28
0.24
0.20
0.16
0.12
0.08
0.04
207Pb/206Pb
1200
1400
1600
1800
2000
2200
2400
2600
238U/206Pb
5
4
3

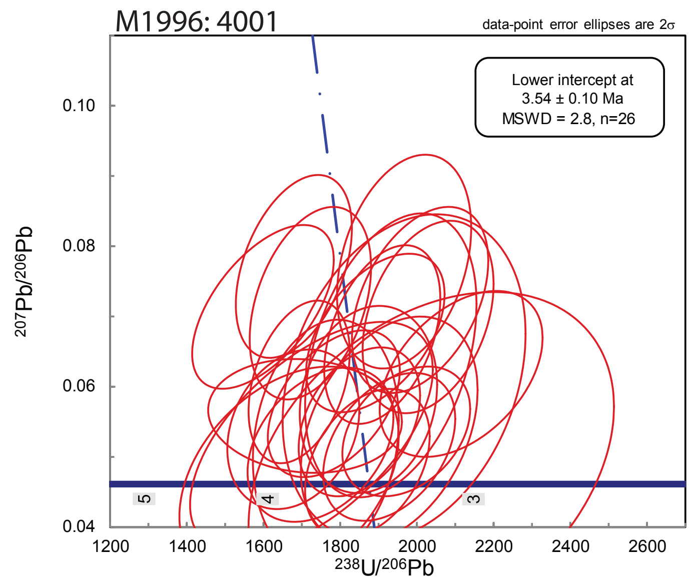
M1996: 4001
data-point error ellipses are 2σ
Lower intercept at
3.54 ± 0.10 Ma
MSWD = 2.8, n=26
0.10
0.08
0.06
0.04
207Pb/206Pb
1200
1400
1600
1800
2000
2200
2400
2600
238U/206Pb
5
4
3

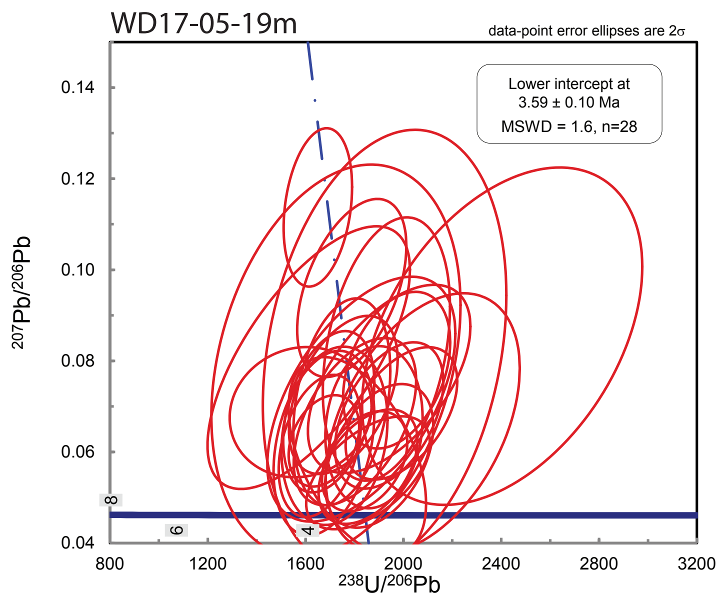
WD17-05-19m
data-point error ellipses are 2σ
Lower intercept at
3.59 ± 0.10 Ma
MSWD = 1.6, n=28
0.14
0.12
0.10
0.08
0.06
0.04
207Pb/206Pb
800
1200
1600
2000
2400
2800
3200
238U/206Pb
8
6
4

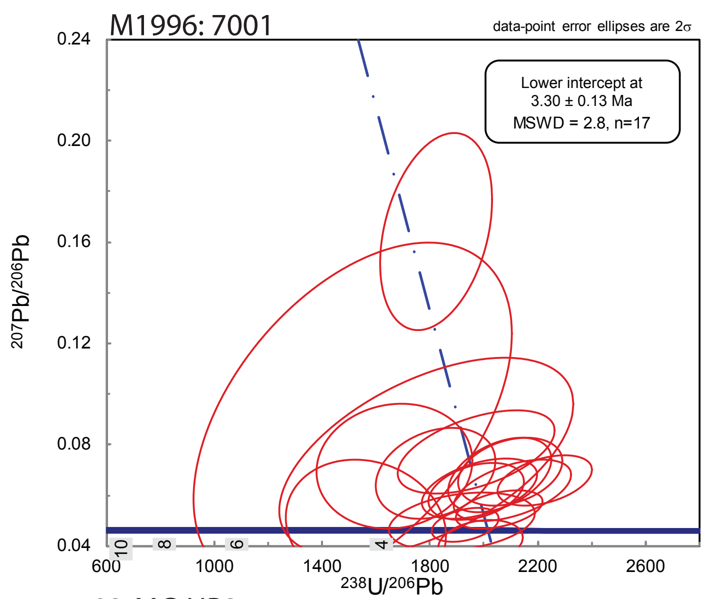
M1996: 7001
data-point error ellipses are 2σ
Lower intercept at
3.30 ± 0.13 Ma
MSWD = 2.8, n=17
0.24
0.20
0.16
0.12
0.08
0.04
207Pb/206Pb
600
1000
1400
1800
2200
2600
238U/206Pb
10
8
6
4

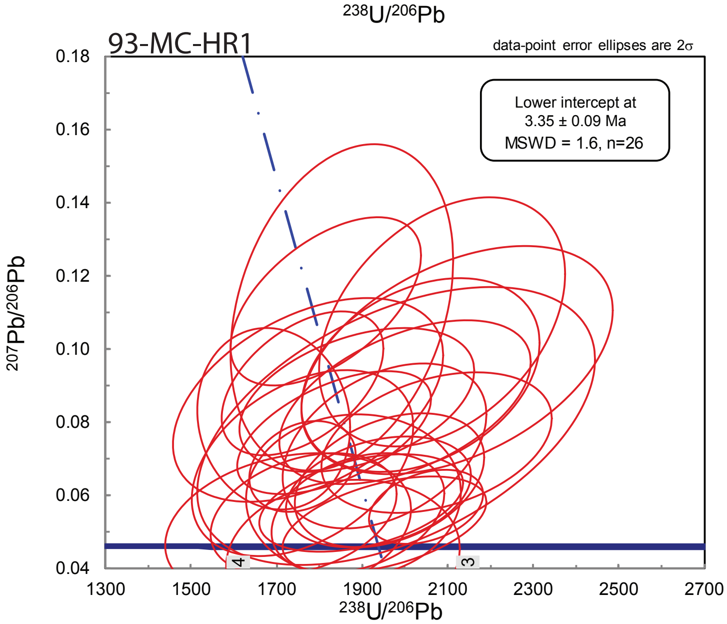
93-MC-HR1
data-point error ellipses are 2σ
Lower intercept at
3.35 ± 0.09 Ma
MSWD = 1.6, n=26
0.18
0.16
0.14
0.12
0.10
0.08
0.06
0.04
207Pb/206Pb
1300
1500
1700
1900
2100
2300
2500
2700
238U/206Pb
4
3

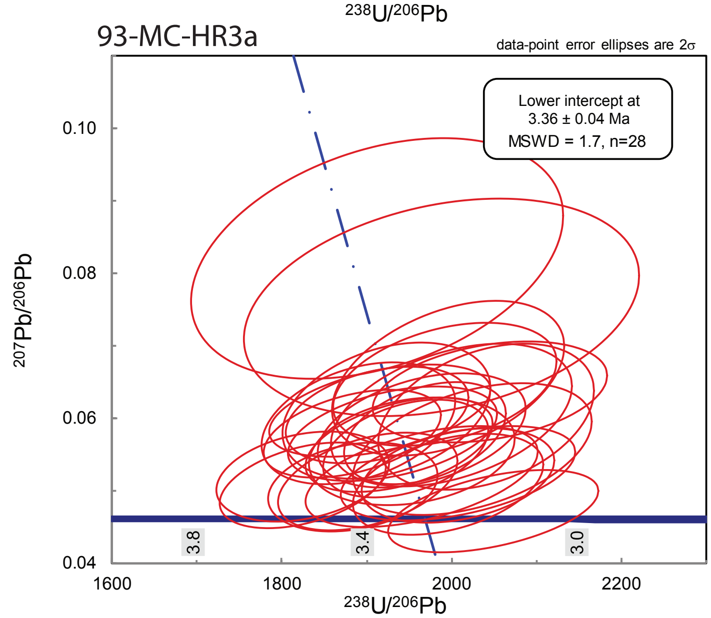
93-MC-HR3a
data-point error ellipses are 2σ
Lower intercept at
3.36 ± 0.04 Ma
MSWD = 1.7, n=28
0.10
0.08
0.06
0.04
207Pb/206Pb
1600
1800
2000
2200
238U/206Pb
3.8
3.4
3.0

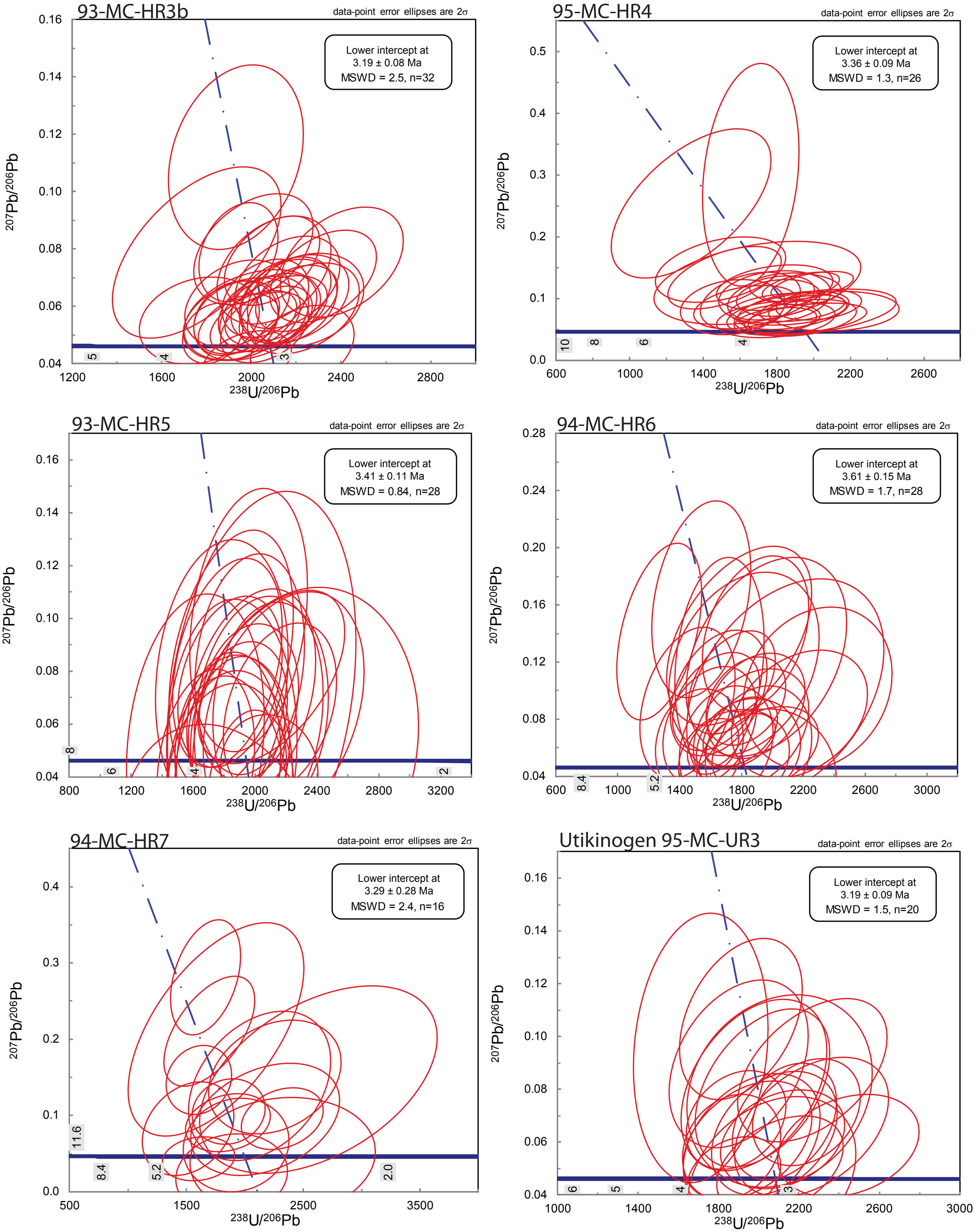
93-MC-HR3b
data-point error ellipses are 2σ
Lower intercept at
3.19 ± 0.08 Ma
MSWD = 2.5, n=32
207Pb/206Pb
238U/206Pb
95-MC-HR4
data-point error ellipses are 2σ
Lower intercept at
3.36 ± 0.09 Ma
MSWD = 1.3, n=26
207Pb/206Pb
238U/206Pb
93-MC-HR5
data-point error ellipses are 2σ
Lower intercept at
3.41 ± 0.11 Ma
MSWD = 0.84, n=28
207Pb/206Pb
238U/206Pb
94-MC-HR6
data-point error ellipses are 2σ
Lower intercept at
3.61 ± 0.15 Ma
MSWD = 1.7, n=28
207Pb/206Pb
238U/206Pb
94-MC-HR7
data-point error ellipses are 2σ
Lower intercept at
3.29 ± 0.28 Ma
MSWD = 2.4, n=16
207Pb/206Pb
238U/206Pb
Utikinogen 95-MC-UR3
data-point error ellipses are 2σ
Lower intercept at
3.19 ± 0.09 Ma
MSWD = 1.5, n=20
207Pb/206Pb
238U/206Pb

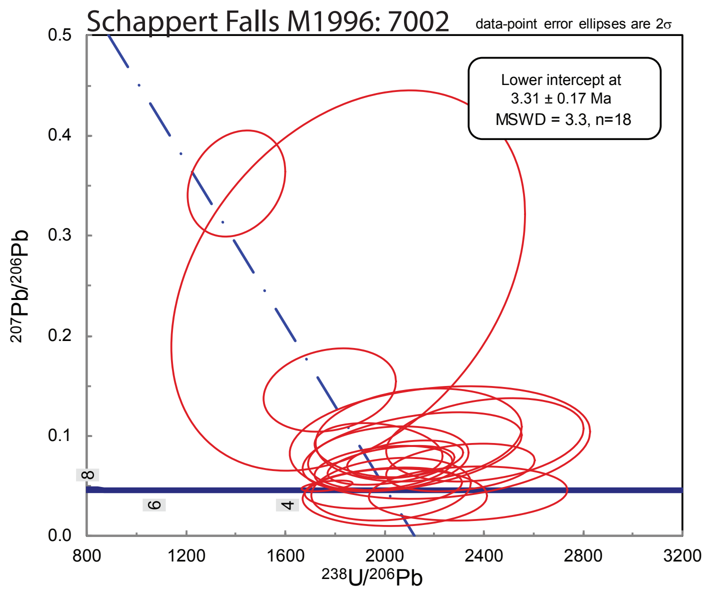
Schappert Falls M1996: 7002
data-point error ellipses are 2σ
Lower intercept at
3.31 ± 0.17 Ma
MSWD = 3.3, n=18
207Pb/206Pb
238U/206Pb
0.5
0.4
0.3
0.2
0.1
0.0
800
1200
1600
2000
2400
2800
3200
8
6
4

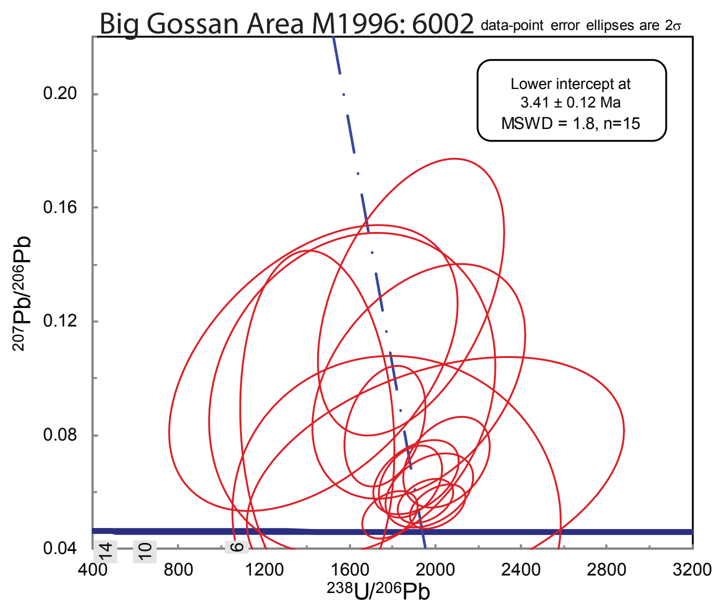
Big Gossan Area M1996: 6002
data-point error ellipses are 2σ
Lower intercept at
3.41 ± 0.12 Ma
MSWD = 1.8, n=15
207Pb/206Pb
238U/206Pb
0.20
0.16
0.12
0.08
0.04
400
800
1200
1600
2000
2400
2800
3200
14
10
6

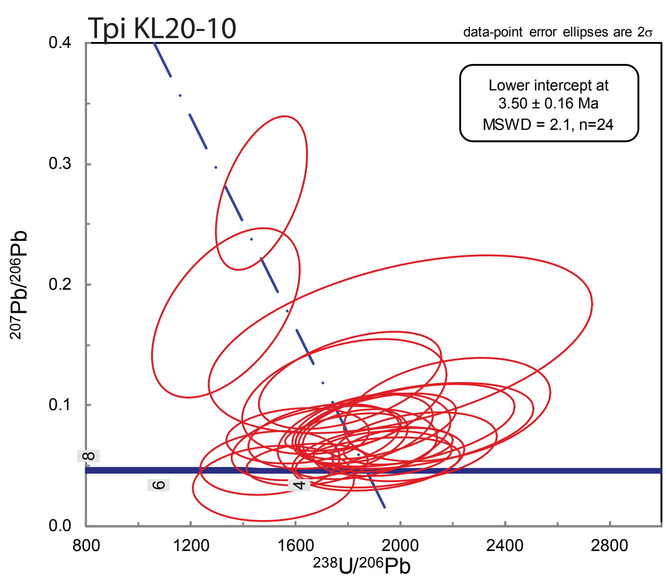
Tpi KL20-10
data-point error ellipses are 2σ
Lower intercept at
3.50 ± 0.16 Ma
MSWD = 2.1, n=24
207Pb/206Pb
238U/206Pb
0.4
0.3
0.2
0.1
0.0
800
1200
1600
2000
2400
2800
8
6
4

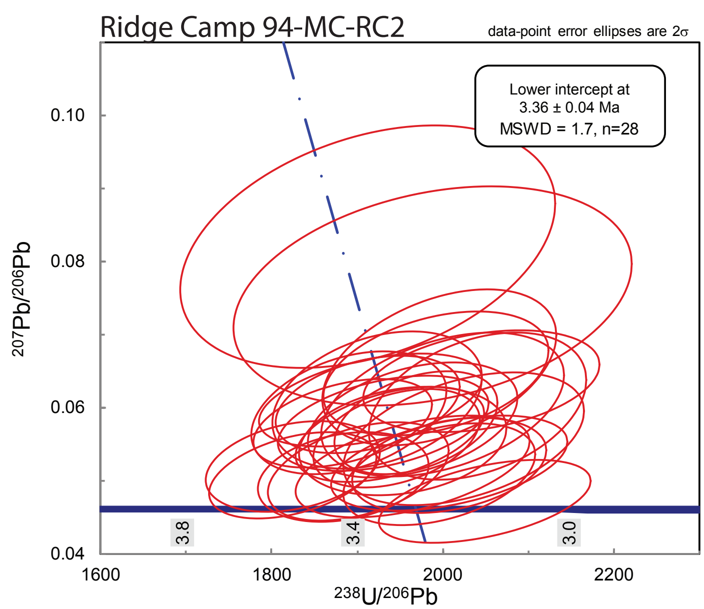
Ridge Camp 94-MC-RC2
data-point error ellipses are 2σ
Lower intercept at
3.36 ± 0.04 Ma
MSWD = 1.7, n=28
207Pb/206Pb
238U/206Pb
0.10
0.08
0.06
0.04
1600
1800
2000
2200
3.8
3.4
3.0

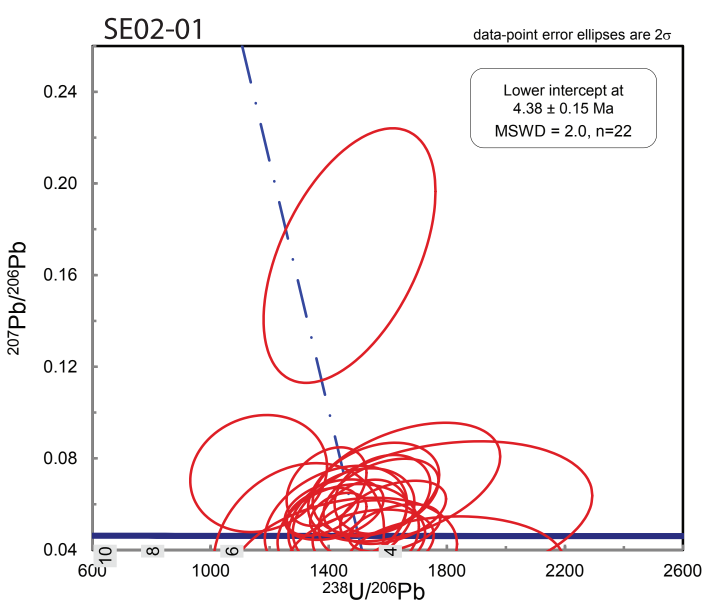
SE02-01
data-point error ellipses are 2σ
Lower intercept at
4.38 ± 0.15 Ma
MSWD = 2.0, n=22
207Pb/206Pb
238U/206Pb
0.24
0.20
0.16
0.12
0.08
0.04
600
1000
1400
1800
2200
2600
10
8
6
4

Appendix G: Xenocrystic Core Ages for Zircons from the Ertsberg-Grasberg Mining District

Zircon ID	Intrusion	207Pb/235U	207Pb/235U error	206Pb/238U	206Pb/238U Error	Error Correlation 206/238 vs. 207/235	Final Age (Ma)	Error (Ma)	Approx U (ppm)	Approx Th (ppm)
GBC6_74_5	Post-Kali	0.3044	0.008	0.04142	0.00088	0.23916	261.6	5.5	439.3	424
GBC6_74_6	Post-Kali	0.384	0.018	0.0517	0.0012	0.78952	325	7.2	600	797
GBC6_96_14	Post-Kali	4.32	0.067	0.2835	0.0059	0.73784	1608	30	327	29
AM96_148_13	Kali	0.2484	0.0094	0.0343	0.0012	0.73514	217.5	7.6	328	242.8
AM96_148_26	Kali	3.763	0.055	0.2767	0.0046	0.5466	1574	23	285.4	327.8
AM96_148_6	Kali	0.395	0.019	0.0534	0.002	0.39384	335	12	163.8	113.7
2007_9	Kali	0.271	0.019	0.0383	0.0021	0.53512	242	13	72.7	68.8
2007_22	Kali	5.415	0.085	0.3422	0.0059	0.60955	1897	28	148.9	60.4
2003_16	Kali	1.32	0.02	0.1401	0.0019	0.64575	847	11	309	166.2
2005_11	Kali	0.315	0.015	0.03868	0.00078	0.22444	244.6	4.8	204	210
GRD32_06_258_10	Kali	5.12	0.26	0.322	0.018	0.9939	1792	90	339	177
GRD41_01_59_8	Kali	0.242	0.013	0.03377	0.00097	0.20928	214.1	6	180.6	83.7
GRD41_01_59_9	Kali	0.351	0.024	0.0494	0.002	0.39984	311	12	136.2	81.1
GRD41_01_59_10	Kali	2.839	0.038	0.2268	0.0031	0.88435	1317	17	731	251
GRD41_01_59_25	Kali	0.3344	0.0099	0.0475	0.001	0.44236	299.8	6.6	178.8	143.9
GRD41_01_348_9	Kali	4.966	0.081	0.3232	0.0041	0.53991	1805	20	305	122.3
KL98_1693_22	Kali	0.319	0.015	0.03974	0.00064	0.46304	251.2	3.9	290.7	121.9
EKI1315_23	Kali	5.152	0.086	0.3261	0.0069	0.73298	1818	33	320.4	230.6
AM96_477_17	Kali	0.2052	0.006	0.02688	0.00048	0.32427	171	3	298	69.9
INF37_02_75_17	Kali	5.117	0.087	0.3265	0.0075	0.70297	1821	36	290	30.7
INF37_02_75_27	Kali	0.1928	0.0092	0.0283	0.0013	0.26112	180	8.4	77.6	76.8
SW05_35	Kali	1.361	0.031	0.1435	0.0051	0.76384	864	29	198.9	377
SW05_12	Kali	0.2619	0.0089	0.0353	0.0015	0.71235	223.6	9.6	2510	460
SW05_13	Kali	0.3714	0.008	0.05053	0.00088	0.31542	317.7	5.4	330	346
SW05_24	Kali	0.328	0.016	0.0383	0.0012	0.44582	242.2	7.2	160.1	102.7
SW05_33	Kali	0.389	0.03	0.0421	0.0023	0.36941	265	14	197.4	217.7
2001_12	Ring Dike	0.363	0.0098	0.04911	0.00086	0.39585	309	5.3	197.6	171.1
95_MC_RD1_3	Ring Dike	0.346	0.019	0.04235	0.0007	0.61122	267.3	4.3	250.2	215
95_MC_RD1_14	Ring Dike	0.216	0.018	0.0294	0.0025	0.86794	187	16	265	119.4
95_MC_RD1_21	Ring Dike	0.288	0.012	0.0397	0.0012	0.28731	251.2	7.7	128.7	121.6
95_MC_RD1_25	Ring Dike	0.213	0.01	0.0306	0.0012	0.63282	194.4	7.4	189.4	142.3
X95_MC_RD1_6	Ring Dike	0.3335	0.0081	0.0465	0.0012	0.80973	293	7.5	771	510
95_MC_RD2_9	Ring Dike	0.3093	0.0077	0.0429	0.00088	0.44124	270.7	5.5	385	288
95_MC_RD2_19	Ring Dike	0.3713	0.0088	0.0502	0.0011	0.26887	315.6	6.8	181.3	125.5
95_MC_RD2_21	Ring Dike	0.356	0.013	0.0486	0.001	0.061322	305.9	6.1	128.2	105
95_MC_RD2_23	Ring Dike	0.248	0.023	0.0312	0.0015	-0.29667	198	9.1	161.3	90.6
95_MC_RD2_24	Ring Dike	0.309	0.012	0.0446	0.0011	0.21213	281.2	6.7	291	334
GRD42_06_389_11	MGI	0.2253	0.0057	0.0319	0.00045	0.42842	202.4	2.8	350	644
GRD42_06_389_14	MGI	0.3544	0.0061	0.04951	0.0005	0.17987	311.5	3	268	171.8
GRD42_06_389_19	MGI	0.412	0.012	0.05133	0.00083	0.21857	322.7	5.1	616	389
GRD42_06_389_26	MGI	0.3578	0.0079	0.04891	0.00074	0.37598	307.8	4.5	283	345
GRD42_06_389_32	MGI	0.3648	0.0072	0.05105	0.00062	0.13195	320.9	3.8	216.3	111.8

Zircon ID	Intrusion	207Pb/235U	207Pb/235U error	206Pb/238U	206Pb/238U Error	Error Correlation 206/238 vs. 207/235	Final Age (Ma)	Error (Ma)	Approx U (ppm)	Approx Th (ppm)
INF42_01_32_27	MGI	0.0227	0.0022	0.001034	0.000065	-0.023147	6.66	0.42	499	30.6
INF42_01_32_28	MGI	0.336	0.0044	0.0467	0.00051	0.16873	294.2	3.2	511	605
INF42_01_32_5	MGI	0.3649	0.0078	0.05037	0.00091	0.21363	316.8	5.6	220	130.6
INF42_01_32_11	MGI	7.33	0.29	0.3592	0.0099	0.58891	1975	47	9.83	12.93
INF42_01_32_17	MGI	5	0.045	0.318	0.0028	0.75395	1780	13	329	227
INF42_01_32_19	MGI	0.3236	0.0049	0.04442	0.00044	0.31532	280.2	2.7	420	469
INF42_01_200_14	MGI	4.737	0.045	0.2993	0.003	0.81324	1687	15	698	293
INF42_01_200_15	MGI	4.062	0.056	0.2482	0.0034	0.92563	1429	18	668	303
MGIAM_J_12	MGI	5.208	0.096	0.3287	0.0068	0.70714	1831	33	181.6	155.9
MGI94_MC_33	MGI	4.301	0.078	0.2714	0.0054	0.67187	1550	28	881	830
GRS93A_0_4	MGI	0.327	0.012	0.0456	0.0013	0.66435	287.3	8.2	977	670
GRS93A_0_10	MGI	5.121	0.096	0.3154	0.0058	0.75457	1767	29	256	286
GRS3_12.FIN2	MGI	0.57	0.011	0.0716	0.0014	0.50059	445.7	8.3	277	73
GRS3_24.FIN2	MGI	0.3675	0.0097	0.049	0.0011	0.58281	308.6	6.6	263	198
PlagDike_19	Plag Dike	0.813	0.015	0.0968	0.0017	0.090989	595.4	9.7	384	8.19
GCZ1_7	Tvs	4.846	0.076	0.3154	0.0047	0.54782	1767	23	62.7	21.53
GCZ2_12	Tvs	5.029	0.046	0.3346	0.0052	0.38164	1860	25	452	40.1
GCZ2_21	Tvs	1.29	0.12	0.1287	0.007	0.45429	787	42	9.7	8.23
GCZ2_30	Tvs	4.76	0.066	0.3205	0.0064	0.25718	1792	31	123	152
NSC2_10	Tvs	4.63	0.1	0.2977	0.0048	0.88207	1680	24	787	16.9
NSC2_22	Tvs	6.34	0.21	0.3249	0.0055	0.76433	1813	27	135.7	65
GRS_DA_30	Dalam Andesite	9.78	0.13	0.4319	0.0038	0.60461	2314	17	143.9	131.5
GRS_DA_24	Dalam Andesite	0.256	0.011	0.03603	0.00076	0.31874	228.2	4.8	126.9	142.1
GRD32_06_46_21	Dalam	0.32	0.018	0.04232	0.00097	0.44528	267.2	6	127.4	113.3
GRS123_0_19	Dalam	10.99	0.38	0.3927	0.0094	0.85863	2132	43	117.9	81.8
GRS123_0_29	Dalam	7.51	0.25	0.368	0.016	0.81969	2020	74	312.4	107.1
KL40_06_416_2	Dalam	6.87	0.28	0.369	0.014	0.77345	2026	63	80.3	40.9
KL40_06_416_13	Dalam	0.3043	0.0098	0.04264	0.0008	0.31989	269.1	4.9	158	174
KL40_06_516_12	Dalam	0.223	0.03	0.0335	0.0021	0.11232	212	13	55.8	60
KL40_06_762_10	Dalam	4.899	0.046	0.3239	0.0037	0.61638	1808	18	568	58.4
KL40_06_762_13	Dalam	0.361	0.016	0.0493	0.0012	0.071484	310.2	7.2	127.9	123.6
KL40_06_762_23	Dalam	0.383	0.014	0.049	0.0011	0.086753	308	6.5	101.8	74.6
1001_26	Ertsberg	0.299	0.025	0.0406	0.0023	0.52833	257	14	122.3	131.7
1002_1	Ertsberg	0.2737	0.0064	0.03783	0.00088	0.6761	239.3	5.5	303.2	218.7
KL1202_7	Ertsberg	0.352	0.02	0.0254	0.0015	0.77031	161.6	9.3	356	180.1
KL1202_15	Ertsberg	0.318	0.014	0.04303	0.00095	0.31609	271.6	5.9	153.7	143.9
TE07_29_30	Ertsberg	0.4079	0.0087	0.0547	0.0011	0.75244	343.6	6.7	456	279
TE07_29_31	Ertsberg	0.3386	0.0095	0.04732	0.00092	0.34353	298	5.7	188.6	125.1
TE07_29_14	Ertsberg	0.273	0.012	0.03847	0.00079	0.034087	243.3	4.9	84.3	85
TE07_29_18	Ertsberg	0.3139	0.0076	0.04346	0.00078	0.62326	274.2	4.8	407	212.3
TE07_29_27	Ertsberg	0.3155	0.0058	0.04383	0.00076	0.41406	276.5	4.7	220.3	243
GBC3_902_3	Ertsberg	0.3565	0.0089	0.04876	0.00085	0.30876	306.9	5.2	358	320
GBC3_902_26	Ertsberg	0.0238	0.0014	0.00312	0.00012	0.278	20.05	0.76	496	100.7

Zircon ID	Intrusion	207Pb/235U	207Pb/235U error	206Pb/238U	206Pb/238U Error	Error Correlation 206/238 vs. 207/235	Final Age (Ma)	Error (Ma)	Approx U (ppm)	Approx Th (ppm)
SEID_297_24	Ertsberg	0.2	0.01	0.02878	0.00068	0.0052073	182.9	4.2	219.5	162.5
AB1_2m_2	Ertsberg	2.444	0.062	0.1861	0.0054	0.79282	1100	29	368	205
AB1_2m_23	Ertsberg	0.4761	0.0095	0.0624	0.001	0.52868	390.2	6.3	174.1	208.2
DOW53_01_30	Ertsberg Sill	0.3165	0.0067	0.0436	0.001	0.60043	275.1	6.3	335	310
DOW53_01_12	Ertsberg Sill	0.3097	0.0074	0.04296	0.00072	0.54444	271.1	4.4	324	338
DOW53_01_17	Ertsberg Sill	0.2828	0.0049	0.04012	0.00055	0.55577	253.5	3.4	668	592
DOW53_01_15	Ertsberg Sill	0.3172	0.0069	0.04375	0.00067	0.38464	276	4.2	274	182.8
DOW53_01_24	Ertsberg Sill	0.2976	0.0064	0.04137	0.00071	0.54665	261.3	4.4	221.9	148.1
5002_24	Karume	5.236	0.079	0.3235	0.0058	0.79254	1810	29	1189	99.3
KL2010_4	Karume	0.2827	0.0075	0.03928	0.00064	0.16057	248.4	4	334	376
KL2010_6	Karume	4.68	0.056	0.2992	0.0044	0.85676	1686	22	443	114.9
KL2010_17	Karume	0.3755	0.0089	0.04943	0.00071	0.22918	311	4.4	155.9	103.9
KL2010_25	Karume	0.296	0.018	0.0408	0.0011	0.007849	257.9	6.7	109.3	120.1
KL2010_28	Karume	3.481	0.027	0.2617	0.0024	0.67093	1499	12	950	1203
KL2010_29	Karume	4.969	0.04	0.3135	0.0024	0.61832	1758	12	285.9	183.6
GBC3_37_4	Karume	0.8108	0.0096	0.09747	0.00062	0.25372	599.6	3.6	381	8.26
GBC6_50_13	Karume	0.2899	0.0081	0.03983	0.00076	0.081155	251.7	4.7	176.1	166.1
KL98_1505_28	Tpi	0.1249	0.0048	0.01782	0.00032	0.31667	113.9	2	146	145
KL98_1505_29	Tpi	1.265	0.013	0.132	0.0011	0.54521	799.1	6.2	394	76.1
KL98_1505_30	Tpi	0.1147	0.004	0.01698	0.00035	-0.0071128	108.5	2.2	168.5	159
KL98_1505_1	Tpi	0.6289	0.0063	0.07941	0.00065	0.37242	492.6	3.9	328	262
KL98_1505_2	Tpi	0.3418	0.0042	0.04691	0.00049	0.43867	295.5	3	413	325
KL98_1505_3	Tpi	0.3364	0.0043	0.0474	0.00037	0.21882	298.5	2.3	384	291
KL98_1505_7	Tpi	0.686	0.01	0.08628	0.00072	0.24703	533.4	4.3	136.3	325
KL98_1505_10	Tpi	0.336	0.017	0.0404	0.00047	0.61536	255.3	2.9	258	160
KL98_1505_11	Tpi	0.372	0.011	0.04764	0.00063	-0.19938	300	3.9	167	80.1
KL98_1505_14	Tpi	0.756	0.016	0.0914	0.0013	0.25371	564.7	7.4	92.2	73.9
KL98_1505_17	Tpi	0.1173	0.0039	0.0175	0.00034	-0.087984	111.8	2.1	179	189
Tpi1460_27	Tpi	0.357	0.014	0.0456	0.001	0.23635	287.7	6.2	456	246.4
Tpi1460_8	Tpi	0.126	0.0053	0.01731	0.00037	0.16054	110.6	2.4	238.2	228.4
Tpi1460_15	Tpi	0.3177	0.0077	0.04552	0.00096	0.36664	286.9	5.9	315	283
Tpi1460_16	Tpi	0.3328	0.0091	0.04631	0.00081	0.31425	291.8	5	263.3	212.5
Tpi1460_21	Tpi	0.3118	0.0088	0.0446	0.0012	0.51872	281.1	7.6	319	348
Tpi1544_30	Tpi	0.458	0.012	0.06	0.0013	0.21419	375.8	8.2	401	318
Tpi1544_1	Tpi	0.1383	0.0095	0.01738	0.00033	0.35292	111.1	2.1	789	459
Tpi1544_5	Tpi	0.3056	0.0077	0.04257	0.0009	0.28547	268.7	5.6	367	298
Tpi1544_6	Tpi	0.2631	0.006	0.03791	0.00088	0.27087	239.8	5.5	179	156
Tpi1544_7	Tpi	0.2976	0.0058	0.04132	0.00072	0.33033	261	4.5	471	521
Tpi1544_15	Tpi	0.1168	0.0045	0.01613	0.00039	0.24627	103.1	2.5	482	727
Tpi1544_16	Tpi	0.1167	0.0044	0.01595	0.00034	0.4527	102	2.2	993	1010
Tpi1544_21	Tpi	0.3347	0.0064	0.04697	0.00096	0.25335	295.9	5.9	267	181.2
Tpi1544_22	Tpi	0.2244	0.0082	0.03154	0.00093	0.37588	200.1	5.8	209.2	228.8
Tpi1544_24	Tpi	0.1091	0.0029	0.01631	0.00041	0.20459	104.3	2.6	301.2	365.2

Zircon ID	Intrusion	207Pb/235U	207Pb/235U error	206Pb/238U	206Pb/238U Error	Error Correlation 206/238 vs. 207/235	Final Age (Ma)	Error (Ma)	Approx U (ppm)	Approx Th (ppm)
Tpi1544_25	Tpi	0.1292	0.004	0.01883	0.00044	0.14094	120.2	2.8	808	816
Tpi1544_27	Tpi	0.2622	0.0087	0.0355	0.0011	0.30903	225	6.8	187.2	181.4
KL98_22_1505_29	Tpi	0.122	0.0041	0.0178	0.0003	0.29987	113.8	1.9	151	145
KL98_22_1505_30	Tpi	1.274	0.013	0.13204	0.00098	0.53162	799.4	5.6	425	78.6
KL98_22_1505_31	Tpi	0.1152	0.0035	0.017	0.00033	0.028484	108.7	2.1	187	169
KL98_22_1505_1	Tpi	0.1002	0.0041	0.01536	0.00036	-0.060571	98.3	2.3	140.3	137.4
KL98_22_1505_2	Tpi	0.6297	0.0063	0.0795	0.00064	0.3716	493.1	3.8	322	257
KL98_22_1505_3	Tpi	0.3425	0.0042	0.04704	0.00048	0.40565	296.3	3	411	324
KL98_22_1505_4	Tpi	0.3367	0.004	0.04737	0.00035	0.21516	298.3	2.2	389	293
KL98_22_1505_8	Tpi	0.688	0.011	0.08634	0.00074	0.25457	533.8	4.4	136.7	329
KL98_22_1505_11	Tpi	0.319	0.012	0.0401	0.00044	0.20871	253.4	2.7	255.2	148.3
KL98_22_1505_12	Tpi	0.3533	0.0081	0.04796	0.00073	-0.00083313	302	4.5	147	78.3
KL98_22_1505_15	Tpi	0.755	0.015	0.0918	0.0012	0.23259	566.2	7.2	92.3	75.5
KL98_22_1505_18	Tpi	0.1187	0.0039	0.01767	0.00035	-0.155	112.9	2.2	177	182
982_17	Tigt	0.278	0.011	0.03642	0.00099	0.17041	230.6	6.1	88.3	51.1
1192_6	Tigt	0.2414	0.0062	0.0331	0.00065	0.17678	209.9	4	343	368
922_3	Tigt	4.73	0.17	0.297	0.01	0.94599	1673	52	105.1	33.8
948_1	Tigt	0.315	0.011	0.04393	0.00089	0.32691	277.1	5.5	136	80
948_4	Tigt	4.66	0.042	0.3004	0.0034	0.72511	1693	17	446	239.9
948_6	Tigt	0.3139	0.0054	0.04415	0.00057	0.24482	278.5	3.5	367	222
948_28	Tigt	11.085	0.072	0.4746	0.0035	0.53049	2503	15	124.5	179
1132_1	Tigt	24.63	0.41	0.6305	0.0077	0.78283	3151	31	108.8	63.8
1132_4	Tigt	0.3688	0.0091	0.04918	0.00058	0.065321	309.5	3.5	273	140.4
1132_11	Tigt	5.151	0.076	0.3288	0.0092	0.79638	1832	45	420	46.1
1132_12	Tigt	11.22	0.14	0.48	0.0051	0.47178	2527	22	136.7	49.6
1132_14	Tigt	0.444	0.015	0.04991	0.00088	0.28605	313.9	5.4	117.3	110
1132_23	Tigt	2.514	0.056	0.2146	0.0038	0.41379	1253	20	68.4	67.16
1132_24	Tigt	0.3504	0.0065	0.04688	0.00056	0.33048	295.3	3.5	345	314
1132_27	Tigt	9.59	0.11	0.4443	0.0037	0.65337	2370	17	168	141
1132_32	Tigt	3.333	0.033	0.2538	0.0023	0.85287	1458	12	730	301
1132_20	Tigt	0.3635	0.0084	0.0496	0.00085	0.79308	312	5.2	470	379
1243_2	Tigt	0.235	0.018	0.0334	0.0016	0.51977	212	10	179	50.5
1243_6	Tigt	0.3461	0.0074	0.04767	0.00073	0.050826	300.2	4.5	191	101
1243_11	Tigt	4.49	0.43	0.243	0.022	0.99687	1390	120	722	259
1243_17	Tigt	0.9	0.2	0.051	0.012	0.99526	321	71	382	389
1243_24	Tigt	1.61	0.13	0.1111	0.009	0.98375	677	52	382.2	138.7
1243_26	Tigt	0.365	0.016	0.04719	0.00088	0.078607	297.2	5.4	84.1	50.4
1243_29	Tigt	0.4031	0.0067	0.05392	0.00073	0.57212	338.5	4.4	533	291
1266_1	Tigt	0.224	0.01	0.0314	0.0014	0.85067	199.3	8.5	313.4	225.7
1266_4	Tigt	2.04	0.35	0.135	0.022	0.99775	800	130	291	64.5
1266_6	Tigt	2.75	0.23	0.181	0.015	0.99669	1076	79	365.4	237.4
1266_14	Tigt	0.3906	0.0036	0.05299	0.00032	0.21191	332.8	2	748	467
1266_16	Tigt	2.322	0.07	0.1903	0.0045	0.97594	1122	24	361	247

Zircon ID	Intrusion	207Pb/235U	207Pb/235U error	206Pb/238U	206Pb/238U Error	Error Correlation 206/238 vs. 207/235	Final Age (Ma)	Error (Ma)	Approx U (ppm)	Approx Th (ppm)
1266_18	Tigt	0.3681	0.0091	0.04902	0.00092	0.29988	308.5	5.7	335	165
1266_25	Tigt	0.3243	0.0082	0.0457	0.0011	0.8866	287.7	6.7	474	204
KL98_1254_14	Tigt	0.3258	0.0072	0.04455	0.00056	0.33297	281	3.4	238	184
KL98_1254_15	Tigt	0.3071	0.0051	0.04356	0.00043	0.18299	274.9	2.7	339	338
KL98_1254_23	Tigt	0.394	0.0095	0.0528	0.0012	0.35215	331.5	7.5	186	249
Tikl1386_18	Tigt	2.394	0.04	0.218	0.0056	0.74682	1276	28	127.1	78.9
KL98_10_21_L_24	Tigt	0.2875	0.0087	0.03932	0.00088	0.46303	248.6	5.4	289.6	121.9
KL98_22_1254_3	Tigt	4.541	0.067	0.296	0.0032	0.78106	1671	16	566	139
KL98_22_1254_15	Tigt	0.3262	0.0068	0.04453	0.00052	0.35146	280.8	3.2	242	184.9
KL98_22_1254_16	Tigt	0.3054	0.0051	0.04346	0.00041	0.25039	274.2	2.5	350	345
KL98_22_1254_24	Tigt	0.405	0.011	0.054	0.001	0.29537	339.3	6.3	180.8	233
1344_1_C2.FIN2	Tigt	5.011	0.046	0.3272	0.0033	0.55725	1824	16	401	315.3
1344_2_C2.FIN2	Tigt	8.055	0.087	0.397	0.0041	0.43491	2155	19	180.2	112
1344_3_C1.FIN2	Tigt	0.433	0.025	0.0401	0.0011	-0.10873	253.1	6.9	64.5	70.2
1344_3_R2.FIN2	Tigt	0.305	0.023	0.0401	0.0014	-0.01805	253.5	8.4	75.6	52.6
1344_8_R1.FIN2	Tigt	8.74	0.14	0.4159	0.005	0.85122	2241	23	513.1	188
1344_8_C2.FIN2	Tigt	7.098	0.081	0.3726	0.0049	0.60951	2041	23	1195	327
1344_10_C1.FIN2	Tigt	0.251	0.011	0.03333	0.0008	0.080537	211.3	5	233	123
1344_10_R2.FIN2	Tigt	0.1654	0.0052	0.02304	0.00047	0.25263	146.8	3	327	187.8
1344_11_C2.FIN2	Tigt	4.315	0.049	0.2779	0.0031	0.66946	1581	16	1533	222.4
1344_14_C1.FIN2	Tigt	1.528	0.018	0.1001	0.0021	0.045232	615	12	562	492.6
6002_35	Big Gossan	11.1	0.16	0.4643	0.0067	0.62921	2458	30	500	365
6002_3	Big Gossan	6.232	0.078	0.3735	0.0044	0.6539	2045	21	382	215
6002_4	Big Gossan	4.76	0.14	0.311	0.0089	0.3821	1745	44	16.9	22.3
6002_5	Big Gossan	12.73	0.2	0.5158	0.006	0.65726	2681	25	76.6	59.12
6002_12	Big Gossan	11.49	0.19	0.493	0.013	0.66966	2584	56	761	621
6002_15	Big Gossan	5.142	0.073	0.339	0.0074	0.86751	1881	36	1226	87.2
6002_16	Big Gossan	11.3	0.15	0.507	0.0072	0.51628	2644	31	1138	557
6002_17	Big Gossan	7.78	0.2	0.3834	0.0055	0.60285	2091	26	138.2	149.4
6002_18	Big Gossan	6.2	0.1	0.3733	0.0071	0.4458	2045	33	254.1	102
6002_21	Big Gossan	4.77	0.1	0.3115	0.0071	0.61225	1753	36	377	105.8
6002_22	Big Gossan	8.14	0.24	0.3878	0.0051	0.13705	2112	24	90.4	134
6002_23	Big Gossan	7.77	0.11	0.3908	0.0065	0.78887	2126	30	728	97.5
6002_25	Big Gossan	0.105	0.037	0.00155	0.00036	0.75823	10	2.3	274	193
6002_26	Big Gossan	8.86	0.16	0.4099	0.0064	0.8466	2214	29	235	146
6002_27	Big Gossan	10.28	0.11	0.4581	0.0057	0.47473	2431	25	245.1	78.9
6002_29	Big Gossan	6.638	0.093	0.3716	0.0063	0.73585	2036	30	588	430
6002_30	Big Gossan	7.93	0.13	0.412	0.0098	0.81429	2238	37	581	551
BG241_32.FIN2	Big Gossan Dike	0.231	0.024	0.02906	0.00087	0.0017492	184.6	5.5	115.3	68.1
BG241_32.FIN2	Big Gossan Dike	0.305	0.018	0.0433	0.0014	0.22067	275	8.8	74.8	64.92
BG241_17.FIN2	Big Gossan Dike	0.3002	0.0038	0.04144	0.00052	0.44732	261.7	3.2	533	318
BG241_20.FIN2	Big Gossan Dike	0.2728	0.0045	0.03827	0.00048	0.11342	242.1	3	293	228
BG241_31.FIN2	Big Gossan Dike	0.3634	0.0066	0.04909	0.00062	0.16345	308.9	3.8	354	24.8

Zircon ID	Intrusion	207Pb/235U	207Pb/235U error	206Pb/238U	206Pb/238U Error	Error Correlation 206/238 vs. 207/235	Final Age (Ma)	Error (Ma)	Approx U (ppm)	Approx Th (ppm)
Kay_14	Kay	0.0471	0.0033	0.00404	0.0002	0.58835	26	1.3	615.1	385
Kay_16	Kay	4.032	0.074	0.2743	0.0047	0.86028	1562	24	185.1	31.6
3001_27	North Grasberg	0.0814	0.0072	0.0059	0.00034	0.40435	37.9	2.2	403.6	224.9
3001_12	North Grasberg	0.489	0.011	0.0651	0.0011	0.054411	406.3	6.8	119.7	100.5
3001_18	North Grasberg	0.3328	0.0072	0.04425	0.00052	0.19679	279.1	3.2	546	114.9
3001_19	North Grasberg	5.65	0.26	0.0468	0.0031	0.040631	295	19	7.37	31.8
3001_22	North Grasberg	0.361	0.0076	0.0493	0.00076	0.089484	310.2	4.7	186	159.4
3001_23	North Grasberg	0.374	0.011	0.05143	0.00072	0.16198	323.3	4.4	167	91.2
TLT_14	Lembah Tembaga	4.906	0.055	0.3215	0.0038	0.54855	1797	18	244.1	143.9
TLT_18	Lembah Tembaga	4.25	0.051	0.2811	0.0045	0.74023	1597	23	563	138
TLT_19	Lembah Tembaga	9.524	0.096	0.4323	0.0038	0.61249	2316	17	142.7	139.6
4001_32	Wanagon	5.578	0.084	0.3552	0.0072	0.73496	1958	34	500	173.1
4001_5	Wanagon	6.01	0.1	0.4042	0.0061	0.55721	2188	28	870	71.2
4001_7	Wanagon	4.81	0.22	0.317	0.012	0.9198	1770	59	80.5	32.7
4001_25	Wanagon	0.349	0.017	0.0462	0.0018	0.46986	291	11	92.4	108
4001_27	Wanagon	5.3	0.13	0.371	0.01	0.86598	2034	47	681	3.78
WD17_05_32	Wanagon	11.07	0.13	0.4827	0.0048	0.52434	2539	21	93.9	366
WD17_05_8	Wanagon	0.0156	0.0019	0.001	0.00013	0.64634	6.46	0.81	393	102.3
WD17_05_6	Wanagon	0.356	0.015	0.0474	0.0013	0.17976	298.7	8.3	68.6	49.3
93_MC_HR1_12	Heat Road Intrusion	0.1239	0.0099	0.0158	0.0011	-0.0069741	100.9	7.2	103.8	78.3
93_MC_HR1_20	Heat Road Intrusion	0.3274	0.0089	0.04355	0.00088	0.19986	274.7	5.4	250	191
7001_31	Heat Road Intrusion	3.531	0.04	0.2692	0.0033	0.49259	1538	17	422	179
7001_2	Heat Road Intrusion	0.414	0.012	0.0546	0.001	0.16332	342.7	6.3	201.2	194.3
7001_4	Heat Road Intrusion	6.57	0.27	0.378	0.014	0.96912	2063	67	1224	215
7001_5	Heat Road Intrusion	6.144	0.086	0.3573	0.0052	0.55076	1969	25	192.8	94.8
7001_7	Heat Road Intrusion	23.19	0.27	0.6434	0.0092	0.63946	3201	36	140.1	210.5
7001_10	Heat Road Intrusion	4.725	0.079	0.3038	0.0059	0.65985	1709	29	400	219.2
7001_17	Heat Road Intrusion	9.48	0.22	0.441	0.01	0.5686	2354	46	719	212.2
7001_18	Heat Road Intrusion	4.82	0.16	0.309	0.0078	0.13244	1735	39	22.21	9.7
7001_20	Heat Road Intrusion	4.898	0.089	0.3163	0.0064	0.65626	1771	31	89.8	26.19
7001_21	Heat Road Intrusion	4.828	0.093	0.3103	0.0078	0.78029	1741	38	148.2	40.6
MC95HR4_6	Heat Road Intrusion	4.31	0.17	0.2963	0.0067	0.70459	1673	33	125.7	60.6
MC95HR4_25	Heat Road Intrusion	0.266	0.011	0.0377	0.00081	0.3005	238.5	5	195.6	232
MC93HR5_6	Heat Road Intrusion	4.93	0.12	0.3184	0.0055	0.032753	1782	27	81.9	14.9
MC93HR5_13	Heat Road Intrusion	5.48	0.27	0.331	0.016	0.68037	1844	78	89.8	74.1
MC93HR5_22	Heat Road Intrusion	0.359	0.022	0.0521	0.002	0.21782	327	12	94	60
MC94HR6_8	Heat Road Intrusion	4.52	0.13	0.292	0.0089	0.42525	1651	45	251.5	61.8
MC94HR6_10	Heat Road Intrusion	0.0021	0.0036	0.00036	0.00012	0.2097	2.33	0.77	104	65.8
94_MC_RC2_17	Ridge Camp	4.592	0.054	0.3002	0.003	0.33634	1692	15	190	110.7
94_MC_RC2_30	Ridge Camp	0.1652	0.006	0.02196	0.00084	0.34863	140	5.3	309	185.2
94_MC_RC2_19	Ridge Camp	1.986	0.067	0.1313	0.0034	0.72267	795	19	87.9	65.8
7002_1	Scappert Falls	0.376	0.012	0.0518	0.001	0.32084	325.4	6.2	85.1	108.2
7002_3	Scappert Falls	0.3356	0.0066	0.04714	0.00067	0.41213	296.9	4.1	335	255

Zircon ID	Intrusion	207Pb/235U	207Pb/235U error	206Pb/238U	206Pb/238U Error	Error Correlation 206/238 vs. 207/235	Final Age (Ma)	Error (Ma)	Approx U (ppm)	Approx Th (ppm)
7002_24	Scappert Falls	5.186	0.054	0.3265	0.0043	0.68517	1821	21	452	25.2
7002_26	Scappert Falls	0.3396	0.0049	0.04703	0.00045	0.17782	296.3	2.8	621	304
7002_27	Scappert Falls	0.4342	0.0091	0.05799	0.00076	0.58119	363.3	4.6	446	431
7002_29	Scappert Falls	0.3098	0.0064	0.04421	0.00077	0.14756	278.8	4.7	307	312
TSE_32	Southeast Intrusion	4.64	0.13	0.2992	0.0062	0.17956	1698	33	29.8	97
TSE_33	Southeast Intrusion	3.41	0.15	0.249	0.01	0.71288	1433	52	138.6	135.9
TSE_34	Southeast Intrusion	6.45	0.16	0.3402	0.008	0.57063	1887	39	139.4	94
TSE_4	Southeast Intrusion	4.113	0.069	0.3005	0.0049	0.46574	1693	24	118.4	118.7
TSE_6	Southeast Intrusion	4.78	0.27	0.3056	0.0093	0.97224	1717	45	146	83.8
TSE_13	Southeast Intrusion	5.15	0.12	0.3287	0.0055	0.70978	1835	26	77.5	96.5
TSE_15	Southeast Intrusion	11.11	0.13	0.4693	0.0065	0.60589	2480	29	90.7	114.8
TSE_16	Southeast Intrusion	9.99	0.26	0.429	0.01	0.64823	2300	46	29.4	111.6
TSE_21	Southeast Intrusion	10.18	0.42	0.45	0.014	0.83925	2392	64	46.6	50.4
TSE_28	Southeast Intrusion	7.572	0.083	0.4103	0.0062	0.75912	2216	28	971	451
TSE_29	Southeast Intrusion	4.112	0.086	0.2793	0.0045	0.85292	1587	23	716	119.1
X95_MC_UR3_31	Utiki River	0.3274	0.0075	0.04489	0.00079	0.17445	283	4.9	356	247
95_MC_UR3_1	Utiki River	0.363	0.0089	0.0489	0.001	-0.012039	307.9	6.3	140.3	121.2
95_MC_UR3_2	Utiki River	0.3281	0.0078	0.04585	0.00069	0.38196	289	4.2	237.9	291.1
95_MC_UR3_3	Utiki River	4.8	0.14	0.3005	0.0094	0.7547	1692	47	574	37.5
95_MC_UR3_6	Utiki River	0.3568	0.0063	0.04957	0.00075	0.3652	311.8	4.6	395	161.6
95_MC_UR3_7	Utiki River	0.364	0.012	0.0501	0.001	0.18202	315	6.3	112.4	66
95_MC_UR3_20	Utiki River	0.3006	0.0074	0.04143	0.00078	0.11101	261.6	4.8	302	362
95_MC_UR3_22	Utiki River	0.369	0.01	0.05039	0.00086	0.47028	317.5	5.4	264	217
95_MC_UR3_23	Utiki River	0.369	0.0086	0.05017	0.00086	0.25343	315.5	5.3	231	199
95_MC_UR3_29	Utiki River	0.34	0.01	0.0474	0.0016	0.68928	299	10	479	274.1

Appendix H: (U-Th)/He Sample Locations

UTM coordinates for each of the zircon and apatite (U-Th)/He samples are listed in the following table. For outcrop samples, GPS coordinates of the sampling location are given. For drill core samples, UTM coordinates of the drill hole collar and the downhole depths are given. Final ages are also reported in this table. The final age and uncertainty is the average and standard deviation of the ages from six single-grain aliquots.

Sample Type	Sample Number	UTM Easting	UTM Northing	Elevation (m)	DDH ID	Depth (m)	Rock Type	Method	Age Ma	Error +/- Ma
Core	INF-37-02 75m	734558	9551182	3045	INF37-02	75	LKI	Apatite (U-Th)/He	2.9	0.2
Outcrop	2004	735180	9550920	3785			LKI	Apatite (U-Th)/He	2.9	0.3
Outcrop	14-SW-05	734971	9551031	3415			EKI	Apatite (U-Th)/He	2.5	0.2
Core	AM96-40-01 148m	18774	22118	2955	AM96-10-09	148	EKI	Apatite (U-Th)/He	2.3	0.2
Core	AM96-40-01 345m	18774	22118	2955	AM96-10-09	345	EKI	Apatite (U-Th)/He	2.5	0.4
Core	AM96-40-01 477m	18774	22118	2955	AM96-10-09	477	EKI	Apatite (U-Th)/He	1.7	0.5
Core	AB1-10-01 382m	735605	9549890	2528	AB1-10-01	382	EKI	Apatite (U-Th)/He	2.8	0.1
Outcrop	14-SW-02	734493	9551570	3255			MGI	Apatite (U-Th)/He	2.9	0.2
Core	INF-42-01 50m	734480	9551489	3051	INF42-01	50	MGI	Apatite (U-Th)/He	2.8	0.2
Core	INF-42-01 250m	734480	9551489	3051	INF42-01	250	MGI	Apatite (U-Th)/He	3.2	0.4
Core	AB1-10-01 500m	735605	9549890	2528	AB1-10-01	500	Plag Dike	Apatite (U-Th)/He	3.1	0.2
Outcrop	1001	735650	9549175	3580			Ertsberg	Apatite (U-Th)/He	2.8	0.4
Core	TEW-08-01 0m	736633	9549336	3145	TEW 08-01	0	Ertsberg	Apatite (U-Th)/He	2.7	0.1
Core	TEW-08-01 500m	736633	9549336	3145	TEW 08-01	500	Ertsberg	Apatite (U-Th)/He	2.9	0.4
Core	TEW-08-01 750m	736633	9549336	3145	TEW 08-01	750	Ertsberg	Apatite (U-Th)/He	2.2	0.4
Core	AB1-10-01 2m	735605	9549890	2528	AB1-10-01	2	Ertsberg	Apatite (U-Th)/He	2.4	0.7
Core	VZW-74S 70m	736381	9549129	3841	VZW-74S	70	Ertsberg	Apatite (U-Th)/He	2.9	0.2
Core	VZW-74S 276m	736381	9549129	3841	VZW-74S	276	Ertsberg	Apatite (U-Th)/He	2.9	0.3
Core	AB1-10-01 578m	735605	9549890	2528	AB1-10-01	578	Karume	Apatite (U-Th)/He	2.8	0.2
Core	KL98-10-21 727m	734101	9550741	3062	KL98-10-21	727	Tigt	Apatite (U-Th)/He	2.4	0.6
Core	KL98-10-21 1192m	734101	9550741	3062	KL98-10-21	1192	Tigt	Apatite (U-Th)/He	2.1	0.3
Outcrop	3001	733820	9553445	4125			North Grasberg	Apatite (U-Th)/He	3.2	0.6
Outcrop	4001	732310	9549690	4025			Wanagon	Apatite (U-Th)/He	2.3	0.2
Outcrop	93-MC-HR2	733630	9550720	4030			Heat Road Dike	Apatite (U-Th)/He	2.3	0.9
Outcrop	93-MC-HR3a	733450	9547180	2760			Heat Road Dike	Apatite (U-Th)/He	2.2	0.6
Outcrop	95-MC-HR4	734020	9550000	3790			Heat Road Dike	Apatite (U-Th)/He	3	0.3
Outcrop	93-MC-HR5	733850	9549560	3535			Heat Road Dike	Apatite (U-Th)/He	2.7	0.3
Outcrop	94-MC-HR6	733690	9549270	3335			Heat Road Dike	Apatite (U-Th)/He	2.6	0.1
Outcrop	93-MC-HR8	733590	9549300	3315			Heat Road Dike	Apatite (U-Th)/He	2.4	0.2
Outcrop	M1996: 2004	735180	9550920	3785			LKI	Zircon (U-Th)/He	2.8	0.2
Core	INF37-02-75m	734558	9551182	3045	INF37-02	75	LKI	Zircon (U-Th)/He	2.9	0.2
Core	INF37-02-275m	734558	9551182	3045	INF37-02	275	LKI	Zircon (U-Th)/He	3	0.2
Core	KL98-10-21-1693m	734100.862	9550740.986	3063	KL98-10-21	1693	LKI	Zircon (U-Th)/He	2.1	0.4
Core	AB1-10-01 205m	735605	9549890	2528	AB1-10-01	205	LKI*	Zircon (U-Th)/He	2.9	0.2
Core	AB1-10-01 382m	735605	9549890	2528	AB1-10-01	382	EKI	Zircon (U-Th)/He	3.2	0.2
Core	AM96-40-09-148m	18774	22118	2955	AM96-40-09	148	EKI	Zircon (U-Th)/He	2.8	0.2
Core	AM96-40-09-344.7m	18774	22118	2955	AM96-40-09	344.7	EKI	Zircon (U-Th)/He	2.8	0.3
Core	AM96-40-09-477m	18774	22118	2955	AM96-40-09	477	EKI	Zircon (U-Th)/He	2.8	0.2
Outcrop	14-SW-05	734971	9551031	3415			EKI	Zircon (U-Th)/He	3.1	0.2
Core	INF42-01-250m	734480.130	9551489.010	3052	INF42-01	250	MGI	Zircon (U-Th)/He	3.2	0.3
Outcrop	14-SW-02	734493	9551570	3255			MGI	Zircon (U-Th)/He	2.9	0.4
Core	INF42-01-50m	734480.130	9551489.010	3052	INF42-01	50	MGI	Zircon (U-Th)/He	3.2	0.2
Core	GRD42-06-362m	734478.897	9551487.066	3046	GRD42-06	362	MGI	Zircon (U-Th)/He	2.9	0.3
Outcrop	90-TM-GRS3	735605	9549890	2528			MGI	Zircon (U-Th)/He	2.9	0.3
Core	GRS-93A 0m	18439	22503.000	4112	GRS-93A	0	MGI	Zircon (U-Th)/He	3.2	0.3
Core	AB1-10-01 500m	735605	9549890	2528	AB1-10-01	500	Plag Dike	Zircon (U-Th)/He	2.7	0.1
Core	NSC-09-02 246m	734334	9552357	4225	NSC-09-02	246	Tvs	Zircon (U-Th)/He	3.1	0.5
Core	GCZ-40-01 59m	734278	9552475	4078	GCZ-41-01	59.1	Tvs	Zircon (U-Th)/He	3.3	0.2
Core	GT-INC-023 22m	734184	9552463	4032	GT-INC-023	22	Tvs	Zircon (U-Th)/He	3.4	0.1

Sample Type	Sample Number	UTM Easting	UTM Northing	Elevation (m)	DDH ID	Depth (m)	Rock Type	Method	Age Ma	Error +/- Ma
Core	GCZ-50-02 105m	734297	9552353	4061	GCZ-50-02	105	Tvs	Zircon (U-Th)/He	3.3	0.3
Outcrop	14-SW-06	734128	9551593	3570			DF	Zircon (U-Th)/He	3.3	0.1
Core	GRS-116 6m	18148	22148	4051	GRS-116	6	DF	Zircon (U-Th)/He	3.1	0.5
Core	GRS-116 200m	18148	22148	4051	GRS-116	200	DF	Zircon (U-Th)/He	3.2	0.2
Core	GRS-119 15m	18473	23171	4150	GRS-119	15	DF	Zircon (U-Th)/He	3.2	0.3
Core	GRS-119 210m	18473	23171	4150	GRS-119	210	DF	Zircon (U-Th)/He	3	0.6
Core	GRS-123 0m	18015	22427	4053	GRS-123	0	DF	Zircon (U-Th)/He	3.3	0.2
Core	GRS-123 200m	18015	22427	4053	GRS-123	200	DF	Zircon (U-Th)/He	3.1	0.2
Core	GRS-128 0m	18117	21735	3989	GRS-128	0	DF	Zircon (U-Th)/He	3.1	0.3
Core	GRS-128 203m	18117	21735	3989	GRS-128	203	DF	Zircon (U-Th)/He	3.3	0.1
Core	AB1-10-01 2m	735605	9549890	2528	AB1-10-01	2	Ertsberg	Zircon (U-Th)/He	2.8	0.3
Core	TEW08-01 0m	736633	9549336	3145	TEW 08-01	0	Ertsberg	Zircon (U-Th)/He	2.5	0.2
Core	TEW08-01 280m	736633	9549336	3145	TEW 08-01	280	Ertsberg	Zircon (U-Th)/He	2.2	0.5
Core	TEW08-01 500m	736633	9549336	3145	TEW 08-01	500	Ertsberg	Zircon (U-Th)/He	2.1	0.4
Core	TEW08-01 750m	736633	9549336	3145	TEW 08-01	750	Ertsberg	Zircon (U-Th)/He	2.3	0.7
Core	TEW08-01 1000m	736633	9549336	3145	TEW 08-01	1000	Ertsberg	Zircon (U-Th)/He	2.1	0.2
Core	TEW08-01 1275m	736633	9549336	3145	TEW 08-01	1275	Ertsberg	Zircon (U-Th)/He	1.6	0.5
Core	GB23-02-56m	736008.208	9549327.231	3791	GB23-02	56	Ertsberg	Zircon (U-Th)/He	2.5	1
Core	ABE01-01-143m	735734.760	9548227.424	2511	ABE-01-01	143	Ertsberg	Zircon (U-Th)/He	2.6	0.6
Core	TEW01-01-75.5m	736482.880	9548606.420	3960	TEW01-01	75.5	Ertsberg	Zircon (U-Th)/He	3	0.1
Core	DMLZC05-01-248m	736232.881	9547348.660	2912	DMLZC05-01	248	Ertsberg	Zircon (U-Th)/He	2.2	0.1
Core	VZW-74S 70m	736381	9549129	3841	VZW-74S	70	Ertsberg	Zircon (U-Th)/He	2.2	0.1
Core	VZW-74S 276m	736381	9549129	3841	VZW-74S	276	Ertsberg	Zircon (U-Th)/He	2.6	0.4
Outcrop	M1996: 1001	735650	9549175				Ertsberg	Zircon (U-Th)/He	2.4	0.4
Core	AB1-10-01 574m	735605	9549890	2528	AB1-10-01	574	Karume	Zircon (U-Th)/He	3.2	0.3
Core	AB1-10-01 578m	735605	9549890	2528	AB1-10-01	578	Karume	Zircon (U-Th)/He	2.9	0.6
Core	KL20-10 3m	735024	9550482	2804	KL20-10	3	Karume	Zircon (U-Th)/He	2.9	0.1
Core	KL98-10-21-727m	734101	9550741	3062	KL98-10-21	727	Tigt	Zircon (U-Th)/He	2.7	0.1
Core	KL98-10-21-841m	734101	9550741	3062	KL98-10-21	841	Tigt	Zircon (U-Th)/He	3.1	0.4
Core	KL98-10-21-922m	734101	9550741	3062	KL98-10-21	922	Tigt	Zircon (U-Th)/He	2.6	0.9
Core	KL98-10-21-948m	734101	9550741	3062	KL98-10-21	948	Tigt	Zircon (U-Th)/He	2.7	0.4
Core	KL98-10-21-982m	734101	9550741	3062	KL98-10-21	982	Tigt	Zircon (U-Th)/He	2.6	0.3
Core	KL98-10-21-1192m	734101	9550741	3062	KL98-10-21	1192	Tigt	Zircon (U-Th)/He	2.1	0.2
Core	KL98-10-21-1243m	734101	9550741	3062	KL98-10-21	1243	Tigt	Zircon (U-Th)/He	2.8	0.3
Core	KL98-10-21-1266m	734101	9550741	3062	KL98-10-21	1266	Tigt	Zircon (U-Th)/He	2.5	0.5
Core	BG-WSH-04 237m	734726	9548458	3184	BG-WGH-04	237	Big Gossan Dike	Zircon (U-Th)/He	2.8	0.2
Outcrop	M1996: 3001	733820	9553445	4125			North Grasberg	Zircon (U-Th)/He	3.1	0.1
Outcrop	M1996: 4001	732310	9549690	4025			Wanagon	Zircon (U-Th)/He	3.1	0.2
Outcrop	93-MC-HR2	733630	9550720	4030			Heat Road Dike	Zircon (U-Th)/He	2.9	0.3
Outcrop	93-MC-HR3a	733450	9547180	2760			Heat Road Dike	Zircon (U-Th)/He	2.6	0.1
Outcrop	95-MC-HR4	734020	9550000	3790			Heat Road Dike	Zircon (U-Th)/He	3.3	0.3
Outcrop	93-MC-HR5	733850	9549560	3535			Heat Road Dike	Zircon (U-Th)/He	3.1	0.3
Outcrop	94-MC-HR6	733690	9549270	3335			Heat Road Dike	Zircon (U-Th)/He	2.6	0.4
Outcrop	93-MC-HR8	733590	9549300	3315			Heat Road Dike	Zircon (U-Th)/He	3	0.4
Outcrop	94-MC-RC2	732240	9544980	2160			Ridge Camp Intusion	Zircon (U-Th)/He	2.1	0.3
Outcrop	91-RW-E'	733500	9549800	3525			Sirga	Zircon (U-Th)/He	detrital	
Outcrop	91-RW-A	737000	9551100	3875			Sirga	Zircon (U-Th)/He	detrital	
Outcrop	15-SW-16	735500	9552300	4060			Sirga	Zircon (U-Th)/He	detrital	

Appendix I: Zircon Diffusion Experiments

The following table reports the results of two step-heating diffusion experiments conducted on single zircon grains from the MGI (sample GRD42-02 389m). In order to quantitatively interpret the zHe ages it is important to understand the diffusion kinetics and retentivity of helium for low radiation damage Grasberg zircons (Guenthner et al., 2013). ^{4}He diffusion experiments were conducted using the methods described by Farley et al. (1999), and the results show that bulk helium diffusion, despite the low radiation damage, is not anomalously low and is consistent with published experimental data on zircon (Reiners et al., 2004). The "effective" closure temperature for zircons from the mining district of 210°C was calculated iteratively for the observed cooling rates (~500°C/myr) using the Dodson equation (Dodson, 1973) and the experimentally derived zircon diffusion kinetics.

Appendix I: MGI Zircon Diffusion Experiment Results

MGI-1

Step #	Average T (°C)	Time (s)	He (ncc)	±	sum%He	ln(D/r2)[1]	±
1	400	7200	1.3846	0.0038	0.073333	-16.54611	0.1682
2	400	7200	0.3111	0.0020	0.089808	-17.2397	0.4017
3	400	7200	0.2514	0.0023	0.103125	-17.2051	0.2652
4	410	7200	0.2968	0.0015	0.118845	-16.88627	0.1840
5	420	7200	0.3473	0.0017	0.137242	-16.5709	0.1322
6	430	7200	0.3854	0.0026	0.157654	-16.30822	0.1278
7	440	7200	0.4015	0.0025	0.178917	-16.11587	0.1205
8	450	7200	0.3731	0.0020	0.198680	-16.05463	0.1044
9	460	7200	0.3350	0.0027	0.216420	-16.04969	0.1035
10	470	7200	0.2788	0.0040	0.231187	-16.14166	0.1368
11	480	7260	0.2467	0.0027	0.244252	-16.1981	0.1385
12	482	10860	0.2474	0.0018	0.257356	-16.5307	0.0975
13	472	10860	0.1226	0.0015	0.263847	-17.18463	0.1362
14	462	10800	0.0717	0.0013	0.267646	-17.68987	0.1662
15	452	10800	0.0474	0.0009	0.270155	-18.08988	0.1787
16	442	10800	0.0313	0.0008	0.271812	-18.49426	0.1993
17	432	10800	0.0215	0.0009	0.272951	-18.86337	0.2651
18	422	10800	0.0145	0.0008	0.273720	-19.2508	0.3509
19	412	10800	0.0100	0.0007	0.274249	-19.62158	0.4215
20	402	10860	0.0072	0.0005	0.274630	-19.95259	0.4579
21	405	10800	0.0073	0.0005	0.275015	-19.93642	0.3942
22	420	10800	0.0117	0.0007	0.275632	-19.46166	0.3056
23	435	10800	0.0205	0.0008	0.276718	-18.89282	0.2377
24	450	10800	0.0375	0.0010	0.278706	-18.28087	0.1730
25	465	10860	0.0565	0.0015	0.281700	-17.86521	0.1576
26	480	10860	0.0933	0.0012	0.286641	-17.3457	0.1105
27	495	10800	0.1433	0.0038	0.294231	-16.88238	0.1248
28	510	10860	0.2204	0.0055	0.305902	-16.41433	0.1394
29	525	10860	0.2824	0.0019	0.320860	-16.10789	0.0922
30	539	10860	0.3463	0.0028	0.339199	-15.8332	0.0541
31	536	10860	0.2682	0.0029	0.353403	-16.0216	0.0734
32	526	10860	0.1596	0.0044	0.361854	-16.49509	0.1272
33	516	10860	0.1054	0.0014	0.367438	-16.88162	0.1423
34	506	10860	0.0682	0.0013	0.371051	-17.29873	0.1107
35	496	10860	0.0466	0.0009	0.373521	-17.66741	0.1253
36	486	10860	0.0340	0.0011	0.375320	-17.97578	0.1463
37	476	10860	0.0238	0.0010	0.376578	-18.32717	0.2010
38	466	10800	0.0195	0.0008	0.377609	-18.51642	0.2024
39	456	10860	0.0135	0.0007	0.378324	-18.88452	0.2342

MGI-2

Step #	Average T (°C)	Time (s)	He (ncc)	±	sum%He	ln(D/r2)	±
1	400	7260	0.1016	0.0013	0.016496	-19.53822	1.2267307
2	400	7260	0.0445	0.0007	0.023721	-19.47262	1.4843054
3	400	7260	0.0442	0.0013	0.030889	-19.17458	1.1580049
4	410	7260	0.0562	0.0010	0.040016	-18.67191	0.927262
5	420	7260	0.0746	0.0011	0.052119	-18.12769	0.6462014
6	430	7260	0.0907	0.0011	0.066841	-17.67634	0.4994485
7	440	7260	0.1035	0.0018	0.083649	-17.30867	0.4430518
8	450	7260	0.1100	0.0018	0.101501	-16.96471	0.4524666
9	460	7260	0.1127	0.0015	0.119804	-16.74572	0.368592
10	470	7200	0.1236	0.0022	0.139860	-16.46899	0.3154519
11	480	7200	0.1232	0.0030	0.159855	-16.31051	0.3428914
12	482	10860	0.1456	0.0030	0.183497	-16.39761	0.2898071
13	472	10800	0.0883	0.0011	0.197827	-16.77	0.3062647
14	462	10860	0.0559	0.0008	0.206902	-17.16152	0.2394116
15	452	10860	0.0368	0.0007	0.212871	-17.53659	0.2553535
16	442	10860	0.0253	0.0008	0.216984	-17.88036	0.3214019
17	432	10860	0.0160	0.0007	0.219578	-18.32238	0.4351766
18	422	10860	0.0109	0.0005	0.221350	-18.6918	0.4791951
19	412	10860	0.0075	0.0006	0.222569	-19.05696	0.5792635
20	402	10860	0.0044	0.0005	0.223280	-19.59076	0.7958996
21	405	10860	0.0061	0.0006	0.224274	-19.25168	0.6141362
22	420	10860	0.0104	0.0006	0.225961	-18.7148	0.4503856
23	435	10860	0.0173	0.0007	0.228777	-18.19067	0.3147911
24	450	10860	0.0284	0.0009	0.233384	-17.6783	0.2480023
25	465	10860	0.0445	0.0009	0.240604	-17.19758	0.1969008
26	480	10860	0.0640	0.0012	0.250998	-16.78778	0.1656046
27	495	10860	0.0903	0.0011	0.265657	-16.38117	0.1299094
28	510	10860	0.1142	0.0015	0.284196	-16.06641	0.1151464
29	525	10800	0.1298	0.0013	0.305260	-15.84208	0.1043668
30	540	10800	0.1472	0.0015	0.329156	-15.61721	0.0890169
31	536	10800	0.0918	0.0022	0.344065	-16.00743	0.144216
32	526	10860	0.0556	0.0010	0.353093	-16.46558	0.1728641
33	516	10800	0.0405	0.0014	0.359661	-16.74656	0.1674408
34	506	10860	0.0271	0.0008	0.364057	-17.13204	0.2069364
35	496	10860	0.0189	0.0007	0.367118	-17.47886	0.1967213
36	486	10860	0.0151	0.0007	0.369572	-17.68921	0.2170258
37	476	10860	0.0109	0.0005	0.371336	-18.01097	0.2524018
38	466	10860	0.0079	0.0005	0.372626	-18.31825	0.2881851
39	456	10860	0.0047	0.0006	0.373381	-18.84956	0.454279

[1] Values for ln(D/a2) calculated from equations described in Fechtig and Kalbitzer (1966) assuming a spherical geometry.

Appendix J: Apatite (U-Th)/He Age Results

The following table contains the apatite (U-Th)/He age results for single-grain apatite aliquots. Six euhedral, inclusion-free apatite were selected and analyzed for each sample, and final reported age is the average and standard deviation of the six aliquots.

Sample	Intrusion	Elevation (m)	Mineral	mass (ug)	ESR	U (ppm)	Th (ppm)	147Sm (ppm)	He (nmol/g)	Ft	Age, Ma	err., Ma
INF37-02-75m-1	LKI	3120	apatite	2.49	44.70	5.6	40.7	57.7	0.2	0.65	3.1	0.18
INF37-02-75m-3	LKI	3120	apatite	2.93	47.24	9.2	63.5	70.6	0.3	0.67	3.2	0.19
INF37-02-75m-4	LKI	3120	apatite	2.69	46.09	6.9	32.7	50.2	0.1	0.66	2.8	0.17
INF37-02-75m-5	LKI	3120	apatite	3.62	51.41	10.9	45.6	66.1	0.2	0.69	3.0	0.18
INF37-02-75m-6	LKI	3120	apatite	6.10	62.20	7.0	33.2	55.9	0.2	0.74	3.0	0.18
INF37-02-75m-7	LKI	3120	apatite	2.79	47.28	9.4	79.8	60.3	0.3	0.67	3.0	0.18
INF37-02-75m-8	LKI	3120	apatite	1.38	38.61	7.4	43.7	45.6	0.2	0.60	2.6	0.15
INF37-02-75m-9	LKI	3120	apatite	5.87	61.67	9.4	41.5	51.3	0.2	0.74	2.7	0.16
INF37-02-75m-10	LKI	3120	apatite	1.89	39.78	11.9	51.6	32.8	0.2	0.61	3.0	0.18
INF37-02-75m-11	LKI	3120	apatite	5.93	59.43	7.7	41.1	63.9	0.2	0.73	3.0	0.18
INF37-02-75m-12	LKI	3120	apatite	2.03	43.57	6.9	95.5	66.3	0.3	0.64	3.3	0.20
INF37-02-75m-13	LKI	3120	apatite	5.42	59.46	6.3	68.5	56.3	0.2	0.73	2.7	0.16
2004-2	LKI	3785	apatite	2.34	45.83	9.7	30.1	53.3	0.2	0.66	3.0	0.18
2004-3	LKI	3785	apatite	1.59	37.99	10.3	38.0	53.8	0.2	0.60	3.2	0.19
2004-4	LKI	3785	apatite	2.33	46.51	5.7	19.9	38.2	0.1	0.67	2.4	0.14
2004-5	LKI	3785	apatite	0.93	32.85	7.3	27.8	49.9	0.1	0.55	2.8	0.17
2004-6	LKI	3785	apatite	1.76	41.20	6.4	29.0	39.5	0.1	0.63	3.1	0.18
14-SW-05-1	EKI	3415	apatite	5.39	47.43	3.1	12.3	24.1	0.1	0.74	2.5	0.15
14-SW-05-2	EKI	3415	apatite	7.88	57.84	2.9	11.0	16.8	0.1	0.78	2.6	0.16
14-SW-05-3	EKI	3415	apatite	4.14	45.87	2.1	7.3	14.6	0.0	0.73	2.5	0.15
14-SW-05-4	EKI	3415	apatite	4.73	48.58	2.6	9.1	13.3	0.0	0.75	2.0	0.12
14-SW-05-5	EKI	3415	apatite	3.69	44.67	3.7	16.1	24.6	0.1	0.73	2.3	0.14
14-SW-05-6	EKI	3415	apatite	9.59	61.02	3.0	12.2	17.0	0.1	0.80	2.4	0.14
14-SW-05-7	EKI	3415	apatite	3.26	42.96	2.0	7.0	11.8	0.0	0.72	2.1	0.13
14-SW-05-8	EKI	3415	apatite	5.54	51.72	3.9	13.5	19.9	0.1	0.76	2.8	0.17
14-SW-05-9	EKI	3415	apatite	4.34	44.82	5.3	18.4	28.0	0.1	0.73	2.8	0.17
14-SW-05-10	EKI	3415	apatite	5.16	48.00	3.5	12.5	20.6	0.1	0.74	2.6	0.15
AM96-40-01-148m-1	EKI	2893	apatite	1.41	37.64	10.6	32.0	29.4	0.1	0.60	2.3	0.14
AM96-40-01-148m-2	EKI	2893	apatite	3.96	53.01	6.8	22.4	29.3	0.1	0.70	2.2	0.13
AM96-40-01-148m-3	EKI	2893	apatite	1.04	33.32	8.7	30.5	42.6	0.1	0.55	2.1	0.13
AM96-40-01-148m-4	EKI	2893	apatite	1.64	38.96	6.6	25.0	43.5	0.1	0.61	2.4	0.14
AM96-40-01-148m-6	EKI	2893	apatite	3.48	51.59	7.7	26.5	34.9	0.1	0.70	2.0	0.12
AM96-40-01-148m-7	EKI	2893	apatite	0.98	33.20	6.3	22.5	33.8	0.1	0.55	2.3	0.14
AM96-40-01-148m-8	EKI	2893	apatite	1.67	41.13	6.2	21.7	37.5	0.1	0.63	2.4	0.14
AM96-40-01-148m-9	EKI	2893	apatite	2.03	41.42	5.2	19.9	36.0	0.1	0.63	2.2	0.13
AM96-40-01-148m-10	EKI	2893	apatite	1.19	34.99	7.4	32.6	48.9	0.1	0.57	2.9	0.17
AM96-40-01-345m-1	EKI	2696	apatite	2.15	44.60	4.7	21.9	38.1	0.1	0.65	1.7	0.10
AM96-40-01-345m-3	EKI	2696	apatite	3.62	50.52	5.8	24.1	55.1	0.1	0.69	2.2	0.13
AM96-40-01-345m-4	EKI	2696	apatite	2.18	40.60	11.2	31.1	43.0	0.2	0.63	3.0	0.18
AM96-40-01-345m-5	EKI	2696	apatite	4.77	56.27	5.6	21.1	39.6	0.1	0.72	2.5	0.15

Sample	Intrusion	Elevation (m)	Mineral	mass (ug)	ESR	U (ppm)	Th (ppm)	147Sm (ppm)	He (nmol/g)	Ft	Age, Ma	err., Ma
AM96-40-01-345m-6	EKI	2696	apatite	8.93	68.25	2.9	9.2	21.4	0.1	0.77	3.0	0.18
AM96-40-01-345m-7	EKI	2696	apatite	3.14	50.05	14.3	61.9	94.1	0.3	0.69	2.9	0.17
AM96-40-01-345m-9	EKI	2696	apatite	4.19	53.25	5.8	25.9	53.2	0.1	0.70	2.5	0.15
AM96-40-01-345m-10	EKI	2696	apatite	4.18	55.50	5.7	26.4	34.0	0.1	0.71	2.2	0.13
AM96-40-01-477m-1	EKI	2564	apatite	2.05	43.47	5.3	25.0	37.5	0.1	0.64	1.8	0.11
AM96-40-01-477m-2	EKI	2564	apatite	2.52	43.43	8.1	30.4	69.5	0.2	0.64	2.9	0.17
AM96-40-01-477m-4	EKI	2564	apatite	1.96	42.65	4.5	20.9	47.0	0.0	0.64	1.0	0.06
AM96-40-01-477m-5	EKI	2564	apatite	0.91	32.33	5.4	21.4	43.2	0.1	0.54	1.7	0.10
AM96-40-01-477m-6	EKI	2564	apatite	3.27	47.53	7.3	35.3	56.4	0.1	0.67	1.8	0.11
AM96-40-01-477m-7	EKI	2564	apatite	1.95	42.11	5.7	25.2	52.5	0.1	0.63	1.4	0.09
AM96-40-01-477m-8	EKI	2564	apatite	2.48	46.46	7.0	31.9	38.5	0.1	0.66	1.4	0.08
AM96-40-01-477m-9	EKI	2564	apatite	1.34	34.78	6.3	27.4	56.2	0.1	0.57	1.8	0.11
AM96-40-01-477m-10	EKI	2564	apatite	1.71	39.01	5.1	22.5	48.1	0.1	0.61	1.4	0.09
AB1-10-01-382m-3	EKI	2528	apatite	1.55	37.26	6.8	31.3	159.4	0.1	0.59	2.7	0.22
AB1-10-01-382m-4	EKI	2528	apatite	1.19	34.19	4.4	16.9	75.5	0.1	0.56	2.9	0.23
14-SW-02-1	MGI	3235	apatite	2.24	43.35	14.2	36.0	61.3	0.3	0.65	3.4	0.21
14-SW-02-2	MGI	3235	apatite	2.60	45.96	12.5	40.4	64.7	0.3	0.66	3.5	0.21
14-SW-02-3	MGI	3235	apatite	1.28	36.02	10.1	34.3	56.8	0.2	0.58	3.3	0.20
14-SW-02-4	MGI	3235	apatite	1.44	37.87	14.6	50.5	64.4	0.3	0.60	3.8	0.23
14-SW-02-5	MGI	3235	apatite	1.94	39.52	10.2	36.1	56.8	0.2	0.61	3.3	0.20
14-SW-02-6	MGI	3235	apatite	1.63	40.36	4.9	22.6	45.1	0.1	0.62	3.0	0.18
14-SW-02-7	MGI	3235	apatite	3.79	51.09	7.4	15.5	24.8	0.1	0.70	2.8	0.17
14-SW-02-10	MGI	3235	apatite	1.53	38.70	22.6	37.5	37.4	0.3	0.61	2.8	0.17
14-SW-02-11	MGI	3235	apatite	4.13	56.99	23.2	40.6	56.9	0.4	0.73	3.2	0.19
14-SW-02-12	MGI	3235	apatite	2.88	47.21	28.0	45.0	40.8	0.4	0.68	2.8	0.17
14-SW-02-13	MGI	3235	apatite	5.86	60.41	18.8	36.1	24.0	0.3	0.74	2.6	0.16
14-SW-02-14	MGI	3235	apatite	1.71	39.57	5.2	31.0	48.8	0.1	0.61	3.1	0.18
INF42-01-50m-2	MGI	3100	apatite	4.88	56.13	19.4	21.6	47.0	0.3	0.73	3.4	0.20
INF42-01-50m-3	MGI	3100	apatite	4.88	56.92	2.6	58.7	57.2	0.2	0.72	3.2	0.19
INF42-01-50m-4	MGI	3100	apatite	3.16	47.53	19.9	22.4	36.6	0.3	0.68	3.6	0.22
INF42-01-50m-5	MGI	3100	apatite	3.01	47.42	3.8	28.0	51.5	0.1	0.67	2.9	0.17
INF42-01-50m-6	MGI	3100	apatite	1.90	42.38	5.8	32.6	43.6	0.1	0.63	3.0	0.18
INF42-01-50m-7	MGI	3100	apatite	2.16	40.32	14.1	16.0	36.6	0.2	0.63	3.7	0.22
INF42-01-50m-8	MGI	3100	apatite	15.21	85.40	2.4	60.0	54.6	0.2	0.80	2.2	0.13
INF42-01-50m-9	MGI	3100	apatite	5.14	55.52	16.3	24.5	50.0	0.3	0.72	3.2	0.19
INF42-01-50m-10	MGI	3100	apatite	20.20	91.81	3.1	79.7	71.7	0.3	0.82	3.3	0.20
INF42-01-50m-11	MGI	3100	apatite	10.40	76.00	2.8	69.9	233.4	0.2	0.78	2.7	0.16
INF42-01-50m-12	MGI	3100	apatite	5.09	60.31	2.8	61.8	212.7	0.2	0.73	2.8	0.17
INF42-01-50m-13	MGI	3100	apatite	2.39	44.60	4.4	51.1	247.6	0.2	0.65	3.1	0.19
INF42-01-50m-14	MGI	3100	apatite	20.04	85.75	2.4	62.9	198.4	0.2	0.81	2.6	0.16
INF42-01-50m-15	MGI	3100	apatite	13.66	75.67	3.4	84.1	278.3	0.3	0.78	2.8	0.17

Sample	Intrusion	Elevation (m)	Mineral	mass (ug)	ESR	U (ppm)	Th (ppm)	147Sm (ppm)	He (nmol/g)	Ft	Age, Ma	err., Ma
INF42-01-250m-1	MGI	3300	apatite	13.55	78.14	2.6	45.2	52.5	0.2	0.79	3.2	0.19
INF42-01-250m-3	MGI	3300	apatite	14.87	81.39	8.1	40.6	50.1	0.3	0.80	3.7	0.22
INF42-01-250m-6	MGI	3300	apatite	10.91	74.57	1.6	46.5	40.9	0.1	0.78	2.7	0.16
AB1-10-01-500m-1	Plag Dike	2528	apatite	10.87	73.47	26.8	75.6	174.3	0.6	0.78	3.3	0.26
AB1-10-01-500m-2	Plag Dike	2528	apatite	2.43	43.76	18.3	65.1	160.2	0.4	0.65	3.2	0.25
AB1-10-01-500m-3	Plag Dike	2528	apatite	3.23	47.79	23.1	81.4	196.7	0.5	0.67	3.0	0.24
AB1-10-01-500m-4	Plag Dike	2528	apatite	2.44	45.70	21.9	73.3	150.4	0.5	0.66	3.4	0.27
AB1-10-01-500m-6	Plag Dike	2528	apatite	7.18	63.76	17.0	48.5	128.9	0.4	0.75	2.9	0.24
1001-2	Ertsberg	3550	apatite	1.74	40.34	2.2	8.5	39.8	0.0	0.62	2.2	0.13
1001-3	Ertsberg	3550	apatite	6.04	61.43	7.0	29.7	100.9	0.2	0.74	2.7	0.16
1001-5	Ertsberg	3550	apatite	1.92	41.18	25.2	63.8	212.6	0.5	0.63	3.4	0.21
1001-6	Ertsberg	3550	apatite	2.86	48.06	32.8	38.4	150.3	0.5	0.68	3.0	0.18
TEW08-01-0m-2	Ertsberg	3145	apatite	15.63	83.82	8.8	38.0	101.2	0.2	0.81	2.6	0.16
TEW08-01-0m-3	Ertsberg	3145	apatite	5.98	60.06	6.0	28.0	59.2	0.1	0.73	2.7	0.16
TEW08-01-0m-4	Ertsberg	3145	apatite	4.34	52.94	7.1	36.2	68.8	0.2	0.70	2.8	0.17
TEW08-01-0m-5	Ertsberg	3145	apatite	5.80	62.66	5.9	28.0	64.7	0.1	0.74	2.8	0.17
TEW08-01-500m-3	Ertsberg	2645	apatite	8.63	71.73	6.1	27.9	115.5	0.2	0.77	3.5	0.21
TEW08-01-500m-4	Ertsberg	2645	apatite	7.15	66.18	9.6	48.9	141.8	0.2	0.76	2.5	0.15
TEW08-01-500m-5	Ertsberg	2645	apatite	3.39	51.39	10.2	22.5	80.2	0.2	0.70	2.8	0.17
TEW08-01-750m-2	Ertsberg	2395	apatite	3.29	51.00	16.4	29.5	69.1	0.2	0.70	2.1	0.13
TEW08-01-750m-3	Ertsberg	2395	apatite	3.04	50.14	14.0	26.8	93.2	0.2	0.69	2.9	0.18
TEW08-01-750m-4	Ertsberg	2395	apatite	1.17	36.76	9.0	23.1	88.5	0.1	0.59	2.1	0.13
TEW08-01-750m-5	Ertsberg	2395	apatite	2.02	42.36	7.6	24.3	64.0	0.1	0.64	1.8	0.11
AB1-10-01-2m-1	Ertsberg	2528	apatite	4.92	58.39	6.9	40.2	207.5	0.1	0.73	1.9	0.15
AB1-10-01-2m-2	Ertsberg	2528	apatite	2.67	46.76	7.1	35.8	182.8	0.1	0.67	2.4	0.19
AB1-10-01-2m-5	Ertsberg	2528	apatite	1.74	39.40	8.7	35.4	135.2	0.2	0.61	3.5	0.28
AB1-10-01-2m-6	Ertsberg	2528	apatite	2.17	44.98	4.4	21.4	108.4	0.1	0.65	1.9	0.15
VZW-74S-70m-1	Ertsberg	3770	apatite	3.33	49.80	21.3	60.6	141.8	0.4	0.69	2.8	0.22
VZW-74S-70m-2	Ertsberg	3770	apatite	2.82	48.33	21.9	69.4	171.3	0.4	0.68	3.0	0.24
VZW-74S-70m-3	Ertsberg	3770	apatite	3.58	50.88	10.2	38.7	119.5	0.3	0.69	3.5	0.28
VZW-74S-70m-4	Ertsberg	3770	apatite	4.83	55.85	26.4	71.8	95.8	0.5	0.72	3.0	0.24
VZW-74S-70m-5	Ertsberg	3770	apatite	4.73	55.78	15.2	46.4	174.3	0.3	0.72	2.5	0.20
VZW-74S-70m-6	Ertsberg	3770	apatite	2.89	46.61	23.1	69.5	175.9	0.4	0.67	2.7	0.22
VZW-74S-276m-2	Ertsberg	3564	apatite	11.01	73.64	14.9	54.8	84.5	0.3	0.78	2.8	0.23
VZW-74S-276m-3	Ertsberg	3564	apatite	4.90	55.83	11.3	47.5	56.0	0.3	0.72	3.2	0.25
VZW-74S-276m-4	Ertsberg	3564	apatite	7.52	66.68	18.8	37.4	121.3	0.3	0.76	2.9	0.23
VZW-74S-276m-5	Ertsberg	3564	apatite	10.36	72.58	9.8	33.8	161.0	0.2	0.78	3.1	0.24
VZW-74S-276m-6	Ertsberg	3564	apatite	5.43	59.04	12.5	35.0	161.6	0.2	0.73	2.8	0.22
AB1-10-01-578m-1	Karume	2528	apatite	1.30	36.51	16.1	31.4	101.6	0.2	0.59	2.4	0.19
AB1-10-01-578m-2	Karume	2528	apatite	2.60	43.21	28.2	47.0	162.5	0.4	0.65	3.0	0.24
AB1-10-01-578m-3	Karume	2528	apatite	0.96	32.51	26.0	32.7	93.8	0.3	0.56	2.5	0.20

Sample	Intrusion	Elevation (m)	Mineral	mass (ug)	ESR	U (ppm)	Th (ppm)	147Sm (ppm)	He (nmol/g)	Ft	Age, Ma	err., Ma
AB1-10-01-578m-4	Karume	2528	apatite	2.51	46.27	23.9	28.9	178.9	0.4	0.67	3.1	0.24
AB1-10-01-578m-5	Karume	2528	apatite	1.79	39.63	24.9	40.2	138.8	0.3	0.62	2.8	0.22
AB1-10-01-578m-6	Karume	2528	apatite	6.56	64.05	24.2	29.3	174.0	0.4	0.76	2.7	0.22
KL98-10-21-727m-1	Tigt	2335	apatite	3.19	50.17	7.5	34.7	38.2	0.1	0.69	2.1	0.12
KL98-10-21-727m-3	Tigt	2335	apatite	6.39	62.72	6.9	30.9	35.1	0.1	0.74	1.3	0.08
KL98-10-21-727m-4	Tigt	2335	apatite	4.42	54.96	5.3	28.0	40.6	0.1	0.71	2.3	0.14
KL98-10-21-727m-6	Tigt	2335	apatite	4.99	56.01	4.8	19.6	49.4	0.1	0.72	2.4	0.14
KL98-10-21-727m-7	Tigt	2335	apatite	7.04	67.99	9.5	44.5	58.8	0.3	0.76	3.2	0.19
KL98-10-21-727m-8	Tigt	2335	apatite	5.20	57.25	5.7	50.3	97.3	0.2	0.72	3.0	0.18
KL98-10-21-727m-9	Tigt	2335	apatite	2.15	45.28	5.1	37.6	53.9	0.1	0.65	2.6	0.16
KL98-10-21-1192m-1	Tigt	1870	apatite	2.37	46.61	7.0	33.8	40.8	0.1	0.66	2.0	0.12
KL98-10-21-1192m-2	Tigt	1870	apatite	9.77	75.08	2.5	13.2	36.8	0.1	0.78	2.3	0.14
KL98-10-21-1192m-3	Tigt	1870	apatite	7.58	69.07	6.9	22.1	24.9	0.1	0.77	1.8	0.11
KL98-10-21-1192m-4	Tigt	1870	apatite	9.16	71.13	2.7	13.0	33.4	0.1	0.77	2.2	0.13
KL98-10-21-1192m-5	Tigt	1870	apatite	1.10	35.15	6.1	25.1	40.2	0.1	0.57	2.2	0.13
KL98-10-21-1192m-6	Tigt	1870	apatite	5.81	58.20	7.1	33.7	43.7	0.1	0.73	2.3	0.14
KL98-10-21-1192m-7	Tigt	1870	apatite	6.01	60.44	4.2	22.4	34.8	0.1	0.73	1.4	0.08
KL98-10-21-1192m-8	Tigt	1870	apatite	2.87	48.03	5.7	27.2	37.0	0.1	0.67	2.4	0.14
3001-2	North Grasberg	4125	apatite	5.19	59.22	10.1	36.7	49.4	0.3	0.73	3.4	0.20
3001-3	North Grasberg	4125	apatite	3.87	52.73	17.7	60.8	49.9	0.4	0.70	3.4	0.20
3001-4	North Grasberg	4125	apatite	3.11	48.53	12.5	57.5	64.2	0.3	0.68	3.4	0.20
3001-5	North Grasberg	4125	apatite	7.49	69.00	9.3	34.0	45.1	0.2	0.77	2.2	0.13
3001-6	North Grasberg	4125	apatite	4.45	57.24	11.7	40.0	48.0	0.3	0.72	3.5	0.21
4001-1	Wanagon	4025	apatite	3.25	49.45	4.1	7.0	114.6	0.0	0.69	1.9	0.12
4001-2	Wanagon	4025	apatite	4.50	56.68	5.0	10.0	141.5	0.1	0.72	2.3	0.14
4001-3	Wanagon	4025	apatite	14.25	83.90	3.3	6.5	92.7	0.1	0.81	2.6	0.16
4001-5	Wanagon	4025	apatite	5.16	59.53	3.6	7.4	102.1	0.1	0.74	2.5	0.15
4001-6	Wanagon	4025	apatite	8.09	66.62	3.8	6.4	108.3	0.1	0.76	2.3	0.14
93-MC-HR2-1	HEAT Rd Intrusion	2900	apatite	26.03	99.84	4.2	27.7	144.3	0.1	0.83	1.4	0.09
93-MC-HR2-2	HEAT Rd Intrusion	2900	apatite	1.67	39.98	1.4	11.4	28.9	0.0	0.61	3.4	0.21
93-MC-HR2-3	HEAT Rd Intrusion	2900	apatite	3.09	51.11	2.6	14.1	100.5	0.0	0.69	1.7	0.10
93-MC-HR2-4	HEAT Rd Intrusion	2900	apatite	4.94	60.01	4.3	28.9	143.8	0.1	0.73	2.0	0.12
93-MC-HR2-6	HEAT Rd Intrusion	2900	apatite	4.69	55.91	4.3	27.0	139.1	0.1	0.71	2.9	0.17
93-MC-HR3a-1	HEAT Rd Intrusion	2760	apatite	9.54	72.21	7.7	18.9	155.2	0.1	0.78	2.1	0.13
93-MC-HR3a-3	HEAT Rd Intrusion	2760	apatite	13.96	81.39	7.0	16.5	151.9	0.1	0.80	2.0	0.12
93-MC-HR3a-4	HEAT Rd Intrusion	2760	apatite	11.63	75.77	6.6	17.2	139.3	0.2	0.79	3.3	0.20
93-MC-HR3a-5	HEAT Rd Intrusion	2760	apatite	10.19	73.81	6.2	14.3	133.2	0.1	0.78	1.8	0.11
93-MC-HR3a-6	HEAT Rd Intrusion	2760	apatite	11.57	77.27	7.8	19.5	160.1	0.1	0.79	1.8	0.11
95-MC-HR4-1	HEAT Rd Intrusion	3790	apatite	11.64	76.02	7.6	37.1	197.9	0.2	0.79	2.7	0.16
95-MC-HR4-2	HEAT Rd Intrusion	3790	apatite	5.08	57.68	8.5	44.4	205.5	0.3	0.72	3.2	0.19
95-MC-HR4-3	HEAT Rd Intrusion	3790	apatite	2.74	48.56	7.8	25.0	131.9	0.2	0.68	3.0	0.18

Sample	Intrusion	Elevation (m)	Mineral	mass (ug)	ESR	U (ppm)	Th (ppm)	147Sm (ppm)	He (nmol/g)	Ft	Age, Ma	err., Ma
95-MC-HR4-4	HEAT Rd Intrusion	3790	apatite	9.40	70.24	8.0	41.0	209.7	0.2	0.77	3.0	0.18
95-MC-HR4-5	HEAT Rd Intrusion	3790	apatite	3.12	49.80	13.0	45.4	218.8	0.3	0.69	3.3	0.20
95-MC-HR4-6	HEAT Rd Intrusion	3790	apatite	4.75	58.30	5.9	19.0	210.5	0.1	0.73	2.6	0.15
93-MC-HR5-1	HEAT Rd Intrusion	3535	apatite	27.06	98.94	4.8	24.7	126.3	0.1	0.83	2.7	0.16
93-MC-HR5-2	HEAT Rd Intrusion	3535	apatite	10.59	73.63	5.2	23.1	118.3	0.1	0.78	2.9	0.18
93-MC-HR5-3	HEAT Rd Intrusion	3535	apatite	9.87	70.83	5.4	21.0	119.1	0.1	0.77	2.8	0.17
93-MC-HR5-4	HEAT Rd Intrusion	3535	apatite	3.65	52.93	3.8	18.0	69.7	0.1	0.70	2.1	0.13
93-MC-HR5-5	HEAT Rd Intrusion	3535	apatite	16.28	85.76	6.2	25.7	184.9	0.2	0.81	2.7	0.16
93-MC-HR5-6	HEAT Rd Intrusion	3535	apatite	1.67	39.71	6.1	24.7	126.2	0.1	0.61	2.9	0.17
94-MC-HR6-1	HEAT Rd Intrusion	3335	apatite	9.51	72.05	10.3	54.4	253.2	0.3	0.77	2.7	0.16
94-MC-HR6-2	HEAT Rd Intrusion	3335	apatite	31.94	104.95	7.9	39.8	180.4	0.2	0.84	2.5	0.15
94-MC-HR6-3	HEAT Rd Intrusion	3335	apatite	8.69	69.15	7.5	40.4	197.8	0.2	0.77	2.5	0.15
94-MC-HR6-4	HEAT Rd Intrusion	3335	apatite	40.25	116.75	6.3	31.8	158.2	0.2	0.86	2.4	0.15
94-MC-HR6-5	HEAT Rd Intrusion	3335	apatite	26.39	100.09	7.3	39.1	189.7	0.2	0.83	2.7	0.16
94-MC-HR6-6	HEAT Rd Intrusion	3335	apatite	27.87	98.30	8.2	40.1	199.9	0.2	0.83	2.6	0.15
94-MC-HR8-1	HEAT Rd Intrusion	3000	apatite	3.23	48.78	7.1	17.8	163.6	0.1	0.68	2.2	0.13
94-MC-HR8-3	HEAT Rd Intrusion	3000	apatite	11.97	78.65	6.8	16.1	151.2	0.1	0.80	2.7	0.16
94-MC-HR8-4	HEAT Rd Intrusion	3000	apatite	1.30	37.02	3.4	10.6	77.6	0.0	0.59	2.2	0.13
94-MC-HR8-5	HEAT Rd Intrusion	3000	apatite	4.16	56.03	1.7	6.6	70.0	0.0	0.72	2.6	0.15
94-MC-HR8-6	HEAT Rd Intrusion	3000	apatite	3.09	51.88	6.1	18.6	143.5	0.1	0.70	2.5	0.15
94MCRC2-2	Ridge Camp	2160	apatite	5.45	60.63	0.1	0.7	0.4	0.0	0.73	0.9	0.05
94MCRC2-5	Ridge Camp	2160	apatite	5.26	61.66	6.5	25.3	119.1	0.1	0.74	2.7	0.16

Appendix K: Zircon (U-Th)/He Age Results

The following table contains the zircon (U-Th)/He age results for single-grain zircon aliquots. Six euhedral zircons, between 80 to 120μm in width, were selected and analyzed for each sample, and final reported age is the average and standard deviation of the six aliquots.

Sample	Intrusion	Elevation (m)	mineral	mass (ug)	ESR	U (ppm)	Th (ppm)	147Sm (ppm)	He (nmol/g)	Ft	Age, Ma	err., Ma
z2004-1	LKI	3785	zircon	4.54	44.87	118.7	77.2	0.5	1.5	0.74	2.8	0.23
z2004-2	LKI	3785	zircon	6.38	52.47	75.4	46.7	0.3	1.0	0.77	2.7	0.21
z2004-3	LKI	3785	zircon	5.76	48.77	435.6	142.2	0.4	6.1	0.76	3.2	0.25
z2004-4	LKI	3785	zircon	6.37	51.02	115.2	76.3	0.3	1.6	0.77	2.9	0.23
z2004-5	LKI	3785	zircon	2.39	38.06	98.3	71.6	0.4	1.0	0.70	2.4	0.19
z2004-6	LKI	3785	zircon	9.22	60.92	94.6	65.9	0.5	1.3	0.80	2.7	0.22
zINF37-02-75m-10	LKI	3120	zircon	4.48	47.68	250.5	448.8	0.5	3.8	0.75	2.7	0.21
zINF37-02-75m-11	LKI	3120	zircon	2.68	38.90	161.7	139.6	0.9	2.0	0.70	2.8	0.22
zINF37-02-75m-12	LKI	3120	zircon	8.12	57.28	91.8	60.5	1.0	1.5	0.79	3.2	0.26
zINF37-02-75m-8	LKI	3120	zircon	14.37	71.44	87.6	63.3	0.2	1.4	0.83	3.0	0.24
zINF37-02-75m-9	LKI	3120	zircon	23.90	81.49	74.0	50.5	0.4	1.0	0.85	2.6	0.21
zINF37-02-275m-1	LKI	3120	zircon	11.66	63.98	141.4	105.3	2.2	2.1	0.81	2.8	0.23
zINF37-02-275m-2	LKI	2920	zircon	9.55	58.89	100.0	77.3	4.3	1.5	0.80	3.0	0.24
zINF37-02-275m-3	LKI	2920	zircon	5.20	49.73	173.8	138.0	16.8	1.0	0.76	1.2	0.10
zINF37-02-275m-4	LKI	2920	zircon	4.68	48.14	88.8	55.1	0.9	1.2	0.76	2.8	0.22
zINF37-02-275m-5	LKI	2920	zircon	3.87	44.99	115.5	90.6	1.3	1.6	0.74	3.0	0.24
zINF37-02-275m-6	LKI	2920	zircon	4.23	47.93	156.4	159.0	1.4	2.7	0.75	3.4	0.27
zINF37-02-275m-7	LKI	2920	zircon	40.58	95.21	182.2	72.9	0.3	3.2	0.87	3.4	0.27
zINF37-02-275m-8	LKI	2920	zircon	17.28	76.57	66.9	49.6	0.3	1.1	0.84	3	0.24
zKL981693-1	LKI*	1414	zircon	6.31	52.18	156.0	113.4	0.4	2.0	0.77	2.6	0.21
zKL981693-2	LKI*	1414	zircon	3.68	41.63	198.9	138.8	0.7	1.7	0.72	1.9	0.15
zKL981693-3	LKI*	1414	zircon	4.98	48.27	150.6	113.8	0.4	1.4	0.75	1.9	0.15
zKL981693-4	LKI*	1414	zircon	2.88	39.29	216.5	187.2	0.5	2.5	0.70	2.5	0.20
zKL981693-5	LKI*	1414	zircon	2.99	40.87	111.0	74.8	0.4	0.9	0.72	1.7	0.14
zAB1-10-01-205m-1	LKI	2528	zircon	10.59	61.37	112.7	62.2	1.3	1.6	0.81	2.9	0.18
zAB1-10-01-205m-2	LKI	2528	zircon	13.29	64.24	247.7	85.9	1.1	3.2	0.82	2.7	0.16
zAB1-10-01-205m-3	LKI	2528	zircon	14.50	68.05	95.7	63.9	1.5	1.3	0.82	2.6	0.16
zAB1-10-01-205m-4	LKI	2528	zircon	10.83	58.84	151.6	101.0	3.1	1.9	0.80	2.5	0.15
zAB1-10-01-205m-5	LKI	2528	zircon	10.38	63.00	92.5	56.0	1.3	1.1	0.81	2.3	0.14
zAB1-10-01-205m-6	LKI	2528	zircon	13.30	64.92	127.2	72.2	0.9	1.8	0.82	2.8	0.17
zAB1-10-01-382m-1	EKI	2528	zircon	17.45	71.78	202.5	106.0	3.9	3.3	0.83	3.2	0.19
zAB1-10-01-382m-2	EKI	2528	zircon	10.40	58.85	116.1	62.6	1.3	1.5	0.80	2.6	0.16
zAB1-10-01-382m-3	EKI	2528	zircon	8.00	54.60	84.5	52.9	0.8	1.1	0.78	2.7	0.16
zAB1-10-01-382m-4	EKI	2528	zircon	12.10	65.71	108.7	63.2	1.2	1.6	0.82	2.9	0.18
zAB1-10-01-382m-6	EKI	2528	zircon	19.45	72.57	78.0	41.3	1.0	1.1	0.83	2.7	0.16
zAM96148-7	EKI	2893	zircon	58.80	111.48	52.2	30.1	0.2	0.8	0.89	3.0	0.24
zAM96148-8	EKI	2893	zircon	3.73	43.52	158.5	108.7	0.5	1.9	0.73	2.6	0.21
zAM96148-9	EKI	2893	zircon	3.80	43.51	145.1	86.0	0.4	1.7	0.73	2.6	0.21
zAM96148-10	EKI	2893	zircon	7.23	54.77	191.3	89.8	0.3	2.9	0.78	3.2	0.26
zAM96148-12	EKI	2893	zircon	8.12	55.54	81.4	50.4	0.3	1.1	0.79	2.9	0.23
zAM96345-7	EKI	2696	zircon	2.39	38.44	120.2	79.2	0.4	1.4	0.70	2.7	0.22
zAM96345-9	EKI	2696	zircon	3.63	43.86	220.6	131.1	0.4	3.2	0.73	3.2	0.25
zAM96345-10	EKI	2696	zircon	4.59	45.70	161.5	109.7	1.4	1.8	0.74	2.4	0.19
zAM96345-11	EKI	2696	zircon	15.45	70.43	88.1	53.9	0.3	1.2	0.83	2.8	0.22
zAM96477-7	EKI	2564	zircon	13.58	66.10	157.0	129.0	0.4	2.3	0.82	2.7	0.22
zAM96477-8	EKI	2564	zircon	7.74	56.29	133.0	93.2	0.4	1.7	0.79	2.5	0.20
zAM96477-9	EKI	2564	zircon	3.78	43.27	148.0	107.2	0.4	1.9	0.73	2.7	0.22

Sample	Intrusion	Elevation (m)	mineral	mass (ug)	ESR	U (ppm)	Th (ppm)	147Sm (ppm)	He (nmol/g)	Ft	Age, Ma	err., Ma
zAM96477-10	EKI	2564	zircon	22.23	79.87	71.2	47.4	0.3	1.2	0.85	3.1	0.25
zAM96477-11	EKI	2564	zircon	5.76	49.61	262.7	137.3	0.5	3.2	0.76	2.7	0.21
zAM96477-12	EKI	2564	zircon	23.14	83.13	57.7	36.5	0.2	0.9	0.85	2.8	0.23
z14SW05-7	EKI	3415	zircon	13.34	63.71	110.2	68.4	0.4	1.7	0.81	3.0	0.24
z14SW05-8	EKI	3415	zircon	4.39	45.45	90.1	63.1	0.6	1.3	0.74	3.0	0.24
z14SW05-9	EKI	3415	zircon	14.96	67.05	99.9	69.9	0.4	1.5	0.82	2.8	0.23
z14SW05-10	EKI	3415	zircon	5.44	50.43	131.3	55.7	0.2	1.7	0.77	2.9	0.23
z14SW05-11	EKI	3415	zircon	5.89	50.39	144.8	125.4	0.3	2.4	0.76	3.3	0.26
z14SW05-12	EKI	3415	zircon	4.75	47.73	165.3	89.6	0.2	2.5	0.75	3.4	0.27
zINF42-01-50m-1	MGI	3100	zircon	34.18	90.18	254.9	96	0.2	4.2	0.87	3.2	0.26
zINF42-01-50m-2	MGI	3100	zircon	43.99	104.56	83.6	66.3	0.3	1.4	0.88	3	0.24
zINF42-01-50m-3	MGI	3100	zircon	15.94	70.01	257.7	144	0.3	4.6	0.83	3.5	0.28
zINF42-01-50m-4	MGI	3100	zircon	10.46	60.19	88.4	59.7	0.5	1.3	0.8	3	0.24
zINF42-01-50m-5	MGI	3100	zircon	20.27	77.88	180.9	54.3	0.2	2.9	0.85	3.3	0.26
zINF42-01-250m-3	MGI	3300	zircon	4.57	47.91	210.5	81.2	18.1	3.1	0.76	3.3	0.26
zINF42-01-250m-4	MGI	3300	zircon	5.56	47.05	292.4	107.9	0.3	4.6	0.75	3.6	0.29
zINF42-01-250m-5	MGI	3300	zircon	16.58	75.7	86.8	62.9	0.3	1.4	0.84	3.1	0.24
zINF42-01-250m-6	MGI	3300	zircon	28.39	87.86	37	30.3	0.2	0.6	0.86	2.8	0.22
zGRD42-06-326m-1	MGI	2700	zircon	8	54.75	341	109	0.3	4.4	0.79	2.8	0.23
zGRD42-06-326m-2	MGI	2700	zircon	5.61	51.22	341.3	217.2	4.5	4.8	0.77	3	0.24
zGRD42-06-326m-3	MGI	2700	zircon	7.97	55.14	1478.3	253.9	0.3	16.3	0.79	2.5	0.2
zGRD42-06-326m-4	MGI	2700	zircon	2.23	36.88	58.7	44.3	0.5	0.7	0.69	2.7	0.22
zGRD42-06-326m-5	MGI	2700	zircon	2.45	37.35	141.7	101.8	0.6	2	0.69	3.3	0.26
zGRD42-06-326m-6	MGI	2700	zircon	6.96	53.95	274	88.4	0.2	4	0.78	3.3	0.26
z14-SW-02-7	MGI	3235	zircon	4.48	47.91	391.6	390.7	0.5	5.1	0.75	2.6	0.21
z14-SW-02-8	MGI	3235	zircon	11.8	66.78	456.3	533.5	0.8	7.8	0.82	3	0.24
z14-SW-02-9	MGI	3235	zircon	4.86	48.94	379.9	402.6	0.7	4.9	0.76	2.5	0.2
z14-SW-02-10	MGI	3235	zircon	5.44	51.08	365.9	408.5	0.7	6.9	0.76	3.6	0.29
z14-SW-02-11	MGI	3235	zircon	6.13	54.33	272.6	299.6	0.6	4	0.78	2.8	0.22
z90TMGRS3-1	MGI	2528	zircon	11.72	63.81	330.8	81.6	0.9	4.2	0.82	2.7	0.22
z90TMGRS3-2	MGI	2528	zircon	17.38	71.19	97.6	104.0	2.4	1.6	0.83	2.9	0.23
z90TMGRS3-3	MGI	2528	zircon	12.58	64.59	300.4	104.8	0.8	4.3	0.82	3.0	0.24
z90TMGRS3-4	MGI	2528	zircon	59.13	116.04	42.5	49.6	1.0	0.7	0.89	2.5	0.20
z90TMGRS3-5	MGI	2528	zircon	12.69	68.06	197.5	124.8	7.1	3.4	0.82	3.3	0.27
zGRS93A0-1	MGI	4113	zircon	25.86	83.70	243.9	130.7	1.2	4.4	0.85	3.5	0.28
zGRS93A0-2	MGI	4113	zircon	35.72	92.85	184.1	68.8	1.8	3.3	0.87	3.6	0.29
zGRS93A0-3	MGI	4113	zircon	19.02	76.18	216.0	79.6	1.3	3.4	0.84	3.2	0.26
zGRS93A0-4	MGI	4113	zircon	22.51	80.72	274.4	140.8	1.7	4.1	0.85	2.9	0.23
zGRS93A0-5	MGI	4113	zircon	39.45	95.16	189.1	98.9	1.1	3.0	0.87	3.0	0.24
zGRS93A0-6	MGI	4113	zircon	21.25	78.49	223.8	121.5	1.6	3.7	0.85	3.3	0.26
zAB1-10-01-500m-2	Plag Dike	2528	zircon	13.29	67.50	479.8	525.4	4.1	7.5	0.82	2.8	0.17
zAB1-10-01-500m-3	Plag Dike	2528	zircon	4.27	45.75	711.4	1018.5	9.6	10.1	0.74	2.7	0.16
zAB1-10-01-500m-4	Plag Dike	2528	zircon	6.49	52.06	502.4	695.7	7.6	7.0	0.77	2.5	0.15
zAB1-10-01-500m-5	Plag Dike	2528	zircon	6.30	53.41	894.4	1073.3	6.5	12.9	0.77	2.7	0.16
zAB1-10-01-500m-6	Plag Dike	2528	zircon	7.66	57.12	451.1	675.3	3.8	6.9	0.79	2.7	0.16
zNSC-09-02-246m-1	Tvs	4225	zircon	3.24	41.40	277.5	172.1	0.3	3.7	0.72	3.0	0.24
zNSC-09-02-246m-2	Tvs	4225	zircon	7.08	52.56	393.6	205.4	0.5	5.8	0.78	3.2	0.25
zNSC-09-02-246m-3	Tvs	4225	zircon	3.15	40.20	472.9	245.6	0.4	7.2	0.71	3.5	0.28
zNSC-09-02-246m-4	Tvs	4225	zircon	2.91	39.64	206.2	181.4	0.7	2.2	0.71	2.3	0.19

Sample	Intrusion	Elevation (m)	mineral	mass (ug)	ESR	U (ppm)	Th (ppm)	147Sm (ppm)	He (nmol/g)	Ft	Age, Ma	err., Ma
zNSC-09-02-246m-5	Tvs	4225	zircon	25.11	83.49	314.7	180.6	0.5	5.0	0.85	3.0	0.24
zNSC-09-02-246m-6	Tvs	4225	zircon	9.59	59.41	245.5	118.8	0.3	4.5	0.80	3.8	0.31
zGCZ-40-01-59m-2	Tvs	4078	zircon	10.95	62.14	215.3	96.7	0.3	3.2	0.81	3.1	0.25
zGCZ-40-01-59m-3	Tvs	4078	zircon	15.24	71.42	258.0	142.5	0.7	4.3	0.83	3.3	0.27
zGCZ-40-01-59m-4	Tvs	4078	zircon	3.47	43.31	232.3	140.1	0.5	3.5	0.73	3.4	0.27
zGCZ-40-01-59m-5	Tvs	4078	zircon	17.21	74.63	235.7	133.1	0.4	4.1	0.84	3.4	0.27
zGCZ-40-01-59m-6	Tvs	4078	zircon	9.47	62.98	149.4	41.1	0.2	2.2	0.81	3.2	0.25
zGT-INC-023-22m-1	Tvs	4032	zircon	11.76	62.48	199.7	107.4	0.3	3.1	0.81	3.2	0.26
zGT-INC-023-22m-2	Tvs	4032	zircon	21.10	78.36	244.3	128.1	0.4	4.2	0.85	3.4	0.27
zGT-INC-023-22m-3	Tvs	4032	zircon	18.13	72.37	261.9	123.3	0.3	4.5	0.83	3.5	0.28
zGT-INC-023-22m-6	Tvs	4032	zircon	14.26	67.05	314.7	183.7	0.4	5.4	0.82	3.4	0.27
zGCZ-50-02-105m-1	Tvs	4061	zircon	5.79	51.87	236.3	174.9	0.4	3.9	0.77	3.4	0.27
zGCZ-50-02-105m-2	Tvs	4061	zircon	4.46	45.45	304.9	153.6	0.4	4.1	0.74	3.0	0.24
zGCZ-50-02-105m-3	Tvs	4061	zircon	5.93	50.34	250.7	128.4	0.4	3.8	0.77	3.2	0.26
zGCZ-50-02-105m-4	Tvs	4061	zircon	4.62	46.65	294.8	144.8	0.4	5.0	0.75	3.8	0.30
z14SW06-10	Dalam Fragmental	3570	zircon	3.99	44.51	450.6	260.9	0.7	7.0	0.74	3.4	0.27
z14SW06-11	Dalam Fragmental	3570	zircon	18.92	73.64	425.0	205.3	0.6	6.8	0.84	3.2	0.26
z14SW06-7	Dalam Fragmental	3570	zircon	22.27	78.40	264.4	178.6	0.4	4.7	0.84	3.4	0.27
z14SW06-8	Dalam Fragmental	3570	zircon	11.05	64.57	246.0	168.2	0.3	3.9	0.81	3.1	0.25
z14SW06-9	Dalam Fragmental	3570	zircon	6.14	50.70	333.6	196.0	0.5	5.4	0.77	3.5	0.28
zGRS1166-1	Dalam Fragmental	4051	zircon	28.49	85.97	200.2	111.7	1.1	2.8	0.86	2.6	0.21
zGRS1166-2	Dalam Fragmental	4051	zircon	41.25	96.70	215.3	106.7	1.1	4.0	0.87	3.5	0.28
zGRS1166-3	Dalam Fragmental	4051	zircon	99.48	129.80	255.8	135.7	2.2	4.6	0.91	3.2	0.26
zGRS1166-4	Dalam Fragmental	4051	zircon	27.82	84.37	218.0	121.3	1.1	4.1	0.86	3.6	0.29
zGRS1166-5	Dalam Fragmental	4051	zircon	22.27	78.94	370.5	193.7	1.7	6.2	0.85	3.3	0.26
zGRS1166-6	Dalam Fragmental	4051	zircon	26.86	81.48	342.0	176.6	1.8	4.3	0.85	2.5	0.20
zGRS116200-1	Dalam Fragmental	3851	zircon	7.03	56.49	2465.6	1109.4	12.0	39.5	0.79	3.4	0.27
zGRS116200-2	Dalam Fragmental	3851	zircon	37.37	92.85	368.8	179.2	2.1	5.9	0.87	3.0	0.24
zGRS116200-4	Dalam Fragmental	3851	zircon	16.59	71.88	252.9	88.2	2.0	4.2	0.83	3.4	0.27
zGRS116200-5	Dalam Fragmental	3851	zircon	18.38	75.67	213.9	113.3	21.8	3.2	0.84	2.9	0.23
zGRS116200-6	Dalam Fragmental	3851	zircon	15.30	68.19	389.7	222.4	1.7	6.7	0.82	3.4	0.28
zGRS11915-1	Dalam Fragmental	4150	zircon	17.75	72.00	98.9	79.9	3.5	1.7	0.83	3.3	0.26
zGRS11915-2	Dalam Fragmental	4150	zircon	15.84	69.10	128.1	102.5	1.9	2.2	0.82	3.2	0.26
zGRS11915-3	Dalam Fragmental	4150	zircon	9.61	59.41	77.0	54.1	2.1	1.2	0.80	3.0	0.24
zGRS11915-4	Dalam Fragmental	4150	zircon	9.55	59.71	88.6	67.9	1.4	1.2	0.80	2.8	0.22
zGRS11915-6	Dalam Fragmental	4150	zircon	6.50	50.93	163.5	69.5	0.9	2.6	0.77	3.5	0.28
zGRS119210-2	Dalam Fragmental	3940	zircon	3.18	41.54	328.6	199.2	30.4	3.1	0.72	2.1	0.17
zGRS119210-3	Dalam Fragmental	3940	zircon	20.86	75.31	349.3	176.3	2.9	5.4	0.84	3.1	0.25
zGRS119210-4	Dalam Fragmental	3940	zircon	8.44	58.64	262.2	42.0	1.5	3.3	0.80	2.8	0.22
zGRS119210-5	Dalam Fragmental	3940	zircon	15.77	71.62	202.3	190.0	1.5	4.1	0.83	3.7	0.30
zGRS119210-6	Dalam Fragmental	3940	zircon	16.81	72.06	221.8	145.4	1.4	3.6	0.83	3.1	0.25
zGRS1230-1	Dalam Fragmental	4053	zircon	52.66	104.81	237.5	149.6	2.4	3.9	0.88	3.0	0.24
zGRS1230-2	Dalam Fragmental	4053	zircon	62.87	111.22	190.2	84.5	1.4	3.5	0.89	3.4	0.27
zGRS1230-3	Dalam Fragmental	4053	zircon	31.86	88.90	296.8	165.2	34.8	5.1	0.86	3.3	0.26
zGRS1230-5	Dalam Fragmental	4053	zircon	11.57	63.00	366.5	349.6	2.4	6.9	0.81	3.5	0.28
zGRS1230-6	Dalam Fragmental	4053	zircon	25.60	82.97	229.8	185.5	2.0	4.0	0.85	3.1	0.25
zGRS123200-1	Dalam Fragmental	3853	zircon	12.34	66.22	440.5	242.5	5.7	6.4	0.82	2.9	0.23
zGRS123200-2	Dalam Fragmental	3853	zircon	21.78	79.05	623.5	391.9	4.5	9.8	0.85	3.0	0.24
zGRS123200-3	Dalam Fragmental	3853	zircon	24.80	83.76	358.0	99.3	1.6	5.5	0.86	3.1	0.25

Sample	Intrusion	Elevation (m)	mineral	mass (ug)	ESR	U (ppm)	Th (ppm)	147Sm (ppm)	He (nmol/g)	Ft	Age, Ma	err., Ma
zGRS123200-4	Dalam Fragmental	3853	zircon	11.29	64.53	274.8	125.7	1.2	3.9	0.82	2.9	0.23
zGRS123200-5	Dalam Fragmental	3853	zircon	30.44	84.80	315.7	194.7	1.7	5.6	0.86	3.3	0.27
zGRS123200-6	Dalam Fragmental	3853	zircon	7.34	52.09	491.0	294.1	3.9	7.4	0.77	3.2	0.25
zGRS1280-1	Dalam Fragmental	3989	zircon	69.34	115.14	314.3	169.8	2.1	5.0	0.89	2.9	0.24
zGRS1280-5	Dalam Fragmental	3989	zircon	7.72	56.40	320.2	260.5	3.0	4.7	0.79	2.9	0.23
zGRS1280-6	Dalam Fragmental	3989	zircon	5.39	47.91	481.4	261.0	29.8	7.5	0.76	3.4	0.27
zGRS128203-1	Dalam Fragmental	3786	zircon	29.61	88.85	254.3	98.3	1.2	4.2	0.86	3.3	0.26
zGRS128203-2	Dalam Fragmental	3786	zircon	83.46	126.30	273.9	126.8	2.9	4.7	0.90	3.2	0.26
zGRS128203-3	Dalam Fragmental	3786	zircon	13.81	64.22	421.2	190.0	1.7	6.3	0.81	3.1	0.25
zGRS128203-4	Dalam Fragmental	3786	zircon	13.73	68.93	365.4	224.4	1.5	6.3	0.83	3.4	0.27
zGRS128203-5	Dalam Fragmental	3786	zircon	11.49	63.74	589.3	287.6	33.8	9.7	0.81	3.4	0.27
zGRS128203-6	Dalam Fragmental	3786	zircon	18.55	76.33	338.5	228.7	1.5	5.8	0.84	3.3	0.26
zAB1-10-01-2m-1	Ertsberg	2528	zircon	9.57	58.20	162.0	94.2	1.0	2.2	0.80	2.8	0.17
zAB1-10-01-2m-2	Ertsberg	2528	zircon	15.01	69.98	57.8	33.1	1.4	0.7	0.83	2.4	0.14
zAB1-10-01-2m-3	Ertsberg	2528	zircon	7.44	56.09	114.6	75.1	1.7	1.4	0.79	2.6	0.15
zAB1-10-01-2m-4	Ertsberg	2528	zircon	7.08	55.17	51.1	32.6	0.7	0.5	0.78	2.1	0.13
zAB1-10-01-2m-5	Ertsberg	2528	zircon	5.30	50.45	94.9	54.8	0.8	1.0	0.77	2.3	0.14
zAB1-10-01-2m-6	Ertsberg	2528	zircon	4.17	47.58	143.6	157.0	1.2	1.9	0.75	2.6	0.16
zTEW08-01-0m-1	Ertsberg	3145	zircon	35.44	97.24	60.4	41.2	1.1	0.8	0.87	2.4	0.19
zTEW08-01-0m-2	Ertsberg	3145	zircon	17.65	72.91	98.6	57.6	0.7	1.4	0.83	2.8	0.22
zTEW08-01-0m-3	Ertsberg	3145	zircon	14.95	73.24	43.2	31.8	0.8	0.5	0.83	2.3	0.18
zTEW08-01-0m-5	Ertsberg	3145	zircon	23.79	84.55	64.6	46.5	1.1	0.8	0.86	2.4	0.19
zTEW08-01-0m-6	Ertsberg	3145	zircon	11.04	65.57	92.8	66.5	0.7	1.2	0.82	2.5	0.20
zTEW08-01-280m-1	Ertsberg	2865	zircon	27.19	85.26	161.1	161.5	1.7	2.5	0.86	2.7	0.22
zTEW08-01-280m-2	Ertsberg	2865	zircon	38.05	98.48	205.9	167.8	1.0	3.0	0.87	2.6	0.21
zTEW08-01-280m-3	Ertsberg	2865	zircon	7.37	57.50	308.1	275.2	3.6	2.0	0.79	1.2	0.10
zTEW08-01-280m-4	Ertsberg	2865	zircon	33.81	94.51	155.9	127.7	3.4	2.0	0.87	2.3	0.19
zTEW08-01-280m-5	Ertsberg	2865	zircon	14.46	72.42	409.0	338.0	2.0	4.8	0.83	2.2	0.18
zTEW08-01-280m-6	Ertsberg	2865	zircon	22.82	80.83	205.0	244.7	2.5	2.8	0.85	2.4	0.19
zTEW08-01-500m-1	Ertsberg	2645	zircon	21.18	80.94	93.5	93.0	1.8	0.9	0.85	1.6	0.13
zTEW08-01-500m-2	Ertsberg	2645	zircon	22.42	84.12	68.4	58.8	2.1	0.9	0.85	2.3	0.19
zTEW08-01-500m-3	Ertsberg	2645	zircon	10.26	64.45	172.4	151.1	2.2	2.3	0.81	2.5	0.20
zTEW08-01-500m-4	Ertsberg	2645	zircon	14.59	71.60	102.4	66.0	3.4	1.1	0.83	2.1	0.17
zTEW08-01-500m-5	Ertsberg	2645	zircon	94.68	136.46	36.2	25.4	1.6	0.5	0.91	2.5	0.20
zTEW08-01-500m-6	Ertsberg	2645	zircon	25.33	85.97	57.8	42.6	1.8	0.5	0.86	1.7	0.14
zTEW08-01-750m-1	Ertsberg	2395	zircon	42.42	100.76	177.3	112.9	1.3	2.4	0.88	2.5	0.20
zTEW08-01-750m-2	Ertsberg	2395	zircon	46.08	105.88	90.7	74.3	1.0	1.2	0.88	2.4	0.19
zTEW08-01-750m-3	Ertsberg	2395	zircon	17.19	74.43	151.0	126.1	5.3	0.8	0.84	1.0	0.08
zTEW08-01-750m-4	Ertsberg	2395	zircon	78.46	125.07	154.2	135.5	1.3	2.5	0.90	2.8	0.22
zTEW08-01-750m-5	Ertsberg	2395	zircon	24.68	84.79	354.9	218.3	1.9	5.1	0.86	2.7	0.22
zTEW08-01-750m-6	Ertsberg	2395	zircon	13.08	69.00	88.3	84.8	1.0	1.0	0.82	2.1	0.17
zTEW08-01-1000m-3	Ertsberg	2145	zircon	8.33	60.02	165.6	127.2	0.6	1.8	0.80	2.1	0.17
zTEW08-01-1000m-4	Ertsberg	2145	zircon	4.55	47.34	441.3	220.7	1.5	3.8	0.75	1.9	0.15
zTEW08-01-1000m-6	Ertsberg	2145	zircon	10.93	66.37	84.1	81.2	0.6	1.0	0.82	2.3	0.18
zTEW08-01-1275m-1	Ertsberg	1870	zircon	15.30	73.97	71.7	46.8	6.2	0.7	0.84	1.9	0.15
zTEW08-01-1275m-2	Ertsberg	1870	zircon	16.78	75.41	58.5	54.4	1.0	0.6	0.84	2.0	0.16
zTEW08-01-1275m-3	Ertsberg	1870	zircon	18.31	74.96	124.6	82.9	1.8	1.4	0.84	2.1	0.17
zTEW08-01-1275m-4	Ertsberg	1870	zircon	20.55	80.66	88.8	68.0	27.2	0.5	0.85	1.1	0.08
zTEW08-01-1275m-6	Ertsberg	1870	zircon	9.64	62.49	113.2	63.4	55.8	0.7	0.81	1.2	0.09

Sample	Intrusion	Elevation (m)	mineral	mass (ug)	ESR	U (ppm)	Th (ppm)	147Sm (ppm)	He (nmol/g)	Ft	Age, Ma	err., Ma
z1001-3	Ertsberg	-	zircon	4.17	44.58	166.1	76.7	0.4	1.7	0.74	2.3	0.18
z1001-4	Ertsberg	-	zircon	12.98	63.92	370.8	980.3	1.4	5.7	0.81	2.2	0.17
z1001-5	Ertsberg	-	zircon	13.83	68.52	70.2	58.0	0.4	0.8	0.82	2.1	0.17
z1001-6	Ertsberg	-	zircon	8.29	58.00	286.6	391.1	1.0	5.0	0.79	3.1	0.25
zGB2302-2	Ertsberg	3791	zircon	4.45	46.3	129.8	61.7	0.6	2.1	0.75	3.7	0.29
zGB2302-3	Ertsberg	3791	zircon	5.28	47.87	107.8	56.5	0.4	1.2	0.76	2.4	0.19
zGB2302-6	Ertsberg	3791	zircon	2.8	39.48	733	353	1.4	4	0.71	1.3	0.1
zABE0101-1	Ertsberg	2511	zircon	15.2	71.98	116.6	99.4	0.3	1.5	0.83	2.4	0.19
zABE0101-2	Ertsberg	2511	zircon	30.41	90.27	321.9	283.6	0.8	4.3	0.86	2.4	0.19
zABE0101-3	Ertsberg	2511	zircon	26.05	84.14	147.5	115.5	0.3	3.1	0.85	3.9	0.31
zABE0101-4	Ertsberg	2511	zircon	33.96	95.61	169.6	113.5	0.3	2.2	0.87	2.4	0.19
zABE0101-5	Ertsberg	2511	zircon	40.12	98.3	214.7	181.3	0.4	2.7	0.87	2.2	0.18
zABE0101-6	Ertsberg	2511	zircon	18.15	76.52	196.9	189.1	0.5	2.7	0.84	2.4	0.19
zAB1-10-01-574m-1	Karume	2528	zircon	65.74	112.99	227.4	74.4	0.8	3.8	0.89	3.2	0.19
zAB1-10-01-574m-3	Karume	2528	zircon	16.45	71.61	824.1	1913.6	6.2	16.1	0.83	2.8	0.17
zAB1-10-01-574m-4	Karume	2528	zircon	24.56	85.17	502.0	1176.3	13.7	9.4	0.85	2.6	0.16
zAB1-10-01-574m-5	Karume	2528	zircon	8.52	58.12	544.5	708.9	5.3	10.4	0.79	3.4	0.21
zAB1-10-01-574m-6	Karume	2528	zircon	10.32	62.95	744.5	1385.9	5.7	13.0	0.80	2.8	0.17
zAB1-10-01-578m-4	Karume	2528	zircon	14.75	69.64	306.9	112.5	1.1	3.3	0.83	2.2	0.13
zAB1-10-01-578m-5	Karume	2528	zircon	17.23	70.65	308.3	163.5	1.0	4.8	0.83	3.1	0.19
zAB1-10-01-578m-6	Karume	2528	zircon	15.64	69.23	357.4	142.6	1.9	5.9	0.83	3.4	0.20
zKL20-10-3m-1	Karume	2804	zircon	36.23	93.67	228.3	82.6	0.2	3.6	0.87	3.1	0.25
zKL20-10-3m-2	Karume	2804	zircon	40.12	94.32	149.6	56.3	0.1	2.2	0.87	2.9	0.23
zKL20-10-3m-3	Karume	2804	zircon	9.24	58.86	259.1	90.4	0.2	3.4	0.8	2.8	0.23
zKL98-10-21-727-1	Tigt	2335	zircon	16.75	69.44	215.3	111.6	0.7	3.0	0.83	2.8	0.22
zKL98-10-21-727-2	Tigt	2335	zircon	4.64	45.70	187.2	130.2	0.4	2.3	0.74	2.6	0.21
zKL98-10-21-727-3	Tigt	2335	zircon	18.14	75.59	68.4	51.0	0.4	0.9	0.84	2.6	0.21
zKL98-10-21-727-4	Tigt	2335	zircon	20.88	80.02	85.4	60.1	0.4	1.1	0.85	2.5	0.20
zKL98-10-21-727-5	Tigt	2335	zircon	29.14	87.42	91.3	55.5	0.4	1.3	0.86	2.6	0.21
zKL98-10-21-727-6	Tigt	2335	zircon	11.24	64.73	259.7	115.9	0.4	3.7	0.82	3.0	0.24
zKL98-10-21-727-7	Tigt	2335	zircon	3.54	43.80	126.9	117.9	0.3	1.6	0.73	2.7	0.21
zKL98-10-21-727-8	Tigt	2335	zircon	19.24	76.30	88.7	71.0	0.3	1.5	0.84	3.2	0.25
zKL98-10-21-727-9	Tigt	2335	zircon	6.67	54.21	89.4	69.7	0.3	1.2	0.78	2.7	0.22
zKL98-10-21-727-10	Tigt	2335	zircon	7.53	56.72	100.9	84.0	0.2	1.5	0.79	2.9	0.23
zKL98-10-21-727-11	Tigt	2335	zircon	2.16	37.53	187.9	142.9	0.3	2.9	0.69	3.6	0.28
zKL98-10-21-727-12	Tigt	2335	zircon	3.61	44.34	80.7	70.9	0.3	1.4	0.73	3.7	0.29
zKL98-10-21-841-2	Tigt	2221	zircon	17.25	69.72	121.4	96.4	1.5	2.1	0.83	3.3	0.26
zKL98-10-21-841-3	Tigt	2221	zircon	21.53	77.91	126.1	111.5	1.4	1.9	0.84	2.7	0.22
zKL98-10-21-841-4	Tigt	2221	zircon	15.53	68.07	105.8	81.3	1.2	1.4	0.82	2.6	0.20
zKL98-10-21-841-5	Tigt	2221	zircon	12.00	62.14	252.0	129.3	1.1	4.0	0.81	3.3	0.26
zKL98-10-21-841-6	Tigt	2221	zircon	26.14	85.86	313.5	184.7	1.8	5.7	0.86	3.4	0.27
zKL98-10-21-922-1	Tigt	2140	zircon	10.58	63.04	372.4	222.5	2.3	5.3	0.81	2.8	0.23
zKL98-10-21-922-2	Tigt	2140	zircon	19.05	76.42	102.9	73.2	1.2	1.3	0.84	2.4	0.19
zKL98-10-21-922-3	Tigt	2140	zircon	39.18	93.12	177.5	119.2	1.1	3.3	0.87	3.4	0.27
zKL98-10-21-922-4	Tigt	2140	zircon	19.09	75.39	86.2	62.6	1.0	1.7	0.84	3.7	0.30
zKL98-10-21-922-5	Tigt	2140	zircon	17.21	75.37	120.7	94.7	2.5	1.1	0.84	1.7	0.14
zKL98-10-21-922-6	Tigt	2140	zircon	27.30	85.07	142.7	73.2	1.5	1.1	0.86	1.5	0.12
zKL98-10-21-948-2	Tigt	2114	zircon	10.33	62.39	221.7	207.9	5.4	2.7	0.81	2.3	0.18
zKL98-10-21-948-3	Tigt	2114	zircon	7.21	53.34	166.7	188.3	13.1	2.0	0.77	2.3	0.18

Sample	Intrusion	Elevation (m)	mineral	mass (ug)	ESR	U (ppm)	Th (ppm)	147Sm (ppm)	He (nmol/g)	Ft	Age, Ma	err., Ma
zKL98-10-21-948-4	Tigt	2114	zircon	24.28	83.88	136.5	74.6	2.3	2.0	0.86	2.8	0.23
zKL98-10-21-948-5	Tigt	2114	zircon	16.54	72.18	284.2	222.3	1.1	5.0	0.83	3.3	0.26
zKL98-10-21-948-6	Tigt	2114	zircon	30.80	89.98	139.6	116.4	1.1	2.3	0.86	3.0	0.24
zKL98-10-21-982-1	Tigt	2080	zircon	5.31	47.87	206.6	187.9	2.0	2.7	0.75	2.6	0.21
zKL98-10-21-982-3	Tigt	2080	zircon	6.45	52.35	93.4	83.4	2.2	1.1	0.77	2.3	0.18
zKL98-10-21-982-4	Tigt	2080	zircon	6.17	50.55	136.1	84.0	2.4	1.8	0.77	2.7	0.22
zKL98-10-21-982-5	Tigt	2080	zircon	4.82	48.23	227.1	156.6	2.0	3.2	0.76	3.0	0.24
zKL98-10-21-982-6	Tigt	2080	zircon	5.97	51.63	91.3	76.4	1.4	1.0	0.77	2.2	0.18
zKL98-10-21-1192-1	Tigt	1870	zircon	5.11	49.97	127.0	93.8	0.4	1.1	0.76	1.8	0.15
zKL98-10-21-1192-2	Tigt	1870	zircon	6.16	53.73	130.2	144.1	0.5	1.4	0.78	2.1	0.17
zKL98-10-21-1192-3	Tigt	1870	zircon	6.05	52.38	142.8	110.9	0.4	1.5	0.77	2.2	0.17
zKL98-10-21-1192-4	Tigt	1870	zircon	3.67	42.93	112.3	74.3	0.5	1.2	0.73	2.3	0.19
zKL98-10-21-1192-5	Tigt	1870	zircon	2.73	40.12	135.6	146.1	2.0	1.3	0.71	1.9	0.16
zKL98-10-21-1192-6	Tigt	1870	zircon	5.48	51.35	111.7	78.8	0.4	1.2	0.77	2.2	0.18
zKL98-10-21-1192-7	Tigt	1870	zircon	23.90	79.69	270.6	144.7	0.5	4.6	0.85	3.3	0.26
zKL98-10-21-1192-8	Tigt	1870	zircon	4.48	45.30	104.2	91.5	0.4	1.6	0.74	3.2	0.26
zKL98-10-21-1192-9	Tigt	1870	zircon	6.39	52.80	172.7	132.5	0.7	2.3	0.77	2.7	0.21
zKL98-10-21-1192-10	Tigt	1870	zircon	5.03	48.91	68.0	51.7	0.3	0.8	0.76	2.6	0.20
zKL98-10-21-1192-11	Tigt	1870	zircon	5.99	53.75	73.7	62.5	0.3	1.0	0.78	2.6	0.21
zKL98-10-21-1243-1	Tigt	1819	zircon	16.42	69.76	292.9	128.8	0.9	4.4	0.83	3.0	0.24
zKL98-10-21-1243-2	Tigt	1819	zircon	13.32	68.38	101.0	85.7	1.4	1.8	0.82	3.3	0.27
zKL98-10-21-1243-3	Tigt	1819	zircon	8.25	55.26	230.5	88.6	0.8	3.0	0.79	2.8	0.22
zKL98-10-21-1243-4	Tigt	1819	zircon	8.66	56.91	107.1	78.2	1.4	1.5	0.79	2.8	0.22
zKL98-10-21-1243-5	Tigt	1819	zircon	6.96	52.94	298.7	183.6	1.7	3.4	0.78	2.3	0.19
zKL98-10-21-1243-6	Tigt	1819	zircon	11.02	62.09	120.3	61.4	1.0	1.5	0.81	2.6	0.21
zKL98-10-21-1266-1	Tigt	1796	zircon	16.56	70.53	263.1	88.5	0.7	3.7	0.83	2.9	0.23
zKL98-10-21-1266-2	Tigt	1796	zircon	25.69	84.38	130.2	125.5	1.3	1.7	0.85	2.4	0.19
zKL98-10-21-1266-3	Tigt	1796	zircon	11.41	66.44	218.7	199.0	1.2	2.3	0.82	1.9	0.15
zKL98-10-21-1266-5	Tigt	1796	zircon	5.56	49.83	92.4	65.5	1.2	1.3	0.76	3.0	0.24
zKL98-10-21-1266-6	Tigt	1796	zircon	4.51	47.76	144.6	88.7	1.6	1.5	0.75	2.2	0.18
zBG-WSH-04-238-1	Big Gossan	3184	zircon	43.37	103.89	81.2	99.7	1.9	1.4	0.88	2.8	0.17
zBG-WSH-04-238-2	Big Gossan	3184	zircon	11.36	64.08	41.2	41.3	1.0	0.6	0.81	2.5	0.15
zBG-WSH-04-238-3	Big Gossan	3184	zircon	17.16	76.45	44.0	37.7	1.4	0.6	0.84	2.5	0.15
zBG-WSH-04-238-4	Big Gossan	3184	zircon	15.96	73.59	159.0	276.7	2.1	2.5	0.83	2.5	0.15
zBG-WSH-04-238-5	Big Gossan	3184	zircon	30.10	87.08	39.4	41.3	1.9	0.5	0.86	2.4	0.14
zBG-WSH-04-238-6	Big Gossan	3184	zircon	9.31	58.13	87.0	115.8	3.0	1.4	0.79	2.8	0.17
z3001-1	North Grasberg	4125	zircon	9.85	61.54	124.1	91.6	0.2	1.8	0.80	2.9	0.23
z3001-2	North Grasberg	4125	zircon	7.73	55.31	321.6	142.4	0.7	4.6	0.79	3.0	0.24
z3001-3	North Grasberg	4125	zircon	6.68	52.11	228.5	95.9	0.3	3.3	0.77	3.2	0.25
z3001-4	North Grasberg	4125	zircon	2.63	38.63	306.5	108.7	0.3	3.8	0.71	3.0	0.24
z3001-5	North Grasberg	4125	zircon	2.72	38.62	288.5	117.0	0.4	3.6	0.70	3.0	0.24
z3001-6	North Grasberg	4125	zircon	4.22	46.89	235.6	94.6	0.3	3.3	0.75	3.2	0.26
z4001-1	Wanagon	4025	zircon	21.58	81.94	170.3	53.1	0.4	2.5	0.85	2.9	0.24
z4001-2	Wanagon	4025	zircon	24.38	83.01	193.2	47.4	0.4	3.0	0.86	3.1	0.25
z4001-3	Wanagon	4025	zircon	9.33	57.08	305.2	66.5	0.4	4.1	0.80	2.9	0.24
z4001-4	Wanagon	4025	zircon	11.10	59.63	290.9	59.8	0.4	4.4	0.80	3.4	0.27
z4001-5	Wanagon	4025	zircon	17.87	70.99	349.5	92.7	0.5	5.5	0.83	3.3	0.26
z4001-6	Wanagon	4025	zircon	18.83	72.73	287.3	86.2	0.5	4.1	0.84	2.9	0.23
z93MCHR2-1	Heat Road Intrusion	2900	zircon	7.68	56.39	76.4	62.8	1.8	1.1	0.79	2.9	0.23

Sample	Intrusion	Elevation (m)	mineral	mass (ug)	ESR	U (ppm)	Th (ppm)	147Sm (ppm)	He (nmol/g)	Ft	Age, Ma	err., Ma
z93MCHR2-2	Heat Road Intrusion	2900	zircon	7.11	55.33	232.0	164.9	1.1	3.6	0.78	3.1	0.25
z93MCHR2-3	Heat Road Intrusion	2900	zircon	4.13	44.56	93.9	76.0	2.0	1.3	0.74	3.0	0.24
z93MCHR2-4	Heat Road Intrusion	2900	zircon	14.44	70.82	36.3	27.6	2.0	0.4	0.83	2.3	0.18
z93MCHR2-6	Heat Road Intrusion	2900	zircon	6.14	49.05	126.3	92.5	1.8	1.8	0.76	3.0	0.24
z93MCHR3a-3	Heat Road Intrusion	2760	zircon	14.28	68.13	398.4	167.8	1.3	5.2	0.82	2.7	0.21
z93MCHR3a-4	Heat Road Intrusion	2760	zircon	10.06	58.20	455.2	180.5	1.2	5.6	0.80	2.6	0.21
z93MCHR3a-5	Heat Road Intrusion	2760	zircon	16.10	72.37	289.7	105.9	0.9	3.5	0.83	2.5	0.20
z93MCHR3a-6	Heat Road Intrusion	2760	zircon	8.58	58.22	309.7	132.0	1.0	3.6	0.80	2.4	0.19
z93MCHR4-1	Heat Road Intrusion	3790	zircon	3.08	41.43	250.4	154.7	1.8	3.1	0.72	2.8	0.23
z93MCHR4-2	Heat Road Intrusion	3790	zircon	5.52	50.22	272.2	136.8	1.4	3.9	0.77	3.1	0.25
z93MCHR4-3	Heat Road Intrusion	3790	zircon	9.75	59.10	272.2	158.8	1.4	4.6	0.80	3.4	0.28
z93MCHR4-5	Heat Road Intrusion	3790	zircon	3.27	40.73	449.4	348.7	4.8	7.3	0.71	3.6	0.29
z93MCHR4-6	Heat Road Intrusion	3790	zircon	7.68	57.06	214.8	134.4	1.5	3.5	0.79	3.3	0.27
z93MCHR5-1	Heat Road Intrusion	3535	zircon	21.50	79.22	116.4	70.5	1.4	1.8	0.85	3.0	0.24
z93MCHR5-3	Heat Road Intrusion	3535	zircon	14.77	68.97	124.7	66.2	0.8	1.9	0.83	3.1	0.25
z93MCHR5-4	Heat Road Intrusion	3535	zircon	10.56	61.79	166.2	125.1	2.7	2.5	0.81	3.0	0.24
z93MCHR5-5	Heat Road Intrusion	3535	zircon	11.51	63.65	190.8	119.0	1.1	3.1	0.81	3.2	0.26
z93MCHR5-6	Heat Road Intrusion	3535	zircon	15.53	67.77	123.7	91.5	1.6	2.0	0.82	3.1	0.25
z93MCHR6-1	Heat Road Intrusion	3335	zircon	18.53	77.39	108.2	61.7	7.3	1.1	0.84	2.0	0.16
z93MCHR6-3	Heat Road Intrusion	3335	zircon	9.67	59.29	147.2	67.8	1.6	1.8	0.80	2.6	0.20
z93MCHR6-4	Heat Road Intrusion	3335	zircon	15.12	71.55	147.5	90.0	1.1	1.9	0.83	2.5	0.20
z93MCHR6-5	Heat Road Intrusion	3335	zircon	24.94	84.16	118.7	83.8	1.2	1.7	0.85	2.7	0.22
z93MCHR6-6	Heat Road Intrusion	3335	zircon	13.76	65.24	375.6	151.8	1.2	5.8	0.82	3.2	0.26
z93MCHR8-1	Heat Road Intrusion	3000	zircon	12.45	62.88	314.5	115.6	0.9	4.8	0.81	3.2	0.26
z93MCHR8-2	Heat Road Intrusion	3000	zircon	16.43	72.89	315.4	102.6	1.5	5.5	0.84	3.6	0.29
z93MCHR8-3	Heat Road Intrusion	3000	zircon	19.90	76.90	372.0	71.2	12.7	4.1	0.85	2.3	0.19
z93MCHR8-4	Heat Road Intrusion	3000	zircon	2.50	36.89	212.2	134.1	2.7	2.9	0.69	3.2	0.25
z93MCHR8-5	Heat Road Intrusion	3000	zircon	7.45	57.45	93.6	27.8	1.1	1.3	0.80	3.0	0.24
z93MCHR8-6	Heat Road Intrusion	3000	zircon	23.07	82.31	38.0	32.0	1.1	0.6	0.85	2.8	0.22
z94MCRC2-2	Ridge Camp	2160	zircon	7.89	56.08	246.3	153.5	2.0	2.5	0.79	2.1	0.17
z94MCRC2-3	Ridge Camp	2160	zircon	5.07	48.13	191.4	151.5	2.4	1.6	0.75	1.7	0.14
z94MCRC2-4	Ridge Camp	2160	zircon	6.39	53.82	114.0	59.8	0.7	1.1	0.78	2.0	0.16
z94MCRC2-5	Ridge Camp	2160	zircon	4.22	45.76	269.0	210.1	1.8	2.6	0.74	2.0	0.16
z94MCRC2-6	Ridge Camp	2160	zircon	4.41	46.54	201.8	176.4	1.9	2.5	0.75	2.5	0.20
zRWV-2	Sirga	3175	zircon	9.67	63.63	71.1	53.0	1.7	3.0	0.81	8.3	0.67
zRWV-3	Sirga	3175	zircon	3.83	42.91	217.3	116.8	2.9	12.7	0.73	13.1	1.05
zRWV-4	Sirga	3175	zircon	7.61	53.73	168.1	273.9	331.2	3.5	0.77	3.6	0.29
zRWV-5	Sirga	3175	zircon	8.56	59.89	226.9	109.8	4.3	23.6	0.80	21.6	1.73
zRWV-6	Sirga	3175	zircon	17.98	75.20	38.4	41.7	2.4	1.1	0.84	5.0	0.40
zSW16-4	Sirga	3175	zircon	9.38	58.30	206.7	78.5	3.1	99.5	0.80	102.1	8.17
zSW16-5	Sirga	4200	zircon	17.47	76.75	59.4	83.7	1.1	135.8	0.84	370.0	29.60
zSW16-6	Sirga	4200	zircon	10.76	64.78	41.4	97.4	8.9	60.6	0.81	213.0	17.04
zSW16-7	Sirga	4200	zircon	7.43	55.99	107.6	54.7	1.0	35.4	0.79	68.9	5.51
zSW16-8	Sirga	4200	zircon	8.63	58.02	145.4	136.6	2.6	54.4	0.79	71.4	5.71
zSW16-9	Sirga	4200	zircon	25.17	81.97	86.3	48.6	1.8	22.9	0.85	50.9	4.07
zUTFCT2-206	FCT		zircon	4.60	46.58	168.1	87.6	1.8	20.1	0.75	26.4	2.11
zUTFCT2-207	FCT		zircon	3.54	44.30	194.1	104.7	3.7	25.8	0.74	29.6	2.36
zUTFCT2-135	FCT		zircon	3.01	40.27	262.3	134.9	4.4	32.6	0.71	28.8	2.30
zUTFCT2-136	FCT		zircon	20.38	79.20	130.7	68.6	0.4	20.1	0.85	30.0	2.40

Sample	Intrusion	Elevation (m)	mineral	mass (ug)	ESR	U (ppm)	Th (ppm)	147Sm (ppm)	He (nmol/g)	Ft	Age, Ma	err., Ma
zUTFCT2-169	FCT		zircon	1.82	35.63	248.2	210.1	1.8	29.8	0.68	27.4	2.19
zUTFCT2-170	FCT		zircon	5.12	50.85	215.3	103.3	1.9	27.3	0.77	27.4	2.19
zUTFCT2-179	FCT		zircon	3.90	42.50	324.9	177.4	1.7	40.7	0.73	28.3	2.26
zUTFCT2-180	FCT		zircon	3.64	43.94	186.2	100.6	1.5	21.9	0.74	26.3	2.10
zUTFCT-586	FCT		zircon	9.13	58.99	216.4	132.7	4.9	25.7	0.80	24.1	1.45
zUTFCT-587	FCT		zircon	3.15	42.65	214.1	119.3	1.6	29.3	0.73	30.8	1.85
zUTFCT2-543	FCT		zircon	7.13	51.91	268.7	138.3	2.5	38.8	0.77	30.8	2.47
zUTFCT2-544	FCT		zircon	3.86	43.81	316.7	173.8	2.8	44.3	0.73	31.2	2.50
zUTFCT2-545	FCT		zircon	4.52	45.94	211.4	128.0	1.5	28.6	0.74	29.4	2.35
zUTFCT2-546	FCT		zircon	6.25	52.61	117.1	74.3	2.4	14.9	0.77	26.5	2.12
zUTFCT3-15	FCT		zircon	23.75	80.22	181.6	98.5	2.5	26.6	0.85	28.3	2.27
zUTFCT3-16	FCT		zircon	7.56	54.56	181.0	94.0	1.5	23.9	0.78	27.9	2.23
zUTFCT2-145	FCT		zircon	14.67	66.21	198.6	103.7	2.5	29.1	0.82	29.5	2.36
zUTFCT2-146	FCT		zircon	8.15	56.13	265.8	134.2	1.3	39.7	0.79	31.3	2.51
zUTFCT2-527	FCT		zircon	11.68	63.08	241.9	112.5	3.5	33.9	0.81	28.8	2.31
zUTFCT2-528	FCT		zircon	11.65	64.65	129.6	91.1	5.0	19.4	0.81	29.3	2.34

Appendix L: Garnet U/Pb Age Results

The following table presents the LA-ICP-MS results for analyzed garnets. For each sample, large garnet crystals were selected from each sample, mounted in epoxy, and polished to expose a clean face of the garnet rim. Backscattered electron images were collected in order to evaluate the zoning within the garnet crystals prior to analysis. Garnet U/Pb analyses were completed at the University of Texas at Austin, using a single collector ThermoFisher Element2 ICP-MS with an attached PhotonMachine Analyte G.2 193 nm ArF Excimer Laser and large-volume Helex sample. The method of Seman et al. (submitted) was used to acquire data: garnets were ablated for 30 s (10 Hz repetition rate, 6 mJ energy, 17% beam attenuation, resulting in a fluence rate of 1.67 J/cm^2) using a large 110 µm spot size in order to maximize count rates. The instrument was tuned in order to maximize ^{238}U counts and minimize the interferences from oxide masses (UO <0.5%).

The results for each garnet spot analysis were compiled on a Tera-Wasserburg plot, and the lower Concordia intercept and its uncertainty are reported as the common lead corrected sample age and uncertainty.

		207Pb/235U	207Pb/235U error	206Pb/238U	206Pb/238U Error	Error Correlation 206/238 vs. 207/235	Final Age (Ma)	Error (Ma)	Approx U (ppm)	Approx Th (ppm)
Big Gossan	BG_1	0.0191	0.0018	0.000573	0.00003	0.58767	3.69	0.19	62.5	0.0
BG240W-06	BG_2	0.0428	0.0017	0.000769	0.000044	0.38522	4.95	0.28	56.5	0.1
Duplicate 1	BG_3	0.0429	0.0017	0.000786	0.000035	0.45457	5.07	0.23	70.3	0.1
	BG_4	0.01169	0.00086	0.000495	0.000026	0.15922	3.19	0.16	76.8	0.1
	BG_5	0.008	0.0011	0.000444	0.000022	0.49931	2.86	0.14	66.6	0.1
	BG_6	0.0155	0.0019	0.000553	0.000027	0.30407	3.57	0.17	59.2	0.0
	BG_7	0.0274	0.0016	0.000632	0.000037	0.31391	4.07	0.24	61.5	0.0
	BG_8	0.00949	0.00095	0.000492	0.000033	0.1886	3.17	0.21	47.0	0.0
	BG_9	0.0191	0.0014	0.000559	0.00003	0.4886	3.6	0.19	45.3	0.0
	BG_10	0.0062	0.001	0.00043	0.000039	0.18922	2.77	0.25	41.9	0.0
	BG_11	0.0261	0.0017	0.00066	0.000039	0.45072	4.25	0.25	48.2	0.0
	BG_12	0.0079	0.0021	0.00046	0.000032	0.079791	2.97	0.2	41.9	0.1
	BG_13	0.0058	0.0013	0.000455	0.000034	0.31966	2.94	0.22	43.9	0.1
	BG_14	0.0103	0.0017	0.000478	0.000041	0.28774	3.08	0.26	31.5	0.0
	BG_15	0.0136	0.0015	0.000524	0.000032	0.40544	3.38	0.2	62.4	0.1
	BG_16	0.00995	0.00067	0.000478	0.000028	0.29538	3.08	0.18	65.8	0.1
	BG_17	0.0251	0.0013	0.000643	0.00004	0.31633	4.14	0.26	52.0	0.0
	BG_18	0.00865	0.0007	0.000443	0.000029	0.14986	2.85	0.19	59.0	0.0
	BG_19	0.00942	0.0009	0.000453	0.000023	0.17853	2.92	0.15	71.8	0.0
	BG_20	0.244	0.017	0.00238	0.00015	0.92964	15.31	0.99	57.9	0.3
	BG_21	0.0161	0.0016	0.000545	0.000032	0.45808	3.51	0.21	92.9	0.0
	BG_22	0.00649	0.00063	0.000469	0.000023	0.21826	3.02	0.15	87.8	0.0
	BG_23	0.0211	0.003	0.000556	0.000043	0.47512	3.58	0.27	44.8	0.6
	BG_25	0.072	0.0037	0.000997	0.000047	0.5857	6.43	0.3	85.1	0.0
	BG_26	0.0088	0.0011	0.000487	0.000033	0.33433	3.14	0.21	54.9	0.0
	BG_27	0.01027	0.00097	0.000471	0.000032	0.48233	3.03	0.21	53.1	0.0
	BG_28	0.0105	0.0011	0.0005	0.000026	0.71477	3.22	0.17	64.7	0.0
	BG_29	0.0219	0.0015	0.00056	0.000028	0.50116	3.61	0.18	71.5	0.0
	BG_30	0.012	0.0027	0.000457	0.000035	0.11735	2.94	0.23	44.9	0.1
	BG_31	0.033	0.0023	0.000711	0.00005	0.37138	4.58	0.32	47.3	0.3
	BG_32	0.0466	0.0035	0.000844	0.000055	0.83401	5.44	0.35	50.7	0.1
	BG_33	0.316	0.018	0.00309	0.00014	0.45602	19.86	0.89	43.2	0.1
	BG_34	0.0655	0.0033	0.000943	0.000058	0.025482	6.08	0.37	54.0	0.0
	BG_35	0.0089	0.0013	0.000482	0.000035	0.42887	3.11	0.23	50.7	0.0
	BG_36	0.0288	0.0018	0.000661	0.00004	0.41299	4.26	0.26	46.7	0.1
	BG_37	0.0072	0.0017	0.000481	0.000031	0.30475	3.1	0.2	48.3	0.1
	BG_38	0.0208	0.0016	0.000605	0.000033	0.30655	3.9	0.21	47.5	0.2
	BG_39	0.00716	0.00079	0.000456	0.000031	0.29065	2.94	0.2	52.0	0.3
	BG_40	0.0373	0.0024	0.000768	0.000049	0.042021	4.95	0.32	50.1	0.4
	BG_41	0.0093	0.0014	0.000476	0.000034	0.33972	3.07	0.22	38.4	2.8
	BG_42	0.0136	0.002	0.000506	0.000037	0.47756	3.26	0.24	44.5	0.3
	BG_43	0.0905	0.0079	0.001235	0.000088	0.71406	7.96	0.56	34.9	0.3
	BG_44	0.563	0.026	0.00502	0.0002	0.3427	32.3	1.3	34.1	0.2
	BG_45	0.0086	0.0013	0.000514	0.000031	0.46006	3.31	0.2	54.1	0.0
	BG_46	0.0182	0.0032	0.000596	0.000047	0.73038	3.84	0.3	42.7	0.1
	BG_47	0.0575	0.0026	0.00088	0.00004	0.47186	5.67	0.26	82.5	0.1
	BG_48	0.033	0.0041	0.00069	0.000042	0.71158	4.44	0.27	56.2	0.4
	BG_49	0.0296	0.0039	0.000704	0.00006	0.42256	4.54	0.38	43.9	0.0
	BG_50	0.011	0.0014	0.000497	0.000038	0.17435	3.2	0.24	47.5	0.1
	BG_51	0.0218	0.0033	0.00061	0.000046	0.58039	3.93	0.29	44.7	0.0
	BG_52	0.0703	0.0047	0.001058	0.000067	0.61177	6.82	0.43	49.4	0.1
	BG_53	0.0126	0.0013	0.000536	0.00003	0.72175	3.45	0.2	63.4	0.2
	BG_54	0.0255	0.0019	0.000591	0.000041	0.19294	3.81	0.26	41.3	0.0
	BG_55	0.0909	0.007	0.001067	0.000086	0.014636	6.87	0.55	11.6	0.1
	BG_56	0.0146	0.0014	0.000506	0.000035	0.27297	3.26	0.23	38.1	0.0
	BG_57	0.014	0.0011	0.000494	0.00003	0.14011	3.18	0.19	45.5	0.4
	BG_58	0.011	0.002	0.00048	0.00003	0.33315	3.09	0.2	60.1	0.1

	207Pb/235U	207Pb/235U error	206Pb/238U	206Pb/238U Error	Error Correlation 206/238 vs. 207/235	Final Age (Ma)	Error (Ma)	Approx U (ppm)	Approx Th (ppm)
BG_59	0.0123	0.002	0.000513	0.000034	0.048501	3.31	0.22	43.2	0.2
BG_60	0.0349	0.0031	0.000697	0.000043	0.74508	4.49	0.27	52.2	0.2
BG_61	0.01366	0.00085	0.000523	0.000031	0.20454	3.37	0.2	75.1	0.1
BG_62	0.00584	0.00067	0.000447	0.000022	0.25347	2.88	0.14	76.2	0.4
BG_63	0.0446	0.0032	0.000797	0.000063	0.46967	5.14	0.41	45.1	0.5
BG_64	0.0111	0.0011	0.00052	0.000037	0.10799	3.35	0.24	44.2	0.6
BG_65	0.0116	0.0027	0.000524	0.000041	0.62426	3.38	0.26	39.6	0.6
BG_66	0.0074	0.0014	0.000488	0.000035	0.0218	3.14	0.22	44.1	0.6
BG_67	0.013	0.0026	0.000473	0.000055	0.015689	3.05	0.35	43.2	0.0
BG_68	0.0125	0.0013	0.000545	0.000033	0.18987	3.51	0.21	48.9	0.0
BG_69	0.0093	0.0012	0.000527	0.000035	0.4117	3.4	0.22	54.0	0.1
BG_70	0.00537	0.00082	0.000459	0.00003	0.42994	2.96	0.19	46.3	0.1
BG_71	0.0574	0.0023	0.000855	0.00005	0.50468	5.51	0.32	55.7	0.2
BG_72	0.00683	0.00074	0.00042	0.000027	0.34373	2.71	0.17	62.0	0.1
BG_73	0.0106	0.0015	0.00052	0.000036	0.71242	3.35	0.23	61.4	0.0
BG_74	0.0128	0.0028	0.000508	0.000041	0.11669	3.28	0.26	41.1	0.1
BG_75	0.0486	0.0055	0.000832	0.00006	0.80474	5.36	0.39	49.2	0.2
BG_76	0.0313	0.0018	0.000684	0.000044	0.56459	4.41	0.28	45.6	0.2
BG_77	0.0185	0.0019	0.000568	0.000042	0.79436	3.66	0.27	53.1	0.7
BG_78	0.0616	0.0036	0.001004	0.000071	0.42445	6.47	0.46	27.9	0.5
BG_79	0.0292	0.0025	0.000654	0.000041	0.63506	4.22	0.27	32.0	0.2
BG_80	0.0285	0.0025	0.000636	0.000048	0.56832	4.1	0.31	29.5	0.2
BG_81	0.0125	0.0012	0.000518	0.000031	0.68787	3.34	0.2	75.4	0.5
BG_82	0.0764	0.0031	0.001027	0.000044	0.47241	6.62	0.29	68.4	0.7
BG_83	0.0272	0.0018	0.000652	0.000037	0.44112	4.2	0.24	65.0	0.6
BG_84	0.0383	0.0031	0.000719	0.000059	0.50337	4.63	0.38	25.8	0.6
BG_85	0.0152	0.0018	0.000548	0.000045	0.66232	3.53	0.29	42.8	0.2
BG_86	0.0062	0.0012	0.000473	0.000031	0.56034	3.05	0.2	48.0	0.3
BG_87	0.0066	0.0013	0.000485	0.000037	0.7763	3.12	0.24	46.2	0.0
BG_88	0.0265	0.0031	0.000644	0.000052	0.59271	4.15	0.33	41.9	0.1
BG_89	0.0175	0.0027	0.000557	0.000043	0.40212	3.59	0.28	42.1	0.2
BG_90	0.00908	0.00085	0.000426	0.000028	0.3377	2.74	0.18	66.2	0.9
BG_91	0.0204	0.0015	0.000539	0.000035	0.54993	3.47	0.23	44.8	0.1
BG_92	0.0173	0.0015	0.000566	0.000037	0.50726	3.65	0.24	48.5	0.0
BG_93	0.0118	0.0012	0.000516	0.000038	0.39075	3.33	0.24	44.0	0.0
BG_94	0.0279	0.0031	0.000628	0.000053	0.68988	4.05	0.34	44.7	0.0
BG_95	0.0085	0.0011	0.000467	0.000038	0.47072	3.01	0.24	38.7	0.0
BG_96	0.0717	0.0031	0.001039	0.000053	0.50023	6.7	0.34	52.8	0.1
BG_97	0.0264	0.0016	0.000646	0.000041	0.19839	4.17	0.26	43.6	0.1
BG_98	0.0114	0.0023	0.000485	0.000046	0.10337	3.12	0.3	22.3	0.0
BG_99	0.0418	0.0069	0.000711	0.000076	0.67874	4.58	0.49	30.5	0.0
BG_100	0.0487	0.0038	0.000813	0.000061	0.79003	5.24	0.39	46.1	0.2
BG_101	0.0073	0.0016	0.00044	0.000032	0.47965	2.84	0.21	47.5	0.2
BG_102	0.0183	0.0021	0.00055	0.000049	0.44708	3.54	0.32	33.3	0.2
BG_103	0.0306	0.003	0.000651	0.000048	0.52465	4.19	0.31	43.3	0.0
BG_104	0.1305	0.0049	0.001478	0.000078	0.51445	9.52	0.5	24.7	0.0
BG_105	0.0766	0.0056	0.00104	0.0001	0.36212	6.68	0.64	20.3	0.0
BG_106	0.0155	0.0012	0.000526	0.000031	0.27106	3.39	0.2	81.2	0.0
BG_107	0.0059	0.0013	0.000463	0.000032	0.73177	2.99	0.21	55.2	0.0
BG_108	0.029	0.0059	0.000674	0.000067	0.86555	4.35	0.43	42.5	0.1
BG_109	0.0182	0.0032	0.000597	0.000042	0.79029	3.85	0.27	45.4	0.0
BG_110	0.0554	0.0068	0.000829	0.000061	0.52896	5.34	0.4	45.0	0.1
BG_111	0.0061	0.001	0.000454	0.000035	0.007797	2.93	0.22	45.0	0.5
BG_112	0.0068	0.0015	0.000445	0.000027	0.59908	2.87	0.17	69.2	0.3
BG_113	0.00785	0.00093	0.000497	0.000043	0.11938	3.2	0.28	70.8	0.1
BG_114	0.029	0.0023	0.000674	0.000059	0.46735	4.34	0.38	40.3	0.3
BG_115	0.0344	0.0031	0.000709	0.000047	0.69267	4.57	0.3	58.9	0.2
BG_116	0.0099	0.0014	0.00049	0.00003	0.75522	3.16	0.19	74.3	0.1
BG_117	0.0222	0.002	0.000583	0.00004	0.66816	3.76	0.26	75.8	0.3

	207Pb/235U	207Pb/235U error	206Pb/238U	206Pb/238U Error	Error Correlation 206/238 vs. 207/235	Final Age (Ma)	Error (Ma)	Approx U (ppm)	Approx Th (ppm)
BG_118	0.01581	0.0009	0.000509	0.00002	0.17871	3.28	0.13	91.0	0.1
BG_119	0.00395	0.00069	0.000453	0.00003	0.16552	2.92	0.19	56.5	0.3
BG_120	0.0115	0.00081	0.000528	0.000023	0.30856	3.4	0.15	91.6	0.3
BG_121	0.0343	0.0068	0.000705	0.000068	0.85387	4.54	0.44	60.7	0.3
BG_122	0.0109	0.0014	0.000478	0.000038	0.42009	3.08	0.24	52.3	0.3
BG_123	0.00633	0.00083	0.000457	0.000034	0.030063	2.95	0.22	45.1	0.3
BG_124	0.00552	0.00073	0.000452	0.000032	0.024665	2.91	0.21	57.2	0.3
BG_125	0.00768	0.00061	0.000444	0.000026	0.05033	2.86	0.17	96.8	0.3
BG_126	0.0086	0.0013	0.000502	0.00004	0.34141	3.24	0.26	42.6	0.3
BG_127	0.0375	0.003	0.000766	0.000048	0.44079	4.94	0.31	50.7	0.2
BG_128	0.00681	0.00072	0.000439	0.000036	0.24256	2.83	0.23	44.1	0.1
BG_129	0.023	0.0016	0.000587	0.000047	0.40505	3.79	0.3	52.1	0.3
BG_130	0.0193	0.0011	0.000594	0.000036	0.30772	3.82	0.23	57.5	0.5
BG_131	0.392	0.02	0.0038	0.00019	0.80241	24.4	1.2	40.8	0.4
BG_132	0.00476	0.00083	0.000478	0.000037	0.033428	3.08	0.24	52.1	0.0
BG_133	0.0064	0.001	0.000443	0.000028	0.0069104	2.86	0.18	47.5	0.0
BG_134	0.307	0.01	0.00305	0.00014	0.4559	19.63	0.87	28.6	0.0
BG_135	0.0067	0.001	0.000486	0.000037	0.27928	3.13	0.24	43.7	0.0
BG_136	0.01054	0.00071	0.000489	0.000024	0.28495	3.15	0.15	78.7	0.1
BG_137	0.011	0.00088	0.000523	0.000028	0.18393	3.37	0.18	77.3	0.1
BG_138	0.0424	0.0025	0.000829	0.000061	0.050017	5.34	0.39	39.7	0.1
BG_139	0.0244	0.002	0.000645	0.000048	0.49122	4.16	0.31	34.8	0.1
BG_140	0.01159	0.00093	0.000529	0.00004	0.15607	3.41	0.26	38.4	0.0
BG_141	0.0172	0.0017	0.000563	0.000044	0.66627	3.63	0.28	52.3	0.3
BG_142	0.00583	0.00077	0.000443	0.000026	0.2041	2.85	0.17	67.4	0.1
BG_143	0.0856	0.0047	0.001127	0.000061	0.4057	7.26	0.4	38.6	0.1
BG_144	0.007	0.00084	0.000482	0.000033	0.078791	3.11	0.21	74.8	0.1
BG_145	0.00608	0.00054	0.00045	0.000022	0.25393	2.9	0.14	97.2	0.2
BG_146	0.0116	0.0012	0.000496	0.000035	0.40066	3.2	0.23	70.7	0.1
BG_147	0.00435	0.00065	0.000462	0.000026	0.063036	2.98	0.17	59.5	0.1
BG_148	0.0268	0.0016	0.000685	0.000036	0.088306	4.41	0.23	49.1	0.7
BG_149	0.0102	0.0015	0.000523	0.000039	0.64014	3.37	0.25	50.9	1.0
BG_150	0.00553	0.00074	0.000483	0.000035	0.25343	3.11	0.23	58.7	0.2
BG_151	0.00495	0.00082	0.00044	0.000038	0.088473	2.84	0.25	32.9	0.0
BG_152	0.00489	0.00054	0.000433	0.00003	0.05369	2.79	0.19	56.5	0.0
BG_153	0.0198	0.003	0.00059	0.000038	0.64434	3.8	0.24	64.8	0.2
BG_154	0.0078	0.0016	0.000445	0.000029	0.02522	2.87	0.19	47.0	0.9
Big Gossan BG240W-06 Duplicate 1									
BG240W_1	0.0103	0.0016	0.000444	0.000024	0.72644	2.86	0.16	70.9	1.4
BG240W_2	0.0084	0.0011	0.000462	0.000024	0.66459	2.98	0.16	76.7	0.8
BG240W_3	0.0127	0.0011	0.000475	0.000021	0.49184	3.06	0.13	89.2	0.2
BG240W_4	0.0118	0.0012	0.000489	0.000024	0.54059	3.15	0.15	93.5	0.2
BG240W_5	0.0227	0.0016	0.000578	0.000023	0.34974	3.72	0.15	84.3	0.4
BG240W_6	0.0122	0.0012	0.000487	0.000022	0.54492	3.14	0.14	82.3	0.3
BG240W_7	0.00855	0.00091	0.000482	0.000021	0.65938	3.11	0.14	114.6	0.1
BG240W_8	0.0121	0.0013	0.000499	0.000023	0.63446	3.22	0.15	84.3	0.4
BG240W_9	0.0109	0.0011	0.000471	0.000023	0.48774	3.04	0.15	85.1	0.9
BG240W_10	0.32	0.24	0.0035	0.0024	0.99778	22	15	76.9	1.4
BG240W_11	0.0188	0.0017	0.000547	0.000027	0.5562	3.53	0.17	70.9	1.0
BG240W_12	0.00862	0.00098	0.000461	0.000025	0.45492	2.97	0.16	80.8	1.0
BG240W_13	0.0178	0.0015	0.000536	0.000026	0.42208	3.45	0.17	75.7	0.6
BG240W_14	0.0136	0.0011	0.000514	0.000021	0.6801	3.31	0.13	97.7	0.1
BG240W_15	0.0132	0.0011	0.000492	0.000023	0.69933	3.17	0.15	76.5	0.3
BG240W_16	0.249	0.013	0.00241	0.00013	0.84427	15.53	0.81	51.3	0.1
BG240W_17	0.0221	0.0026	0.000581	0.000036	0.77547	3.75	0.23	60.7	0.5
BG240W_18	0.0104	0.0015	0.000472	0.000026	0.69301	3.05	0.17	70.4	0.1
BG240W_19	0.018	0.0014	0.000579	0.000031	0.53509	3.73	0.2	69.0	0.1
BG240W_20	0.0223	0.0025	0.000598	0.000037	0.76838	3.85	0.24	53.0	0.1
BG240W_21	0.0134	0.0024	0.000524	0.00004	0.7152	3.38	0.26	50.7	0.2

		207Pb/235U	207Pb/235U error	206Pb/238U	206Pb/238U Error	Error Correlation 206/238 vs. 207/235	Final Age (Ma)	Error (Ma)	Approx U (ppm)	Approx Th (ppm)
	BG240W_22	0.0065	0.001	0.000475	0.00003	0.48884	3.06	0.19	77.0	0.6
	BG240W_23	0.00492	0.0007	0.000429	0.000021	0.40401	2.77	0.14	99.2	0.3
	BG240W_24	0.0171	0.0017	0.000582	0.000034	0.7353	3.75	0.22	70.1	0.1
	BG240W_25	0.0142	0.0018	0.000578	0.000048	0.17825	3.72	0.31	65.5	0.0
	BG240W_26	0.0279	0.0037	0.000621	0.000038	0.74453	4	0.24	61.8	0.0
	BG240W_27	0.0666	0.0055	0.000919	0.000055	0.81015	5.92	0.35	64.7	0.1
	BG240W_28	0.0327	0.0025	0.000646	0.000031	0.6309	4.16	0.2	101.6	0.0
	BG240W_29	0.0304	0.0036	0.000688	0.000059	0.42308	4.43	0.38	74.6	0.4
	BG240W_30	0.0082	0.0016	0.000505	0.000032	0.56446	3.25	0.21	57.3	0.1
	BG240W_31	0.00483	0.00062	0.000447	0.000025	0.016728	2.88	0.16	71.4	0.2
	BG240W_32	0.00474	0.00077	0.000456	0.000024	0.56472	2.94	0.16	73.8	0.3
	BG240W_33	0.0262	0.0015	0.000619	0.000027	0.20599	3.99	0.17	78.2	0.4
	BG240W_34	0.00579	0.00084	0.000437	0.000022	0.4646	2.82	0.14	77.5	0.4
	BG240W_35	0.0154	0.0018	0.000547	0.000035	0.54261	3.52	0.22	64.9	0.5
	BG240W_36	0.0165	0.002	0.00055	0.00003	0.80363	3.55	0.2	72.4	0.3
	BG240W_37	0.0272	0.0022	0.00061	0.000024	0.29788	3.93	0.16	76.3	0.3
	BG240W_38	0.00824	0.00078	0.000492	0.000027	0.15801	3.17	0.18	94.0	0.4
	BG240W_39	0.00419	0.00062	0.000475	0.000021	0.22787	3.06	0.14	101.2	0.4
	BG240W_40	0.00505	0.00049	0.000466	0.000021	0.047568	3.01	0.13	113.6	0.3
	BG240W_41	0.0783	0.005	0.001065	0.000053	0.7828	6.86	0.34	54.0	0.1
	BG240W_42	0.0329	0.0034	0.000715	0.000038	0.63779	4.6	0.25	86.4	0.1
	BG240W_43	0.00761	0.00077	0.000459	0.00002	0.20777	2.96	0.13	80.2	0.1
	BG240W_44	0.0207	0.0017	0.000586	0.000025	0.44879	3.78	0.16	113.2	0.1
	BG240W_45	0.00731	0.00093	0.000492	0.000026	0.2687	3.17	0.16	75.2	0.1
	BG240W_46	0.035	0.0026	0.000734	0.000032	0.51112	4.73	0.2	64.0	0.1
	BG240W_47	0.00695	0.0008	0.000473	0.000022	0.25865	3.05	0.14	78.2	0.4
	BG240W_48	0.0388	0.0054	0.000757	0.000056	0.82837	4.88	0.36	44.4	0.2
	BG240W_49	0.0635	0.0061	0.000962	0.000073	0.92768	6.2	0.47	50.8	0.0
	BG240W_50	0.0181	0.0016	0.000554	0.000033	0.0062737	3.57	0.22	47.9	0.0
97-CG-134	CG134_1	0.0177	0.0017	0.00058	0.00004	0.13212	3.74	0.26	42.1	0.0
	CG134_2	0.019	0.0019	0.00054	0.000036	0.15133	3.48	0.23	39.1	0.0
	CG134_3	0.0417	0.0045	0.000739	0.000073	0.31123	4.76	0.47	17.9	0.1
	CG134_4	0.0182	0.0018	0.000566	0.000028	0.5379	3.65	0.18	52.6	0.0
	CG134_5	0.0434	0.0054	0.000728	0.000075	0.30337	4.69	0.48	15.0	0.1
	CG134_6	0.0177	0.0018	0.000585	0.000035	0.11279	3.77	0.22	41.1	0.0
	CG134_7	0.0386	0.003	0.000716	0.000043	0.3483	4.61	0.28	32.4	0.0
	CG134_8	0.0153	0.0015	0.000502	0.000028	0.07125	3.23	0.18	49.4	0.0
	CG134_9	0.0315	0.0069	0.00078	0.00012	0.26324	5.05	0.78	6.9	0.2
	CG134_10	0.0235	0.0056	0.00058	0.0001	0.10556	3.72	0.66	6.6	0.1
	CG134_11	0.0115	0.0044	0.000575	0.000096	0.029206	3.71	0.62	8.8	0.1
	CG134_12	0.0162	0.0046	0.00059	0.0001	0.044784	3.79	0.67	7.1	0.1
	CG134_13	0.072	0.012	0.00101	0.00013	0.4617	6.52	0.84	7.0	0.0
	CG134_14	0.0239	0.0056	0.00065	0.00012	0.0085113	4.18	0.74	6.8	0.1
	CG134_15	0.0324	0.0058	0.000755	0.000096	0.37243	4.86	0.62	9.3	0.1
	CG134_16	0.0219	0.0061	0.00064	0.0001	0.29048	4.15	0.67	7.3	0.0
	CG134_17	0.00381	0.00096	0.000416	0.00003	0.0068441	2.68	0.19	37.4	0.0
	CG134_18	0.0063	0.0016	0.000462	0.000046	0.14687	2.98	0.3	31.0	0.0
	CG134_19	0.0165	0.0026	0.000577	0.000051	0.37391	3.72	0.33	28.4	0.0
	CG134_20	0.0139	0.0018	0.000523	0.000033	0.39683	3.37	0.21	38.1	0.0
	CG134_21	0.0153	0.0017	0.000546	0.000032	0.19434	3.52	0.21	39.4	0.0
	CG134_22	0.00472	0.00093	0.000451	0.000031	0.13306	2.91	0.2	44.2	0.0
	CG134_23	0.0081	0.0014	0.000471	0.000035	0.11103	3.04	0.22	36.0	0.2
	CG134_24	0.0067	0.0011	0.000492	0.000028	0.15861	3.17	0.18	39.9	0.0
	CG134_25	0.0114	0.0014	0.000501	0.000033	0.11852	3.23	0.21	41.7	0.1
	CG134_26	0.012	0.0014	0.00052	0.000034	0.018851	3.35	0.22	44.3	0.0
	CG134_27	0.0108	0.0014	0.000505	0.000035	0.07555	3.26	0.22	42.2	0.1
	CG134_28	0.0085	0.0013	0.000495	0.000034	0.11967	3.19	0.22	43.1	0.0
	CG134_29	0.0101	0.0013	0.000449	0.000032	0.14241	2.89	0.21	41.6	0.0

		207Pb/235U	207Pb/235U error	206Pb/238U	206Pb/238U Error	Error Correlation 206/238 vs. 207/235	Final Age (Ma)	Error (Ma)	Approx U (ppm)	Approx Th (ppm)
	CG134_30	0.024	0.0043	0.000623	0.000064	0.44806	4.02	0.41	22.5	0.1
	CG134_31	0.0108	0.0017	0.000522	0.000043	0.053523	3.36	0.28	31.0	0.0
	CG134_32	0.0107	0.0018	0.000537	0.000037	0.046069	3.46	0.24	33.1	0.0
	CG134_33	0.0112	0.0022	0.000483	0.000047	0.14052	3.11	0.3	23.0	0.0
	CG134_34	0.008	0.0016	0.000469	0.000036	0.27937	3.02	0.23	34.3	0.1
	CG134_35	0.007	0.0014	0.000482	0.000039	0.15109	3.1	0.25	36.0	0.0
	CG134_36	0.0112	0.0023	0.000515	0.000057	0.056917	3.32	0.37	18.4	0.1
	CG134_37	0.0117	0.0024	0.000515	0.000041	0.19745	3.32	0.27	23.7	0.1
	CG134_38	0.0069	0.0018	0.000501	0.000047	0.1244	3.23	0.3	24.1	0.1
	CG134_39	0.016	0.002	0.000538	0.000034	0.38665	3.46	0.22	37.9	0.0
	CG134_40	0.066	0.0074	0.00095	0.00013	0.33442	6.11	0.81	7.5	0.1
	CG134_41	0.0833	0.0095	0.00102	0.00013	0.22441	6.55	0.83	7.3	0.1
	CG134_42	0.0976	0.0086	0.00111	0.00011	0.076202	7.15	0.73	8.4	0.0
	CG134_43	0.0332	0.0048	0.000681	0.00008	0.19709	4.39	0.52	12.4	0.2
	CG134_44	0.294	0.021	0.00296	0.00021	0.71963	19.1	1.4	12.3	0.2
	CG134_45	0.0044	0.0011	0.00045	0.000032	0.094727	2.9	0.21	41.4	0.0
	CG134_46	0.009	0.0016	0.000448	0.000038	0.49627	2.89	0.24	33.3	0.0
	CG134_47	0.035	0.0052	0.000675	0.000083	0.46837	4.35	0.54	11.5	0.0
	CG134_48	0.135	0.012	0.00174	0.00015	0.57984	11.21	0.97	9.9	0.1
	CG134_49	0.0471	0.0061	0.000763	0.000086	0.37343	4.92	0.56	12.4	0.0
						0				
97-CG-135a	CG135a_15	2.676	0.088	0.02392	0.00098	0.42688	152.9	6.1	2.3	0.0
	CG135a_14	1.018	0.03	0.00948	0.00031	0.50568	60.8	2	13.1	0.2
	CG135a_20	0.738	0.04	0.00693	0.00035	0.9725	44.5	2.3	131.2	0.0
	CG135a_37	0.605	0.057	0.00563	0.00049	0.98754	36.2	3.2	99.6	3.5
	CG135a_38	0.304	0.015	0.00299	0.00019	0.15787	19.2	1.2	7.9	0.0
	CG135a_13	0.289	0.023	0.00274	0.0002	0.61499	17.7	1.3	11.7	0.2
	CG135a_33	0.0493	0.006	0.000835	0.000052	0.8245	5.38	0.33	115.0	0.4
	CG135a_40	0.0493	0.002	0.000834	0.00003	0.35599	5.38	0.19	133.3	0.3
	CG135a_48	0.037	0.0011	0.00074	0.000019	0.17783	4.77	0.12	163.7	0.0
	CG135a_22	0.0299	0.0011	0.000681	0.000017	0.27728	4.39	0.11	178.6	0.1
	CG135a_18	0.0317	0.0027	0.000671	0.00004	0.64589	4.32	0.26	42.3	0.8
	CG135a_35	0.03	0.0022	0.000643	0.000025	0.50218	4.14	0.16	127.8	2.5
	CG135a_31	0.0174	0.0028	0.000618	0.000048	0.72461	3.98	0.31	29.8	0.4
	CG135a_41	0.0203	0.0013	0.000602	0.000019	0.60704	3.88	0.12	188.6	0.1
	CG135a_11	0.0238	0.0037	0.000596	0.000058	0.25706	3.84	0.37	15.5	0.9
	CG135a_30	0.0183	0.0028	0.00057	0.000037	0.78142	3.67	0.24	79.1	0.1
	CG135a_1	0.021	0.0012	0.000565	0.000018	0.49354	3.64	0.12	118.9	0.0
	CG135a_8	0.0164	0.0012	0.000536	0.000027	0.29817	3.46	0.17	77.8	0.3
	CG135a_23	0.0138	0.001	0.000518	0.00002	0.82799	3.34	0.13	159.2	0.0
	CG135a_5	0.0144	0.0017	0.000517	0.000025	0.39413	3.33	0.16	68.3	0.0
	CG135a_27	0.01156	0.00089	0.000508	0.000021	0.26424	3.27	0.14	120.5	0.2
	CG135a_28	0.01145	0.00081	0.000505	0.000021	0.15064	3.26	0.13	121.4	0.1
	CG135a_36	0.01105	0.00079	0.000504	0.00002	0.36666	3.25	0.13	122.6	1.9
	CG135a_32	0.0109	0.001	0.000498	0.000016	0.41462	3.21	0.1	198.8	0.0
	CG135a_6	0.00928	0.00098	0.000489	0.000024	0.37704	3.15	0.16	72.9	0.0
	CG135a_12	0.0117	0.0011	0.000488	0.000024	0.13397	3.15	0.15	57.6	0.2
	CG135a_47	0.00626	0.00062	0.00048	0.000015	0.33841	3.09	0.1	161.8	0.2
	CG135a_7	0.0089	0.0016	0.000461	0.00003	0.75875	2.97	0.19	52.7	0.4
	CG135a_34	0.00619	0.00058	0.000461	0.000019	0.10292	2.97	0.12	122.6	1.2
	CG135a_29	0.00645	0.00084	0.00046	0.000024	0.091928	2.97	0.15	71.7	0.1
	CG135a_39	0.00662	0.00071	0.000457	0.000017	0.23013	2.94	0.11	109.2	0.0
	CG135a_19	0.0071	0.0011	0.000453	0.000028	0.011825	2.92	0.18	48.4	0.8
	CG135a_9	0.00523	0.00051	0.000453	0.000016	0.11229	2.92	0.1	132.5	0.1
	CG135a_44	0.0038	0.00037	0.000446	0.000015	0.012411	2.872	0.097	199.9	0.0
	CG135a_21	0.00573	0.00055	0.000444	0.000015	0.21747	2.861	0.095	164.5	0.0
	CG135a_46	0.00404	0.00035	0.000443	0.000015	0.10512	2.852	0.097	169.5	0.1
	CG135a_24	0.00553	0.00063	0.000441	0.000017	0.013752	2.84	0.11	114.4	0.2
	CG135a_25	0.00512	0.00048	0.00044	0.000017	0.095655	2.84	0.11	132.0	0.1

		207Pb/235U	207Pb/235U error	206Pb/238U	206Pb/238U Error	Error Correlation 206/238 vs. 207/235	Final Age (Ma)	Error (Ma)	Approx U (ppm)	Approx Th (ppm)
	CG135a_45	0.00401	0.00044	0.000438	0.000017	0.71862	2.82	0.11	179.9	0.0
	CG135a_42	0.00324	0.00032	0.000437	0.000014	0.020096	2.816	0.087	186.1	0.0
	CG135a_3	0.00919	0.00096	0.000434	0.000022	0.13028	2.8	0.14	78.9	0.5
	CG135a_49	0.00447	0.00078	0.000434	0.000019	0.33157	2.8	0.12	77.6	0.6
	CG135a_26	0.00332	0.00043	0.000434	0.000017	0.11268	2.8	0.11	110.2	1.5
	CG135a_16	0.00465	0.00052	0.000433	0.000016	0.024155	2.79	0.1	130.1	0.0
	CG135a_2	0.00542	0.00066	0.000431	0.000016	0.06448	2.78	0.1	137.1	0.0
	CG135a_43	0.00376	0.00043	0.000426	0.000016	0.25462	2.74	0.1	172.0	0.1
253 7858	X7858_5	1.71	0.16	0.0154	0.0013	0.9319	98.2	8.5	8.2	0.2
	X7858_34	0.878	0.077	0.00781	0.00065	0.66486	50.1	4.1	3.9	0.1
	X7858_23	0.77	0.1	0.0073	0.00093	0.97814	46.8	6	8.4	0.0
	X7858_42	0.348	0.075	0.00348	0.00064	0.99385	22.4	4.1	15.9	0.4
	X7858_39	0.297	0.015	0.003	0.00016	0.5569	19.3	1	20.4	0.1
	X7858_53	0.2877	0.0063	0.002888	0.000074	0.14615	18.59	0.47	47.1	0.1
	X7858_20	0.274	0.018	0.00287	0.00017	0.60449	18.5	1.1	16.9	0.2
	X7858_43	0.255	0.017	0.00265	0.00017	0.79996	17.1	1.1	21.9	0.1
	X7858_12	0.225	0.028	0.00245	0.00038	0.058163	15.8	2.4	2.1	0.2
	X7858_18	0.212	0.013	0.00227	0.00016	0.5283	14.6	1	14.3	0.1
	X7858_19	0.167	0.015	0.00196	0.00017	0.72584	12.6	1.1	15.1	0.0
	X7858_16	0.161	0.011	0.00194	0.00012	0.20752	12.5	0.78	10.2	0.0
	X7858_17	0.142	0.014	0.00168	0.00015	0.78701	10.82	0.97	14.8	0.1
	X7858_59	0.1219	0.0052	0.00156	0.000077	0.39448	10.05	0.5	33.3	1.5
	X7858_6	0.123	0.011	0.00155	0.00016	0.0099333	10	1	7.0	1.3
	X7858_21	0.1201	0.009	0.00144	0.00013	0.24425	9.27	0.84	10.8	0.0
	X7858_36	0.093	0.011	0.0012	0.00013	0.67437	7.7	0.85	8.8	0.2
	X7858_47	0.0841	0.0051	0.001115	0.000079	0.26024	7.19	0.51	19.7	0.1
	X7858_41	0.0808	0.0067	0.001016	0.000075	0.33161	6.55	0.48	16.3	0.1
	X7858_31	0.049	0.0059	0.00095	0.0001	0.10624	6.11	0.64	8.1	1.4
	X7858_50	0.0587	0.0034	0.000937	0.000059	0.02879	6.04	0.38	22.4	0.1
	X7858_14	0.0599	0.0064	0.00092	0.0001	0.093985	5.95	0.64	9.8	1.8
	X7858_26	0.0467	0.0045	0.000907	0.000072	0.0058856	5.84	0.46	13.1	0.6
	X7858_55	0.06	0.011	0.0009	0.0001	0.85823	5.8	0.66	36.3	0.7
	X7858_25	0.0464	0.0056	0.000885	0.000094	0.074192	5.7	0.6	11.0	1.4
	X7858_57	0.0553	0.0032	0.000881	0.000047	0.22502	5.67	0.3	35.7	0.5
	X7858_32	0.0564	0.0073	0.00087	0.00011	0.3525	5.63	0.73	9.0	0.4
	X7858_9	0.0553	0.0068	0.000865	0.000097	0.055709	5.57	0.62	8.9	1.4
	X7858_10	0.0543	0.0056	0.000859	0.000081	0.040673	5.54	0.52	10.2	1.6
	X7858_51	0.0466	0.0044	0.000837	0.00006	0.84428	5.39	0.39	38.1	0.3
	X7858_24	0.0492	0.0067	0.00083	0.00012	0.28486	5.37	0.77	9.7	0.0
	X7858_30	0.0533	0.005	0.000825	0.000084	0.059108	5.32	0.54	11.3	1.2
	X7858_48	0.0485	0.0033	0.000814	0.000053	0.026546	5.24	0.34	18.8	0.2
	X7858_45	0.0455	0.0057	0.000804	0.000067	0.14768	5.18	0.43	18.2	0.4
	X7858_37	0.0387	0.0085	0.00079	0.00012	0.72554	5.11	0.75	7.0	0.4
	X7858_2	0.0418	0.0067	0.000767	0.000097	0.56696	4.94	0.62	10.0	0.0
	X7858_33	0.0435	0.0053	0.00076	0.0001	0.14169	4.86	0.66	9.0	1.3
	X7858_27	0.0471	0.0051	0.000757	0.000078	0.099374	4.88	0.5	12.2	1.1
	X7858_8	0.0428	0.0045	0.000748	0.000082	0.10931	4.82	0.53	12.1	0.6
	X7858_4	0.0327	0.0038	0.000722	0.000079	0.067466	4.65	0.51	11.5	1.2
	X7858_46	0.0332	0.0039	0.00072	0.000069	0.022304	4.64	0.44	12.9	1.3
	X7858_54	0.0318	0.002	0.000712	0.000036	0.19409	4.59	0.23	53.3	0.0
	X7858_7	0.0281	0.0044	0.00071	0.0001	0.076799	4.55	0.67	8.8	0.0
	X7858_29	0.0365	0.0052	0.000688	0.000082	0.080264	4.43	0.53	9.0	0.2
	X7858_60	0.0302	0.0018	0.000676	0.00004	0.17195	4.36	0.26	41.7	0.4
	X7858_3	0.0179	0.0044	0.000655	0.000091	0.084601	4.22	0.58	7.9	1.2
	X7858_15	0.0208	0.0031	0.000652	0.000069	0.061551	4.2	0.45	13.1	0.0
	X7858_28	0.0343	0.0043	0.00065	0.000078	0.15039	4.19	0.5	10.4	1.2
	X7858_22	0.0214	0.0041	0.000639	0.000092	0.10494	4.12	0.59	10.0	0.0
	X7858_44	0.0284	0.0032	0.000625	0.000056	0.23418	4.03	0.36	18.0	0.2

		207Pb/235U	207Pb/235U error	206Pb/238U	206Pb/238U Error	Error Correlation 206/238 vs. 207/235	Final Age (Ma)	Error (Ma)	Approx U (ppm)	Approx Th (ppm)
	X7858_58	0.0201	0.0016	0.000619	0.000068	0.0043642	3.99	0.44	40.8	0.7
	X7858_56	0.0188	0.0015	0.000573	0.000034	0.08379	3.69	0.22	40.8	0.6
	X7858_38	0.0169	0.0034	0.000531	0.000043	0.23699	3.42	0.28	21.2	0.0
	X7858_49	0.0171	0.0021	0.000522	0.000051	0.022523	3.36	0.33	20.2	0.1
	X7858_52	0.0089	0.0011	0.000498	0.000039	0.091801	3.21	0.25	41.4	0.2
253 7859	X7859_26	1.79	0.17	0.0148	0.002	0.11361	94	13	0.5	0.0
	X7859_14	1.52	0.15	0.0144	0.002	0.37495	92	13	0.5	0.0
	X7859_27	1.5	0.1	0.0126	0.0011	0.022539	81.3	7.1	0.8	0.0
	X7859_25	1.37	0.11	0.0122	0.0013	0.43281	78	8.1	1.2	0.1
	X7859_41	0.8	0.088	0.0082	0.0011	0.36104	52.3	6.9	1.1	0.3
	X7859_49	0.379	0.033	0.00379	0.00036	0.043773	24.4	2.3	2.3	0.2
	X7859_53	0.269	0.04	0.00327	0.0004	0.77341	21.1	2.5	4.5	0.2
	X7859_3	0.305	0.02	0.00298	0.00023	0.15489	19.1	1.5	5.8	0.2
	X7859_43	0.218	0.048	0.00292	0.00064	0.78083	18.7	4.1	1.7	0.1
	X7859_29	0.221	0.039	0.0026	0.00042	0.91877	16.7	2.7	2.6	0.2
	X7859_47	0.223	0.021	0.00258	0.00034	0.027391	16.6	2.2	2.4	0.2
	X7859_20	0.242	0.018	0.00237	0.00021	0.36679	15.2	1.3	6.2	0.2
	X7859_1	0.215	0.013	0.00227	0.00017	0.15143	14.8	1.1	7.3	0.3
	X7859_45	0.147	0.018	0.0018	0.00023	0.049738	11.6	1.5	3.0	0.2
	X7859_40	0.145	0.019	0.00176	0.00018	0.5712	11.3	1.2	9.0	0.4
	X7859_56	0.152	0.018	0.00173	0.00023	0.19795	11.1	1.5	3.8	0.1
	X7859_55	0.131	0.016	0.00164	0.00019	0.4066	10.5	1.2	11.4	0.6
	X7859_33	0.101	0.016	0.00159	0.00026	0.50464	10.2	1.6	15.4	0.1
	X7859_6	0.1408	0.0075	0.00154	0.000095	0.18774	9.92	0.61	15.3	0.0
	X7859_13	0.1114	0.0087	0.00147	0.00013	0.041446	9.47	0.86	7.7	1.4
	X7859_48	0.073	0.013	0.00147	0.00023	0.0044351	9.5	1.5	3.1	0.2
	X7859_19	0.1143	0.0064	0.001395	0.000083	0.15073	8.98	0.53	17.0	0.3
	X7859_54	0.073	0.013	0.00133	0.00029	0.00355	8.6	1.9	6.8	0.3
	X7859_59	0.0645	0.0097	0.00114	0.0002	0.049917	7.3	1.3	4.9	0.2
	X7859_37	0.0616	0.0064	0.001054	0.000095	0.36182	6.79	0.61	17.0	0.2
	X7859_51	0.061	0.011	0.00105	0.00019	0.0060037	6.7	1.2	3.6	0.2
	X7859_21	0.068	0.011	0.00104	0.00012	0.62415	6.73	0.78	9.5	0.3
	X7859_18	0.067	0.0063	0.00098	0.00011	0.016676	6.34	0.73	7.6	0.9
	X7859_5	0.0582	0.0032	0.000878	0.000054	0.049191	5.66	0.35	28.4	1.0
	X7859_7	0.0514	0.0035	0.000875	0.00005	0.091093	5.64	0.32	31.4	1.6
	X7859_9	0.046	0.0035	0.000776	0.000053	0.016354	5	0.34	24.1	2.0
	X7859_30	0.0276	0.0061	0.00077	0.00011	0.025908	4.94	0.73	6.2	0.2
	X7859_8	0.0386	0.0026	0.00075	0.000042	0.062353	4.84	0.27	38.1	1.0
	X7859_28	0.0295	0.003	0.000739	0.000083	0.052574	4.76	0.54	15.7	0.3
	X7859_4	0.0394	0.0029	0.000724	0.00005	0.0043168	4.66	0.32	26.4	0.6
	X7859_32	0.028	0.0028	0.000683	0.000055	0.23492	4.4	0.35	26.2	0.3
	X7859_2	0.0279	0.004	0.000678	0.000071	0.16056	4.37	0.46	14.8	0.2
	X7859_36	0.0204	0.003	0.000668	0.000077	0.010379	4.31	0.5	17.1	0.2
	X7859_38	0.0264	0.0029	0.000657	0.00004	0.11761	4.23	0.26	30.1	0.2
	X7859_34	0.0246	0.0057	0.000636	0.000066	0.83315	4.1	0.43	21.9	0.5
	X7859_15	0.0269	0.0031	0.000625	0.000047	0.008593	4.03	0.3	20.7	1.0
	X7859_57	0.0192	0.0071	0.0006	0.00013	0.048469	3.9	0.84	5.0	0.2
	X7859_10	0.0223	0.0016	0.000598	0.000032	0.031246	3.85	0.2	48.7	0.1
	X7859_23	0.0253	0.004	0.000588	0.000075	0.11865	3.79	0.48	11.6	0.8
	X7859_24	0.0211	0.0033	0.000576	0.000059	0.054423	3.71	0.38	13.5	0.6
	X7859_39	0.0204	0.0028	0.000561	0.000052	0.06011	3.62	0.33	18.4	0.5
	X7859_31	0.015	0.0029	0.000553	0.000056	0.17984	3.56	0.36	24.7	0.2
	X7859_35	0.0094	0.0018	0.000533	0.000044	0.065532	3.44	0.28	25.3	0.5
	X7859_52	0.0124	0.0039	0.000503	0.000079	0.43371	3.24	0.51	10.3	0.5
	X7859_44	0.0153	0.0054	0.000487	0.000096	0.62401	3.14	0.62	9.6	0.3
	X7859_17	0.009	0.0012	0.000484	0.00003	0.041431	3.12	0.19	47.2	0.1
	X7859_11	0.0092	0.0016	0.000478	0.00003	0.017974	3.08	0.19	46.0	0.4
	X7859_12	0.0131	0.0019	0.000475	0.000049	0.099005	3.06	0.31	21.2	0.9

253 7860

	207Pb/235U	207Pb/235U error	206Pb/238U	206Pb/238U Error	Error Correlation 206/238 vs. 207/235	Final Age (Ma)	Error (Ma)	Approx U (ppm)	Approx Th (ppm)
X7859_16	0.0081	0.0018	0.00044	0.000045	0.083709	2.83	0.29	20.6	1.1
X7860_9	0.37	0.18	0.0039	0.0017	0.98915	25	10	6.7	0.0
X7860_14	0.277	0.051	0.00306	0.00056	0.87939	19.7	3.6	3.1	0.0
X7860_45	0.254	0.027	0.00268	0.00027	0.72389	17.3	1.8	6.1	0.0
X7860_32	0.234	0.02	0.00263	0.00028	0.7269	16.9	1.8	5.5	0.0
X7860_39	0.193	0.016	0.00204	0.00022	0.4116	13.1	1.4	5.9	0.0
X7860_8	0.143	0.012	0.00186	0.00018	0.185	12	1.2	6.1	0.1
X7860_38	0.155	0.01	0.00186	0.00014	0.090153	11.98	0.92	8.5	0.0
X7860_2	0.178	0.023	0.00183	0.00032	0.35467	11.8	2	3.0	0.0
X7860_51	0.116	0.01	0.00141	0.00012	0.39315	9.06	0.77	7.2	0.0
X7860_54	0.099	0.024	0.00139	0.00026	0.93631	9	1.7	8.8	0.0
X7860_48	0.097	0.0091	0.0013	0.00012	0.097205	8.34	0.79	8.6	0.0
X7860_26	0.095	0.014	0.00128	0.00016	0.76573	8.2	1	7.7	0.0
X7860_44	0.1087	0.0083	0.00126	0.00012	0.036166	8.1	0.77	8.2	0.1
X7860_37	0.0727	0.0072	0.0011	0.0001	0.17637	7.1	0.65	8.4	0.0
X7860_31	0.0719	0.0079	0.00105	0.00011	0.26758	6.78	0.68	9.0	0.0
X7860_55	0.0718	0.0068	0.001021	0.000089	0.070722	6.58	0.57	10.0	0.0
X7860_28	0.0635	0.009	0.00101	0.00013	0.84061	6.48	0.83	9.6	0.0
X7860_58	0.0656	0.0064	0.00096	0.00011	0.07939	6.22	0.7	8.8	0.0
X7860_34	0.0546	0.0062	0.00091	0.0001	0.072385	5.87	0.64	8.1	0.0
X7860_56	0.0548	0.0072	0.00086	0.000096	0.053841	5.54	0.62	8.7	0.0
X7860_46	0.0478	0.0059	0.000823	0.000094	0.054977	5.3	0.6	8.9	0.0
X7860_12	0.0148	0.0074	0.00082	0.00019	0.0042467	5.3	1.2	3.8	0.0
X7860_11	0.034	0.0088	0.00079	0.00016	0.17553	5.1	1	3.8	0.0
X7860_22	0.0391	0.0068	0.00073	0.00013	0.11942	4.72	0.82	6.5	0.0
X7860_36	0.0294	0.0057	0.000719	0.000088	0.015539	4.64	0.57	9.0	0.0
X7860_43	0.0422	0.0062	0.000703	0.000091	0.34232	4.53	0.59	8.6	0.0
X7860_52	0.0332	0.0048	0.000702	0.000093	0.0063342	4.52	0.6	8.2	0.0
X7860_60	0.0377	0.0049	0.000666	0.000085	0.026042	4.29	0.55	9.2	0.0
X7860_21	0.0242	0.0044	0.00065	0.0001	0.14755	4.17	0.64	7.6	0.0
X7860_47	0.0146	0.0043	0.000632	0.000089	0.12427	4.07	0.58	8.1	0.0
X7860_6	0.0106	0.0063	0.00063	0.00012	0.07116	4.04	0.76	5.3	0.0
X7860_15	0.0207	0.007	0.00063	0.00012	0.10754	4.04	0.79	5.2	0.0
X7860_18	0.0064	0.0054	0.00063	0.00014	0.085156	4.06	0.89	5.2	0.0
X7860_41	0.0175	0.0037	0.000602	0.000083	0.10764	3.88	0.53	10.1	0.0
X7860_29	0.0113	0.0034	0.000593	0.000074	0.091726	3.82	0.48	9.5	0.0
X7860_59	0.0326	0.0054	0.000593	0.000091	0.19573	3.82	0.59	8.6	0.0
X7860_17	0.0116	0.0051	0.00059	0.00012	0.097023	3.78	0.79	5.9	0.0
X7860_20	0.0368	0.009	0.00059	0.00014	0.17758	3.77	0.88	4.5	0.0
X7860_1	0.0095	0.0067	0.00058	0.00012	0.0054751	3.74	0.79	4.6	0.0
X7860_53	0.0156	0.004	0.000577	0.000085	0.053402	3.72	0.54	8.1	0.0
X7860_16	0.0061	0.0061	0.00057	0.00013	0.035256	3.69	0.84	4.5	0.0
X7860_49	0.0195	0.0049	0.000566	0.000085	0.001373	3.65	0.54	8.6	-0.1
X7860_7	0.0101	0.0062	0.00056	0.00011	0.219	3.58	0.73	5.3	0.1
X7860_40	0.0202	0.0053	0.000552	0.000097	0.054513	3.55	0.62	7.0	0.1
X7860_4	0.0014	0.0077	0.00055	0.00018	0.095083	3.5	1.2	3.2	0.0
X7860_50	0.0114	0.0046	0.000532	0.000085	0.079694	3.43	0.55	7.5	0.0
X7860_33	0.0145	0.0086	0.00052	0.00016	0.14213	3.4	1	3.4	0.0
X7860_35	0.0112	0.0044	0.000514	0.000097	0.14802	3.31	0.63	7.0	0.0
X7860_27	0.0114	0.0036	0.000513	0.000073	0.059511	3.31	0.47	9.5	0.0
X7860_24	0.0054	0.0042	0.00051	0.00011	0.15164	3.28	0.7	6.2	0.0
X7860_30	0.0165	0.0046	0.000505	0.000082	0.0038654	3.26	0.53	9.2	0.0
X7860_23	0.026	0.0058	0.000479	0.000091	0.6125	3.08	0.59	7.2	0.0
X7860_13	0.0153	0.0074	0.00046	0.00013	0.059149	2.96	0.85	4.1	0.0
X7860_5	0.0076	0.0059	0.00041	0.00012	0.12913	2.66	0.79	4.9	0.0
X7860_10	0.0166	0.0081	0.00041	0.00014	0.095752	2.66	0.93	3.7	0.0

		207Pb/235U	207Pb/235U error	206Pb/238U	206Pb/238U Error	Error Correlation 206/238 vs. 207/235	Final Age (Ma)	Error (Ma)	Approx U (ppm)	Approx Th (ppm)
253 7861	X7861_12	0.572	0.051	0.00553	0.00041	0.82573	35.5	2.6	9.6	0.0
	X7861_15	0.482	0.023	0.00483	0.00022	0.5766	31	1.4	12.5	0.3
	X7861_1	0.453	0.017	0.00443	0.00021	0.40074	28.5	1.4	10.9	0.2
	X7861_13	0.276	0.093	0.00288	0.00091	0.98397	18.5	5.7	14.6	0.1
	X7861_14	0.22	0.061	0.00242	0.00053	0.9896	15.5	3.4	15.4	0.3
	X7861_29	0.176	0.019	0.00207	0.00018	0.87952	13.3	1.2	25.7	0.0
	X7861_60	0.0944	0.0036	0.001245	0.000053	0.23967	8.02	0.34	34.1	0.0
	X7861_11	0.0883	0.0044	0.001201	0.000061	0.18105	7.73	0.4	25.0	0.1
	X7861_55	0.0812	0.0036	0.001184	0.000054	0.080608	7.63	0.35	33.8	0.0
	X7861_56	0.0764	0.0037	0.001056	0.000055	0.0066898	6.81	0.35	31.4	0.0
	X7861_28	0.0748	0.0098	0.001042	0.000099	0.74661	6.71	0.64	23.6	0.0
	X7861_19	0.0629	0.008	0.00101	0.0001	0.95353	6.54	0.66	25.2	0.1
	X7861_47	0.0704	0.0039	0.001	0.000071	0.09273	6.44	0.45	19.5	0.1
	X7861_2	0.066	0.013	0.00098	0.00014	0.99105	6.28	0.87	26.4	0.0
	X7861_52	0.0655	0.0039	0.000948	0.000052	0.17516	6.11	0.33	26.4	0.1
	X7861_42	0.0605	0.0041	0.000932	0.000049	0.068663	6.01	0.31	28.2	0.0
	X7861_26	0.0614	0.0036	0.000927	0.000051	0.068289	5.98	0.33	28.3	0.0
	X7861_41	0.046	0.0031	0.000867	0.00005	0.053835	5.59	0.32	26.9	0.0
	X7861_27	0.0481	0.0037	0.000832	0.000062	0.066926	5.36	0.4	26.3	0.0
	X7861_48	0.0463	0.0033	0.000832	0.000064	0.16179	5.36	0.41	19.3	0.0
	X7861_50	0.055	0.012	0.000811	0.00009	0.53914	5.22	0.58	27.0	0.1
	X7861_35	0.0407	0.0033	0.000794	0.000058	0.34362	5.12	0.37	25.2	0.1
	X7861_30	0.0394	0.0034	0.000769	0.000052	0.23334	4.95	0.33	23.7	0.1
	X7861_53	0.0375	0.0029	0.000745	0.000043	0.17168	4.8	0.28	26.4	0.0
	X7861_45	0.0384	0.0029	0.000742	0.000056	0.044472	4.78	0.36	24.5	0.0
	X7861_7	0.0278	0.0033	0.000728	0.000062	0.16059	4.69	0.4	17.0	0.0
	X7861_16	0.0322	0.0024	0.000704	0.000049	0.10119	4.54	0.32	28.0	0.1
	X7861_49	0.0289	0.0052	0.000702	0.000065	0.95608	4.53	0.42	26.4	0.0
	X7861_32	0.0236	0.0023	0.000676	0.000045	0.019343	4.36	0.29	26.5	0.0
	X7861_18	0.0256	0.0031	0.000671	0.000048	0.75715	4.33	0.31	31.5	0.1
	X7861_36	0.0232	0.003	0.000662	0.000051	0.038282	4.27	0.33	27.4	0.0
	X7861_6	0.0248	0.0036	0.00066	0.000074	0.028385	4.25	0.47	11.6	0.0
	X7861_58	0.0194	0.0018	0.000616	0.000039	0.0097739	3.97	0.25	33.0	0.0
	X7861_24	0.0237	0.0035	0.000615	0.000057	0.55909	3.97	0.37	19.6	0.1
	X7861_37	0.0172	0.0021	0.000601	0.000046	0.052949	3.87	0.3	27.9	0.0
	X7861_46	0.0181	0.0023	0.00059	0.000043	0.07542	3.8	0.28	25.0	0.0
	X7861_34	0.0166	0.0019	0.000569	0.000046	0.11677	3.67	0.29	26.7	0.1
	X7861_20	0.0169	0.0022	0.000556	0.000042	0.00045165	3.58	0.27	23.8	0.0
	X7861_17	0.0154	0.0019	0.000552	0.000037	0.056231	3.56	0.24	26.7	0.2
	X7861_59	0.0108	0.0016	0.000539	0.000038	0.086784	3.47	0.24	33.8	0.0
	X7861_38	0.0071	0.0014	0.000538	0.000043	0.0099737	3.47	0.28	28.5	0.1
	X7861_5	0.0134	0.002	0.000534	0.00004	0.023723	3.44	0.26	28.4	0.1
	X7861_43	0.0062	0.0012	0.000521	0.000046	0.10589	3.35	0.29	26.7	0.0
	X7861_31	0.0113	0.0015	0.000519	0.000043	0.040768	3.34	0.28	28.9	0.0
	X7861_39	0.0111	0.0016	0.000514	0.000039	0.11392	3.31	0.25	29.0	0.0
	X7861_33	0.0068	0.0014	0.000509	0.000043	0.064318	3.28	0.28	25.8	0.0
	X7861_9	0.0075	0.0014	0.000483	0.000039	0.048919	3.11	0.25	26.7	0.1
	X7861_44	0.0083	0.0013	0.000483	0.000037	0.016015	3.11	0.24	28.8	0.0
	X7861_10	0.0071	0.0014	0.000482	0.000037	0.017402	3.11	0.24	27.7	0.0
	X7861_40	0.006	0.0013	0.000482	0.000039	0.093525	3.11	0.25	29.3	0.0
	X7861_3	0.007	0.0017	0.000476	0.00005	0.003875	3.07	0.32	24.4	0.1
	X7861_22	0.0065	0.0014	0.000462	0.000042	0.13642	2.98	0.27	28.3	0.0
	X7861_4	0.004	0.0012	0.000448	0.000039	0.089077	2.89	0.25	25.6	0.0
	X7861_8	0.0073	0.0014	0.000434	0.000036	0.0078061	2.8	0.23	29.6	0.0
	X7861_25	0.0083	0.0023	0.000434	0.000047	0.023981	2.8	0.31	16.7	0.2
	X7861_23	0.0048	0.0025	0.000423	0.000067	0.089278	2.72	0.43	13.2	0.0
BG14W-07 65m Core-Rim Experiments	BG14W-core1_1	0.00655	0.00071	0.000471	0.000021	0.065526	3.03	0.13	70.1	0.4
	BG14W-core1_2	0.1701	0.0048	0.001823	0.000054	0.38179	11.74	0.35	51.1	0.4
	BG14W-core1_3	0.00387	0.00055	0.000419	0.000023	0.075866	2.7	0.15	64.6	0.3
	BG14W-core1_4	0.0656	0.0053	0.000901	0.00006	0.53721	5.8	0.39	44.7	0.3
	BG14W-core1_5	0.0238	0.002	0.000602	0.000033	0.36909	3.88	0.21	52.2	0.2
	BG14W-core1_6	0.0219	0.002	0.000564	0.000027	0.40364	3.64	0.17	71.9	0.1
	BG14W-core1_7	0.0326	0.003	0.000657	0.000031	0.75686	4.24	0.2	63.0	0.1
	BG14W-core1_8	0.256	0.014	0.00249	0.00013	0.84619	16.05	0.84	56.8	0.3

	207Pb/235U	207Pb/235U error	206Pb/238U	206Pb/238U Error	Error Correlation 206/238 vs. 207/235	Final Age (Ma)	Error (Ma)	Approx U (ppm)	Approx Th (ppm)
BG14W-core1_9	0.121	0.011	0.00152	0.00013	0.3316	9.77	0.81	60.9	0.3
BG14W-core1_10	0.065	0.0054	0.000989	0.000062	0.60335	6.37	0.4	58.0	0.5
BG14W-core1_11	0.0936	0.008	0.001151	0.000072	0.79802	7.42	0.46	49.4	0.2
BG14W-core1_12	0.392	0.012	0.00366	0.00012	0.63997	23.58	0.8	52.4	0.2
BG14W-core1_13	0.0519	0.006	0.000807	0.000055	0.80248	5.2	0.35	65.1	0.1
BG14W-core1_14	0.036	0.004	0.000742	0.00005	0.21306	4.78	0.32	74.5	0.0
BG14W-core1_15	0.0121	0.0015	0.000508	0.000029	0.31309	3.27	0.19	65.7	0.1
BG14W-core1_16	0.0275	0.0021	0.000604	0.000026	0.15765	3.89	0.17	72.4	0.1
BG14W-core1_17	0.0703	0.0074	0.000975	0.000064	0.77236	6.28	0.41	71.3	0.0
BG14W-core1_18	0.0395	0.0057	0.000785	0.00005	0.66748	5.06	0.32	67.5	0.0
BG14W-core1_19	0.0424	0.0035	0.000738	0.000041	0.53621	4.75	0.26	54.8	0.1
BG14W-core1_20	0.279	0.013	0.00258	0.00011	0.79039	16.63	0.72	52.3	0.1
BG14W-core1_21	0.021	0.0017	0.000604	0.000034	0.28428	3.89	0.22	49.4	0.1
BG14W-core1_22	0.0162	0.0014	0.000532	0.000029	0.27358	3.43	0.19	66.9	0.0
BG14W-core1_23	0.0293	0.0021	0.000649	0.000027	0.13182	4.18	0.18	72.2	0.0
BG14W-core1_24	0.0074	0.0011	0.000446	0.000024	0.37486	2.87	0.15	71.4	0.0
BG14W-core1_25	0.0184	0.0024	0.000566	0.000033	0.60318	3.65	0.21	69.3	0.0
BG14W-core2_1	0.0134	0.0018	0.000532	0.000035	0.43619	3.43	0.23	37.1	0.7
BG14W-core2_2	0.0341	0.0036	0.000716	0.000048	0.54769	4.62	0.31	36.9	0.7
BG14W-core2_3	0.0567	0.0035	0.000874	0.000045	0.323	5.63	0.29	38.3	0.6
BG14W-core2_4	0.0541	0.0052	0.000875	0.000056	0.62283	5.64	0.36	39.7	0.4
BG14W-core2_5	0.0089	0.0016	0.000467	0.00003	0.017368	3.01	0.19	39.8	0.4
BG14W-core2_6	0.0578	0.0032	0.000881	0.000042	0.26213	5.68	0.27	38.7	0.5
BG14W-core2_7	0.0488	0.0041	0.000802	0.000055	0.4579	5.17	0.35	37.1	0.7
BG14W-core2_8	0.222	0.011	0.00234	0.00011	0.63808	15.09	0.73	34.5	0.7
BG14W-core2_9	0.1266	0.007	0.001515	0.000072	0.40852	9.76	0.46	33.7	0.7
BG14W-core2_10	0.0789	0.0077	0.00114	0.0001	0.37118	7.34	0.67	31.1	0.8
BG14W-core2_11	0.0129	0.0043	0.000524	0.000041	0.039122	3.37	0.27	32.7	1.1
BG14W-core2_12	0.0181	0.0023	0.000556	0.000043	0.12777	3.58	0.27	32.4	0.9
BG14W-core2_13	0.0728	0.0048	0.001081	0.00006	0.48002	6.96	0.39	34.2	0.8
BG14W-core2_14	0.0672	0.0033	0.000928	0.000046	0.27639	5.98	0.3	37.5	0.8
BG14W-core2_15	0.0641	0.0043	0.000897	0.000052	0.39785	5.78	0.33	39.2	0.7
BG14W-core2_16	0.0583	0.004	0.000878	0.000068	0.17716	5.66	0.44	21.9	0.5
BG14W-core2_17	0.0159	0.0016	0.000562	0.000045	0.073295	3.62	0.29	34.3	0.9
BG14W-core2_18	0.0719	0.0055	0.00104	0.000059	0.43198	6.7	0.38	32.4	1.0
BG14W-core2_19	0.0124	0.0018	0.000498	0.000037	0.0020675	3.21	0.24	31.2	1.1
BG14W-core2_20	0.0206	0.0028	0.000543	0.000043	0.57352	3.5	0.28	29.1	1.6
BG14W-core2_21	0.0303	0.0054	0.000684	0.000052	0.58283	4.41	0.33	29.7	2.5
BG14W-core2_22	0.0265	0.0026	0.000641	0.000047	0.20229	4.13	0.3	31.9	2.3
BG14W-core2_23	0.0147	0.0023	0.000525	0.000049	0.30595	3.38	0.32	33.5	1.4
BG14W-core2_24	0.0211	0.0031	0.000589	0.000054	0.24351	3.8	0.35	32.3	1.0
BG14W-core2_25	0.249	0.013	0.00246	0.00014	0.65022	15.86	0.88	29.2	0.7
BG14W-core3_1	0.0317	0.0032	0.000716	0.000046	0.42272	4.61	0.29	58.0	0.7
BG14W-core3_2	0.0115	0.0013	0.000547	0.000031	0.081633	3.53	0.2	56.9	0.6
BG14W-core3_3	0.0109	0.0013	0.000514	0.000027	0.0080557	3.31	0.18	57.6	0.5
BG14W-core3_4	0.0146	0.0015	0.00053	0.000029	0.14421	3.41	0.19	56.4	0.5
BG14W-core3_5	0.00708	0.00084	0.00045	0.000027	0.25743	2.9	0.18	58.9	0.4
BG14W-core3_6	0.0154	0.0051	0.00054	0.000039	0.3146	3.48	0.25	58.3	0.5
BG14W-core3_7	0.0066	0.0011	0.0005	0.000034	0.10758	3.22	0.22	60.4	0.5
BG14W-core3_8	0.0501	0.0029	0.000783	0.000041	0.10365	5.05	0.26	49.5	0.5
BG14W-core3_9	0.0089	0.0015	0.000515	0.000038	0.015792	3.32	0.24	59.2	0.5
BG14W-core3_10	0.0471	0.004	0.000804	0.000061	0.32402	5.18	0.39	61.8	0.6
BG14W-core3_11	0.0195	0.0018	0.00054	0.000029	0.19376	3.48	0.19	67.6	0.6
BG14W-core3_12	0.0092	0.0013	0.000476	0.000028	0.51644	3.07	0.18	69.3	0.6
BG14W-core3_13	0.062	0.0041	0.00092	0.000064	0.20635	5.93	0.41	49.2	0.5
BG14W-core3_14	0.0158	0.0016	0.000549	0.00003	0.31771	3.54	0.2	66.1	0.5
BG14W-core3_15	0.0105	0.0027	0.000484	0.000026	0.025388	3.12	0.17	69.4	0.5
BG14W-core3_16	0.00509	0.0007	0.000441	0.000022	0.073143	2.84	0.14	70.4	0.5
BG14W-core3_17	0.0209	0.002	0.0006	0.000041	0.11527	3.86	0.27	59.1	0.6
BG14W-core3_18	0.0379	0.006	0.000688	0.000051	0.10559	4.44	0.33	56.9	0.5
BG14W-core3_19	0.0133	0.0015	0.000543	0.000033	0.4712	3.5	0.22	56.8	0.6
BG14W-core3_20	0.0412	0.0042	0.000706	0.000039	0.042209	4.55	0.25	54.4	0.7
BG14W-core3_21	0.0178	0.0019	0.000572	0.000036	0.69828	3.68	0.23	54.8	0.7
BG14W-core3_22	0.0207	0.0048	0.000556	0.000041	0.043733	3.59	0.27	59.7	0.7

	207Pb/235U	207Pb/235U error	206Pb/238U	206Pb/238U Error	Error Correlation 206/238 vs. 207/235	Final Age (Ma)	Error (Ma)	Approx U (ppm)	Approx Th (ppm)
BG14W-core3_23	0.0273	0.0024	0.000664	0.000033	0.36327	4.28	0.21	63.0	0.7
BG14W-core3_24	0.0924	0.0049	0.001171	0.000062	0.34744	7.54	0.4	51.9	0.6
BG14W-core3_25	0.0732	0.0035	0.001032	0.000043	0.41796	6.65	0.28	67.9	0.8
BG14W-rim1_1	0.0091	0.0039	0.000448	0.000024	0.027169	2.89	0.16	52.2	0.7
BG14W-rim1_2	0.00503	0.0006	0.000418	0.000022	0.02618	2.69	0.14	67.1	0.1
BG14W-rim1_3	0.00453	0.00065	0.000446	0.000024	0.068654	2.87	0.15	64.9	0.0
BG14W-rim1_4	0.0099	0.0011	0.000479	0.00002	0.52165	3.09	0.13	100.6	0.0
BG14W-rim1_5	0.00545	0.00055	0.000449	0.000018	0.1892	2.89	0.12	101.6	0.0
BG14W-rim1_6	0.00731	0.00069	0.000465	0.00002	0.05869	3	0.13	102.1	0.0
BG14W-rim1_7	0.0122	0.001	0.000524	0.000021	0.064267	3.38	0.14	92.2	0.0
BG14W-rim1_8	0.0175	0.0013	0.000527	0.000025	0.096248	3.4	0.16	68.3	0.0
BG14W-rim1_9	0.01206	0.00092	0.000518	0.000021	0.17085	3.34	0.14	80.9	0.0
BG14W-rim1_10	0.01121	0.00073	0.0005	0.000023	0.0045762	3.23	0.15	93.4	0.0
BG14W-rim1_11	0.0202	0.0012	0.000562	0.000023	0.027996	3.62	0.15	62.0	0.0
BG14W-rim1_12	0.00628	0.00067	0.000465	0.000019	0.0014714	2.99	0.12	85.5	0.1
BG14W-rim1_13	0.00335	0.00056	0.000439	0.000028	0.010835	2.83	0.18	72.1	0.2
BG14W-rim1_14	0.00451	0.00058	0.000449	0.000024	0.022587	2.89	0.16	73.7	0.3
BG14W-rim1_15	0.0191	0.0016	0.00054	0.000025	0.21178	3.48	0.16	66.8	0.8
BG14W-rim1_16	0.0921	0.0044	0.001184	0.000047	0.5476	7.63	0.3	56.9	0.6
BG14W-rim1_17	0.00508	0.00064	0.000446	0.000025	0.086768	2.88	0.16	67.3	0.4
BG14W-rim1_18	0.0337	0.0019	0.000678	0.000031	0.049983	4.37	0.2	60.0	0.5
BG14W-rim1_19	0.0388	0.0035	0.000737	0.000042	0.74638	4.75	0.27	70.9	0.6
BG14W-rim1_20	0.00568	0.00068	0.000433	0.000024	0.24611	2.79	0.15	69.5	0.7
BG14W-rim1_21	0.00726	0.00074	0.00048	0.000024	0.12362	3.1	0.15	69.6	1.3
BG14W-rim1_22	0.00787	0.0007	0.000477	0.000023	0.0044821	3.08	0.15	72.8	0.8
BG14W-rim1_23	0.1407	0.0063	0.001592	0.000074	0.4907	10.26	0.48	33.1	0.3
BG14W-rim1_24	0.0117	0.0011	0.000504	0.00003	0.21445	3.25	0.19	52.9	0.6
BG14W-rim1_25	0.00501	0.00063	0.000414	0.000022	0.012512	2.67	0.14	71.0	0.5
BG14W-rim2_1	0.0039	0.00059	0.000444	0.000021	0.22367	2.86	0.14	74.4	0.0
BG14W-rim2_2	0.013	0.0013	0.000511	0.000029	0.0074563	3.29	0.18	66.3	0.0
BG14W-rim2_3	0.0346	0.0023	0.000703	0.000034	0.11075	4.53	0.22	59.9	0.0
BG14W-rim2_4	0.0268	0.0024	0.000657	0.000036	0.56589	4.23	0.23	58.5	0.0
BG14W-rim2_5	0.015	0.0029	0.000521	0.000032	0.14591	3.36	0.21	64.6	0.0
BG14W-rim2_6	0.00719	0.00092	0.000442	0.00002	0.082844	2.85	0.13	68.1	0.0
BG14W-rim2_7	0.009	0.001	0.000487	0.000023	0.40264	3.14	0.15	97.6	0.0
BG14W-rim2_8	0.00884	0.00069	0.000473	0.000018	0.11549	3.05	0.12	98.8	0.0
BG14W-rim2_9	0.0265	0.0014	0.000608	0.000025	0.34736	3.92	0.16	102.3	0.0
BG14W-rim2_10	0.01157	0.00097	0.000494	0.000023	0.23596	3.18	0.15	100.3	0.0
BG14W-rim2_11	0.00549	0.00072	0.000463	0.000023	0.08897	2.99	0.15	94.9	0.0
BG14W-rim2_12	0.0089	0.0011	0.000459	0.000026	0.10756	2.96	0.16	58.4	0.0
BG14W-rim2_13	0.0183	0.0022	0.00061	0.000034	0.36198	3.93	0.22	42.2	0.0
BG14W-rim2_14	0.017	0.0023	0.000518	0.000036	0.29093	3.34	0.23	40.4	0.1
BG14W-rim2_15	0.0684	0.0044	0.001013	0.000093	0.081067	6.53	0.6	28.9	0.1
BG14W-rim2_16	0.0153	0.0018	0.00054	0.000039	0.20016	3.48	0.25	41.3	0.0
BG14W-rim2_17	0.0894	0.0074	0.00121	0.0001	0.33499	7.79	0.66	31.8	0.1
BG14W-rim2_18	0.04	0.0034	0.000806	0.000051	0.091916	5.19	0.33	32.6	0.4
BG14W-rim2_19	0.0083	0.0013	0.000472	0.000033	0.088678	3.04	0.21	39.8	0.1
BG14W-rim2_20	0.0234	0.0019	0.000627	0.000035	0.15205	4.04	0.23	48.1	0.1
BG14W-rim2_21	0.0095	0.0015	0.000517	0.000033	0.54826	3.33	0.22	52.0	0.1
BG14W-rim2_22	0.0175	0.0019	0.000523	0.00003	0.043521	3.37	0.19	48.3	0.0
BG14W-rim3_1	0.0157	0.00093	0.000519	0.000023	0.059076	3.34	0.15	84.7	0.2
BG14W-rim3_2	0.0178	0.0012	0.000533	0.000026	0.0698	3.44	0.17	81.7	0.2
BG14W-rim3_3	0.1685	0.0075	0.00182	0.000079	0.10429	11.72	0.51	52.7	0.0
BG14W-rim3_4	0.00485	0.00079	0.000468	0.00003	0.30439	3.02	0.19	54.0	0.0
BG14W-rim3_5	0.0364	0.0029	0.000722	0.000044	0.57687	4.65	0.28	48.0	0.0
BG14W-rim3_6	0.0607	0.0042	0.000961	0.00006	0.35918	6.19	0.39	44.4	0.0
BG14W-rim3_7	0.046	0.004	0.000798	0.000045	0.092522	5.14	0.29	47.4	0.0
BG14W-rim3_8	0.0193	0.0016	0.000583	0.000034	0.26439	3.75	0.22	53.6	0.0
BG14W-rim3_9	0.0078	0.0011	0.000476	0.000033	0.43734	3.07	0.21	54.7	0.1
BG14W-rim3_10	0.009	0.00096	0.000498	0.000022	0.57579	3.21	0.14	78.9	0.4
BG14W-rim3_11	0.0222	0.002	0.000622	0.00003	0.64856	4.01	0.2	86.3	0.1
BG14W-rim3_12	0.012	0.0015	0.0005	0.000026	0.76104	3.22	0.17	70.2	0.2
BG14W-rim3_13	0.00576	0.00083	0.000473	0.000024	0.26433	3.05	0.16	60.8	0.3
BG14W-rim3_14	0.00537	0.00077	0.000443	0.000023	0.049737	2.85	0.15	63.0	0.4

		207Pb/235U	207Pb/235U error	206Pb/238U	206Pb/238U Error	Error Correlation 206/238 vs. 207/235	Final Age (Ma)	Error (Ma)	Approx U (ppm)	Approx Th (ppm)
	BG14W-rim3_15	0.0067	0.001	0.000448	0.000031	0.068013	2.89	0.2	53.2	0.1
	BG14W-rim3_16	0.0131	0.0012	0.000503	0.000022	0.10865	3.24	0.14	66.7	0.0
	BG14W-rim3_17	0.0118	0.0013	0.000507	0.000023	0.12326	3.27	0.15	61.4	0.0
	BG14W-rim3_18	0.00425	0.00061	0.000429	0.000025	0.11493	2.77	0.16	63.8	0.1
	BG14W-rim3_19	0.0309	0.0018	0.000676	0.000031	0.23327	4.36	0.2	102.2	0.0
	BG14W-rim3_20	0.00632	0.00062	0.000451	0.000019	0.022019	2.91	0.12	101.7	0.0
	BG14W-rim3_21	0.0136	0.0018	0.000522	0.000032	0.51821	3.36	0.2	63.9	0.0
	BG14W-rim3_22	0.00634	0.00091	0.000426	0.000026	0.15504	2.74	0.17	70.6	0.0
	BG14W-rim3_23	0.0411	0.0026	0.000721	0.000038	0.19481	4.65	0.24	56.9	0.1
	BG14W-rim3_24	0.0062	0.001	0.000444	0.00003	0.061303	2.86	0.19	48.9	0.1
	BG14W-rim3_25	0.0139	0.0019	0.000551	0.000039	0.14274	3.55	0.25	52.8	0.1
	BG14W-rim3_26	0.009	0.0013	0.000503	0.000027	0.066627	3.24	0.17	55.3	0.0
	BG14W-rim3_27	0.00502	0.00091	0.000439	0.00003	0.0088889	2.83	0.19	40.0	0.0
	BG14W-rim3_28	0.0069	0.0011	0.000462	0.000026	0.49925	2.98	0.16	54.1	0.0
	BG14W-rim3_29	0.0066	0.0015	0.000444	0.000029	0.079105	2.86	0.18	55.9	0.0
	BG14W-rim3_30	0.0154	0.0016	0.000536	0.000033	0.051417	3.46	0.21	53.2	0.0
	BG14W-rim3_31	0.025	0.0018	0.000605	0.000034	0.13921	3.9	0.22	52.5	0.1
	BG14W-rim3_32	0.0245	0.0029	0.00063	0.00004	0.56921	4.06	0.26	59.1	0.0
	BG14W-rim3_33	0.016	0.0016	0.00052	0.000028	0.2902	3.35	0.18	63.2	0.1
DOM-91M-6	DOM_91M_6_1	0.084	0.0055	0.001134	0.000074	0.26163	7.31	0.47	17.1	3.8
	DOM_91M_6_2	0.0709	0.0047	0.00102	0.000065	0.16536	6.57	0.42	20.1	4.1
	DOM_91M_6_3	0.0443	0.0036	0.000742	0.000064	0.074518	4.78	0.41	20.0	2.7
	DOM_91M_6_4	0.0357	0.0025	0.000666	0.000035	0.21708	4.29	0.22	46.2	0.1
	DOM_91M_6_5	0.0505	0.0037	0.000767	0.000053	0.18077	4.94	0.34	22.4	3.0
	DOM_91M_6_6	0.0326	0.0029	0.000704	0.000046	0.65754	4.54	0.29	29.4	0.3
	DOM_91M_6_7	0.1256	0.005	0.001541	0.000068	0.20078	9.93	0.44	23.9	1.8
	DOM_91M_6_8	0.0517	0.0045	0.00089	0.000063	0.023057	5.73	0.4	20.8	2.9
	DOM_91M_6_9	0.0585	0.0041	0.000878	0.000064	0.078061	5.66	0.41	18.7	3.5
	DOM_91M_6_10	0.295	0.026	0.00311	0.00026	0.75221	20	1.7	20.6	2.4
	DOM_91M_6_11	0.474	0.024	0.00434	0.0002	0.42176	27.9	1.3	8.1	3.0
	DOM_91M_6_12	0.115	0.011	0.00148	0.00012	0.76626	9.5	0.8	49.1	1.4
	DOM_91M_6_13	0.0967	0.0056	0.001209	0.000074	0.24726	7.79	0.48	20.2	1.3
	DOM_91M_6_14	0.023	0.0031	0.000584	0.000046	0.63939	3.76	0.3	21.6	0.0
	DOM_91M_6_15	0.0477	0.004	0.000722	0.000054	0.025189	4.65	0.34	28.3	0.1
	DOM_91M_6_16	0.0231	0.0034	0.000592	0.000053	0.73858	3.82	0.34	27.0	0.0
	DOM_91M_6_17	0.0106	0.0033	0.000469	0.000069	0.41555	3.02	0.45	14.9	0.0
	DOM_91M_6_18	0.0386	0.0046	0.000741	0.000067	0.77551	4.78	0.43	22.7	0.4
	DOM_91M_6_19	0.15	0.01	0.00158	0.00013	0.45781	10.18	0.81	11.2	1.3
	DOM_91M_6_20	0.156	0.011	0.001651	0.000099	0.30722	10.63	0.64	21.2	3.2
	DOM_91M_6_21	0.337	0.015	0.00335	0.00015	0.57614	21.54	0.94	17.5	1.6
	DOM_91M_6_22	0.112	0.011	0.00143	0.00012	0.8511	9.2	0.78	20.2	2.1
	DOM_91M_6_23	0.099	0.011	0.00126	0.00013	0.3524	8.14	0.81	10.7	1.7
	DOM_91M_6_24	0.0859	0.0091	0.00117	0.00014	0.19278	7.51	0.89	8.5	1.3
	DOM_91M_6_25	0.0577	0.0067	0.00098	0.00012	0.029234	6.3	0.76	8.3	1.4
	DOM_91M_6_26	0.213	0.014	0.00221	0.00016	0.019686	14.2	1	8.7	1.3
	DOM_91M_6_27	0.169	0.015	0.00167	0.00016	0.56892	10.7	1	8.8	0.2
	DOM_91M_6_28	0.0953	0.0084	0.00119	0.00013	0.40724	7.66	0.82	11.2	0.5
	DOM_91M_6_29	0.521	0.025	0.00463	0.00024	0.71344	29.7	1.5	18.2	1.3
	DOM_91M_6_30	0.0905	0.0062	0.001123	0.00009	0.23774	7.23	0.58	16.5	2.9
	DOM_91M_6_31	0.1546	0.0079	0.001702	0.000096	0.29336	10.96	0.61	20.3	0.9
	DOM_91M_6_32	0.1036	0.0062	0.001238	0.000078	0.25732	7.98	0.5	19.9	3.3
	DOM_91M_6_33	0.279	0.013	0.00284	0.00016	0.17698	18.3	1	18.2	3.1
	DOM_91M_6_34	0.958	0.033	0.00849	0.00032	0.62234	54.5	2	19.2	2.8
	DOM_91M_6_35	0.507	0.011	0.00453	0.00017	0.39902	29.1	1.1	26.2	2.9
	DOM_91M_6_36	3.01	0.21	0.0245	0.0018	0.093503	156	11	1.4	3.9
	DOM_91M_6_37	1.021	0.08	0.00914	0.0007	0.8579	58.6	4.5	9.3	1.0
	DOM_91M_6_38	0.135	0.011	0.00158	0.00012	0.59351	10.21	0.8	15.6	2.7
	DOM_91M_6_39	1.197	0.083	0.01014	0.00077	0.63782	65	4.9	8.6	0.7
	DOM_91M_6_40	0.1124	0.0065	0.001264	0.000073	0.1075	8.15	0.47	20.5	3.5
	DOM_91M_6_41	0.0414	0.0042	0.000767	0.000055	0.35281	4.94	0.35	20.8	2.7
	DOM_91M_6_42	0.111	0.0062	0.001376	0.000069	0.091975	8.86	0.44	21.2	3.6
	DOM_91M_6_43	0.0265	0.0029	0.000662	0.000054	0.081046	4.27	0.34	18.0	4.0
	DOM_91M_6_44	0.19	0.017	0.00185	0.00015	0.79127	11.94	0.97	12.3	0.4

		207Pb/235U	207Pb/235U error	206Pb/238U	206Pb/238U Error	Error Correlation 206/238 vs. 207/235	Final Age (Ma)	Error (Ma)	Approx U (ppm)	Approx Th (ppm)
	DOM_91M_6_45	0.129	0.011	0.00141	0.00011	0.24403	9.1	0.73	10.9	1.1
	DOM_91M_6_46	0.413	0.029	0.00408	0.00027	0.80217	26.2	1.8	16.8	2.4
	DOM_91M_6_47	0.0589	0.0075	0.00094	0.00011	0.58344	6.04	0.69	11.9	1.9
	DOM_91M_6_48	0.468	0.016	0.00439	0.0002	0.22148	28.3	1.3	10.4	0.6
	DOM_91M_6_49	0.403	0.023	0.00381	0.00024	0.24644	24.5	1.6	9.0	1.5
	DOM_91M_6_50	0.773	0.069	0.00682	0.00057	0.95431	43.8	3.7	15.0	4.9
DOM-100a	DOM100a_1	0.171	0.029	0.00159	0.00028	0.3039	10.2	1.8	2.1	0.5
	DOM100a_2	0.281	0.032	0.00283	0.00038	0.05383	18.2	2.5	1.8	0.3
	DOM100a_3	0.514	0.053	0.00498	0.00065	0.093861	32	4.2	1.0	0.9
	DOM100a_4	0.121	0.022	0.00145	0.00031	0.0028016	9.4	2	1.9	0.5
	DOM100a_5	0.559	0.054	0.00628	0.00069	0.17358	40.3	4.4	1.3	1.2
	DOM100a_6	0.134	0.023	0.00167	0.00034	0.017909	10.7	2.2	1.5	1.2
	DOM100a_7	0.128	0.013	0.00154	0.00017	0.1059	9.9	1.1	5.5	3.8
	DOM100a_8	0.144	0.021	0.00157	0.00026	0.036748	10.1	1.7	2.5	0.7
	DOM100a_9	0.102	0.017	0.00151	0.00023	0.75399	9.7	1.5	4.5	2.1
	DOM100a_10	0.368	0.062	0.0028	0.00076	0.051343	18	4.9	0.8	0.5
	DOM100a_11	0.216	0.028	0.00228	0.00029	0.020043	14.7	1.9	2.0	0.4
	DOM100a_12	0.98	0.14	0.0091	0.0014	0.37706	58.1	8.9	0.5	0.7
	DOM100a_13	0.214	0.023	0.00207	0.00033	0.16024	13.3	2.1	2.5	0.9
	DOM100a_14	1.18	0.14	0.0109	0.0018	0.42715	70	12	1.1	0.2
	DOM100a_15	0.301	0.013	0.00296	0.00017	0.27018	19.1	1.1	10.6	5.3
	DOM100a_16	0.137	0.023	0.00165	0.00028	0.0096882	10.6	1.8	1.9	1.2
	DOM100a_17	0.267	0.057	0.00265	0.00076	0.07228	17	4.9	0.6	0.5
	DOM100a_18	0.218	0.025	0.00235	0.00028	0.4319	15.1	1.8	3.6	1.6
	DOM100a_19	0.14	0.019	0.0016	0.00024	0.09424	10.3	1.6	3.3	1.1
	DOM100a_20	0.379	0.032	0.00369	0.00035	0.28382	23.7	2.3	2.9	2.0
	DOM100a_21	0.165	0.029	0.00161	0.00038	0.35422	10.3	2.4	1.7	1.5
	DOM100a_22	0.253	0.024	0.0026	0.00027	0.18651	16.7	1.7	2.9	1.3
	DOM100a_23	0.23	0.021	0.00212	0.00021	0.14354	13.6	1.3	4.8	1.7
	DOM100a_24	0.0446	0.0076	0.00093	0.00014	0.0606	5.97	0.9	4.0	1.7
	DOM100a_25	1.57	0.08	0.01346	0.00093	0.34165	86.1	5.9	1.9	0.7
	DOM100a_26	0.524	0.071	0.00642	0.00096	0.0067153	41.2	6.1	0.7	0.7
	DOM100a_27	3.42	0.18	0.0306	0.0016	0.35854	194	9.9	2.2	0.7
	DOM100a_28	0.431	0.044	0.0037	0.00041	0.3205	23.8	2.7	3.0	2.1
	DOM100a_29	0.241	0.03	0.00297	0.00049	0.1448	19.1	3.1	1.3	1.3
	DOM100a_30	0.793	0.03	0.00736	0.00031	0.27103	47.3	2	5.0	1.8
	DOM100a_31	0.106	0.015	0.00157	0.00028	0.059939	10.1	1.8	2.2	2.1
	DOM100a_32	0.333	0.035	0.00309	0.0004	0.19696	19.9	2.6	2.1	1.4
	DOM100a_33	0.082	0.014	0.00111	0.00021	0.13484	7.2	1.3	2.8	0.5
	DOM100a_34	2.437	0.085	0.0215	0.0011	0.43853	137.3	6.7	2.2	0.4
	DOM100a_35	0.27	0.025	0.00284	0.00036	0.098855	18.2	2.3	2.6	0.1
	DOM100a_36	0.368	0.048	0.00355	0.0005	0.44966	22.8	3.2	2.1	0.4
	DOM100a_37	0.147	0.019	0.00174	0.00026	0.049708	11.2	1.7	2.9	0.5
	DOM100a_38	0.184	0.022	0.00193	0.00026	0.54578	12.5	1.7	3.2	0.4
	DOM100a_39	0.431	0.039	0.00418	0.00052	0.14	26.9	3.3	1.6	0.8
	DOM100a_40	0.093	0.012	0.00125	0.00019	0.11388	8.1	1.2	3.3	0.4
	DOM100a_41	0.585	0.082	0.0058	0.001	0.16209	37.5	6.6	0.6	0.8
	DOM100a_42	0.498	0.073	0.00457	0.00082	0.10685	29.3	5.3	0.7	0.8
	DOM100a_43	0.103	0.016	0.00127	0.00024	0.045059	8.2	1.6	2.6	0.5
	DOM100a_44	1.64	0.22	0.016	0.0023	0.60207	102	14	0.5	0.5
	DOM100a_45	0.396	0.045	0.00354	0.0004	0.69768	22.8	2.5	5.1	3.3
	DOM100a_46	2.06	0.22	0.017	0.0021	0.046695	108	13	1.4	1.0
	DOM100a_47	1.234	0.047	0.01006	0.00034	0.53609	64.5	2.2	9.8	4.4
	DOM100a_48	0.202	0.033	0.00267	0.00054	0.020001	17.5	3.5	1.2	1.0
	DOM100a_49	1.67	0.16	0.0145	0.0014	0.86409	92.3	8.7	2.2	0.5
	DOM100a_50	1.13	0.12	0.0083	0.0011	0.60503	53.4	6.9	1.1	1.0
KL20-04-373m	KL_1	20.3	1.7	0.169	0.015	0.98439	993	79	7.2	4.7
	KL_2	28.5	3.2	0.226	0.024	0.97443	1280	120	7.2	4.4
	KL_3	14.5	1.2	0.1151	0.0098	0.97498	695	55	10.7	3.4
	KL_4	24.1	2.4	0.199	0.02	0.97838	1140	100	4.3	2.6
	KL_5	14.43	0.66	0.1178	0.005	0.96502	716	28	9.5	4.0
	KL_6	15.9	1.6	0.131	0.013	0.98601	780	75	9.2	5.2

		207Pb/235U	207Pb/235U error	206Pb/238U	206Pb/238U Error	Error Correlation 206/238 vs. 207/235	Final Age (Ma)	Error (Ma)	Approx U (ppm)	Approx Th (ppm)
	KL_7	22.8	1.7	0.177	0.012	0.92999	1048	66	8.4	3.9
	KL_8	13.2	1	0.1087	0.009	0.95047	664	52	4.9	5.2
	KL_9	21.6	2	0.171	0.015	0.96133	1003	81	4.6	3.5
	KL_10	2.6	0.28	0.0219	0.0023	0.97462	139	14	4.4	2.5
	KL_11	0.381	0.055	0.00343	0.00036	0.040299	22.1	2.3	6.0	1.4
	KL_12	3.34	0.34	0.028	0.0029	0.9668	177	18	6.0	5.9
	KL_13	17.5	1.7	0.142	0.014	0.98169	844	76	4.1	3.9
	KL_14	39.8	2.8	0.324	0.023	0.97517	1780	110	5.9	4.4
	KL_15	18.5	1.3	0.152	0.011	0.98304	902	60	7.1	3.2
	KL_16	8.7	1.3	0.072	0.011	0.98645	438	62	5.6	3.7
	KL_17	27.5	2.6	0.223	0.021	0.98639	1270	100	5.9	7.4
	KL_18	20.2	1	0.1662	0.0084	0.97544	986	46	6.1	4.8
	KL_19	0.393	0.057	0.00376	0.00047	0.64849	24.1	3	3.8	2.4
	KL_20	1.58	0.29	0.0132	0.0023	0.98598	84	15	9.1	5.9
	KL_21	28.6	4	0.232	0.032	0.93905	1290	160	10.4	3.9
	KL_22	10.43	0.83	0.0846	0.0064	0.98213	513	34	17.5	9.2
	KL_23	21.9	2.7	0.182	0.021	0.99076	1050	110	11.6	3.8
	KL_24	82.2	5.8	0.698	0.06	0.9934	3280	170	6.1	4.1
	KL_25	18.3	2.4	0.151	0.02	0.95698	852	98	3.8	3.1
	KL_26	23.2	1.7	0.187	0.013	0.9641	1105	72	5.6	3.5
	KL_27	1.49	0.15	0.01161	0.00089	0.1946	74.4	5.7	11.8	9.8
	KL_28	1.674	0.09	0.0146	0.00085	0.86138	93.4	5.4	10.9	14.0
	KL_29	22.2	2	0.187	0.017	0.9708	1086	94	4.1	4.5
	KL_30	47.8	4.3	0.397	0.035	0.9714	2100	160	4.8	4.5
	KL_31	1.3	0.27	0.0121	0.0024	0.99114	77	15	5.0	4.3
	KL_32	4	1.1	0.0326	0.0083	0.99801	190	42	11.1	14.8
	KL_33	1.61	0.3	0.013	0.0023	0.98153	83	14	7.5	2.6
	KL_34	0.65	0.091	0.00561	0.0008	0.84343	36	5.1	4.6	15.2
	KL_35	0.89	0.11	0.00775	0.00091	0.88641	49.7	5.8	4.4	2.6
	KL_36	16.3	1.8	0.13	0.014	0.99428	776	76	4.6	6.8
	KL_37	9.96	0.74	0.0784	0.0054	0.96856	484	32	4.4	5.7
	KL_38	7	1.9	0.057	0.015	0.97904	340	83	4.6	3.4
	KL_39	32.8	4.2	0.271	0.035	0.9969	1480	160	8.2	3.1
	KL_40	4.61	0.54	0.0373	0.0044	0.95988	234	27	4.9	2.7
	KL_41	32.8	2.7	0.259	0.02	0.98675	1460	100	8.8	3.8
	KL_42	18	2.9	0.152	0.024	0.95641	880	120	6.2	5.5
	KL_43	19.1	3.5	0.16	0.029	0.98805	900	150	3.7	2.5
	KL_44	1.32	0.11	0.01101	0.00085	0.87137	70.5	5.4	7.7	4.3
	KL_45	6.1	0.62	0.0502	0.005	0.96651	314	30	3.5	3.7
	KL_46	1.9	0.22	0.016	0.0018	0.98587	102	11	13.1	0.7
	KL_47	5.14	0.56	0.0419	0.0046	0.98554	263	28	10.4	5.2
DMLZITL3-02	DMLZ_1	0.583	0.079	0.00508	0.00069	0.15829	-	-	1.2	0.0
119m	DMLZ_2	0.022	0.017	0.00064	0.00031	0.028778	-	-	1.8	0.1
	DMLZ_3	0.118	0.041	0.00108	0.00052	0.056882	-	-	0.9	0.0
	DMLZ_4	0.129	0.044	0.0006	0.00054	0.17904	-	-	0.9	0.0
	DMLZ_5	0.09	0.02	0.00131	0.00033	0.35818	-	-	2.2	0.0
	DMLZ_6	0.161	0.042	0.00252	0.00054	0.019524	-	-	1.5	0.0
	DMLZ_7	0.27	0.34	0.00098	0.00033	0.0061489	-	-	2.0	0.0
	DMLZ_8	1.65	0.19	0.0125	0.0016	0.66607	-	-	0.9	0.0
	DMLZ_9	0.191	0.061	0.00206	0.00074	0.17548	-	-	0.9	0.0
	DMLZ_10	0.317	0.091	0.003	0.0011	0.024477	-	-	0.5	0.0
	DMLZ_11	0.08	0.04	0.00103	0.00055	0.03017	-	-	1.0	0.0
	DMLZ_12	0.164	0.024	0.00195	0.00032	0.50741	-	-	3.2	0.0
	DMLZ_13	0.17	0.032	0.00162	0.00028	0.53196	-	-	2.8	0.0
	DMLZ_14	0.08	0.027	0.00081	0.00038	0.12282	-	-	1.7	0.0
	DMLZ_15	0.094	0.043	0.0008	0.0005	0.12796	-	-	1.1	0.0
	DMLZ_16	0.182	0.037	0.00165	0.00039	0.026143	-	-	1.9	0.0
	DMLZ_17	0.033	0.018	0.00105	0.00033	0.17898	-	-	2.4	0.0
	DMLZ_18	0.048	0.02	0.00088	0.00027	0.070189	-	-	2.5	0.0
	DMLZ_19	0.29	0.14	0.0039	0.0022	0.0010801	-	-	1.6	0.0
	DMLZ_20	0.68	0.14	0.0071	0.0011	0.1602	-	-	0.8	0.0
	DMLZ_21	0.248	0.063	0.00211	0.00074	0.27627	-	-	0.9	0.0
	DMLZ_22	0.131	0.045	0.00163	0.00063	0.20871	-	-	1.2	0.0

		207Pb/235U	207Pb/235U error	206Pb/238U	206Pb/238U Error	Error Correlation 206/238 vs. 207/235	Final Age (Ma)	Error (Ma)	Approx U (ppm)	Approx Th (ppm)
	DMLZ_23	0.062	0.037	0.00098	0.00044	0.069089	-	-	1.2	0.0
	DMLZ_24	0.55	0.064	0.0043	0.00083	0.041124	-	-	1.1	0.0
	DMLZ_25	0.019	0.038	0.00092	0.00059	0.19489	-	-	1.0	0.0
	DMLZ_26	0.055	0.03	0.00055	0.00048	0.12347	-	-	1.5	0.0
	DMLZ_27	0.107	0.047	0.00073	0.00069	0.28737	-	-	0.8	0.0
	DMLZ_28	0.05	0.031	0.00076	0.00043	0.090808	-	-	1.3	0.0
	DMLZ_29	0.14	0.05	0.00038	0.00061	0.058428	-	-	1.0	0.0
	DMLZ_30	0.534	0.052	0.00607	0.00068	0.089911	-	-	1.4	0.0
	DMLZ_31	3.98	0.31	0.031	0.0028	0.018928	-	-	0.5	0.0
	DMLZ_32	0.286	0.056	0.00222	0.0006	0.18205	-	-	1.0	0.0
	DMLZ_33	0.102	0.034	0.00113	0.00041	0.072153	-	-	1.4	0.0
	DMLZ_34	0.066	0.021	0.001	0.00031	0.023048	-	-	2.5	0.0
	DMLZ_35	0.39	0.046	0.00366	0.00062	0.37031	-	-	1.7	0.0
	DMLZ_36	0.049	0.023	0.00116	0.00047	0.33242	-	-	1.5	0.0
	DMLZ_37	0.026	0.037	0.00054	0.00053	0.01436	-	-	0.9	0.0
	DMLZ_38	0.037	0.023	0.00055	0.00033	0.072638	-	-	1.7	0.0
	DMLZ_39	0.178	0.035	0.00129	0.00039	0.15693	-	-	1.7	0.0
	DMLZ_40	0.074	0.016	0.00127	0.00024	0.24997	-	-	3.0	0.1
	DMLZ_41	0.135	0.018	0.00177	0.00022	0.1306	-	-	3.6	0.1
	DMLZ_42	0.807	0.052	0.0066	0.00052	0.30359	-	-	2.0	0.0
	DMLZ_43	0.777	0.087	0.0068	0.001	0.64224	-	-	1.2	0.0
	DMLZ_44	0.203	0.017	0.00232	0.00022	0.027834	-	-	4.7	0.1
	DMLZ_45	0.149	0.018	0.00149	0.00022	0.062042	-	-	4.1	0.2
	DMLZ_46	0.283	0.042	0.00296	0.00046	0.0059113	-	-	1.7	0.0
	DMLZ_47	0.143	0.017	0.00169	0.00018	0.036494	-	-	4.4	0.1
	DMLZ_48	0.0187	0.0083	0.00044	0.00015	0.17584	-	-	4.3	0.1
	DMLZ_49	0.192	0.042	0.00225	0.00054	0.53735	-	-	1.5	0.0
GB24-01 382m	GB24_01_1	0.82	0.1	0.0091	0.0014	0.11432	-	-	0.5	0.0
	GB24_01_2	0.238	0.08	0.0033	0.0013	0.13575	-	-	0.4	0.0
	GB24_01_3	1.32	0.13	0.0118	0.0014	0.35046	-	-	0.7	0.1
	GB24_01_4	1.03	0.13	0.0066	0.0012	0.1125	-	-	0.6	0.1
	GB24_01_5	1.28	0.12	0.0116	0.0012	0.32477	-	-	0.9	0.1
	GB24_01_6	4.4	0.33	0.0372	0.0026	0.43704	-	-	0.6	0.1
	GB24_01_7	1.61	0.19	0.0141	0.0018	0.1264	-	-	0.5	0.0
	GB24_01_8	0.43	0.16	0.0016	0.0015	0.18926	-	-	0.4	0.0
	GB24_01_9	0.82	0.1	0.0054	0.0012	0.092855	-	-	0.6	0.1
	GB24_01_10	3.2	0.24	0.0295	0.0027	0.22489	-	-	0.4	0.0
	GB24_01_11	0.298	0.079	0.00368	0.00086	0.12581	-	-	0.7	0.1
	GB24_01_12	0.03	0.11	0.0028	0.0015	0.0089354	-	-	0.3	0.0
	GB24_01_13	1.11	0.15	0.0089	0.0017	0.14422	-	-	0.4	0.1
	GB24_01_14	0.21	0.15	0.0014	0.0017	0.087792	-	-	0.3	0.0
	GB24_01_15	1.14	0.24	0.0124	0.0024	0.25352	-	-	0.3	0.0
	GB24_01_16	2.84	0.44	0.0201	0.0044	0.26843	-	-	0.1	0.0
	GB24_01_17	7.82	0.77	0.0656	0.007	0.39259	-	-	0.2	0.0
	GB24_01_18	4.73	0.5	0.0379	0.0038	0.054425	-	-	0.3	0.0
	GB24_01_19	2.09	0.5	0.02	0.0053	0.57932	-	-	0.2	0.0
	GB24_01_20	1.96	0.36	0.0206	0.0039	0.052238	-	-	0.2	0.0
	GB24_01_21	2.71	0.83	0.0197	0.0062	0.024828	-	-	0.1	0.0
	GB24_01_22	7.69	0.76	0.0512	0.0067	0.51104	-	-	0.2	0.0
	GB24_01_23	3.07	0.4	0.0278	0.0051	0.05939	-	-	0.2	0.0
	GB24_01_24	5.24	0.46	0.0475	0.0049	0.44683	-	-	0.2	0.0
	GB24_01_25	3.18	0.45	0.0242	0.0047	0.34625	-	-	0.2	0.0
	GB24_01_26	2.67	0.32	0.0204	0.0033	0.21439	-	-	0.3	0.0
	GB24_01_27	2.15	0.39	0.0191	0.0047	0.41547	-	-	0.2	0.0
	GB24_01_28	3.96	0.61	0.0334	0.0062	0.39301	-	-	0.2	0.0
	GB24_01_29	25.9	2.6	0.216	0.022	0.90509	-	-	0.2	0.0
	GB24_01_30	23.6	1.9	0.213	0.02	0.85396	-	-	0.2	0.0
	GB24_01_31	0.66	0.1	0.0076	0.0011	0.23649	-	-	0.6	0.1
	GB24_01_32	0.789	0.073	0.0072	0.001	0.12681	-	-	1.0	0.1
	GB24_01_33	1.5	0.23	0.0157	0.0034	0.14545	-	-	0.2	0.0
	GB24_01_34	0.86	0.15	0.0081	0.0018	0.13536	-	-	0.4	0.0
	GB24_01_35	0.814	0.096	0.0082	0.0012	0.039523	-	-	1.0	0.1
	GB24_01_36	2.24	0.32	0.0215	0.0036	0.17399	-	-	0.4	0.0

	207Pb/235U	207Pb/235U error	206Pb/238U	206Pb/238U Error	Error Correlation 206/238 vs. 207/235	Final Age (Ma)	Error (Ma)	Approx U (ppm)	Approx Th (ppm)
GB24_01_37	1.26	0.11	0.0109	0.0013	0.022485	-	-	0.9	0.1
GB24_01_38	1.07	0.13	0.0085	0.0015	0.01938	-	-	0.6	0.1
GB24_01_39	1.79	0.28	0.0153	0.0023	0.041782	-	-	0.5	0.1
GB24_01_40	1.5	0.16	0.0123	0.0017	0.71483	-	-	0.8	0.1
GB24_01_41	3.02	0.44	0.0235	0.004	0.4304	-	-	0.2	0.0

Appendix M: Garnet Rare Earth Element Results

The following table contains the garnet rare earth element results for samples dates using the new garnet U/Pb LA-ICP-MS method. Trace elements were measured using a the same LA-ICP-MS instrumental setup. Rare earth element results are reported in ppm.

	La (ppm)	La Int2SE	Ce (ppm)	Ce Int2SE	Pr (ppm)	Pr Int2SE	Nd (ppm)	Nd Int2SE	Sm (ppm)	Sm Int2SE	Eu (ppm)	Eu Int2SE	Gd (ppm)	Gd Int2SE
BG240W_1	12.76	0.56	30.3	1.3	2.52	0.15	4.99	0.41	0.208	0.092	1.19	0.13	-0.24	0.14
BG240W_2	10	0.55	26.9	1.3	2.25	0.14	4.73	0.41	0.228	0.089	1.13	0.1	0.03	0.18
BG240W_3	10.99	0.48	29	1	2.6	0.11	5.61	0.34	0.286	0.089	1.26	0.11	0.05	0.2
BG240W_4	12.77	0.6	31.6	1.6	2.44	0.13	5.46	0.4	0.23	0.1	1.2	0.14	0.2	0.16
BG240W_5	13.28	0.53	31	1.4	2.57	0.13	5.52	0.42	0.353	0.088	1.04	0.11	0.18	0.15
BG240W_6	12.01	0.48	34.5	1.6	3.45	0.14	8.48	0.54	0.239	0.098	1.7	0.17	0.13	0.19
BG240W_7	11.71	0.62	30.9	1.5	2.93	0.18	6.56	0.47	0.41	0.13	1.5	0.15	0.14	0.18
BG240W_8	10.63	0.47	26.3	1.2	2.13	0.11	4.56	0.38	0.252	0.096	1	0.11	0.11	0.21
BG240W_9	10.12	0.47	26.5	1.1	2.21	0.12	5.2	0.46	0.28	0.1	1.22	0.13	0.19	0.2
BG240W_10	7.39	0.34	44.1	1.5	9.59	0.35	48.4	2.1	5.3	0.47	8.64	0.39	1.38	0.27
BG240W_11	14.5	0.71	37.7	1.7	2.69	0.14	5.41	0.46	0.97	0.16	1.53	0.14	1.07	0.29
BG240W_12	14.95	0.79	44.9	1.8	3.9	0.2	7.47	0.51	1.15	0.2	2.22	0.2	1.08	0.25
BG240W_13	8.24	0.43	49	2.4	9.44	0.35	45.5	2	4.09	0.28	8.07	0.35	1.48	0.29
BG240W_14	7.22	0.45	29.6	1.4	4.33	0.25	12.91	0.73	0.86	0.17	2.91	0.15	0.47	0.17
BG240W_15	11.75	0.41	32.5	1.1	2.81	0.14	8.45	0.61	1.83	0.26	1.46	0.14	2.1	0.28
BG240W_16	10.68	0.51	32.8	1.1	2.56	0.13	4.27	0.35	0.34	0.11	1.71	0.15	0.2	0.18
BG240W_17	15.54	0.72	55.8	2.2	5.89	0.28	13	0.75	0.85	0.13	3.63	0.24	0.35	0.21
BG240W_18	3.73	0.28	11.26	0.73	0.727	0.065	1.86	0.26	0.41	0.14	0.44	0.057	0.36	0.21
BG240W_19	9.59	0.4	53.3	2.1	9.56	0.39	38.9	1.6	2.77	0.3	7.55	0.4	1.27	0.2
BG240W_20	7.04	0.33	42.9	1.6	9.28	0.33	47.6	1.8	4.76	0.46	8.67	0.42	1.86	0.36
DOM91M_1	7.29	0.36	42.7	2	7.58	0.35	35.7	1.6	5.7	0.55	1.8	0.16	2.75	0.28
DOM91M_2	8.8	0.31	48.8	1.9	8.37	0.43	39.5	1.8	5.79	0.39	1.98	0.14	2.89	0.35
DOM91M_3	9.45	0.52	48.8	2	8.47	0.34	35.7	1.5	4.73	0.37	1.91	0.16	1.93	0.26
DOM91M_4	5.48	0.33	32.7	1.6	6.34	0.26	32.3	1.3	6.99	0.46	1.71	0.2	5.2	0.48
DOM91M_5	2.34	0.16	13.56	0.76	2.19	0.15	13.47	0.9	4.94	0.52	2.01	0.14	4.03	0.43
DOM91M_6	1.73	0.11	14.84	0.71	3.2	0.16	22.7	1.3	8.49	0.51	3.19	0.2	7.61	0.66
DOM91M_7	3.22	0.2	25.1	1.1	4.39	0.2	18.35	0.85	3.19	0.36	1.44	0.13	1.9	0.34
DOM91M_8	3.37	0.28	21.5	1.4	4.51	0.27	25.8	1.5	7.79	0.58	2.46	0.2	6.61	0.44
DOM91M_9	2.32	0.17	17.4	1.1	3.94	0.19	24.79	0.97	8.73	0.6	2.89	0.26	6.97	0.6
DOM91M_10	2.85	0.19	17.2	1	2.85	0.2	15.78	0.79	4.18	0.4	1.45	0.15	2.85	0.42
DOM91M_11	1.064	0.074	14.05	0.72	4.39	0.24	32.4	1.9	6.47	0.5	3.81	0.22	2.32	0.24
DOM91M_12	0.929	0.075	14.03	0.6	5.04	0.27	38.6	1.9	7.92	0.64	4.87	0.26	1.96	0.33
DOM91M_13	1.027	0.098	14.69	0.73	5.37	0.24	38.1	1.3	7.34	0.54	5.09	0.29	1.97	0.24
DOM91M_14	0.833	0.071	12.07	0.53	4.24	0.23	30.6	1.3	5.87	0.5	4.24	0.29	1.54	0.33
DOM91M_15	3.29	0.18	21.42	0.92	4.44	0.2	25.3	1.2	7.78	0.39	3.3	0.19	6.72	0.66
DOM91M_16	3.29	0.18	23.7	1	5.02	0.25	25.7	1.4	4.45	0.36	1.95	0.13	1.79	0.22
DOM91M_17	2.35	0.18	21.2	0.78	4.5	0.14	22.19	0.96	4.49	0.55	1.28	0.12	2.11	0.38
DOM91M_18	2.63	0.18	23.5	1.3	4.7	0.2	21	1.1	2.18	0.31	1.2	0.1	0.88	0.22
DOM91M_19	1.717	0.097	14.53	0.64	3.48	0.2	25.2	1.5	10.96	0.77	4.66	0.32	9.7	0.64
DOM91M_20	1.68	0.12	12.75	0.49	3.15	0.13	21.23	0.95	8.59	0.51	2.4	0.19	7.18	0.6
DOM100a_1	0.235	0.034	4.07	0.26	1.523	0.094	11.58	0.67	3.16	0.38	1.65	0.15	1.41	0.27
DOM100a_2	0.203	0.041	3.05	0.17	1.225	0.081	10.33	0.55	3.46	0.4	1.46	0.13	2	0.34
DOM100a_3	0.176	0.03	3.13	0.23	1.051	0.079	7.57	0.47	2.59	0.32	0.915	0.099	1.3	0.28
DOM100a_4	0.032	0.024	0.959	0.064	0.471	0.049	4.79	0.37	2.41	0.31	0.79	0.12	1.95	0.36
DOM100a_5	0.537	0.062	6.87	0.33	2.06	0.12	15.19	0.95	5.95	0.59	3.27	0.24	4.88	0.58
DOM100a_6	0.357	0.046	4.93	0.28	1.53	0.11	11.64	0.82	3.74	0.35	1.89	0.17	2.55	0.37
DOM100a_7	0.793	0.099	9.13	0.59	2.89	0.2	23.3	1.4	6.14	0.46	2.49	0.17	3.6	0.53
DOM100a_8	1.073	0.063	14.9	0.71	5.05	0.23	36.7	1.7	9.96	0.73	3.83	0.21	6.88	0.63
DOM100a_9	0.058	0.028	1.043	0.072	0.419	0.043	3.65	0.3	1.99	0.3	0.705	0.098	1.53	0.37
DOM100a_10	0.036	0.018	0.961	0.064	0.419	0.044	4.7	0.43	2.5	0.34	0.721	0.093	1.34	0.34
DOM100a_11	0.38	0.057	6.54	0.3	1.446	0.077	7.52	0.54	1.3	0.23	0.67	0.12	0.7	0.24
DOM100a_12	0.51	0.046	7.39	0.33	1.73	0.1	7.23	0.62	0.51	0.14	0.417	0.082	0.29	0.18

	Tb (ppm)	Tb Int2SE	Dy (ppm)	Dy Int2SE	Ho (ppm)	Ho Int2SE	Er (ppm)	Er Int2SE	Tm (ppm)	Tm Int2SE	Yb (ppm)	Yb Int2SE	Lu (ppm)	Lu Int2SE	Hf (ppm)	Hf Int2SE
BG240W_1	0.009	0.012	-0.022	0.043	-0.0028	0.0056	0.016	0.056	-0.0065	0.0052	0.04	0.049	0.006	0.01	-0.011	0.046
BG240W_2	0.003	0.01	0.017	0.04	0.0045	0.0073	-0.024	0.051	0.0011	0.006	-0.018	0.043	-0.0073	0.004	-0.009	0.05
BG240W_3	0.029	0.015	0.043	0.05	0.0026	0.0082	-0.049	0.046	0.008	0.011	-0.016	0.036	0.0007	0.0093	-0.009	0.054
BG240W_4	0.004	0.013	0.046	0.055	0.0031	0.0086	0.044	0.06	-0.001	0.0068	-0.013	0.035	0.0071	0.0087	0.01	0.05
BG240W_5	0.024	0.014	0.151	0.065	0.015	0.01	0.055	0.043	0.0036	0.0088	0.004	0.044	0.006	0.01	0.034	0.059
BG240W_6	0.013	0.012	0.043	0.05	0.0093	0.0098	0.047	0.054	0.0083	0.0085	0.008	0.037	-0.0051	0.0055	-0.01	0.044
BG240W_7	0.017	0.014	0.053	0.055	0.0011	0.0061	0.007	0.049	-0.0032	0.0062	0.042	0.051	0.0006	0.0079	-0.011	0.042
BG240W_8	0.001	0.01	0.033	0.047	0.0038	0.0076	0.005	0.047	-0.0007	0.0076	0.003	0.048	-0.0009	0.0066	-0.013	0.042
BG240W_9	0.009	0.012	0.115	0.074	0.0044	0.0073	0.007	0.049	0.0004	0.0088	0.053	0.053	0.0089	0.0098	0.138	0.084
BG240W_10	0.126	0.033	0.38	0.12	0.089	0.02	0.173	0.072	0.023	0.01	0.068	0.055	0.017	0.012	-0.04	0.029
BG240W_11	0.159	0.033	0.9	0.13	0.184	0.023	0.55	0.1	0.058	0.018	0.36	0.093	0.044	0.017	0.234	0.074
BG240W_12	0.123	0.027	0.92	0.13	0.19	0.027	0.57	0.11	0.07	0.02	0.415	0.099	0.061	0.017	0.125	0.052
BG240W_13	0.185	0.038	0.82	0.12	0.197	0.035	0.58	0.12	0.043	0.019	0.315	0.094	0.058	0.022	0.117	0.072
BG240W_14	0.08	0.021	0.61	0.12	0.098	0.023	0.317	0.063	0.046	0.015	0.387	0.087	0.05	0.019	0.55	0.11
BG240W_15	0.321	0.044	2.33	0.28	0.498	0.047	1.55	0.15	0.216	0.033	1.42	0.18	0.173	0.03	0.47	0.1
BG240W_16	0.018	0.014	0.129	0.051	0.017	0.013	0.111	0.063	0.0045	0.0076	0.064	0.038	0.014	0.01	0.217	0.082
BG240W_17	0.072	0.02	0.62	0.11	0.119	0.027	0.287	0.097	0.048	0.018	0.199	0.074	0.014	0.015	0.156	0.061
BG240W_18	0.047	0.014	0.291	0.064	0.048	0.015	0.092	0.049	0.0172	0.0091	0.165	0.068	0.028	0.012	0.36	0.1
BG240W_19	0.146	0.028	1.02	0.14	0.169	0.038	0.49	0.12	0.065	0.022	0.295	0.083	0.055	0.018	0.11	0.071
BG240W_20	0.21	0.036	1.22	0.19	0.201	0.029	0.378	0.088	0.053	0.021	0.298	0.093	0.038	0.013	0.04	0.054
DOM91M_1	0.313	0.045	1.44	0.16	0.151	0.027	0.5	0.12	0.047	0.016	0.426	0.099	0.076	0.022	0.15	0.066
DOM91M_2	0.282	0.04	1.36	0.19	0.137	0.028	0.461	0.077	0.057	0.02	0.28	0.086	0.057	0.018	0.116	0.066
DOM91M_3	0.225	0.036	0.92	0.14	0.127	0.025	0.272	0.058	0.042	0.016	0.259	0.072	0.066	0.019	0.032	0.051
DOM91M_4	0.695	0.065	3.29	0.32	0.525	0.062	1.24	0.18	0.152	0.029	0.9	0.14	0.137	0.034	0.281	0.088
DOM91M_5	0.532	0.079	2.7	0.33	0.428	0.05	0.95	0.14	0.095	0.025	0.63	0.12	0.083	0.025	0.089	0.054
DOM91M_6	0.947	0.067	5.21	0.4	0.823	0.076	1.86	0.17	0.206	0.03	1.29	0.15	0.166	0.028	0.384	0.087
DOM91M_7	0.257	0.042	1.01	0.16	0.134	0.031	0.235	0.063	0.0236	0.0098	0.204	0.075	0.014	0.0088	0.08	0.049
DOM91M_8	0.99	0.081	5.4	0.41	0.852	0.053	2.12	0.2	0.336	0.044	1.79	0.22	0.183	0.033	0.81	0.15
DOM91M_9	1.06	0.1	5.76	0.45	1.069	0.09	2.58	0.24	0.367	0.044	2.18	0.22	0.3	0.046	1.12	0.17
DOM91M_10	0.346	0.039	1.64	0.24	0.197	0.025	0.399	0.093	0.05	0.015	0.31	0.11	0.04	0.013	0.102	0.053
DOM91M_11	0.15	0.033	0.5	0.1	0.045	0.012	0.155	0.072	0.0097	0.0082	0.137	0.068	0.0124	0.0093	0.107	0.073
DOM91M_12	0.112	0.026	0.308	0.086	0.023	0.013	0.046	0.051	-0.0032	0.0059	-0.025	0.031	0.0072	0.0094	0.003	0.058
DOM91M_13	0.128	0.03	0.194	0.067	0.011	0.013	0.041	0.049	-0.0032	0.0053	0.017	0.045	0.0052	0.0094	-0.008	0.052
DOM91M_14	0.12	0.018	0.287	0.093	0.035	0.018	0.102	0.064	0.0012	0.0066	0.045	0.047	0.006	0.0073	0.012	0.052
DOM91M_15	0.945	0.088	5.21	0.44	0.96	0.1	2.26	0.27	0.259	0.041	1.74	0.3	0.232	0.042	1.58	0.3
DOM91M_16	0.125	0.028	0.435	0.094	0.039	0.012	0.109	0.055	0.0017	0.0067	0.043	0.054	0.0056	0.0066	0.027	0.045
DOM91M_17	0.153	0.031	0.74	0.17	0.087	0.022	0.184	0.059	0.02	0.011	0.23	0.079	0.033	0.012	1.51	0.22
DOM91M_18	0.095	0.022	0.54	0.13	0.078	0.015	0.197	0.062	0.023	0.012	0.108	0.057	0.021	0.013	0.66	0.14
DOM91M_19	1.311	0.097	6.81	0.4	1.04	0.093	2.33	0.22	0.254	0.035	1.64	0.19	0.218	0.032	0.55	0.1
DOM91M_20	1.054	0.072	5.89	0.38	1.096	0.087	2.57	0.23	0.316	0.038	2.07	0.21	0.295	0.034	1.9	0.22
DOM100a_1	0.121	0.026	0.56	0.1	0.086	0.019	0.25	0.078	0.036	0.014	0.098	0.058	0.036	0.013	0.43	0.11
DOM100a_2	0.194	0.034	1.06	0.16	0.137	0.02	0.248	0.078	0.049	0.016	0.22	0.084	0.011	0.011	0.081	0.065
DOM100a_3	0.099	0.029	0.54	0.1	0.063	0.018	0.074	0.046	0.012	0.011	0.112	0.068	0.0072	0.0084	0.033	0.05
DOM100a_4	0.204	0.024	0.93	0.13	0.124	0.023	0.244	0.086	0.028	0.015	0.055	0.055	0.012	0.0093	0.031	0.051
DOM100a_5	0.612	0.06	3.12	0.32	0.516	0.061	1.2	0.13	0.123	0.026	0.99	0.16	0.129	0.035	0.47	0.11
DOM100a_6	0.277	0.035	1.38	0.16	0.172	0.026	0.57	0.11	0.059	0.017	0.42	0.1	0.065	0.019	0.588	0.097
DOM100a_7	0.47	0.052	2.18	0.17	0.459	0.061	1.22	0.15	0.168	0.036	1.46	0.21	0.212	0.033	4.71	0.38
DOM100a_8	0.819	0.069	4.13	0.36	0.638	0.056	1.52	0.15	0.208	0.039	1.33	0.24	0.172	0.034	1.41	0.16
DOM100a_9	0.168	0.036	0.91	0.15	0.112	0.027	0.306	0.086	0.042	0.017	0.196	0.097	0.031	0.016	0.066	0.085
DOM100a_10	0.119	0.031	0.478	0.089	0.062	0.019	0.092	0.056	0.0037	0.0078	-0.023	0.038	0.0083	0.0099	-0.039	0.048
DOM100a_11	0.048	0.017	0.281	0.09	0.03	0.013	0.044	0.043	0.016	0.011	0.096	0.058	0.0035	0.0076	0.034	0.065
DOM100a_12	0.01	0.011	-0.023	0.032	0.0095	0.0086	0.023	0.048	0.0084	0.0088	0.03	0.058	0.0046	0.0066	0.056	0.054

	La (ppm)	La Int2SE	Ce (ppm)	Ce Int2SE	Pr (ppm)	Pr Int2SE	Nd (ppm)	Nd Int2SE	Sm (ppm)	Sm Int2SE	Eu (ppm)	Eu Int2SE	Gd (ppm)	Gd Int2SE
DOM100a_13	0.323	0.049	3.55	0.39	1.11	0.14	8.6	1.1	4.34	0.6	1.98	0.28	3.22	0.59
DOM100a_14	0.112	0.035	1.98	0.17	0.716	0.068	6.09	0.44	2.36	0.33	0.84	0.11	0.97	0.23
DOM100a_15	0.313	0.051	4.61	0.23	1.588	0.097	12.21	0.72	3.49	0.39	1.78	0.16	2.1	0.44
DOM100a_16	0.112	0.029	2.15	0.16	0.997	0.076	9.52	0.66	3.27	0.39	1.71	0.15	1.75	0.36
DOM100a_17	0.053	0.025	1.47	0.11	0.66	0.068	6.87	0.5	2.67	0.33	1.55	0.12	1.7	0.3
DOM100a_18	0.05	0.024	1.002	0.096	0.424	0.062	4.95	0.43	2.55	0.36	0.678	0.079	1.22	0.31
DOM100a_19	0.058	0.027	0.849	0.071	0.406	0.046	4.02	0.28	2.25	0.27	0.57	0.11	1.55	0.3
DOM100a_20	0.289	0.039	4.2	0.32	1.056	0.071	6.83	0.46	2.63	0.39	1.42	0.16	2.26	0.4
EESS_1	9.28	0.41	23.89	0.98	2.019	0.096	4.91	0.46	0.228	0.08	2.04	0.18	-0.11	0.17
EESS_2	8.42	0.4	8.9	0.37	0.506	0.053	0.93	0.16	0.079	0.055	0.295	0.09	0	0.18
EESS_3	9.6	0.43	18.58	0.98	1.287	0.086	2.37	0.27	0.133	0.055	0.97	0.11	0.3	0.18
EESS_4	8.77	0.47	21.2	1.2	1.837	0.084	4.47	0.34	0.276	0.095	1.97	0.16	0.13	0.19
EESS_5	5.62	0.25	17.92	0.54	2.09	0.11	6.73	0.46	0.69	0.17	2.75	0.15	0.38	0.24
EESS_6	9.02	0.47	11.07	0.56	0.612	0.048	1.01	0.21	0.019	0.04	0.444	0.09	-0.01	0.12
EESS_7	11.91	0.69	18	0.9	1.219	0.087	2.74	0.36	0.166	0.083	0.764	0.09	0.08	0.15
EESS_8	12.37	0.77	15.79	0.87	0.842	0.068	1.44	0.26	0.167	0.083	0.54	0.12	0.09	0.13
EESS_9	10.11	0.51	8.07	0.42	0.444	0.046	0.97	0.17	0.197	0.085	0.187	0.07	0	0.17
EESS_10	5.4	0.32	4.91	0.25	0.303	0.027	0.73	0.16	0.184	0.099	0.147	0.084	0.06	0.17
Ertsberg_1	0.014	0.032	0.308	0.052	0.13	0.026	2.31	0.29	4.26	0.42	5.9	0.35	9.86	0.98
Ertsberg_2	0.013	0.024	0.231	0.038	0.121	0.022	1.83	0.23	3.68	0.35	5.4	0.28	9.1	0.71
Ertsberg_3	0.001	0.024	0.112	0.026	0.072	0.023	1.28	0.24	2.41	0.38	1.97	0.17	4.82	0.65
Ertsberg_4	0.016	0.021	0.105	0.028	0.091	0.025	1.35	0.25	2.82	0.29	4.2	0.28	8.6	0.62
Ertsberg_5	0.033	0.029	0.148	0.03	0.085	0.026	1.41	0.2	3.64	0.44	5.48	0.35	9.38	0.71
Ertsberg_6	0.024	0.028	0.166	0.029	0.087	0.025	1.43	0.23	3.54	0.45	5.09	0.32	8.35	0.79
Ertsberg_7	0.038	0.023	0.713	0.076	0.376	0.037	5.03	0.38	3.65	0.37	9.52	0.61	3.66	0.39
Ertsberg_8	0.398	0.059	0.447	0.057	0.019	0.011	0.021	0.068	0.019	0.044	-0.017	0.059	0.01	0.18
Ertsberg_9	0.179	0.03	0.311	0.034	0.022	0.012	0.063	0.063	0.028	0.039	0.083	0.074	0.05	0.17
Ertsberg_10	0.763	0.072	0.809	0.064	0.022	0.012	-0.008	0.04	0.011	0.042	0.074	0.061	0.19	0.22
Kucing_Liar_1	31.2	1.6	138.6	6.8	18.43	0.9	58.3	2.3	8.34	0.55	3.07	0.19	6.43	0.52
Kucing_Liar_2	92.3	2.7	268.5	8.9	17.66	0.58	27.5	1.3	2.24	0.37	1.233	0.088	1.25	0.32
Kucing_Liar_3	35.6	1.6	215.7	9.8	26.8	1.1	95.5	3.9	14.45	0.77	3.71	0.24	8.71	0.6
Kucing_Liar_4	16.37	0.76	111.4	4.7	17.27	0.65	77.7	3.4	16.1	1.1	3.72	0.21	12.46	0.82
Kucing_Liar_5	21.88	0.82	129.2	5.3	14.85	0.52	43.9	1.7	6.93	0.56	2.52	0.19	4.69	0.57
Kucing_Liar_6	6.13	0.43	47.5	2.6	9.33	0.42	49.6	2.2	10.77	0.7	3.72	0.24	9.74	0.55
Kucing_Liar_7	18.74	0.66	126.6	3.9	18.15	0.62	73	2.3	12.61	0.79	3.51	0.21	7.84	0.61
Kucing_Liar_8	13.75	0.56	105.9	4.3	17.16	0.65	78.6	3	15.4	1.1	3.64	0.19	10.48	0.63
Kucing_Liar_9	29.4	1.2	144.9	4.4	17.85	0.57	73.1	2.2	14.87	0.8	3.41	0.23	9.23	0.58
Kucing_Liar_10	17.64	0.76	94.1	3.8	14.32	0.45	55.1	1.7	10.01	0.62	3.18	0.19	7.72	0.62
Kucing_Liar_11	30.3	1.2	125	5.4	15.13	0.58	60	2.6	14.35	0.79	3.19	0.24	13.26	0.81
Kucing_Liar_12	16.77	0.67	95.5	4	14.38	0.63	63.6	2.7	9.46	0.74	3.43	0.21	5.47	0.5
Kucing_Liar_13	34	1.1	129.3	4.7	11.77	0.49	44.4	1.8	11.2	0.71	2.55	0.19	9.02	0.79
Kucing_Liar_14	29	1	160.7	5.5	19.42	0.69	69.3	2.8	10.36	0.72	3.53	0.23	8.15	0.65
Kucing_Liar_15	32.3	1.4	176	8.9	20.56	0.75	69.1	2.8	10.21	0.68	3.43	0.18	7.44	0.53
Kucing_Liar_16	30	1.2	127.9	4.6	16.15	0.65	67.3	3.1	12.45	0.82	3.56	0.19	9.16	0.7
Kucing_Liar_17	18.23	0.83	79.8	3.9	10.39	0.39	44.1	1.8	9.54	0.67	3.19	0.17	8.14	0.76
Kucing_Liar_18	69.4	2.6	183.6	7.3	12.17	0.46	31.9	1.3	5.48	0.49	2.05	0.15	4.27	0.47
Kucing_Liar_19	9.83	0.57	76.3	3.6	11.7	0.53	50.3	2.2	6.38	0.54	2.7	0.21	2.66	0.31
Kucing_Liar_20	7.41	0.37	44.5	2.4	5.82	0.23	24.2	1.3	5.24	0.4	1.9	0.12	4.61	0.5
97_CG_134_1	3	0.22	19	1.3	3.1	0.23	10.33	0.76	0.71	0.17	1.11	0.11	0.73	0.22
97_CG_134_2	5.07	0.28	43.6	2.8	7.41	0.41	25.1	1.3	0.98	0.16	2.6	0.16	0.41	0.17
97_CG_134_3	0.649	0.065	12.71	0.7	5.14	0.29	47.9	2.9	14.8	1	8.25	0.59	4.14	0.42
97_CG_134_4	0.837	0.076	13.76	0.55	5.29	0.27	49.1	2.1	15.14	0.96	8.65	0.4	3.56	0.49
97_CG_134_5	0.719	0.088	11.73	0.71	4.49	0.21	43.1	2.5	12.27	0.69	6.13	0.34	3.46	0.37

	Tb (ppm)	Tb Int2SE	Dy (ppm)	Dy Int2SE	Ho (ppm)	Ho Int2SE	Er (ppm)	Er Int2SE	Tm (ppm)	Tm Int2SE	Yb (ppm)	Yb Int2SE	Lu (ppm)	Lu Int2SE	Hf (ppm)	Hf Int2SE
DOM100a_13	0.411	0.065	1.77	0.23	0.267	0.047	0.49	0.1	0.089	0.02	0.36	0.11	0.06	0.016	0.204	0.069
DOM100a_14	0.134	0.026	0.5	0.13	0.053	0.016	0.121	0.05	0.0095	0.0088	0.129	0.054	0.014	0.011	0.067	0.057
DOM100a_15	0.259	0.041	1.21	0.16	0.127	0.025	0.42	0.1	0.05	0.016	0.227	0.075	0.021	0.011	0.078	0.073
DOM100a_16	0.259	0.035	1.24	0.18	0.23	0.042	0.63	0.1	0.106	0.035	0.51	0.13	0.068	0.018	2.08	0.22
DOM100a_17	0.175	0.041	1.12	0.15	0.171	0.026	0.45	0.11	0.073	0.023	0.395	0.09	0.058	0.022	2.08	0.23
DOM100a_18	0.118	0.03	0.47	0.11	0.044	0.016	0.038	0.063	0.0042	0.0088	0.076	0.08	0.0042	0.0095	0.024	0.043
DOM100a_19	0.156	0.029	0.78	0.16	0.076	0.019	0.183	0.086	0.0108	0.0081	0.096	0.058	-0.0002	0.0082	0.003	0.056
DOM100a_20	0.25	0.04	1.39	0.18	0.187	0.032	0.458	0.096	0.054	0.016	0.34	0.1	0.05	0.017	0.138	0.068
EESS_1	0.015	0.016	0.119	0.074	0.01	0.011	0.051	0.061	0.009	0.01	0.081	0.05	0.0019	0.0082	0.046	0.054
EESS_2	0.013	0.012	0.205	0.075	0.05	0.017	0.195	0.065	0.025	0.012	0.146	0.072	0.0095	0.0093	0.005	0.043
EESS_3	0.008	0.012	0.112	0.065	0.016	0.01	0.068	0.062	0.009	0.012	0.044	0.052	-0.0032	0.0058	-0.027	0.041
EESS_4	0.01	0.013	0.172	0.07	0.028	0.013	0.059	0.054	0.0148	0.0089	0.086	0.055	0.006	0.01	0.029	0.06
EESS_5	0.011	0.015	0.015	0.049	0.007	0.01	0.03	0.061	0.006	0.011	0.068	0.063	0.006	0.012	0.058	0.062
EESS_6	0.005	0.011	0.11	0.078	0.0147	0.0094	0.052	0.055	0.0162	0.0099	0.108	0.067	0.013	0.012	0.018	0.05
EESS_7	0.002	0.012	0.084	0.057	0.034	0.014	0.097	0.052	0.015	0.01	0.066	0.044	0.0039	0.0083	0.016	0.05
EESS_8	0.01	0.014	0.112	0.054	0.047	0.015	0.124	0.068	0.016	0.011	0.029	0.048	0.0088	0.008	0.033	0.073
EESS_9	0.003	0.011	0.078	0.064	-0.0057	0.0049	0.045	0.053	0.0025	0.0077	-0.01	0.049	-0.0051	0.0058	0.01	0.062
EESS_10	0.008	0.014	0.053	0.068	0.0012	0.0076	-0.036	0.035	0.0018	0.0089	0.025	0.041	0.0034	0.0093	0.013	0.056
Ertsberg_1	1.71	0.12	9.76	0.63	1.67	0.12	4.39	0.39	0.559	0.062	3.75	0.36	0.468	0.061	5.22	0.41
Ertsberg_2	1.7	0.11	10.24	0.6	1.8	0.13	4.71	0.27	0.657	0.062	3.96	0.26	0.571	0.069	3.64	0.31
Ertsberg_3	0.822	0.093	4.47	0.37	0.842	0.082	2.05	0.25	0.291	0.042	2.1	0.27	0.318	0.063	1.31	0.18
Ertsberg_4	1.57	0.12	10.73	0.53	1.9	0.14	4.47	0.33	0.598	0.062	3.85	0.29	0.499	0.062	0.42	0.11
Ertsberg_5	1.92	0.11	12.64	0.67	2.33	0.16	5.38	0.26	0.781	0.054	4.54	0.38	0.631	0.067	2.14	0.2
Ertsberg_6	1.67	0.14	10.03	0.65	1.68	0.13	4.07	0.35	0.57	0.072	4.17	0.43	0.555	0.07	3.01	0.36
Ertsberg_7	0.414	0.047	1.25	0.16	0.101	0.019	0.132	0.071	0.002	0.01	0.035	0.047	0.0029	0.0093	0.02	0.057
Ertsberg_8	0.0048	0.0084	-0.016	0.036	-0.0041	0.0057	-0.038	0.037	-0.008	0.0059	-0.051	0.028	0.0061	0.0082	-0.073	0.033
Ertsberg_9	-0.001	0.01	0.102	0.062	-0.0019	0.0062	0.01	0.051	-0.0079	0.0054	0.03	0.043	0.0041	0.0074	0.02	0.046
Ertsberg_10	0.003	0.013	0.006	0.039	0.003	0.0071	-0.011	0.043	-0.0017	0.0061	0.004	0.048	-0.0088	0.0038	0.039	0.067
Kucing_Liar_1	0.936	0.077	5.94	0.38	1.035	0.073	2.69	0.24	0.42	0.058	2.72	0.3	0.421	0.057	7.4	0.63
Kucing_Liar_2	0.086	0.022	0.65	0.15	0.103	0.028	0.285	0.091	0.046	0.018	0.288	0.098	0.041	0.015	0.79	0.21
Kucing_Liar_3	1.072	0.087	5.64	0.46	0.928	0.064	2.58	0.25	0.36	0.041	2.45	0.24	0.315	0.036	0.57	0.11
Kucing_Liar_4	1.83	0.16	10.49	0.82	1.83	0.12	5.02	0.37	0.663	0.064	4.78	0.44	0.625	0.063	7.5	1.5
Kucing_Liar_5	0.753	0.08	4.58	0.41	0.871	0.06	2.4	0.25	0.376	0.053	2.6	0.24	0.4	0.057	8	1.7
Kucing_Liar_6	1.43	0.1	9.17	0.61	1.78	0.14	4.67	0.38	0.69	0.057	4.63	0.32	0.601	0.053	14.74	0.77
Kucing_Liar_7	1.057	0.092	5.7	0.37	0.901	0.079	2.28	0.18	0.31	0.036	2.15	0.23	0.299	0.035	2.58	0.33
Kucing_Liar_8	1.5	0.1	9.41	0.52	1.621	0.097	4.37	0.33	0.575	0.06	3.88	0.27	0.594	0.055	6.17	0.34
Kucing_Liar_9	1.269	0.096	6.83	0.47	1.151	0.085	3.24	0.19	0.407	0.052	3.07	0.28	0.359	0.048	2.21	0.15
Kucing_Liar_10	1.106	0.083	6.31	0.42	1.228	0.073	3.26	0.22	0.462	0.042	3.1	0.25	0.485	0.067	6.9	0.5
Kucing_Liar_11	2.01	0.14	12.43	0.66	2.29	0.14	6.01	0.3	0.925	0.083	5.89	0.43	0.852	0.069	12.88	0.84
Kucing_Liar_12	0.731	0.071	3.8	0.28	0.685	0.067	1.79	0.2	0.245	0.031	1.94	0.2	0.237	0.034	4.03	0.27
Kucing_Liar_13	1.27	0.12	8.08	0.49	1.482	0.09	3.96	0.22	0.547	0.052	3.82	0.28	0.517	0.057	11.03	0.63
Kucing_Liar_14	1.031	0.091	6.1	0.36	1.075	0.067	3.29	0.28	0.485	0.042	3.06	0.31	0.48	0.055	3.79	0.29
Kucing_Liar_15	1.093	0.098	6.48	0.43	1.223	0.083	3.2	0.23	0.511	0.056	3.2	0.31	0.44	0.046	4.48	0.36
Kucing_Liar_16	1.32	0.11	8.18	0.56	1.501	0.097	3.98	0.24	0.564	0.051	3.39	0.31	0.47	0.048	2.87	0.29
Kucing_Liar_17	1.266	0.094	8.14	0.46	1.541	0.092	4.42	0.36	0.656	0.064	4.29	0.36	0.628	0.045	21.25	0.92
Kucing_Liar_18	0.591	0.05	3.23	0.28	0.58	0.049	1.4	0.11	0.224	0.027	1.33	0.18	0.188	0.031	1.69	0.28
Kucing_Liar_19	0.253	0.046	1.37	0.16	0.23	0.034	0.578	0.097	0.091	0.027	0.66	0.11	0.087	0.017	1.84	0.27
Kucing_Liar_20	0.871	0.085	6.24	0.42	1.406	0.085	4.33	0.3	0.66	0.075	5.13	0.36	0.687	0.051	10.32	0.73
97_CG_134_1	0.069	0.02	0.487	0.096	0.112	0.025	0.324	0.08	0.031	0.017	0.173	0.082	0.025	0.013	-0.026	0.03
97_CG_134_2	0.02	0.013	0.047	0.053	0.018	0.013	0.074	0.044	0.0095	0.0091	0.001	0.037	-0.0018	0.0043	-0.004	0.048
97_CG_134_3	0.143	0.031	0.267	0.084	0.038	0.015	0.046	0.052	0.0042	0.0075	-0.003	0.039	0.014	0.012	0.032	0.052
97_CG_134_4	0.148	0.03	0.231	0.093	0.022	0.01	0.086	0.067	0.0027	0.0065	0.027	0.05	0.0062	0.0076	0.042	0.049
97_CG_134_5	0.146	0.027	0.586	0.089	0.074	0.022	0.218	0.088	0.019	0.01	0.212	0.07	0.016	0.011	0.199	0.073

	La (ppm)	La Int2SE	Ce (ppm)	Ce Int2SE	Pr (ppm)	Pr Int2SE	Nd (ppm)	Nd Int2SE	Sm (ppm)	Sm Int2SE	Eu (ppm)	Eu Int2SE	Gd (ppm)	Gd Int2SE
97_CG_134_6	0.626	0.064	10.66	0.5	4.05	0.18	36.7	1.9	10.17	0.84	6.27	0.34	2.61	0.35
97_CG_134_7	1.85	0.3	15.5	1.9	1.84	0.11	5.58	0.45	0.7	0.2	0.71	0.13	0.23	0.17
97_CG_134_8	0.852	0.088	7.92	0.39	1.46	0.1	7.2	0.47	1.3	0.28	0.65	0.12	0.54	0.25
97_CG_134_9	0.565	0.068	3.48	0.32	0.72	0.14	4.26	0.94	0.77	0.24	0.5	0.12	0.22	0.16
97_CG_134_10	0.937	0.079	11.37	0.66	1.86	0.13	6.05	0.45	0.405	0.094	0.829	0.098	0.06	0.14
97_CG_135a_1	26.9	1.4	83	3.7	7.79	0.33	18.4	1.1	0.95	0.19	2.18	0.16	0.36	0.2
97_CG_135a_2	19.84	0.9	87.5	2.7	12.13	0.45	42.6	1.8	3.36	0.34	4.08	0.25	1.24	0.24
97_CG_135a_3	14.2	0.59	83.1	3.2	15.79	0.65	84.7	3.1	13.06	0.64	8.81	0.42	5.51	0.44
97_CG_135a_4	10.86	0.46	69.9	2.6	14.26	0.57	79.9	3.4	15.67	0.96	8.68	0.41	8.06	0.68
97_CG_135a_5	13.97	0.65	81.4	3.8	15.6	0.67	82.1	3.5	12.83	0.78	8.53	0.37	5.55	0.6
97_CG_135a_6	13.93	0.6	82.3	3.7	15.04	0.61	75.3	2.9	11.15	0.82	7.72	0.4	4.82	0.48
97_CG_135a_7	22.7	1.3	96	4.5	12.14	0.49	41.6	1.5	3.42	0.45	4.46	0.24	1.05	0.22
97_CG_135a_8	25.6	1.3	72.6	2.7	5.96	0.23	11.28	0.73	0.52	0.13	2.37	0.18	0.29	0.18
97_CG_135a_9	28	1.2	98.8	5.1	10.33	0.48	27.6	1.3	1.17	0.2	4.04	0.21	0.41	0.18
97_CG_135a_10	17.61	0.87	85.2	3.4	13.3	0.56	57.6	2.2	6.47	0.6	7.66	0.47	2.3	0.31
7858_1	0.338	0.054	3.81	0.27	1.339	0.096	13.45	0.7	7.67	0.65	4.46	0.3	4.66	0.56
7858_2	0.565	0.057	5.63	0.23	1.94	0.12	18.8	1	9.93	0.61	4.83	0.23	4.47	0.53
7858_3	2.55	0.16	9.52	0.38	1.034	0.076	2.69	0.33	0.37	0.14	0.242	0.072	0.47	0.26
7858_4	2.73	0.18	7.87	0.36	0.666	0.066	1.69	0.2	0.077	0.054	0.206	0.094	0.08	0.18
7858_5	0.81	0.11	4.89	0.29	1.27	0.14	11.3	1.3	2.85	0.49	1.5	0.22	1.65	0.27
7858_6	0.774	0.094	3.14	0.2	0.511	0.054	3.89	0.39	1.79	0.3	1.31	0.14	1.3	0.28
7858_7	0.392	0.07	3.42	0.39	1.048	0.083	9.83	0.72	5.04	0.46	3.24	0.26	4.15	0.47
7858_8	0.395	0.064	3.38	0.16	1.293	0.093	13.49	0.78	6.87	0.57	4.59	0.27	4.01	0.51
7858_9	2.29	0.19	7.92	0.36	0.936	0.075	3.47	0.34	0.84	0.15	0.554	0.082	0.86	0.26
7858_10	0.581	0.044	5.7	0.29	1.92	0.13	17.9	1.2	6.7	0.43	4.62	0.24	2.17	0.35
7858_11	2.17	0.15	19.82	0.84	4.18	0.18	15.36	0.71	0.38	0.11	1.84	0.14	0.2	0.14
7858_12	0.781	0.085	6.62	0.33	2.21	0.11	19.5	1.1	6.41	0.5	4.68	0.31	1.83	0.29
7858_13	0.582	0.076	5.51	0.32	1.62	0.11	15.01	0.83	4.23	0.42	4.24	0.29	1.27	0.32
7858_14	0.516	0.054	5.29	0.24	1.76	0.1	16.09	0.83	5.32	0.48	4.49	0.27	1.51	0.38
7858_15	1.73	0.18	18.66	0.95	4.33	0.22	16.54	0.84	0.3	0.1	2.07	0.2	0.27	0.18
7858_16	1.81	0.14	18.82	0.82	4.14	0.21	14.95	0.96	0.182	0.086	1.81	0.15	0.13	0.16
7858_17	3.06	0.21	23.1	1.1	3.62	0.19	9.66	0.74	0.157	0.069	1.18	0.12	0.01	0.15
7858_18	1.54	0.11	15.75	0.72	3.39	0.16	12.61	0.63	0.34	0.11	1.5	0.1	-0.15	0.14
7858_19	5.01	0.38	35.8	1.8	6.24	0.29	21.4	1.1	0.42	0.11	1.91	0.16	-0.16	0.17
7858_20	2.89	0.16	26.5	1.2	4.67	0.19	14.02	0.74	0.31	0.1	1.71	0.16	0.21	0.21
7859_1	0.248	0.04	5.19	0.31	1.88	0.13	10.14	0.8	0.6	0.14	1.47	0.15	0.2	0.18
7859_2	0.481	0.082	6.53	0.53	1.74	0.18	8.21	0.78	0.393	0.096	1.03	0.11	0.15	0.19
7859_3	0.328	0.049	3.16	0.27	1.04	0.12	6.04	0.57	1.23	0.24	1.26	0.14	0.6	0.2
7859_4	1.144	0.092	15.41	0.62	4.12	0.21	21.3	1	1.28	0.22	2.34	0.16	0.15	0.2
7859_5	1.13	0.14	14.6	1.3	3.82	0.25	17.83	0.98	0.78	0.19	1.74	0.16	0.32	0.19
7859_6	1.422	0.095	6.44	0.26	1.214	0.065	10.01	0.91	3.2	0.39	1.67	0.18	1.74	0.27
7859_7	1.65	0.11	5.93	0.31	0.788	0.059	4.4	0.45	1.55	0.29	0.92	0.13	1.05	0.31
7859_8	1.008	0.087	5.08	0.23	1.273	0.079	9.66	0.61	3.13	0.36	1.97	0.17	1.56	0.28
7859_9	0.114	0.029	1.67	0.17	0.5	0.07	4.61	0.66	1.58	0.3	1.25	0.27	0.75	0.22
7859_10	0.847	0.081	1.96	0.22	0.434	0.05	2.86	0.3	0.55	0.12	0.581	0.092	0.26	0.17
7859_11	1.5	0.13	17.54	0.92	4.07	0.23	14.7	1	0.267	0.09	1.5	0.16	0.2	0.22
7859_12	1	0.24	13.6	1.9	3.68	0.35	20.1	1.8	1.15	0.25	2.36	0.22	0.27	0.24
7859_13	1.35	0.15	16.9	1.2	4.33	0.22	20	1	0.86	0.2	2.25	0.22	-0.04	0.16
7859_14	1.35	0.2	16.3	1.4	4.15	0.22	21.1	1.2	1.15	0.22	2.54	0.2	0.03	0.23
7859_15	1.75	0.13	21.61	0.83	5.15	0.22	20.54	0.87	0.47	0.13	2.45	0.22	0.03	0.18
7859_16	2.01	0.18	23.6	1.7	5.44	0.27	22.5	1.1	0.65	0.18	2.54	0.17	0.06	0.18
7859_17	0.766	0.096	10.99	0.75	3.41	0.19	17.8	1	0.9	0.17	1.99	0.18	0.1	0.18
7859_18	0.71	0.11	12	1.3	3.11	0.17	14.14	0.77	0.39	0.12	1.47	0.13	0.19	0.22

	Tb (ppm)	Tb Int2SE	Dy (ppm)	Dy Int2SE	Ho (ppm)	Ho Int2SE	Er (ppm)	Er Int2SE	Tm (ppm)	Tm Int2SE	Yb (ppm)	Yb Int2SE	Lu (ppm)	Lu Int2SE	Hf (ppm)	Hf Int2SE
97_CG_134_6	0.107	0.03	0.334	0.082	0.052	0.013	0.077	0.067	0.015	0.011	0.094	0.052	0.017	0.01	0	0.04
97_CG_134_7	0.033	0.017	0.136	0.071	0.015	0.014	0.037	0.056	0.017	0.011	0.064	0.059	0.0094	0.008	-0.008	0.04
97_CG_134_8	0.055	0.023	0.154	0.07	0.0202	0.0086	0.057	0.061	0.0086	0.0081	0.056	0.059	0.002	0.0064	-0.034	0.038
97_CG_134_9	0.016	0.012	0.058	0.051	-0.0011	0.0061	0.034	0.034	0.0023	0.0067	-0.02	0.027	0.002	0.006	0.031	0.043
97_CG_134_10	0.017	0.011	0.075	0.044	0.028	0.015	0.076	0.048	0.0159	0.0085	0.044	0.053	0.005	0.008	0.068	0.05
97_CG_135a_1	0.031	0.016	0.289	0.094	0.043	0.015	0.192	0.08	0.023	0.011	0.08	0.049	0.026	0.013	0.123	0.058
97_CG_135a_2	0.122	0.024	0.578	0.096	0.095	0.026	0.274	0.087	0.028	0.013	0.213	0.091	0.021	0.013	0.103	0.053
97_CG_135a_3	0.617	0.051	3.71	0.33	0.697	0.056	2.01	0.21	0.247	0.035	1.47	0.17	0.191	0.031	0.59	0.12
97_CG_135a_4	1.014	0.065	6.13	0.45	1.208	0.079	3.46	0.28	0.498	0.052	2.81	0.26	0.339	0.042	1.84	0.2
97_CG_135a_5	0.604	0.055	3.72	0.28	0.693	0.06	1.86	0.21	0.258	0.037	1.48	0.2	0.168	0.027	0.69	0.11
97_CG_135a_6	0.519	0.046	3.01	0.22	0.513	0.061	1.23	0.13	0.174	0.036	0.94	0.13	0.12	0.021	0.3	0.069
97_CG_135a_7	0.107	0.02	0.45	0.1	0.073	0.021	0.2	0.08	0.0225	0.0087	0.247	0.066	0.02	0.011	0.14	0.061
97_CG_135a_8	0.015	0.013	0.157	0.068	0.056	0.018	0.149	0.059	0.017	0.012	0.092	0.058	0.023	0.014	0.056	0.043
97_CG_135a_9	0.021	0.012	0.071	0.051	0.0094	0.0084	0.057	0.055	0.0051	0.0087	0.031	0.036	0.0059	0.0076	0.03	0.039
97_CG_135a_10	0.198	0.037	0.73	0.12	0.121	0.029	0.324	0.093	0.042	0.016	0.286	0.076	0.018	0.011	0.012	0.043
7858_1	0.228	0.032	0.564	0.095	0.052	0.014	0.063	0.048	0.01	0.012	0.085	0.062	0.006	0.011	-0.022	0.051
7858_2	0.305	0.049	0.69	0.15	0.053	0.016	0.028	0.051	0.0047	0.0096	0.029	0.055	0.013	0.012	0.035	0.055
7858_3	0.077	0.034	0.24	0.16	0.05	0.026	0.193	0.098	0.019	0.014	0.176	0.086	0.02	0.015	0.042	0.05
7858_4	0.01	0.013	0.01	0.041	0.0105	0.0098	0.018	0.038	-0.0046	0.006	-0.04	0.031	-0.0007	0.008	0.037	0.061
7858_5	0.219	0.039	1.31	0.18	0.195	0.03	0.372	0.077	0.043	0.015	0.351	0.096	0.043	0.022	0.015	0.06
7858_6	0.105	0.027	0.55	0.11	0.084	0.021	0.299	0.086	0.026	0.016	0.265	0.065	0.027	0.014	0.169	0.068
7858_7	0.43	0.049	1.7	0.17	0.215	0.029	0.398	0.093	0.051	0.017	0.261	0.084	0.03	0.015	0.031	0.043
7858_8	0.214	0.042	0.67	0.14	0.071	0.021	0.047	0.064	0.015	0.015	0.067	0.061	-0.004	0.01	-0.049	0.052
7858_9	0.119	0.026	0.53	0.14	0.09	0.02	0.258	0.089	0.036	0.016	0.221	0.092	0.035	0.015	0.096	0.056
7858_10	0.123	0.034	0.15	0.078	0.013	0.0087	0.052	0.058	-0.008	0.0058	0.067	0.048	0.0068	0.0085	-0.002	0.048
7858_11	0.006	0.013	0.03	0.045	0.0079	0.0072	0.01	0.058	0.012	0.011	-0.008	0.039	-0.0027	0.0091	0.101	0.076
7858_12	0.077	0.022	0.098	0.066	0.0005	0.0093	0.032	0.056	-0.001	0.008	0.084	0.072	0.007	0.012	0.021	0.054
7858_13	0.032	0.017	0.026	0.057	0.01	0.011	-0.018	0.041	0.009	0.014	-0.044	0.037	-0.0033	0.0091	0.016	0.058
7858_14	0.05	0.019	0.163	0.079	0.002	0.01	0.03	0.065	-0.0063	0.0066	0.037	0.06	0.006	0.012	0.113	0.074
7858_15	0.002	0.011	0.033	0.061	0.005	0.0085	0.024	0.059	-0.0021	0.008	0.059	0.064	-0.0005	0.0093	0.071	0.055
7858_16	0.018	0.014	0.019	0.047	0	0.0069	0.013	0.06	0.005	0.012	0.04	0.051	-0.0007	0.0093	-0.005	0.042
7858_17	0.006	0.01	0.019	0.039	0.0067	0.0085	-0.027	0.041	0.0051	0.0079	-0.027	0.036	0.008	0.011	0.048	0.054
7858_18	0.004	0.013	0.045	0.055	0.0037	0.0072	0.022	0.058	-0.0024	0.009	0.041	0.053	0.0017	0.0082	0.112	0.066
7858_19	0	0.012	0.026	0.056	0	0.008	0.026	0.053	0.0042	0.0097	-0.004	0.038	-0.0023	0.0092	0.005	0.045
7858_20	-0.001	0.011	0.026	0.04	0.009	0.012	0	0.046	0.006	0.011	-0.02	0.048	0.0064	0.0084	0.028	0.059
7859_1	0.029	0.017	0.21	0.068	0.036	0.016	0.115	0.061	0.014	0.014	0.147	0.069	0.017	0.012	0.015	0.051
7859_2	0.03	0.017	0.106	0.052	0.034	0.017	0.076	0.045	0.026	0.015	0.138	0.078	0.003	0.013	0.03	0.06
7859_3	0.078	0.023	0.51	0.12	0.066	0.018	0.248	0.069	0.013	0.011	0.191	0.063	0.024	0.013	0.092	0.076
7859_4	0.013	0.015	0.021	0.04	0.0019	0.0091	0.02	0.062	0.0068	0.0096	0.035	0.047	-0.0075	0.0062	0.057	0.051
7859_5	0.0035	0.0095	0.045	0.05	0.019	0.011	0.081	0.053	0.0046	0.009	0.027	0.047	0.0006	0.0088	-0.002	0.051
7859_6	0.214	0.039	0.81	0.11	0.118	0.027	0.3	0.1	0.056	0.022	0.188	0.064	0.046	0.018	0.054	0.06
7859_7	0.115	0.028	0.63	0.13	0.123	0.02	0.263	0.069	0.034	0.016	0.288	0.089	0.047	0.022	0.057	0.066
7859_8	0.179	0.029	0.63	0.12	0.076	0.021	0.208	0.074	0.027	0.015	0.189	0.078	0.025	0.015	0.035	0.055
7859_9	0.077	0.027	0.45	0.12	0.093	0.024	0.235	0.069	0.042	0.018	0.27	0.11	0.043	0.014	0.064	0.046
7859_10	0.03	0.016	0.2	0.074	0.04	0.018	0.135	0.058	0.019	0.014	0.142	0.097	0.02	0.016	0.001	0.051
7859_11	0.012	0.014	0.054	0.06	0.01	0.013	0.057	0.045	0.0022	0.0095	0.008	0.052	-0.0044	0.0077	0.038	0.06
7859_12	0.007	0.014	0.066	0.056	0.0031	0.0096	0.038	0.057	-0.0063	0.0077	-0.003	0.043	0.0038	0.0096	0.044	0.056
7859_13	0.009	0.014	0.035	0.059	0.013	0.012	-0.001	0.041	0.0024	0.0081	0.016	0.05	0.001	0.01	-0.019	0.055
7859_14	0.015	0.013	0.008	0.053	0.0023	0.0089	-0.02	0.05	0.0007	0.0089	-0.019	0.041	-0.0016	0.009	0.028	0.063
7859_15	0.005	0.013	0.061	0.064	-0.0014	0.0093	0.009	0.058	-0.0045	0.0079	0.075	0.054	-0.0052	0.0069	0.05	0.056
7859_16	0.015	0.014	0.034	0.065	0.006	0.011	-0.03	0.05	0.003	0.012	0.005	0.062	-0.0011	0.0088	0.028	0.061
7859_17	0.008	0.015	0.043	0.051	-0.0055	0.0063	0.027	0.051	-0.0066	0.0063	-0.007	0.042	-0.0034	0.0083	0.041	0.061
7859_18	0.006	0.012	0.028	0.057	0.0101	0.0097	0.045	0.06	0.008	0.011	0.042	0.06	0.0013	0.0087	0.053	0.058

	La (ppm)	La Int2SE	Ce (ppm)	Ce Int2SE	Pr (ppm)	Pr Int2SE	Nd (ppm)	Nd Int2SE	Sm (ppm)	Sm Int2SE	Eu (ppm)	Eu Int2SE	Gd (ppm)	Gd Int2SE
7859_19	1.38	0.21	16.7	1.8	3.98	0.2	18.9	1.2	1.08	0.29	2.34	0.18	0.17	0.18
7859_20	2.33	0.2	26.4	1.3	5.26	0.25	18.4	1.2	0.42	0.11	1.66	0.11	0.14	0.24
7860_1	1.38	0.11	4.09	0.22	0.475	0.036	1.88	0.25	0.152	0.085	0.25	0.11	0.2	0.23
7860_2	1.65	0.11	3.39	0.16	0.308	0.04	0.92	0.16	0.103	0.068	0.134	0.078	0.07	0.2
7860_3	1.03	0.1	2.89	0.15	0.333	0.039	1.17	0.18	0.303	0.097	0.228	0.082	0.6	0.25
7860_4	2.27	0.14	4.48	0.21	0.376	0.04	1.15	0.21	0.168	0.09	0.199	0.088	0.26	0.22
7860_5	1.098	0.091	2.83	0.16	0.259	0.032	0.87	0.12	0.272	0.088	0.24	0.11	0.37	0.2
7860_6	0.851	0.072	2.35	0.15	0.262	0.042	1.12	0.17	0.199	0.076	0.197	0.093	0.45	0.23
7860_7	0.725	0.066	1.91	0.1	0.206	0.023	0.98	0.13	0.21	0.11	0.183	0.093	0.32	0.17
7860_8	0.844	0.093	2.21	0.11	0.243	0.025	1.11	0.19	0.216	0.097	0.189	0.088	0.44	0.21
7860_9	1.103	0.068	3.05	0.17	0.345	0.044	1.28	0.22	0.25	0.095	0.156	0.069	0.41	0.27
7860_10	1.012	0.077	2.78	0.15	0.318	0.037	1.5	0.32	0.315	0.097	0.213	0.063	0.47	0.22
7860_11	5.01	0.22	5.2	0.3	0.14	0.021	0.109	0.08	0.002	0.036	0.115	0.075	0.02	0.16
7860_12	9.63	0.46	27.08	0.97	1.88	0.11	2.39	0.28	0.026	0.047	0.55	0.076	-0.01	0.14
7860_13	8.85	0.44	32.6	1.3	3.18	0.17	5.92	0.42	0.078	0.051	0.753	0.098	0.03	0.2
7860_14	9.06	0.35	31.8	1.3	2.81	0.13	4.58	0.33	0.045	0.051	0.6	0.12	0.08	0.17
7860_15	8.95	0.36	21.08	0.8	1.4	0.11	1.73	0.21	-0.022	0.025	0.452	0.09	0.12	0.17
7860_16	12.88	0.6	23.03	0.93	1.136	0.083	0.94	0.18	0.06	0.067	0.271	0.084	-0.02	0.19
7860_17	8.39	0.35	12.95	0.55	0.827	0.067	1.22	0.19	0.015	0.042	0.159	0.093	-0.14	0.13
7860_18	10.34	0.56	30.6	1.3	2.26	0.13	4.14	0.37	0.093	0.058	0.511	0.086	0.05	0.16
7860_19	7.26	0.31	33.2	1.4	4.55	0.17	13.49	0.74	0.6	0.17	0.89	0.1	0.25	0.22
7860_20	8.94	0.32	33.5	1.2	3.45	0.15	7.36	0.64	0.126	0.081	0.79	0.13	0.06	0.17
7861_1	10.15	0.55	46	1.9	6.43	0.33	20.9	1.1	1.06	0.19	2.05	0.19	0.45	0.22
7861_2	8.42	0.4	34.9	1.5	4.13	0.18	11.73	0.72	0.39	0.11	1.39	0.17	0.18	0.17
7861_3	5.91	0.28	23.9	1	2.44	0.14	3.71	0.33	0.008	0.044	0.68	0.1	-0.05	0.14
7861_4	11.66	0.61	50.7	1.7	6.3	0.26	17.85	0.87	0.58	0.14	1.8	0.17	0.17	0.15
7861_5	10.06	0.47	43.2	1.9	5.59	0.27	15.07	0.7	0.45	0.13	1.63	0.15	0.11	0.2
7861_6	10.47	0.4	47.9	2	6.76	0.28	21.3	1.1	1	0.18	1.98	0.18	0.52	0.2
7861_7	11.27	0.68	48.7	2.4	6.57	0.27	20.57	0.96	0.98	0.18	1.84	0.15	0.48	0.26
7861_8	9.06	0.38	40.4	1.6	6.15	0.23	21.39	0.84	1.72	0.21	1.97	0.17	0.6	0.19
7861_9	10.42	0.49	46.3	2.1	6.56	0.31	24.4	1.3	1.31	0.22	1.87	0.15	0.76	0.26
7861_10	9.37	0.36	44.8	1.8	6.85	0.28	26.9	1.4	1.85	0.26	2.28	0.2	0.75	0.21
7861_11	9.46	0.39	33.7	1.1	3.9	0.19	13.19	0.87	1.03	0.16	1.36	0.12	0.18	0.18
7861_12	11.01	0.51	33.8	1.4	3.4	0.17	9.38	0.71	0.49	0.13	1.06	0.12	-0.02	0.16
7861_13	11.37	0.68	36.3	1.8	3.47	0.2	9.02	0.64	0.31	0.11	1.14	0.13	0.14	0.16
7861_14	15.48	0.76	44	2.2	3.92	0.19	8.96	0.52	0.46	0.12	1.12	0.15	0.32	0.22
7861_15	11.48	0.48	35.7	1.2	3.91	0.17	12.25	0.66	0.86	0.16	1.19	0.1	0.44	0.18
7861_16	11.9	0.52	36.4	1.5	3.54	0.16	9.43	0.58	0.78	0.15	1.15	0.15	0.32	0.15
7861_17	10.49	0.63	35	1.7	4.04	0.16	12.3	0.75	0.88	0.19	1.26	0.15	0.17	0.18
7861_18	6.98	0.41	16.9	0.73	1.36	0.069	2.59	0.29	0.095	0.057	0.45	0.069	0.09	0.13
7861_19	6.65	0.29	22.89	0.95	2.98	0.23	13.7	1.7	1.53	0.3	1.17	0.16	0.5	0.18
7861_20	10.34	0.41	37.1	1.3	4.64	0.17	15.5	1	0.88	0.17	1.38	0.12	0.24	0.16

	Tb (ppm)	Tb Int2SE	Dy (ppm)	Dy Int2SE	Ho (ppm)	Ho Int2SE	Er (ppm)	Er Int2SE	Tm (ppm)	Tm Int2SE	Yb (ppm)	Yb Int2SE	Lu (ppm)	Lu Int2SE	Hf (ppm)	Hf Int2SE
7859_19	0.006	0.012	0.005	0.053	0.025	0.012	0.032	0.056	0.0001	0.0088	0.017	0.065	-0.0053	0.0063	0.022	0.061
7859_20	0.012	0.014	0.004	0.045	0.016	0.012	0.024	0.048	0	0.01	0.011	0.052	0.0048	0.0091	0.021	0.047
7860_1	0.019	0.015	0.24	0.083	0.034	0.014	0.124	0.065	0.018	0.013	0.079	0.064	0.016	0.014	0.066	0.054
7860_2	-0.001	0.01	0.091	0.067	-0.0027	0.0059	-0.01	0.049	0.01	0.01	0.029	0.05	-0.0018	0.0077	0.036	0.06
7860_3	0.073	0.021	0.71	0.13	0.158	0.03	0.56	0.1	0.066	0.02	0.55	0.11	0.102	0.027	0.03	0.06
7860_4	0.05	0.016	0.36	0.1	0.049	0.013	0.184	0.063	0.038	0.015	0.158	0.061	0.02	0.012	0.067	0.066
7860_5	0.059	0.02	0.46	0.1	0.124	0.026	0.46	0.11	0.047	0.016	0.472	0.098	0.077	0.024	0.022	0.05
7860_6	0.086	0.026	0.58	0.12	0.124	0.029	0.44	0.11	0.075	0.025	0.362	0.092	0.069	0.02	-0.005	0.051
7860_7	0.03	0.016	0.174	0.079	0.039	0.014	0.129	0.066	0.01	0.011	0.181	0.081	0.024	0.014	-0.006	0.037
7860_8	0.036	0.019	0.334	0.085	0.07	0.021	0.21	0.076	0.044	0.014	0.206	0.081	0.032	0.013	-0.005	0.046
7860_9	0.065	0.021	0.321	0.098	0.07	0.018	0.189	0.067	0.03	0.017	0.164	0.082	0.032	0.013	0.06	0.054
7860_10	0.046	0.021	0.505	0.092	0.107	0.019	0.318	0.099	0.06	0.019	0.41	0.1	0.063	0.023	-0.002	0.05
7860_11	0	0.012	0.049	0.059	0.0018	0.0074	0.04	0.065	0.0038	0.0096	-0.007	0.048	-0.0005	0.0091	-0.015	0.056
7860_12	-0.0091	0.0081	0	0.036	0.008	0.0089	0.006	0.045	-0.0037	0.0078	-0.013	0.047	-0.0048	0.0068	0.005	0.066
7860_13	-0.0042	0.0095	0.022	0.046	0.003	0.01	-0.002	0.041	-0.0098	0.0056	0.022	0.051	0.004	0.012	-0.052	0.04
7860_14	-0.005	0.0082	-0.004	0.038	0.0019	0.009	0.007	0.045	0.0004	0.0085	-0.034	0.045	0.005	0.01	-0.021	0.043
7860_15	0.005	0.011	-0.008	0.042	-0.0008	0.0098	0.006	0.055	0.0032	0.008	-0.013	0.043	-0.0032	0.0079	-0.037	0.034
7860_16	0.006	0.014	0.031	0.052	0.0011	0.0073	-0.012	0.047	-0.0064	0.0064	0.003	0.041	-0.0005	0.0077	0.004	0.046
7860_17	-0.0117	0.0084	-0.005	0.045	-0.0056	0.0062	0.021	0.048	-0.0025	0.0061	0.01	0.036	0.01	0.01	0.026	0.062
7860_18	0.005	0.012	0.023	0.04	0.006	0.01	0.01	0.048	0.0048	0.0092	0.006	0.04	0.0018	0.0092	-0.008	0.05
7860_19	-0.006	0.0084	0.025	0.04	-0.0036	0.0058	-0.058	0.033	0.0022	0.0081	-0.009	0.036	0.0037	0.0095	0.032	0.061
7860_20	-0.0034	0.0092	0.029	0.051	0.0052	0.0091	-0.008	0.047	-0.0002	0.0096	0.035	0.055	-0.0012	0.0076	-0.001	0.056
7861_1	0.035	0.022	0.085	0.058	0.0135	0.009	0.047	0.046	0.003	0.01	-0.008	0.041	0.018	0.014	-0.011	0.041
7861_2	0.019	0.014	0.004	0.043	0.016	0.012	-0.011	0.032	0.009	0.013	0.014	0.048	0.0048	0.0078	-0.029	0.042
7861_3	0.004	0.013	-0.009	0.035	0.0068	0.0081	0.014	0.032	0.0047	0.0098	-0.002	0.04	0.016	0.014	0.059	0.051
7861_4	0.016	0.014	0.069	0.069	0.005	0.0072	0.016	0.046	0.004	0.01	-0.03	0.04	-0.0029	0.007	0.041	0.055
7861_5	0.022	0.015	-0.003	0.038	0.0093	0.0076	-0.002	0.041	0.012	0.01	-0.031	0.031	-0.0091	0.0077	-0.04	0.029
7861_6	0.025	0.016	0.087	0.066	0.0029	0.0079	0.019	0.044	0.011	0.01	0.016	0.053	-0.003	0.01	0.107	0.063
7861_7	0.023	0.016	0.146	0.069	0.021	0.011	0.061	0.047	0.009	0.014	0.092	0.067	0.0035	0.0091	-0.001	0.034
7861_8	0.119	0.025	0.48	0.1	0.085	0.023	0.24	0.07	0.0081	0.0087	0.111	0.059	0.023	0.01	0.131	0.071
7861_9	0.074	0.02	0.384	0.088	0.059	0.018	0.165	0.07	0.01	0.013	0.023	0.041	0.0057	0.0098	0.03	0.044
7861_10	0.06	0.023	0.263	0.079	0.058	0.02	0.146	0.063	0.007	0.01	0.044	0.054	0.009	0.009	0.023	0.04
7861_11	0.028	0.017	0.031	0.043	0.006	0.01	0.045	0.05	0.026	0.011	0.016	0.04	0.015	0.013	0.164	0.075
7861_12	0.004	0.01	0.051	0.045	0.0038	0.0074	0.011	0.041	0.014	0.012	-0.015	0.043	0.008	0.011	0.043	0.053
7861_13	0.01	0.013	0.037	0.05	-0.0003	0.0076	0.016	0.043	0.014	0.013	-0.041	0.035	0.019	0.014	-0.011	0.043
7861_14	0.01	0.014	0.127	0.059	0.037	0.016	0.124	0.052	0.0135	0.0081	0.113	0.067	0.012	0.015	0.032	0.048
7861_15	0.06	0.021	0.216	0.074	0.043	0.016	0.073	0.052	0.022	0.011	0.148	0.058	0.023	0.014	0.073	0.065
7861_16	0.031	0.016	0.119	0.064	0.023	0.012	0.071	0.04	0.0055	0.0091	0.017	0.044	0.011	0.013	0.07	0.043
7861_17	0.026	0.016	0.141	0.066	0.02	0.012	0.027	0.048	0.012	0.012	0.074	0.063	0.004	0.0077	-0.009	0.041
7861_18	0.021	0.015	0.039	0.046	0.0122	0.0094	0.027	0.046	0.0008	0.0094	0.057	0.046	0.014	0.01	0.195	0.092
7861_19	0.035	0.018	0.099	0.051	0.011	0.01	0.032	0.043	-0.0025	0.0073	0.004	0.041	0.0024	0.0089	0.296	0.089
7861_20	0.008	0.012	0.096	0.058	0.009	0.012	0.071	0.068	0.005	0.0094	0.035	0.054	0.0039	0.0098	0.096	0.049

References

Arribas, A., Hedenquist, J.W., Itaya, T., Okada, T., Concepcion, R.A., and Garcia, J.S., 1995, Contemporaneous formation of adjacent porphyry and epithermal Cu-Au deposits over 300 ka in northern Luzon, Philippines: Geology, v. 23, p. 337-340.

Bali, E., Audetat, A., and Keppler, H., 2011, The mobility of U and Th in subduction zone fluids—an indicator of oxygen fugacity and fluid salinity: Contributions in Mineralogy and Petrology, v. 161, p. 597–613.

Baker, T., Achetberg, E.V., Ryan, C.G, and Lang, J.R., 2004, Composition and evolution of ore fluids in a magmatic-hydrothermal skarn deposit: Geology, v. 32, p. 117-120.

Ballard, J.R., Palin, J.M., Williams, I.S., Campbell, I.H., and Faunes, A., 2001, Two ages of porphyry intrusion resolved for the super-giant Chuquicamata copper deposit of northern Chile by ELA-ICP-MS and SHRIMP: Geology, v. 29, p. 383-386.

Barra, F., Alcota, H., Rivera, S., Valencia, V., Munizaga, F., and Maksaev, V., 2013, Timing and formation of porphyry Cu-Mo mineralization in the Chuquicamata district, northern Chile: New constraints from the Toki cluster: Mineralium Deposita, v. 48, p. 629-651.

Baumgartner, R., Fontboté, L., Spikings, R., Ovtcharova, M., Schaltegger, U., Schneider, J., Page, L., and Gutjahr, M., 2009, Bracketing the age of magmatic-hydrothermal activity at the Cerro de Pasco epithermal polymetallic deposit, Central Peru: A U-Pb and $^{40}Ar/^{39}Ar$ study: Economic Geology, v. 104, p. 479-504.

Baxter, E.F., and Scherer, E.E., 2013, Garnet geochronology: Timekeeper of tectono-metamorphic processes: Elements, v. 9, p. 433-438.

Blundy, J., Mavrogenes, J., Tattitch, B., Sparks, S., and Gilmer, A., 2015, Generation of porphyry copper deposits by gas-brine reaction in volcanic arcs: Nature Geoscience, v. 8, p. 235-240.

Bowman, E., 2017, Investigating magmatic evolution using mafic enclaves in the Kali Dikes of the Grasberg Igneous Complex, Papua, Indonesia: Bachelors of Science thesis, University of Texas at Austin, 107 pp.

Brown, I.M., 1990, Quaternary glaciations of New Guinea: Quaternary Science Reviews, v. 9, p. 273-280.

Burnham, C.W., 1979, Magmas and hydrothermal fluids: in H.L. Barnes, ed., Geochemistry of hydrothermal ore deposits, Wiley-Interscience, New York, p. 71-136.

Burnham, C.W., and Ohmoto, H., 1980, Late-stage processes of felsic magmatism: Mining Geology Special Issue 8, p. 1-11.

Burton, K.W., and O'Nions, R.K., 1991, High-resolution garnet chronometry and the rates of metamorphic processes: Earth and Planetary Science Letters, v. 107, p. 649-671.

Burton, K.W., Kohn, M.J., Cohen, A.S., and O'Nions, R.K., 1995, The relative diffusion of Pb, Nd, Sr and O in garnet: Earth and Planetary Science Letters, v. 133, p. 199-211.

Campbell, I.H., Ballard, J.R., Palin, J.M., Allen, C., and Faunes, A., 2006, U-Pb zircon geochronology of granitic rocks from the Chuquicamata-El Abra porphyry copper belt of

Northern Chile: Excimer laser ablation ICP-MS analysis: Economic Geology, v. 101, p. 1327-1344.

Campos, E., Wijbrans, J., Andriessen, P.A.M., 2009, New thermochronologic constrains on the evolution of the Zaldivar porphyry copper deposit, Northern Chile: Mineralium Deposita, v. 44, p. 329-342.

Candela, P.A., and Holland, H.D., 1984, The partitioning of copper and molybdenum between silicate melts and aqueous fluids: Geochemica et Cosmochimica Acta, v. 48, p. 373-380.

Candela, P.A., and Piccoli, P.M., 2005, Magmatic processes in the development of porphyry-type ore systems: Economic Geology, v. 100, p. 25-37.

Cannell, J., Cooke, D.R., Walshe, J.L., and Stein, H., 2005, Geology, mineralization, alteration, and structural evolution of the El Teniente porphyry Cu-Mo deposit: Economic Geology, v. 100, p. 979-1003.

Catchpole, H., Kouzmanov, K., Bendezu, A., Ovtcharova, M., Spikings, R., Stein, H., and Fontboté, L., 2015, Timing of porphyry (Cu-Mo) and base metal (Zn-Pb-Ag-Cu) mineralization in a magmatic-hydrothermal system – Morococha district, Peru: Mineralium Deposita, v. 50, p. 895-922.

Cathles, L.M., Erendi, A.H.J., and Barrie, T., 1997, How long can a hydrothermal system be sustained by a single intrusive event?: Economic Geology, v.92, p.766-771.

Cathles, L.M., and Shannon, R., 2007, How potassium silicate alteration suggests the formation of porphyry ore deposits begins with the nearly explosive but barren expulsion of large volumes of magmatic water: Earth and Planetary Science Letters, v. 262, p. 92-108.

Chiaradia, M., Vallance, J., Fontboté, L., Stein, H., Schaltegger, U., Coder, J., Richards, J., Villeneuve, M., and Gendall, I., 2009, U-Pb, Re-Os, and ^{40}Ar/^{39}Ar geochronology of the Nambija Au-skarn and Pangui, porphyry Cu deposits, Ecuador: Implications for the Jurassic metallogenic belt of the Northern Andes: Mineralium Deposita, v. 44, p. 371-387.

Chiaradia, M., Schaltegger, U., Spikings, R., Wotzlaw, J.F., and Ovtcharova, M., 2013, How accurately can we date the duration of magmatic-hydrothermal events in porphyry systems?: Economic Geology, v. 108, p. 565-584.

Chelle-Michou C., Chiaradia M., Selby D., Ovtcharova M., and Spiking R., 2015, High-resolution geochronology of the Coroccohuayco porphyry-skarn deposit, Peru: A rapid product of the Incaic orogeny: Economic Geology, v. 110, p. 423-443.

Cline, J.S., and Bodnar, R.J., 1991, Can economic porphyry copper mineralization be generated by a typical calc-alkaline melt?: Journal of Geophysical Research, v. 96, p. 8113-8126.

Cloos, M., 2001, Bubbling magma chambers, cupolas, and porphyry copper deposits: International Geology Review, v. 43, p. 285-311.

Cloos, M., and Housh, T.B., 2008, Collisional delamination: Implications for porphyry-type Cu-Au ore formation in New Guinea: Arizona Geological Society Digest, v. 22, p. 235-244.

Cloos, M., Sapiie, B., Quarles van Ufford, A., Weiland, R.J., Warren, P.Q., and McMahon, T.P., 2005, Collisional delamination in New Guinea: The geotectonics of subducting slab breakoff: Geological Society of America Special Paper 400, 51 pp.

Cloos, M., and Sapiie, B., 2013, Porphyry copper deposits: strike-slip faulting and throttling cupolas: International Geology Reviews: v. 55, p. 43-65.

Core, D.P., Kesler, S.E., and Essene, E.J., 2006, Unusually Cu-rich magmas associated with giant porphyry copper deposits: Evidence from Bingham, Utah: Geology, v. 34, p. 41-44.

Deckart, K., Clark, A.H., Celso, A.A., Ricardo, V.R., Bertens, A.N., Mortensen, J.K., and Fanning, M., 2005, Magmatic and hydrothermal chronology of the giant Rio Blanco porphyry copper deposit, Central Chile: Implications of an integrated U-Pb and $^{40}Ar/^{39}Ar$ database: Economic Geology, v. 100, p. 905-934.

Dewey, J.F., and Bird, J.M., 1970, Mountain belts and the new global tectonics: Journal of Geophysical Research, v. 75, p. 2625-2647.

DeWolf, C.P., Zeissler, C.J., Halliday, A.N., Mezger, K., and Essene, E.J., 1996, The role of inclusions in U-Pb and Sm-Nd garnet geochronology: Stepwise dissolution experiments and trace uranium mapping by fission track analysis: Geochimica et Cosmochimica Acta, v. 60, p. 121-134.

Dilles, J.H., 1987, The petrology of the Yerington Batholith, Nevada: Evidence for the evolution of porphyry copper ore fluids: Economic Geology, v. 82, p. 1750-1789.

Dodson, M.H., 1973, Closure temperature in cooling geochronological and petrological systems: Contributions in Mineralogy and Petrology, v. 40, p. 259-274.

Dong-Deng, X., Li, J., and Wen, G., 2015, U-Pb geochronology of hydrothermal zircons from the Early Cretaceous iron skarn deposits in the Handan-Xingtai District, North China Craton: Economic Geology, v. 110, p. 2159-2180.

Dziggel, A., Wulff, K., Kolb, J., Meyer, F.M., and Lahaye, Y., 2009, Significance of oscillatory and bell-shaped growth zoning in hydrothermal garnet: Evidence from the Navachab gold deposit, Namibia: Chemical Geology, v. 262, p. 262-276.

Edwards, A., Hine, R., Morrison, F., and Windrim, D., 1990, The regional tectonics of the Tasman orogenic system, eastern Australia: Journal of Structural Geology, v. 12, p. 519-543.

Einaudi, M.T., Meinert, L.D., and Newberry, R.J., 1981, Skarn deposits: Economic Geology, v. 75, p. 317–391.

Farley, K.A., Reiners, P.W., and Nenow, V., 1999, An apparatus for high-precision helium diffusion measurements from minerals: Analytical Chemistry, v. 71, p. 2059-2061.

Farley, K.A., 2000, Helium diffusion from apatite: General behavior as illustrated by Durango fluroapatite: Journal of Geophysical Research, v. 105, p. 2903-2914.

Flint, D.E., 1972, Geology of the Ertsberg Copper Deposit, Irian Barat, Indonesia: Bulletin of National Institute of Geology and Mining, Bandung, v. 4, p. 23-28.

Flowers, R.M., Ketcham, R.A., Shuster, D.L., and Farley, K.A., 2009, Apatite (U-Th)/He thermochronometry using a radiation damage accumulation and annealing model: Geochimica et Cosmochimica Acta, v. 73, p. 2347-2365.

Flynn, R.T., and Burnham, C.W., 1978, An experimental determination of rare earth partition coefficients between a chloride containing vapor phase and silicate melts: Geochimica et Cosmochimica Acta, v. 42, p. 685-701.

Gaspar, M., Knaack, C., Meinert, L.W., and Moretti, R., 2008, REE in skarn systems: A LA-ICP-MS study of garnets from the Crown Jewel gold deposit: Geochimica et Cosmochimica Acta, v. 72, p. 185-205.

Gière, R., and Sorensen, S.S., 2004, Allanite and other REE-rich epidote-group minerals: Reviews in Mineralogy and Geochemistry, v. 56, p. 431-493.

Goutorbe, B., Lucazeau, F., and Bonneville, A., 2008, Surface heat flow and the mantle contribution on the margins of Australia: Geochemistry, Geophysics, Geosystems, v. 9, p. 1-14.

Gregory, C.H., 2004, Subsurface meso-scale structural geology and petrology near Big Gossan ore body, Ertsberg (Gunung Bijih) mining district, Irian Jaya, Indonesia: M.S. Thesis, The University of Texas at Austin, 253 pp.

Guo, X., Navrotsky, A., Kukkadapu, R.K., Engelhard, M.H., Lanzirotti, A., Newville, M., Ilton, E.S., Sutton, S.R., and Xu, H., 2016, Structure and thermodynamics of uranium-containing iron garnets: Geochimica et Cosmochimica Acta, v. 189, p. 269-281.

Gustafson, L.B., and Hunt, J.P., 1975, The porphyry copper deposit at El Salvador, Chile: Economic Geology, v. 87, p. 1566-1583,

Guenthner, W.R., Reiners, P.W., Ketcham, R.A., Nasdala, L. and Giester, G., 2013, Helium diffusion in natural zircon: Radiation damage, anisotropy, and the interpretation of zircon (U-Th)/He thermochronology: American Journal of Science, v. 313, p. 145-198.

Haack, U.K., and Gramse, M., 1972, Survey of garnets for fossil fission tracks: Contributions to Mineralogy and Petrology, v. 34, p. 258-260.

Hamilton, W.B., Tectonics of the Indonesian region: US Geological Survey Professional Paper 1078, 345 pp.

Hantsche, A.L., 2013, Rare earth and trace element analysis of anhydrite veins from the Ertsberg mining district, Papua, Indonesia: Bachelors of Science thesis, University of Texas at Austin, 85 pp.

Harris, A.C., Dunlap, W.J., Reiners, P.W., Allen, C.M., Cooke, D.R., White, N.C., Campbell, I.H., and Golding, S.D., 2008, Multimillion year thermal history of a porphyry copper deposit: application of U-Pb, $^{40}Ar/^{39}Ar$ and (U-Th)/He chronometers, Bajo de Alumbrera copper-gold deposit, Argentina: Mineralium Deposita, v. 43, p. 295-314.

Hastings, J.S., and Harrold, J.L., 1988, Geology of the Beal gold deposit, German Gulch, Montana: in Schafer, R.W., Cooper, J.J., and Vikre, P.G., eds., Bulk mineable precious metal deposits of the western United States, Geological Society of Nevada, Reno, p. 207-220.

Hedenquist, J.W., and Browne, P.R.L., 1989, The evolution of the Waiotapu geothermal system, New Zealand, based on the chemical and isotopic composition of its fluids, minerals, and rocks: Geochimica et Cosmochimica Acta, v. 53, p. 2235-2257.

Hedenquist, J.W., and Lowenstern, J.B., 1994, The role of magmas in the formation of hydrothermal ore deposits: Nature, v. 370, p. 519-527.

Hedenquist, J.W., and Thompson, J.F.H., 1995, The ascent of magmatic fluid: discharge versus mineralization: Magmas, fluids, and ore deposits: Mineralogical Association of Canada Short Course, v. 23, p. 263-289.

Henley, R.W., and McNabb, A., 1978, Magmatic vapor plumes and ground-water interaction in porphyry copper emplacement: Economic Geology, v. 73, p. 1-20.

Henley, R.W., King, P.l., Wykes, J.L., Renggli, C.J., Brink, F.J., Clark, D.A., and Troitzsch, U., 2015, Porphyry copper deposit formation by sub-volcanic sulphur dioxide flux and chemisorption: Nature Geoscience, v. 8, p. 210-215.

Henry, C.D., Elson, H.B., McIntosh, W.C., Heizler, M.T., and Castor, S.B., 1997, Brief duration of hydrothermal activity at Round Mountain, Nevada, determined from $^{40}Ar/^{39}Ar$ geochronology: Economic Geology, v. 92, p. 807-826.

Hickey, K.A., Barker, S.L.L., Dipple, G.M., Arehart, G.B., and Donelick, R.A., 2014, The brevity of hydrothermal fluid flow revealed by thermal halos around giant gold deposits: Implications for Carlin-type gold systems: Economic Geology, v. 109, p. 1461-1487.

Holdren, G.C., and Turner, K., 2010, Characteristics of Lake Mead, Arizona-Nevada: Lake and Reservoir Management, v. 26, p. 230-239.

Housh, T., and McMahon, T.P., 2000, Ancient isotopic characteristics of Neogene potassic magmatism in Western New Guinea (Irian Jaya, Indonesia): Lithos, v. 50, o. 217-239.

Hu, R.Z., Wei, W.F., Bi, X.W., Peng, J.T., Qi, Y.Q., Wu, L.Y., and Chen, Y.W., 2012, Molybdenite Re–Os and muscovite $^{40}Ar/^{39}Ar$ dating of the Xihuashan tungsten deposit, central Nanling district, South China: Lithos, v. 150, p. 111-118.

Ito, H., 2014, Zircon U-Th-Pb dating using LA-ICP-MS: Simultaneous U-Pb and U-Th dating on the 0.1 Ma Toya Tephra, Japan: Journal of Volcanology and Geothermal Research, v. 289, p. 210-233.

Jedlicka, R., Faryad, S.W., and Hauzenberger, C., 2015, Prograde metamorphic history of UHP granulites from the Moldanubian Zone (Bohemian Massif) revealed by major element and Y + REE zoning in garnets: Journal of Petrology, v. 56, p. 2069-2088.

Jingwen, M., Zhaochong, Z., Zuaheng, Z., and Andao, D., 1999, Re-Os isotopic dating of molybdenites in the Xiaoliugou W (Mo) deposit in the northern Qilian mountains and its geological significance, Geochimica et Cosmochimica Acta, v. 63, p. 1815-1818.

Jung, S., and Mezger, K., 2003, U-Pb garnet chronometry in high-grade rocks – case studies from the central Damara orogen (Namibia) and implications for the interpretation of Sm-Nd garnet ages and the role of high U-Th inclusions: Contributions to Mineralogy and Petrology, v. 146, p. 382-396.

Kessel, R., Schmidt, M.W., Ulmer, P., and Pettke, T., 2005, Trace element signature of subduction-zone fluids, melts and supercritical liquids at 120-180 km depth: Nature, v. 437, p. 724-427.

Ketcham, R., 2005, Forward and inverse modeling of low-temperature thermochronometry data: Reviews in Mineralogy and Geochemistry, v. 58, p. 275-314.

Kouzmanov, K., and Pokrovski, G.S., 2012, Hydrothermal controls on metal distribution in porphyry Cu (-Mo-Au) systems: Special Publication of the Society of Economic Geologists, v. 16, p. 573-618.

Leys, C.A., Cloos, M., New, B.T.E., and MacDonald, G..D., 2012, Copper-Gold ± Molybdenum Deposits of the Ertsberg-Grasberg District, Papua, Indonesia: Society of Economic Geologists, Special Publication 16, p. 215-235.

Lima, S.M., Corfu, F., Neiva, A.M.R., and Ramos, J.M.F., 2012, U-Pb ID-TIMS dating applied to U-rich inclusions in garnet, American Mineralogist, v. 97, p. 800-806.

Lowell, J.D., and Guilbert, J.M., 1970, Lateral and vertical alteration-mineralization zoning in porphyry ore deposits: Economic Geology, v. 65, p. 373–408.

Ludwig, K.R., 1998, On the treatment of concordant uranium-lead ages: Geochimica et Cosmochimica Acta, v. 62, p. 665-676.

McDowell, F.W., McMahon, T.P., Warren, P.Q., and Cloos, M., 1996, Pliocene Cu-Au Bearing Igneous Intrusions of the Gunung Bijih (Ertsberg) District, Irian Jaya, Indonesia: K-Ar Geochronology: Journal of Geology, v. 104, p. 327-340.

McInnes, B.I.A., Evans, N.J., Fu, F.Q., and Garwin, S., 2005, Application of thermochronology to hydrothermal ore deposits: Reviews in Mineralogy and Geochemistry, v. 58, p. 467-498.

McMahon, T.P., 1994, Pliocene intrusions in the Gunung Bijih (Ertsberg) mining district, Irian Jaya, Indonesia; Petrology and mineral chemistry: International Geology Review, v. 36, p. 820-849.

McMahon, T.P., 1999, The Ertsberg intrusion and the Grasberg Complex: Contrasting styles of magmatic evolution and Cu-Au mineralization in the Gunung-Bijih (Ertsberg) Mining District, Irian Jaya, Indonesia: Bulletin Geologi, v. 31, p. 123-132.

MacDonald, G.D., and Arnold, L.C., 1994, Geological and geochemical zoning of the Grasberg Igneous Complex, Irian Jaya, Indonesia: Journal of Geochemical Exploration, v. 50, p. 143-178.

Maksaev, V., Munizaga, F., McWilliams, M., Fanning, M., Mathur, R., Ruiz, J., and Zentilli, M., 2004, New chronology for El Teniente, Chilean Andes, from U-Pb, Ar/Ar, Re-Os, and fission-track dating: Implications for the evolution of a supergiant porphyry Cu-Mo deposit: Society of Economic Geologists Special Publication 11, p. 1-40.

Marsh, T.M., Einaudi, M.T., and McWilliams, M., 1997, $^{40}Ar/^{39}Ar$ Geochronology of Cu-Au and Au-Ag mineralization in the Potrerillos District, Chile: Economic Geology, v. 92, p. 784-806.

Meinert, L.D., Hefton, K.K., Mayes, D., and Tasiran, I., 1997, Geology, zonation, and fluid evolution of the Big Gossan Cu-Au skarn deposit, Ertsberg district, Irian Jaya: Economic Geology, v. 92, p. 509–526.

Meinert, L.D., Hedenquist, J.W., Satoh, H., and Matsuhisa, Y., 2003, Formation of anhydrous and hydrous skarn in Cu-Au ore deposits by magmatic fluids: Economic Geology, v. 98, p. 147–156.

Meinert, L.D., Dipple, G., and Nicolescu, S., 2005, World skarn deposits: Economic Geology, v. 100, p. 299-336.

Mertig, H.J., Rubin, J.N., and Kyle, J.R., 1994, Skarn Cu-Au orebodies of the Gunung Bijih (Ertsberg) district, Irian Jaya, Indonesia: Journal of Geochemical Exploration, v. 50, p. 179–202.

Metrich, N. and Rutherford, M.J. 1992, Experimental study of chlorine behavior in hydrous silicic melts: Geochimica et Cosmochimica Acta, v. 56, p. 607-616.

Mezger, K., Essene, E.J., and Halliday, A.N., 1992, Closure temperatures of the Sm-Nd system in metamorphic garnets: Earth and Planetary Science Letters, v. 113, p. 397-409.

Mezger, K., Hanson, G.N., and Bohlen, S.R., 1989, U-Pb systematics of garnet: Dating the growth of garnet in the Late Archean Pikwitonei granulite domain at Cauchon and Natawahunan Lakes, Manitoba, Canada: Contributions to Mineralogy and Petrology, v. 101, p. 136-148.

Mizuta, T., and Scott, S.D., 1997, Kinetics of iron depletion near pyrrhotite and chalcopyrite inclusions in sphalerite: The sphalerite speedometer: Economic Geology, v. 92, p. 772-783.

Mpodozis, C., and Cornejo, P., 2012, Cenozoic tectonics and porphyry copper systems of the Chilean Andes: Economic Geology, Special Publication 16, p. 329-360.

Mungall, J.E., Brenan, J.M., Godel, B., Barnes, S.J., and Gaillard, F., 2015, Transport of metals and sulphur in magmas by flotation of sulphide melt on vapour bubbles: Nature Geoscience, v. 8, p. 216-219.

New, B.T.E., 2006, Controls of copper and gold distribution in the Kucing Liar Deposit, Ertsberg Mining District, West Papua, Indonesia [PhD Dissertation]: Australia, James Cook University, 272 pp.

Norton, D., 1982, Fluid and heat transport phenomena typical of copper-bearing pluton environments: Southeastern Arizona: *in* Titley, S.R. (Ed), Advances in the Geology of Porphyry Copper Deposits, Southwestern North America, University of Arizona Press, Tucson, Arizona, p. 59-72.

O'Connor, G.V., Soebari, L., and Widodo, S., 1994, Upper Miocene-Pliocene magmatism of the Central Range Mobile Belt, Irian Jaya, Indonesia: 4th Asia/Pacific Mining Conference, pp. 1–27.

Park, C., Song, Y., Chi, S.J., Kang, I., Yi, K., and Chung, D., 2013, U-Pb (SHRIMP) and K-Ar age dating of intrusive rocks and skarn minerals at the W-skarn in Weondong Deposit: Journal of the Mineralogical Society of Korea, v. 3, p. 161-174.

Parrish, R.R., 1990, U-Pb dating of monazite and its application to geological problems: Canadian Journal of Earth Sciences, v. 27, p. 1435-1450.

Parsons, A.B., 1933, The porphyry coppers: American Institute of Mining and Metallurgical Engineers, 581 pp.

Pasteris, J.D., 1996, Mount Pinatubo volcano and 'negative' porphyry copper deposit: Geology, v. 24, p. 1075-1078.

Paterson, J.T., and Cloos, M., 2005a, Grasberg porphyry Cu-Au deposit, Papua, Indonesia: 1. Magmatic history *in* Porter, T.M. (Ed), Super Porphyry Copper & Gold Deposits: A Global Perpspective: Adelaide, PCG Publishing, p. 313-329.

Paterson, J.T., and Cloos, M., 2005b, Grasberg porphyry Cu-Au deposit, Papua, Indonesia: 2. Pervasive hydrothermal alteration *in* Porter, T.M. (Ed), Super Porphyry Copper & Gold Deposits: A Global Perpspective: Adelaide, PCG Publishing, p. 330-355.

Paton, C., Hellstrom, J., Paul, B., Woodhead, J., and Hergt, J., 2001, Iolite: Freeware for the visualization and processing of mass spectrometric data: Journal of Analytical Atomic Spectrometry, v. 26, p. 2508-2518.

Peng, J., Zhou, M., Hu, R., Shen, N., Yuan, S., Bi, X., Du, A., and Qu, W., 2006, Precise molybdenite Re-Os and mica Ar-Ar dating of the Mesozoic Yaoganagxian tungsten deposit, central Nanling district, South China: Mineralium Deposita, v. 41, p. 661-669.

Pennington, J., and Kavalieris, I., 1997, New advances in the understanding of the Grasberg copper-gold porphyry system, Irian Jaya, Indonesia: Pacific Treasure Trove – Copper-Gold Deposits of the Pacific Rim: Annual Convention and Trade Show of the Prospectors and Developers Association of Canada, p. 79-97.

Penniston-Dorland, S.C., 1997, Veins and alteration envelopes in the Grasberg Igneous Complex, Gunung Bijih (Ertsberg) District, Irian Jaya, Indonesia: Masters of Science thesis, University of Texas at Austin, 402 pp.

Penniston-Dorland, S.C., 2001, Illumination of vein quartz textures in a porphyry copper ore deposit using scanned cathodoluminescence: Grasberg Igneous Complex, Irian Jaya, Indonesia: American Mineralogist, v. 86, p. 652-666.

Pollard, P.J., and Taylor, R.G., 2002, Paragenesis of the Grasberg Cu-Au deposit, Irian Jaya, Indonesia: results from logging section 13: Mineralium Deposita, v. 37, p. 117-136.

Pollard, P.J., Taylor, R.G., and Peters, L., 2005, Ages of intrusion, alteration, and mineralization at the Grasberg Cu-Au deposit, Papua, Indonesia: Economic Geology, v. 100, p. 1005-1020.

Prendergast, K., Clarke, G.W., Pearson, N.J., and Harris, K., 2005, Genesis of pyrite-Au-As-Zn-Bi-Te zones associated with Cu-Au skarns: Evidence from Big Gossan and Wanagon gold deposits, Ertsberg District, Papua, Indonesia: Economic Geology, v. 100, p. 1021-1050.

Pribnow, D.F.C., Kinoshita, M., and Stein, C.A., 2000, Thermal data collection and heat flow recalculations for ODP Legs 101-180: Institute for Joint Geoscientific Research, GGA, Hannover, Germany, p. 101-180.

Quarles van Ufford, A., 1996, Stratigraphy, structural geology, and tectonics of a young forearc-continent collision, western Central Range, Irian Jaya (Western New Guinea), Indonesia: Ph.D. dissertation, University of Texas at Austin, 420 pp.

Quarles van Ufford, A., and Cloos, M., 2005, Cenozoic tectonics of New Guinea: American Association of Petroleum Geologists Bulletin, v. 89, p. 119-140.

Reiners, P.W., Farley, K.A., and Hickes, H.J., 2002, He diffusion and (U-Th)/He thermochronometry of zircon: initial results from Fish Canyon Tuff and Gold Butte: Tectonophysics, v. 349, p. 297-308.

Reiners, P.W., Spell, T.L., Nicolescu, S. and Zanetti, K.A., 2004, Zircon (U-Th)/He thermochronometry: He diffusion and comparisons with ^{40}Ar/^{39}Ar dating: Geochemica et Cosmochimica Acta, v. 68, p, 1857-1887.

Reynolds, P., Ravenhurst, C., Zentilli, M., and Lindsay, D., 1998, High-precision ^{40}Ar/^{39}Ar dating of two consecutive hydrothermal events in the Chuquicamata porphyry copper system, Chile: Chemical Geology, v. 149, p. 45-60.

Rice, C.M., Steele, G.B., Barford, D.N., Boyce, A.J., and Pringle, M.S., 2005, Duration of magmatic, hydrothermal, and supergene activity at Cerro Rico de Potosi, Bolivia: Economic Geology, v. 100, p. 1647-1656.

Richards, J.P., 2003, Tectono-magmatic precursors for porphyry Cu-(Mo-Au) deposit formation: Economic Geology, v. 98, p. 151-1533.

Richards, J.P., 2005, Cumulative factors in the generation of giant calc-alkaline porphyry Cu deposits, *in* Porter, T.M. (Eds), Super Porphyry Copper & Gold Deposits: A Global Perpspective: Adelaide, PCG Publishing, p. 7-25.

Richards, J.P., 2009, Postsubduction porphyry Cu-Au and epithermal Au deposits: Products of remelting of subduction-modified lithosphere: Geology, v. 37, p. 247-250.

Richards, J.P., 2011, Magmatic to hydrothermal metal fluxes in convergent and collided margins: Ore Geology Reviews, v. 40, p. 1-26.

Richards, J.P., 2013, Giant ore deposits formed by optimal alignment and combinations of geological processes: Nature Geoscience, v. 6, p. 911-916.

Richards, J.P., 2015, The oxidation state, and sulfur and Cu contents of arc magmas: implications for metallogeny: Lithos, v. 233, p. 27-45.

Ronacher, E., Jeremy, J.P., Villeneuve, M.E., and Johnston, M.D., 2002, Short life-span of the ore-forming system at the Porgera gold deposit, Papua New Guinea: Laser ^{40}Ar/^{39}Ar dates for roscoelite, biotite, and hornblende: Mineralium Deposita, v. 37, p. 75-86.

Rubin, J.N., and Kyle, J.R., 1998, The Gunung Bijih Timur (Ertsberg East) skarn complex, Irian Jaya, Indonesia: Geology and genesis of a large magnesian, Cu-Au skarn: Mineralized intrusion-related skarn systems, Mineralogical Association of Canada Short Course, v. 26, p. 245-288.

Rusk, B., and Reed, M., 2002, Scanning electron microscope-cathodoluminescence analysis of quartz reveals complex growth histories in veins from the Butte porphyry copper deposit, Montana: Geology, v. 30, p. 727-730.

Sapiie, B., 1998, Strike-slip faulting, breccia formation and porphyry Cu-Au mineralization in the Gunung Bijih (Ertsberg) mining district, Irian Jaya, Indonesia: Ph.D. Dissertation, University of Texas at Austin, 304 pp., 4 plates.

Sapiie, B., and Cloos, M., 2004, Strike-slip faulting in the core of the Central Range of west New Guinea: Ertsberg Mining District, Indonesia: Geological Society of America Bulletin, v. 116, p. 277-293.

Sapiie, B., and Cloos, M., 2013, Strike-slip faulting and veining in the Grasberg giant porphyry Cu-Au deposit, Ertsberg (Gunung Bijih) mining district, Papua, Indonesia: International Geology Review, v. 55, p. 1-42.

Scharer, U., 1984, The effect of initial ^{230}Th disequilibrium on young U-Pb ages: the Makalu case, Himalaya: Earth and Planetary Science Letters, v. 67, p. 191-204.

Scherer, E.E., Cameron, K.L., and Blichert-Toft, J., 2000, Lu-Hf garnet geochronology: Closure temperature relative to the Sm-Nd system and the effects of trace mineral inclusions: Geochimica et Cosmochimica Acta, v. 64, p. 3413-3432.

Schoene, B., 2014, U-Th-Pb geochronology *in* Holland, H.D., and Turekian, K.K. (Eds), Treatise on Geochemistry 2nd Edition: Toronto, Elsevier, 9144 p.

Seedorff, E., Dilles, J.H., Proffett, J.M., Einaudi, M.T., Zurcher, L., Stavast, W.J.A., Johnson, D.A., and Barton, M.D., 2005, Porphyry deposits: Characteristics and origin of hypogene features: Economic Geology, v. 100, p. 251-298.

Seman S., Stockli, D.F., and McLean N.M. (in review, 2017) U-Pb geochronology of grossular-andradite garnet. Chemical Geology

Shinohara, H., Iiyama, J.T., and Matsuo, S., 1989, Partition of chlorine compounds between silicate melt and hydrothermal solutions: 1. Partition of NaCl-KCl: Geochimica et Cosmochimica Acta, v. 53, p. 2617-2630.

Shinohara, H., and Hedenquist, J.W., 1997, Constraints on magma degassing beneath the Far Southeast porphyry Cu-Au deposit, Philippines: Journal of Petrology, v. 83, p. 1741-1752.

Sibson, R.H., 1989, Earthquake faulting as a structural process: Journal of Structural Geology, v. 11, p. 1-14.

Sillitoe, R.H., 2005, Supergene oxidized and enriched porphyry copper and related deposits: Economic Geology, v. 100, p. 723-768.

Sillitoe, R.H. 2010, Porphyry copper systems: Economic Geology, v. 100, p. 3-41.

Sillitoe, R.H., and Bonham, H.F., 1984, Volcanic landforms and ore deposits: Economic Geology, v. 79, p. 1286-1298.

Simmons, S.F., and Brown, K.L., 2006, Gold in magmatic hydrothermal solutions and the rapid formation of a giant ore deposit: Science, v. 314, p. 288-291.

Smit, M.A., Scherer E.E., and Mezger, K., 2013, Lu-Hf and Sm-Nd garnet geochronology: Chronometric closure and implications for dating petrological process: Earth and Planetary Science Letters, v. 381, p. 222-233.

Smith, M.P., Henderson, P., Jeffries, T.E.R., Long, J., and Williams, C.T., 2004, The rare earth elements and uranium in garnets from the Beinn an Dubhaich aureole, Skye, Scotland, UK: Constraints on processes in a dynamic hydrothermal system: Journal of Petrology, v. 45, p. 457-484.

Smye, A.J., and Stockli, D.F., 2014, Rutile U-Pb age depth profiling: A continuous record of lithospheric thermal evolution: Earth and Planetary Science Letters, v. 408, p. 171-182.

Stockli, D., 2005, Application of low-temperature thermochronometry to extensional tectonic settings: Reviews in Mineralogy and Geochemistry, v. 58, p. 411-448.

Suwardy, E., 1995, Grasberg open pit map May 1995: P.T. Freeport Indonesia (unpublished internal report).

Tapster, S., Condon, D.J., Naden, J., Noble, S.R., Petterson, M.G., Roberts, N.M.W., Saunders, A.D., and Smith, D.J., 2016, Rapid thermal rejuvenation of high-crystallinity magma linked to porphyry copper deposit formation; evidence from the Koloula porphyry prospect, Solomon Islands: Earth and Planetary Science Letters, v. 442, p. 206-217.

Tera, F., and Wasserburg, G.J., 1972a, U-Th-Pb systematics in three Apollo 14 basalt and the problem of initial Pb in lunar rocks: Earth and Planetary Science Letters, v. 14, p. 281-304.

Tera, F., and Wasserburg G.J., 1972b, U–Th–Pb systematics in lunar highland samples from the Luna 20 and Apollo 16 missions: Earth and Planetary Science Letters, v. 17, p. 36–51.

Theodore, T.G., and Blake, D.W., 1978, Geology and geochemistry of the West orebody and associated skarns, Copper Canyon porphyry copper deposits, Lander County, Nevada (with a section on electron microprobe analyses of andradite and diopside by N.G. Banks): U.S. Geological Survey Professional Paper 798-C, 85 pp.

Titley, S.R., and Hicks, C.L. (eds), 1966, Geology of the porphyry copper deposits, Southwestern North America: The University of Arizona Press, Tucson, Arizona, pp. 287.

Titley, S.R., 1975, Geological characteristics and environment of some porphyry copper occurrences in the Southwestern Pacific: Economic Geology, v. 70, p. 499-514.

Tomkins, A.G., and Mavrogenes, J.A., 2003, Generation of metal-rich felsic magmas during crustal anataxis: Geology, v. 31, p. 765-768.

Tosdal, R.M., and Richards, J. P., 2001, Magmatic and structural controls on the development of porphyry Cu ± Mo ± Au Deposits: Society of Economic Geologists Reviews, v. 14, p. 157-181.

Trautman, M., 2013, Hidden intrusions and molybdenite mineralization beneath the Kucing Liar skarn, Etsberg-Grasberg mining district, Papua, Indonesia: Masters of Science thesis, University of Texas at Austin, 336 pp.

Ulrich, T., Gunther, D., and Heinrich, C.A., 1999, Gold concentrations of magmatic brines and the metal budget of porphyry copper deposits: Nature, v. 399, p. 676-679.

Valencia, V.A., Ruiz, J., Barra, F., Geherls, G., Ducea, D., Titley, S.R., and Ochoa-Landin, L., 2005, U-Pb zircon and Re-Os molybdenite geochronology from La Caridad porphyry copper deposit: Insights for the duration of magmatism and mineralization in the Nacozari District, Sonora, Mexico: Mineralium Deposita, v. 40, p. 175-191.

Van Dongen, M., Weinberg, R., Tomkins, A., Armstrong, R., and Woodhead, J., 2010, Recycling of Proterozoic crust in Pleistocene juvenile magma and rapid formation of the Ok Tedi porphyry Cu-Au deposit, Papua New Guinea: Lithos, v. 114, p. 282-292.

Van Nort, S.D., Atwood, G.W., Collinson, T.B., Flint, D.C., and Potter, D.R., 1991, Geology and mineralization of the Grasberg porphyry copper-gold deposit, Irian Jaya, Indonesia: Mining Engineering, v. 30, p. 300-303.

Von Quadt, A., Erni, M., Matinek, K., Moll, M., Peytcheva, I., and Heinrich, C.A., 2011, Zircon crystallization and the lifetimes of ore-forming magmatic-hydrothermal systems: Geology, v. 39, p. 731-734.

Warnaars, F.W., Smith, W.H., Bray, R.E., Lanier, G., and Shafiqullah, M., 1978, Geochronology of igneous intrusions and porphyry copper mineralization at Bingham, Utah: Economic Geology, v. 73, p. 1242-1249.

Weiland, R.J., and Cloos, M., 1996, Pliocene-Pleistocene asymmetric unroofing of the Irian fold belt, Irian Jaya, Indonesia: Apatite fission-track thermochronology: Geological Society of America Bulletin, v. 108, p. 1438-1449.

Wilkinson, B.H., and Kesler, S.E., 2007, Tectonism and exhumation in convergent margin orogens: Insights from ore deposits: Geology, v. 115, p. 611-627.

Williams, T.J., Candela, P.A., and Piccoli, P.M., 1995, The partitioning of copper between silicate melts and two-phase aqueous fluids: An experimental investigation at 1 kbar, 800°C and 0.5 kbar, 850°C: Contributions in Mineralogy and Petrology, v. 121, p. 388-399.

William-Jones, A.E., and Heinrich, C.A., 2005, Vapor transport of metals and the formation of magmatic-hydrothermal ore deposits: Economic Geology, v. 100, p. 1287-1312.

Yang, W.B., Niu, H.C., Shan, Q., Sun, W.D., Zhang, H., Li, N.B., Jiang, Y.H., and Yu, X.Y., 2014, Goechemistry of magmatic and hydrothermal zircon from the highly evolved Baerzhe alkaline granite: Implications for Zr-REE-Nb mineralization: Mineralium Deposita, v. 49, p. 451-470.

Yudintsev, S.V., Lapina, M.I., Ptashkin, A.G., Ioudintseva, T.S., Utsunomiya, S., Wang, L.M., and Ewing, R.C., 2002, Accommodation of uranium into the garnet structure: Materials Research Society Proceedings, v. 713, p. 28-32.

Zhao, W.W., Zhou, M.F., and Chen, W.T., 2016, Growth of hydrothermal baddeleyite and zircon in different stages of skarnization: American Mineralogist, v. 101, p. 2689-2700.

Vita

Stephanie Wafforn was born in Chapleau, Ontario. She graduated from Dr. Charles Best Secondary School in 2007 and attended Queen's University from 2007 to 2011, where she received a B.S. in Geological Sciences, with a minor in Geography, earning Honors with Distinction and the Medal in Geological Sciences. Stephanie then completed a M.S. at Oregon State University, studying the structural geology of the Mount Polley porphyry copper deposit in south-central British Columbia, under the advisement of Dr. John Dilles and Dr. Andrew Meigs. Stephanie has accepted a Postdoctoral Fellow position at the University of Texas at Austin.

Email: steffiwafforn@yahoo.ca

This thesis was typed by the author.